Sound Transmission in the Middle Ear

Dissertation
zur
Erlangung der naturwissenschaftlichen Doktorwürde
(Dr. sc. nat.)
vorgelegt der
Mathematisch-naturwissenschaftlichen Fakultät
der
Universität Zürich
von

Rahel Gerig

von
Bütschwil SG

Promotionskomitee:

Prof. Dr. Dr. Oliver Ullrich (Vorsitz)
Prof. Dr. Alexander Huber (Leitung der Dissertation)
Prof. Dr. Norbert Dillier
Prof. Dr. Franz E. Weber

Zürich, 2015

Dedicated to my brothers Lukas and Andreas

Acknowledgements

A number of people have generously given time, advice, encouragement and valuable information for my Ph.D.

I would like to express my deepest gratitude to my supervisor Prof. Dr. med. Alexander Huber, my responsible professor Prof. Dr. Dr. Oliver Ullrich, and the other members of my steering committee Prof. Dr. sc. techn. Norbert Dillier and Prof. Dr. rer. nat. Franz E. Weber to make this thesis possible and for their encouragement and insightful comments. My very sincere gratitude goes to Prof. Dr. Dr. Oliver Ullrich for taking the lead and support of this thesis. I would also specially thank Dr.-Ing. Pascal Ziegler who immediately agreed to evaluate this thesis as an external reviewer.

I am particularly grateful to Prof. Dr. med. Alex Huber, who offered his continuous advice and encouragement throughout the course of this thesis. Thanks to him I had the opportunity to unhesitatingly incorporate into otologic research and participate at various highly interesting projects ongoing in our group 'biomechanics of hearing'. He also gave me the opportunity to meet colleagues from otologic research and otologic industry worldwide at conferences and meetings, what highly motivated me to advance the ongoing projects.

Thanks to Dr. Jae Hoon Sim for all the spadework he did for this project. This thesis would not have been possible without his great knowledge and expertise about middle-ear mechanics.

The support of Dr. med. Christof Röösli was essential for this study, since he dissected the temporal bones for my measurements. Additionally he was 'the otology expert' and a valuable advisor anytime. Special thanks to you! Thanks as well to Dr. med. Adrian Dalbert for the support with the time-consuming drilling of the bones, and being a great (office) colleague. I also want to thank the pathology department of the University hospital Zurich for supporting us with temporal bones.

I am very grateful for the well-established collaboration of our group with the University of Stuttgart (Institute of Engineering and Computational Mechanics), especially with my co-workers Dipl.-Ing. Sebastian Ihrle and Dr.-Ing. Albrecht Eiber, who contributed decisive to my biomechanical knowledge and deeply interesting (subject-specific) conversations.

I would like to thank all former and current members of the 'biomechanics of hearing'-group and ENT-colleagues that enriched my time as a Ph.D. student: Ivo Dobrev (for his indispensable help with coding in matlab and being a great desk and lab neighbor), Flurin Pfiffner (for his effort in the group, all the constructive advices, and the collaboration in the stapedotomy study), Konrad Thöle and Dominik Péus ('the experts' of sheep temporal bone drilling), Lukas Prochazka (for his great 'fluid dynamic' expertise, matlab tips and being a great colleague), Lichun Zhang and Dr. Xie (thanks for giving me insights into the Chinese culture and being great colleagues), Dr. (!) med. Christian Fausch and Dr. med. Christian Meerwein (thanks for all the fun, the foundation of the research intelligence agency and the success at the FaoL – it was a great time!), Bebeka Gjoksi and Colette Hemsley (for pure women power, interdisciplinary discussions and lovely coffee hours), Rita Jauch and Patrizia Rauso, V. Seematter, Silva Stutz, CI-(coffee)-team (Wai Kong Lai, Markus Schmid, René Holzreuter, Bernd Strauchmann, Andrea Kegel, Stephanie Maassen, Michael Büchler, Jenny

Appleton-Huber, Anja Kietzmann, Franziska Conod, Stephanie Diehl, Helena Lichtensteiger…). I would also like to thank Dr. Dorothe Veraguth for the support and the access to the audiology facilities.

My sincere thanks also go to the colleagues from SCANCO (SCANCO Medical AG, Brüttisellen, Switzerland) for the support with the micro-CT scans and the corresponding valuable advises – it was always fun to improve my micro-CT-data-processing skills in Brüttisellen.

A special thank to the research group of the department of emergency surgery of the University hospital Zurich, especially PD Dr. sc. nat. Paolo Cinelli, for giving us the opportunity to scan the micro-CT samples directly at the hospital. Thank you Paolo for the support!

Many thanks to the Swiss National Science Foundation (SNSF) for funding (# 138726) and, therefore, for making this project possible. This project was also a part of a DACH (D-A-CH) founded project – as a collaboration of the Swiss National Science Foundation (SNSF) and the German Research Foundation (DFG).

This dissertation wouldn’t have been possible without the support of my family. Already during my studies, my mother Ruth and Peter were always available for a hike or a short trip to Italy for emergency shopping including gelato, vino, pasta and pizza. You did and still do enrich my life - as well as my brothers Lukas and Andreas to whom I dedicate this work. Since I can remember you always supported me personal and jobwise. I still admire your good advices! Thanks to Nadia and Cordelia for completing our full evening’s discussions. Many thanks to my father Joe, Enza and ‘almost sister’ Morena, my Italian part of the family, for the tireless support.

A special thank to all my friends that accompanied my daily life as a Ph.D. student; especially Linda Oesterle, Claudia Röösli, Axel Beel, Janine Löpfe, Karin Baumann, Leonie Gschwend, Evelyn Fischer, (…). Schön, dass es euch gibt!

Nicolas, my love, you shared all my ups and downs - and made ‘ups’ out of the ‘downs’. You let me forget unsuccessful measurements or imminent exams. Your analytic thinking built a respectable contrast to my emotional energy and evoked new inputs and insights for my work. I will never forget our numerous short trips on weekends, our rides to Köln (to Carla, Haki, Dorian and Viola) and lazy Sunday evenings. I still don’t understand your passion for old (junk?) cars, but I’m looking forward to discuss that issue with you until the end of my life.

Rahel Gerig

Summary

Hearing is the perception of vibration – a series of variations in air pressure. It involves several mechanisms: the vibrations are collected at the outer ear and travel via the ear canal to the eardrum, where the air pressure variations get transformed into mechanical vibrations. These vibrations are then conveyed by the middle-ear ossicles to the inner ear, where finally a signal is formed that stimulates the brain – resulting in sound perception. It is generally accepted that the middle ear evolutionary developed to overcome the impedance mismatch between air outside the ear and the fluid in the inner ear; more than 99% of the vibrations would be rejected by the borderline between air and fluid without a bridging system like the middle ear.

The field of research in 'middle-ear mechanics' focuses on the anatomical features and function of the middle ear, which includes the eardrum, the three ossicles malleus, incus and stapes, and the joints between the ossicles. The ossicular chain is attached to the middle ear cavity by suspensory attachments like muscles, ligaments and tendons.

The eardrum is the only structure of the middle ear that is accessible without dissection. Therefore, some studies presented intraoperative measurements, but most of the measurements to investigate the middle-ear sound transmission were performed on cadaveric temporal bones. It is known from the literature that the temporal model is a valuable model of the middle ear function compared to live subjects.

The stapes is the smallest bone in the human body with a width of less than 3 mm and a height less than 3.5 mm. The largest ossicle is the malleus with a length of less than 9 mm. The resulting motion magnitudes under acoustic stimulation at physiologically relevant levels are in the nanometer-range. This requires highly precise measurement systems as for example the Laser Doppler Vibrometer (LDV), which has a high sensitivity (0.3 μm/s) that can measure e.g. displacements of around 0.008 nm at 6 kHz.

This dissertation investigates the sound transmission in the middle ear with focus on the joint between malleus and incus; the incudo-malleolar joint (IMJ). The physiological behaviors and functional roles of IMJ in human ears is provided by a series of four measurements, which include 1) middle-ear sound transfer function, 2) behavior of the IMJ under directional dynamic forces, 3) behavior of the IMJ under quasi-static loads, and 4) relative motion between the malleus and incus under sound-induced acoustic stimulation. Overall, the findings suggest a frequency-dependent mobility of the human IMJ under dynamic stimulation in the physiological range, especially above 2-3 kHz. Thus, the IMJ induces a loss in middle-ear sound transmission at higher frequencies.

In the literature, the mobility of the IMJ under acoustic stimulation at physiologically relevant levels is still under debate. While it appeared that the IMJ is mobile under all the different types of stimulation in the investigations in the scope of this thesis, the four different approaches show different aspects of the functional roles of the IMJ.

In the *first measurement*, six fresh human temporal bones were acoustically stimulated at physiologically relevant levels (90-110 dB SPL, 0.25-8 kHz). The 3-D motion of the stapes was constructed from motions of about 100 measurement points on the stapes footplate, measured using a scanning LDV system. The measurements were made for two different

conditions of the IMJ: (1) normal IMJ and (2) artificially immobilized IMJ. The artificial immobilization of the IMJ was confirmed by measuring the relative motion between the malleus and the incus before and after the immobilization. Comparison between the measurements under two different IMJ conditions revealed that the immobilization of the IMJ causes increase in the magnitudes of the piston-like motion of the stapes, and the increase was frequency-dependent. The increase was prominent at high frequencies above 2 kHz. The magnitude ratios of the rocking-like motions to the piston-like motion were similar for both IMJ conditions. Such results suggest that the mobility of the IMJ in normal ears causes middle-ear sound transmission loss under physiologically relevant levels of acoustic stimulation without a change of the stapes motion pattern, especially at frequencies above 2 kHz.

In the *second measurement*, five isolated malleus-incus-complexes (MICs) from fresh human temporal bones were used. The isolated malleus-incus complex was glued to a custom-made sample holder in a way that the malleus was fixed but the incus was still mobile, and thus relative motion between the two bones is possible. The excitation was dynamic using an electro-dynamic shaker (0.01–10 kHz, sweep, multi-sine, single sine) with three different excitation directions: inferior-superior, anterior-posterior, and lateral-medial. Simultaneously, the 3-D motion of the MIC was measured using a 3-D LDV system. No relative motion between malleus and incus below 3 kHz was observed in the preliminary data analysis. However, above 3 kHz, relative motion in the IMJ was observed, which increased with increasing frequency. The pattern of the relative motion was dependent on the excitation direction, suggesting that the mobility of the IMJ is directional allowing larger relative motion for specific directions.

The same five MICs mounted on the sample holder were also used for the *third measurement*, but in this measurement the incus was loaded with quasi-static forces. The quasi-static forces were applied to multiple points on the incus with the magnitude of the force increasing gradually. The amplitudes of the quasi-static forces were controlled and measured by a load cell. Simultaneously, the 3-D motion of the incus was measured using a 3-D LDV system. The preliminary results show spatial motion patterns different from the corresponding patterns under dynamic excitation. Viscous behavior of the IMJ was also observed, indicating energy dissipation at the IMJ. When the large magnitude of the quasi-static force was applied, the surfaces of the two ossicles contacted and slid against each other. Patterns of the sliding motion followed the surface profiles of the two ossicles at the IMJ. The observations in this measurement are considered as a role of protection mechanism of the IMJ under large static pressure change.

In the *fourth measurement*, 3-D motions of the malleus and incus were constructed by measuring the 3-D motion components of several points on each of the two ossicles using a 3-D LDV system, in one frozen and two fresh human temporal bones. The stimulation was delivered via a loudspeaker to an artificial ear canal (90-110 dB SPL, 0.5-5 kHz). Relative motion between malleus and incus was observed. This relative motion increased with increasing frequency. The incus motion at the lenticular process was smaller than the malleus motion at the umbo at high frequencies.

The middle-ear sound transmission in reconstructed ears may differ from the physiological situation. For example during stapes surgery as a treatment for otosclerosis, the fixed stapes structure is removed and replaced with an artificial stapes: a stapes prosthesis. In our ongoing study about the quality of hearing after stapes surgery (n=21), audiometric tests (pure tone audiogram, test for distortions at different frequencies and loudness levels) and a questionnaire (APOSE) were assessed. The subjective satisfaction of the subjects was positive three months after surgery: 80 % of the 15 subjects (3 months after surgery) state to hear better and none of the subjects state to hear worse compared to before surgery. This finding was confirmed with the audiometric results: the pure tone average (for 0.5, 1, 2, and 3 kHz) gain was 21±12 dB HL three months after surgery compared to before surgery. However, 52 % of the subjects report distortions in the questionnaire and 59% in the audiometric tests at least once during the three months follow up. Most distortions were subjectively reported at ‘loud sounds’, which was consistent with the audiometric observations.

The findings of a frequency-dependent mobility of the human IMJ need to be integrated in the future into existing virtual middle-ear models, which serve as a base to develop and improve middle-ear prostheses. The aim is to further develop and improve middle-ear prostheses, and to optimize the quality of perceived sound.

Zusammenfassung

Hören ist die Wahrnehmung von Schwingungen, verursacht durch wiederholte Schwankungen des Luftruckes. Verschiedene Mechanismen sind daran beteiligt: die Schwingungen werden im Aussenohr gesammelt und durch den Gehörgang ans Trommelfell weitergeleitet, wo die Schwankungen des Luftdrucks in mechanische Schwingungen umgewandelt werden. Diese Schwingungen werden über die Ossikel an das Innenohr geleitet, wo schlussendlich ein Impuls entsteht, der im Gehirn die Empfindung des Hörens auslöst. Es ist allgemein anerkannt, dass sich das Mittelohr während der Evolution entwickelt hat, um die Impedanz-Unterschiede zwischen der Luft im Aussenohr und der Flüssigkeit im Innenohr zu überbrücken; ohne das Mittelohr als Überbrückungssystem würden über 99% der Schwingungen am Grenzbereich zwischen Luft und Flüssigkeit verloren gehen.

Die Mittelohrmechanik-Forschung konzentriert sich auf die Anatomie und Funktion des Mittelohres. Dieses umfasst das Trommelfell, die drei Ossikel Hammer, Amboss und Steigbügel und die Gelenke zwischen den Ossikeln. Mit den dazugehörigen Muskeln, Bändern und Sehnen sind die Ossikel in der Paukenhöhle aufgehängt.

Das Trommelfell ist die einzige Struktur des Mittelohres, die von aussen sichtbar ist. Deshalb wurden die meisten Messungen der Schallübertragung im Mittelohr an Felsenbeinen von Kadavern – oder selten auch intraoperativ – gemessen. Die Literatur zeigt, dass Mittelohre von Kadavern vergleichbare Schallübertragungseigenschaften zeigen wie bei Lebenden.

Der Steigbügel ist der kleinste Knochen im menschlichen Körper mit einer Breite von weniger als 3 mm und einer Höhe von weniger als 3.5 mm. Das grösste Ossikel ist der Hammer mit einer Länge von weniger als 9 mm. Die Schwingungen dieser Ossikel unter physiologisch relevanter akustischer Stimulation liegen im Bereich von Nanometern. Dies erfordert hochpräzise Messsysteme wie zum Beispiel das Laser Doppler Vibrometer (LDV), welches eine Sensitivität von 0.3 μm/s aufweist, d.h es können sogar Bewegungen von circa 0.008 nm bei 6 kHz gemessen werden.

Im Rahmen dieser Dissertation wurde die Schallübertragung im Mittelohr analysiert mit Fokus auf das Gelenk zwischen Hammer und Amboss: das Hammer-Amboss-Gelenk (HAG). Das physiologische Verhalten und die Funktion des menschlichen HAGs wurde in vier verschiedenen Messreihen untersucht: 1) die Mittelohr-Übertragungsfunktion, 2) Verhalten des HAG unter direktionaler dynamischer Anregung, 3) Verhalten des HAGs unter quasi-statischer Belastung, und 4) die relative Bewegung zwischen Hammer und Amboss unter schallinduzierter akustischer Anregung.

Die Resultate zeigen im Allgemeinen eine frequenzabhängige Bewegung des HAGs unter dynamischer Anregung im physiologischen Bereich, vor allem für Frequenzen größer als 2-3 kHz. Das heisst also, dass es im HAG bei hohen Frequenzen zu einem Schallübertragungsverlust kommt.

In der Literatur wird die Beweglichkeit des HAGs unter akustischer Anregung im physiologischen Bereich diskutiert. Die Untersuchungen im Rahmen dieser Dissertation haben gezeigt, dass das HAG unter verschiedenen Anregungsformen beweglich ist.

In der *ersten Messreihe* wurden sechs frische menschliche Felsenbeine bei physiologisch relevanter Lautstärke (90-110 dB SPL, 0.25-8 kHz) akustisch stimuliert. Mit einem

scannenden LDV wurden circa 100 Punkte auf der Steigbügel Fussplatte gemessen und die 3-D Bewegung des Steigbügels berechnet. Die Messungen wurden unter zwei verschiedenen HAG-Zuständen durchgeführt: 1) mit dem normalen HAG und 2) mit einem künstlich fixierten HAG. Die künstliche Fixierung des HAGs wurde mit einer Messung der relativen Bewegung zwischen dem Hammer und dem Amboss überprüft – vor und nach der Fixierung des HAGs. Der Vergleich zwischen den Messungen der Bewegung des Stapes mit normalem und fixiertem Gelenk zeigte, dass durch die Fixierung des HAGs die Magnitude der kolbenförmigen Bewegung frequenzabhängig zunahm. Auffallend war die Zunahme der kolbenförmigen Bewegung bei den hohen Frequenzen über 2 kHz. Das Verhältnis der Kippbewegungen zu den kolbenförmigen Bewegungen war mit und ohne Fixierung des HAGs ähnlich. Das Resultat zeigt also, dass die Bewegung im HAG unter physiologsicher akustischer Stimulation im normalen Ohr zu einem Schalleitungsverlust führt, ohne dass das Bewegungsmuster des Stapes beeinflusst wird.

In der *zweiten Messreihe* wurden fünf isolierte Hammer-Amboss-Komplexe (HAKs), bestehend aus Hammer, HAG und Amboss aus frischen menschlichen Felsenbeinen entnommen. Die HAKs wurden so auf einer Probenhalterung angebracht, dass der Hammer fest mit der Halterung verklebt war und sich der Amboss frei bewegen konnte. So war noch eine relative Bewegung im HAG möglich. Mit einem elektrodynamischen Shaker wurde eine dynamische Anregung mit (0.01 – 10 kHz, Multisinus, Sweep, Einzelsinus) aus verschiedenen Richtungen appliziert: von inferior-superior, von anterior-posterior und von lateral-medial. Gleichzeitig wurde die 3-D Bewegung des HAKs mit einem 3-D LDV gemessen. Die vorläufigen Resultate zeigen, dass bei Frequenzen unter 3 kHz keine relativen Bewegungen im HAG vorkommen. Bei Frequenzen über 3 kHz wurden relative Bewegungen im HAG beobachtet, die mit steigender Frequenz weiter zunahmen. Die Bewegungsmuster und die Amplituden der relativen Bewegungen waren abhängig von der Anregungsrichtung. Dies weist darauf hin, dass das HAG für spezifische relative Bewegungsrichtungen direktional grössere Bewegungen zulässt als für andere.

Dieselben fünf HAKs, bereits auf der Probenhalterung angebracht, wurden auch für die *dritte Messreihe* verwendet. In dieser Messreihe wurde der Amboss mit einer quasi-statischen Kraft belastet. Diese quasi-statische Kraft wurde an verschiedenen Messpunkten auf den Amboss appliziert und dabei die Intensität der Kraft graduell erhöht. Die Amplituden der quasi-statischen Kraft wurden mit einer Kraftmesszelle gemessen und kontrolliert. Gleichzeitig wurde mit einem 3-D LDV die 3-D Bewegung des Amboss an verschiedenen Punkten gemessen. Die vorläufigen Resultate zeigen andere Bewegungsmuster als unter dynamischer Anregung. Es wurde ein viskoelastisches Verhalten des HAGs beobachtet, was auf einen Energieverlust im HAG hinweist. Wenn das HAG mit grossen Kräften belastet wurde, zeigte sich, dass die Gelenkoberflächen von Hammer und Amboss aufeinandertrafen und aneinander glitten. Das Muster der gleitenden Bewegung folgte den anatomischen Oberflächenprofilen der Gelenksoberflächen von Hammer und Amboss. Diese Gleitbewegungen gelten als Schutzfunktion des HAGs für das Innenohr bei grossen Druckveränderungen.

In der *vierten Messreihe* wurden die 3-D Bewegungen an verschiedenen Punkten auf Hammer und Amboss in einem gefrorenen und zwei frischen menschlichen Felsenbeinen mit einem 3-D LDV gemessen. Die Ossikel wurden mit einem Lautsprecher in einem künstlichen Gehörgang angeregt (90-110 dB SPL, 0.5-5 kHz). Es zeigten sich relative Bewegungen zwischen Hammer und Amboss. Diese relativen Bewegungen nahmen mit zunehmender

Frequenz weiter zu. Die Bewegungen des Amboss am Processus lenticularis waren kleiner als die Bewegungen des Hammers am Umbo.

Die Schalleitung in einem rekonstruierten Ohr kann sich von einem normalen Ohr unterscheiden. Bei der Stapedotomie-Operation zur Behandlung von Otosklerose wird der pathologisch fixierte Steigbügel entfernt und durch einen künstlichen Steigbügel, einer Steigbügel-Prothese, ersetzt. In unserer laufenden Studie über die Qualität des Hörens nach einer Stapedotomie-Operation (n=21) werden audiometrische Tests (Reintonaudiogramme und Tests für die Erfassung von subjektiv wahrgenommenen Verzerrungen bei verschiedenen Lautstärken und Frequenzen) durchgeführt und ein Fragebogen (APOSE) von den Studienpatienten beantwortet. Die ersten Ergebnisse zeigen, dass die subjektive Zufriedenheit der Patienten drei Monate (n=15) nach der Operation gut ist: 80% von den 15 Studienteilnehmern gaben im Fragebogen an ‚besser' zu hören als vor der Operation. Kein Patient gab an, dass sich sein Hören verschlechtert habe. Ähnliche Ergebnisse zeigen auch die audiometrischen Tests: die durchschnittliche Luftleitungs-Hörschwelle im Reintonaudiogramm zeigt eine Verbesserung von 21±12 dB HL drei Monate postoperativ im Vergleich zu vor der Operation. Allerdings gaben 52 % der Studienpatienten während den ersten drei Monaten im Fragebogen an, dass sie im Alltag Verzerrungen wahrnahmen. Auch in den audiometrischen Test wurden von 59 % der Studienpatienten mindestens einmal in dieser Zeit Verzerrungen wahrgenommen. Im Fragebogen und bei den audiometrischen Test wurden Verzerrungen subjektiv am meisten bei ‚lauten Tönen' angegeben.

Die gewonnenen Erkenntnisse über die frequenz-abhängige Beweglichkeit des HAGs sollten zukünftig in bestehende virtuelle Mittelohr-Modelle integriert werden. Diese Modelle können als Basis für die Entwicklung und Optimierung von Mittelohr-Prothesen eingesetzt werden. Das Ziel ist es, die Mittelohr-Prothesen und die wahrgenommene Hörqualität weiter zu verbessern.

Table of contents

Preface: The sense of hearing

The five traditionally recognized senses hearing, sight, taste and touch come along in modern physiology with the senses for temperature, kinesthetic, pain, balance and various internal stimuli. Thus, hearing is one out of a multitude of senses that humans are able to perceive and plays a very important role. *First*, hearing is our most important sense for communication. The melody, emphasis, pitch and volume of a voice greatly influence the message of a conversation. This is essential to observe irony, goodwill, rejection and retention of the dialogue partner. Therefore, hearing has an often-underestimated emotional and social function.

„Nicht sehen trennt den Menschen von den Dingen. Nicht hören trennt den Menschen vom Menschen.“ Immanuel Kant

„Blindness separates people from things. Deafness separates people from people.“ Immanuel Kant

Second, hearing informs and alerts. Twenty-four hours a day the ear detects sound from surroundings, unlike the eyes that are closed during sleep. Sounds like alarm bells or crying of a baby is then interpreted in the brain and provokes awakening as an alert. Even during daytime the perception of sounds like announcements in public transports or phone conversations simplify human’s everyday life. *Third*, hearing is important for orientation in space. The source of a sound can be detected, what is of high significance for the orientation in the dark or the behavior in road traffic. *Fourth*, a normal hearing is important for the speech and language development in young children. Unborn children already begin to recognize important sounds in their environment, such as the voice of their mother or primary caretaker – they associate these familiar sounds with safety and security later on. As they grow, babies begin to mimic the things heard and with the feedback from their own hearing they control their voice. The ear is the first sensory organ to develop in the womb and is fully functional at birth. *Fifth,* hearing opens the gate to the fascinating world of sounds and all the emotional moments we associate with it e.g. music, laughing of family and friends, waves at the sea, raindrops at the window, wind blowing through the trees in the forest…

The ear has an outstanding resolution and can perceive sound in a wide range that is either extremely soft or extremely loud, and everything in between. The ratio between the quietest sound and the pain threshold is 1:1’000’000. It is even possible to hear a single instrument out of an ensemble (Scheich et al. 1998) or to concentrate on one dialog in a crowded room brimming with multiple conversations (‘cocktail party effect’) (Asari et al. 2006). The disadvantage of such a sensitive organ is that it is harder to inhibit. There is no physical reflex for shutting out sound. Instead, the brain controls how the ear obtains information (Hubel et al. 1959, Hillyard et al. 1973, Woldorff et al. 1993). This regulation of auditory inputs in the brain, a phenomenon known as ‘auditory attention’, requires many complex interactions in the brain (Fritz et al. 2007).

According to the World Health Organization (WHO), 15% of the world population are affected by hearing loss. However, the importance of good hearing and the consequences of hearing loss are still underestimated. The number of people affected by hearing loss rises due to the demographic aging of our society and the growing noise pollution in our environment. The disadvantage from untreated hearing loss range from disadvantages at work, relationship problems and social isolation, and even to depression. Especially for children born with significant hearing loss (annually over 665'000 according to the UN children’s fund Unicef) the consequences of a missed treatment are severe concerning the development of speech and language. Therefore, hearing research is important now – and for the future.

I. Background

I.I Introduction

Because hearing is important and impaired hearing has a direct impact on the life and welfare of the affected people, research on hearing began already more then 200 years ago. Nowadays, researchers from several fields such as medicine, acoustics, mechanics, physiology and psychology work together in close cooperation to develop methods and devices to improve hearing in affected people.

Several hearing-research fields developed due to the increasing complexity with increasing knowledge about the process of hearing. Our group is specialized in the field of 'biomechanics of hearing'. This dissertation focuses on the mechanics of the middle ear; the sound transmission in the middle ear. The sound is transmitted from the tympanic membrane via three ossicles to the inner ear. The three ossicles malleus, incus and stapes are connected by joints. One of these joints, the incudo-malleolar joint (IMJ), interfaces the malleus head and the incus body.

The main interest of this dissertation is whether the IMJ is mobile under acoustic stimulation in the physiological range. Therefore, the background chapter mainly focuses on the description of the middle ear (see chapter I.III.2) with focus on the morphology of the middle-ear ossicles (see chapter I.III.2.4) and joints (see chapter I.III.2.4.4). The morphology of the IMJ is extensively discussed in chapter I.III.2.4.4.1 due to its importance in this dissertation. The mobility of the incudo-malleolar joint was measured with three different approaches (see chapter III.1, III.2, and III.3). Therefore, the background chapter also includes a collection of all important works known to the author according the mobility of the human incudo-malleolar joint from the year 1851 to 2005 (see chapter I.III.2.5.3.2 and I.III.2.5.3.3) including a table for better overview (Table I.6). The comparison of the previous works and the findings of this dissertation are compared in the discussion in chapter IV.

This work should support future researchers to improve and develop middle-ear prostheses, to elucidate the influence of the IMJ to age-related hearing loss, and to describe the function of the IMJ (e.g. protection function for the inner ear in case of large pressure changes). The findings of this dissertation may be included into virtual models that are used to simulate the behavior of the normal and diseased middle ear. Such models are also used to improve and develop middle-ear prostheses.

A pathologically immobilized stapes (e.g. in case of otosclerosis) results in an impaired middle-ear sound transmission. As a consequence, the patients suffer from conductive hearing loss. A possible treatment is the stapes surgery, where the immobilized stapes is removed and replaced with a prosthesis. Preliminary results of a patient study focusing on the sound quality after stapes surgery are presented in chapter III.IV.

Several ongoing project of our group with contribution of the author are listed in chapter III.V, and some of the results are presented in the background chapter: Whole head measurement regarding bone conduction via the skull and soft tissue (see chapter I.III.6), intra-acoustic receiver project (ICAR) for the later development of a fully implantable cochlear implant (see chapter I.III.3.2.3), and monitoring the changes in cochlear function after cochlear implant surgery using electrocochleography (ECoG) (see chapter I.III.3.2.2.1.3.3).

I.II Sound: physical properties and perception

Sound can be described as a wave motion in air (stimulus) or as an excitation of the hearing mechanism that results in the perception of sound (sensation) (Everest & Pohlmann 2009). Sound is characterized by numerous different basic phenomena. Parts of these phenomena are objective, like frequency that specifies the number of waveform repetitions per unit of time (Hertz, Hz) and can be measured on an oscilloscope or frequency counter. Contrary, pitch is a subjective property of sound. According to the American National Standards Institute (ANSI, 1994), pitch is the attribute of sound according to which sounds can be ordered on a scale from low to high. For example, the ear perceives different pitches for soft and loud 100 Hz tones (Everest & Pohlmann 2009). Frequency and pitch are analogous, but not equal. Thus, the interaction between the physical properties of sound and our perception of them confronts us with complex issues.

Hearing is the ability to perceive sound by detecting vibrations. This chapter explains how these vibrations emerge and explains acoustical terms used later on in this dissertation.

I.II.1 The sine wave

The sine way can be illustrated with the oscillation of an undamped spring-mass system around the equilibrium (see Figure I.1). The weight (mass) on the spring is pulled down and the spring pulls the weight back, and however, its inertia will carry it even beyond the origin position. The weight will continue to oscillate, and moves in what is called *simple harmonic motion*. This oscillation or vibration of the weight is possible because of the elasticity of the spring and the inertia of the weight. All media to be capable of conducting sound must possess elasticity and inertia.

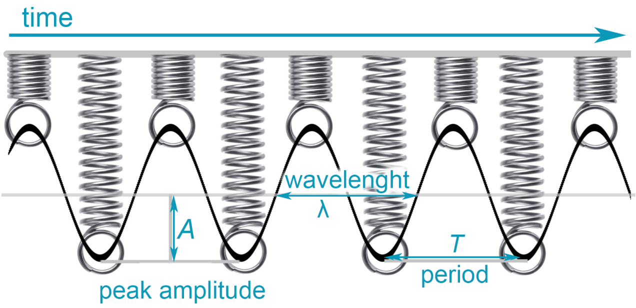

Figure I.1 Simple harmonic motion.

The frequency of sound defined by the wavelength λ is colloquially known as the tone pitch (high sound – deep sound) and the amplitude A as the intensity (soft sound – loud sound).

I.II.2 Propagation of sound in media

Sound is conducted in all elastic media; gases (e.g air), liquids (e.g water) and solids (e.g steel). In air, instead of the weight on the spring, particles are displaced. The air particle is made to vibrate about its equilibrium position by the energy of a passing sound wave because of the elastic forces of the air and the inertia of the air particle (Everest & Pohlmann 2009) (see Figure I.2). For sound waves travelling in air (or other gaseous medium), the particles move in the direction the sound is travelling which is called *longitudinal waves*. The velocity of a particle is maximal at its equilibrium position and is very small – less than 0.013 m/s – for even a loud sound (Everest & Pohlmann 2009). In general, the speed of sound increases with the stiffness (the resistance of an elastic body to deformation by an applied force) of the material, decreases with the density, and is given by the Newton-Laplace equation, where K is a coefficient of stiffness and ρ is the density:

$$c = \sqrt{\frac{K}{\rho}}$$

The speed of a sound wave in air depends upon the properties of the air, mostly the temperature, and the humidity. In dry air at 20 °C (ρ = 1.2041 kg·m^{-3}), at sea level, the speed of sound is 343 m/s or 1.234 km/h. Without a medium, like in vacuum or outer space, sound cannot be propagated.

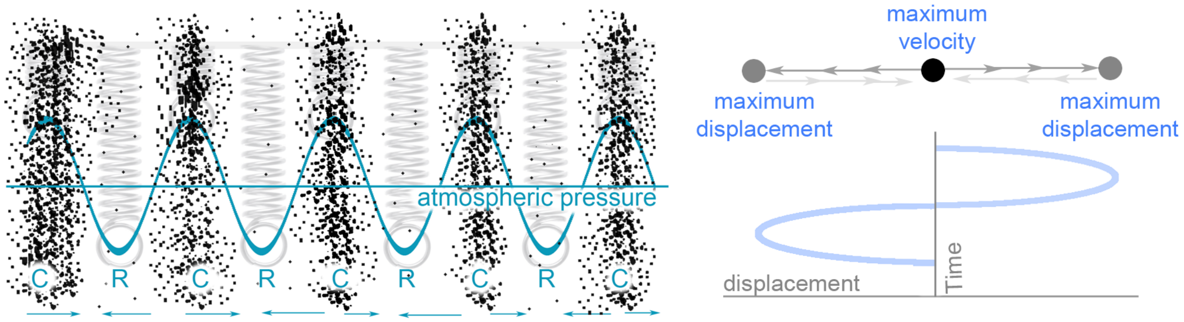

Figure I.2 (left) Sound waves travelling through a medium change localized air particle density: C= Compression (region of high pressure) and R = Rarefaction (region of low pressure). Modified after Everest & Pohlmann (Everest & Pohlmann 2009). (right) Equilibrium position of an air particle. An air particle is made to vibrate about its equilibrium position by the energy of a sound wave, caused by the elastic forces and the inertia of the particle. Modified after Everest & Pohlmann (Everest & Pohlmann 2009).

I.II.3 Amplitude

Amplitude is the objective measurement of the degree of change (positive or negative) in atmospheric pressure (the compression and rarefaction of air molecules) caused by sound waves. Sounds with greater amplitude will produce greater changes in atmospheric pressure from high pressure to low pressure (Hass 2003). The amplitude A of a sound wave defines the intensity of the perceived sound – soft sound or loud sound (see Figure I.1).

I.II.4 Wavelength and frequency

For periodic waves, e.g. sine waves, the distance a wave travels in the time it takes to complete one cycle is defined as wavelength λ (see Figure I.1). The frequency f specifies the number of cycles per second, measured in hertz (Hz) (Everest & Pohlmann 2009). The frequency f of a sinusoidal wave is equal to the phase velocity v of the wave divided by the wavelength λ of the wave. Wavelength and frequency are inversely related.

$$\mathrm{f} = \frac{\mathrm{v}}{\lambda} \quad \text{and} \quad \lambda = \frac{\mathrm{v}}{\mathrm{f}}$$

As noted, the speed of sound in air is about 1.234 km/h at normal conditions and therefore the wavelength becomes:

$$\lambda = \frac{\mathrm{v}}{\mathrm{f}} = \frac{1.234\ \mathrm{km/h}}{\mathrm{f}}$$

I.II.4.1 Complex waves

Most waves like in speech and music are not sinusoidal and are considered to as complex waves. However, as long as it is periodic, it can be reduced to sine components. Joseph Fourier was the first to prove that any complex periodic waveform can be synthesized from sine waves of different frequencies, different amplitudes, and different time relationships (phase) (Everest & Pohlmann 2009).

I.II.5 Harmonics, harmonic distortions

Figure I.3 shows simple sine waves with given amplitudes (A_1, A_2, A_3, A_5) and frequencies (f_1, f_2, f_3, f_5). By combining these waves, the resultant is obtained. This complex waveform can be disassembled again to f_1, f_2, f_3, *and* f_5 sine components by either acoustical or electronic filters. The sine wave with the lowest frequency (f_1) is called the fundamental. Sine wave f_2 is called the second harmonic, and sine wave f_3 is the third harmonic. These whole number multiples of the fundamental sine wave are called harmonic distortion. Harmonic distortion may be expressed in terms of the relative strength of individual components in decibels (dB), as total harmonic distortion (THD) or the Root Mean Square (RMS).

f_1 = fundamental, $f_2 = 2 * f_1$ = second harmonic, $f_2 = 3 * f_1$ = third harmonic,

$f_n = n * f_1$ = n harmonic

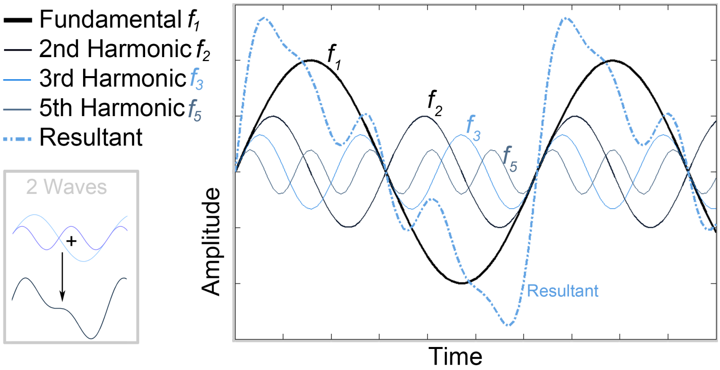

*Figure I.3 Harmonic distortions shown for five sinus waves (y = A · sin(ax)): y1 = sin(t); y2=sin(2*t)/2; y3=sin(3*t)/3; y5=sin(5*t)/5. The resulting wave (resultant) is the sum of all five waves yall=y1+y2+y3+y5.*

I.II.5.1 Standing sound waves (longitudinal standing waves)

A 'standing wave' is a phenomenon that result when two sinusoidal wave trains of the same frequency are moving in opposite directions in the same space and interfere with each other. It arises from the combination of reflection and interference and, therefore, can occur only in confined spaces like strings or air columns e.g. tubes. So called ‘nods’ are the specific points where the amplitude is minimal and the points appearing to stand still. At these points the two waves add with opposite phase and diminish each other. They can even cancel each other out, if the two waves have the same amplitude. Contrary, ‘antinods’ are the specific points where the two waves add with the same phase and reinforce each other, which result in maximal amplitude at these points. Standing waves only appear at specific frequencies, depending on the length of the tube (and it’s harmonics). In a tube that is closed at one end (see Figure I.4), the standing wave pattern that has an anti-node at the open end and a node at the closed end of the tube is called the *first mode*. The pressure is the highest at the closed end and, therefore, the velocity is minimal (node). This pattern exactly comprises quarter of a circle: 0° to 90° or $\frac{\lambda}{4}$. This $\frac{\lambda}{4}$ is as well the wavelength of its frequency of vibration. Furthermore, this is the first resonant frequency, which is the fundamental frequency.

$fundamental\ frequency\ (f) = \frac{v}{\lambda} = \frac{v}{4L}$ with L = length of the tube and λ = wavelenght

For that reason, a tube that is closed at one end is called ‘quarter-wavelength resonator’. These tubes can only produce odd modes of vibration and odd harmonics of the fundamental frequency (f_1, f_3, f_5, f_7...), because a node can only occur at one end.

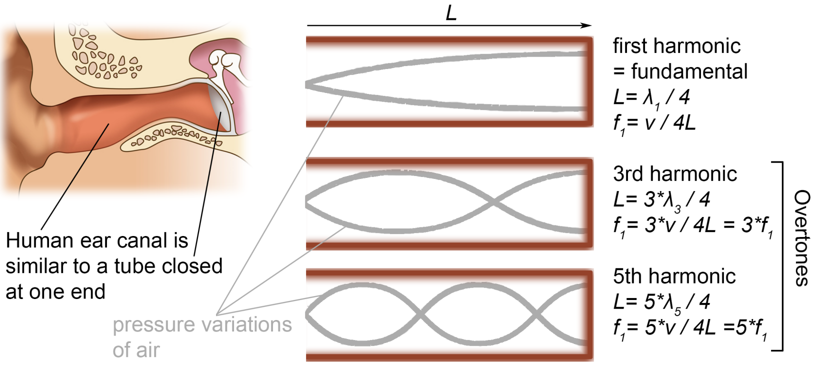

Figure I.4 The human ear canal is similar to a tube closed at one end (tympanic membrane). Therefore, the model of standing waves in tubes with one closed end is shown in this figure for the first, third and fifth harmonic.

I.II.6 Phase

Phase (φ) is the particular point in the cycle of a waveform, measured as an angle in degrees (°) (see Figure I.5 A). It is normally not an audible characteristic of a single wave. Two waves with the same frequency are ‘in phase’ if they have the same phase. The phase is a very important factor in the interaction of one wave with another – the resulting wave can be diminished or amplified according to the phase shift (see Figure I.5 B). The phase of wave refers to a sinusoidal function with the amplitude A, frequency f and phase φ as follows:

$$x(t) = A * \cos(2\pi f t + \varphi)$$

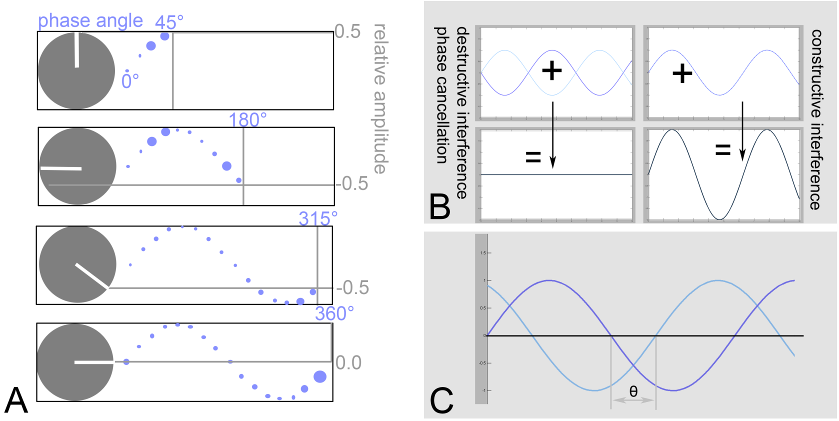

Figure I.5 (A) If a wheel rotates counterclockwise, the sine wave reaches its peak positive amplitude when the spoke has traveled 90° from its starting point, with a relative amplitude of +1. At 180° from the starting point, the amplitude of the sine wave has returned to 0. The sine wave reaches returns to 0 as it returns to its starting point of 360° or 0° (B) Interference of two waves; destructive and constructive (C) Phase shift θ. A & B Modified after (Haas 2003).

The cosine wave has exactly the same shape as a sine wave and would sound exactly the same all by itself, but is distinguished by the fact that it's cycle begins 90° out of phase to a sine wave, or at +1.

When waveforms of either the same or differing phases are combined, they interfere with each other create a new composite wave. Two waves with the same frequency and phase (see Figure I.5 B, right) will combine to create a single sound of greater amplitude (= constructive interference). Two identical waves 180° out of phase (see Figure I.5 B, left) will cancel each other out (= phase cancellation = destructive interference).

The phase shift θ describes the "shift" from zero phase (see Figure I.5 C).

I.II.7 Sound level

The power of sound is measured in Watt ($W=Nm/s$) and is a measurement of the amplitude A over time t *(Hass 2003)*. Together with the distance to the sound source, power is combined to *sound intensity* ($I=W/m^2$). *Sound intensity level* (L) is a logarithmic measure of the sound intensity in comparison to a reference level. The ratio of two sound intensities (I_0, I_1) is:

$$L_1 = 10log_{10}\left(\frac{I_1}{I_0}\right)$$

The sound intensity level (L) is measured in decibel (dB), which a dimensionless quantity. Sound pressure is usually more accessible to measure than sound intensity. Therefore, the sound-pressure level (SPL) is used more often.

$$SPL = 10log_{10}\left(\frac{p^2}{p_{ref}^2}\right) \text{ with } p_{ref}^2 = 20\mu\text{Pa} \Rightarrow SPL = 10log_{10}\left(\frac{p}{20\mu Pa}\right) \Rightarrow p = (20 * 10^{-6}) * SPL$$

where SPL = sound-pressure level in dB, p = acoustic pressure (e.g. in mPa), $pref$ = acoustic reference pressure.

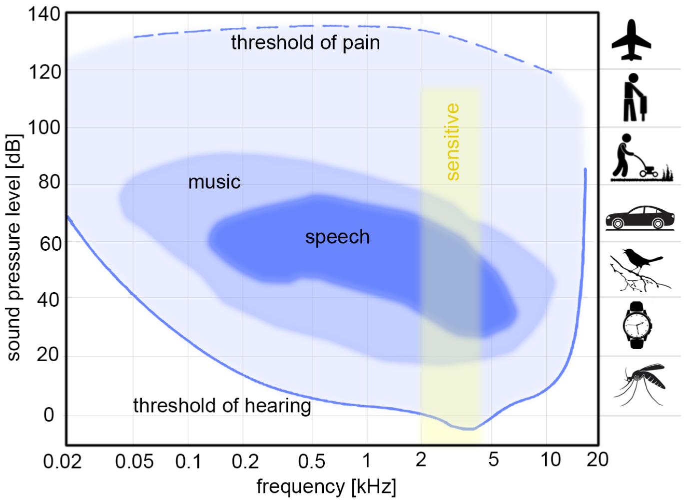

Figure I.6 Range of human audibility with normal hearing. Also indicated are the areas encompassed by music and speech and the area between 2000 Hz and 4000 Hz, where the human ear is most sensitive. Modified after (Fastl & Zwicker 2007) with kind permission of Springer Berlin © 2007, Psychoacoustics. Facts and models, pp. 17, figure 2.1.

I.II.8 Perceived loudness of tones

The perceived level of loudness for a given sound or noise is described in 'phon'. It is based on equal loudness contours, where 0 phons at 1,000 Hz is set at 0 decibels, the threshold of hearing at that frequency (see Figure I.7) (Truax 1999). The hearing threshold of 0 phons lies along the lowest equal loudness contour, and if the intensity level at 1,000 Hz is raised to 20 dB the second curve is followed (Truax 1999). Thus, the relationship between the decibel and phon scale at 1,000 Hz is exact, but because of the way the ear discriminates against or in favor of sounds of varying frequencies, the phon curve varies considerably (Truax 1999). The sounds with the same 'phon'-value are equally loud. However, 'phon' is not usable to measure the relationship between sounds with different loudness; e.g. 10 phons is sufficient to produce the impression that a sine tone is twice as loud (Truax 1999).

Loudness is a subjective measure of the sound pressure in acoustics. To measure this difference in loudness, the 'sone' scale of subjective loudness was invented; one 'sone' is arbitrarily taken to be 40 phons at any frequency, i.e. at any point along the 40 phon curve on the graph (see Figure I.7) (Truax 1999). The relationship between phons and sones is: Phon = 40 + 10 $\log_2$ (sone).

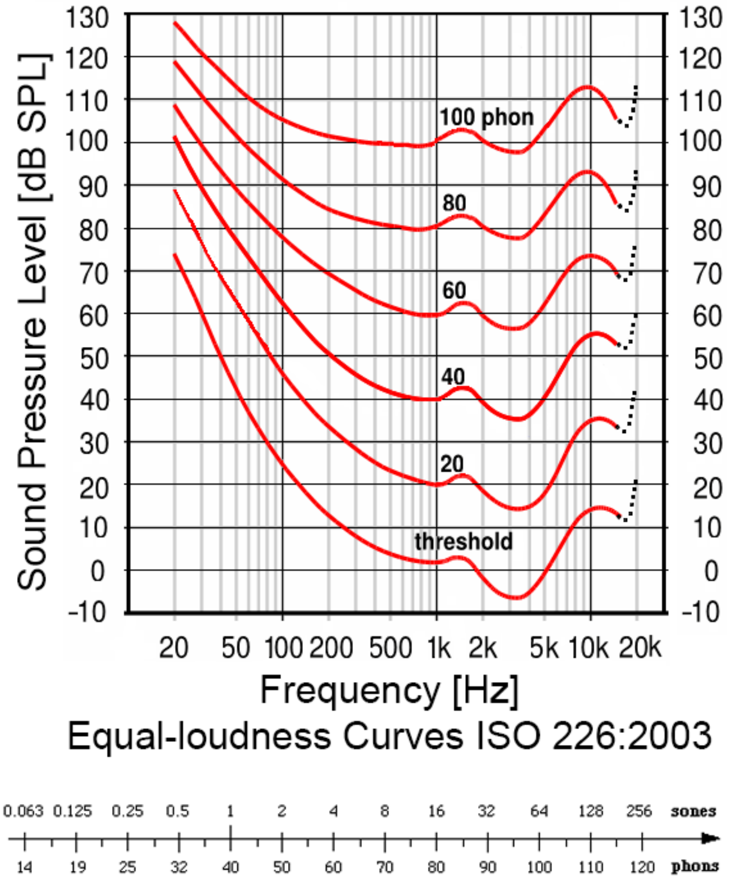

Figure I.7 Phon. Equal loudness contours for pure tones and normal threshold of hearing for persons aged 18-25 years, using free-field hearing from ISO recommendation R226. Reprinted from (Truax 1999).

I.II.9 Acoustic impedance

Sound waves travel through materials with different properties. The acoustic impedance of different materials (e.g. water, bone, muscle, cochlear fluid) explicitly differs. The acoustic impedance (Z) is defined as

$$Z = \rho v$$

where ρ is the density in kg/m^3 and v is the acoustic velocity in m/s at which sound propagates in this medium.

Acoustic impedance is for example important in the determination of acoustic transmission and reflection at the boundary of two materials having different acoustic impedances (see chapter I.II.9).

Compared to water, the density of air is lower by a factor of about 825, and sound propagates slower in air by a factor of about 4.32. Accordingly, the ratio of the impedance between water and air is about 3564 (see Table I.1).

parameter		water	air	ratio
density	ρ	998.21 kg/m^3	1.21 kg/m^3	825
velocity (at 20°)	v	1482 m/s	343.2 m/s	4.32
acoustic impedance	Z	1’479’347.2 Ns/m^3 =147’934.7 ohm/cm^3	415.3 Ns/m^3 = 41.5 ohm/cm^3	3564.7

Table I.1 Comparison of the acoustical properties in water and air: density, propagation velocity and acoustic impedance. The ratio is calculated by dividing the property of water by the corresponding property of air.

The energy that gets reflected due to the impedance mismatch is defined as

$$Reflected\ energy = \left(\frac{Z_1 - Z_2}{Z_1 + Z_2}\right)^2 * 100\%$$

The amount of transmitted energy (T) from one medium to another depends on the ratio (r) between the impedance of both adjacent media as defined as

$$T = transmitted\ energy = total\ energy - reflected\ energy$$

$$= \left(\frac{4 * Z_1 Z_2}{(Z_1 - Z_2)^2}\right) * 100 \ = \frac{4 * r}{(r + 1)^2}$$

In case of energy is transmitted from air to water, the transmitted energy (T) is 0.11%:

$$T = \frac{4 * r}{(r + 1)^2} = \frac{4 * 3564.7}{(3564.7 + 1)^2} \ = \ 0.001121 \ = \ 0.11\%$$

Hence, 99.9 % of sound will be reflected from the borderline between both media to air. Consequently only 0.11% will be transmitted to water.

I.III Morphology and physiology of the ear

The auditory pathway can structurally be divided into three different parts: external ear, middle ear and inner ear (see Figure I.8). The external ear is composed of the pinna and the external ear canal. The middle ear is separated from the external ear by the eardrum. The ossicular chain including malleus, incus, and stapes is located in the middle-ear cavity. The stapes is connected to the bony capsule termed cochlea of the inner ear. These structures, along the way of the travelling sound waves from the environment to the inner ear, are described in detail in this chapter.

Some figures presented in this chapter include 3-D reconstructions from micro-CT data obtained in the context of this dissertation (for example Figure I.20).

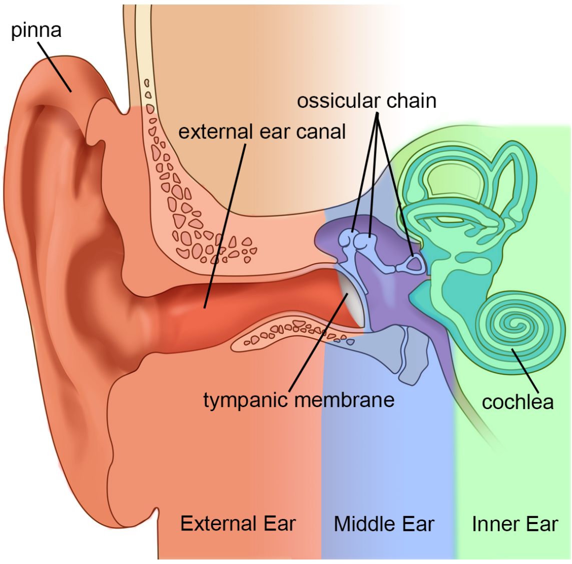

Figure I.8 The auditory pathway. Sound is travelling from the outer ear via the middle ear to the inner ear.

I.III.1 External ear

The external ear includes the pinna (or auricle) and the external ear canal (external auditory meatus).

I.III.1.1 Pinna (auricle)

The anatomy and function of the pinna, and its role in sound localization as a part of the external ear are discussed in this chapter.

I.III.1.1.1 Anatomy of the pinna

The pinna is the only visible portion of the ear and often colloquially called ‘the ear’. It is composed of a thin plate of elastic cartilage (see Figure I.9) (except the earlobe), a small amount of subcutaneous fat, and is covered with skin. The skin contains sebaceous glands, sweat glands, and hair. Ligaments and muscles (see Figure I.9) link the pinna to the surrounding parts, and the pinna is connected to the external ear canal with fibrous tissue. Humans do not have the ability to move their pinna with the auriculares muscles in order to focus hearing in a certain direction like many mammals, because the muscles declined by losing the relevance of their maneuverability. The detailed structures of the pinna are described in Figure I.9. The pinna merges with the cartilaginous part of the external ear canal.

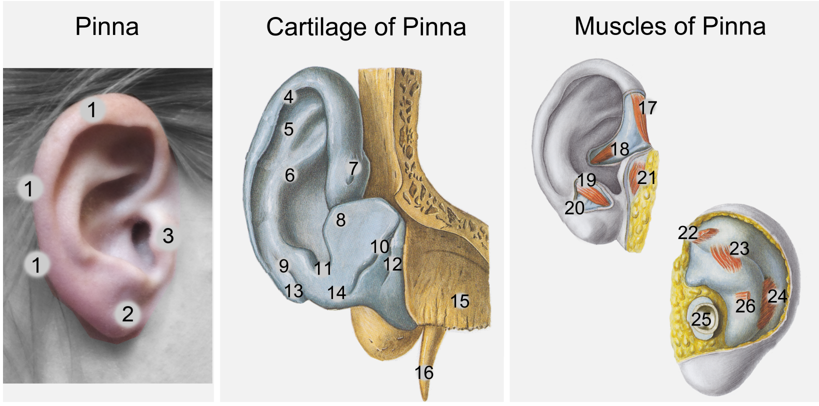

Figure I.9 Schema of the external ear. Right ear of a women: (1) helix , (2) lobulus (earlobe), (3) tragus. Illustration of the cartilage of the pins: (4) helix, crus helicis, (5) scapha, (6) antihelix, (7) spina helicis, (8) lamina tragi, (9) fissura antitragohelicina, (10) incisurae cartilaginis meatus acoustici, (11) incisura intertragica, (12) (see 10), (13) cauda helicis, (14) cartilago meatus acustici, (15) os temporale, pars tympanica, (16) processus styloideus. Illustration of the muscles in the pinna: (17) M. helicis major, (18) M. helicis minor, (19) M. antitragicus, (20) cauda helicis, (21) M. tragicus, (22) Lig. auriculare superius, (23) M. obilquus auriculae, (24) M. transversus auriculae, (25) Meatus acusticus externus, (26) Lig. auriculare posterius. Modified after Sobotta (Putz & Pabst 2005).

I.III.1.1.2 Function of the pinna

The pinna collects sound and channels it via the external ear canal on the tympanic membrane (ear drum). For low frequencies the pinna behaves similar to a reflector dish, directing sounds toward the ear canal. Its value seems to be more complex for high frequencies. To determine the sound pressure gain or loss due to the pinna, a microphone outside the ear and at the entrance of the external ear canal monitors the sound from a loudspeaker. The difference between the two measurements shows the impact of the pinna, also described as the 'transfer function' (TF) from the free field to the entrance of the external ear canal. In Figure I.10 0 dB means that the pinna has no influence, positive values show the amount of gain provided by the pinna and, contrary, negative values show the transmission loss. As mentioned before, the pinna has a higher impact on high frequencies (> 1k Hz) then on low frequencies (< 1k Hz).

$$Transfer\ function = TF = \frac{signal\ output}{signal\ input} = \frac{Pressure_{ear\ canal}}{Pressure_{freefield}}$$

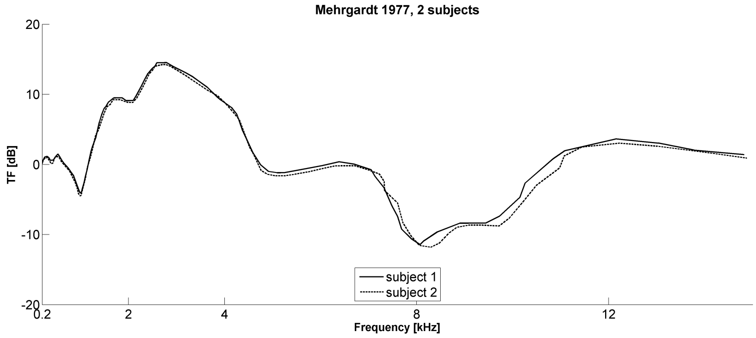

Figure I.10 Transfer function from the free field to the entrance of the external ear canal; up to 0.6 kHz the pinna has almost no influence to the transfer function (TF ≈ 0). Modified after Mehrgardt & Mellert (Mehrgardt & Mellert 1977)

How does sound from a specific point in the free field arrive at the eardrum? The general term 'head-related transfer function' (HRTF) describes the changes caused by diffraction and reflections off the human body (e.g. head, shoulders, torso and ears), and is individually based on the anatomical variations of human. Likewise, the HRTF is the sound transfer function from free field to the eardrum:

$$Transfer\ function = TF = \frac{signal\ output}{signal\ input} \Rightarrow\ HRTF = \frac{Pressure_{eardrum}}{Pressure_{freefield}}$$

This evaluation of amplitudes plays an important role in sound localization (see chapter I.III.1.1.3). Furthermore, the HRTF strongly depends on the position of the loudspeaker related to the subject tested (Figure I.11 B, Figure I.12). In previous studies, the HRTF is shown with the loudspeaker directly in front of the subject (Figure I.11 A). The HRTF is highly frequency dependent; pressure gain of 15 dB to 20 dB was observed between 2 and 5 kHz, whereas pressure losses occurred at higher frequencies (8 – 10 kHz).

However, while passing the pinna, sound goes through a filtering process. The filtering effect of the human pinna preferentially selects sounds in the frequency range of human speech (Blauert 1997). Thus, sounds entering the pinna get frequency dependent modulated (amplified or attenuated), with an effect that can be described mathematically by linear transfer functions or 'pinna filters' (Wightman & Kistler 1989, Hofman et al. 1998). One of these filters is the 'pinna notch'. This effect is due to the delay that occurs because some of the sounds that enter the ear travel directly to the canal, and others get first reflected off the pinna contours. The reflected sound waves enter the ear canal with a very slight delay. Such a delay turns into phase cancellation, where the frequency component is virtually eliminated if its wave period is twice the delay period. The following effect of significant dropping of neighboring frequencies is known as the pinna notch. A spectral transformation is performed by the pinna for incoming sound which enable enables the process of vertical sound localization (Middlebrooks & Green 1991). The importance of this function has also been shown in narrow-band sound localization studies (Middlebrooks 1992) and pinna-occlusion experiments (Oldfield & Parker 1984).

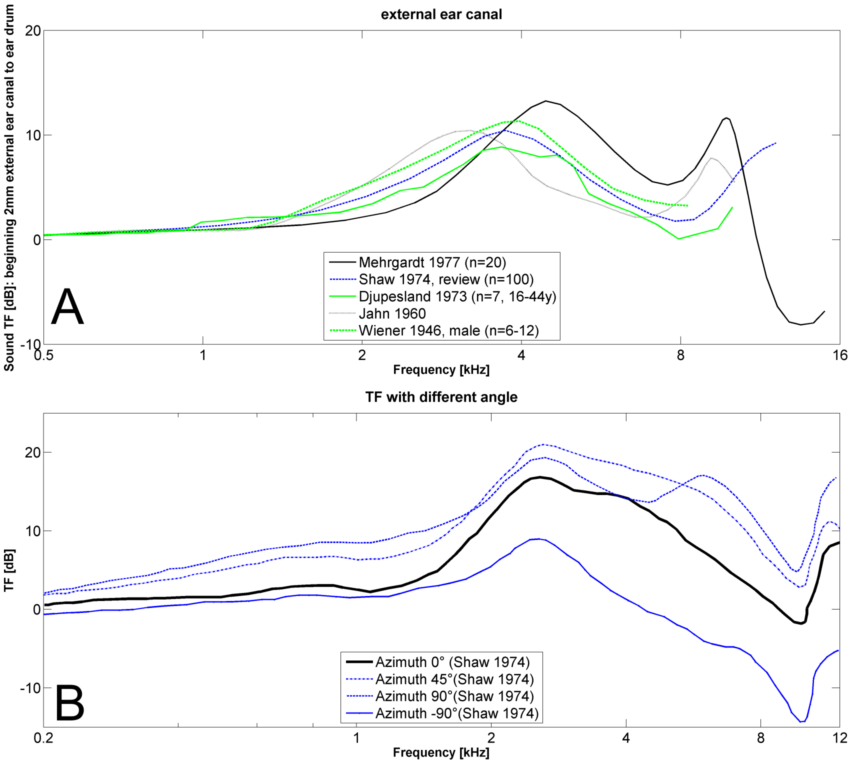

Figure I.11 (A) Average HRTF (sound level at the eardrum compared with outside the ear) for sound presented from loudspeaker directly in front of subject (azimuth=0°). Modified after (Hellström 1995, Mehrgardt & Mellert 1977, E. A. Shaw 1974, Wiener & Ross 1946). (B) HRTFs vary with the horizontal and vertical angles at witch sound arrive at the pinna. The graph shows the HRTF between free field and pinna at four different azimuth with data Modified after Shaw et al. 1974 (E. A. Shaw 1974).

I.III.1.1.3 Role of the external ear in sound localization

An important function of the pinna is the contribution to the localization of sound. Humans can locate sounds in three dimensions (distance, directions: above/below, right/left, front/rear) with only two ears. This is possible due to the close collaboration of the brain, inner ear and pinna. The auditory system uses several cues for sound localization, including differences in time and intensity between ears, spectral information, timing analysis, correlation analysis, and pattern matching. Localization can be described in terms of three-dimensional position: the azimuth or horizontal angle, the elevation (zenith, altitude) or vertical angle, and the distance (for static sounds) or velocity (for moving sounds) (see Figure I.12) (Roads 1994). Roads described that the “azimuth of a sound is signaled by the difference in arrival times between the ears, by the relative amplitude of high-frequency sounds (the shadow effect), and by the asymmetrical spectral reflections from various parts of our bodies, including torso, shoulders, and pinnae” (Roads 1994).

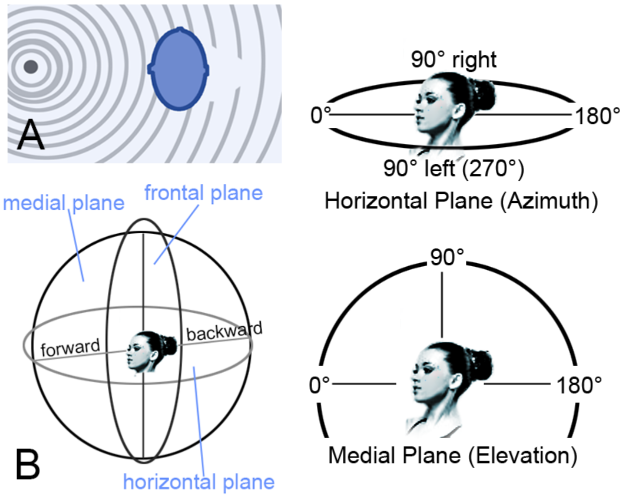

Figure I.12 The pinna plays an important role in sound localization. (A) The head is like an ‘acoustic shadow’ for the ear farer away from the sound source, because the head obstructs the path of sound. (B) For example with 0 degrees (0°) azimuths sound source directly in front of the listener, 90° to the right, and 180° with sound source directly behind the listener.

The auditory system analyzed the following information to determine the horizontal (or azimuth plane) input direction (see Figure I.12): Interaural time differences (ITD) and Interaural level differences (ILD). Both, ITD and ILD, depend on the ‚acoustic shadow’ of the head. ITD are evaluated from the phase delay (at low frequencies) and group delays (at high frequencies) (Blauert 1997). ILD are highly frequency dependent and they increase with increasing frequency. Depending on the frequency, either ILD, LTD or both are important. Below 800 Hz, mainly ITD (phase delays) are evaluated (Wightman & Kistler 1992, Macpherson & Middlebrooks 2002). For these frequencies (80Hz – 800 Hz) the dimension of the head are smaller than the half wavelength of sound and, therefore, the auditory system is able to determine the phase delays between both ears. The ILD is too small in this range to contribute to sound location. Contrary, for frequencies above 1600 Hz mainly ILD are evaluated (Wightman & Kistler 1992, Macpherson & Middlebrooks 2002)). At these high frequencies, more than one wavelength fits in-between the source and the ear and therefore ITD is inapplicable – similar like for elevation of the sound source or distinction between sound source on the front or rear. Between 800 Hz and 1600Hz both mechanisms, ITD and ILD, play a role. Humans can discern ITD small as 10 microseconds and ILD small as 0.5 dB (Blauert 1997). Localization accuracy is 1 degree for sources (sinusoidal signals) in front of the listener (from the median plane) and 7 degrees for sources to the sides (from 75°) (Mills 1958, Bennemann et al. 2013, DeLiang Wang & Brown 2006, Blauert 1997).

I.III.1.2 External ear canal (external auditory meatus)

I.III.1.2.1 Anatomy of the external ear canal

The external ear canal is approximately 7 mm in diameter and 2.5 cm long (John A. Seikel et al. 2005). Ear canal volume ranges between 0.68 to 2.54 ml with a mean of 1.11 ml for females and 1.35 ml for males (Hellström 1995). The lateral third of the canal is continuous with the cartilage from the pinna, and firmly attached to the circumference of the auditory process of the temporal bone. The medial two-thirds of the canal are composed of bone of the temporal bone. It is marked, except at its upper part, by a narrow channel, the tympanic sulcus, in which the circumference of the tympanic membrane is attached. The canal has a S-like shape that goes slightly upwards in the cartilaginous part and slightly downward towards the tympanic membrane. The canal and the outer surface are covered with very thin skin. Only the thick subcutaneous tissue of the cartilaginous part of the canal contains hair, sebaceous glands (producing oily liquid) and ceruminous glands (producing wax). By producing cerumen (ear-wax) the ear protects itself from harmful bacteria and fungi, and therefore, prevents infections. In front of the osseous part is the condyle of the mandible, which is frequently separated from the cartilaginous part by a part of the parotid gland. The movements of the jaw, though, influence the lumen of this portion. Behind the osseous part are the mastoid cells of the temporal bone, separated from the canal by a thin layer of bone. These mastoid cells, which can be felt as a bump in the skull behind the pinna, also contain air, which is ventilated through the middle ear (Sade 1992).

I.III.1.2.2 Function of the external ear canal

The ear canal also amplifies the sounds traversing it. Acoustically, the external ear canal is approximately a tube-like duct, closed at the inner end by the eardrum (standing sound waves chapter I.II.5.1). Therefore, with a tube closed at one end, the resonance effect of the ear canal increases sound pressure at the eardrum at certain frequencies. A primary peak is noted around 3 to 4kHz caused by the quarter-wave tube resonance effect, where the 2.5-cm tube is one-quarter wavelength. In the ear, the arriving and reflected sound waves produce an anti-node at the eardrum. Consequently, the amplitude of the sound pressure of standing waves is maximal at the eardrum. Figure I.13 shows the effect of resonance in the ear canal by the transfer function:

$$TF = \frac{Pressure_{Eardrum}}{Pressure_{entrance\ external\ ear\ canal}}$$

Previous studies show that the primary resonance in the tube amplifies the sound pressure at the eardrum by approximately 10 to 15 dB at the major resonance at about 4 kHz, and there is a secondary weaker resonance at 9 kHz. Additionally, a plane wave striking the front of the head will be diffracted. This diffraction also increases sound pressure at the ears at midrange frequencies, which combines to make the ear most sensitive to midrange frequencies, the same frequencies important for speech (Everest & Pohlmann 2009).

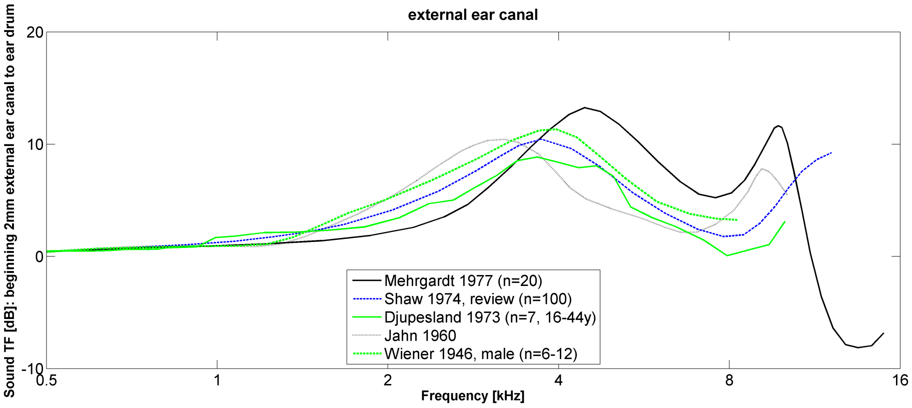

Figure I.13 Transfer function of the external ear canal (Mehrgardt & Mellert 1977, E. A. Shaw 1974, Djupesland & Zwislocki 1973, Jahn 1960, Wiener & Ross 1946).

The exact sound transmission characteristics of the canal are given by its shape, volume, length, variation in cross-section area along the canal, the acoustic properties of the wall, and acoustic impedance of the tympanic membrane and the middle ear (Hudde & Engel 1998a, Hudde & Engel 1998b, Hudde & Engel 1998c, Wiener & Ross 1946, Mehrgardt & Mellert 1977, Gerhardt et al. 1987).

I.III.2 Middle Ear

The middle ear is an air-filled space, which is normally sealed laterally by the tympanic membrane. Sound waves are conveyed via the external ear canal to the tympanic membrane, which vibrates under sound pressure. Here, the energy of sound waves gets transformed into mechanical vibrations, which proceed via the three small bones, ossicular chain (malleus, incus, stapes), to the inner ear. The following subchapters describe the anatomy and function of the middle-ear structures in detail, due to the importance of these topics in this work.

I.III.2.1 Tympanic membrane

This chapter describes the anatomy and function of the tympanic membrane in the middle ear.

I.III.2.1.1 Anatomy of the tympanic membrane

The size, orientation, structure, thickness and the changes with age of the tympanic membrane are discussed in the following subchapters.

I.III.2.1.1.1 Size and orientation of the tympanic membrane

The tympanic membrane is placed at the medial end of the external ear canal and normally seals the air-filled middle ear cavity (see Figure I.14). It has a particular orientation, which allows it to have a larger surface than the ear canal section itself. The area of the tympanic membrane is approximately 85 mm^2; however, only about two-third (56.7 mm^2) of this area vibrates effectively (G. Békésy 1960). Its vertical axis ranges from 8.5 to 10 mm while the horizontal axis ranges from 8 to 9 mm (Wajnberg 1987). The angles of tympanic membrane to the external ear canal seem to diverse in a wide range between different individuals. In many textbooks a typical angle of 55° (Lockhart 1965) formed with both floor and anterior wall of the external ear canal is described. However, several authors measured diverse angles between the tympanic membrane and the external ear canal in the past (see Table I.2) (Todd 2009, Salvinelli et al. 1991, Lockhart 1965, Cable & Tadros 1982, Smelt et al. 1988). Recently, McManus et al. found the tympanic membrane to be angled at a mean value of 34° (range 16 to 45°) to the parasagittal plane and 42° (range 22 to 58°) to the axial plane (n=39) (McManus et al. 2012) (see Figure I.15).

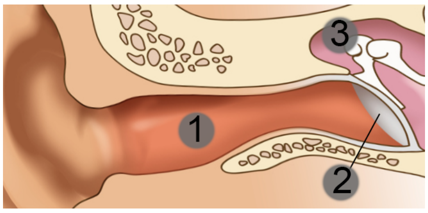

Figure I.14 Schematic drawing of the external ear canal (1), the tympanic membrane (2) and the malleus (3).

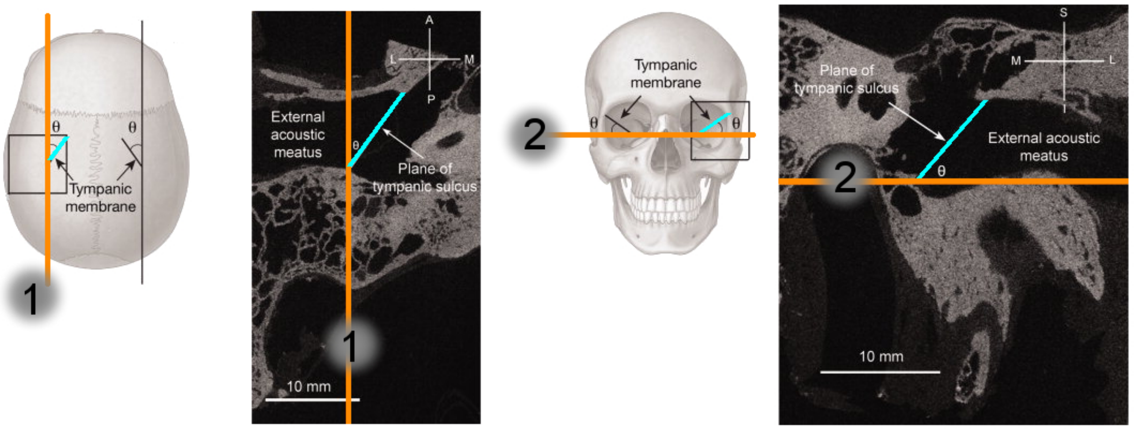

Figure I.15 Axial (left) and coronal (right) micro-CT images from the left temporal bone. (1) parasagittal plane, (2) horizontal plane, the tympanic membrane is marked with the light blue line. (M) medial, (L) lateral, (A) anterior, (P) posterior, (S) superior, (I) inferior. Modified after McManus et al 2012 (McManus et al. 2012), from Lauren J. McManus, Patrick J. D. Dawes, Mark D. Stringer; "The orientation of the tympanic membrane", Clinical Anatomy 2014, Copyright © 2011 Wiley-Liss, Inc.

Study	Angle between tympanic membrane and defined structure	Angle in degrees [°]
(Lockhart 1965)	Tympanic membrane & both floor and anterior wall of the external ear canal	55°
(Cable & Tadros 1982) n=50	Antero-superiorly to posterio-inferiorly	30°
(McManus et al. 2012) n=39	Tympanic membrane & parasagittal plane	34° (range 16 to 45°)
	Tympanic membrane & axial plane	42° (range 22 to 58°)
(Salvinelli et al. 1991) n=280	Tympanic membrane & central canal axis of the external ear canal	43°
	Plane of tympanic membrane & anterior-inferior ear canal wall	19°
(Smelt et al. 1988) n=18 n=33	External canal axis (viewed from antero-inferior aspect)	47°
	Plane of tympanic membrane & anterior-inferior external ear canal wall	17°
(Todd 2009) n=41	View from lateral through the external ear canal to anteriorly	40° to 60° (median: 55°)
	View from lateral through the external ear canal to antero-inferiorly	50° to 70° (median: 60°)
	View from lateral through the external ear canal to inferiorly	70° to 80° (median: 75°)

Table I.2 Angles between the tympanic membrane and the external ear canal.

I.III.2.1.1.2 Structure and thickness of the tympanic membrane

The periphery of the tympanic membrane is firmly attached to the tympanic sulcus, a groove in the wall of the tympanic cavity, by a fibro-cartilaginous ring called the annular ligament or tympanic annulus. The tympanic annulus has a small defect in its posterior edge due to a tiny interruption known as notch of Rivinus. The tympanic membrane is shaped like a flat cone pointing into the middle ear, respectively, concave outward. In physiological conditions, the cone has an angle of 132–139° (Kirikae 1960) a cone depth of 1.42–1.5 mm (Lee et al. 2006, Koike et al. 2002). The peak of this inward-cone is called the umbo. Here, the first of the three ossicles from the middle ear (manubrium of the malleus) is attached to the membrane. The attachment of the malleus varies along the manubrium: the lateral process of the malleus and the umbo are firmly attached to the tympanic membrane, while in the midway region, between the lateral process and the umbo, the manubrium separates slightly from the tympanic membrane (Ferrazzini 2003). The manubrium is laterally visible through the tympanic membrane and divides the latter anatomically into a smaller anterior and a larger posterior quadrant. Functionally, the tympanic membrane is divided into two parts: pars flaccida and pars tensa. The pars flaccida is the small superior portion of the tympanic membrane and attaches it to the temporal bone at notch of Rivinus. Structurally, the pars flaccida is relatively thick and only consists of two layers: the most lateral layer of the tympanic membrane that continuous with the skin of the external ear canal (epidermal layer) and the most medial layer that continues with the mucous membrane of the middle ear (mucosal epithelial layer, see chapter I.III.2.2.1). The large pars tensa amounts about 90% of the tympanic membrane. This part of the tympanic membrane is almost translucent. Although, it contains two more layers than the pars flaccida in between the epidermal and mucosal epithelial layer: radial collagen fiber layer and circumferential collagen fiber layer (fibrous layers) (see Figure I.16). Radial fibers extend from the tympanic annulus to the umbo (see Figure I.16). A critical feature for vibratory behavior of the tympanic membrane is the thickness. Large inter-specimen variability in thickness between different human tympanic membranes is described in the literature. A recent study found the thinnest thickness in the central region between umbo and manubrium (50-70 µm) and largest near the peripheral rim of the pars tensa and around the umbo (100-120 µm) (Van der Jeught et al. 2013) (see Figure I.17).

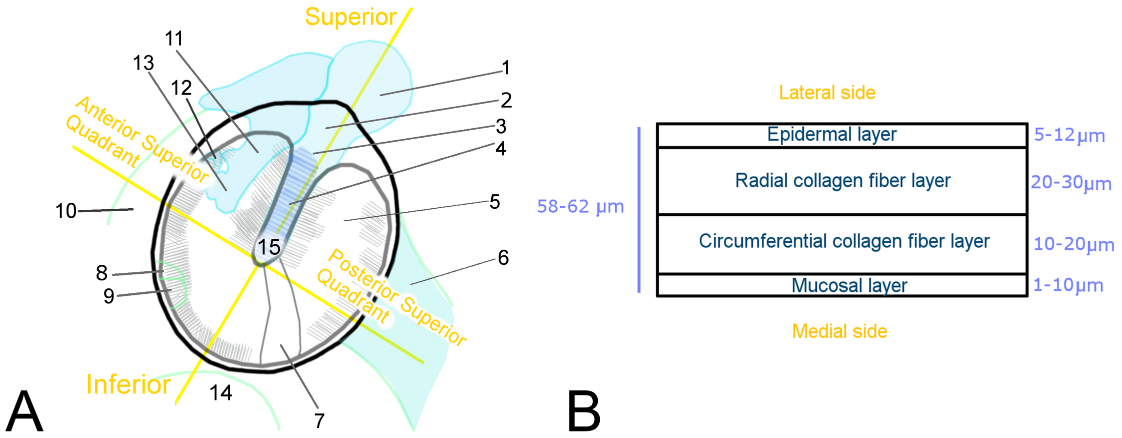

Figure I.16 (left) (1) malleus (head), (2) pars flaccida in Notch of Rivinus, (3) short (= lateral) process of malleus, (4) manubrium of malleus, (5) pars tensa, (6) Eustachian tube, (7) cone of light, (8) fibrous annulus, (9) round window, (10) facial canal, (11) long process of incus, (12) stapes, (13) lenticular process, (14) jugular bulb, (15) Umbo. Modified after (Paparella 2009). (right) Schematic diagram of a tympanic membrane cross-section trough Pars tensa. Modified after (Daphalapurkar et al. 2009)with data from (Lim 1970, Fay et al. 2005) with permission of © Elsevier, Journal of the mechanical behavior of biomedical materials 2 (2009) pp. 82–92.

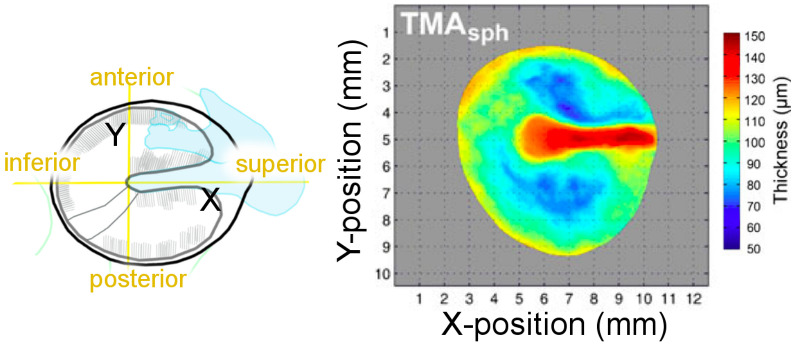

Figure I.17 Average thickness map of the human TM: TMs of 5 TB, measured by optical coherence tomography OCT. Modified after (Van der Jeught et al. 2013) by Springer and the JARO, 14, 2013, 490, Full-field thickness distribution of human tympanic membrane obtained with optical coherence tomography, Van der Jeught, S., Dirckx, J. J., Aerts, J. R., Bradu, A., Podoleanu, A. G., Buytaert, J. A., figure 5, D 2013 Association for Research in Otolaryngology with kind permission of Springer Science and Business Media.

I.III.2.1.1.3 Changes with age of the tympanic membrane

At birth, the tympanic membrane is nearly the same size as that of adults (Smelt et al. 1988), but the angle of the tympanic membrane to the ear canal is much flatter; the children's membrane lies flush with the outer rim of the base of the skull (Smelt et al. 1988). Tillaux et al. found an 10° angle (Tillaux 1980) antero-inferiorly – others found the membrane in the horizontal plane (Smelt et al. 1988). With growing up, the tympanic membrane adapts to the growing process of the skull and becomes steeper. Ruah et al. demonstrated that the tympanic membrane is a structure that changes continuously throughout life; with aging, the tympanic membrane becomes less vascular, less cellular, more rigid, and less elastic (Ruah et al. 1991).

I.III.2.1.2 Function of the tympanic membrane

In the previous chapter (I.II.5.1) the external ear canal was described as a tube closed at one end. Acoustically this is not the case; the tympanic membrane absorbs acoustic energy from the external ear canal, transform it into mechanical vibration and transmit it to the ossicular chain. This transition (of acoustic energy into mechanical vibration) at the tympanic membrane is defined by different parameters such as the tension of the membrane, its mass and shape, the middle ear cavity, and the load and stiffness of the ossicular chain. It is impressive that this 50-120 µm thick membrane absorbs very small pressure changes of 20 µPa at the hearing threshold, and compensates up to 120 kPa from the atmospheric pressure changes (Jensen & Bonding 1993). The function of the tympanic membrane is related to the function of the middle-ear ossicles (see chapter I.III.2.5.).

I.III.2.2 Tympanic cavity (middle ear cavity)

The tympanic cavity is an air-filled cavity behind the tympanic membrane that includes three ossicles: malleus, incus, and stapes. These three ossicles of the ossicular chain in the middle ear play the main role in this dissertation and therefore are described in detail in the following paragraphs. The manubrium (or handle) of the malleus is connected to a part called umbo of the tympanic membrane. The head of the malleus is connected to the body of the incus which itself is connected to the stapes. The stapes is the smallest bone in the human body and is connected to the oval window of the inner ear. Two joints exist in the middle ear: the incudo-malleolar-joint between the malleus and the incus, and the incudo-stapedial-joint between the incus and stapes.

I.III.2.2.1 Mucosal lining

The tympanic cavity is lined throughout a thin membrane with endodermal origin that is continuous with that of the auditory tube, the tympanic antrum, and the mastoid cells (Goycoolea & De Souza 2012). It is directly bound to the periosteum of the bone, and also covers the middle-ear structures and their ligaments (see chapter I.III.2.4) (Goycoolea & De Souza 2012). The mucosa includes a superficial epithelial layer (secretory cells, ciliated cells, non-specialized cells) separated from the deep connective layer by a basement membrane (Brémond & Coquin 1972). The purpose of this mucosa is to maintain an air-filled cavity such that middle ear can perform its function of sound permission (Goycoolea & De Souza 2012). The mucosa forms various folds and pouches e.g., the anterior and posterior pouches (of von Troltsch), which are related to the anterior and the posterior ligaments of the malleus respectively (see chapter I.III.2.4.1.1) (Goycoolea & De Souza 2012). This mucosal lining (or mucoperiosteum) consists of epithelium, connective tissue and periosteum proper; details of these different tissues are nicely illustrated in the 'atlas of otologic surgery and magic otology' of (Goycoolea & De Souza 2012), and is not discussed further in this work.

I.III.2.2.2 Orientation in the middle ear cavity

The volume of the cavity ranges from 0.5 cm^3 (0.51 ± 0.04 ml) to 1 cm^3 (Whittemore et al. 1998, Gyo et al. 1986). The posterior portion of the tympanic cavity, which includes the malleus and the incus, is called the 'epitympanic recess' or the 'attic' (Gelfand 2009). A schematic analogy of the cavity as a 'box-model' is shown in Figure I.18 A. The thin bony 'tegment tympani' separates the tympanic cavity from the brain cavity above (Gelfand 2009). Laterally, the cavity is separated from the jugular vein below. Anterior, are the opening of the Eustachian tube and the internal carotid artery canal located. The tensor tympani semicanal containing the tensor tympani muscle is on the anterior side as well. The cochleariform process (not illustrated) on the anterior/medial side is wrapped with the tendon of the tensor tympani muscle. A prominent bulge on the medial wall appears due to the promontory of the basal turn of the cochlea. The oval window with the stapes attached to it and the round window are located at the medial wall as well. Superior to the oval window is the facial nerve canal prominence. The mastoid is located behind (posterior) to the posterior wall. To fix the stapedius muscle on the posterior wall, the 'pyramid' protrude from the posterior wall.

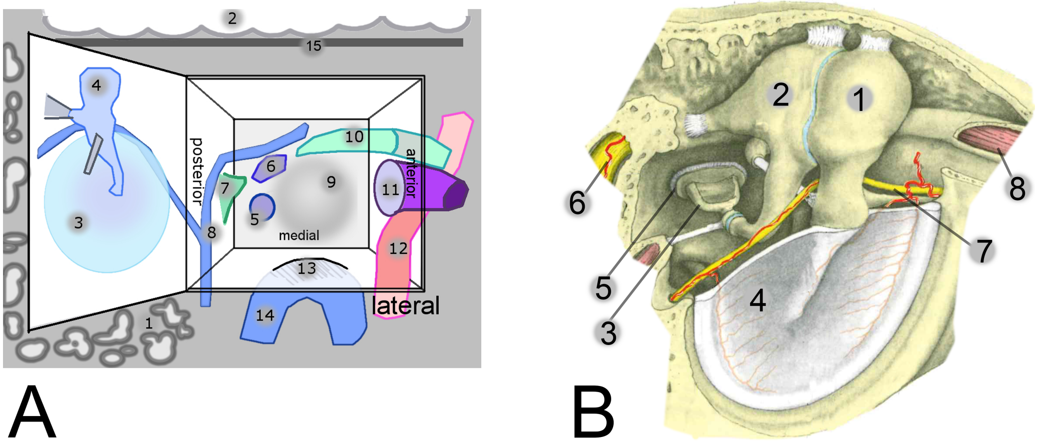

Figure I.18 (A) Schematic illustration of the middle ear cavity with the lateral wall folded to the left: (1) mastoid bone behind posterior wall, (2) temporal lobe of the brain, (3) tympanic membrane, (4) malleus, (5) round window, (6) oval window with stapes attached from lateral side (not illustrated), (7) pyramid, (8) chorda tympani, (9) promontory, (10) tensor tympani tendon, (11) Eustachian tube, (12) carotid artery, (13) jugular bulb, (14) jugular vein (15) tegment tympani. Modified after (Gelfand 2009, hawkelibrary 2014). (B) Middle-ear structures: (1) malleus, (2) incus, (3) stapes, (4) tympanic membrane, (5) annular ligament of the stapes, (6) facial nerve, (7) Chorda tympani, (8) tensor tympani muscle. Modified after (Rauber & Kopsch 1987). Permission for reprint achieved © Georg Thieme Verlag KG.

I.III.2.3 Eustachian tube

Unlike the open ear canal, the air of the middle ear is not in direct contact with the atmosphere outside the body. The Eustachian tube connects the middle ear to the upper throat (nasopharynx) and is ventilated through the nose. The function of the Eustachian tube is to protect, drain and ventilate the middle ear (Bockers 2013, Leuwer & Koch 1999). It is normally closed but opens from time to time during activities such as yawning, swallowing, and chewing due to contraction of palatine muscles (Sproat et al. 2014). In adults, the Eustachian tube has a length of 35-37 mm and an anteromedial gradient of 2 cm or descending angle of 45° (Leuwer & Koch 1999). The tube is structured into pars ossea (covered by bony tissue) beginning at the cavum tympani and a pars cartilaginea (covered by lamina medialis, lamina lateralis and lamina membranacea) that reaches the nasopharynx (Bockers 2013). This pars cartilaginea builts the functional part of the Eustachian tube that allows the ventilation of the middle ear and therefore equalization to atmospheric pressure. This keeps the air pressure equal either side of the eardrum, which is necessary for transmission of sound and therefor for a proper hearing. Furthermore, fresh supplies of air are needed for the cells that line the middle ear.

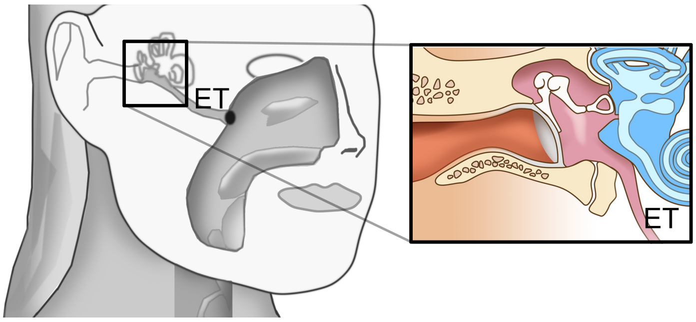

Figure I.19 The Eustachian tube (ET) connects the middle ear to the upper throat.

I.III.2.4 Anatomy of the ossicles in the middle ear

The ossicles malleus, incus and stapes form the coupling between the vibration of the outer ear (tympanic membrane, respectively) and the forces exerted on the oval window of the inner ear. The anatomy of the malleus (see I.III.2.4.1), Incus (see I.III.2.4.2), stapes (see I.III.2.4.3) and the two joints (IMJ I.III.2.4.4.1, ISJ I.III.2.4.4.2) are described in the following subchapters.

A unique future of the ossicles is that they are completely enveloped by mucosa, continuous with the middle ear (see chapter I.III.2.2.1) (Goycoolea & De Souza 2012). The epithelium of the ossicles is almost entirely squamous; taller ciliated cells are rarely found (Goycoolea & De Souza 2012).

I.III.2.4.1 Malleus ('hammer', 'mace')

The malleus is the largest and most lateral of the three auditory ossicles. It has a weight of 21.2 to 30.7 mg (n= 54) and height of 7.1 to 8.8 mm (n= 60) (Todd & Creighton 2013). Anatomical landmarks of the malleus are described in Figure I.20. The malleus is attached to tympanic membrane; its attachment part is named manubrium or handle of the malleus, which extends from the lateral process of the malleus to the umbo. This is the tightest connection between the ossicular chain and the ossicles, although, the middle part of the manubrium is not intimately connected with the fibrous layer of the tympanic membrane in human (Aernouts et al. 2012). The manubrium separates slightly from the fibrous layer of the tympanic membrane so that its only attachment is a fine fold of mucous membrane (Gulya & Schuknecht 1995, M. D. Graham et al. 1978, Salih et al. 2012). Superiorly, the lateral malleal process terminates the manubrium, which is often visible otoscopically from the medial side between the pars tensa and the pars flaccida (see fig TM). The head of the malleus connects the malleus to the incus and therefore builds the anterior part of the incudo-malleolar joint (IMJ see chapter I.III.2.4.4.1).

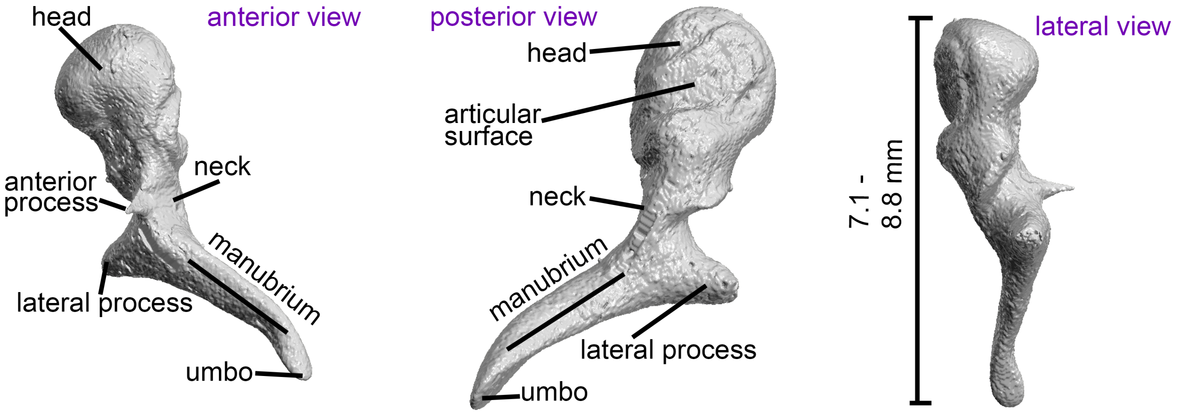

Figure I.20 Malleus (right ear) from anterior view, posterior view, and lateral view: head, neck, anterior process, lateral process (short process), manubrium, umbo, articular surface.

I.III.2.4.1.1 Suspensory attachment of malleus to the tympanic cavity

The middle ear ossicles are suspensory attached to the tympanic cavity. Several descriptions of the attachments of the malleus have been reported; the authors disagree through the number of identified suspensory attachments of the malleus to the tympanic cavity from two (Koike et al. 2002) to five (Beer et al. 1996). Nowadays, four suspensory attachments consisting of the tensor tympani tendon, the anterior attachment, the lateral attachment, and the superior attachment are generally accepted (Gray & Lewis 1918, Schuknecht 1974, Gan et al. 2002, J.H. Sim & Puria 2008). The anterior and the lateral attachment are commonly described as suspensory ligaments consisting of collagen fibers, while the superior attachment is sometimes considered to be a thin fold of mucous membrane consisting of a thin layer of epithelium (J.H. Sim & Puria 2008). The lateral ligament connects the neck of the malleus and the lateral wall of the tympanic cavity with a shape like a fan. Together with the opposed laterally pars flaccida, inferiorly the lateral process of the malleus and the outer attic wall superiorly, it encloses a small air filled chamber (recess) called Prussak's space. The anterior ligament (or 'axial ligament' Helmholtz 1868) rises from the neck of the malleus and reaches into the petrotympanic fissure (U. Willi 2003) that runs from the temporomandibular joint to the tympanic cavity (Eckerdal 1991). The superior malleal ligament weakly connects the head of the malleus and the wall of the superiorly epitympanic recess (U. Willi 2003). Furthermore, the malleus is connected via the tensor tympani tendon to one of two middle-ear muscles; the tensor tympani muscle. The tendon connects the manubrium close to the neck of the malleus to the tensor tympani muscle, which is attached to the medial wall of the tympanic cavity near the entrance of the Eustachian tube. When contracting, it pulls the manubrium of the malleus inward, displacing the tympanic membrane inwards by stretching it (Aage R. Møller 2000). It is innervated by the trigeminal nerve (CN V) (Aage R. Møller 2000). It may dampen sounds conducted through bone, such as those produced from chewing or even speech – but not under voluntary control (Mason 2011).

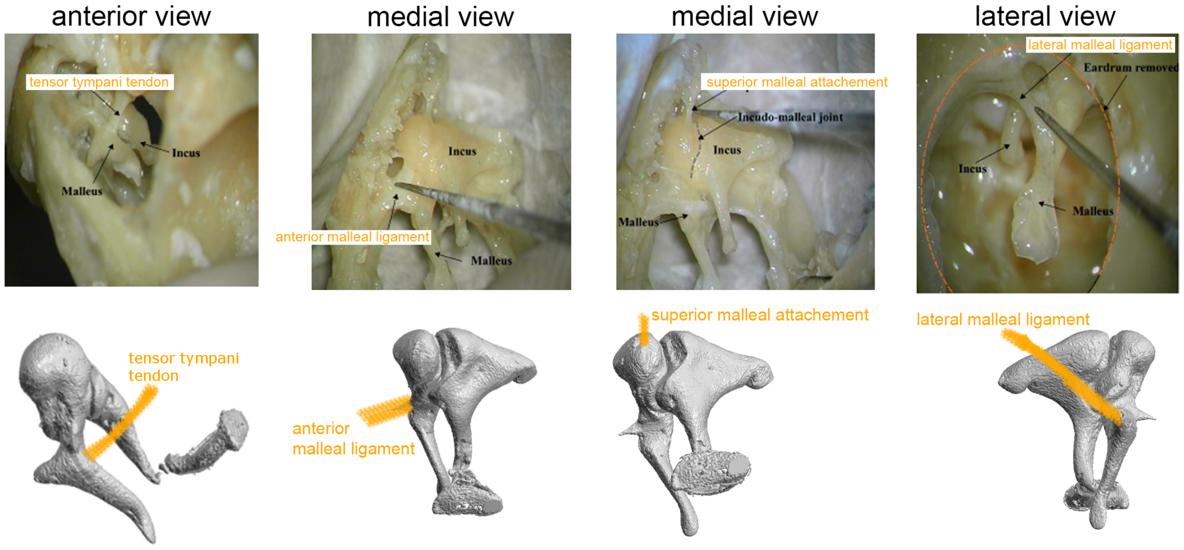

Figure I.21 Microscopic view and schematic illustration of malleal suspensory attachments; tensor tympani tendon, the anterior malleal attachment, the lateral malleal attachment, and the superior malleal attachment. Microscopic view Modified after Springer and JARO - Journal of the Association for Research in Otolaryngology, 9(1), 2007, 5-21, "Soft Tissue Morphometry of the Malleus–Incus Complex from Micro-CT Imaging", Sim JH, Puria S., figure 1, © Springer Science and Business Media, with kind permission of Springer Science and Business Media. (J.H. Sim & Puria 2008).

I.III.2.4.2 Incus ('anvil')

The incus is positioned between the malleus and the stapes. It has a weight of 24.4 to 37.4 mg (n= 66) and height of 6.5 ± 0.3 mm (n= 68) (Todd & Creighton 2013). Anatomical landmarks of the incus are described in Figure I.22. The head of the incus forms the posterior part of the incudo-malleolar joint. Its short process (see Figure I.22) projects to the posterior side with a length of 5.0 ± 0.3 mm (n= 68) (Todd & Creighton 2013). Inferiorly, the incus projects by a long process, which terminates with a small appendix called 'lenticular process' of the incus. This region, including the connection of the long process of the incus to the head of the stapes by the lenticular process, is called the 'distal incus' (Chien et al. 2009a). A recent anatomic study revealed wide variations of diameters and shape of the long process of incus; between 0.52 mm and 1.15 mm at the level of 1.5 mm far from the tip of the long process, which is the most common site for stapes prosthesis attachment (Toth et al. 2013). The tip of the incus, the lenticular process, rises medially and forms the lateral part of the incudo-stapedial joint. The best nomenclature for the lenticular process is still uncertain (Graboyes et al. 2011); originally, the lenticular process was thought to be a separate ossicle (n=9 of 270 cadaveric human temporal bones (Chien et al. 2009a)), contrary, later studies revealed that it was actually attached to the incus by a thin strut or pedicle (n=261 of 270 cadaveric human temporal bones (Chien et al. 2009a)).

The chorda tympani nerve, which originates from the taste buds in the front of the tongue, crosses the long process laterally and joins the facial nerve (cranial nerve VII) inside the facial canal. Often, the access and view to the long process of the incus is disabled by this nerve (see Figure I.18 B, (7) chorda tympani).

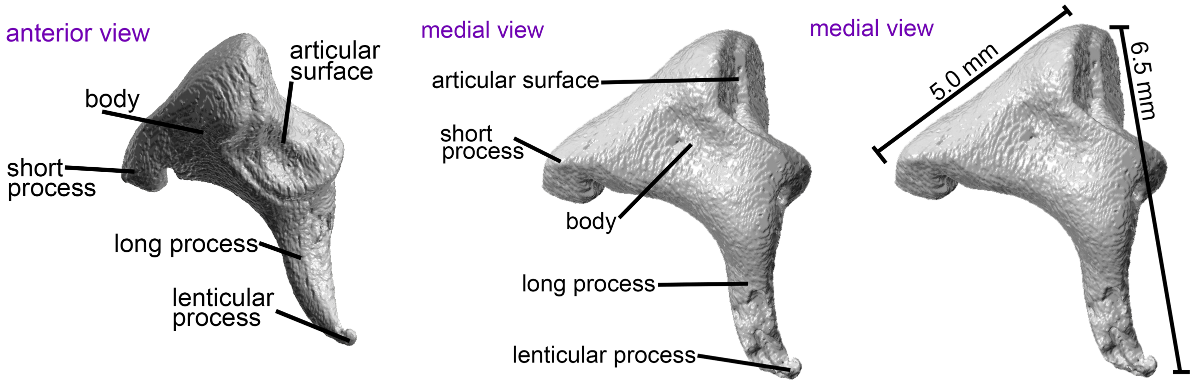

Figure I.22 Incus from anterior and medial view: articular surface, body, short process (short limb, crus breve), lenticular process, long process (long limb, crus longum).

I.III.2.4.2.1 Suspensory attachment of incus to the tympanic cavity

The incus is connected to the tympanic cavity with a short, thick band (Gray & Lewis 1918), which attaches the short process of the incus (mainly on the medial and lateral parts) to the epitympanic recess wall (U. Willi 2003, J.H. Sim & Puria 2008). Sometimes, this ligament is referred to as the posterior ligament of the incus. The geometry is more complicated than for the ligaments of the malleus; the ligament connects the short process of the incus to the bony wall of the tympanic cavity on the medial and lateral side – hence, this ligament split itself to two strands that are still connected through the inferior and posterior parts of the short process of the incus (J.H. Sim & Puria 2008).

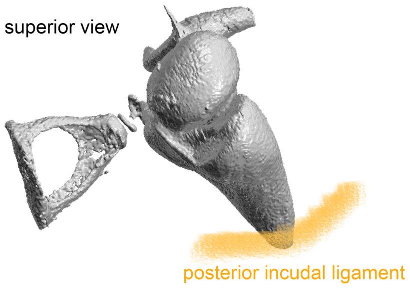

Figure I.23 Schematic illustration of the posterior incudal ligament.

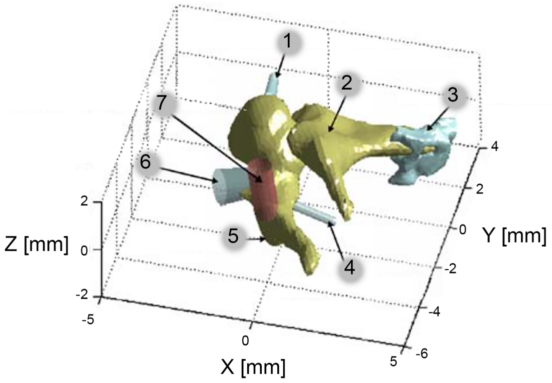

Figure I.24 Simplified features of the suspensory attachments of the malleus-incus-complex: (1) superior malleal attachment, (2) incus, (3) posterior incudal ligament, (4) lateral malleal ligament, (5) malleus, (6) anterior malleal ligament, (7) tensor tympani tendon. Modified after Springer and JARO - Journal of the Association for Research in Otolaryngology, 9 (1), 2007, 5-21, "Soft Tissue Morphometry of the Malleus–Incus Complex from Micro-CT Imaging", Sim JH, Puria S., figure 10, © Springer Science and Business Media, with kind permission of Springer Science and Business Media (J.H. Sim & Puria 2008).

I.III.2.4.3 Stapes ('stirrup')

The smallest bone of the human body, the stapes, is connected to the incus via the incudo-stapedial joint. The head of the stapes builds the medial aspect of this joint. Medially, two crura form a sort of archway over the stapes footplate. Anatomical nomenclature is described in Figure I.25. The stapes has a weight of 3.3 ± 0.6 mg (n=17) (Ferrazzini 2003). The height (h) of the stapes is 3.28 ± 0.21 mm, the long length of the footplate (a) is 2.81 ± 0.158 mm and short length of the footplate (b) is 1.27 ± 0.109 mm with a resulting footplate area of 3.03 ± 0.331 mm^2 (n=53) (J.H Sim et al. 2013). The wider anterior crus width at shoulders is 398 µm (range of 333-500 µm) and the narrower posterior crus width at shoulders is 386 µm (range of 285-600 µm) (Farahani & Nooranipour 2008). The angle between the crura is 19.5 degrees (range, 15-24 degrees) (Farahani & Nooranipour 2008). Our group described the precise anatomical properties of the stapes in a publication of 2003 (J.H Sim et al. 2013); an intrinsic frame (defined based on the geometry of the medial surface of the stapes footplate) was used to examine and quantify the asymmetrical shapes. The anterior length a_{ant} was defined as the length from the centroid of the medial surface of the footplate (origin of intrinsic frame) to the anterior edge of the footplate through the long axis (x-axis). This a_{ant} was then compared to the posterior length a_{pos}, which was defined as the length from the origin to the posterior edge (see Figure I.26 and

Figure I.27). Analogously, the superior and inferior lengths were defined as lengths along the short axis (y-axis) and were compared with each other.

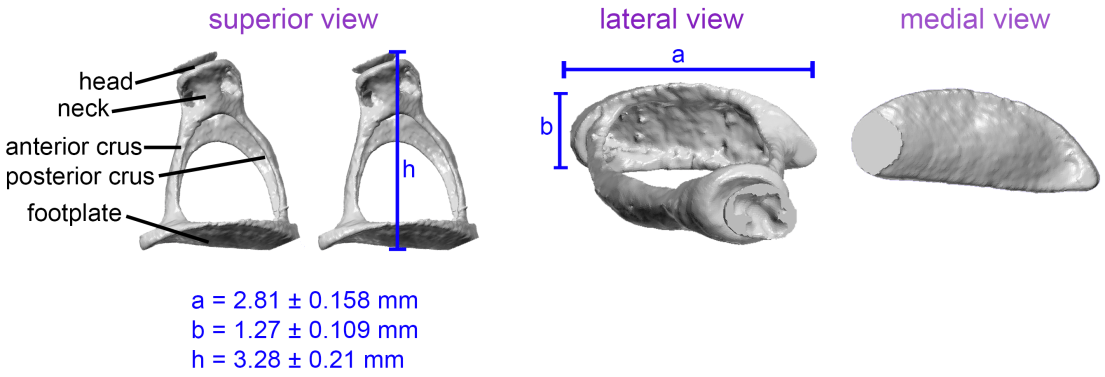

Figure I.25 Superior, lateral and medial view of the stapes; head, neck, anterior crus, posterior crus, footplate (base).

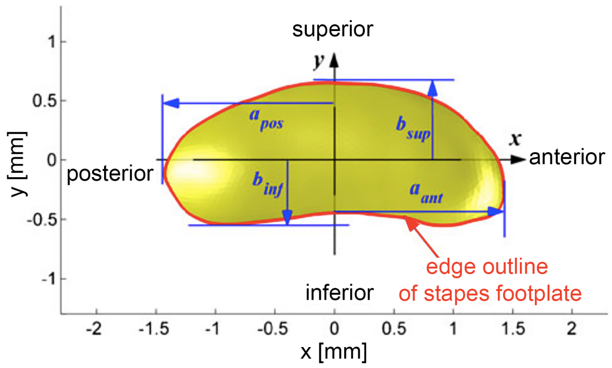

Figure I.26 References for the asymmetry of the stapes footplate in an intrinsic frame. The outline of the footplate is shown in the x–y plane (red). Modified after Springer and JARO - Journal of the Association for Research in Otolaryngology, 9(1), 2007, 5-21, "Characterization of Stapes Anatomy: Investigation of Human and Guinea Pig", Sim, J. H., Röösli, C., Chatzimichalis, M., Eiber, A., Huber, A. M., figure 3, © Springer Science and Business Media, with kind permission of Springer Science and Business Media. (J.H Sim et al. 2013).

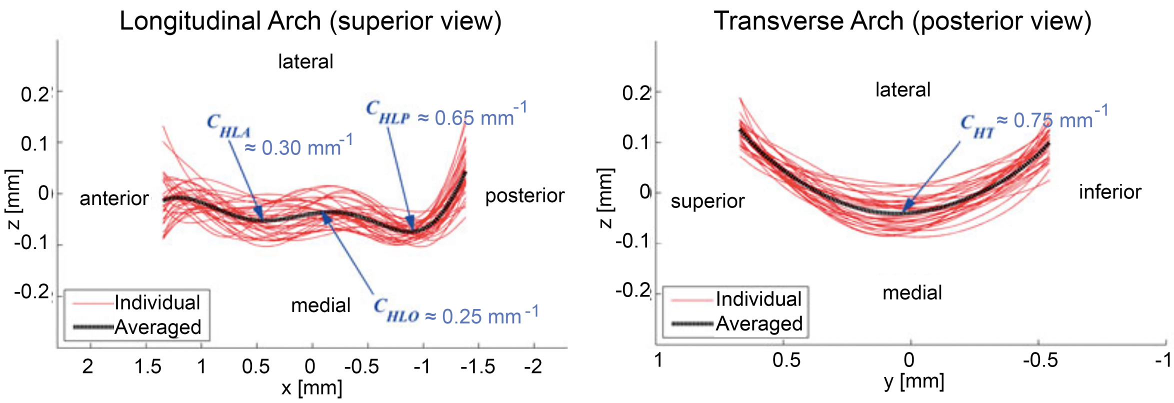

Figure I.27 Surface profiles of the footplate in 29 human stapes. The red lines show the diversity of the longitudinal arch of the medial surface along the long axis (x-axis) and the diversity of the transverse arch of the short axis (y-axis). The curvatures are labeled in the graph: curvature of the averaged longitudinal around the origin (C_{HLO}), in the convex regions of the anterior (C_{HLA}) and in the posterior (C_{HLP}) parts. The transverse arch of the medial surface along the short axis (y-axis) in the human stapes was convex medially, and its curvature is marked as (C_{HT}) in the graph. Modified after Springer and JARO - Journal of the Association for Research in Otolaryngology, 9(1), 2007, 5-21, "Characterization of Stapes Anatomy: Investigation of Human and Guinea Pig", Sim, J. H., Röösli, C., Chatzimichalis, M., Eiber, A., Huber, A. M., figure 5 (B and C), © Springer Science and Business Media, with kind permission of Springer Science and Business Media (J.H Sim et al. 2013).

I.III.2.4.3.1 Suspensory attachment of stapes to the tympanic cavity

The stapes is connected to the incus with the ISJ, to the tympanic cavity by the stapedial muscle, and to the oval window of the inner ear by the annular ligament. These suspensory attachments of the stapes are described in the following subchapters.

I.III.2.4.3.1.1 Annular ligament

The slightly irregular oval stapes footplate is connected to oval window in the cochlear wall by the annular ligament. This connection is also named 'stapedio-vestibular joint' (see Figure I.28). It provides a sealed but mobile boundary for transmission of ossicular movement into cochlear fluid (Wolff & Bellucci 1956). Elastic fibers are prominent near the surface of the ligament (Michaels & Hellquist 2001). Shear stress of the annular ligament is induced as the stapes follows piston-like motion and rocking-like motion forms (Gan et al. 2011). A space lined by connective tissue in the posterior part of the ligament is present in approximately seventy percent adult specimens (Bolz & Lim 1972); however, it is not clear whether this space should be considered a modified synovial joint, a bursa, or a degenerative change caused by aging (S.N. Merchant & Nadol 2010). The thinner anterior part of the annular ligament (n=37) has a width between 22 µm (middle part) and 40 µm (toward the inner ear); the wider posterior part of the annular ligament (n=37) has a width between 50 µm (middle part) and 85 µm (toward the inner ear) (Cherukupally et al. 1998). Looking at the mechanical properties, the fibrous annular ligament is a typical viscoelastic material (Gan et al. 2011). This directly affect the acoustic-mechanical transmission to the cochlea; a reduced movement of the stapes, due to otosclerosis of the stapes footplate or/and abnormal ossification of the annular ligament, cause conductive hearing loss (Gan et al. 2011, S. N. Merchant et al. 2001, Schuknecht & Barber 1985).

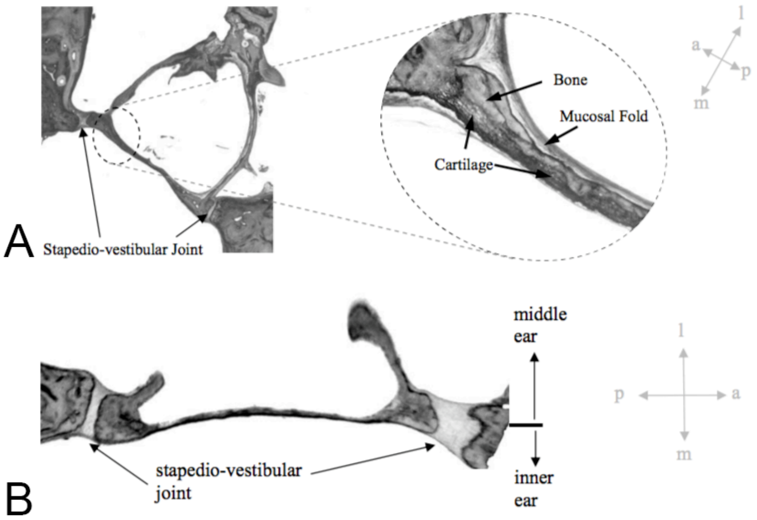

Figure I.28 Microscopic section showing the stapedio-vestibular joint, where the annular ligament connects the stapes footplate with the oval window of the cochlea. From the TB collection, ENT-Dept. University Hospital Zurich. TBs are fixed with Heidenhain-Sussa, decalcified and embedded in celloidin. The axes for orientation are p= posterior, a= anterior, m = medial, l= lateral. The blocks were serially cut at a thickness of 20 µm in the horizontal plane and stained with hematoxilin-eosin. Reprinted with kind permission of Dr.sc.techn. Mattia Ferrazzini (Ferrazzini 2003): (A) Figure II.10 pp.20 and (B) Figure II.14 pp. 22.

I.III.2.4.3.1.2 Stapedial muscle and stapedial reflex

The stapes is connected to the tympanic cavity via the stapedial muscle (or 'stapedius muscle'). Along with the tensor tympani it is one of the two muscles in the middle ear. It is the smallest striate muscle of the body (Aage R. Møller 2000). Its tendon spans between the neck of the stapes to the opening of a bony shell in the pyramidal eminence on the posterior (or mastoid) wall of the tympanic cavity. Most of the muscle is located in the bony canal (Aage R. Møller 2000). The stapedial muscle is innervated by the facial nerve (CN VII) (Aage R. Møller 2000). Various functions are attributed to this muscle. For example it improves hearing in noise acting as a low-frequency filter; the excitation of the muscle results in a stimulus level–dependent attenuation of low-frequency (<1kHz) ossicular chain vibration reaching the cochlea (Wilson & Margolis 1991). Furthermore, it protects the cochlea against acoustic trauma by reflexive contractions of the stapedius muscle evoked by loud sounds (Hilding & Fletcher 1960, Zakrisson & Borg 1974, Zakrisson et al. 1975). This reflexive contraction is afferent mediated by the cochlear nerve and efferent by the stapedial branch of the facial nerve (Borg 1968, Musiek & Baran 2007). The contracted stapedial muscle pulls the stapes in a direction that is perpendicular to its piston-like motion, tilting the stapes such as it rotates around the posterior ligament (Aage R. Møller 2000). A recent study shows that the stapedius reflex appears to offer some protection from the upward spread of masking of speech by background low-frequency noise at moderate levels, but not at high levels (Aiken et al. 2013).

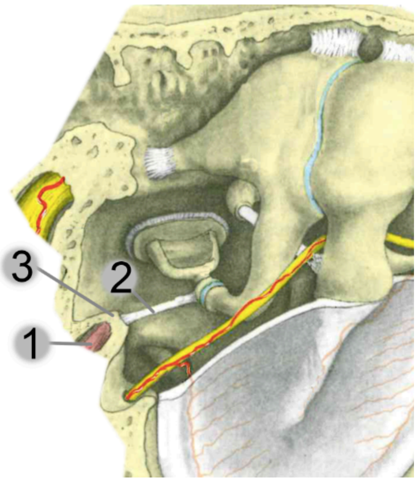

Figure I.29 Illustration of the stapedial muscle (1), the stapedial tendon (2) and the pyramidal eminence (3) in the middle ear. Modified after (Rauber & Kopsch 1987). Permission for reprint achieved © Georg Thieme Verlag KG.

I.III.2.4.4 Anatomy of the joints in the middle ear

The middle ear comprises two joints: the incudo-malleolar joint (IMJ) and the incudo-stapedial joint (ISJ). The IMJ connects the malleus and incus, and the ISJ connects the incus and the stapes.

I.III.2.4.4.1 Incudo-malleolar joint ('malleo-incudal joint', 'incudo-malleal joint', 'incudo-mallear joint', 'articulatio incudomallearis')

The main studies of this disseration (see chapter III.I to III.III) are focused on the function of the IMJ under acoustic and quasi-static excitation. Therefore, this chapter describes the anatomy of the IMJ in detail including the historical background and the recent knowledge.

I.III.2.4.4.1.1 Historical background of the anatomy of the incudo-malleolar joint (IMJ)

The anatomy and physiology of the IMJ evoked many discussions among scientists. Findings of descriptions of the IMJ in literature are ordered chronologically in the following paragraph. Controversial discussions about the anatomy and the physiology of the joint continued in the 20th century – as well about the function of the IMJ (see also chapter I.III.2.5.3).

Valsalva described the IMJ already in 1707. He found that the connection between malleus and incus did not allow motion between the ossicles: "habetur immobilis articulation cum malleo" (Valsalva 1707). First detailed comments about the anatomy of the human IMJ were made at the end of the 18th century in the work of Sömmerring (von Sömmerring 1791). He described the connection between the malleus and the incus already as a sort of joint with two articular surfaces covered with cartilage and held together with a tenuous skinny capsule.

> *"der Amboss… ist winklig zur Verbindung mit dem Hammer ausgeschnitten, und bildet daher zwei Gelenkflächen"…"Durch sehr zarte, fast nur häutige, wenigstens nicht augenscheinlich sehnige Gelenkkapselchen werden die überknorpelten glatten Gelenksflächen des Hammers und des Ambosses… zusammengehalten"*. (von Sömmerring 1791)

Pappenheim (Pappenheim 1840) found a fold of the synovial structure (“Synovialfalte”) that extended from the medial side into the IMJ. Against the generally considered opinion at that time, Barkow (Barkow 1841) stated that the connection between malleus and incus wasn’t a true joint, and that no cartilage, which would reduce or even eliminate the sound transmission via the ossicular chain, covers the surfaces of the ossicles.

Broman describes in his work “Die Entwicklungsgeschichte der Gehorknöchelchen beim Menschen” the historical development of the ossicles until the end of the 19th century (Broman 1899). According to his work, Luschka (Luschka 1858) confirmed the findings of Sömmerring; he found a 0.4 mm thick hyaline cartilage with round cells, a membrane connecting malleus und incus, and therefore defines this connection as a true joint. Contrary, Magnus doubted that a true joint exists and assumed only a connection of elastic tissue between the ossicles like in the spine (Magnus 1861). Helmholtz described in his foundational work “Sensations of Tone” the incudo-malleolar joint as curved depression of a rather irregular form, like a saddle (H. Helmholtz 1863). Toynbee also described the ‘convex surfaces of the lower and posterior part of the head of the malleus’ which articulated with the ‘concavity on the anterior part of the body of the incus’ connected with ligaments (Toynbee 1865). Brunner shared the opinion of Sömmerring, Luschka and Helmholtz of the true joint with joint capsule, and articular surfaces covered with hyaline cartilage - not covered with endothelial cells (Brunner 1870). Looking at a successfully collection of histological cuts through the IMJ, Rüdinger discovered for the fist time a prominent meniscus that separated the joint surfaces (Rüdinger 1870). Therefore, he proposed the IMJ to constitute a true joint with a movable disc in between (= meniscus). In his opinion the meniscus was not found in previous studies due to the preparation techniques applied. Rüdinger's discoveries were confirmed by Körner (Körner 1878), who was his former student (Schmidt 1903). Körner added on that this meniscus doesn’t intergrowth with the hyaline cartilage and pervades the whole length of the joint. Mach & Kessel described the existence of a fibrocartilaginous disc that partly connected the two articular surfaces in all IMJs (Mach & Kessel 1874). Also, Politzer obtained that fibrous structures were posteriorly prolonged into a uniform cartilaginous (‘wedge-shaped’) meniscus (Politzer 1884). Siebenmann wasn’t in agreement with Körner and other authors (Schmidt 1903, Druss 1928) according the existence of a symphysis (= fibrocartilaginous fusion between two bones) and doubted a meniscus how Rüdiger originally described it (Siebenmann 1898). In Siebenmann’s opinion, the IMJ is not a real ‘free joint’ and the ‘meniscus’ is adnate via star-shaped cells to the hyaline cartilage and not freely movable. Motivated by his mentor Prof. Siebenmann, Schmidt published in 1903 his work about the anatomy and ontogenesis (fetal, newborn, infantine and adult middle ears) of the ossicular joints (Schmidt 1903). He used microscopy and the magnifying glass to investigate the 12 adult sequences of sections, which where stained with several staining techniques enabling better classification of tissue. One example of a drawing of his work is shown in Figure I.30. He divided the investigated joints into two groups; the "meniscoide" form with a meniscus, a fibrocartilaginous structure, which fully or partly divides a joint cavity, and a "symphysoide" form where the ossicles are connected via fibrocartilage. Finally, he classified all observed forms as ‘intermediate’; the ossicles were connected with fibrocartilaginous tissue, which partly divided the joint with a cleft or continuously blended into each other. A totally free meniscus was not observed. He concludes that the incudo-malleolar joint is a ‘loose symphysis’, with occurrence of intermediate forms like meniscus-joints also referred to as diarthrodial joints. He never found a typical diarthrodial joint, nevertheless, he didn’t deny the existence of a such. Doran compared in his study the morphology of the ossicles in several mammalian species and described the articular surfaces assuming the incudo-malleolar joint being a true joint (Doran 1878, Doran 1876).

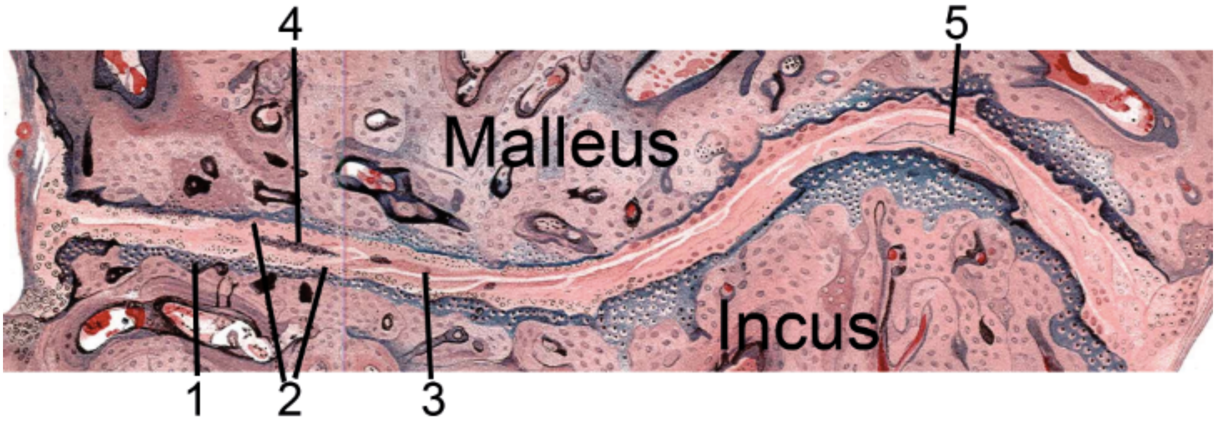

Figure I.30 Drawing of a human incudo-malleolar Schmidt 1903; "Symphysoide" form of the incudo-malleolar joint of a 22-year-old man: (1) zone of ossification, (2) hyalin covering of the joint, (3) conjunction-zone, (4) calcareous deposits within the conjunction-zone. Modified after Springer and Zeitschrift für Ohrenheilkunde, Bergmann, Bd 43, Zur Anatomie und Entwicklungsgeschichte der Gelenksverbindung der Gehörknöchelchen beim Menschen, 1903, figure 11, Schmidt, C., with kind permission of Springer Science+Business Media.

In 1911, Frey compared the anatomy of the IMJ between several mammals, including humans (Frey 1911). He doubted the accuracy of the previous histological studies. The IMJ was classified as ‘partially ankylosed’ with connective tissue in his work and, thus mobility in the joint was disclaimed. In his opinion the connection between malleus and incus ‘never’ fulfills the criteria to be a true joint; neither a simple joint nor a joint with a meniscus. He was convinced, that under physiological stimulation no motion occurs in the joint.

Also other authors briefly characterized the IMJ as a true joint regarding the histology of the ossicles (Altmann 1965, Beck 1978, Covell & Feinmesser 1959, Eysell 1870, Lempert 1945).

I.III.2.4.4.1.2 Recent studies about the anatomy of the incudo-malleolar joint (IMJ)

This chapter focuses on the recent knowledge of the anatomy of the IMJ. Currently, it is assumed that the IMJ is a true diarthrodial joint that contains synovial fluid inside the joint capsule, a discus between the two articular surfaces of the malleus and incus, and that a fibrous joint capsule surrounds it.

I.III.2.4.4.1.2.1 Synovial joint

The IMJ is nowadays considered to be a synovial joint, also known as diarthrodial joint or diarthrosis, connecting the malleus and incus at its articular surfaces (Schuknecht 1974, Marquet 1981, Etholm & Belal 1974). Analogously, according to the Terminologia Anatomica (Federative Committee on Anatomical Terminology (FICAT) & International Federation of Associations of Anatomists 1998) the two middle ear joints are classified as synovial joints (FMA:60064). A synovial joint is generally defined as “a point where two bones are separated by a narrow, encapsulated space filled with lubricating synovial fluid; most such joints are relatively mobile” (Saladin 2012) (see Figure I.31). Other synovial joints in the human body are for example knee, shoulder, hip and elbow. The main structural difference from synovial joints to other joints is the existence of a capsule surrounding the articulating surface of the synovial joint and the presence of lubricating synovial fluid within this capsule. The incudo-malleolar joint is presumed to contain synovial fluid as well (see Figure I.33) (Marquet 1981, Hüttenbrink & Pfautsch 1987). Sim et al. describe the fluid as a “sticky fluid, which is contained by the fibrous wall along its boundary” (see Figure I.32) (J.H. Sim & Puria 2008).

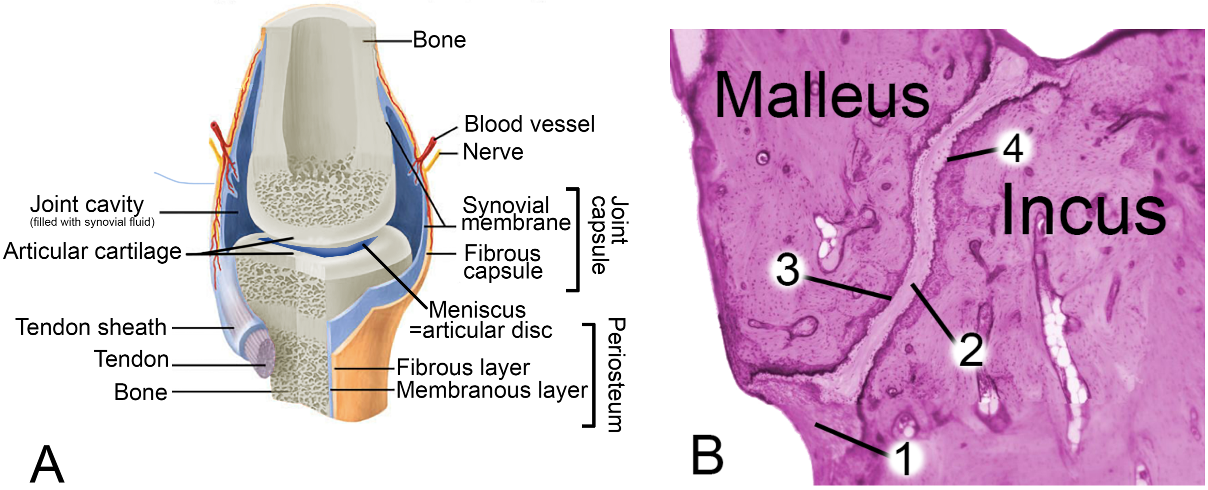

Figure I.31 (A) Schematic drawing of a synovial joint. Modified after (Saladin 2012). (B) Microscopic section of the IMJ: (1) joint capsule, (2) meniscus (articular disc), (3) articular cartilage of the malleus, (4) articular cartilage of the incus. This was a sample from the temporal bone collection of the ENT-Department University Hospital Zurich. The samples were fixed with Heidenhain-Sussa, decalcified and embedded in celloidin. The blocks were serially cut at a thickness of 20 µm in the horizontal plane and stained with hematoxilin-eosin.

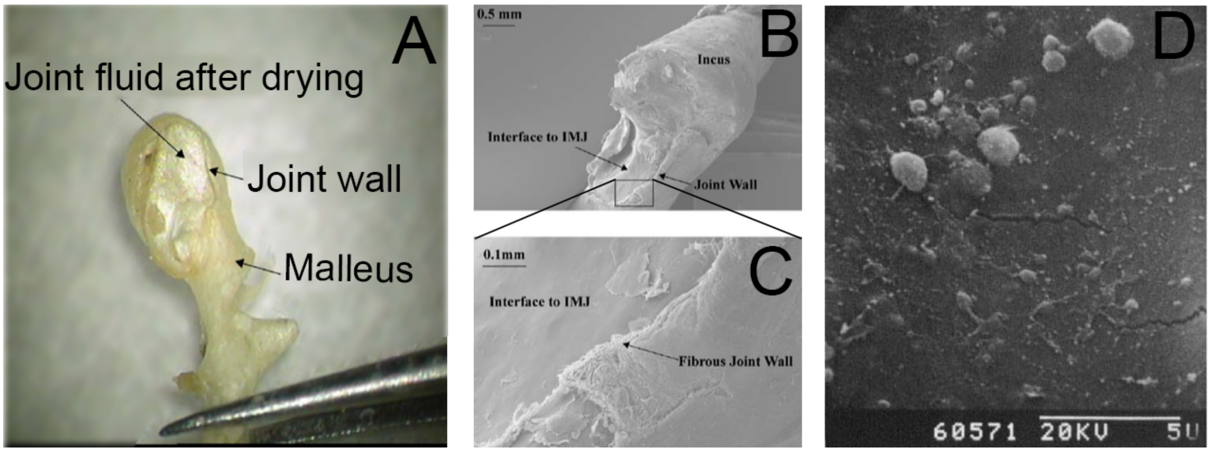

Figure I.32 The articular surfaces of the malleus and incus of the incudo-malleolar joint (IMJ). (A) Microscopic view of the articular surface of the malleus after drying of the joint fluid for 30 min (B) SEM photo of articular surface of the incus (C) SEM photo of the fibrous structure at the joint wall. Modified after Springer and JARO - Journal of the Association for Research in Otolaryngology, 9(1), 2007, 5-21, “Soft Tissue Morphometry of the Malleus–Incus Complex from Micro-CT Imaging”, Sim JH, Puria S., figure 2, © Springer Science and Business Media, with kind permission of Springer Science and Business Media. (J.H. Sim & Puria 2008)

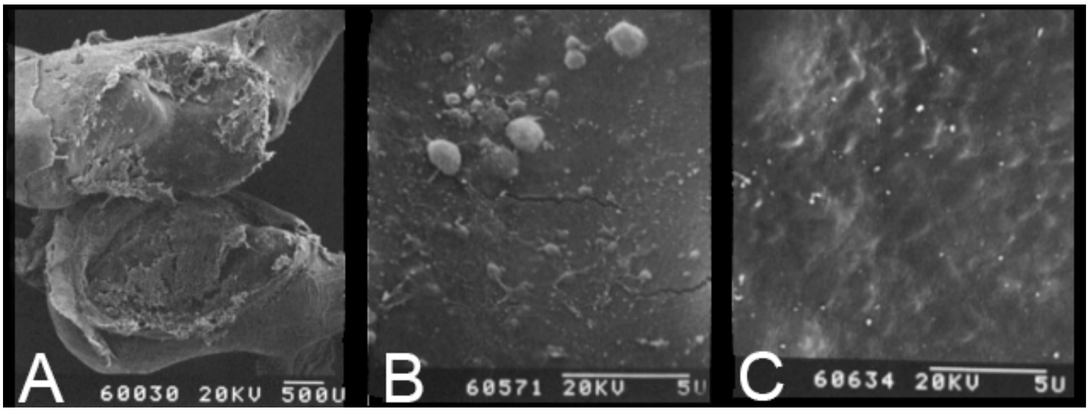

Figure I.33 (A) SEM picture (14x) of opened IMJ with lifted meniscus (B) The articular surfaces seem homogeny smooth in the SEM pictures. The collagen fibers are not visible because they are covered by cartilage. Small flakes of dried protein components of the synovial fluid stick on the articular surface shown in the picture, (c) smooth hyaline cartilage surface of the malleus with removed synovial fluid and removed meniscus. Only small exaltations of 1-2 µm are detectible. The collagen fibers are embedded into the hyaline cartilage (matrix built of proteoglycans) and only visible after pathological changes. The meniscus contained visible collagen fibers and was not firmly attached to the joint; thus, the meniscus was not grown together with the cartilage. Reprinted from (Hüttenbrink & Pfautsch 1987). Permission for reprint achieved from Thieme, © Georg Thieme Verlag KG.

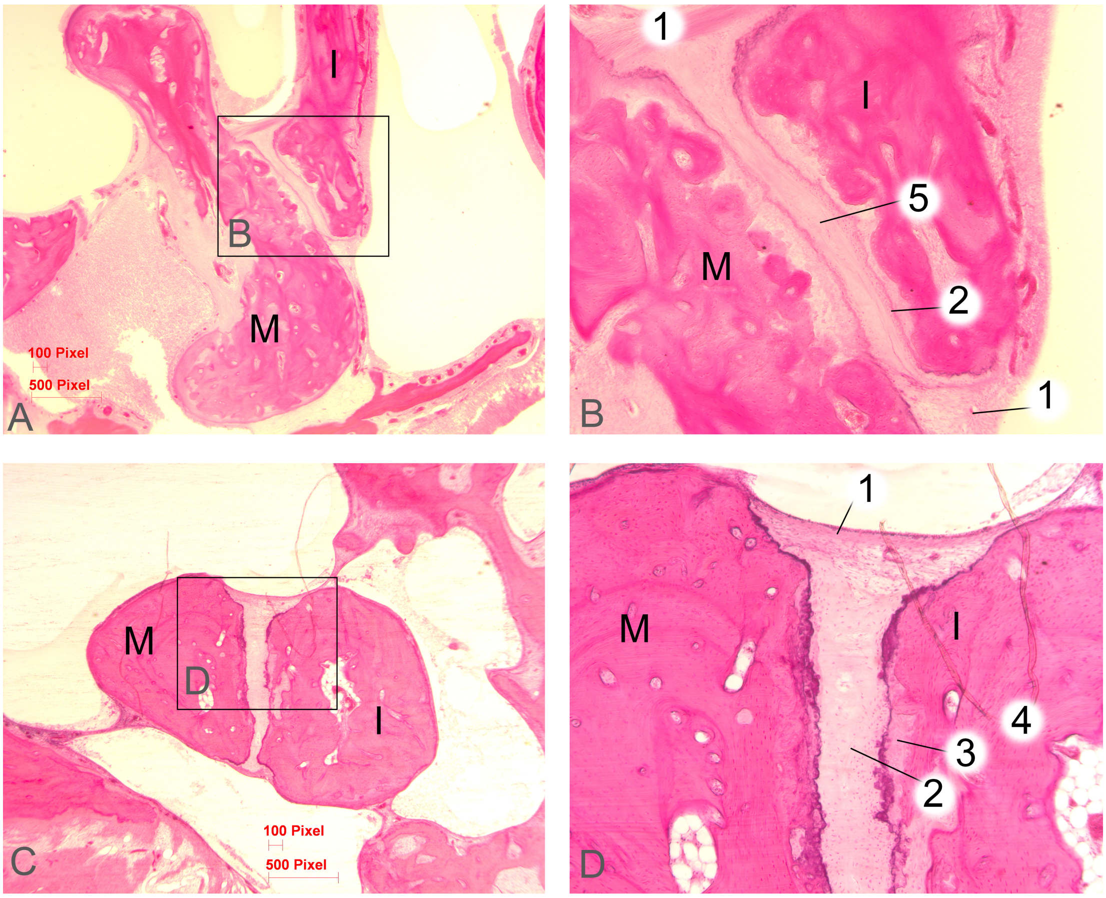

Figure I.34 Microscopic sections of the IMJ: (M) malleus, (I) incus, (1), joint capsule, (2) cartilage tissue (3) calcified cartilage, (4) bony tissue, (5) meniscus. This was a sample from the temporal *bone collection of the ENT-Department University Hospital Zurich. The samples were fixed with Heidenhain-Sussa, decalcified and embedded in celloidin. The blocks were serially cut at a thickness of 20 µm in the horizontal plane and stained with hematoxilin-eosin.*

Marquet reported from his observations with horizontal, sagittal and frontal cross-sections of the IMJ that one can imagine the articular surface of the malleus as a small 'ball', corresponding to a homologue facet and a cap on the incudal side (Marquet 1981). The malleolar surface has a slightly convex surface in its lateral half, until the 'ball' appears, where it becomes finally concave (Marquet 1981) (see Figure I.35). Accordingly, the articular surfaces of the incudo-malleolar joint are saddle-shaped (Etholm & Belal 1974, Ars 1989). A layer of hyaline cartilage covers both, the articular surface of malleus and incus (Marquet 1981, Hüttenbrink & Pfautsch 1987, Harty 1964). Additionally, very thin fibrous structures (similar to intra-articular ligaments) sprout from the articular surfaces and prolong posteriorly into a smooth cuneiform cartilaginous meniscus (Politzer 1884, Marquet 1981). Similarly, Wolff et al. described this interarticular disc as a structure filling the space in the joint, and she denied an expansion throughout the inter-ossicular space (Wolff et al. 1957). Hüttenbrink & Pfautsch (Hüttenbrink & Pfautsch 1987) found the meniscus to be loose and not to be connected to the cartilage of the joint (see Figure I.33). Furthermore, it exists no muscular mechanism to sustain articular surface contact of the IMJ and therefore the joint entirely depends on the elastic capsular component (Harty 1964).

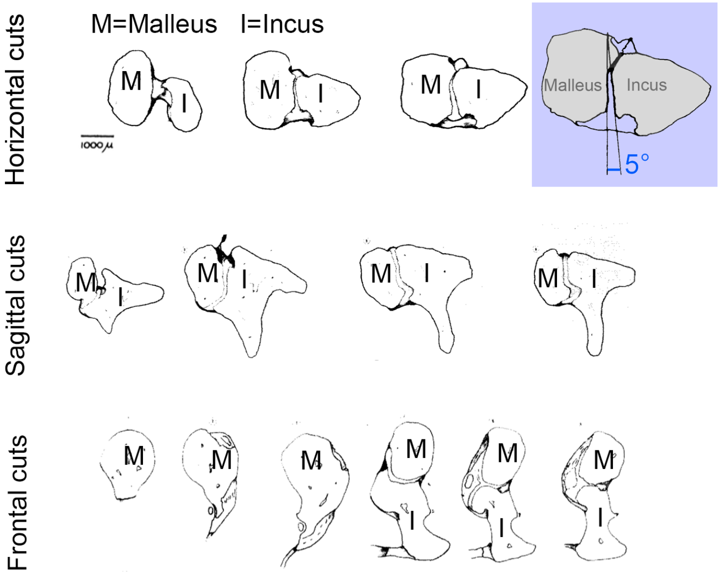

Figure I.35 Marquet's drawing of the horizontal, sagittal and frontal cross-sections of the IMJ, and of the 5° angle between malleus and incus (marked in blue). Modified after (Marquet 1981) with kind permission of JLO (1984) Ltd, Journal of Laryngology and Otology, Marquet J., 1981; 95: 543-565, The incudo-malleal joint, figures 11-14.

Gussen (Gussen 1971) found in a histological study with 152 samples (age range: birth to 88 years) that the articular cartilage of the IMJ appears to be secondary or chondroid cartilage, formed and maintained by the synovial cells of the joint space. Furthermore, she considered the articular cartilage to be epiphyseal cartilage, forming chondroid cartilage and chondroid bone normally within the deep cartilage of the joint.

Microscopic sections of the IMJ are presented in Figure I.34.

I.III.2.4.4.1.2.2 Fibrous joint capsule

The two articular surfaces are connected by thin fibrous structures along the boundary building the capsule of the joint (J.H. Sim & Puria 2008). The joint tension is maintained efficiently by the elastic capsule, contrary to ordinary synovial joints that preserve the intra-articular contact by the local muscle tone, which is absent in the IMJ (Harty 1953). Harty categorizes the joint capsule into three layers; an inner or deeper layer of synovial membrane, the intermediate fibrous capsule, and an external layer of mucous membrane continuous with that of the middle ear (Harty 1964, Etholm & Belal 1974). The synovial membrane lines the joint cavity entirely except on the articular cartilage (Harty 1964, Etholm & Belal 1974). “This synovial membrane is classed as the fibrous type (Key 1932) where only a small range of slide movement occurs between the fibrous capsule and underlying synovial membrane” (Harty 1964). The fibrous component of the IMJ is composed of parallel bundles of elastic fibers (Davies 1948, Harty 1953). “The majority of these fibers pass at right angles to the joint line from the juxta-articular margin of one bone to that of the other” (Harty 1964). The joint capsule has a variable thickness (Marquet 1981). Marquet reported in his measurements with horizontal serial sections of the incudo-malleolar joint that the thickness of the fibrous ligaments reached 200 µm and 700 µm on the lateral and medial aspects (Marquet 1981). The gap between the two surfaces widens posteriorly and builds an angle estimated at 5 degrees which faces medially (see Figure I.35) (Marquet 1981). The superior and inferior articular ligaments are very similar to one another in thickness and generally thin, except the thicker upper ligament on the medial side (Marquet 1981). Today, techniques like scanning electron microscopy (SEM) and micro-scale x-ray computed tomography (micro-CT) are used in addition to microscope observations. Sim & Puria used micro-CT imaging (resolution 10 µm) to obtain the inertial properties of the ossicles (J.H Sim et al. 2007) and soft tissue morphometry (J.H. Sim & Puria 2008) in the human middle ear. Micro-CT imaging is known to be a suitable method for imaging high-density tissue such as bones e.g ossicles, but it could also be used for soft tissue in the middle ear with under modified and optimized scan conditions; scan properties were found to be optimal with a X-ray source at 55 keV, 145 µA, and integration time up to 2.000 ms (J.H. Sim & Puria 2008). They found the fibrous structures to be thickened on its medial and lateral aspects (J.H. Sim & Puria 2008), where the articular space is fairly large (Marquet 1981). The minimum and maximum thicknesses of the tissue layer of the IMJ were 0.04 mm and 0.32 mm reported by Sim & Puria from microCT data (J.H. Sim & Puria 2008), respectively, 0.02 mm and 0.36 mm reported by Wolff from microscopic photos of horizontal cuts (Wolff et al. 1957). Wolff et al. describe the ligament enclosing the IMJ as well much thicker on the medial side than on the lateral side of the ossicles; spreading fanlike from the anteromedial surface of the incus (0.3 mm), narrowing (medial 0.15 mm, lateral 0.02 mm) through the joint space and spreading again (0.36 mm) on the posteromedial surface of the malleus (Wolff et al. 1957).

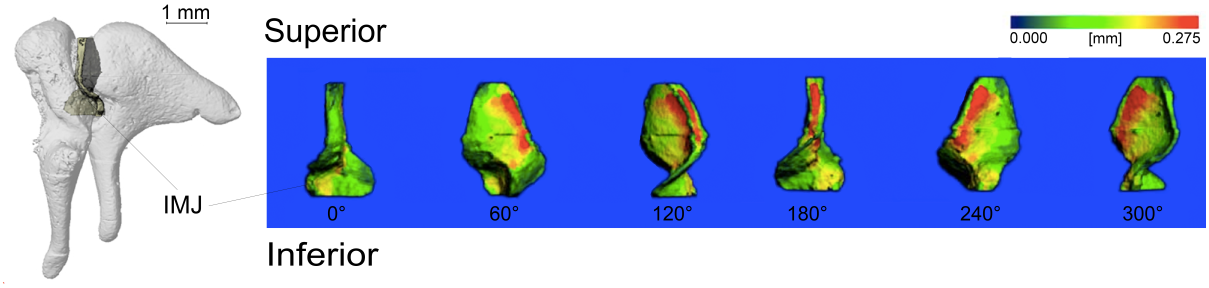

Figure I.36 (left) Incudo-malleolar complex with incudo-malleolar-Joint (IMJ) illustrated in green. This microCT picture is reprinted with kind permission of Jae Hoon Sim and was created within the *context of his PhD thesis (J.H Sim 2007). (right) Thickness map of an incudo-malleolar joint from one ear. Each subplot is a clockwise rotation of 60° steps. Modified after Springer and JARO - Journal of the Association for Research in Otolaryngology, 9(1), 2007, 5-21, "Soft Tissue Morphometry of the Malleus–Incus Complex from Micro-CT Imaging", Sim JH, Puria S., figure 13, © Springer Science and Business Media, with kind permission of Springer Science and Business Media. (J.H. Sim & Puria 2008).*

An example of a thickness map of an incudo-malleolar joint is shown in Figure I.36. The thickness is calculated by the distance transformation (DT) method, which fits spheres into the volume (J.H. Sim & Puria 2008). The thickness varies from about 0.05 mm (dark green) to 0.275 mm (red). The minimum thickness appeared between the lateral side and the center of the joint, and near the inferior side (J.H. Sim & Puria 2008). The maximum thickness in all samples appeared on the medial side and aligned along the anterior–posterior direction at this surface (J.H. Sim & Puria 2008). The mean maximal thickness was 0.32 mm (SEM 0.029), the mean minimal thickness 0.04 mm (SEM 0.005), the mean contact area onto the malleus 5.84 mm^3 (SEM 0.55), the mean contact area onto the incus 6.33 mm^3 (SEM 0.67), and the mean volume was 1.23 mm^3 (SEM 0.28) (J.H. Sim & Puria 2008). The smallest thickness of the joint corresponded to the smallest ossicles distance and vice versa. Incus contact area was larger than contact area onto malleus for each sample. Variations in the joint volume are large (SEM > 20% of mean value) (J.H. Sim & Puria 2008).

Lauxmann et al. (Lauxmann et al. 2012a) determined the rupture forces of the IMJ – mainly to calculate the risks for incus luxation or subluxation during stapes surgery; the IMJ was severely injured at 894 mN rupture force in the anterior- posterior direction and 695 mN in the lateral-medial direction. Micro-ruptures occurred already at forces around 568 mN in the anterior-posterior direction and in the lateral-medial direction at 406 mN.

I.III.2.4.4.1.3 Blood supply of the ossicles and the joints

The blood supply to the ossicles is provided by pathways from many folds of the peritoneum and other membranes that are attached to the ossicles (Schuknecht 1974). Small blood vessels intervene the elastic capsule of the IMJ and the overlying mucous membrane (Harty 1964). The distribution and the number of blood vessels may be related to the regions where internal bone modeling is processed (Marotti et al. 1998, Chen et al. 2008). These regions are very limited and restricted to certain regions, namely, the head of the stapes, the body of the incus and the head of the malleus (Marotti et al. 1987, Marotti et al. 1998). In these regions, arterioles and venules running inside large vascular canals predominate, whereas there are relatively few capillaries (responsible for blood exchange), due to the lack of Haversian canals (tubes around narrow channels) compared with compact bone in other skeletal segments (Marotti et al. 1987).

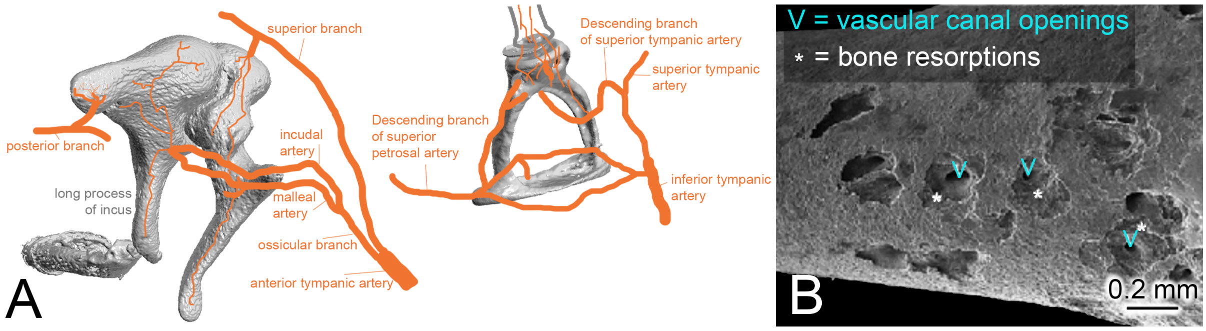

Figure I.37 Illustration of the blood supply of the middle-ear ossicles. Modified after Cummings Otolaryngology: Head and Neck Surgery 2010 (Flint & Cummings 2010). (B) Long process of the incus of a ninety-three-year-old male. Some bone resorptions occurred along the vascular canal openings on the surface of the long process of the incus. Modified after 'Annals of Anatomy - Anatomischer Anzeiger', Vol. 190, H. Chen, T. Okumura, S. Emura, S. Shoumura, "Scanning electron microscopic study of the human auditory ossicles", figure 2b, pp. 53–58. Copyright 2007, with permission from Elsevier (Chen et al. 2008).

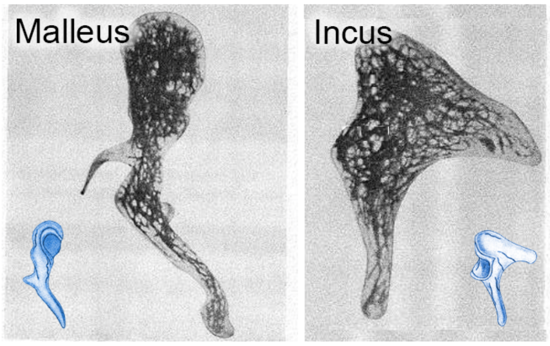

Figure I.38 Blood vessels shown in a 'transparent' malleus and incus. Kirikae observed the blood vessels of the human auditory ossicles microscopically by means of transparent specimens and serial histologic sections. Modified after (Kirikae 1960) with kind permission of Kensuke Goto, Senior Editor, Manager of International Liaison, University of Tokyo Press.

I.III.2.4.4.1.4 The effect of aging on the middle-ear and remodeling of the ossicles

The middle ear ossicles show very early ossification; they reach their adult size in the fetus, and their growth ends at 4 years, changing from a cavity- to a compact-structure (Olszewski 1990, Cisneros Gimeno et al. 2009). This change explains the increase of weight of the malleus from birth (20.15 ± 0.6 mg) to adult (24.9 + 0.7 mg) (Marquet 1981). It should be added that malleus and the incus lack epiphysis and metaphysis, and their growth remains constant with minimum remodeling (Cisneros Gimeno et al. 2009). The development of the ossicles is described in chapter I.IV. Hence, aging begins before birth and continues throughout life with different mechanisms for different parts of the body and different individuals. Most studies of the effects of aging on hearing focused on changes in the cochlea. The age-related hearing loss is also termed presbycusis. However, the middle ear could influence the age-related hearing loss as well. Glorig and Davis (Glorig & Davis 1961) found in their audiometric study (164 men, 25-80 y) a consistent air bone gap for high frequencies and attributed this finding to an age-related conductive hearing loss in the middle ear (see Figure I.39).

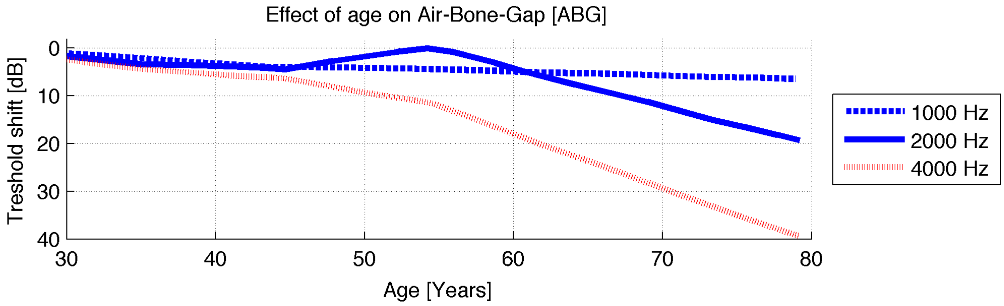

Figure I.39 Glorig and Davies found an age-related increase of the air bone gap for high frequencies. The mean thresholds of the 20-30 year old group were used as the reference levels. The air-bone-gap (= difference between the threshold for hearing by bone conduction and by air conduction) for three different frequencies is shown (20-30y n=35, 30-40y n=41, 40-50y n=26, 50-60y n=22, 60y n=26). Modified after (Glorig & Davis 1961).

Harty (Harty 1953) studied the elastic tissue of the middle-ear from 12 human temporal bones (birth to 84y) by staining with orcein, which has a specific affinity for elastic fibers. He found that the capsule of the IMJ and ISJ were composed entirely of elastic tissue which showed a tendency to fragment and split with advancing age (Harty 1953). Around 20 years later, Etholm and Belal published their histological study of the age-related (senile) changes in the middle-ear (Etholm & Belal 1974). They classified these changes of the middle-ear joints (IMJ and ISJ) into three grades: I mild, II moderate and III severe (see Table I.3).

Grade	**Capsule**	**Articular Cartilage**		**Joint -Space**
		Articular Cartilage	**Disc**	
I Mild		Fraying, Vacuolation, Fibrillation		
II Moderate	Hyalinization	Thinning, Clacification	Hyaline deposits	Narrowing
III Severe	Calcification	Diffuse Calcification	Calcium deposits	Obliteration

Table I.3 Histopahtological grading of IMJ-arthritis. Reprinted from (Etholm & Belal 1974) with kind permission of Ann Otol Rhinol Laryngol, Copyright © 1974, © SAGE Publications.

All of the 125 samples (birth to 96 years) were allocated to one of these grades; fusion of the articular surface with complete obliteration of the joint was described only in four IMJs and two ISJs. The gradual changes increased with advancing age; none of the individuals under one year of age showed arthritic changes, while all individuals over 70 years showed grade II to III in the joints. Contrary to Glorig and Davis, Etholm and Belal did not believe in a relation between the arthritic changes in the joints and the age-related hearing loss. They only found one case (out of 26 over the age of 70) of arthritic changes that correlated with conductive hearing loss (ABG). It remained unclear weather the fusion of the joints were enough to cause immobilization of the joint, and weather mild conductive hearing loss can give an audiologic picture other than the air-bone-gap (i.e. lowering the bone conduction thresholds at high frequencies). Similarly, Gussen (Gussen 1971) described a progressing degenerative arthritis of the IMJ with advancing age; including the loss of surface demarcation, focal surface defects, and foci of thinning and absence of the intra-articular disc with approximation of uneven, calcified joint surfaces. Furthermore, she already observed IMJ changes at early age that were consisted of globule formation and cell clustering in the superficial cartilage layer, with gradual transformation to a chondro-osseous matrix at the surface (Gussen 1971). Savic & Djeric (Savić & Djerić 1988) studied the histopathologic features of degenerative changes in the IMJ in adults. They found degenerative changes in 40% of the cases; including atrophy, fibrosis, hyalinization and calcification. In agreement with Harty, they only noted obliteration of the articular space in few cases.

As mentioned already in chapter I.III.2.4.4.1.3, the regions of remodeling of the ossicles are very limited and restricted to certain regions, namely, the head of the stapes, the body of the incus and the head of the malleus (Marotti et al. 1987, Marotti et al. 1998). Chen et al. (Chen et al. 2008) examined 34 samples (mallei, incudes and stapedes) using scanning electron microscope (SEM) to compare the bone surface type among different regions of auditory ossicles. The percentage area of the resorbing surface was the highest on the long process of the incus and the neck of stapes, nevertheless, resorbing surfaces were found on the remaining areas of the incus and stapes as well. They considered that the malleus maintained in stable condition, because bone-forming or resorbing surfaces were identified. However, the long process of the incus and the neck of the stapes demonstrated marked bone resorption. No significant correlation between the age and the area of resorbing surface was determined.

I.III.2.4.4.2 Incudo-stapedial joint (ISJ)

The ISJ connects the incus and stapes in the middle ear (see Figure I.40 & Figure I.41). It is a 'typical ball and socket joint' (Etholm & Belal 1974) with a convex surface of the lenticular process of the incus and a concave surface of the head of the stapes. Karmody et al. (2009) described the anatomy of the ISJ in detail in 86 temporal bones from 51 subjects, aged 12 to 104 years, by light microscopy and three- dimensional images of computer-based reconstructions. Similar to the IMJ, the ISJ is classified as a synovial joint (see Figure I.40) consisting of a joint capsule, cartilage, meniscus (articular disk), and synovial fluid as observed from scanning electron microscopy (SEM) (Djeric et al. 1987, Karmody et al. 2009), computer tomography (Yamada et al. 1999) and histology (H Wang et al. 2006, Fausch & Röösli 2015, Ogando et al. 2013).

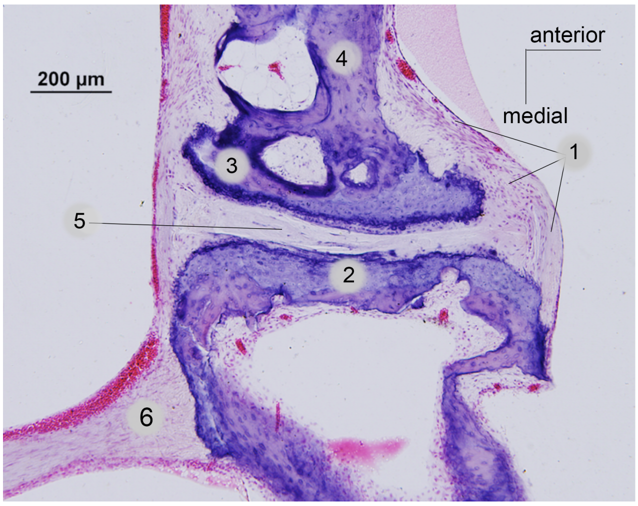

Figure I.40 The incudo-stapedial joint (ISJ): (1) joint capsule, (2) stapes head, (3) Plate of the lenticular process of the incus, (4) Pedicle of the lenticular process of the incus, (5) Fibrocartilaginous disc, (6) stapedius tendon. Microscopic view of histological cut reprinted with permission of MD Christof Röösli, Division of Otorhinolaryngology, Head and Neck Surgery, *UniversityHospital Zurich, in context of his work with the samples of the Massachusetts Eye and Ear Infirmary (MEEI), Boston.*

Marquet found this true diarthrodial joint to have a small antero-inferior part with more laxity than the postero-superior part (Marquet 1981).

I.III.2.4.5 Position of ossicles

The ossicular structures are illustrated in Figure I.42 and Figure I.41 for a better overview. The position of the ossicles is maintained the suspensory attachments, ligaments and muscles in the middle ear (see Figure I.42). The tensor tympani muscle and the stapedius muscle modify the action of the ossicles (S.N. Merchant & Nadol 2010). The IMJ and ISJ do not provide any muscular mechanism to sustain the articular surface contact, thus, the joints are only held together by the fibrous joint capsule.

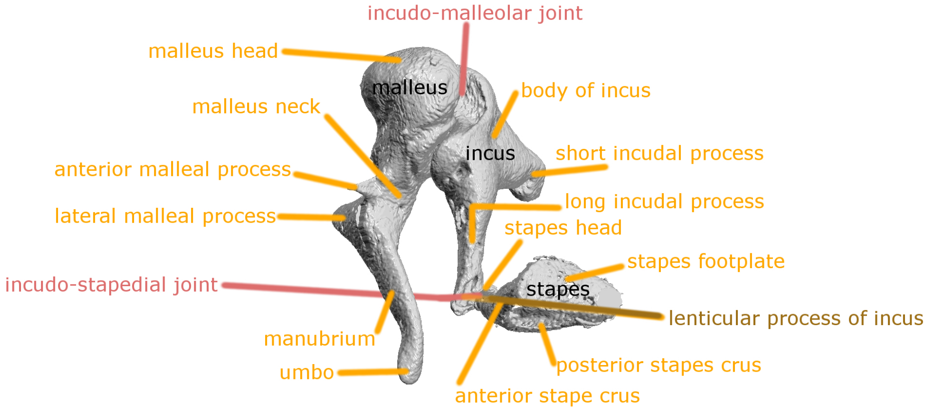

Figure I.41 Anatomical description of the middle ear ossicles and their suspensory attachments.

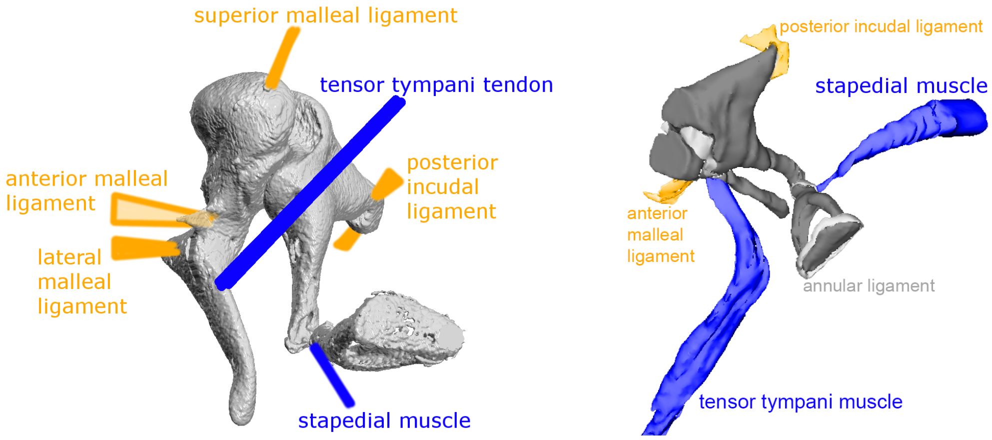

Figure I.42 Overview of attachments in the middle ear. Malleus: tensor tympani tendon, the anterior malleal attachment, the lateral malleal attachment, and the superior malleal attachment. Incus: posterior incudal ligament from inferior and posterior parts of the short process of the incus to the bony wall of the tympanic cavity on the medial and lateral side. Illustration on the right side was modified after the model of the Massachusetts Eye and Ear (MIT, Boston, USA). "The model was made under the supervision of Drs. M. Charles Liberman and Saumil Merchant by Haobing Wang and Clarinda Northrop. Model development was supported by a core grant from the NIDCD (P30 DC05209)".http://www.masseyeandear.org/research/otolaryngology/investigators/laboratories/eaton-peabody-laboratories/epl-imaging-resources/3-d-model-of-human-temporal-bone/. With kind permission of Haobing Wang.

I.III.2.4.6 Orientation of the ossicles in the skull

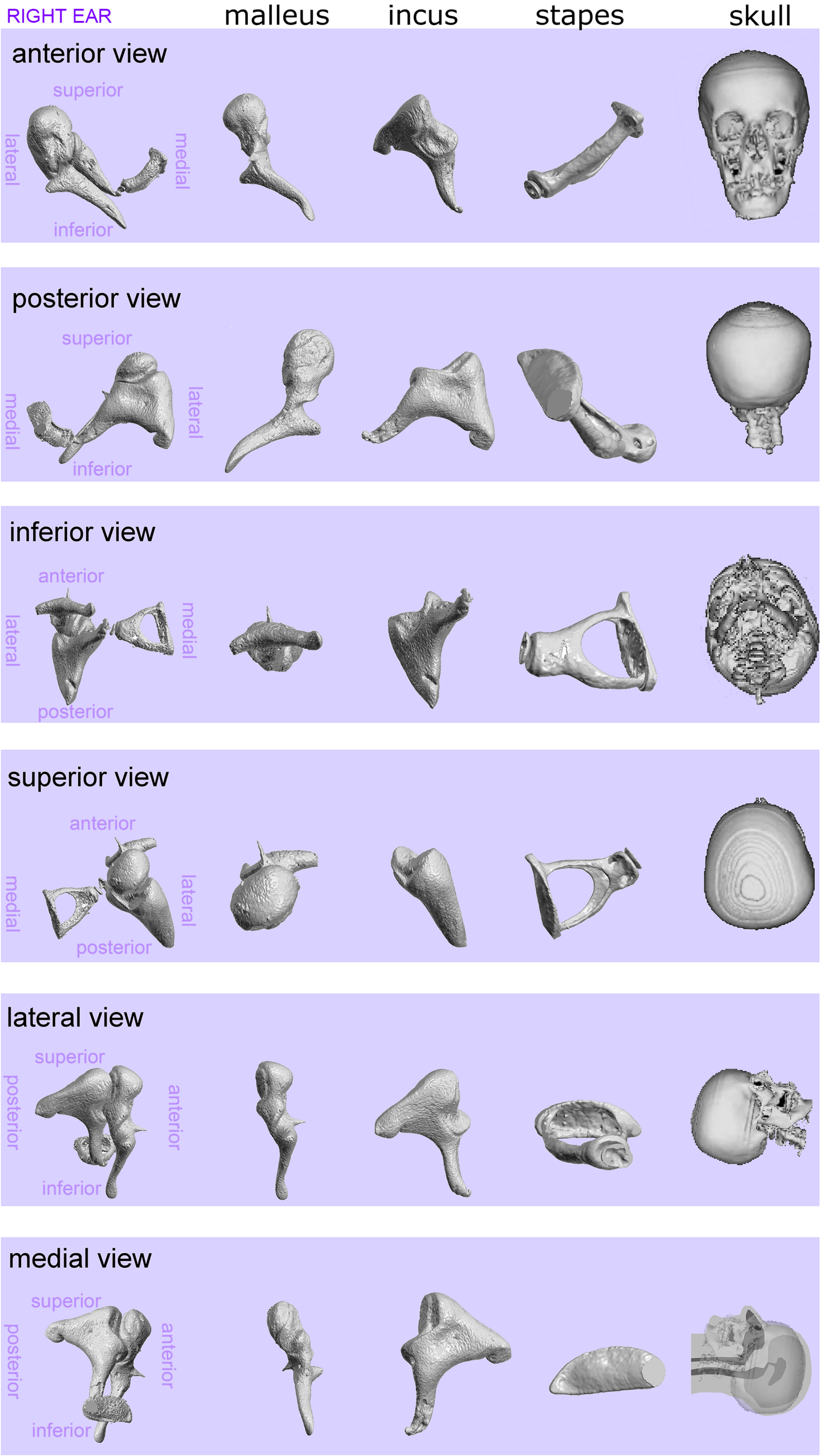

Figure I.43 Orientation of the ossicles: right ear. 3-D reconstruction of the ossicles from micro-CT data from anterior, posterior, inferior, superior, lateral and medial view.

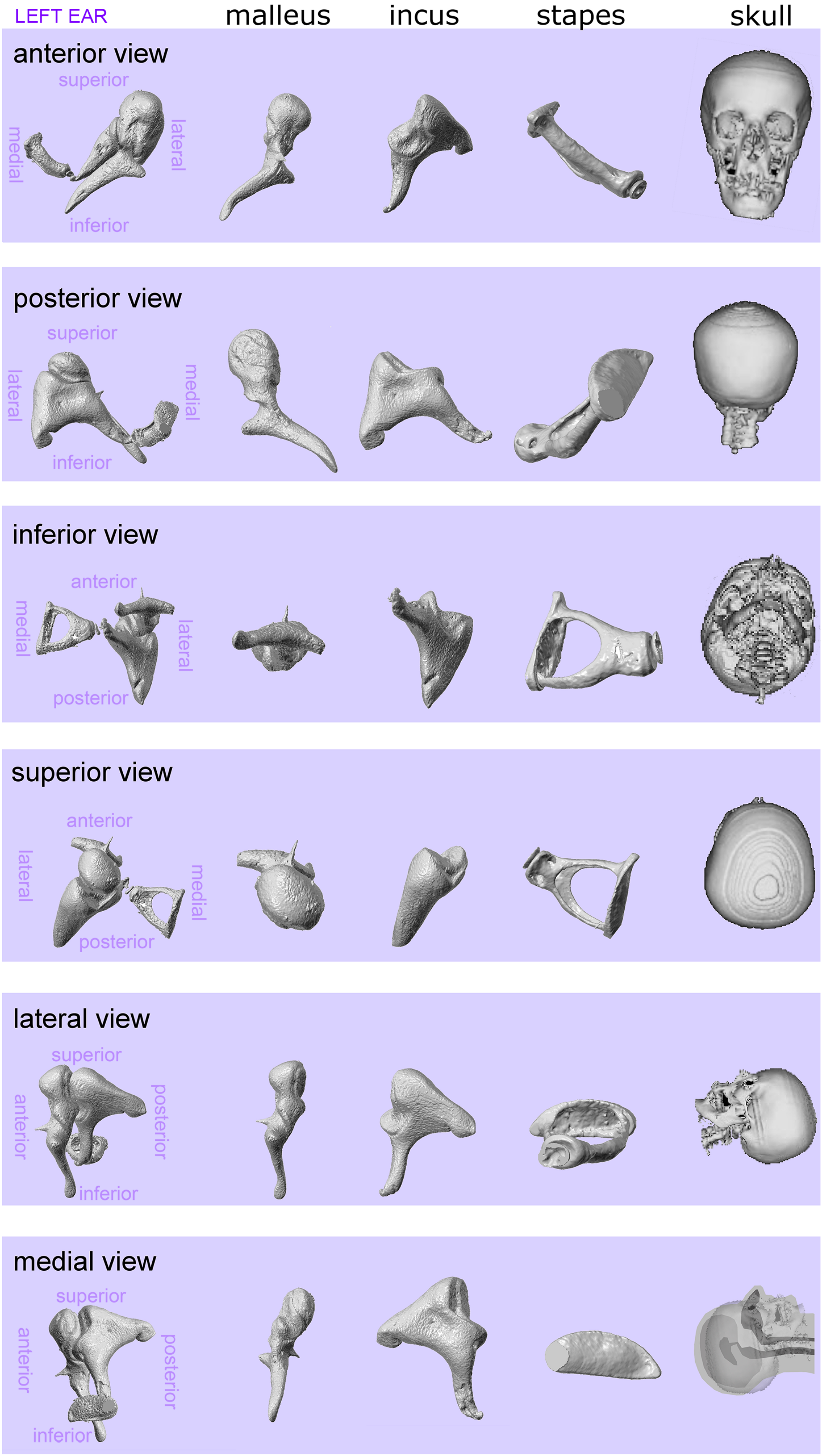

Figure I.44 Orientation of the ossicles: left ear. 3-D reconstruction of the ossicles from micro-CT data from anterior, posterior, inferior, superior, lateral and medial view.

I.III.2.5 Function of ossicles in the middle ear

The function of the middle ear is the transformation of the acoustic energy from the external ear into mechanical vibrations. The tympanic membrane absorbs this acoustic energy from the external ear canal, transforms it into mechanical vibration and transmits it to the ossicular chain. This conversion of acoustic energy into mechanical vibration at the tympanic membrane is defined by different parameters such as the tension of the membrane, its mass and shape, the volume of the middle ear cavity, and the load and stiffness of the ossicular chain. This function of the middle ear is crucial to match the acoustic impedance between the sound waves in air and the fluid of the inner ear (see chapter I.III.2.5.1).

I.III.2.5.1 Impedance mismatch between air and cochlear fluid

Transmitting sound energy from a tenuous medium such as air into a dense medium like the fluid in the cochlea poses challenges. The impedance of the cochlear fluid is much greater than the impedance of air. As a result, about 99.9 % of the sound energy would be reflected from the cochlear fluid and only about 0.1 % of it would be actually transmitted (see also chapter I.II.9 about acoustic impedance). The impedance of the cochlea might not exactly equal the value of water (as calculated in chapter I.II.9), but it can be expected to have similar magnitude. This 99.9% energy transmission loss expressed in decibels equals -30 dB (Bronzino & Peterson 2006). Therefore, the task of the middle ear is to overcome this impedance mismatch by acting as a mechanical transformer, which amplifies the original signal in a way that energy is boosted and can be efficiently transmitted to the cochlear fluid. This amplification mechanism is accomplished by the combination of three mechanical principles:

1. Principle of the hydraulic lever ratio
2. Principle of the lever ratio of the ossicular chain
3. Principle of the curved membrane lever ratio

These three principles are discussed in the following subchapters in detail (chapter I.III.2.5.1.1, I.III.2.5.1.2, I.III.2.5.1.3). It will illustrate that the middle ear transformer ratio implicates a combination of several mechanical principals. Generally, the middle ear has to overcome the great impedance differences at the borderline of air and inner ear, and thereby prevents from significant transmission losses. Thus, the main function of this transformer ratio is to transmit the vibration from the tympanic membrane efficiently to the inner ear by decreasing the displacement magnitude and increasing the force along the ossicular chain to reach a satisfying stimulation of the sensory cells in the inner ear (see Figure I.45). Theoretical calculation of the total transformer ratio is extremely difficult, as all of these principles are frequency dependent. Furthermore, the transformer ratio should be tested experimentally with an intact middle ear in order to achieve fairly reliable results. But the access to the ossicles and the other structures of interest is difficult due to the enclosed embedding of the middle ear.

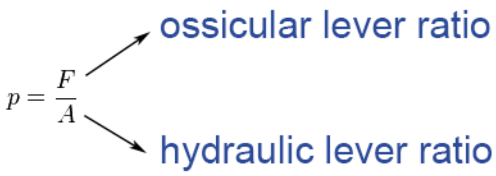

Figure I.45 The sound transmission overcomes the impedance mismatch by the ossicular lever ratio, which is based on the lever action of malleus and incus (Lever$_{Malleus}$ *>> Lever*$_{Incus}$*), and the hydraulic lever ratio, which is based on the difference in size of the tympanic membrane and the stapes footplate (Size*$_{TympanicMembrane}$ *>> Size*$_{StapesFootplate}$*).*

I.III.2.5.1.1 Principle of the hydraulic lever ratio

The surface area of the tympanic membrane is many times that of the stapes footplate. The principle of the hydraulic lever ratio is based on this difference in size and the property of pressure acting as force per area ($p = \frac{F}{A}$) (see Figure I.45). The hydraulic lever concentrates acoustic energy at the oval window and results from the 15- to 26-fold difference in vibratory surface of the tympanic membrane compared with the smaller area of the stapes footplate (von Helmholtz 1869, G. Békésy 1960, Wever & Lawrence 1954). This is thought to be the main impedance matching mechanism and is manifested in the transfer function as well. This is only true if the two surfaces act as a piston; but the stapes is footplate moves mainly piston-like but also includes rocking-like motion (J. H. Sim et al. 2010a), and the tympanic membrane is however a complex, flexible structure and all its parts do not vibrate with the same displacement. The effective area of the tympanic membrane needs to be defined in order to calculate the effective area ratio. Wever and Lawrence (1954) defined the effective area as the "area that a piston would needs to displace the same volume when its whole face moves with the amplitude of the center of the drum membrane" (Wever & Lawrence 1954). Nowadays, quantifying this area is still very challenging and intense research on this topic is going on. The sound-induced vibration patterns of the tympanic membrane are highly frequency dependent and vary from simple in-phase displacement patterns to more complex patterns with many spatial maxima and minima moving with different phase angles as frequency increases (Tonndorf & Khanna 1970, Decraemer et al. 1989, S. M. Khanna & Tonndorf 1972b, Rosowski et al. 2009, Cheng et al. 2010). At high frequencies, vibratory patterns starting to be restricted in size and break up into "quasi-independent sub-patterns" (Tonndorf & Khanna 1970). Recently, Cheng et al. (Cheng et al. 2013) observed the sound-induced motions of the surface of the tympanic membrane using stroboscopic holography in cadaveric human temporal bones at frequencies between 0.2 and 18 kHz. By using a simple two-wave model they were able to separate out different wave motion patterns and identify frequencies and regions where the patterns of motion were consistent with: (1) simple modal motion (at low frequencies, where phase angle is constant on the TM surface, and by the presence of nodes at higher frequencies) (2) dominant traveling-wave-like motions (regions where the phase angle changes regularly with location), and (3) a combination of a larger low-order (low spatial frequency) modal disturbance and a smaller high-order (high spatial frequency) traveling-wave-like motion. These results were found to be consistent with the previous interpretations (de La Rochefoucauld & Olson 2010, Cheng et al. 2010, Rosowski et al. 2011). The contribution of these different motion patterns to middle ear function is the topic of their current studies. Thus, the hydraulic principle is frequency dependant and therefore the effective transformer ratio, which is based on it, becomes frequency dependent as well. Therefore, constant values indicated in the literature must be considered with caution.

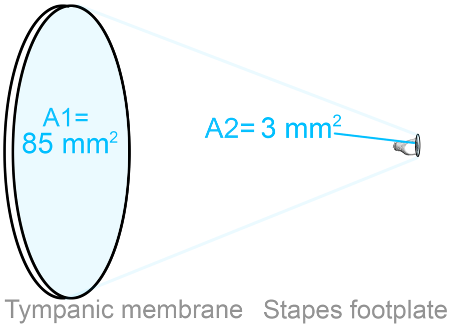

Figure I.46 The principle of the hydraulic lever ratio. This principle is based on this difference in size and the property of pressure acting as force per area (P=F/A) of the tympanic membrane (A1 ≈ 85 mm^2*) and the stapes footplate (A2≈ 3* mm^2*).*

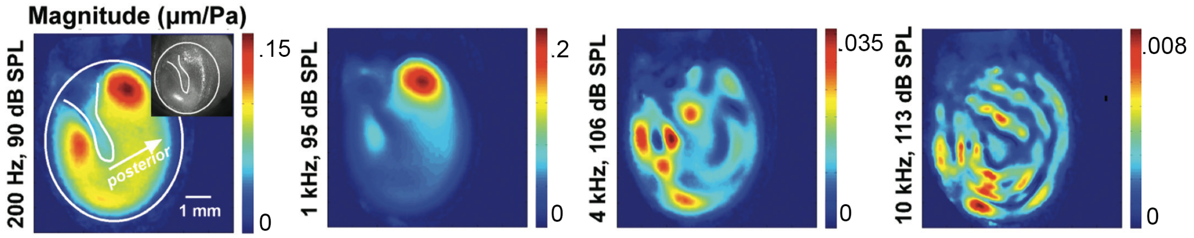

Figure I.47 Tympanic membrane surface displacement normalized to stimulus sound pressure; measured by stroboscopic holography on one temporal bone (TB 10_5). The displacement magnitude color bars are shown on the right side of each plot and the stimulus frequency and levels are given on the left side of each plot. (Cheng et al. 2013) Reprinted with permission from J. Acoust. Soc. Am. 133 (2), © 2013, Acoustic Society of America: Melville, NY, figure 2, "Wave motion on the surface of the human tympanic membrane: holographic measurement and modeling analysis". Cheng JT, Hamade M, Merchant SN, Rosowski JJ, Harrington E, Furlong C.

I.III.2.5.1.2 Principle of the lever ratio of the ossicular chain

The principle of the lever ratio is based on the given condition that the arm of the malleus (manubrium) is longer than that of the incus (long process), and this produces a lever action that increases the force and decreases the velocity at the stapes. Thus, the mechanical lever system amplifies the force exerted on the tip of the umbo; an increase in force equals the decrease in displacement. Additionally, the difference in lengths between the two ossicles also corresponds to a pressure gain at the incus equivalent to the length ratio of the two ossicles. Békésy reported a n approximately 1.3 times longer arm of the malleus than of the incus (G. Békésy 1960).

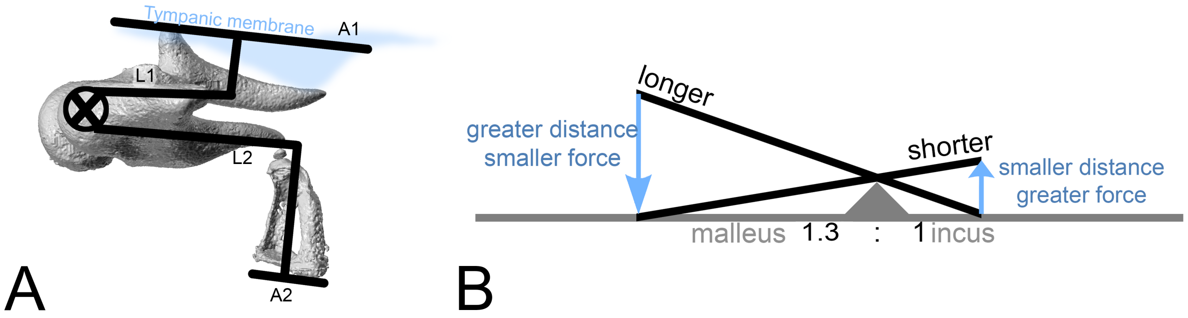

Figure I.48 (A) Principle of the lever ratio of the ossicular chain: L1 lever arm of the malleus (manubrium), L2 lever arm of the incus (long process). (B) Model of the malleus and incus as a simple lever.

However, the concepts of the ossicular lever ratio varied between different studies. The different concepts of the ossicular lever ratio are listed in Table I.4 in chronological order.

Concepts of the ossicular lever ratio			Lever ratio of this concept
1869 Helmholtz (von Helmholtz 1869)	Single lever arm concept; two lever arms but both reside in the same line. First lever arm: from posterior incudal ligament to the umbo Second lever arm: from lenticular process of the incus back to the posterior incudal ligament The axis of rotation is perpendicular to the orientation of the lever arm. The exact position is not described. Method: anatomical observation	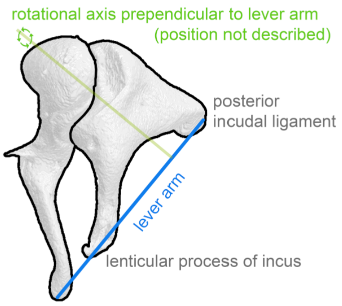 *Modified after (Wever & Lawrence 1954)*	1.5 : 1
1930 Dahmann (Dahmann 1930)	Two lever arm concept; both arising from the same rotational axis which passes through the anterior malleal ligament and the posterior incudal ligament. System with fixed axes. First lever arm: Perpendicularly to rotational axis; force arm, spanning the distance between the umbo and the rotation axis Second lever arm: Perpendicularly to rotational axis; resistance arm, running from the lenticular process of the incus to the rotation axis. Method: dynamic stimulation of the middle ear. Additionally; measured dynamic umbo displacement. Asymmetrical movement	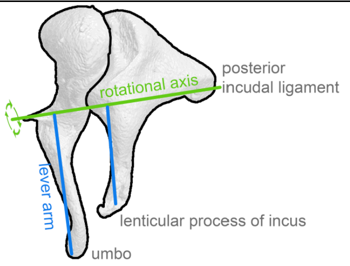 *Modified after (Wever & Lawrence 1954)*	1.3 : 1

	of umbo. Disappearance of asymmetry after removal of stapes; resistance exerted by the stapes through its attachment to the oval window with ligaments caused the resilience of the IMJ.		
1937 Stuhlman (Stuhlman 1937)	Lever ratio depending on mobilization of the IMJ. Method: oversized ossicular chain model under different conditions: First condition: immobile IMJ Second condition: mobile IMJ, because he assumed that the asymmetric motion of the umbo observed by Dahmann was caused by a loose coupling of the malleus and incus within the IMJ. Different lever ratios for first and second condition.	see Figure I.58	IMJ immobile (rigid body): 1.27 : 1 IMJ mobile (loose coupling): Inward motion 2 : 1 Outward motion 1 : 1

Table I.4 Concepts of the ossicular lever ratio

I.III.2.5.1.3 Principle of the curved membrane lever ratio

The tympanic membrane transforms airborne environmental sound into a mechanical stimulus by converting the acoustic wave into vibration of the middle ear ossicles. The principle of the curved membrane lever ratio will convert this ‘low pressure, high displacement vibrations’ of the acoustic wave into ‘high pressure, low displacement vibrations’ suitable for driving cochlear fluids.

One of the oldest theories of the principle of the curved membrane lever ratio was postulated by Helmholtz (von Helmholtz 1869). He proposed that the tympanic membrane provides a catenary lever that assists the transformation function of the middle ear; having large displacements in the middle of the anterior and posterior curved sections compared to small displacements of the manubrium. A catenary is the curve that an idealized hanging rope assumes under its own weight when supported only at its ends. The catenary lever can be illustrated by a rope suspended between two walls as shown in Figure I.49. The force acting on the walls is larger than the force of the weight of the rope. This force acting on the walls is even increased if the rope is taut. Additionally, this force will again increase, if a small additional weight is placed in the center of the curved rope (see Figure I.49 B). In case of the human tympanic membrane, the membrane curves its rim towards the umbo, due to the arrangement of the radial and circular fibers of the tympanic membrane. Each radial fiber would play the part of the rope, using the example of the rope for imagination. The tympanic membrane is firmly attached to the mobile umbo. The conical was of the tympanic membrane can be changed like the curvature of a suspended rope, assuming that the radial fibers are relatively inelastic and the circular fibers relatively compliant (U. Willi 2003). Hence, the vibration is concentrated on the manubrium of the malleus. During the rarefaction phase of a sound wave, the curvature will slightly increase due to the displacement of the center portion of the tympanic membrane, and the umbo is displaced with smaller amplitude but greater force (see Figure I.49 C). The size of the tympanic membrane also plays an important role in collecting the force at the membrane and transmits it to the umbo; the larger the area, the larger the transmitted force. Similarly, the longer the rope, the greater is the exerted force on the wall.

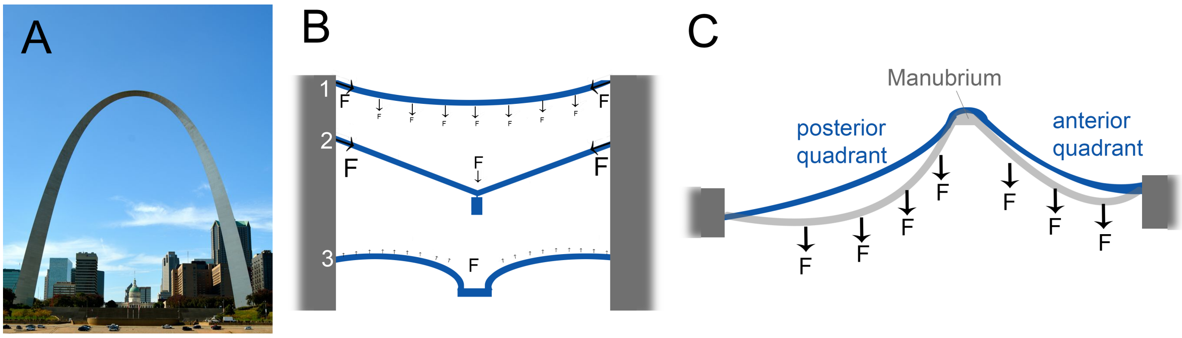

Figure I.49 The principle of the curved membrane lever ratio. (A) The Gateway Arch in St. Louis (Missouri U.S.) has the form of a catenary. It is the world's tallest arch (192 m). Planned by Eero Saarinen and Hannskarl Bandel in 1947 and constructed between 1963 – 1965 (National Park Service 2010). (B1, B2) Illustration of the catenary as a rope suspended between two walls. (B2) The force acting on the walls is larger than the force of the weight of the rope. Modified after Willi 2003 (U. Willi 2003). (B3) Applied to the middle ear, each radial fiber would play the part of the rope. The small forces are now regularly spread over the tympanic membrane surface. The forces exerted on the walls in (B1) and (B2) are now exerted on the umbo. Modified after Willi 2003 (U. Willi 2003). (C) The principle of the curved curved membrane lever ratio involves an increase in force at the manubrium because it moves with less displacement than the curved eardrum membrane. Illustrations (B) and (C) were modified after (Tonndorf & Khanna 1970).

Békésy (Békésy 1941) wasn't in agreement with Helmholtz (von Helmholtz 1869); he interpreted tympanic membrane motion as hinged plate movement (at least below 2 kHz). Later, Tonndorf and Khanna measured full-field displacement magnitude maps of the tympanic membrane in cats and human cadaver ear with time-averaged holography (Tonndorf & Khanna 1972a, S. M. Khanna & Tonndorf 1972b). They were consistent with Helmholtz' theory and observed smaller motions at connections with the umbo and the manubrium as compared to the area between the manubrium and the annulus. In 2010, Cheng et al. measured tympanic membrane motion with stroboscopic holography, which yields both magnitude and phase information of the displacement pattern. They measured maximal human tympanic membrane displacements of 0.3 µm for a 1 kHz stimulus at 90 dBSPL. As described in chapter I.III.2.5.1.1, Cheng et al. (Cheng et al. 2013) recently published holographic measurements and modeling analysis of the wave motion on the surface of the human tympanic membrane (see Figure I.47). The motion pattern of the tympanic membrane is nowadays assumed to be highly frequency dependent.

I.III.2.5.2 Overall middle ear gain

An intact ossicular chain is important to normal hearing function (S.N Merchant & Rosowski 2003). Its interruption introduces a hearing loss of 60 dB in humans (Peake et al. 1992). Similar losses have also been reported in other species e.g. in cat (Wever et al. 1948). The 'input' of the middle ear at the umbo of the malleus is not equal the 'output' at the stapes or to the pressure changes in the cochlea, respectively. Thus, the middle ear significantly influences the sound transmission.

The measurements of the transfer function measured by *relative displacement of umbo and stapes* is frequency-dependent (see Figure I.50) in fresh human temporal bones and live humans

(Ramirez-Garcia 1980, Kringlebotn & Gundersen 1985, Vlaming & Feenstra 1986, Brenkman et al. 1987, Hato et al. 2001, Gyo et al. 1987, Goode et al. 1994) suggest the middle ear becomes increasingly inefficient above 1000 Hz (see Figure I.50). The major decrease of the transfer function is between 1-3 kHz, which is important for the range of frequency of speech understanding in humans (0.3 and 3 kHz). This transfer function of the middle ear is different in animals: 1500 Hz for cat (Guinan & Peake 1967, Buunen & Vlaming 1981) and 4000 Hz for guinea pig (Wilson & Johnstone 1975).

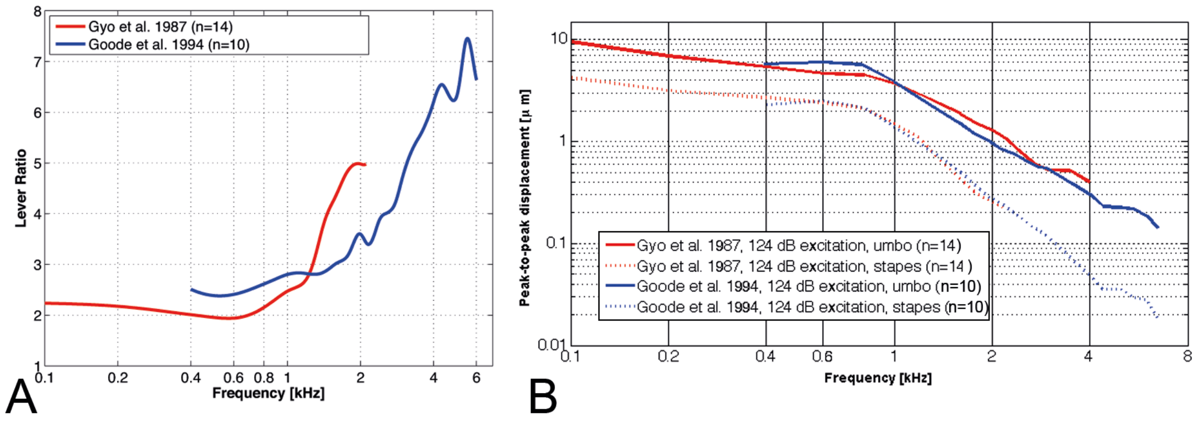

Figure I.50 Transfer function and displacement of umbo (malleus) vs. stapes. (A) Transfer function of umbo vs. stapes head. (red) Transfer function measured by relative displacement between the umbo and the stapes head by Gyo et al. 1987. The transfer function was 3.6-4.2 dB up to 0.8 kHz and then increased reaching a peak of 7.9 dB at 2.2 kHz, and decreasing slightly at higher frequencies. This result was different to the widely accepted ratio of 1.31 suggested by Dahmann at that time (see chapter I.III.2.5.3.2.6). Modified after (Gyo et al. 1987). (blue) The transfer function (umbo displacement vs. stapes footplate displacement) measured by Goode et al. 1994. The transfer function had a mean value of about 2-2.5 dB up to 1.8 kHz and reached a peak of 6.6 dB at 6 kHz. Additionally, the umbo has a broader frequency dependence than the stapes (see chapter I.III.2.5.3.3.1) Modified after (Goode et al. 1994), Figure 1 pp. 148. (B) Frequency-dependent umbo and stapes displacement. Modified after (Goode et al. 1994, Gyo et al. 1987).

The transfer function of the middle ear measured by the relative magnitude between the *pressure in the ear canal and the relative pressure in the cochlea* (scala vestibuli, basal turn) was obtained in human temporal bones in 2009 by Nakajima et al. (Nakajima et al. 2009). They presented the first simultaneous sound pressure measurements in scala vestibuli and scala tympani of the cochlea in human cadaveric temporal bones (see Figure I.51). The microscale pressure sensors necessary for the measurements were developed by Olson (Olson 1998). Nakajima et al. found the pressure to be up to 20 dB larger in the inner ear than at the tympanic membrane in humans (see Figure I.51). Our group has assembled a microscale pressure sensor as well; see chapter I.III.3.2.3 for more details about the project. Intracochlear pressure in human temporal bones has previously also been examined by Puria et al. (Puria et al. 1997), Aibara et al. (Aibara et al. 2001) and O'Connor & Puria (O'Connor & Puria 2006) with different methods.

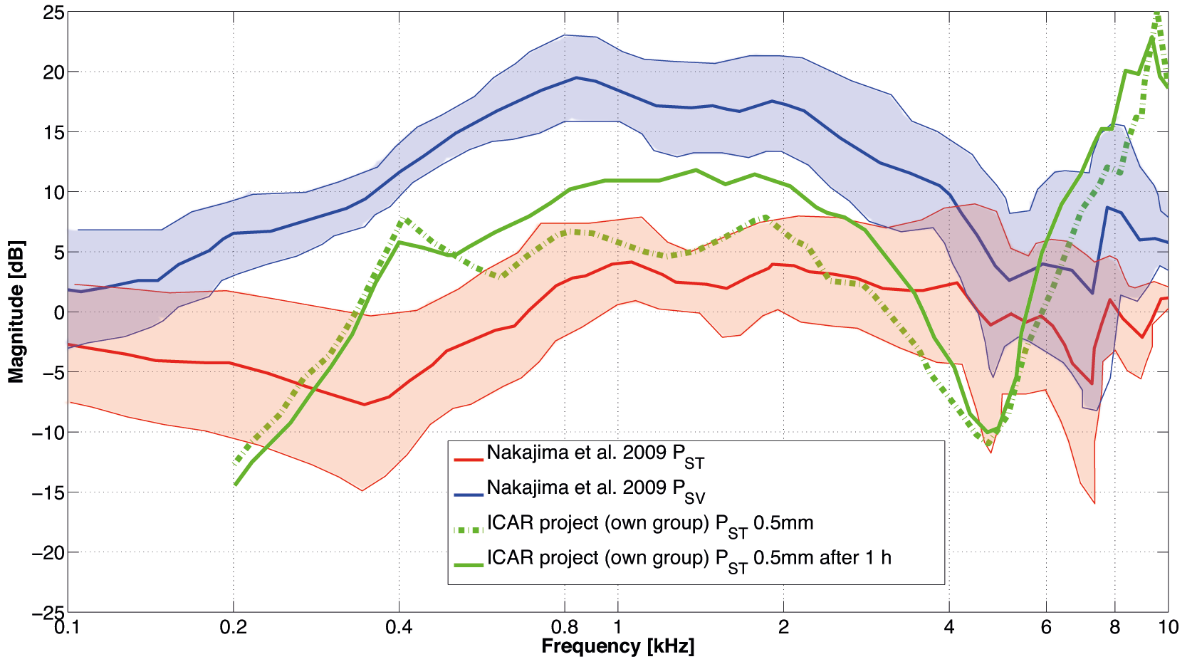

Figure I.51 Pressure measurements in the scala tympani and scala vestibuli of the human cochlea. The pressures were normalized to the reference pressure ($P_{Ear\ Canal}$) in the ear canal. (red) Pressure in scala tympani (P_{ST}) and (blue) in scala vestibuli (P_{SC}) by Nakajima et al. 2009 (mean and standard deviation, n=6) (Nakajima et al. 2009), and a preliminary test of our group with the intracochlear acoustic receiver (ICAR) in a human cochlea (0.5 mm insertion of sensor and 0.5 mm insertion of the sensor after 1 hour) (see I.III.3.2.3). Modified after (Nakajima et al. 2009, Pfiffner et al. 2015).

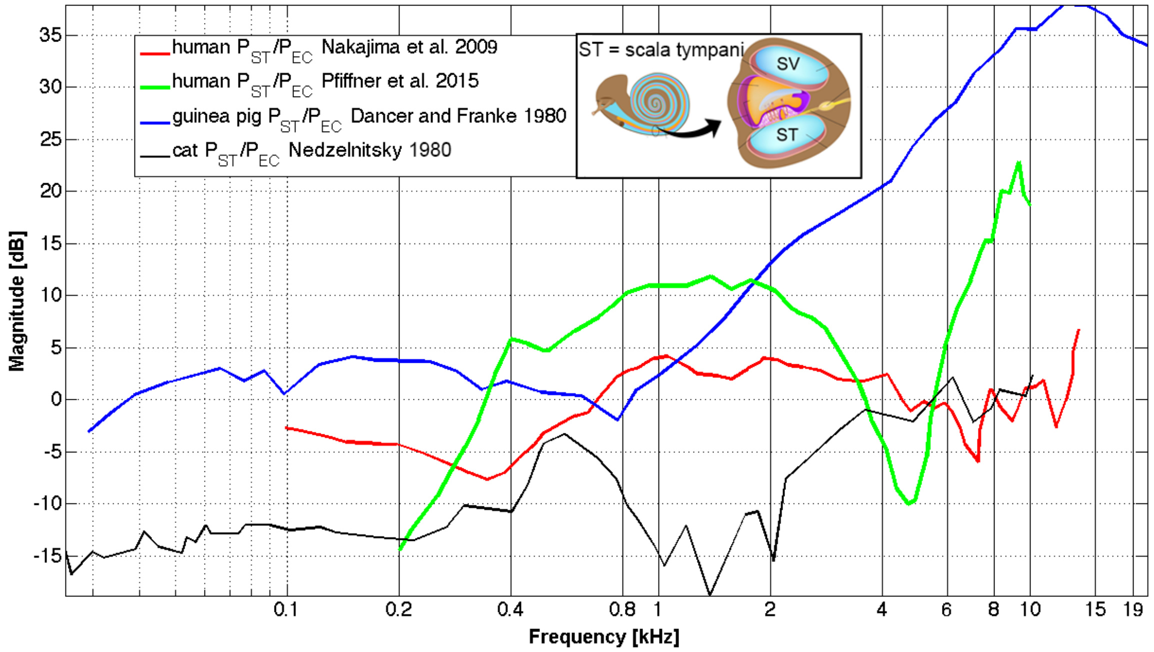

Figure I.52 Pressure measurements in the scala tympani (P_{ST}) in human and animals (anatomy of the cochlea see chapter I.III.3.2.1). The pressure was normalized to the reference pressure in the ear canal (P_{EC}). (red) P_{ST} in human measured by Nakajima et al. 2009, a preliminary measurement of our group with the intracochlear acoustic receiver (ICAR) in a human cochlea in P_{ST} (0.5 mm insertion of sensor after 1h) (see I.III.3.2.3), P_{ST} in guinea pig measured by Dancer and Franke in

1980 (mean, n=5, CI 95 %), and (black) P_{ST} in cat measured by Nedzelnitsky 1980 (median, n=6) (Nedzelnitsky 1980). Modified after (Nakajima et al. 2009, Pfiffner et al. 2015, Dancer & Franke 1980, Nedzelnitsky 1980).

The roll-offs (dB/octave) above 1 kHz in the middle-ear transfer function (see Figure I.50 B) were extensively reviewed in the dissertation of Urban Willi (see Table I.5). Possible reasons for the increasing inefficiency for frequencies higher than 1 kHz could be (modified after Goode et al. 1994): 1) The decrease in the tympanic membrane function at higher frequencies due to the breaking up into smaller vibrating portions rather than a piston-like motion (Tonndorf & Khanna 1972a), 2) the mobility in the middle-ear joints (see chapter I.III.2.5.3), 3) the 3 kHz-Carhart notch: a decrease of the effective sound transmission at 3 kHz produced by a mastoid cavity (Gyo et al. 1986, McElveen et al. 1982).

	Hato et al. 2001	**Kurokawa 1995**	**Gyo et al. 1987**	**Kringlebotn & Gundersen 1984**	**Ramirez-Garcia 1980**	**Goode et al. 1994**	**Willi 2003**
SPL-umbo	-9 dB		-9 dB			-9 dB	-8.5 dB
SPL-LPI							-14 dB
SPL-stapes	-13.2 dB	-13.6 dB	-15 dB			-14 dB	
SPL-rw				-15 dB	-16 dB		
umbo-LPI							-5.5 dB
umbo-stapes	-4.2 dB		- 6 dB			-5 dB	

Table I.5 Roll-offs (dB/octave) reviewed by Urban Willi (U. Willi 2003). The displacement measurements were performed at the umbo of the malleus, the lenticular process of the incus (LPI), the stapes and the round window (rw) with the sound pressure level (SPL) at the tympanic membrane as a reference. Reprinted with kind permission of Urban Willi from (U. Willi 2003).

I.III.2.5.3 Function and mobility of the incudo-malleolar joint (IMJ)

Even though many investigations have been made to determine the roles of the IMJ, its specific functions still under debate. The main question discussed in this dissertation is whether the IMJ is mobile under acoustic excitation of physiologically-relevant levels (see chapter III.I to III.III). Does the IMJ amplify vibrations received from the tympanic membrane? Or does it have the function of damping the sound in order to protect the inner ear from noise? Or does its function change, depending on the stimulation frequency? In the following subchapters the historical background and the current scientific explanations of the function of the joint are described in very detail, because of the importance of this topic for this dissertation. The comparison of the measured data in the scope of this dissertation to the literature is discussed in chapter IV.III.

I.III.2.5.3.1 Overview

The following subchapters summarize the historical (see chapter I.III.2.5.3.2) and more recent (see chapter I.III.2.5.3.3) findings according the mobility and function of the IMJ of each author separately. This is important because several different measurement methods, sample preparations and sample handlings were used, what makes it difficult to compare the findings of the different authors (see chapter IV.III). With increasing knowledge about the IMJ function, several biases in earlier measurement were observed, as for example the effect of drying of the middle-ear structures (see chapter IV.II.3.1), the effect of a drained cochlea (change of impedance at oval window resulting in slight decrease in stapes footplate displacement at low frequency < 1 kHz (Lord et al. 2001)), and the post-mortem time of the cadavers (see chapter IV.II.3.2) on the transfer function of the middle ear. It is still under debate whether the measurement temperature (different temperature in cadaver and in live subject) (see chapter IV.II.3.3), and the age and gender of the donor (see chapter IV.II.3.4) influence the middle-ear sound transmission.

I.III.2.5.3.2 Historical background of the function of the incudo-malleolar joint

The IMJ was defined as a joint already in the 18th (von Sömmerring 1791, Luschka 1858) (see also chapter I.III.2.4.4.1.1). In the 19th century, Weber also considered the IMJ to represent a true joint but negated functional mobility during the transmission of sound (Weber 1851).

The historical background of the anatomy of the IMJ was described in chapter I.III.2.4.4.1.1 in detail. This chapter serves as a chronological review of the historical findings about the function and mobility of the IMJ. An overview of all authors and their findings is presented Table I.6.

I.III.2.5.3.2.1 H. von Helmholtz

Helmholtz (von Helmholtz 1869) was the first who investigated the anatomy of the IMJ in detail with respect to its function. He described the anterior ligament and the posterior part of the ligament as forming together a common rotational axis for the motion of the incudo-malleolar complex. In his opinion, the shape of the IMJ surface crucially affected the function of the joint, as working similarly to a 'cog mechanism' (Ger. 'Uhrschlüsselgelenk') (see Figure I.53 C).

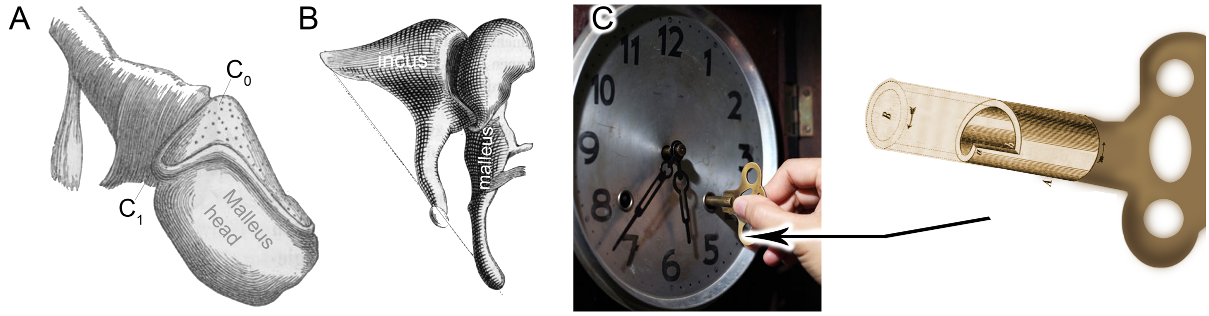

Figure I.53 Helmholtz investigated the anatomy of the IMJ in detail with respect to its function. (a) His illustration shows the malleus separated from the incus; C_0 and C_1 are described as cogs (dt. 'Sperrzähne'), (B) Incudo-malleolar complex with cogs toothed, (C) 'watch-key mechanism' ('Uhrschlüsselgelenk'); as a help for imagination of Helmholtz' theory "...the handle cannot be turned in one direction without carrying the steel shell with it, while in the opposite direction it meets with only light resistance" (H. Helmholtz et al. 1873). Figures (A) and (B) are modified after *(von Helmholtz 1869) figure 8 pp. 28 (A) and figure 9 pp. 38 (B), with kind permission of Bouvier Verlag, Bonn, Germany.*

Helmholtz proposed that the ligamentary connection by the articular capsule was relatively loose and, therefore, the two ossicles had an additional degree of freedom. Malleus and incus moved together, but the resilience of the IMJ allowed a moderate degree of independent mobility. The joint admitted slight rotation about the rotational axis, as it is the case in the watch-key mechanism. When the malleus moved outward (excursion), the incus only followed partly the malleus motion. This indicated that the joint allowed a small amount of gliding between the two ossicles, and that the malleus temporarily disengaged from the incus. The articular capsule and the cartilage covering the articular surfaces restricted the amount of spreading between both ossicles. Contrary, when the malleus moved inward (incursion), the cog surfaces toothed firmly and the incus followed the inward motion of the malleus. Hence, the inward motion was restricted by the cog mechanism. In a second step he removed the stapes. Therefore, the incus was now decoupled from the cochlear load and followed the inward and outward motions of the malleus likewise. He assumed that the 'cog mechanism' was developed to move the incus inward despite the cochlear load and the flexibility of the articular capsule. Helmholtz investigated the IMJ macroscopically and made his conclusions from rough mechanical testing. His assumptions, therefore, have to be associated with static mechanics rather than with the dynamic behavior of the ossicular chain. Additionally, he described the IMJ as a protection mechanism for the stapes-joints and the inner ear. Due to the resilience of the articular capsule during an outward motion, a drastic decrease in pressure of the external ear canal did not harm the delicate stapes structures. And, the inward motion was restricted by the flexibility of the tympanic membrane. Thus, the inner ear was protected from drastic pressure changes.

I.III.2.5.3.2.2 A. Buck

Helmholtz was the impulse and supporter for Albert Buck's studies in 1869 (Buck 1869). Confusingly, on the one hand, Buck (Buck 1869) agreed with Weber (Weber 1851) and Helmholtz (von Helmholtz 1869), and concludes that the ossicles vibrate together as a whole. On the other hand, he showed different displacement amplitudes for the malleus and incus and therefore a functional mobility of the IMJ (see Figure I.54). He made experiments under dynamic stimulation (organ pipe) at low frequencies (6, 110, 220 and 400 Hz) and reported the change of the light spot (from lamp focused on ossicle) reflecting on the ossicles to follow the displacement amplitude. The displacement amplitudes of the malleus head and the incus body close to the IMJ was found to be different in all eleven temporal bones he examined (average age: 32 years). Additionally, he provided evidence that the vibration of the malleus where twice the vibration of the incus, and four times the vibration of the stapes (lever ratio between umbo, lenticular process of the incus and stapes; 4:2:1). Hence, the transmission ratio between malleus and incus was 2:1 (Buck 1869).

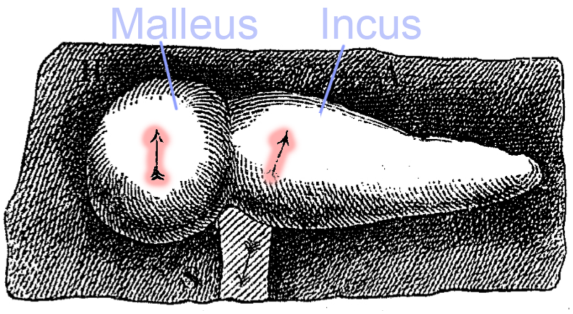

Figure I.54 Different motion directions of malleus and incus measured with Buck's method of following the shiny points on the ossicles provoked by a focused light beam. Modified with kind permission of Springer Science+Business Media after (Buck 1869), figure 1, Arch Augen Ohrenheilkd..

I.III.2.5.3.2.3 A. Politzer

In almost the same period, Politzer showed in experiments with variable static air pressure in the external ear canal that the IMJ yields to a significant excursion of the malleus and only a small displacement of the incus, which confirmed Helmholtz' findings (Politzer 1873, Politzer 1862). This was observed with glass filaments that were glued on both malleus and incus. He further described the lever ratio of the ossicles; during an inward motion of the malleus, the malleus moved the most, followed by he lenticular process of the incus, and to the smallest degree the stapes. Hence, he observed a decline of the motion degree along the ossicular chain, what he equates with a condensation of the sound wave along the ossicular chain due to the scale difference between tympanic membrane and stapes footplate findings (Politzer 1873, Politzer 1862). This was confirmed four years later by Schmiedekam (Schmiedekam 1868). On the one hand, Politzer shared the idea of a 'cog mechanism' as described by Helmholtz where the incus completely followed the inward motion of the malleus. On the other hand, contrary to Helmholtz, Politzer assumed the IMJ to be functionally mobile, similar to Buck (Buck 1869). Contrary to Helmholtz (von Helmholtz 1869), Politzer (Politzer 1873) assigned the articular capsule of the IMJ the responsibility for the lever effect by yielding to the malleus inward and not only the 'cogs' as described by Helmholtz. Thus, Politzer proposed the mobility of the IMJ to cause the lever effect. Additionally, he addressed as well a protection mechanism of the IMJ with a weekend signal arriving at the cochlea (Politzer 1862), and refers to the agreement with Ludwig who already described the protection mechanism in 1852 (Ludwig 1852). Politzer was a former student of Toynbee (see also chapter I.III.2.4.4.1.1).

I.III.2.5.3.2.4 E. Mach & J. Kessel

Mach and Kessel (Mach & Kessel 1874) observed the motion of the ossicles during sound stimulation based on the angular deflection of light beams reflecting from tiny mirrors on the ossicles. They stated that their method of mounting the mirrors with wax to the ossicles shouldn't change the ossicular motion as much as Helmholtz's method with gluing glass fibers on the ossicles. They used a pipe with 256 Hz for the sound stimulation. The sound pressure levels are not indicated. In general, Mach and Kessel agreed with Weber (Weber 1851), Politzer (Politzer 1864) and Helmholtz (von Helmholtz 1869).

In a second measurement, the ossicles were powdered with gold bronze and stroboscopic light measurements were performed to describe the ossicular motion. The stroboscopic observations were performed as well under acoustic stimulation with the pipe at 256 Hz and several higher harmonics. Due to the smaller magnitude of motion at higher harmonics, Mach and Kessel formulated their conclusion for the 256 Hz measurements. They fount the IMJ to be flexible under static pressure and under dynamic sound pressure alterations (Mach & Kessel 1874). Additionally, during static excitation (+0.0052 at ≈ 509.9 Pa ≈ 148 dB SPL), less motion of the stapes was found than for the malleus.

As described in chapter I.III.2.5.3.2.1, Helmholtz concluded from his macroscopic investigations that the incursion of the malleus was smaller that its excursion at the same sound pressure level. He also described that during the excursion, the capsule of the IMJ relaxed and a gap resulted between the articular surfaces. So far Mach and Kessel coincided with Helmholtz's investigations; they found during the excursion that the cog left the pit and the synovial fluid penetrated the resulting gap, which caused the articular capsule to bulge in channel-shaped. Correspondingly, during incursion the cog entered the pit and the capsule bulged out due to the displacement of the synovial fluid. Contrary to Helmholtz they also stated that as soon as the cog is locked in place, the articular edges at the medio-superior portion of the IMJ diverged (articular capsule tensed), whereas the latero-inferior portion approached (articular capsule relaxed). The excursion of the malleus was reduced to a quarter in case of immobilization of the IMJ with wax.

They also emphasized the complexity of the ossicular motion, pointing out the necessity of several degrees of freedom to describe the motion of the malleus in the three-dimensional space.

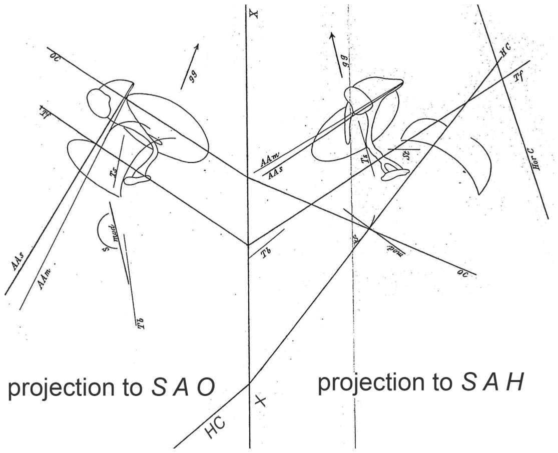

Figure I.55 Draft from Mach and Kessel's publication 'topography and the mechanics of the middle ear' from 1874 (Mach & Kessel 1874) (Projections of the right ear) to illustrate the complexity of the ossicular motion in the three-dimensional space. Reprinted with kind permission of the "Österreichische Akademie der Wissenschaften"; Mach, E.; Kessel. J.: "Beiträge zur Topographie und Mechanik des Mittelohres." In: Sitzungsberichte der Kaiserlichen Akademie der Wissenschaften: Mathematisch- NatunNissenschaftIiche Classe 69, Wien: 1874. S. 221-243.

I.III.2.5.3.2.5 O. Frank

Frank (Frank 1923) was one of the authors, together with (Dahmann 1930, Stuhlman 1937), that introduced the mobility of the IMJ into the interpretation of middle-ear mechanics. He developed a mathematical model implicating the air in the external ear canal, the tympanic membrane, the ossicular chain and the middle ear cavity (as acoustic resonator, Helmholtz resonator). Additionally, he stated the importance of the cochlear load. For his model, he considered the masses of all ossicles and the elasticity coefficients of all ligaments involved. The columella in amphibians, reptiles and birds is homologues to the human stapes and is the single ossicle that directly connects the tympanic membrane to the cochlea. Frank stated, that contrary to the columella in birds, the existence of the incus added a new mass and the coupling between the tympanic membrane and the inner ear decreased. Thus, he suggested the malleus and incus behave like two separate bodies and therefore ascribes elastic properties to the IMJ. Frank saw a direct connection between the development from the single-ossicle ear (columella) to the thee-ossicle ear (as in humans) with additional appearance of a second middle-ear muscle (tensor tympani muscle) during evolution for the three-ossicle ear. In his opinion, independent effects of both muscles (tensor tympani muscle at malleus (see chapter I.III.2.4.1.1) and stapedius muscle at stapes (see chapter I.III.2.4.3.1)) can only be performed by partly decoupling the ossicular chain. He clearly stated that the sound transmission in the single-ossicle ear (columella) is better than in humans due to the sound transmission losses appeared as an unavoidable side effect of the three-ossicle ear. Frank did not observe any cog mechanism as described by Helmholtz (von Helmholtz 1869), even so he did not preclude its existence because he did not focus on these aspects in his experiments.

I.III.2.5.3.2.6 D. Dahmann

The second author that introduced the mobility of the IMJ into the interpretation of middle-ear mechanics was Dahmann. Dahmann experimentally examined the static and dynamic behavior of the IMJ and finally suggested a functional role for the IMJ (Dahmann 1930, Dahmann 1929). Additionally, he reported that the transmission loss due to the relative motions between the malleus and incus were approximately compensated by the lever ratio of the malleus and incus. Some of his findings are presented in the following paragraph in detail.

In his publication from 1929 (Dahmann 1929), Dahmann pointed out the difficulties that occur according measurements in the middle ear, hence the middle-ear structures are not visible without any preparation, which may influence the behavior of the middle-ear (e.g. muscles) and differs from the physiological situation. Therefore, he stated to keep the sources of errors during the measurements as small as possible by…

- … using non-fixed specimens as fresh as possible; maximal 24 hours post mortem, based on Frank's (Frank 1923) findings, which reported that the mechanical conditions in temporal bones matched those in live human subjects (Dahmann 1930)
- … using stimuli that correspond to the physiological stimulation (in daily life)
- … using a measurement technique that affects the mechanical properties of the ossicles as little as possible, respectively, as non-invasive as possible.

Dahmann (Dahmann 1929, Dahmann 1930) used an optical technique to measure the displacement of the ossicles, which was already established by Mach & Kessel (Mach & Kessel 1874). This method implicated the fixation of tiny mirrors on the ossicles, and mapping the deflected light beam during stimulation occurring from the simultaneous illumination of the middle ear (see chapter I.III.2.5.3.2.4). A mirror had a less weight then 1 mg and, thus, Dahmann assumed the weight was nearly negligible. Indeed, this weight is low compared to the mass of the malleus (21.2 to 30.7 mg (Todd & Creighton 2013)) and the incus (24.4 to 37.4 mg (Todd & Creighton 2013)). An advantage of this optical technique is that it can be used for measurements under dynamic and static excitation, since the absolute position of the ossicles by the light deflection is mapped.

To compare the motion of the three ossicles, Dahmann fixed a tiny mirror on each ossicle in fresh human temporal bones (Dahmann 1929). **Static excitation** was applied using two different pressures (incursion/compression of +60 mmHg and excursion/aspiration -60 mmHg). In the intact system with intact inner ear and ossicular chain, the incursion showed smaller displacement than the excursion (1). The ratio was approximately 3:5. Additionally, a loss of displacement along the ossicular chain occurred (2); the malleus showed the largest displacement, followed by the incus, and to the smallest amount the stapes. In a second setup, where the ossicular chain was separated from the cochlear, both effects (1 & 2) disappeared; the incus did not follow the motion of the malleus anymore. Therefore, Dahmann concluded that the loss of displacement along the ossicular chain was not an effect of the lever ratio, which would be similar after the separation of the ossicles from the cochlea. Hence, a *transmission loss* occurred in the joints of the middle ear and, therefore, the joints were regarded as flexible. Dahmann explained the mobility of the joint as a result of the motions of the stapes that were drastically limited by the annular ligament (see chapter I.III.2.4.3.1.1). Hence, a relatively large displacement from the malleus could not be transmitted by the stapes, and was may attenuated already in the ligaments of the IMJ before reaching the stapes.

Dahmann (Dahmann 1929, Dahmann 1930) found similar results under acoustic **dynamic excitation**; the incursion was smaller than the excursion (1), the displacements along the ossicular chain were reduced (2), and both effects (1 & 2) disappeared by decoupling the ossicular chain from the cochlea.

In 1930, Dahmann indicated the problem of drying out of the samples during the measurements, which is still a challenge nowadays with modern measurement setups (see chapter III.I.9.1). In this publication he focused on the static and dynamic stimulation of the Incudo-malleolar complex. He was still open-minded according the functionality of the joint and stated three possibilities: (1) The IMJ was immobilized, (2) The IMJ is mobile and the malleus and incus could move freely, (3) The IMJ is mobile and malleus and incus are coupled together by fibrously tissue (joint capsule). Finally, he stated that relative motion occurred between malleus and incus and, therefore the joint was flexible. However, he stated that the lever ratio of the ossicular chain was not evolved in order to amplify pressure along the ossicular chain from the tympanic membrane to the stapes, but rather to dynamically balance the dissipations along the chain, especially in the IMJ. As already mentioned above, he reported that transmission loss due to the relative motions between the malleus and incus were approximately compensated by the lever ratio of the malleus and incus. Hence, he assumed that the middle-ear mechanism is oriented on the weakest excitations and, therefore, uses the lever ratio to compensate the transmission losses of the joints.

In another measurement setup, Dahmann (Dahmann 1929) investigated the effect of experimentally applying strain to the tendons of the middle-ear muscles; the tensor tympani (see chapter I.III.2.4.1.1) and the stapedial muscle (see chapter I.III.2.4.3.1). This additional strain resulted in smaller displacement of the ossicles and, therefore, he concluded their function as a protecting mechanism to protect the inner ear from excessive stimulation. The middle-ear joints played an important role in this case of increasing the tension on the tendons as well. As soon as the stapes motion exceeded a certain amount of displacement, which could not be transmitted anymore via the oval window due to the fixation of the stapes with the annular ligament to the oval window, the residual energy terminated in the middle-ear joints. Therefore, Dahmann mainly described the function of the IMJ as a protection mechanism (see chapter I.III.2.5.3.6).

I.III.2.5.3.2.7 G. von Békésy

Georg von Békésy won the Nobel Prize in Physiology or Medicine 1961 "for his discoveries of the physical mechanism of stimulation within the cochlea" (Nobel Media AB 2014. Web. 3 Jan 2015.). He also significantly influenced the general description of the ossicular motion. A assembly of his publications are collected in the book "Experiments in Hearing" (G. Békésy 1960). Dynamic measurements of the middle-ear vibrations in response to physiologic acoustical stimulation are in the range of micro- and nanometers and are therefore difficult to assess. Békésy faced this problem and made such measurements using a capacitive probe (G. Békésy 1941). Békésy described the capacitive probe as "a piece of metal foil that is attached to the vibrating surface and a second fixed electrode placed a short distance away. These two conducting surfaces then form the plates of a condenser, and when one plate is vibrating the variations in capacity give a measure of the vibratory amplitude" (G. Békésy 1941, Georg Von Békésy & Wever 1960). The cochlea was drained for the measurement preparation, which could have influenced the results due to the lower impedance at the oval window.

Sound delivered to the tympanic membrane induced the ossicular chain to move approximately as a rigid body with the malleus– incus complex rotating about one axis – without any role of the IMJ; "However, a movement in the joint between the malleus and incus could usually not be observed (cf. Helmholtz 1869); this joint is apparently ankylosed." (G Békésy 1936b, G. Békésy 1941). This statement of Békésy is surprising looking at the observations he did. His observations are described in the following paragraphs.

The pressure-transformation ratio from the tympanic membrane to the stapes (see Figure I.56) was described as independent of the frequency up to 2400 Hz (G. Békésy 1941). The prominent drop of the ratio at higher frequencies (> 2400 Hz) was completely disregarded by Békésy.

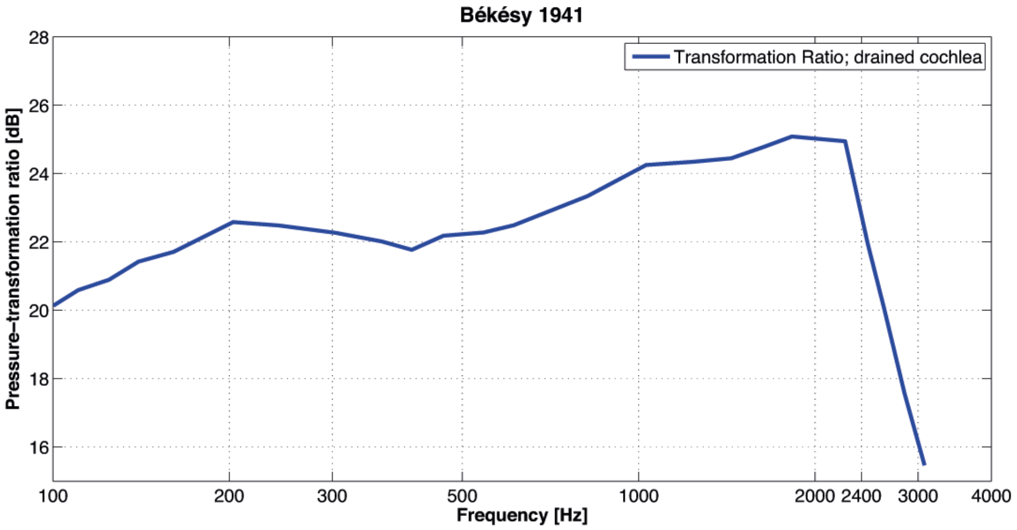

Figure I.56 The transformation ratio from the tympanic membrane to the stapes with a drained cochlea is shown under stimulation of 0.1 Pa (≈ 74 dB SPL). Modified after (G. Békésy 1941).

The rotational axis passed through the center of mass of the incudo-malleolar complex for higher frequencies from the anterior malleal ligament to the posterior incudal ligament (see Figure I.57 A) (G. Békésy 1941). This theory was in agreement with Bárány (Bárány 1938), who showed that for all mammals the distribution of mass was about the rotational axis.

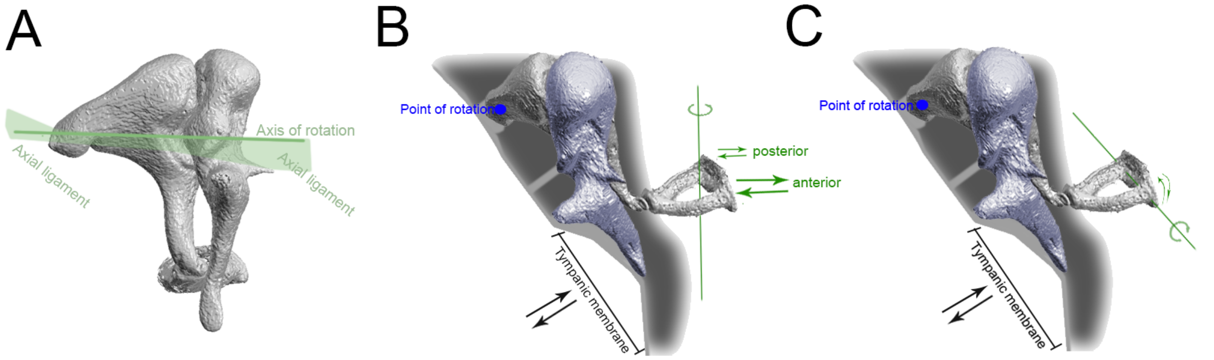

Figure I.57 (A) Lateral view of the ossicles showing the axis of rotation through the malleus-incus-complex from the anterior malleal ligament to the posterior incudal ligament (G. Békésy 1941). (B & C) Different degrees of freedom at different sound intensities; the point of rotation is marked in blue (G Békésy 1936b). (B) At moderate sound intensities (below the threshold of feeling): "As the footplate of the stapes is fastened at its anterior end by looser ligaments than at its posterior end, it executes a rotational movement about a vertical axis running through the posterior edge of the footplate. In this rotation the fluid is pressed into the cochlear canal, especially by the anterior portion of the footplate" (G Békésy 1936b). (C) At excessive sound pressure (above the threshold of feeling): "If the amplitude of motion of the eardrum was made still greater…" (than shown in 'B') "…this form of vibration finally came to a sudden end and consistently went over into another form in which the stapes rotated about an axis running longitudinally through the footplate. Then the fluid of the inner ear merely shifts from the upper half of the footplate to the lower, without causing any displacement in the cochlear canal. As the footplate of the stapes is rather small, this is a means of limiting the transmission of an excessive vibration of the eardrum to the fluid of the inner ear" (G Békésy 1936b). Modified after (Georg Von Békésy & Wever 1960).

For moderate sound pressures (see Figure I.57 B), the increase of pressure caused the manubrium to move to inferior, along with the lower portion of the incus. The movement of the stapes was described as rotating around an axis near the posterior edge of the footplate, such as the anterior part of the footplate had a greater displacement than the posterior part (see Figure I.57 B) (G Békésy 1936b).

For excessive sound pressures (see Figure I.57 C), the complex motion of the ossicular chain did not only rotate about a fixed rotational axis, but about a point (see Figure I.57 C; 'Point of rotation') formed by the short process of the incus and the wall of the middle-ear (G Békésy 1936b).

Thus, the ossicular motion showed several degrees of freedom at different sound pressure levels (G Békésy 1936b). Békésy saw in this new and innovative idea of different modes of vibration (see Figure I.57 B & C) a protection mechanism for the inner ear at high sound pressure stimulation. The transition from one motion mode to the other was possible due to the rotational point (see Figure I.57 B & C) and was explained as a saturation of elongation of the ligaments and the stiffness of the footplate, followed by a change in the volume displacement at the oval window. For frequencies above 100 Hz, a superimposed motion mode (mixture of *B* and *C*) at high sound pressure was observed. Differently, for low frequencies (especially below 20 Hz) at high sound pressure levels a sharply separated form of *C* was detected. Therefore, for low frequencies the protection mechanism reduced the loudness more efficiently (shown also elsewhere for 5 Hz and 10 Hz (G Békésy 1936)) than for frequencies above 100 Hz (G Békésy 1936b).

This protection mechanism derives according to Békésy from the joints in the middle-ear (G Békésy 1936b). Békésy stated that distortion like rattling between the ossicles could occur, if the contact force was smaller then the stimulation force (G Békésy 1936). For low sound pressure levels the elastic joint capsule was able to prevent from these distortions. For high sound pressure levels the ligaments were not strong enough and, additionally, the middle-ear muscles had the function to press the stapes against the incus (tighten the ISJ), while at the same time the ligaments of the IMJ got stretched to avoid distortions in the joints (G Békésy 1936b). Békésy doubted a protective function of the middle-ear muscles; e.g. the tensor tympani only showed a "slight effectiveness in protecting against sound pressures…" (G Békésy 1936b).

I.III.2.5.3.2.8 O. Stuhlman

Stuhlman (Stuhlman 1937) aimed to show mechanical characteristics of the ossicular chain in a oversized model (see Figure I.58). The 20x model of an 'average adult ear' was built after precisely looking at the anatomy and dimensions of the ossicles. The model allowed changing the stiffness of the springs between the ossicles from tight to loose. In case of an immobile IMJ, the lever ratio was 1.27:1. Contrary, if the IMJ was mobile (loose springs), the displacement and force were transmitted in a nonlinear and asymmetrical way from the malleus to the stapes; such as the inward motion (lever ratio 2:1) of the malleus handle differed from the outward motion (1:1). Hence, the IMJ only dislocated during the inward motion. Stuhlman described the IMJ as a "mechanical protective device against great inwardly directed pressures" to protect the sensitive sensory cells of the inner ear (see chapter I.III.2.5.3.6).

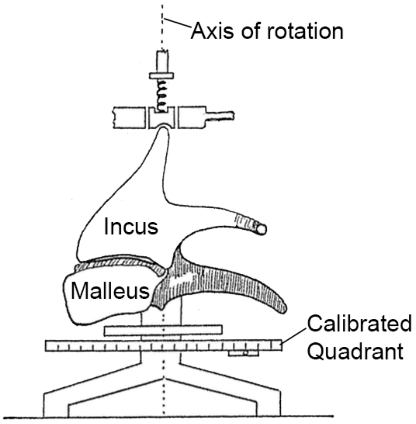

Figure I.58 Illustration of Stuhlman's oversized ossicular chain model. Adapted with permission from J. Acoust. Soc. Am. 9, © 2005, Acoustic Society of America: Melville, NY, figure 3, "The nonlinear transmission characteristics of the auditory ossicles" (Stuhlman 1937).

I.III.2.5.3.2.9 E. Bárány

Bárány (Bárány 1938) assumed that the motion of the ossicular chain is about one single axis "under action of moderate forces" as described by Dahmann (see chapter I.III.2.5.3.2.6). He doubted that this theory with one degree of freedom is true for high frequencies or large amplitudes as well due to the "elastic connections" of the ossicular chain with the walls of the middle ear. Assuming the single rotation axis, Bárány described the IMJ as a rigid body without any movement between malleus and incus. He referred to the anatomical description of the rigid IMJ by Frey (Frey 1911) (see chapter I.III.2.4.4.1.1), and disagreed with Helmholtz' theory (H. Helmholtz et al. 1873).

I.III.2.5.3.2.10 N. W. Gill

Gill (Gill 1951) examined the movements of the tympanic membrane and the ossicles with stroboscopic illumination under dynamic stimulation. The method of stroboscopic illumination was elaborated before by (Mach & Kessel 1874, Lucae 1901, G. von Békésy 1949, Perlman 1945, Kobrak 1941). The measurements were performed in fresh human temporal bones (intact cochlea) and in the living rabbit. A pure sinus wave (0.5-4 kHz) around 120 dB was used to excite the middle ear. In the human temporal bones he found "the heads of the malleus and incus move together as one. Even at very high sound pressure levels they do not separate (Gill 1951) pp. 413" (see Figure I.59).

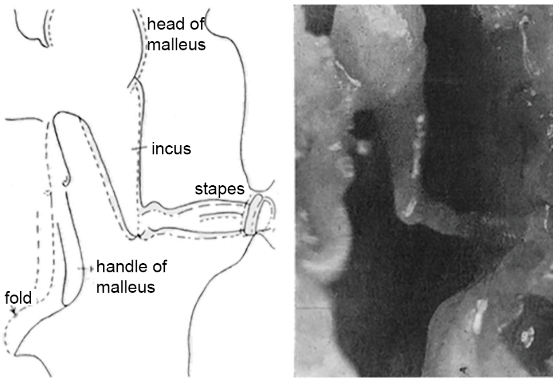

Figure I.59 Illustration and photograph of the ossicular motion at 300 Hz by Gill. Modified after Gill, N. W. 1951, Some observations on the conduction mechanism of the ear, J Laryngol Otol vol 65 (6), pp. 404-13, figure 3, with kind permission of Journal of Laryngology and Otology, JLO (1984) Ltd.

I.III.2.5.3.2.11 H. G. Kobrak

Kobrak (Kobrak 1959) observed the function of the IMJ under three different stimulation forms and different methods:

1. Static air pressure (high pressure changes; 1-4 cc H_2O (≈134 dB – 143 dB): Kobrak observed a phase lag between malleus and incus during static air pressure changes as an evidence of the mobile IMJ in fresh human temporal bones. The method for the static air pressure measurements was the same as applied by Mach & Kessel (1874) and Dahmann (1930) using small mirrors glued on the head of the ossicles, and the rotations were recorded by the light reflections of the mirrors. The angle of rotation was calculated from the length of the light beam. Kobrak found that the rotations of the incus were smaller than the rotations of the malleus. This finding was in agreement to previous reports (Politzer 1862, Politzer 1873, von Helmholtz 1869, Dahmann 1930, Stuhlman 1937).
2. Motion picture study: During both – inward and outward motion – the incus lagged behind the malleus in fresh human temporal bones. Hence, the IMJ was observed again to be mobile.
3. Acoustical stimulation with motion-picture recordings: Under acoustic stimulation of physiologically-relevant levels, the long process of the incus slightly lagged behind (but parallel) to the movements of the manubrium of the malleus. The motion amplitudes of the long process of the incus were smaller than those of the manubrium. Thus, the IMJ was shown to be mobile at the frequencies measurable with this technique (low frequencies).

The sound pressures that he applied were very high and only low frequencies were measured. However, Kobrak described a transmission loss from malleus to incus during the middle-ear sound transmission due to the ‘looseness’ of the IMJ.

Kobrak stated that the function of the middle-ear muscles was a protection mechanism for the inner ear. He found a correlation between the tone intensity and the strength of muscle contraction; “the stronger the tone, the greater the contraction” (Kobrak 1959).

I.III.2.5.3.2.12 I. Kirikae

Kirikae (Kirikae 1960) carefully observed the middle-ear structures and it mechanics including the morphology, size, weight, correlation to age, blood supply (see chapter I.III.2.4.4.1.3, Figure I.37), bony cortex, split line arrangement, folds of mucosa, suspensory ligaments the density, the center of gravity, and the position of the axis of rotation of the ossicles – in a impressive detailed manner. A 15x model was built for stress distribution measurements.

One chapter of his 157 pages document (Kirikae 1960) is devoted to the "experimental study on vibration of the human auditory ossicles" (page 95 to 110). Fresh human temporal bones (18-38 years) were prepared sacrificing the tensor tympani muscle (see chapter I.III.2.4.1.1), superior malleal attachment (see chapter I.III.2.4.1.1), and Kirikae also mentions to disconnect the long process of the incus from the middle-ear cavity (no attachments described in modern literature, see chapter I.III.2.4.2.1). The cochlea was drained for the measurements, where access to the stapes was needed. Measurements were conducted several hours postmortem. However, Kirikae was convinced that the postmortem effect didn't influence his measurements, referring to previous publications (Frank 1923, G. Békésy 1960), which described that no change of the elasticity of the ligaments, the joint capsule and the tympanic membrane occurs within several hours postmortem to those of living subjects.

Two methods were used to measure the ossicular motion; an optical method and an electrical method. Four temporal bones were measured.

1. Optical method; under pressure excitation and acoustic excitation (close to sine wave)
   120-1000 Hz, 110-140 dB
   The results according the IMJ mobility are only shown for 400 Hz and 800 Hz at 140 dB.
   Double-exposure photographs under strobe illumination
2. Electrical method; acoustic excitation (close to sine wave)
   200-2400 Hz, 110-140 dB
   The results according the IMJ mobility are only shown for 400 Hz and 800 Hz at 140 dB.
   Electric condenser & cathode ray oscillograph

By focusing on measurement in in the audible frequency range under 'adequate intensity' of the stimulus, Kirikae concluded that the IMJ was immobile and moved as one rigid body. This immobile IMJ was approved for all frequencies (120-1000 Hz) and intensities (110-140 dB) with the optical method (see Figure I.60). No optical measurements with frequencies above 1000 Hz under acoustic stimulation were performed and only the results for 400 Hz and 800 Hz were presented.

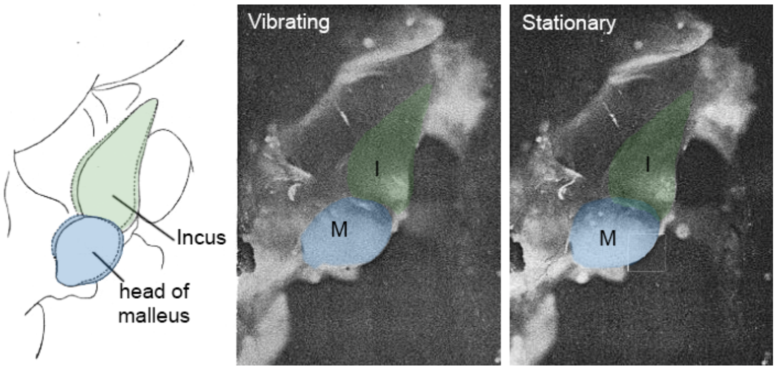

Figure I.60 Vibration of the malleus-incus-complex shown with double exposure photography. The dotted line shows the effect of the vibration. Modified after (Kirikae 1960).

Contrary, a mobile IMJ was observed under static pressure changes above 154 dB with the optical method.

With the electrical method, the IMJ showed again an immobile behavior with no phase lag between malleus and incus for all frequencies (200-2400 Hz) and intensities (110-140 dB) by measuring the phase difference.

Thus, Kirikae (1960) concluded from his optical and electrical measurement that the malleus and incus vibrate as a rigid body up to 140 dB SPL for up to 1000 Hz, respectively 2400 Hz. He also stated that the rotation axis was fixed and the lever ratio constant with frequency.

Kirikae strongly believed in a protection function of the IMJ; a 'buffer action' for high sound pressure levels that were eventually supported by the contraction of the tensor tympani muscle (see chapter I.III.2.4.1.1). He stated that this protection function only takes place at very high sound pressure levels and, otherwise, 'both ossicles are compactly united with articulation' (Kirikae 1960).

I.III.2.5.3.2.13 M. Harty

Davies (Davies 1948) and Harty (Harty 1953, Harty 1964) studied the morphology of the middle-ear joints, which they assumed to be true. They found the capsules to be mainly composed of elastic tissue. Harty (Harty 1964) assumed that the IMJ allows sliding and rotation at the joint surfaces to protect the 'delicate' ear-structures. However, he also found the IMJ to "provide enough articular cohesion to allow the ossicular chain to function as a physiological unit." Thus, under physiological conditions he assumed the IMJ to be immobilized.

I.III.2.5.3.2.14 B.S. Elpern

Elpern et al. (Elpern et al. 1965) experimentally immobilized the IMJ. They found no significant changes in the transmission of sound to the round window due to the immobilization. Thus, their findings suggested that the IMJ was functionally immobilized. Refering to Békésy's method (Georg von Békésy 1942), a pure tone stimulus (0.25-8 kHz, around 110 dB) was applied to the meatus of human temporal bones. A small tube inserted into the round window niche and a condenser microphone connected to the tube then measured the volume displacement of the round window. Nineteen temporal bones were measured (20 to 48 hours post-mortem).

The change in sound transmission (in dB) is also presented for four other fixation sites in Elpern's work (Elpern et al. 1965); head of the malleus, incus, ISJ, and tendon of the stapedius muscle. They assumed that "arthritis, congenital fixation and similar lesions affecting these sites may be considered functionally insignificant" – same for the immobilization of the IMJ.

No information was given about possible drying effects before or during the measurements. The IMJ may was already immobilized before measurements due to drying of middle-ear structures. Additionally, the immobilization was not checked and, thus, the IMJ may was not immobilized sufficiently. The results need to be interpreted with care, because Elpern et al. used the difference between SPL at the tympanic membrane and the volume velocity of the round window membrane as the transfer function. Thus, the tympanic membrane, the ossicular chain, and the inner ear are included in this transfer function. The admittance of the umbo strongly refers to the transfer function of the ossicular chain; a decrease of the transfer function of the ossicular chain du to the immobilization of the IMJ results in a decrease of the umbo admittance (U. Willi et al. 2002, Dahmann 1930, Weistenhöfer & Hudde 2000). Thus, a conclusion about the functionality of the IMJ is uncertain to draw from these measurements.

I.III.2.5.3.2.15 J. Marquet

Marquet et al. (Marquet et al. 1973) considered the IMJ as 'vibrate as one unit' in their mechanical model of the middle ear. Thus, he assumed no mobility in the joint by malleus and incus moving in 'the same amplitude and phase' but, however, he assumed mobility in the ISJ (Marquet et al. 1973).

Eight years later, Marquet (Marquet 1981) explained the behavior of the IMJ from his observations of the IMJ anatomy (see also chapter I.III.2.4.4.1). He made serial cross-sections of the IMJ in three different planes to show its possible three-dimensional motions. In his opinion, the "articular facets permits three-dimensional movement" (Marquet 1981). Contrary to his previous report, he found the IMJ anatomy to allow relative rotations between the malleus and incus. Marquet (1981) assumed a flexion of nearly 500 µm of the long process of the incus on the handle of the malleus (see Figure I.61).

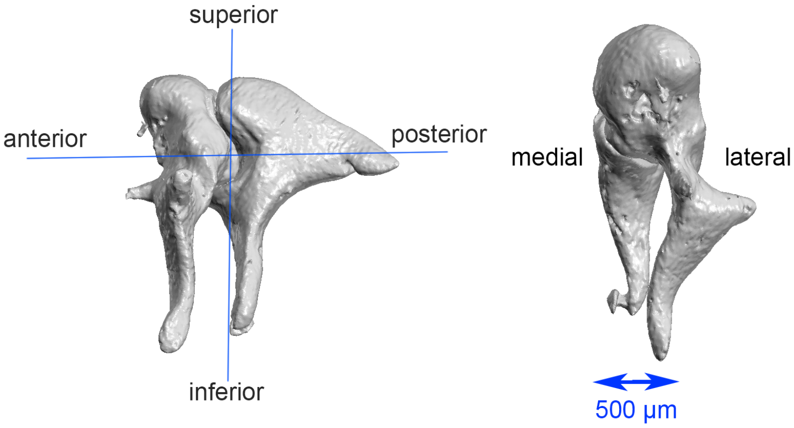

Figure I.61 Orientation of the malleus-incus complex for better understanding of Marquet's observations.

I.III.2.5.3.2.16 W. Cancura

Cancura (Cancura 1980) reported that the IMJ is not flexible under physiological stimulation. However, the IMJ was flexible under large static pressure fluctuations, which may serve as a protection mechanism of the middle ear to protect the sensitive inner ear structures. Furthermore, no fixed pivot was found for the malleus and incus. An adjusting of the pivot to each oscillation form of the tympanic membrane was concluded, especially for higher frequencies.

In detail, an electromagnetic probe was used for static examinations on 12 human temporal bones with removed tympanic membrane. A precisely adjustable force was applied to a certain point on the malleus with this small electromagnet. Simultaneously, the displacement was measured in microns by using a metal core that reached into a coil of an oscillator. This oscillator frequency changed according to the longitudinal shift of the probe. The resistance of the ossicles was determined from the ratio between the applied force and the shift of the probe. Furthermore, the result of the oscillator was compared to a second oscillator (reference oscillator); the shift (equals the shift of the probe tip) was read at the micrometer drive.

Forces of 5 mN and 10 mN were applied to certain points on the Malleus (see Figure I.62 a). The greatest displacement was detected at the umbo, a smaller displacement at the middle of the manubrium and a considerably smaller displacement at the lateral process of the malleus.

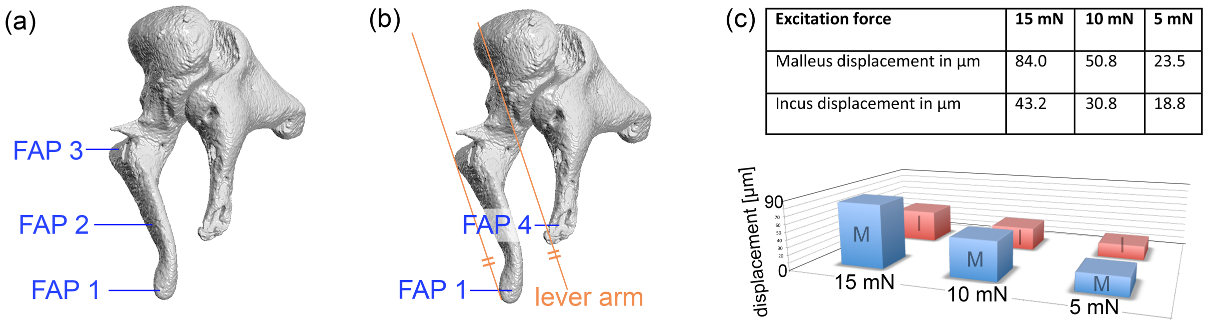

Excitation force	15 mN	10 mN	5 mN
Malleus displacement in µm	84.0	50.8	23.5
Incus displacement in µm	43.2	30.8	18.8

Figure I.62 Cancura used different force application points (FAP) for the static measurements. (a) FAP at the umbo (FAP 1), middle of the manubrium (FAP 2) and lateral process (FAP 3) of the malleus. (b) FAP at the umbo (FAP 1) and at the long process of the incus close to the lenticular process (FAP 4). (c) The IMJ showed an elastic behavior under static excitation at 15 mN, 10 mN and 5 mN; the differences of the displacement were the more pronounced the greater the forces applied were. Modified after (Cancura 1980).

To check the flexibility of the joint, 10 human temporal bones were prepared and force was applied on the malleus and the incus (see Figure I.62 b). Cancura assumed these two points (FAPs) to be on the same lever arm and (see chapter I.III.2.5.3.2.6, Figure I.62), therefore, the IMJ is showing elastic properties if the displacement of FAP 1 and FAP 4 is different. Differences in displacement were found for all excitations with 5 mN, 10 mN and 15 mN; the differences were the more pronounced the greater the forces applied were (see Figure I.62 c). The displacements started to be equal at/below 1 mN applied force. Hence, no transmission loss occurred below 1 mN. This 1 mN corresponds to an acoustic stimulation of about 120 dB. Therefore, Cancura concluded that on one hand the IMJ is not flexible within the human auditory area, and on the other hand the IMJ becomes more and more flexible under great sound intensities.

I.III.2.5.3.2.17 T. Gundersen

Gundersen (Gundersen 1971)concluded that the no movement appeared in the IMJ up to 125 dB (n= 15). A stroboscope was used to measure the movement of malleus and incus, and a maximum of 2 dB difference was observed between the movement of the malleus head and the corpus of the incus under acoustic stimulation between 0.06-2 kHz.

Five years later, Gundersen and Høgmoen (Gundersen & Høgmoen 1976) used time averaged holography (similar like (Tonndorf & Khanna 1972a)) to characterize the motion of the ossicular chain in the area of the IMJ. Again, the IMJ was found to be immobile for acoustical transmission; below 800 Hz a common rotational axis between malleus and incus with no transmission losses (up to 1.5 kHz) was obtained (Gundersen & Høgmoen 1976). They found the IMJ only to be mobile under large pressure change; visible as a 'discontinuity or deflection of the straight fringes by transition from malleus to incus' (see Figure I.63).

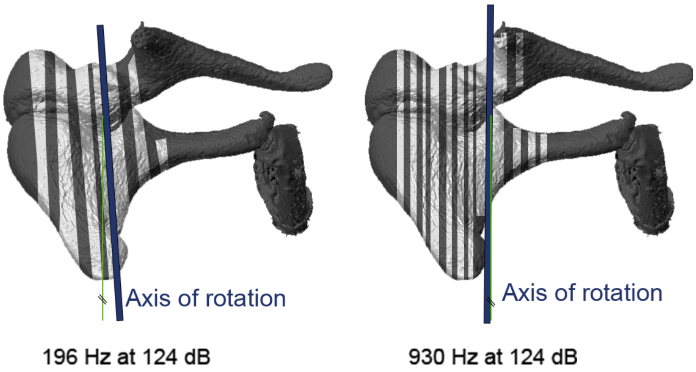

Figure I.63 Illustration of the time averaged holography measurements of Gundersen & Høgmoen (1976). The

Thirty-two fresh human temporal bones (6-48 h post-mortem) were investigated under acoustic stimulation (0.1-10 kHz, most measurements <2 kHz and 100-125 dB SPL). Aluminium powder with a negligible mass (0.03 mg/cm^2) was applied to the surface of the ossicles to increase the reflectivity. No phase information could be obtained with this measurement method. To avoid any effect of drying, the temporal bones were kept moist during the measurements.

Unfortunately, a part of the semicircular canals and vestibulum were removed to visualize the IMJ from the medial side; "without removing these parts of the cochlea it was impossible , to see both the tip of the manubrium body of the malleus and the long crus of the incus." Gundersen (Gundersen & Høgmoen 1976, Gundersen 1971) found no effect on the ossicular motion due to removal of these structures. Contrary, several other authors described a significant effect of draining the cochlea on the ossicular motion (the resistance at the lenticular process of incus changes). Therefore, Gundersen & Høgmoen's results cannot be stated to show the functionality of a normal middle ear. Willi (U. Willi 2003) found similar results according the IMJ-mobility up to 2 kHz with an experimentally drained cochlea.

The ossicular chain was described as a 'lever around an axis'. However, the axis of rotation was found to change with frequencies. The lever ratio was smaller at the resonance frequency of the middle ear (0.8-0.9 kHz (Gundersen, 1971)), and larger at frequencies below and above this point (Gundersen & Høgmoen 1976).

Gundersen & Høgmoen (1976) also performed measurements looking at the muscles in the middle ear. "In order to apply a force, simulating the natural contraction of tensor tympani, the muscle was dissected free and a thread was fastened to it, making it possible to apply the force in the direction of natural contraction." The magnitude of force was only described for animals; finally, a force of 10-50 g to tensor tympani and 1-10 g to stapedius were applied (between 0.3-1 kHz, between 114-134 dB). "Traction in the tympanic muscles attenuated the vibration amplitudes and reduces the transmission of amplitude from malleus to incus. This is a result of movement in the joint between malleus and incus." The authors concluded that this mobility in the joint was considered to be a protecting mechanism (see chapter I.III.2.5.3.6).

Gundersen also focused on the "frequency characteristics of the middle ear" (Kringlebotn & Gundersen 1985) (see chapter I.III.2.5.2).

I.III.2.5.3.2.18 K. Gyo

Gyo et al. (Gyo et al. 1987) visually measured the motion of the umbo, the lenticular process of the incus and the stapes head under a microscope. Similar to Guinan & Peake (1967), a video measuring system and a stroboscope as a light source were utilized. Sound-induced ossicular motion down to 0.3 µm could be measured. The cochlea was left intact. Measurements in the same work showed that the drainage of the cochlea significantly influenced the ossicular motion. The measurements were performed in 14 fresh human temporal bones; used immediately (< 24 post mortem) or stored in thimersal in the fridge (used within 3 days post mortem). The authors paid attention to carefully avoiding effects of drying; the artificial openings were closed and the sample periodically moistened with saline. They found diverse results for the stimulation below and above 1 kHz. Below 1 kHz, the umbo rotated around an axis near the neck of the malleus. Above 1 kHz, the direction of the umbo movement changed 'slightly' and a rotational component appeared additionally to the piston-like movement.

A frequency dependent transfer function from umbo to head of the stapes (lever ratio) was obtained. This lever ratio was 1.9 below 1 kHz and gradually increasing with frequency above 1.2 kHz with a peak at 2.2 kHz – and decreasing slightly at higher frequencies. This finding was contrary to Dahmann's ratio of 1.31, which was largely accepted by this time (see chapter I.III.2.5).

According the mobility of the IMJ they mentioned that the frequency-dependent transfer function could be explained by 'a loosening' of the IMJ. The sound-induced displacement of the umbo was more than twice the displacement of the long process of the incus. This ratio even increased for higher frequencies > 1 kHz (see Figure I.64). They experimentally immobilized one IMJ by placing a 'polyethylene strut between the malleus handle and the long process of the incus, and glued both ends' to eliminate 'any possible loose coupling of the joint'. The displacement of the incus did not increase due to the artificial immobilization. However, the authors held the opinion that the IMJ is functionally immobile and, thus, the IMJ allows no relative motion between malleus and incus – referring also to Kirikae (1960), Gundersen and Høgmoen (1976) and Elpern et al. (1965). They concluded that the frequency dependent transfer function of the middle ear could be produced by a frequency dependent orientation of the rotational axis of the IMJ, thus, corresponding to its lever ratio. Phase data could not be obtained. Additionally, they assumed a transmission loss in the ISJ.

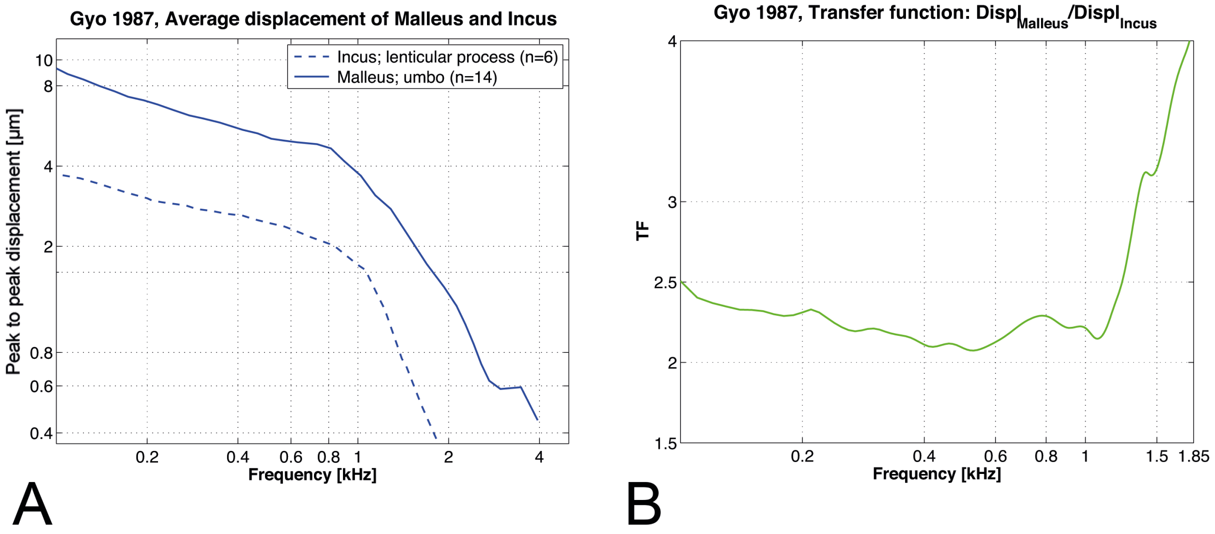

Figure I.64 (A) Average displacement at the umbo (malleus) and the lenticular process (incus) at 124 dB SPL excitation. (B) Transfer function between the displacement of the umbo (malleus) and the lenticular process (incus). The magnitude of the sound-induced displacement of the umbo was more than two times greater than the displacement of the lenticular process of the incus. Modified after (Gyo et al. 1987).

I.III.2.5.3.2.19 K. B. Hüttenbrink

Several authors described the fine structures of the ossicles with the scanning electron microscope (SEM) technology (Terrahe et al. 1970, Terrahe et al. 1971a, Terrahe et al. 1971b, Brownson & Marovitz 1972b, Brownson & Marovitz 1972a, Casselbrant 1979, M.D. Graham 1985, Hassmann & Chodynicki 1978, Lim 1970, Möller 1982). Hüttenbrink & Pfautsch (Hüttenbrink & Pfautsch 1987) focused on the description of the IMJ with SEM (n = 17 fresh temporal bones). They describe the morphology of the middle-ear joints (see chapter I.III.2.4.4.1). Based on their findings they conclude that the IMJ is a true diarthrodial joint and, therefore, motion in he joint is possible. However, they believed that motion in the joint only occurs under high-pressure changes, and that the IMJ serves as a protection mechanism for the inner ear under such conditions. Referring to previous works (Gundersen & Høgmoen 1976, Tonndorf & Khanna 1966) they describe the IMJ to be functionally immobilized under acoustic excitation of physiologically-relevant levels.

One year later, Hüttenbrink published his elaborate work about the 'mechanics of the middle-ear' (Hüttenbrink 1988a, Hüttenbrink 1988b). Again, he stated that the IMJ was functionally immobilized for acoustical transmission, whereas it was mobile during changes of static air pressure (from 148 dB to 166 dB) (Hüttenbrink 1988c). Due to this mobility of the IMJ, the direction of the movement of the lenticular process changed under static pressure changes (see Figure I.65). Contrary, with an experimentally immobilized IMJ, the movement of the lenticular process and the stapes was inward and outward under static pressure changes (Hüttenbrink 1988c). Although the umbo displacement was reduced by one half, the inward and outward motion of the stapes increased three times. The measurements were performed in 14 fresh human temporal bones – carefully moistened, because he described changes due to effect of drying or freezing of the samples.

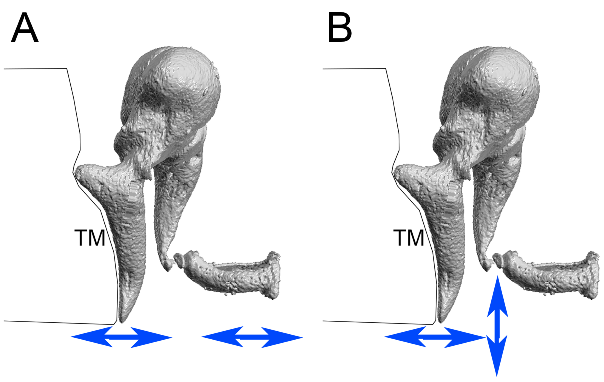

Figure I.65 Hüttenbrink found the malleus handle to change from an inward and outward motion under acoustic physiological stimulation to a predominantly upward and downward movement of the lenticular process under static pressure changes due to the mobility in the IMJ (148 to 166 dB). TM= tympanic membrane. Modified after (Hüttenbrink 1988c).

The movements of the umbo, the lenticular process and the stapes head were registered with an optical technique and videotaped radiographic examinations. For the optical technique, relevant points on the ossicles were marked with aluminium powder, lighted with an optic fiber, and the movement (displacement down to 1 µm) observed under microscopic magnification (max. 1250x). Hüttenbrink (Hüttenbrink 1988c) assumed that in vivo the ossicular motion would be greater due the body temperature due to the viscoelasticity of the IMJ (Marquet et al. 1973).

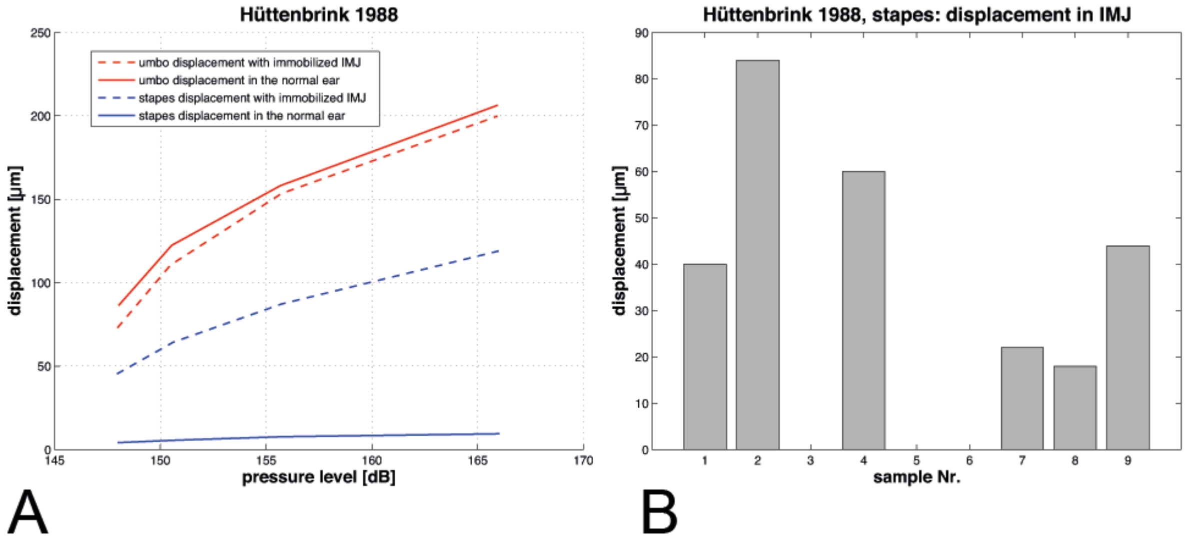

Figure I.66 (A) Stapes motion increased after immobilization of the IMJ under static pressure stimulation. Modified after (Hüttenbrink 1988d) with 10 mmH_2O = 1 p/cm2 = 98,0665 Pa = 133.81 dB SPL. (B) Relative motion in the IMJ measured in difference of stapes displacement due to the immobilized IMJ at 186 dB (400 mmH_2O) stimulation. Six out of nine temporal bones showed mobility at the IMJ under this condition.

In a second step, the IMJ was immobilized with Histoacryl (Fa. Braun) glue in the joint cleft in eight samples. This resulted in a reduction of the in-and-out movement of the malleus by one half in all specimens. The decrease of the umbo mobility was not significant in all six temporal bones. With the immobilized IMJ, the stapes is pushed (and pulled out) of the oval window 'considerably further than in the normal ear'; the inward and outward movement of the piston was considerably increased after the IMJ immobilization.

The ratio of the inward and outward motion of malleus, incus and stapes was found to be 21:1.8:1 (Hüttenbrink 1988c), in contrary to previous presented ratios of 4:2:1(M:I:S) (Buck 1869, Kobrak 1959) and 4:1 (M:S) (Bezold 1880). With the immobilized IMJ this ratio decreased to 4.2:2.2:1 (Hüttenbrink 1988c) what in Hüttenbrink's opinion could be a evidence that the drying effect (see chapter III.I.9.1) biased previous works.

The mobility of the IMJ was confirmed intraoperatively in 18 revisions of normal middle ears (e.g. prominent bulb of jugular vein) (Hüttenbrink 1988c). Furthermore, only 16 out of 30 otosclerosis patients showed intraoperatively an 'outward motion of the malleus' typical for motion in the IMJ by pulling the lenticular process backwards.

Again five years later, Hüttenbrink (Hüttenbrink 1992) described an imaginary rotational axis to be located outside the ossicles, resulting in a piston like vibration of the complete ossicular chain. Thus, again he stated that the ossicular chain acts as one single unit with no relative motion in the IMJ under physiological relevant stimulation.

I.III.2.5.3.2.20 C. J. Brenkman and J. J. Grote

Brenkman and Grote (Brenkman et al. 1987) aimed to use a measurement setup to measure ossicular motion without influencing the structure and function of the ear, thus without opening the cochlea or change the middle-ear anatomy, and with a sensitivity to measure displacements down to 1 nm. They found the SQUID (superconducting quantum interference device) magnetometer (W.L.C. Rutten et al. 1982, W. L. Rutten et al. 1986) to be an appropriate solution, where "mechanical vibrations are transformed into magnetic flux variations by gluing (with glass ionomer cement) a small magnet to the middle-ear structure under study (umbo and anterior crus of the stapes)" (Brenkman et al. 1987). The main goal was to compare the input-displacement (umbo) and the output-displacement (stapes) of the middle ear in 14 human temporal bones (48-86 years) from 0.2-10 kHz at 80 dB (loudspeaker, logarithmic sweep). No influence of the mass (1.5 mg) of the magnet was assumed after testing for mass-influence.

The umbo displacement was not parallel to the stapes displacement. Brenkman and Grote mentioned an energy loss in the middle-ear due to mobile joints as a possible reason for this. However, they concluded the IMJ to be functionally immobilized referring to several previous works (H. Helmholtz 1868, Dahmann 1930, Dahmann 1929, Stuhlman 1937, Wever & Lawrence 1954, G. Békésy 1941, Tonndorf & Khanna 1972a, Bárány 1938, Kirikae 1960, A.R. Møller 1961, Elpern et al. 1965, Cancura 1980). Thus, their explanation for the transmission loss in the middle ear was the inter-individual differences and a change of the transformer ratio as a function of frequency (e.g change of middle-ear axis and/or a mobile ISJ).

I.III.2.5.3.3 More recent studies about function of the incudo-malleolar joint (> year 1993)

Improvements in measurement technology have led to more precise results and a remarkable increase of the knowledge about the ossicular physiology over the last 20 years. Studies focusing the function of the IMJ since 1993 are reviewed in the following subchapters.

I.III.2.5.3.3.1 R. L. Goode

Goode et al. (Goode et al. 1993) previously measured the umbo displacement with an LDV system (see chapter II.IV) in 4 live subjects (6 ears) and in 15 fresh human temporal bones. He found similar umbo motion in the temporal bone model and the live subjects. The post-mortem effect is discussed in chapter IV.II.3.2.

In 1994, Goode et al. (Goode et al. 1994) measured ossicular motion by LDV in 20 fresh human temporal bones (stored in merthiolate solution at 5°C, mean age 68.9 between 53 and 87 years). The measurements were performed within 6 days after death. The reflection of the stapes footplate was improved by placing a piece of reflective foil with cyanoacrylate cement. A pure-tone stimulus was applied to the tympanic membrane through a speculum (104, 114, 124 dB SPL, from 0.2-6 kHz (malleus and incus), 0.4-6kHz (stapes respectively). They believed in an immobile IMJ under physiological stimulation, referring to (Gundersen 1971, Gundersen & Høgmoen 1976). However, the displacement of the umbo was more than two times greater than that of the stapes, and had a broader frequency dependence than the stapes displacement (see Figure I.67) (Goode et al. 1994). The phase of umbo and stapes displacement showed that the stapes lags behind the umbo. They also found a decrease of 12-15 dB/octave in the middle-ear transfer function between 1 and 3 kHz (Goode et al. 1994) (see Figure I.67). This increase of the lever ratio above 1 kHz was not attributed to the IMJ in their work, however, they stated that it is "thought to be caused by translational movement of the ossicular rotation axis near the short process (pp. 145)" of the incus (Goode et al. 1994). In detail, they are assuming slippage influenced the ossicular motion by influencing the "laxity in the ossicular rotation axis, which lies on a line between the anterior malleolar ligament and the posterior incudal ligament close to the short process of the malleus. (pp. 151)" (Goode et al. 1994). They assumed this axis not to be fixed, but moving in and out as well as rotating; referring to previous works that showed that this movement causes a decrease in efficiency of the lever action at higher frequencies and a shift of axis of rotation (Gundersen & Høgmoen 1976, Gundersen 1971). In their previous work (Goode et al. 1993) they found this slippage to cause a transmission loss of about -4 to -6 dB per octave above 1 kHz (umbo & stapes).

Looking at the transfer function from the umbo of the malleus to the short process of the incus, the mean umbo displacement was minimum 1.8 times greater than the mean incus displacement for all measured frequencies (0.2-6 kHz) (see Figure I.68). The transfer function (short process of incus/ umbo of malleus) was about 2 above 1.8 kHz – and even greater for the lower frequencies. Goode et al. (1994) only measured the 2-D vibration of the ossicles. They assumed that this increase in the lever ratio was caused by an increasing 'translation displacement of the rotational axis' above 1 kHz referring to the work of (Aritomo 1989) and (Gundersen & Høgmoen 1976, Gundersen 1971). However, they assumed that the IMJ was immobile under physiological stimulation and bend at high static pressures, referring to (Gundersen & Høgmoen 1976, Gundersen 1971).

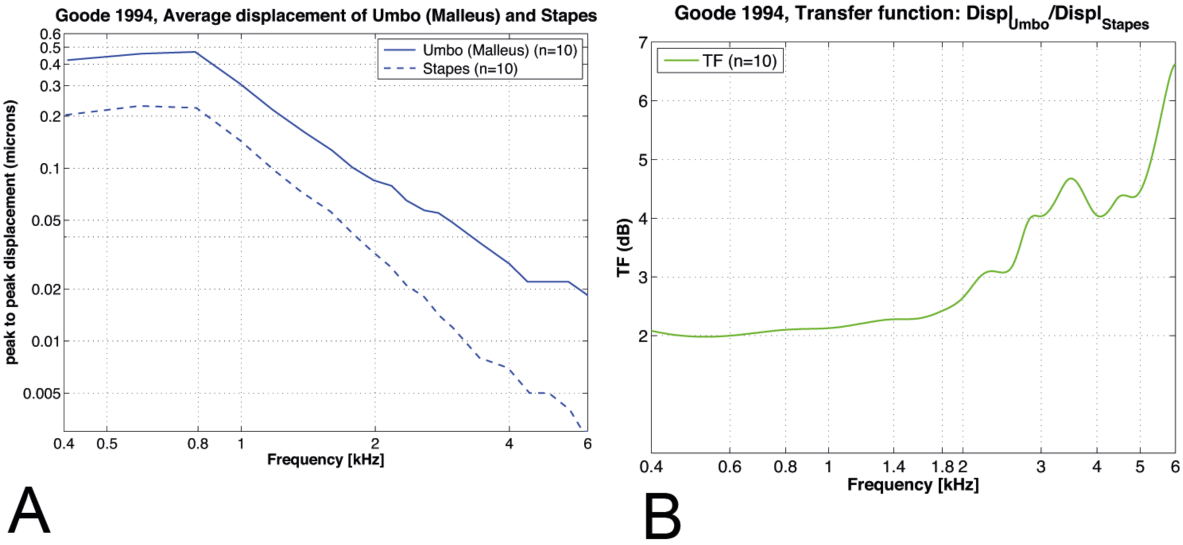

Figure I.67 Mean of umbo and stapes footplate displacement in ten human temporal bones (mean age 72 years from 65-80 years) at 104 dB SPL stimulation at the tympanic membrane. The mean umbo displacement rolled off at -10.4 dB per octave from 1-4 kHz. The mean stapes displacement rolled off at -13-4 dB per octave from 1-4 kHz. (B) Transfer function; lever ratio (umbo displacement/stapes footplate displacement) calculated from data of (A). The lever ratio had a mean value of about 2-2.5 dB up to 1.8 kHz and reached a peak of 6.6 dB at 6 kHz. Modified after (Goode et al. 1994), Figure 1 pp. 148.

At the MEMRO conference in 1997 Goode stated in a discussion about the work of Huber et al. (A. Huber et al. 1997) that they assumed that "one of the reason for the loss of energy between the umbo and stapes (pp. 87)" is maybe in the IMJ. Therefore, they glued the IMJ and saw no difference due to the immobilization. However, they assumed that the immobilization of the joint was maybe not successfully performed.

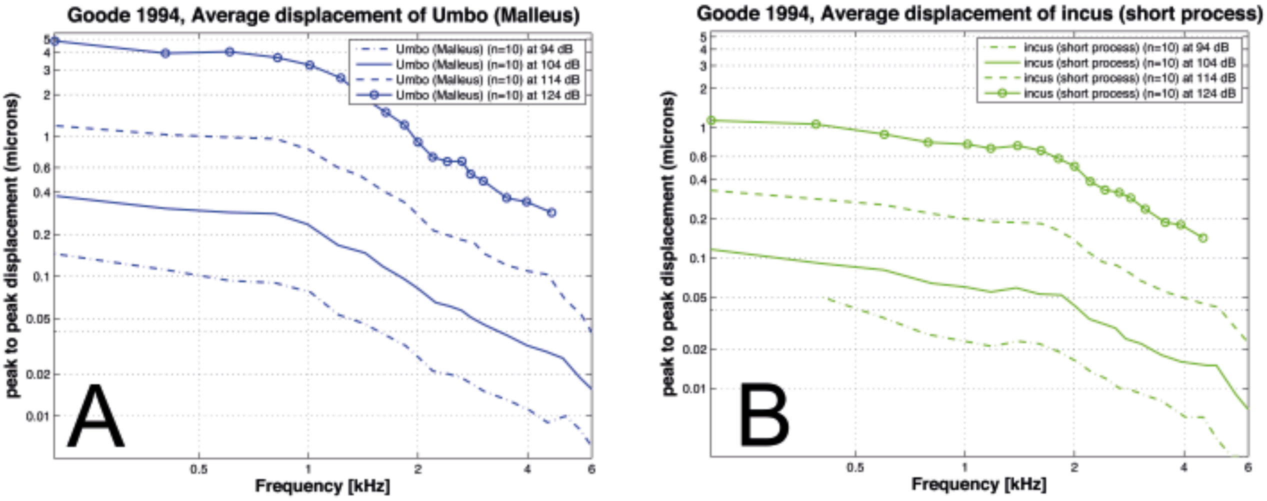

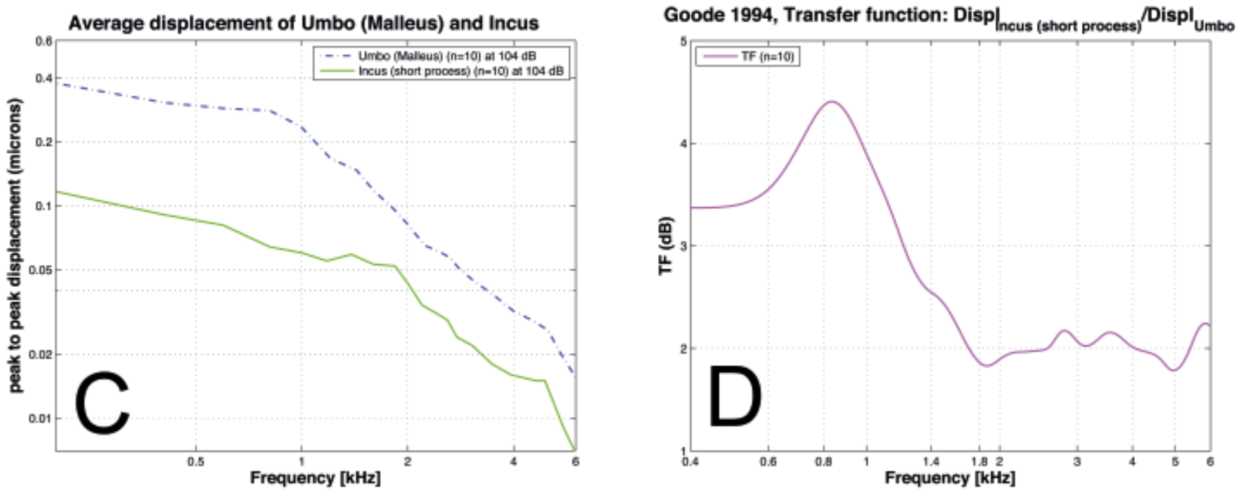

Figure I.68 Mean displacement of umbo (malleus) (A) and incus (short process) (B) in ten human temporal bones at different sound pressure levels. The mean displacement for umbo and incus at 104 dB SPL is shown in (C). The transfer function (incus/umbo) (D) was positive for all measured frequencies; the mean umbo displacement was greater than the mean incus displacement for all measured frequencies (0.2-6 kHz). Modified after (Goode et al. 1994).

I.III.2.5.3.3.2 H. L. Tay and R.P. Mills

Tay and Mills studied the mobility of the IMJ at different sound pressure levels (Tay & Mills 1996). Ossicular motion of two fresh frozen human temporal bones were analysed by photography technique, including a microscope (25x magnification) and superimposing of images. The maximal displacement of the long process of the incus was less than 100 µm. It is doubtful, whether the statement that "the malleus and incus are united by a firm pseudoarthrodial joint and move as a unit except at extremely high intensities" (Tay & Mills 1996) can be concluded with the present measurement method. According the axis of rotation of malleus and incus, they were in agreement with Békésy (Von Békésy 1960) who found the rotational axis to pass from the anterior malleal ligament to the posterior incudal ligament (see chapter I.III.2.5.3.2.7).

I.III.2.5.3.3.3 F. Schön and J. Müller

Schön and Müller disagreed that the malleus and incus rotate about a fixed axis (Schön & Müller 1999). Instead, a more complex vibration pattern was shown on frozen temporal bones. No changes occurred after defrosting and refreezing the bones. Nevertheless, the authors assumed possible changes to the living subjects due to the different condition of the tissue. Linearity was given in the range from 25 to 105 dB at 1 kHz stimulation with an earphone. A pseudo-white noise from 0 to 10 kHz was chosen for the stimulus. The velocity of the ossicles was measured with a single point LDV (see chapter II.IV).

Measuring the motion of the lenticular process and the stapes showed larger difference than explainable only by the slippage in the ISJ. Therefore, a slippage in the IMJ was assumed, the inner ear was removed and the middle ear opened for further measurements. Then, under acoustical stimulation the motion of the incus and malleus was scanned at different points. For the frequency range between 0 and 1 kHz the malleus and incus rotated about a single axis. For higher frequencies (1 to 10 kHz) the nature of motion changed. Thus, the role of the IMJ in sound transmission was dependent on frequency.

In a second stimulation form electrostatic forces were applied to the middle-ear. The authors saw as advantages of this new applied technique that (1) no contact with the ossicles was needed for the local stimulation, (2) force could be produced proportional to the exciting voltage and with the same phase, (3) force was independent of the frequency. The disadvantage was that the magnitude of force was not easily adjustable to a known value. Again, the stapes was removed for the measurements. Additionally, the eardrum and the malleus were fixed by glass ionomer cement. Hence, the incus was only mobile if the IMJ allowed relative motion between the two ossicles. Schön and Müller found the IMJ to be 'compliant'. Nevertheless, they were not convinced whether this relative motion in the joint also appears 'during the process of hearing' (Schön & Müller 1999).

I.III.2.5.3.3.4 W. F. Decraemer & S. M. Khanna

Decraemer et al. especially, but not only, described the ossicular motion in animal (cat, gerbil) (Decraemer et al. 1991, Decraemer & Khanna 1997, Decraemer & Khanna 2000, Decraemer & Khanna 2004, Decraemer et al. 2014) (see chapter I.III.2.5.3.5.1 & I.III.2.5.3.5.2).

They developed a technique to obtain the complete 3-D motions of the ossicular chain (Decraemer et al. 1994). First, they measured 3-D motion of the manubrium of the malleus in anesthetized cats (Decraemer & Khanna 1997), and then they also measured the 3-D motion of the stapes in temporal bones (Decraemer & Khanna 1999b). In 1999, they presented for the first time the 3-D motion of the entire ossicular chain in the cat ear (Decraemer & Khanna 1999) (see chapter I.III.2.5.3.5.1).

For the human ossicular chain, preliminary data on the complete 3-D motion was shown at the ARO meeting (Decraemer & Khanna 2001). The study was based on LDV measurements of the spatial motion of the ossicles, using a compound heterodyne laser-interferometer/confocal-scanning-microscope system (Decraemer & Khanna 2001). A 'substantial amount slippage' was found between the malleus an incus under acoustic stimulation. This slippage was even found at very low frequencies. The authors were careful with the interpretation of their findings, because the measurements were performed in only two temporal bones of the same donor (left ear and right ear). It was "not clear whether this slippage is due to post mortem and/or conservation effects of the bone or a genuine feature" (Decraemer & Khanna 2001). The 3-D anatomical data was obtained to calculate the 3-D movement of the ossicles, assuming the ossicles to have the properties of rigid bodies. The motion modes of malleus and incus became more complex at higher frequencies, without showing any common rotation axis (nor free, nor defined, nor stable, nor common). These observations were made in both ears of the donor.

Two years later, Decraemer et al. (Decraemer et al. 2003) published their work about the three-dimensional modeling of the middle-ossicles of human and cat using a commercial high-resolution X-Ray CT scanner. This is of interest to obtain the frame registration data for 3-D motion measurements with the LDV (see chapter III.V.5.1). Decraemer et al. (Decraemer et al. 2002) also used the geometrical data of a 3-D model for the interpretation and validation of experimental e.g of middle-ear vibrations.

In 2004, Decraemer and Khanna (Decraemer & Khanna 2004) used again a LDV system and micro-CT data to measure and model the spatial ossicular motion under acoustic stimulation. Measurements were performed from five different LDV-viewing angles changed by the goniometer about a vertical and a horizontal axis. Coordinates of several 'anatomical' points that defined the position of the ossicular chain during the experiment were also measured. The 3-D components of the ossicular motion was determined by the five measurements under different angle; including the rotation and translation amplitude and phase for the x, y and z motion components (see earlier publication for details of procedures (Decraemer & Khanna 1997, Decraemer & Khanna 1999, Decraemer & Khanna 1999b)). The already mentioned micro-CT scans were used to generate a model of the ossicular chain after segmentation (Decraemer et al. 2003). Additionally, anatomical landmarks (e.g. annulus or part of external ear-canal) were also modeled and served for the development of an intrinsic reference system (Decraemer & Khanna 1999b, Decraemer & Khanna 1999, Decraemer et al. 2003, Decraemer et al. 2002). In a next step the 'anatomical frame' and the 'measurement frame' were aligned. It allowed the animation of the model and the visualization of the 3-D motion of the entire chain – the motion could be studied from any angel. The spatial ossicular motion was calculated for 12 different frequencies. Samples of five cats and four humans were measured. The results for the cat temporal bones are described in chapter I.III.2.5.3.5.1. In humans (n=4), they reported again 'large slippage' between incus and malleus even at low frequencies, indicating a mobile IMJ (Decraemer & Khanna 2004) – like in the first human data set presented at ARO (Decraemer & Khanna 2001). The inter-individual differences were quite large. Ossicular motions became more and more complex with increasing frequency. In Figure I.69 the ossicular motion of one human temporal bone is shown; the malleus showed much larger displacement than the incus. Thus, this showed possible motion in the IMJ. They also compared their results to Willi et al. (U. Willi et al. 2002) and found a perfect match of the rotation component when the z-axis was aligned along the ligament axis perpendicular to the footplate (piston-like component).

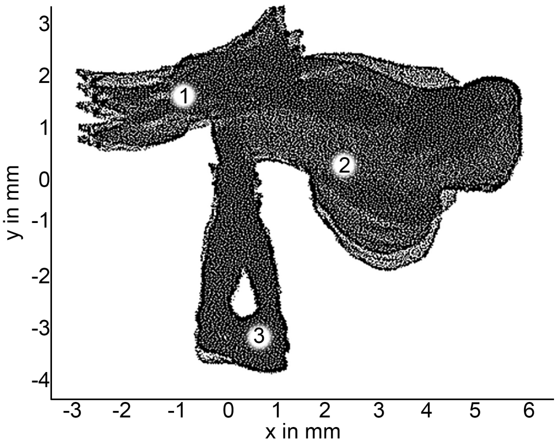

Figure I.69 (1) Malleus, (2) incus, (3) stapes. Ossicular motion of the temporal bone of a 83 year old female donor at 1000 Hz. Displacements were scaled up by a factor of 2000 (to make them visible on the plot). The 'slippage' in the IMJ was described by Decraemer et al. as 'remarkable'. Modified after "Measurement, visualization and quantitative analysis of complete three-dimensional kinematical data sets of human and cat middle ear", Decraemer, W.F., Khanna, S.M., In: Gyo, K., Wada, H., Hato, N., Koike, T. (Eds.), Middle Ear Mechanics in Research and Otology. World Scientific, Singapore, with kind permission of World Scientific Publishing Co Pte Ltd, Copyright © 2014 World Scientific (Decraemer & Khanna 2004).

Recently, Decraemer et al. (Decraemer et al. 2014) observed the 3-D motion of the ossicles in the gerbil (see chapter I.III.2.5.3.5.2). For all examined species – including human, cat, and gerbil – the vibration mode became more complex and more relative motion was seen in the IMJ and ISJ at higher frequencies (Decraemer et al. 2014). The vibration mode was expected to change with the mass of the ossicles; the larger the ossicle (human > cat > gerbil) the larger the mass – and therefore, the vibration mode change occurs at lower and lower frequencies. Indeed, the vibration mode was found to become complex at ~2 kHz in human, at ~3 to 4 kHz in cat, and at ~8 to 10 kHz in gerbil. They doubted that the large slippage in the human IMJ 'that looked as thought a decoupling between malleus and incus took place, … really happens in the healthy living ear' (Decraemer et al. 2014). For the five different human temporal bones that they measured, they found the incus rotation to be about 0.8 of the malleus rotation at low frequencies, and only 0.15 of the malleus rotation above 2 kHz – similar to the large slippage found by Sim et al. (J. H. Sim et al. 2004) and Willi et al. (U. Willi et al. 2002). They argue that their measurements of human ossicular vibration (Decraemer & Khanna 2004) were biased in two ways:

1. Age bias: The measurements were performed in temporal bones of elderly donors. Thus, most of the donors were expected to suffered from high-frequency hearing loss, which may also involved a middle-ear component (see chapter IV.II.3.4).
2. Post-mortem bias: The measurements were performed with a minimum of three or four days after death (see chapter IV.II.3.2). A post mortem stiffening may occurred (e.g., of the annular ligament) "although this is not supported by Chien et al. (Chien et al. 2009b) who did not find substantial differences in stapes motion between living human and temporal bone measurements" (Decraemer et al. 2014).

Decraemer et al. (Decraemer et al. 2014) suggested further measurement to answer the question whether the slippage in the IMJ in human middle ears is genuine or a post mortem artefact.

I.III.2.5.3.3.5 A. Huber

The 1st Symposium 'Middle ear mechanics in research and otosurgery' (MEMRO) in Dresden in 1996 was initiated by K.-B. Hüttenbrink. At this symposium, Huber et al. presented their findings about the vibration of the ossicles in the three dimensional space (A. Huber et al. 1997). They found the IMJ to be mobile at higher frequencies (see Figure I.70). In detail, four fresh frozen human temporal bones stored (no longer than 6 days in merthiolate solution after defrosting) were used for the experiments. Acoustical stimulation (pure tones from 100 Hz to 10 kHz) was used at moderate sound pressure levels (74 to 110 dB). The motion of the ossicles was measured with an LDV system (see chapter II.IV) at different points on the ossicles, with reflective balls positioned held by capillary force (to improve the signal-to-noise ratio). The ossicles were assumed to be rigid bodies without banding; based on preliminary data that showed no bending in the handle of the malleus within the speech frequencies (see chapter II.II). Therefore, in the three-dimensional space 6 degrees of freedom needed to be determined (see chapter III.II.2). The motion of the ossicles was measured at these points (six per ossicle) where the balls were attached. Three points where measured for the x-axis, two points for the y-axis and one for the z-axis. The rotational axis was defined as the point with the minimal translational movement in each ossicle, and finally, the rotational axis of the malleus and the incus had 'virtually the same rotation axis'. The axis was through the anterior malleolar ligament and the short process of incus at 500 Hz, and moved slightly superior with increasing the frequency.

As mentioned, they found the IMJ to be mobile at higher frequencies, showing differences in displacement and phase angle between the umbo and the lenticular process of the incus (see Figure I.70). This ‘could not be explained by the rotational axis’; the malleus and incus moved about the same axis. Thus, relative motion occurred in the IMJ. The ‘slippage’ in the IMJ at high frequencies was around 6 dB transmission loss (see Figure I.70). Huber et al. also observed this slippage quantitatively in a computer animation; showing a minimal ‘slippage’ at low frequencies below 1 kHz – increasing at higher frequencies.

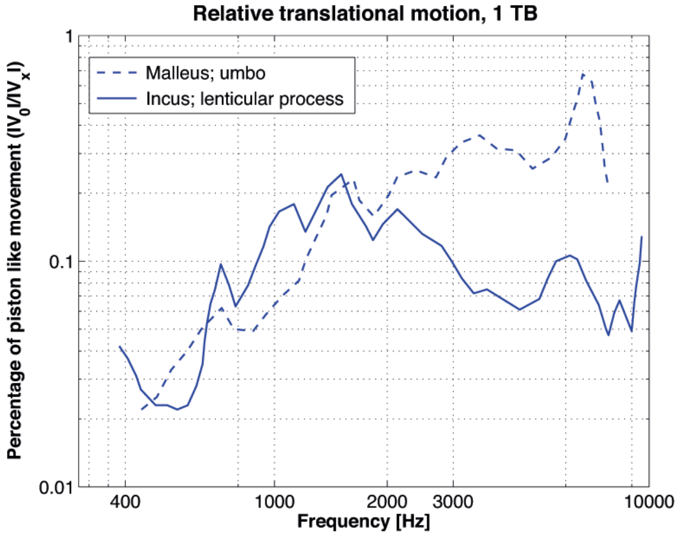

Figure I.70 Huber et al. showed ‘slippage’ in the IMJ. The relative translational motion is shown between the malleus (umbo) and the incus (lenticular process) in the three-dimensional space for one temporal bone at 80 dB SPL. The percentage of the piston like motion was calculated $IV_0//IV_xI$; Vx was the velocity vector at the umbo and at the lenticular process respectively. Modified after (A. Huber et al. 1997) Fig 2.

I.III.2.5.3.3.6 C.F.E. Offergeld

Similar to Cancura, Offergeld was confident that the function of the joints (ISJ and IMJ) is a protection function for the inner ear during high-pressure changes by decoupling the ossicular chain (C.F.E. Offergeld 2000, Cancura 1980). He refers to a previous study (Hüttenbrink 1988d), where the displacement of the stapes increased three times under high-pressure stimulation, if the joints were immobilized. Therefore, the displacement of the stapes with a LDV system (see chapter II.IV) were measured for the normal human middle-ear (10 fresh temporal bones) and with immobilized middle-ear joints (C.F.E. Offergeld 2000). The process of the artificial immobilization of the IMJ was described as follows: “After opening the superior joint capsule, the synovial fluid was removed by suction and a droplet of Cyanoacrylate (Histoacryl ®) was administered to the joint cleft. Tiny mechanical movements of the ossicles led to correct distribution of cyanoacrylate throughout the incudo-malleal joint (intracapsular fixation), with no danger of fixation of ligaments, ossicles, tympanic membrane and/or tympanic cavity from leakage of glue material (Offergeld 2000).” Offergeld stated that he used the same method as Hüttenbrink described (Hüttenbrink 1988c). A decrease of the stapes displacement at low frequencies and a small increase at high frequencies was examined after the immobilization of both joints (ISJ & IMJ) (see Figure I.71). According to this resonance shift to higher frequencies after immobilization of the joint, Offergeld concluded that the ossicular chain may not be "absolutely stiff for acoustic sound transfer" (C.F.E. Offergeld 2000). However, the differences of the stapes displacement were in the range of 5-10 dB and, therefore, it was assumed to be unlikely that this effect is clinically relevant.

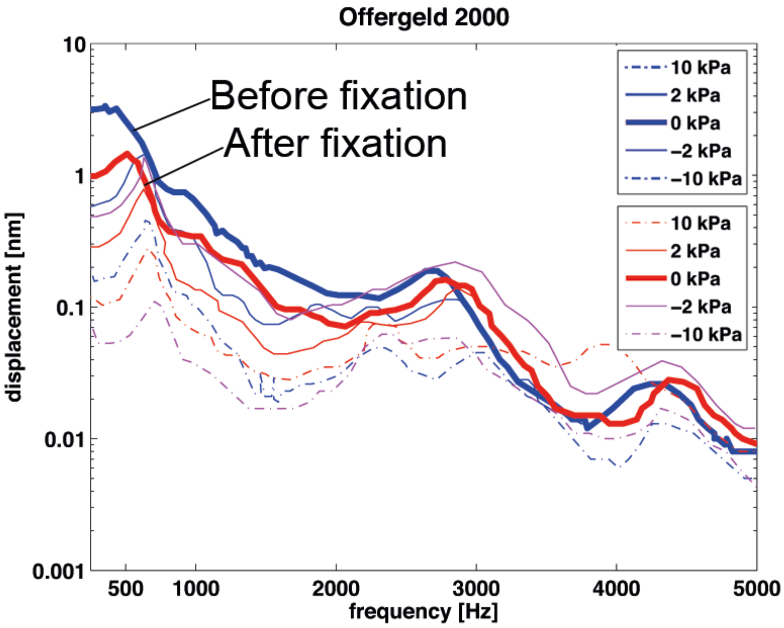

Figure I.71 Displacement of the stapes before and immobilization of the joints in the middle ear under different pressure conditions. At 0 kPa (94 dB SPL at 1000 Hz), a decrease of the stapes displacement at low frequencies and a small increase at high frequencies was examined after the immobilization of both joints (red lines). This is a simplified and condensed illustration of the data shown in the graphs of (C.F.E. Offergeld 2000).

Looking at the influence of high-pressure changes on the displacement of the stapes, Offergeld found a decrease between 250 Hz and 3 kHz (maximal drop at ± 10 kPa) in normal middle ears. Contrary to the normal-middle ear condition, the immobilization of the joints leads to a "more accentuated and sudden decrease" of the displacement of the stapes at low frequencies and an increase at high frequencies (C.F.E. Offergeld 2000).

In a second study, Offergeld (C. Offergeld et al. 2007) showed the consequences of the immobilization of the single IMJ, single ISJ and both joints, to show their effect on the function of the reconstructed middle-ear (e.g. prosthesis). Twelve fresh human temporal bones were measured; six with immobilization of the IMJ first, followed by the ISJ – and six with the immobilization of the ISJ first, followed by the immobilization of the IMJ. The immobilization of the joints was performed using cyanoacrylate glue (Histoacryl®); "A droplet of Histoacryl® was administered into the joint cleft and distributed properly within" (C. Offergeld et al. 2007). The sound excitation was a multisinus of 94 dB SPL at 1 kHz between 125 Hz and 5 kHz. The stapes vibration was measured with an LDV system.

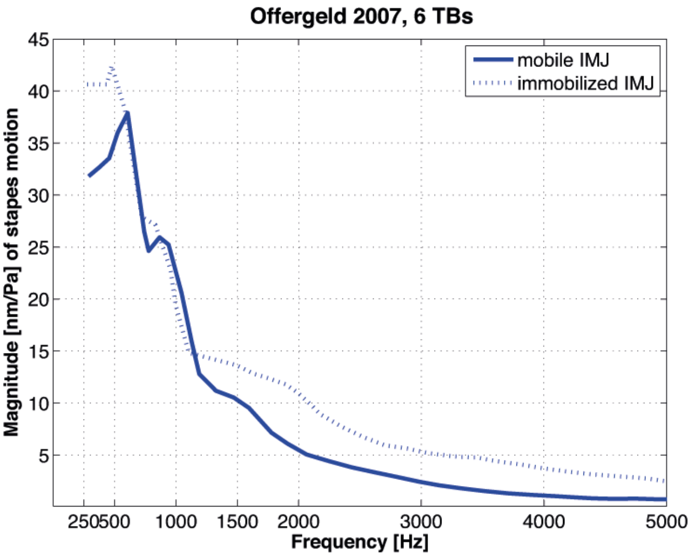

Figure I.72 Magnitude of the stapes motion with mobile IMJ and after immobilization of the IMJ; with 94 dB SPL at 1 kHz. The magnitude increases less than 10 dB at middle and high frequencies (1.2 kHz to 5 kHz) after immobilization of the IMJ. Modified after (C. Offergeld et al. 2007)

After the immobilization of the IMJ, the stapes motion amplitude increased between 1.2 and 5 kHz. This increase was less than 10 dB for all the frequencies. The immobilization of the ISJ showed additionally a decrease of the stapes motion amplitude at low frequencies (below 1.2 kHz). Immobilizing both joints showed again a decrease at low frequencies and more prominent increase at higher frequencies (1.2 kHz to 5 kHz).

I.III.2.5.3.3.7 U. Willi

Willi – a former PhD student in the Department of Otorhinolaryngology of the University Hospital of Zürich – composed a very detailed dissertation (U. Willi 2003) about the IMJ-mobility in human temporal bones. He found the IMJ to be flexible represented by a relative motion difference of the two ossicles at physiologically relevant levels (75-90 dB SPL). A clear difference between the motions of the two bones was found in the rotational component along the axis through the short process of the incus and the head of the malleus. These relative motions between the malleus and the incus contributed to the steep slope in the middle-ear TF between 1 and 3 kHz (see Figure I.75).

In detail, the motion of incus and malleus were examined in nine fresh human temporal bones using a scanning laser doppler vibrometer (SLDV) (see chapter II.IV.1.3) (U. Willi et al. 2002). Two types of acoustic stimuli were used; a multi-sine (to measure the IMJ-motion) and a periodic chirp (to measure at the umbo or the lenticular process of the incus) (U. Willi et al. 2002). The SLDV measures the vibration in one direction. Therefore, only three out of six degrees of freedom (see chapter II.II.2) of the vibration for each, malleus and incus, could be reconstructed (see Figure I.73); one translational (*vt*; towards SLDV-Beam) and two rotational (ω_x, ω_y; orthogonal plane to SLDV-beam) components.

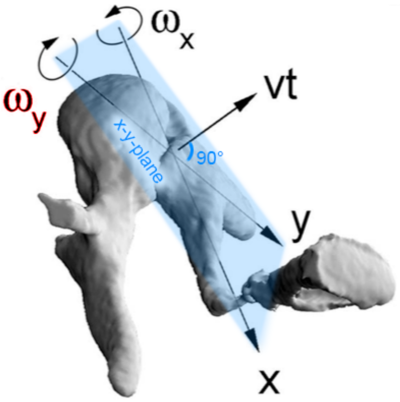

Figure I.73 Three motion components for the ossicular motion at the IMJ; one translational (vt; towards SLDV-Beam) and two rotational (ω_x, ω_y; orthogonal plane to SLDV-beam) components. Modified after Hearing research, Vol. 137, Willi, U., Ferrazzini, M. A., Huber, A. M., "The incudo-malleolar joint and sound transmission losses", figure 2, pp. 32-44. Copyright 2002, with permission from Elsevier Science (U. Willi et al. 2002).

The transfer function was calculated as follows:

$$TF = \frac{vibration\ amplitude\ of\ the\ incus}{vibration\ amplitude\ of\ malleus} = \frac{\underline{R_I}}{\underline{R_M}} = \frac{R_I}{R_M} \times e^{-i\omega(\varphi_I - \varphi_M)} \quad \text{(U. Willi et al. 2002)}$$

The TF becomes 1 if the IMJ allows no relative motion between the two ossicles, when the three components (vt, ω_x and ω_y) are equal. Thus, the IMJ would be functionally immobilized. Contrary, if the IMJ is mobile, a value of the TF < 1 indicates a transmission loss for some components. The mean of the TFs for the three motion components are shown in Figure I.74; all motion components showed a frequency dependent transmission loss to different extent (see Figure I.74). However, the ω_x-component was found to be "negligible small", and the vt-component was smaller compared to the ω_y-component (U. Willi et al. 2002). Additionally, the vt-component showed large inter-individual differences. Only R-ω_y showed similar characteristics for all nine temporal bones. Willi et al. regarded this rotation about the y-axis (ω_y) as "the most important component because the amplitude and phase of its TF approximate very well those of the TF between the umbo and the lenticular process of the incus" (U. Willi et al. 2002). This dominant ω_y transmission losses coincidence with the findings of Goode et al (Goode et al. 1994) (see chapter I.III.2.5.3.3.1), who described a decrease of 12-15 dB/octave in the middle-ear TF between 1 and 3 kHZ similar to Willi et al.

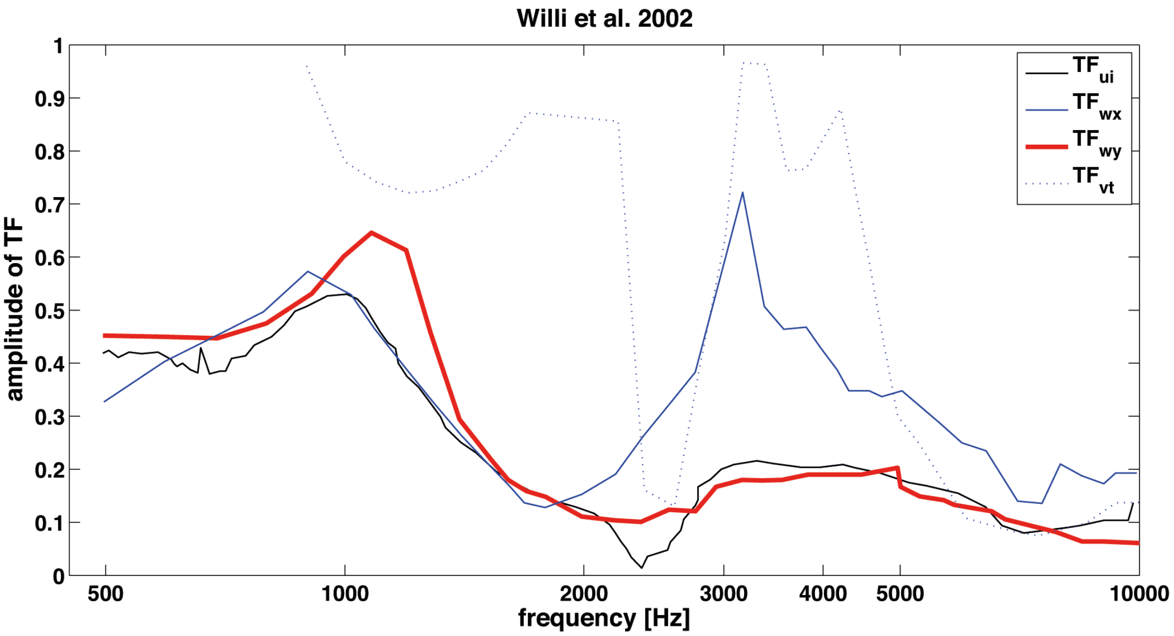

Figure I.74 Mean amplitudes of TFs at the IMJ (R-ω_x, R-ω_y and R-vt) and between the umbo and the lenticular process of the incus (R-ui) at 90 dB SPL. Below 2 kHz; R-ui is approximately by R-ω_x and R-ω_y. The dip in R-ui is only present in R-vt. R-ω_y showed a similar frequency response like R-ui. Modified after Hearing research, Vol. 137, Willi, U., Ferrazzini, M. A., Huber, A. M., "The incudo-malleolar joint and sound transmission losses", figure 7, pp. 32-44. Copyright 2002, with permission from Elsevier Science (U. Willi et al. 2002).

A small transmission loss occurred at low frequencies (below 1 kHz), followed by a steep loss between 1 and 3 kHz and high transmission losses between 3 kHz and 10 kHz.

The IMJ was experimentally immobilized in a next step, to show that the sound transmission losses are a consequence of the joint flexibility (U. Willi 2003). He opened the joint capsule with a sickle knife and infused acrylic resin in order to entirely immobilized the IMJ. However, the loss of sound transmission caused by the flexibility of the joint could almost be compensated by the gain in sound transmission achieved by the immobilization of the IMJ (see Figure I.75). An effect was only prominent above 1.5 kHz (see Figure I.75); this effect was frequency dependent and increased with increasing frequency (up to +10 dB between 4 and 10 kHz).

From both measurements Willi finally concluded that "the IMJ constitutes an elastic component of the ossicular chain, which causes significant sound transmission losses (about -10 dB) at higher frequencies (> 3 kHz). However, at the low frequencies (< 1 kHz) sound transmission is not affected by the rigidity of the IMJ" (U. Willi 2003).

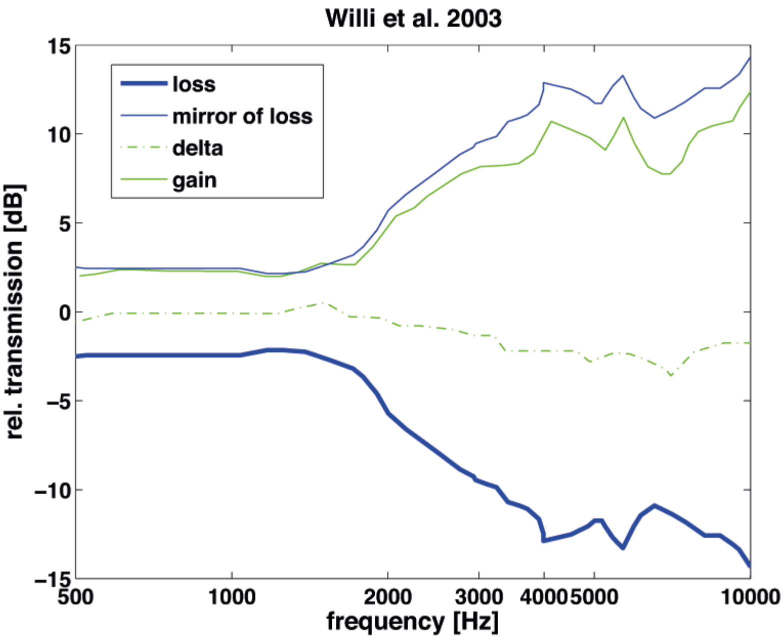

Figure I.75 Immobilization of the IMJ in 14 human temporal bones. The loss of sound transmission caused by the flexibility of the joint (loss) could almost be compensated by the gain in sound transmission (gain) achieved by the immobilization of the IMJ, which is shown by the green dashed line (delta). Modified after (U. Willi 2003) with kind permission of Urban Willi.

Willi also examined a possible effect of the post-mortem time, gender and age of the donor on sound transmission (U. Willi 2003). None of these factors significantly influenced the measurement, however, a tendency of a decreased sound transmission at high frequencies (> 3 kHz) was observed.

I.III.2.5.3.3.8 T. Zahnert

Zahnert (Zahnert 2003) focused on the laser measurement techniques in hearing research. In this context he also published LDV data on umbo and stapes motion with an intact human ossicular chain, an artificially immobilized IMJ and a subluxated IMJ (see Figure I.76) under acoustic stimulation (0.25-5 kHz). The sound transmission with an artificially immobilized IMJ with glue was similar to the normal middle-ear sound transmission; only a small increase of the stiffness of the ossicular chain up to the first resonance frequency resulting in a loss of stapes motion magnitude of approximately 5 dB was reported by Zahnert (2003, pp. 168). Figure I.76 B shows the comparison between the stapes motion with a mobile versus immobilized IMJ. It is assumed that only one measurement is presented, and though the result needs to be interpreted with care. However, Zahnert assumed the IMJ to be mobile (see Figure I.77). The umbo vibration only showed small changes after the subluxation of the IMJ, contrary, the stapes motion diminished up to -20 dB.

Five years later, Zahnert (Zahnert 2007) published the vibration mode of the human ossicular chain at 4 kHz (see Figure I.77). He also referred to the measurements of Decraemer et al. (Decraemer & Khanna 2000, Decraemer et al. 1991) that showed a complex vibration mode with translational and rotational motion components at higher frequencies under acoustic stimulation (see chapter I.III.2.5.3.3.4).

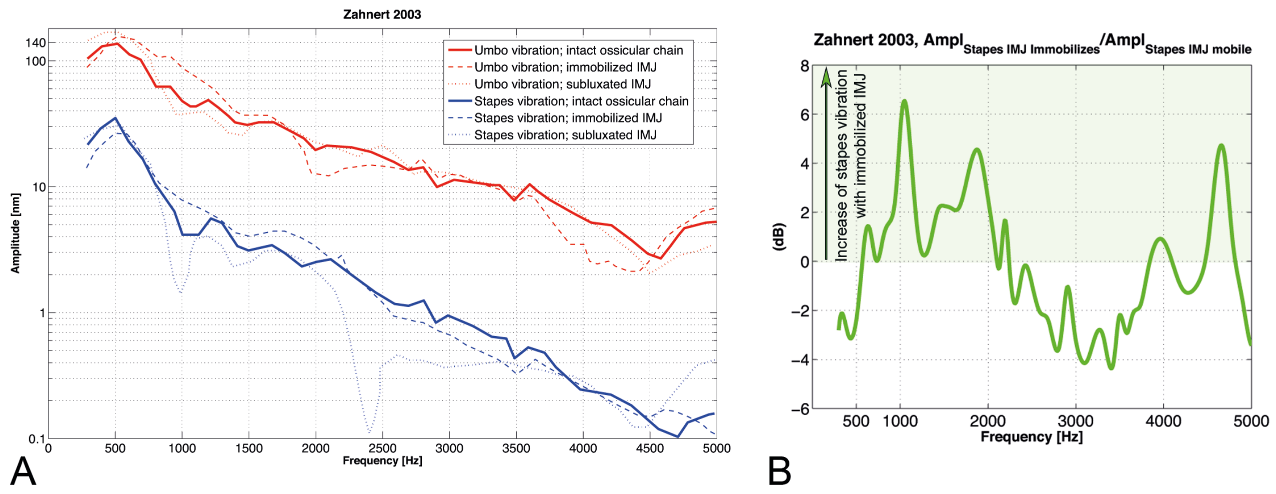

Figure I.76 (A) Vibration amplitude of the umbo and stapes; with an intact ossicular chain, artificially immobilized IMJ and subluxated IMJ. (B) Stapes motion with immobilized vs. mobile IMJ. The immobilization of the IMJ induced changes of the stapes motion of around 6 dB at 1 kHz. Modified after (Zahnert 2003).

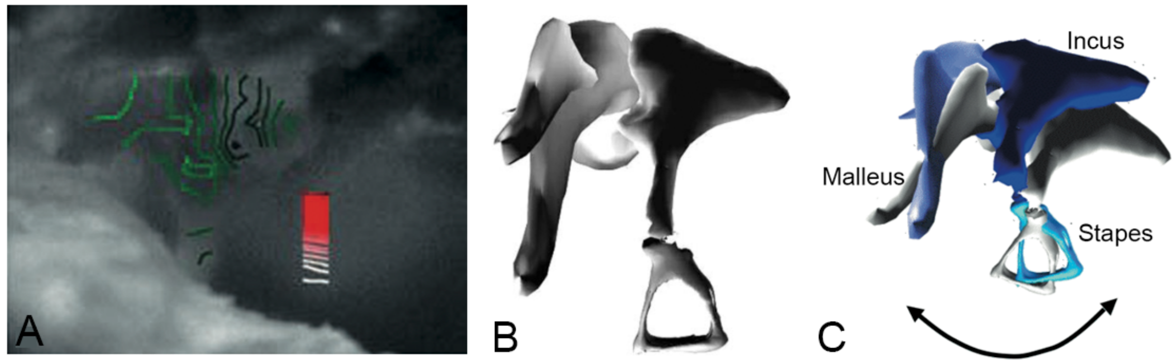

Figure I.77 (A) LDV measurement at the IMJ; relative motion in the IMJ with rotation of the malleus visible due to iso-amplitude lines at 2.5 kHz 90°. (B) Model of slippage in the IMJ (C) Vibration mode of a human ossicular chain showing the complex vibration mode at 4 kHz. Modified after (Zahnert 2007, Zahnert 2003). Permission for reprint of A and B achieved from © Georg Thieme Verlag KG and (C) reprinted with kind permission of TU Dresden.

I.III.2.5.3.3.9 J.H. Sim

Sim et al. (J. H. Sim et al. 2004) described the behavior of the IMJ in the isolated malleus-incus complex, where the stapes and eardrum were dissected and the malleus-incus complex was driven by a tiny magnet attached to the umbo and current conducting coil mounted around the annulus rim of the eardrum. With the laser Doppler vibrometer, relative rotations between the malleus and incus were observed clearly for a rotation component along the anterior-to-posterior direction at low frequencies (270 Hz to 4 kHz) (J. H. Sim et al. 2004). More precisely, the motion of the malleus-incus complex was almost purely rotational motion about the axis orthogonal to the malleus handle, below the first resonance (550 Hz). With increasing frequencies, the motion became more complex and slippage between the two ossicles at the IMJ was detected (J. H. Sim et al. 2004). The rotational motion about the axis orthogonal to the malleus handle at the joint was observed for all frequencies, while the rotation about the axis perpendicular to the plane of the tympanic annulus at the joint was observed only at 4 kHz (J. H. Sim et al. 2004).

I.III.2.5.3.3.10 H. Nakajima

The work by Nakajima et al. (Nakajima et al. 2005) reported that the IMJ also provided flexibility for different physiological states of the middle-ear ossicular chain. The measurements were performed with a chirp (0.025-20 kHz) with a RMS level of 105–114 dB SPL, and the ossicular motion was measured with a LDV system “focused on a 0.25 mm^2 reflector made of 50 µm diameter polystyrene micro beads glued on plastic tape”. The physiological states were changed by means of ‘fixation’ of the ossicles, respectively, attachments of ossicles to the surrounding temporal bone. These ‘fixations’ showed an effect on the umbo and stapes velocity; “fixations of the stapes or incus produce larger reductions in sound-induced stapes velocity (as much as 40–50 dB with extensive stapes fixation), than reductions in umbo velocity (typically less than 10 dB). Fixations of the malleus produce similar-sized changes in both umbo and stapes velocity.” Thus, the study reported a difference between the relatively small change in umbo velocity and the decrease in stapes velocity, which indicated flexibility in the ossicular chain between the incus and the umbo; most likely due to flexibility in the IMJ (Nakajima et al. 2005). Their finding of a significant flexing of the two ossicular joints was in agreement with previous reports (Gyo et al. 1987, Goode et al. 1994, U.B. Willi et al. 2004, U. Willi et al. 2002, Decraemer & Khanna 2004).

Furthermore, Nakajima et al. suggested that an additional improvement in hearing occurred during evolution with an increase in the stiffness of the IMJ, as “it ceased to constrain jaw motion and was involved only in coupling acoustic signals” (Nakajima et al. 2005).

I.III.2.5.3.4 Table with overview of functional mobility of the IMJ during sound transmission

	IMJ **immobile** during sound transmission	IMJ **mobile** during sound transmission	investigation properties	artificial immobi-lization of the IMJ
19th Century				
(Weber 1851)	“Beide Gehörknöchelchen sind zwar durch ein Gelenk verbunden, welches aber so gebildet ist, dass es denselben in der auf die Achsensenkrechten Drehungsebene keine Bewegung gegen einander gestattet, so dass sie sich also nur gemeinschaftlich in derselben bewegen können, wie es der Fall sein würde, wenn sie gar kein Gelenk hätten und nur ein einziges Knochenstück wären”		macroscopically	
(von Helmholtz 1869) see chapter I.III.2.5.3.2.1	“Malleus and incus moved together, but…”	”…the resilience of the IMJ allows a moderate degree of independent mobility”	macroscopically, rough mechanical testing	
(Politzer 1864, Politzer 1873) see chapter I.III.2.5.3.2.3		x	Optical method: glass fibers glued on ossicles, variable static air pressure	
(Buck 1869) see chapter I.III.2.5.3.2.2	”ossicles move as a whole, but…”	“… different displacement amplitudes for malleus and	Optical method: reflecting light spots,	

		incus”	dynamic stimulation at low frequencies	
(Mach & Kessel 1874) see chapter I.III.2.5.3.2.4		x	Optical methods: Method 1: stroboscopy Method 2: mirrors glued on ossicles	immobilization of the IM with wax; reduced excursion of malleus
20st Century				
(Frey 1911) see chapter I.III.2.4.4.1.1	x		morphology	
(Frank 1923) see chapter I.III.2.5.3.2.5		x	mathematical model	
(Dahmann 1930, Dahmann 1929) see chapter I.III.2.5.3.2.6	(x fixed rotation axis)	**transmission loss** due to relative motion in the IMJ is compensated by the lever ratio	optical method, mirrors glued on ossicles, static and dynamic stimulation	
(Stuhlman 1937) see chapter I.III.2.5.3.2.8		motion during inward motion of malleus handle	oversized model (20x)	
(Bárány 1910, Bárány 1938, G. Békésy 1960, G. Békésy 1939, G Békésy 1936b) see chapter I.III.2.5.3.2.9 and chapter I.III.2.5.3.2.7	malleus-incus complex as a rigid body, without acknowledging its articular movement		dynamic stimulation, capacitive probe measurement	
(Gill 1951) see chapter I.III.2.5.3.2.10	“the heads of the malleus and incus move together as one. Even at very high sound pressure levels they do not separate.”		optical method: stroboscopic light	
(Kobrak 1959) see chapter I.III.2.5.3.2.11		x static x dynamic x motion picture study	optical method: mirrors glued on ossicle, static and dynamic stimulation, motion picture study, high sound pressure levels	
(Kirikae 1960) see chapter I.III.2.5.3.2.12	up to 140 dB immobile IMJ	at very high static pressure (154 dB)	optical method: double-exposure photographs, electrical method: condenser & cathode ray oscillograph	
(Harty 1964) see chapter I.III.2.5.3.2.13	immobile IMJ under physiological conditions	mobile IMJ under excessive stimulation	morphology	
(Elpern et al. 1965) see chapter I.III.2.5.3.2.14	x		Dynamic stimulation, condenser microphone at round window	no changes in the round window displacement with immobilized IMJ
(Fischler et al. 1967)	common axis of rotation (with drained cochlea): “the vibrations of the tympanic membrane at the umbo and along the junction with the malleus were in synchrony with those of the stapes”		capacitive-probe vibration meter	
(Gundersen 1971, Gundersen & Høgmoen 1976) see chapter I.III.2.5.3.2.17	x x		stroboscope time average holography	
(Marquet et al. 1973) see chapter I.III.2.5.3.2.15		x	mechanical model	
(Marquet 1981) see chapter I.III.2.5.3.2.15	x		morphology	
(Cancura 1980) see	immobilized under	mobile under large sound	static excitation with a	

chapter I.III.2.5.3.2.16	physiological stimulation	pressure stimulation; above 1 mN static excitation (≈ around 120 dB)	electromagnetic probe, metal core in coil of oscillator	
(Brenkman et al. 1987) see chapter I.III.2.5.3.2.20	IMJ functionally immobilized		SQUID, dynamic stimulation	
(Gyo et al. 1987) see chapter I.III.2.5.3.2.18	functionally immobilized IMJ, change of rotational axis of IMJ	'loosening' of the IMJ, transfer function increases above 1 kHz	dynamic, video measuring system, stroboscope, require high non-physiologic sound pressure levels	incus motion did not increase with immobilized IMJ
(Hüttenbrink & Pfautsch 1987, Hüttenbrink 1988d, Hüttenbrink 1988c) see chapter I.III.2.5.3.2.19	Immobilized under physiological excitation immobilized under physiological excitation	Motion possible under high sound pressure levels Motion possible under high sound pressure levels (6 out of 9 samples showed mobility in the IMJ)	Morphology, SEM Static air pressure changes, optical technique and videotaped radiographic examinations	
(Goode et al. 1993, Goode et al. 1994) see I.III.2.5.3.3.1	immobilized under physiological excitation	found difference in malleus and incus motion, but stated that this was caused by 'translation displacement of the rotational axis', bending at high pressure changes	Dynamic excitation, LDV	statement of Goode in Huber et al. 1997; no change found due to insufficient immobilization?
(Tay & Mills 1996) see chapter I.III.2.5.3.3.2	immobilized under physiological excitation	mobile at extremely high sound pressure levels	photography technique, superimposing images	
(A. Huber et al. 1997) see chapter I.III.2.5.3.3.5		Mobile IMJ at higher frequencies	dynamic stimulation, LDV	
(Schön & Müller 1999) see chapter I.III.2.5.3.3.3		x they were not uncertain whether the IMJ is also mobile in the process of hearing	dynamic stimulation, LDV	
(Decraemer & Khanna 1999, Decraemer & Khanna 2001, Decraemer et al. 2014) see chapter I.III.2.5.3.3.4		'substantial amount of slippage' in the IMJ – even at low frequencies (only 2 samples); only post-mortem effect 'large amount of slippage' in the IMJ – even at low frequencies recently; doubted whether the slippage 'really happens in the living ear'	LDV, dynamic stimulation LDV, micro-CT, dynamic stimulation LDV, dynamic stimulation	
21st Century				
(C.F.E. Offergeld 2000, C. Offergeld et al. 2007) see chapter I.III.2.5.3.3.6	5-10 dB difference in stapes motion; unlikely that this effect is clinically relevant	ossicular chain may not be "absolutely stiff for acoustic sound transfer"	LDV, dynamic stimulation	frequency-dependent changes
(U. Willi 2003, U. Willi et al. 2002) see chapter I.III.2.5.3.3.7		x > 1 kHz	SLDV, acoustic stimulation	frequency-dependent changes
(Zahnert 2003) see chapter I.III.2.5.3.3.8		x	SLDV, acoustic stimulation	almost no change
(J. H. Sim et al. 2004) see chapter I.III.2.5.3.3.9		x	Isolated MIC, tiny magnet as stimulator, LDV	
(Nakajima et al. 2005) see chapterI.III.2.5.3.3.10		x	LDV, dynamic stimulation	

Table I.6 Overview of functional mobility of the IMJ during sound transmission

I.III.2.5.3.5 Function of the IMJ in mammals

Many studies regarding the IMJ mobility and function were based on measurements in animals (e.g., cat, guinea pig, chinchilla, gerbil, rabbit). These measurements cannot directly be adapted to humans due to the differences in the anatomy. Nevertheless, in-vivo measurements in the middle ear are rather realizable than in humans. Intra-operative measurements of acoustically stimulated stapes motion were performed for the first time by Huber et al. (A Huber et al. 2001) by means of LDV (see chapter IV.II.3.2) methods. Puria et al. (Puria et al. 2007) found the IMJ to be fused in some animals like guinea pig (J.J. Zwislocki 1963, Henson 1974) and chinchilla and, thus, there is no mobility in the IMJ (Puria & Steele 2010b). However, there are some findings that show mobility in the IMJ of specific animals e.g., cat and gerbil. The larger the ossicles of the species are (human>cat>gerbil), “the larger the mass is, and, due to inertial effects (mass or inertial moments), it is reasonable to expect that the vibration mode will change at lower and lower frequencies” (more complex vibration modes starting at ~2 kHz in human, ~3 to 4 kHz in cat, and ~8 to 10 kHz in gerbil) (Decraemer et al. 2014). Relative motion between the malleus and incus was found in all three species at high frequencies (Decraemer et al. 2014). The findings for cat and gerbil are listed in the following subchapters by author.

I.III.2.5.3.5.1 Cat

The anatomy of the middle ear of the cat is illustrated in Figure I.78. Mobility of the IMJ in cats was discussed by several authors (Tonndorf & Khanna 1966, Guinan & Peake 1967, Decraemer & Khanna 2000, Decraemer & Khanna 2004).

Tonndorf & Khanna (Tonndorf & Khanna 1966) found the IMJ in living cats to be immobile for frequencies above 50-60 Hz. Similar findings have been published three years before by Møller (A.R. Møller 1963). They suggested that the IMJ mimics an ‘friction clutch’ and, therefore, only transmits the acoustic energy without any loss at frequencies greater than 50-60 Hz. Below this 50-60 Hz, the IMJ yielded under pressure. Tonndorf & Khanna assumed a protective function of the IMJ for the inner ear to high pressure changes at low frequencies (e.g., explosion). To obtain the ossicular motion in cats, they stimulated the ossicles to vibrate either acoustically or by another vibrating system. Then, the necessary sound pressure or the deflection amplitude was registered, such that the voltage of the cochlear microphone was 10 μV at the round window. The same method was applied by Wever & Lawrence (Wever & Lawrence 1954), which obtained the transfer function between malleus handle and stapes for the first time in living cats.

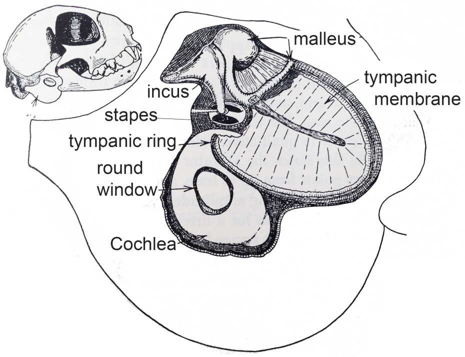

Figure I.78 Anatomy of the middle ear of the cat. Modified after (Wever & Lawrence 1954) Fig 34 pp. 103 with kind permission of Princeton University Press.

One year later, (Guinan & Peake 1967) measured the ossicular motion with stroboscopic illumination (acoustic stimulation 0.03-10 kHz up to 130 dB) in living cats as well and found relative motion between malleus and incus at higher frequencies (above 3 kHz). The stapes and the incus moved slower than the malleus. They felt that slippage in the IMJ as the most likely explanation, although they could not exclude bending of malleus and incus.

In 1991, Decraemer et al. (Decraemer et al. 1991) obtained the mode of vibration of the cat manubrium by measuring its vibration in response to acoustic stimulus between the umbo and the lateral process of the malleus with a heterodyne interferometer. They found the malleus vibration to be frequency dependent: purely translational at some frequencies, rotational at others and mixed at most frequencies. Thus in cats, the classical concept of the malleus rotating around a fixed axis running from the anterior malleolar to the posterior incudal ligament fits to their measurements only at low frequencies. In 1997, Decraemer demonstrated again that the ossicular chain is probably not absolutely stiff for acoustic sound transfer in cats. The malleus, incus and stapes performed 3-D movements during acoustic sound stimulation that were independent of each other, especially at high frequencies (Decraemer & Khanna 1997). Again three years later, Decraemer & Khanna (Decraemer & Khanna 2000) showed mobility in the IMJ and ISJ in fresh temporal bones of cats in their three-dimensional analysis of ossicular vibrations by use of a confocal heterodyne interferometer. A pure tone stimulus (between 80 and 90 dB) was applied. In 2003, Decraemer et al. (Decraemer et al. 2003) published their work about the three-dimensional modelling of the middle-ossicles of human and cat using a commercial high-resolution X-Ray CT scanner.

Decraemer & Khanna confirmed their findings again in 2004 (Decraemer & Khanna 2004), that both human (see chapter I.III.2.5.3.3.4) and cat showed a mobile IMJ, but its frequency dependence is species dependent.

I.III.2.5.3.5.2 Gerbil

Mobility in the IMJ of gerbils was described by de La Rochefoucauld et al. (de La Rochefoucauld et al. 2010) and Decraemer et al. 2014 (Decraemer et al. 2014).

De La Rochefoucauld et al. (de La Rochefoucauld et al. 2010) measured the gain in sound transmission due to the middle ear in gerbil using two different interferometers previously described by (de la Rochefoucauld et al. 2008). The pressure gain between the ear canal and the cochlea was around 25 dB from 2-40 kHz. Additionally, they measured ossicular motion at the umbo, the long process of the manubrium and across the IMJ (80-100 dB). They described a significant delay across the IMJ with additional small delays along the malleus and incus, indicating mobility in the IMJ (see Figure I.79 and in detail: de La Rochefoucauld et al. 2010; Fig.7 and Fig.8).

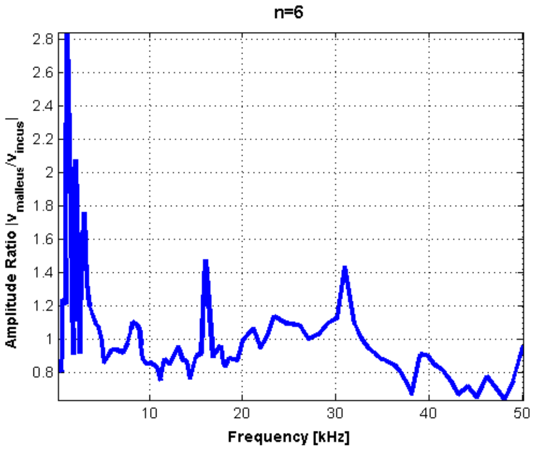

Figure I.79 Mean of six measurements of the ratio of the velocity amplitude across the IMJ in gerbil indicating relative motion in the joint.

Decraemer et al. (Decraemer et al. 2014) studied the three dimensional ossicular motion in gerbils. At higher frequencies (> 8 kHz) the vibration mode became more complex and “more and more relative motion was seen in the IMJ and ISJ” (Decraemer et al. 2014). In their work, they published the vibration modes of several animals at different frequencies (see Decraemer et al. 2014). The ear was stimulated with an earphone in the gerbil’s ear canal (0.25-50 kHz, 80-90 dB), and a reference microphone was placed as well at the edge of the ear canal. The ossicular motion was measured with a non-commercial heterodyne laser interferometer combined with an optical microscope. The same setup was already described by Khanna et al. (S. M Khanna et al. 1996). An intrinsic frame from the measurement data was measured, and an anatomical frame from the reconstructed middle-ear data from micro-CT was calculated (see chapter II.V). Then, the **translation displacements** of the malleus and incus (x-axis from tip of anterior malleolar process (AMP) to posterior incudal process (PIP), and z-axis parallel to piston-like motion of stapes (e.g., see Figure I.80), and the **rotational components** were calculated (see III.II.3.1). The instantaneous rotation axis (“screw axis concept”, spatial location of the screw axis, changes from instant to instant) was shown for the different gerbils to determine the rotational axes from the motion itself. The mode of vibration of malleus and incus of gerbil varied strongly with frequency. Thus, they assumed that the classical model (fixed-axis rotation) is only approximately valid for the gerbil at relatively low frequencies below 10 kHz. No ‘principal axes’ for ossicular chain could be found, contrary to Kirikae’s findings in human temporal bones (Kirikae 1960).

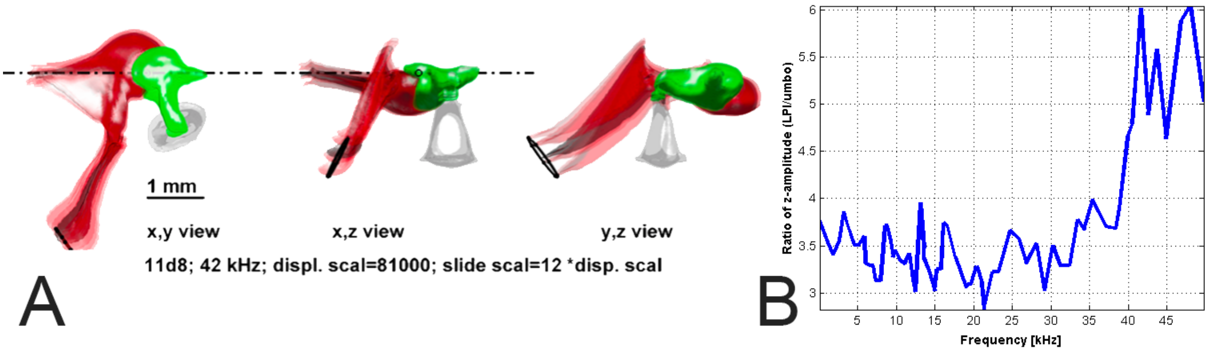

Figure I.80 (A) Motion animation of malleus and incus of a gerbil at 42 kHz. Reconstruction of the gerbil ossicles from micro-CT data. (B) The ratios of the z displacements (parallel to the piston-like direction of the stapes motion) of the umbo relative to the displacement at the lenticular process of the incus (LPI) for one anesthetized gerbil. Reprinted with permission from JARO. Vol. 15, © Springer, figure 12 (A), figure 16 (B), "Three-Dimensional Vibration of the Malleus and Incus in the Living Gerbil". W. F. Decraemer, O. de La Rochefoucauld, W. R. J. Funnell, E. S. Olson (Decraemer et al. 2014).

Buytaert et al. (Buytaert et al. 2011) aimed to assess precise morphological data of the middle ear in gerbils. They combined data from high-resolution micro-CT recordings (showing bony structures in high resolution) with data from high-resolution orthogonal-plane fluorescence optical-sectioning microscopy (OPFOS) (showing both bone and soft tissue in 'unprecedented quality'). The goal was to improve middle ear finite- element modeling (FEM). The IMJ and ISJ were visible as a tight connection by the OPFOS (see Figure I.81). However, they did not find any fluid or open space in the IMJ of the gerbil. The thickness of the IMJ varied from nearly 0 to 51 µm (Buytaert et al. 2011).

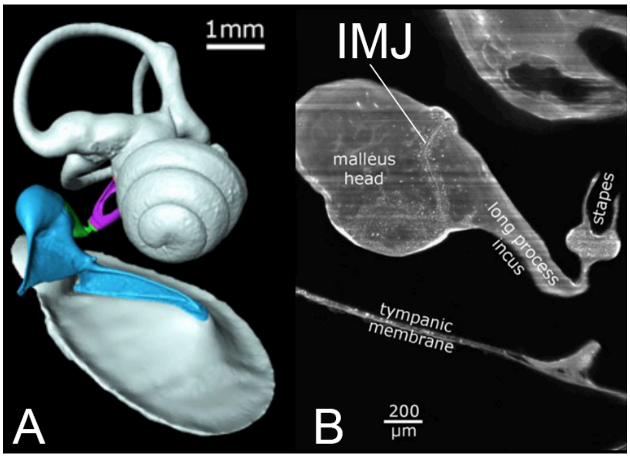

Figure I.81 Reconstruction of a gerbil ear by a combined micro-CT and OPFOS. (A) Malleus (blue), incus (green), and stapes (magenta) (voxel size is 8.5×8.5×8.5 µm) (B) IMJ of the gerbil (pixel size 1.5×1.5 µm). Reprinted and modified after (Buytaert et al. 2011), Springer and the JARO, 12 (6), 2011, Realistic 3D computer model of the gerbil middle ear, featuring accurate morphology of bone and soft tissue structures, Buytaert, J.A., Salih, W. H., Dierick, M., Jacobs, P., Dirckx, J.J., figure 4A and figure 2B, © 2011 Association for Research in Otolaryngology, with kind permission of Springer Science and Business Media.

I.III.2.5.3.6 Protection mechanism

The mobility of the IMJ is still debated. Our projects show changes of the sound transmission in the middle ear after immobilization of the IMJ and, therefore, suggest mobility in the joint under acoustic stimulation of physiologically-relevant levels (see chapter IV.I). Possible functions of the IMJ are discussed in chapter IV.IV. One possibility is a protection mechanism that protects the sensitive structures of the inner ear against high static pressure changes. Several researchers support this idea (Dahmann 1930, Dahmann 1929, G Békésy 1936b, Stuhlman 1937, Kobrak 1959, Kirikae 1960, Gundersen & Høgmoen 1976, Hüttenbrink & Pfautsch 1987, Hüttenbrink 1988a, Hüttenbrink 1988b, Hüttenbrink 1997, Cancura 1980, C.F.E. Offergeld 2000). In case of an immobilization of the middle-ear joints, Offergeld (2000) suggest a three times higher displacement of the stapes footplate into the vestibulum in situations where the ambient pressure changes e.g. wind, swallowing, sneezing, flying or diving. It is not clear whether this is also a possible reason for hearing loss, tinnitus or vertigo in cases of a pathological joint immobilization. Additionally to the researchers that found the IMJ to be mobile under physiological stimulation, some only found slippage in the IMJ with unphysiologically high pressure (Tonndorf & Khanna 1966, Guinan & Peake 1967), where a protection mechanism for the inner ear would be beneficial.

I.III.2.5.3.7 Models of the middle ear

The results of ossicular vibration measurements can serve as a base for the development of middle-ear model. These models then can be helpful to understand the effect of various anatomic modifications (e.g., due to surgery, diseases or accidents) on middle ear sound transmission.

The first mathematical model was developed by Frank (Frank 1923) implicating the acoustic resonator of the middle-ear cavity (Helmholtz resonator) as well as the ossicular chain and the cochlear load.

Modeling of the middle ear using a circuit mode (analog model) has been described by several authors e.g., (A.R. Møller 1961, J.J Zwislocki 1962, E. A. G. Shaw & Stinson 1981, Lynch 1981, Killion & Clemis 1981, Kringlebotn 1988) and was reviewed by Shera and Zweig (Shera & Zweig 1992).

“Finite element modeling has distinct advantages in modeling the middle ear over circuit models that correspond indirectly with its structure and geometry” (Chou et al. 2011). The first finite element (dynamic) model of the middle ear was published by Funnell and Laszlo in 1987 (Funnell et al. 1987), which simulated the cat tympanic membrane. Later on, inertial and damping effects and footplate and cochlear impedance were added to this model (Funnell et al. 1987), and a three-dimensional finite element model of the cat middle ear was later developed (Ladak & Funnell 1996). In 1988, Lesser and Williams (Lesser & Williams 1988) created a 2-D cross-sectional finite element model of the human tympanic membrane with the malleus. They also analyzed the static displacements of the tympanic membrane and malleus under a uniform load (Lesser & Williams 1988). Some authors also examined the effects of several tympanic membrane parameters on the natural frequencies in a finite element model of the human tympanic membrane (Lesser et al. 1991, Williams & Lesser 1990, Williams et al. 1995). Wada et al. (Wada et al. 1992) created a 3-D finite element model of the middle ear to investigate vibration patterns at resonance frequencies in normal and pathologic middle ears including the tympanic membrane and ossicles; considering also the cochlear impedance and stiffness of the annular ligament of the tympanic membrane. Some years later, finite element models with more accurate middle ear geometry were presented (Beer et al. 1997, Beer et al. 1999). Beer et al. (Beer et al. 1997, Beer et al. 1999) obtained the middle ear geometry by laser scanning microscopy. An other 3-D model including the tympanic membrane, the ossicles, and some attached soft tissues was created by Prendergast et al. (Prendergast et al. 1999). Koike et al. reported an updated and refined finite element in 2002 (Koike et al. 2002). Several authors compared the transfer characteristics of the middle ear using finite element models to previous studies (Sun et al. 2002, Gan et al. 2002, Gan et al. 2006). In 2011, Chou et al. (Chou et al. 2011) developed a finite element model for analysis of the naturally resonant frequency of in- vivo human ossicles. Recently, Volandri et al. developed a numerical model for pathological and academic purposes (Volandri et al. 2011, Volandri et al. 2012, Zhao et al. 2009).

Much research was undertaken on the modeling of the middle ear. Nevertheless, it remains a large uncertainty in the development of a dynamic model for the transfer function characteristics of the human middle ear – several issues can influence the models (Ahn et al. 2013):

1. The inter-individual differences of the geometrical structures of the middle are large (Voss et al. 2008) e.g, differences in energy reflectance between Caucasians and Chinese (Voss et al. 2008, Shahnaz & Bork 2006). Thus, the dynamic response of the middle ear varies mainly due to these differences.
2. The material properties of the different middle-ear components such as the tympanic membrane, joints, tendons, and ligaments, have much uncertainty (Volandri et al. 2011, Volandri et al. 2012).

Therefore, it remains important to validate the models using experimental data.

Recently, Ihrle et al. (Ihrle et al. 2013) modeled the middle ear in a nonlinear elastic multibody system, where the tympanic membrane and the air in the ear canal as well as in the tympanic cavity were considered as elastic bodies.

I.III.2.5.4 Function of the incudo-stapedial joint

The function of the ISJ is not clear yet and data on the functionality ISJ is scarce. However, Zwislocki (J.J Zwislocki 1962) assumed that the flexing of the ISJ is more prominent then that of the IMJ because of the more robust size and more faceted contact surfaces. A degree of flexibility between the incus and stapes in mammals seems likely, considering e.g. in the cat the mainly piston-like motion of the stapes as opposed to the rotational motion of the incus (Funnell et al. 2005). This flexibility of the ISJ may be the case in human as well. A clinical study reported a air bone gap of 11 to 16 dB on cases (n=30) of fibrous ankylosis (=stiffness of a joint due to abnormal adhesion) of the ISJ (Szpunar & Miszke 1970).

In 1987, Gyo et al. (Gyo et al. 1987) found the sound transmission loss at the incudo-stapedial joint to be negligible below 1 kHz; the difference in the displacement between the stapes head and the lenticular process of the incus was less than 2 dB.

Zahnert et al. (Zahnert 2003) found the immobilization of the ISJ to result in a sound transmission loss of 6 dB up to the first resonance (1 kHz) frequency using LDV ossicular vibration measurements at the umbo and the stapes head.

Zhang and Gang (Zhang & Gan 2011) report the experimental measurement of the mechanical properties of the human ISJ with an analytical approach and finite element modeling to describe the mechanical parameters of the ISJ. Eight ISJ samples from human cadaver temporal bones were harvested to measure the tension, compression, and perform stress relaxation and failure tests in a micro- material testing system. They concluded that the ISJ is a viscoelastic structure with nonlinear stress–strain relationship; the ISJ sustained higher force in compression than in tension (Zhang & Gan 2011).

Recently, Alian et al. (Alian et al. 2013) examined the effect of increasing the stiffness of the ISJ with applying cyanoacrylate (=strong fast-acting adhesive) to the ISJ. The joint was assumed as immobilized, if no movement was visually detectable in the ISJ itself while pushing the ossicles with a microsurgical needle. Additionally, they found the incus and stapes moving completely unison after immobilization by measuring the velocity magnitude of the umbo and the stapes (see Figure I.82). A LDV (OFV-302 laser head, OFV-3000 vibrometer controller; Polytec PI) was used to measure ossicular motion. The acoustic stimuli were generated in form of frequency sweeps from 0.2 to 8 kHz at 90 dB SPL. Their results showed that stiffening the ISJ produced an almost equal decrease in peak-to-peak displacement at both the umbo and the stapes footplate, consistent with an increase in ossicular impedance. The decrease was mainly between 400 and 1000 Hz with a statistically significant mean magnitude loss of 6 dB at 740Hz (see Figure I.82) (Alian et al. 2013). Therefore, stiffening of the ISJ resulted only in a very small decrease of the stapes magnitude at 740 Hz, and is probably clinically insignificant.

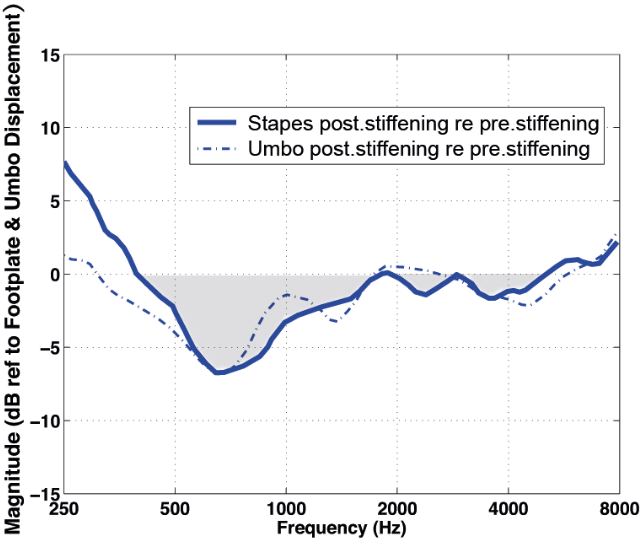

Figure I.82 The stapes footplate vibrations after stiffening are plotted referenced to the stapes footplate vibrations before stiffening (mean values of 5 samples). The ordinates express the ratio in dB displacement. The grey-shaded area shows the stapes footplate vibrations that decreased after stiffening the ISJ (mainly 0.4-1 kHz) with a maximum of 6 dB difference at 740 Hz (significant difference HSD, α = 0.05). Measurements below 400 Hz were may contaminated by background vibration noise. Data were smoothened using a Gaussian kernel with 25 degrees of freedom (Alian et al. 2013). Modified after (Alian et al. 2013).

In a very recent study, the separation of the ISJ did not reduce significantly the middle ear function, even though a decrease in stapes velocity after ISJ separation was found by a single point LDV for all samples (n=5, fresh human temporal bones) (Szymanski et al. 2014). The mean stapes velocity was reduced for 1 dB at 800 Hz, up to 9 dB in frequencies above 1 kHz, and even more reduced at higher frequencies (Szymanski et al. 2014).

Several authors described that abnormalities in the ISJ, such as disarticulation and ankylosis, can induce severe conductive hearing loss or even deafness (Holler & Greenberg 1972, R. J. Sim & Chang 2008, Suzuki et al. 2008).

I.III.2.6 Function of the middle ear muscles and tendons

The function of the suspensory attachments is described in each corresponding chapter: chapter I.I.1.1.1.1 for the malleus (tensor tympani muscle, Figure I.83 Nr. 8), chapter I.I.1.1.2.1 for the incus, and chapter I.I.1.1.3.1 for the stapes (stapedius muscle).

Kobrak (1959) stated that the function of the middle-ear muscles was a protection mechanism for the inner ear. He found that "the stronger the tone", the greater the muscle contraction of the middle-ear muscles. Also Marquet (1981) argued that the middle-ear ossicles should keep the ossicular chain under tension, mainly to prevent from excessive displacement during high pressure changes (von Helmholtz 1869, Wever & Lawrence 1954). Wever and Lawrence (1954) found that the ossicles are "remarkable fragile" when the tendons of the muscles are cut. The middle-ear muscles are also thought to keep the ossicles in an optimal vibrating position for sound transmission (Marquet 1985).

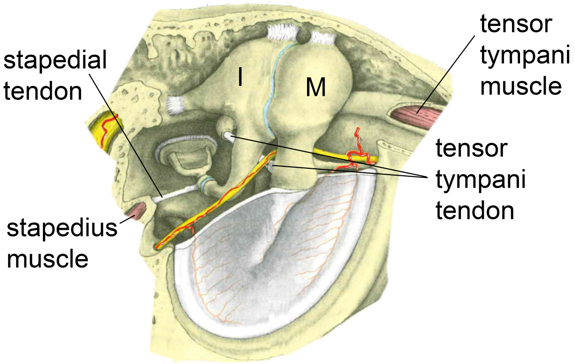

Figure I.83 Middle-ear muscles and the corresponding tendons: (M) malleus, (I) incus. Modified after (Rauber & Kopsch 1987). Permission for reprint achieved © Georg Thieme Verlag KG.

I.III.3 Inner ear

The inner ear consists of the bony labyrinth situated within the petrous part of the temporal bone, a hollow cavity in the temporal bone, with two imbedded organs:

1. Vestibular system: serve as the body's balance organ. The vestibular system is irrelevant for sound transmission, hence, only a brief overview of this organ is given in this work (see chapter I.III.3.1).
2. Cochlea: converting mechanical stimuli from the middle ear into electrochemical impulses, which are passed on to the brain via the auditory nerve (see chapter I.III.3.2).

I.III.3.1 Anatomy and function of the vestibular system

This sensory system provides information about movement and sense of balance to the brain. As movements consist of rotations and translations, the vestibular system comprises two components. On one hand the semicircular canal system, which indicates rotational movements, and on the other hand otoliths, which indicate linear accelerations. The structures of the vestibular system are described in Figure I.84 in detail.

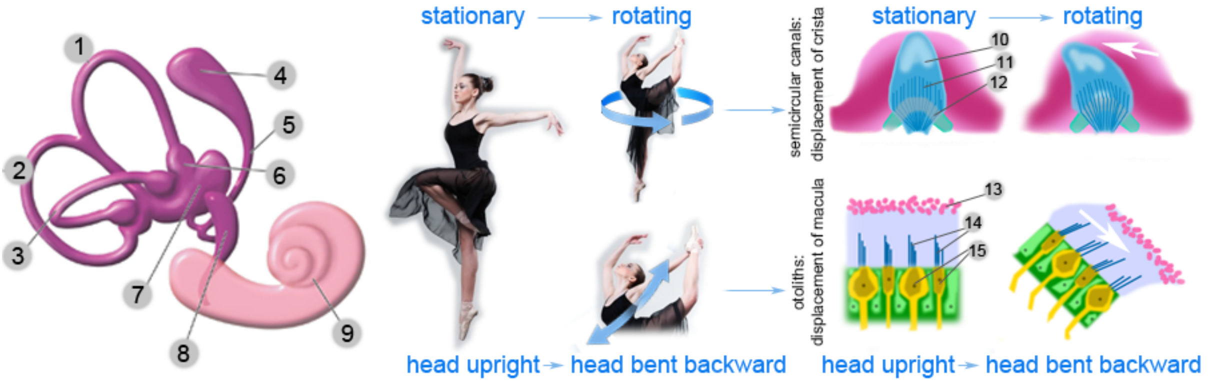

Figure I.84 vestibular system: (1) anterior semicircular canal, (2) posterior semicircular canal, (3) lateral (horizontal) semicircular canal, (4) endolymphatic sac, (5) endolymphatic duct, (6) ampulla, (7) utricle, (8) saccule, (9) cochlea, (10) cupula, (11) hair bundles, (12) hair cells, (13) otoconia on otolithic membrane, (14) kinocilum & stereocilia, (15) hair cells.

I.III.3.1.1 Semicircular canal system

To detect any angular acceleration, like for example circular motion such as turning one's had, each ear contains three semicircular canals (see figure Figure I.84). The canals are filled with fluid (endolymph). They are approximately orthogonal to each other, and are called the horizontal (or lateral), the anterior semicircular canal (or superior) and the posterior (or inferior) semicircular canal. Each of these canals has an ampulla containing the receptor organ called crista, which contains the vestibular hair cells that transduce the mechanical movement of fluid that pushes on the top part of crista called 'cupula' to electrical signals (Gelfand 2009).

I.III.3.1.2 Otoliths

Whereas the semicircular canals respond to rotations, the otolithic organs (see Figure I.84) sense gravity and linear accelerations (such as front-back, right-left, or up-down) (Gelfand 2009). The two otoliths are called utricle and saccule. Both respond to the deflection of the cilia of their sensory receptor organs called maculae, which happens if the otolith bears down on the otolith membrane during movement (Gelfand 2009). While most of the utricular signals elicit eye movements, the majority of the saccular signals projects to muscles that control our posture.

I.III.3.2 Cochlea

The cochlea (Latin for 'snail') is the essential organ of hearing. It is the part of the inner ear, which transforms fluid motion into electrical energy that leads to the sense of hearing in the brain.

I.III.3.2.1 Anatomy of the Cochlea

The cochlea looks similar to a snail shell (see Figure I.85) with its coiled structure consisting of 2 ½ to 2 ¾ turns (Swartz & Loevner 2011). It is surrounded by a compact bony structure; the otic capsule, the hardest bone in the body. 'This is desirable, so that vibrations of fluid in the cochlea are reflected and not absorbed by the temporal bone' (Rask-Andersen et al. 2012). The cochlea lies against the lateral end of the internal acoustic meatus, its basal coil forms the promontory of the middle ear, and its apex is directed anterolaterally. The outer cochlear wall has a mean length of 42.0 mm; the first turn represented 53% of the total length (Erixon et al. 2009). The structures of the cochlea are shown in Figure I.85 in detail.

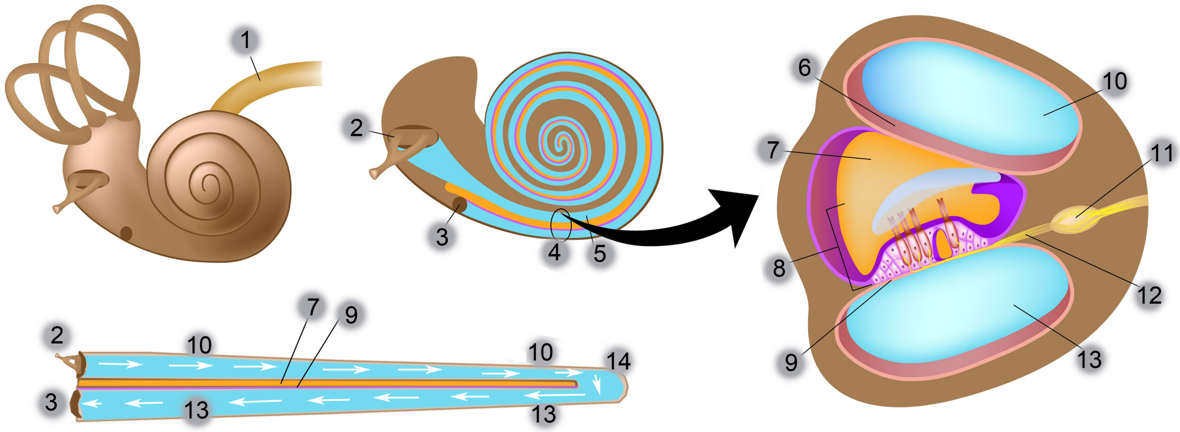

Figure I.85 Cochlea: 1 cochlear never, 2 stapes at the oval window of the cochlea, 3 round window, 4 scala vestibuli & scala tympani, 5 scala vestibuli with perilymph, 6 vestibular membrane, 7 cochlear duct with endolymph, 8 organ of corti (scala media), 9 basilar membrane, 10 scala vestibuli with perilymph, 11 spiral ganglion, 12 cochlear nerve fibre, 13 Scala tympani with perilymph, 14 Helicotrema

A bony core, the modiolus, transmits the cochlear nerve and contains the spiral ganglion. The osseous spiral lamina winds around the modiolus like the thread of a screw. The cochlear duct extends from this lamina to the wall of the cochlea. Therefore, the cochlea is divided into three ducts: a scala vestibuli anteriorly and a scala tympani posteriorly, separated by the cochlear duct that is part of the membranous labyrinth (see Figure I.85). The scala vestibuli begins after the oval window and passes to the apex of the cochlea, where the two scalae meets each other (helicotrema). The scala tympani returns near the round window, which is closed by a membrane. The round window is linked to the tympanic cavity via this membrane. Within the membranous labyrinth is a fluid called endolymph (see Figure I.85). The space between the outer wall of the membranous labyrinth and the wall of the bony labyrinth is filled with a fluid called perilymph. Perilymph communicates with the CSF via the cochlear aqueduct (Rask-Andersen et al. 2012). These two fluids, endolymph and perilymph, differ in their ionic concentration: high levels of potassium (K^+ 150 mM) and low levels of Sodium (Na^+ 40 mM) are found in the endolymph, while perilymph has high levels of sodium (Na^+ 138mM) and low levels of (K^+ 6.9mM) (Ealy et al. 2011).

I.III.3.2.1.1 Organ of Corti on basilar membrane

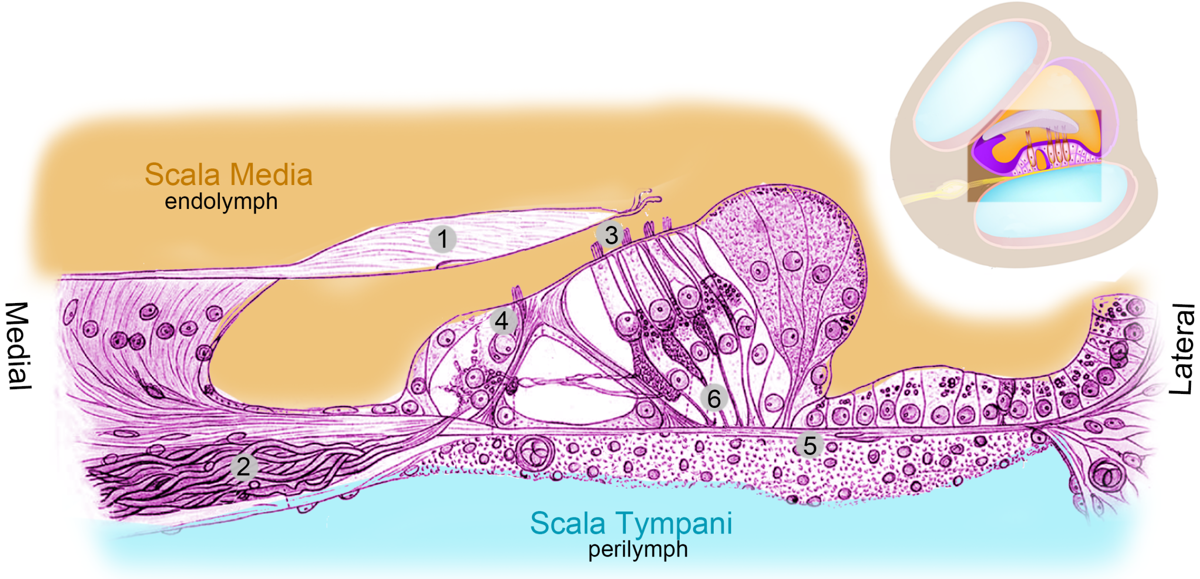

Figure I.86 The organ of Corti (purple colored): (1) Tectorial membrane, (2) myelinated cochlear nerve fibers, (3) outer hair cells, (4) inner h air cell, (5) basilar membrane, (6) deiters cells. Modified after (Raphael & Altschuler 2003).

The organ of Corti (see Figure I.86) is placed on the basilar membrane in the cochlear duct filled with endolymph. This sensorineural end organ for hearing includes polarized epithelial cells (hair cells and supporting cells) of placodal origin (membranous labyrinth), a specialized basement membrane with a layer of matrix called basilar membrane, nerve endings and the tectorial membrane (Raphael & Altschuler 2003). The organ of Corti is approximately 150 µm wide (Fettiplace & Hackney 2006). There are two types of hair cells; inner hair cells and outer hair cells. Both, inner hair cells and outer hair cells, differ by their shape and the pattern of their stereocilia. In the human cochlea, there are about 3’500 inner hair cells and about 12’000 outer hair cells (John M. Graham 2009). This number is incredibly low compared to millions of photo-receptors in the retina (around 60 million rods and around 3 million cones (Jonas et al. 1992)). In addition, hair cells are inable to proliferate because they differentiate and reach their final number very early in development (around 10 weeks of fetal gestation); from this stage on our cochlea can only lose hair cells (Pujol Rémy 2013).

I.III.3.2.2 Function of the Cochlea

The vibrations of the stapes at the oval window of the cochlea lead to movements of the fluid in the cochlear ducts and generate a traveling wave on the basilar membrane. The two ducts of the cochlea responsible for transmission of pressure are the scala vestibule and the scala tympani. The third duct (cochlear duct) includes the sensitive organ of Corti, which detects pressure impulses and responds with electrical impulses, which travel along the auditory nerve to the brain. The pressure created by the waves generated at the oval window gets relieved at the round window. The cochlea is tonotopically organized: the basal turn of the cochlea senses high frequencies and the apical turn senses low frequencies (see Figure I.87). ‘For a complex sound signal such as music or speech, many momentary peaks are produced, constantly shifting in amplitude and position along the basilar membrane’ (Everest & Pohlmann 2009).

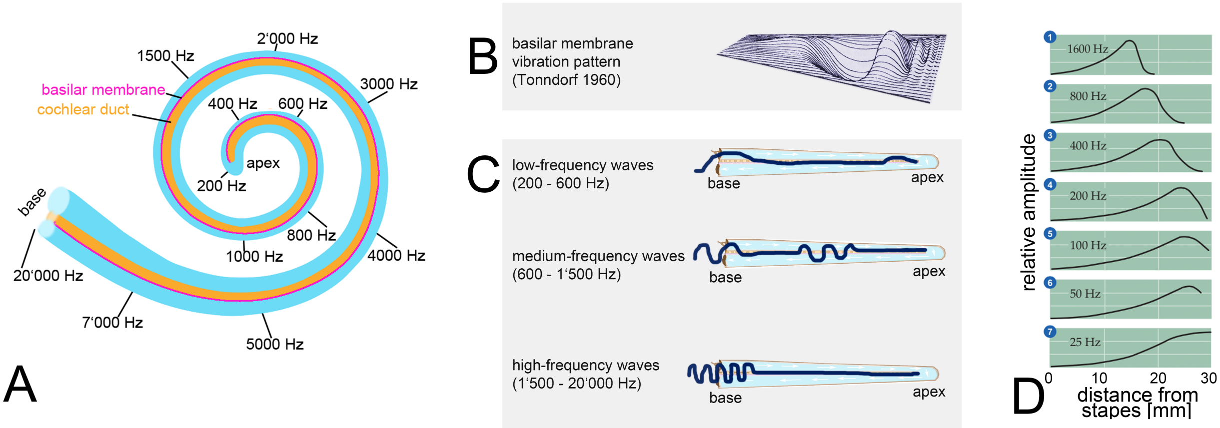

Figure I.87 (A) Tonotopic organization of the cochlea. (B) Expected vibration pattern of the basilar membrane. Modified after (Tonndorf 1960). (C) Basilar membrane motions at different frequencies. The basilar membrane motion is depending on the frequency. For low frequencies, the basilar membrane moves mainly in the apex, and for high frequencies in the base of the cochlea. Modified after (Everest & Pohlmann 2009) based on (v. Békésy 1953). (D) Amplitude of the traveling wave along the basilar membrane for different frequencies (i.e., 1–7) where the traveling wave reaches its maximum amplitude varies directly with the frequency of stimulation. Figure D is modified after (Purves & Williams 2001) Neuroscience, Third Edition (2004), figure 12.5 pp. 293, with kind permission of Sinauer Associates, Inc., Publishers, Sunderland, MA, USA.

I.III.3.2.2.1 Senosorineural mechanism

I.III.3.2.2.1.1 Theories for senosorineural mechanism

Previously, two kinds of classical theories have attempted to explain how the basilar membrane vibrations are converted into neural signals that distinguish between different frequencies (see (Gelfand 2009) p. 64/65 for more detailed information);

1. Resonance place theory, (Hermann von Helmholtz 1896), segmented basilar membrane, only segments of cochlea respond to frequency (place-by-place basis)
2. Temporal (or frequency) theories, e.g. (Rutherford 1886) “telephone theory”, entire cochlea responds as a whole to all frequencies, not only peak transmitted

Nowadays, it is assumed that both theories were wrong. It is believed that temporal and place coding exists. Place coding operates according to the traveling wave model of Békésy (v. Békésy 1953, Von Békésy 1980) (see Figure I.87), which describes how frequency is coded by place in the cochlea. The basilar membrane gets wider toward the top; therefore, a gradation of stiffness exists along the length of the basilar membrane; from stiffest at the base (near stapes, widest diameter) to least stiff at the apex (near helicotrema, smallest diameter) (Gelfand 2009) (see Figure I.87). This creates a special kind of wave pattern always travelling from the base up to the apex, called the traveling wave. Even though neurons cannot respond to all of the individual cycles, it has been shown that they can follow the periodicity of a sound for frequencies as high as 5000 Hz on a probability basis, even though they actually fire in response to fewer cycles (Gelfand 2009, Kiang 1965). For mainly lower frequencies, the increasing curvature cochlear spiral has an enhancing effect because it concentrates vibrations toward the outer wall of the duct (Manoussaki et al. 2006).

I.III.3.2.2.1.2 Effect of rocking like stapes motion on the fluid flow in the cochlea

A recent paper published from (Edom et al. 2013) of our and our collaborating group from the IFD (ETH, Switzerland) modeled the effect of rocking stapes motions on the fluid in the cochlea and on the basilar membrane motion by numerical simulations. The peak amplitudes of the basal membrane motion were compared and their dependence on the frequency and model geometry (stapes position and cochlear channel height) were investigated (see Figure I.88). Both, the piston-like and the rocking-like component of the stapes movement generate a traveling wave in the fluid and on the basilar membrane (with differences only in the basal region). Edom et al. found that the peak amplitudes for the rocking-like stapes motion were lower and decreased as frequency decreased. Contrary, the peak amplitudes for the piston-like motion increased as frequency decreased. The basilar motion was dominated by the piston-like motion under normal conditions (when the cochlea was activated by both stapes movements at the same time). However, the rocking-like motion may lead to hearing if no piston-like motion is present or possible.

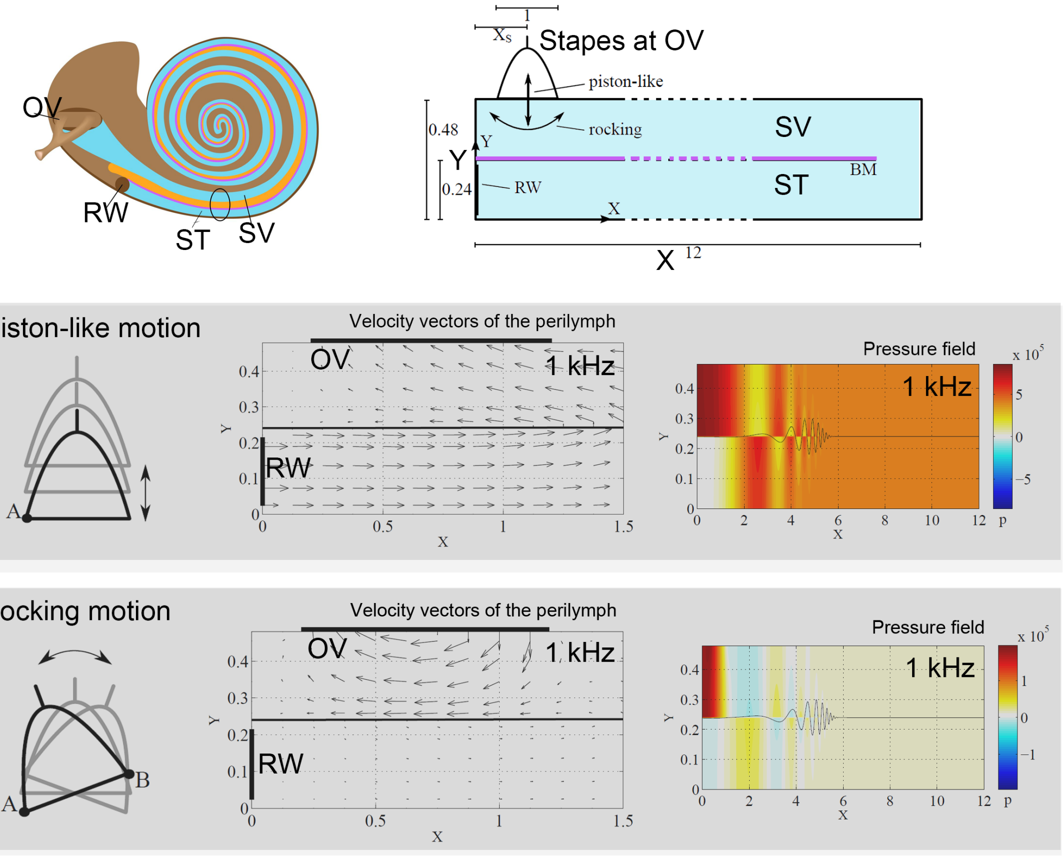

Figure I.88 Effect of the rocking stapes motions on the cochlear fluid and the basilar membrane motion: (OV) oval window of the cochlea, (RW) round window of the cochlea, (ST) scala tympani, (SV) scala vestibuli. The model is shown on top right. Modified and reprinted with permission from Edom, E., et al. (2013). "The effect of rocking stapes motions on the cochlear fluid flow and on the basilar membrane motion." J Acoust Soc Am 134(5): 3749-3758. Copyright (Edom et al. 2013), Acoustic Society of America.

I.III.3.2.2.1.3 Hair cells

Hence, a given inward motion will cause the fluids in the cochlea to be displaced downward, pushing downward on the basilar membrane; a given outward motion will displace the fluids and the basilar membrane upward. This vibratory stimulation is then translated into the bending of the hair cell stereocilia. The stereocilia protrude from the apical domain of the hair cells; bathing in the surrounding endolymph. Stereocilia transform the mechanical energy of sound waves activated due to the bending into electrical signals for the hair cells. The inner hair cells are the true sensory cell type, sending impulses via the auditory nerve (Raphael & Altschuler 2003). Contrary, outer hair cells are used to enhance the performance of the cochlea, qualitatively (increased selectivity) and quantitatively (increased sensitivity) (Raphael & Altschuler 2003). Their innervation to and from the CNS is also totally different. The hair cells are stimulated by the upward displacement of the basilar membrane which bends the stereociliary bundles of the hair cells against the acellular tectorial membrane (Fettiplace & Hackney 2006).

I.III.3.2.2.1.3.1 Inner hair cells

It is assumed, that the inner hair cells are mainly stimulated by the motion of the tectorial membrane and consequent drag of the surrounding fluid while the membrane is displaced (Dallos et al. 1972). The deflection of the hair-cell stereocilia opens mechanically gated ion channels that allow potassium to enter the cell; this influx of positive ions from the endolymph in scala media depolarizes the cell, resulting in a receptor potential (Purves & Williams 2001). This receptor potential opens voltage gated calcium channels in the hair cell membrane; calcium ions then enter the cell and trigger the release of neurotransmitters at the basal end of the cell onto the auditory nerve endings (Purves & Williams 2001). The neurotransmitters diffuse across the synapse (narrow space between the hair cell and a nerve terminal), where they then bind to receptors and thus trigger action potentials in the nerve. Hence, the mechanical sound signal is converted into an electrical nerve signal. An unusual adaptation of the hair cell in repolarization of the hair cell is that potassium serves to depolarize the cell as well, enabling the hair cell's potassium gradient to be largely maintained by passive ion movement alone (Purves & Williams 2001). The perilymph in the scala tympani has a very low concentration of positive ions. Therefore, the electrochemical gradient makes the positive ions flow through channels to the perilymph (Purves & Williams 2001). Each signal from the inner hair cell is related to the brain via 10 to 20 afferent fibres of the VIIIth cranial nerve (Fettiplace & Hackney 2006).

I.III.3.2.2.1.3.2 Outer hair cells

Outer hair cells cilia (see Figure I.89) are shared because they are attached to the tectorial membrane (Gelfand 2009). They have both, sensory and motor capabilities (Fettiplace & Hackney 2006). The innervation of the outer hair cells is mainly efferent and only sparsely afferent (Fettiplace & Hackney 2006). Efferent signals from the olivocochlear bundle (part of VIIIth cranial nerve, also known as the auditory-vestibular nerve) use the capability of motility (electromotility) of the outer hair cells; which influences the cochlear sensitivity (Fettiplace & Hackney 2006, Gelfand 2009). Hence, the cochlear amplifier enhances the signal received by the inner hair cells (cochlear amplifier (Davis 1983)). This active process also appears to be responsible for the ability of the cochlea to produce sounds called otoacoustic emissions that can be measured with a sensitive microphone in the ear canal (Gelfand 2009).

There is still controversy concerning the precise mechanism of the hair cell activation. ‘Mechanical manipulations of the cochlea and measurements of the passive and active displacements of the basilar membrane in the normal and postmortem cochleas provide evidence that the outer hair cells are activated directly by the fluid pressures induced in the cochlea by low-level sound, and not indirectly by a passive traveling wave’ (Sohmer 2012).

Details of the hair cell activation are illustrated in Figure I.89.

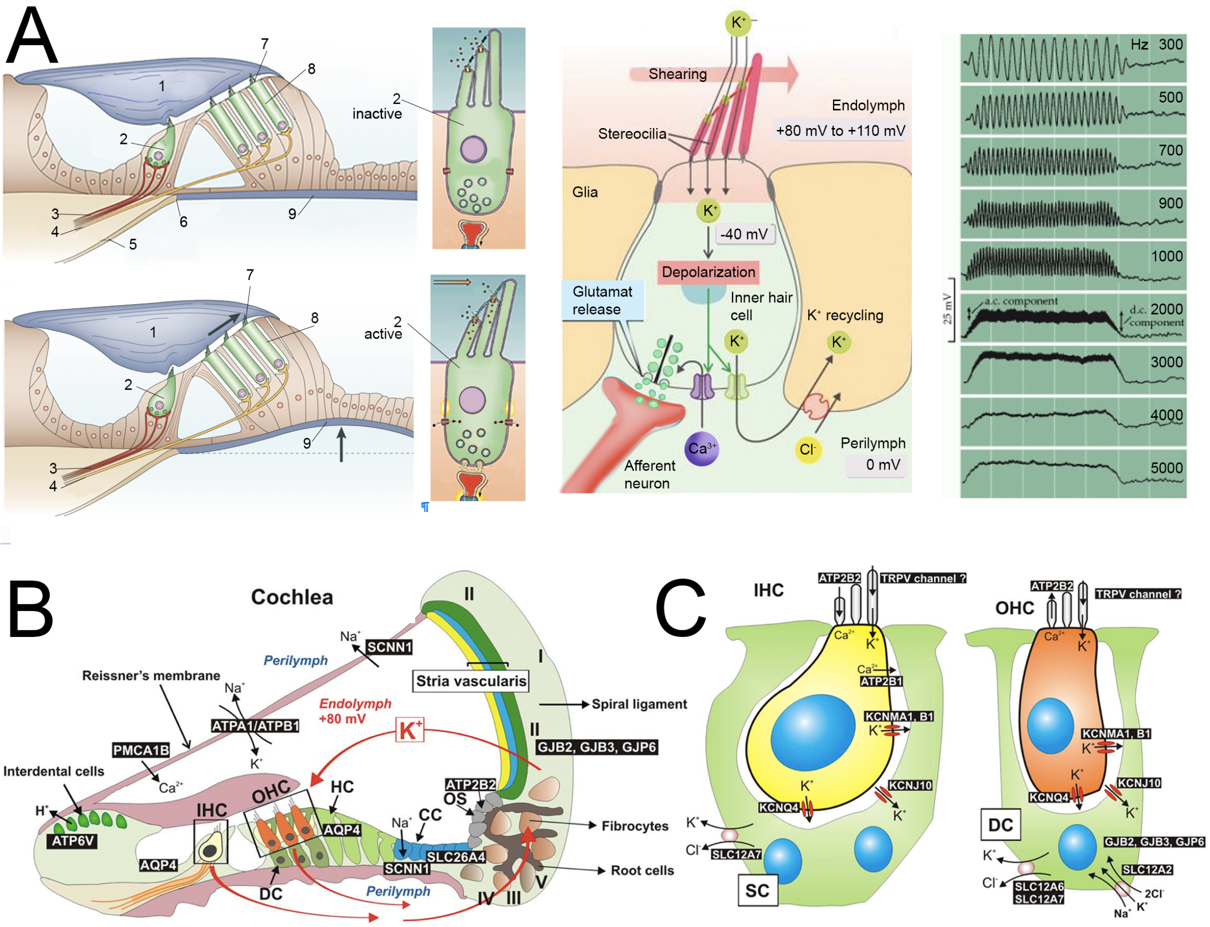

*Figure I.89 (**A**) Cross section through the cochlear duct and hair cell activation: (E) Endolymph, (P) perilymph, (1) tecotorial membrane, (2) inner hair cell, (3) afferent neuron, (4) efferent neuron, (5) osseous spiral lamina, (6) hinge point, (7) hair bundle, (8) outer hair cell, (9) basilar membrane. Modified after (Fettiplace & Hackney 2006, Purves & Williams 2001, Tanner-Thies 2011). (**B**) Molecular processes in the cochlea: (IHC) inner hair cell, (OHC) outer hair cell (**C**) Illustration of the inner hair cell (IHC) and the outer hair cell (OHC). Gene names of expressed ion channels and transporters are illustrated: Deiter's cells (DD), Claudius' cells (CC), Hensen's cells (HC), outer sulcus cells (OS), supporting cells (SC), specialized fibrocyte types (I–V). Reprinted from Lang et al. 2007, Copyright © 2014, The American Physiological Society (Lang et al. 2007).*

I.III.3.2.2.1.3.3 Cochlear microphonic

The receptor potentials, produced during the process of hair cell activation, can be monitored with electrodes. One of these receptor potentials is an alternating current signal that represents the stimulus waveform, called the cochlear microphonic (Gelfand 2009). The other receptor potential, which appears as a deviation or shift in the direct current baseline, is the summating potential (Gelfand 2009). Our group (Dalbert et al. 2015a) recently monitored changes in cochlear function during cochlear implantation using electrocochleography (ECoG) and correlated the changes to postoperative hearing preservation. Extracochlear ECoG was found to be a reliable tool to assess cochlear function during cochlear implantation (see I.III.3.2.3) (e.g., trauma of the cochlea followed by a partial or complete loss of the acoustic residual hearing). In 20 patients, the ECoG was measured extracochlear near the round window at two different time points: before (1) and after (2) the insertion of the cochlear implant electrode (Dalbert et al. 2015b). In nine patients, further measurements were performed during the electrode implantation and during follow-up consultations by using the implanted cochlear electrode as the recording electrode itself (Dalbert et al. 2015b). The acoustic stimulus was a tone burst at 250 Hz, 500 Hz and 1000 Hz. Ninety percent (18/20) of the cochlear implant subjects had ECoGs that were measurable (Dalbert et al. 2015b). Almost all (94 %, 17/18) showed no changes indicating acute trauma in the extracochlear measurements during the implantation of the electrode (Dalbert et al. 2015b). Only one patient showed a large decrease of the ECoG signals, which was also associated with a complete loss of hearing four weeks after surgery (Dalbert et al. 2015b).

I.III.3.2.3 Cochlear Implant

Patients who are suffering of a severe hearing loss or deaf because of a damage of the sensory hair cells in the cochlea (see I.III.3.2.2.1.3) can choose a surgical implantation of a cochlear implant (CI) as a treatment. In these patients, the implants often can enable sufficient hearing for better understanding of speech. Even though the quality of sound is different from natural hearing, with less sound information being received and processed by the brain, many patients are able to hear and understand speech and environmental sounds. The CIs currently on the market consist of (NIH Publication No. 11-4798 2013):

- a microphone → behind the ear (Figure I.90 A)
- a speech processor → behind the ear (Figure I.90 A)
  (to select and arrange sounds picked up by the microphone)
- a transmitter and receiver/stimulator → implanted under the skin (Figure I.90 B Nr. 1)
  (they receive signals from the speech processor and convert them into electric impulses)
- an electrode array → implanted in the cochlea (Figure I.90 B Nr. 2)
  (consists of a group of electrodes that collects the impulses from the stimulator and sends them to different regions of the auditory nerve)

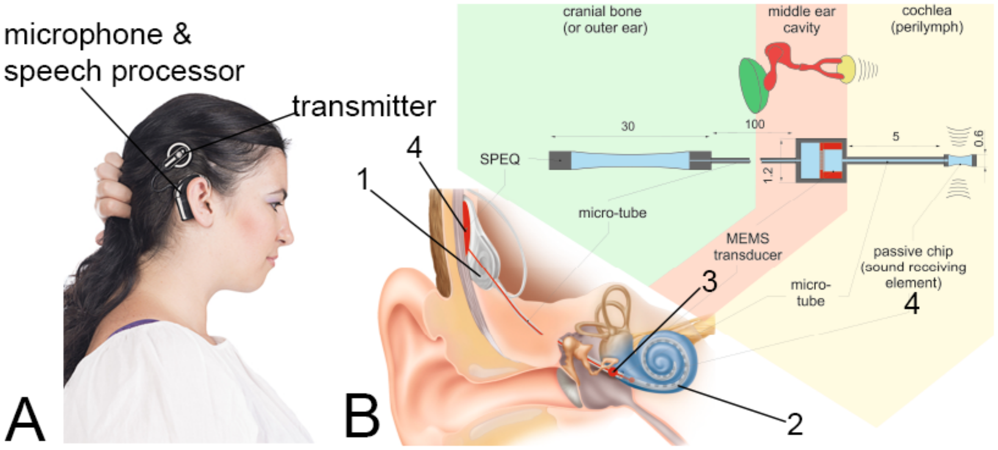

Figure I.90 Cochlear implant (CI): (A) A CI recipient wearing a CI currently available on the market showing the microphone and the speech processor behind the ear. (B) Illustration of the intra-

cochlear acoustic receiver (ICAR) of our group: (1) transmitter and receiver/stimulator, (2) electrode array, (3) Microelectromechanical system (MEMS) pressure transducer, (4) pressure equalizing system (SPEC). Modified after (Pfiffner et al. 2015).

The goal nowadays is to improve and develop the devices and processing-strategies that e.g., allow recipients to hear better in noise, and enjoy music. Future totally implantable CI systems could deliver significant safety benefits and improve the quality of life e.g., by using the CI even while sleeping, showering and swimming. Our group (Dept. Otorhinolaryngology, Head and Neck Surgery, University Hospital Zurich, Switzerland) is currently developing and validating an intra-cochlear acoustic receiver (ICAR) for future totally implantable CI systems (see Figure I.90 B) in collaboration with the Institute of Fluid dynamics (IFD) (Swiss Federal Institute of Technology (ETHZ), Switzerland) and the Cochlear Technology Centre Belgium (Mechelen, Belgium). The replacement of the external microphone with a fully implanted ICAR is a crucial step towards this totally implantable CI. The idea is to integrate the sensor into a CI electrode and situated in the scala tympani (see Figure I.90 B Nr. 2). The Microelectromechanical system (MEMS) pressure transducer is placed in the middle ear cavity (see Figure I.90 B Nr. 3). The pressure in the cochlea varies if a sound wave arrives at the cochlea (see chapter I.III.3.2.2.1.2). Diaphragms of the sound receiving element (see Figure I.90 B Nr. 4) causes pressure variations within the inert gas in the micro tube, which in turn are registered by the MEMS pressure transducer (see Figure I.90 B Nr. 3). The idea is to finally convert this signal to an electric impulse of the electrode array placed in the cochlea (similar to a currently available CI), which then stimulates the auditory nerve fibers. Corresponding patents certificates are: 61/901,272 (CID02124USPR1) and 62/013,829 (CID02125USPR1).

First measurements of the inner ear pressure in sheep (see Figure I.91) and human temporal bones were already performed. The preliminary results (Pfiffner et al. 2015) showed a good response of the sensor (see Figure I.51, magenta line). The gain ($\text{pressure}_{\text{scala tympany}}/\text{pressure}_{\text{ear canal}}$) was measured at maximal acoustic stimulation at two different insertion depths and two different instances. An example for the gain at 1 mm insertion depth and 1h after the first measurement is shown in figure Figure I.51. The aim in the ongoing measurements is mapping the inner ear pressure at different access positions and different insertion depths in human and sheep temporal bones. This will be useful later on to find the optimal insertion position for the ICAR in totally implantable CI systems.

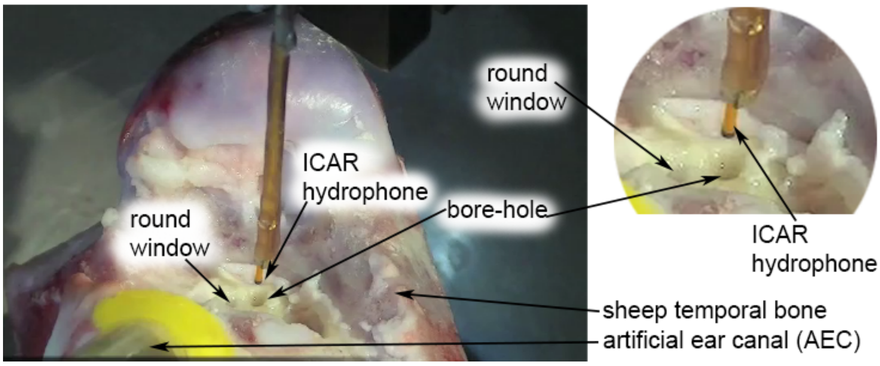

Figure I.91 Measurement of the intra-cochlear pressure with the intra-cochlear acoustic receiver (ICAR) in a sheep temporal bone under acoustic stimulation via the artificial ear canal.

I.III.4 Central auditory system

This chapter is thought to complete description of how sound travels via the middle ear to the inner ear – and finally provokes a stimulus in the brain that results in perception of sound. This chapter is not of main interest for the measurement series performed in the scope of this dissertation and, therefore, only severs as a short overview.

The receptor potential of the hair cells stimulates the release neurotransmitters (by the hair cell) and stimulates an all-or-none action potential in the auditory nerve fiber. This action potential is then forwarded via the auditory pathway to ultimate target of afferent auditory information; the auditory cortex (see Figure I.92). Although the auditory cortex has a number of subdivisions, the area can be divided into a primary area and peripheral areas. The primary auditory cortex (A1) is located on the superior temporal gyrus in the temporal lobe (Purves & Williams 2001). It receives point-to-point input from the ventral division of the medial geniculate complex (Purves & Williams 2001). Both, medial geniculate complex and A1, contain a precise tonotopic map (Purves & Williams 2001). Thus, frequencies close to each other in the cochlea are represented in topologically neighboring regions in the brain as well (see Figure I.92). The peripheral areas of the auditory cortex receive more diffuse input and therefore are less precise in their tonotopic organization (Purves & Williams 2001).

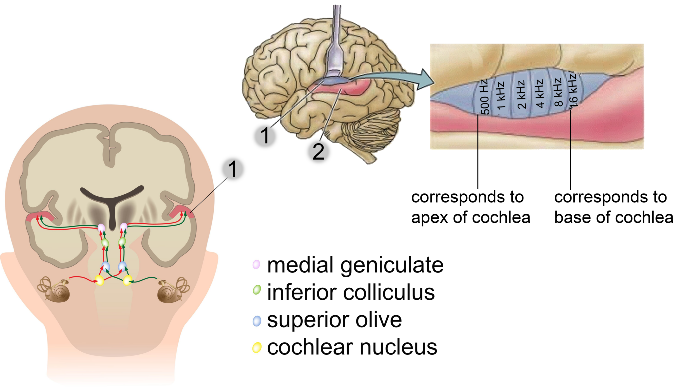

Figure I.92 The auditory pathway: (1) primary auditory cortex, (2) secondary auditory cortex. The primary auditory cortex has a tonotopic organization, as shown in the illustration of a segment of A1. Tonotopic organization is modified after (Purves & Williams 2001) Neuroscience, Third Edition (2004), figure 12.15 pp. 309, with kind permission of Sinauer Associates, Inc., Publishers, Sunderland, MA, USA.

I.III.5 The temporal bone

Figure I.93 shows the ear structures in relation to the skull and the brain. The auditory system is imbedded in each of the temporal bones (see Figure I.94), which are situated at sides and base of the skull and lateral to the temporal lobes of the brain. The different anatomical landmarks of the temporal bone are labeled in the illustration Figure I.94.

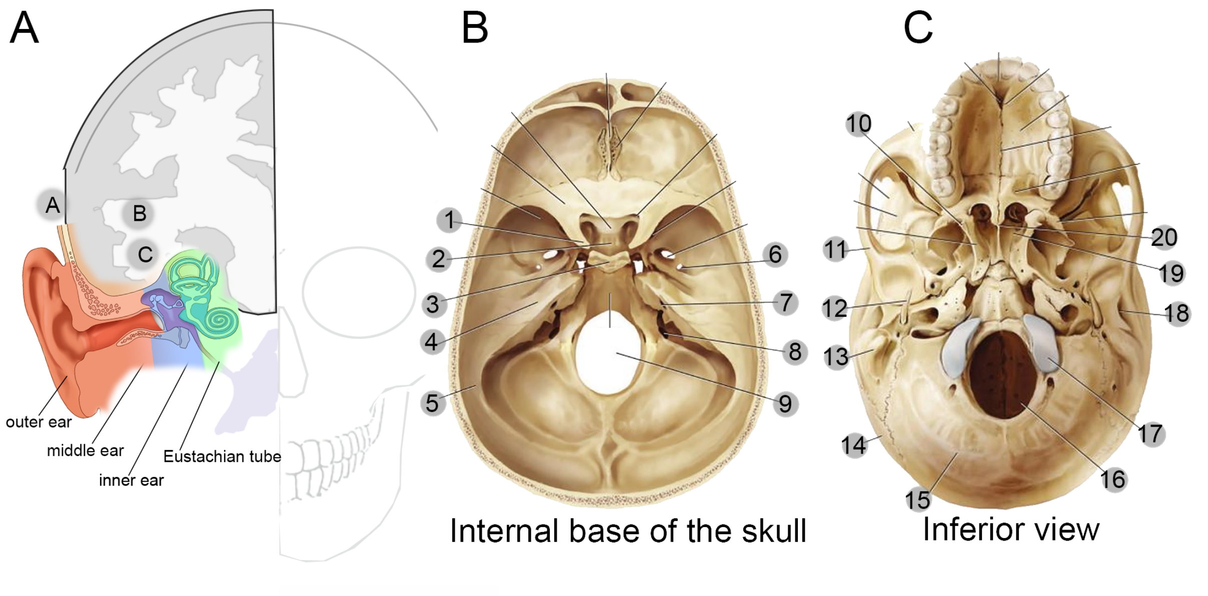

Figure I.93 (left) Illustration of the auditory system in relation to the skull and the brain after 'courtesy of Abbott Laboraties' (A) epitympanic recess, (B) auditory cortex, (C) temporal lobe. (B) Illustration of a human skull from internal view: (1) anterior clinoid process, (2) hypophyseal fossa, (3) posterior clinoid process, (4) ***temporal bone****, (5) parietal bone, (6) foramen ovale, (7) internal auditory meatus, (8) jugular foramen, (9) foramen magnum. (C) Illustration of a human skull from inferior view: (10) hamulus, (11) zygomatic process, (12) styloid process, (13) mastoid process, (14) parietal bone, (15) occipital bone, (16) foramen magnum, (17) occipital condyle, (18) external auditory meatus, (19) vomer, (20) posterior nasal spine. Modified after (B) (John A. Seikel et al. 2005) figure 6.8 pp. 312 and (C) (J. Seikel et al. 2013) figure 4.7 pp. 210 with kind permission of From Seikel/Drumright/Seikel. Essentials of Anatomy and Physiology for Communication Disorders (with CD-ROM), 2E. © 2014 Delmar Learning, a part of Cengage Learning, Inc. Reproduced by permission. www.cengage.com/permissions.*

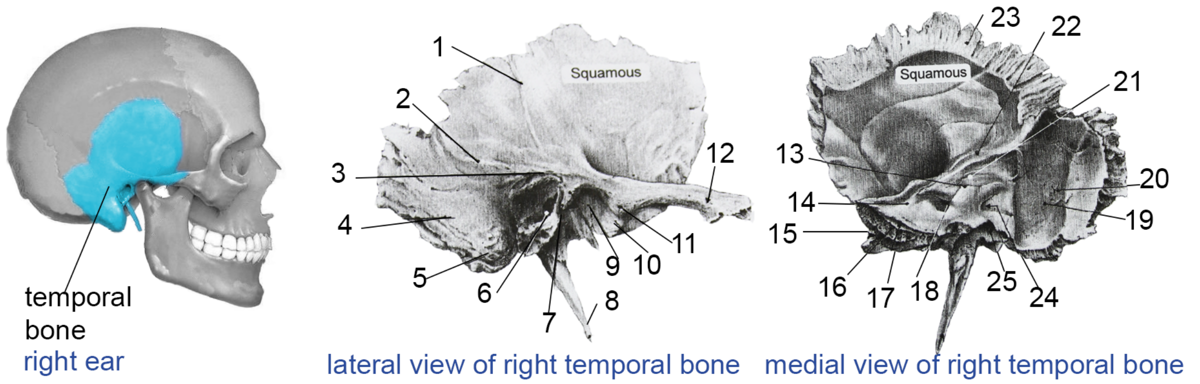

Figure I.94 Human temporal bone: (1) groove for posterior deep temporal artery, (2) temporal line, (3) suprameatal triangle, (4) mastoid, (5) mastoid process, (6) external auditory meatus, (7) tympanic crest, (8) styloid process, (9) mandibular (glenoid) fossa, (10) temporal condyle, (11) anterior zygomatic tubercle, (12) zygomatic process, (13) arcuate eminence, (14) superior petrosal sulcus, (15) orifice of carotid canal, (16) occipital margin, (17) inferior petrosal sulcus, (18) internal auditory meatus, (19) sigmoid sulcus, (20) mastoid foramen, (21) petrous, (22) superior petrosal sulcus, (23) parietal margin, (24) vestibular aequaduct, (25) pyramidal fossa. Lateral and medial views of the right temporal bone modified after (Gelfand 2009) who reprinted from (Proctor 1989).

I.III.6 Bone conduction pathways

In most cases, humans hear sound because sound waves travel in air through the ear canal (see I.III.1.2) and the middle ear ossicles (see I.III.2) to the inner ear (see I.III.3). In the cochlea (see I.III.3.2), the sound pressure creates a travelling wave on the basilar membrane (see I.III.3.2.1.1) and the sensory cells in the cochlea respond to the pressure with a signal to the auditory nerve (see I.III.3.2.2.1). This route for sound transmission is known as 'air conduction route'. However, a second route exists as well for sound transmission; "sound can also be transmitted as vibrations in the skull bone, cartilage, and soft tissues that finally cause the bone around the cochlea to vibrate and result in a perception of sound (Stenfelt & Goode 2005). This route is often referred to as bone conduction even if it involves other structures than bone *per se* (Stenfelt 2014)". Our group (Dept. Otorhinolaryngology, Head and Neck Surgery, University Hospital Zurich, University Zurich, Switzerland) presented preliminary results of diverse bone conduction measurements at the Annual MidWinter Meetings of the Association for Research in Otolaryngology (ARO) in 2013 (Röösli et al. 2013), 2014 (Röösli et al. 2014b, JH Sim et al. 2014, Röösli et al. 2014a) and 2015 (Röösli et al. 2015). The diverse projects are described in the following paragraphs.

As mentioned above, the bone conduction hearing is considered to include several pathways including ear canal radiation, inertia of the ossicles and cochlear fluid, compression and expansion of the skull, and pressure transmission through soft tissues. Until today, the importance and mechanism (e.g., frequency dependence) of these pathways is not fully clear (Stenfelt & Goode 2005). Many controversial discussions are going on, especially according the contribution of the pathway via non-osseous skull contents such as brain content and cerebrospinal fluid (CSF). Among others, understanding of linear mechanical vibration properties is important to understand head injury with skull fractures and to develop equipment for preventing injury (McKnight et al. 2013). The skull seems to behave in a more complex way than a spherical shell that supports bending and stretching parallel to the surface. Our group aims to investigate this wave propagation with direct stimulation of the skull bone taking the different modes of wave propagation into account. The correlation between intracranial pressure and skull vibration on the promontory (in cadaveric human whole heads) for bone conduction stimulation (Röösli et al. 2013). The propagation speed of the traveling wave is also calculated, and it is compared with the time interval of promontory motion and cranial pressure between stimulation at ipsi-mastoid and stimulation at contra- mastoid. The hypothesis is, that the modes of wave propagation on the skull -bone depends on frequency, and that the skull-bone vibration and intracranial pressure change is related each other.

Three human cadaver heads were stimulated with a bone-anchored hearing aid (BAHA)(100 dB bone conductive stimuli, 0.1-10 kHz) (see Figure I.95). The stimulation was performed with a 5-N steel headband at mastoid, forehead, eye, and neck – and additionally with a percutaneous implanted BAHA at the mastoid and forehead. The changes in the intracranial pressure at the center of the head were measured with a hydrophone. Simultaneously, the motion of the cochlear promontory was measured by a scanning LDV system (see chapter II.IV). Frequency dependency of the intracranial pressure differed from the corresponding skull bone vibration, and the intracranial attenuation could be estimated from the difference of skull bone vibration between the ipsi- and the contralateral sides. This may show that the non-osseous skull pathways contribute to bone conduction hearing in some frequencies (Röösli et al. 2013). Further measurements showed that the magnitude of the transferred force was similar for both the BAHA "coupled to the screw" and "positioned with the headband", whereas the phase with "positioned with the headband" showed larger phase delay than with "coupled to the screw" above 1 kHz (Röösli et al. 2014b, Röösli et al. 2014a). Additionally, the skull bone vibrations showed near rigid-body motion at low frequencies below 0.5 kHz, and clear traveling waves were observed at high frequencies above 2 kHz, for both conditions (see Figure I.95) (Röösli et al. 2014b, Röösli et al. 2014a). Only the direction of the wave propagation changed (speed of wave propagation was of a similar magnitude) for both stimulation sites (Röösli et al. 2014b, Röösli et al. 2014a). According the intracranial pressure (measured with the hydrophone) under stimulation with the BAHA at the mastoid, the pressure was larger in the ipsi-lateral position than in the other positions at high frequencies (JH Sim et al. 2014). For the stimulation at the forehead, the pressures were similar for all five positions (JH Sim et al. 2014). However, the intra-cranial sound pressure magnitudes were relatively uniform for stimulation with the BAHA attached to the mastoid and the forehead. Only the intra-cranial pressure in the ipsi-lateral position with stimulations at the mastoid had larger magnitudes than in other positions with other stimulations sites (JH Sim et al. 2014). Our group very recently focused on the bone conduction pathway trough non-osseous contents by directly stimulating the dura of a whole cadaveric head (Röösli et al. 2015). A craniotomy was performed and, then, a bone conducting hearing aid (Bonebridge, Med-El) was attached to the dura stimulating with a stepped-sine (0.1-10 kHz) directly to the transducer (Röösli et al. 2015). The cochlear promontory motion was measured using again the LDV and the intracranial pressure was measured with a hydrophone (Röösli et al. 2015). The magnitudes of the intracranial pressure were similar to the promontory motion above 1.4 kHz, suggesting that the non-osseous contents interact with bone vibrations in this frequency range (Röösli et al. 2015).

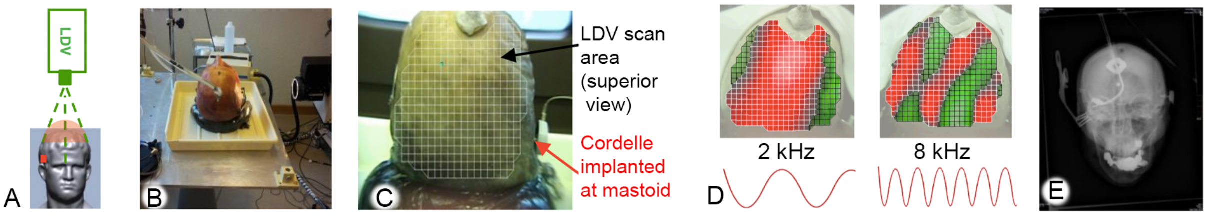

Figure I.95 Wave propagation in the skull bone during bone conduction stimulation: Measurement setup included a BAHA (= Cordelle) (A,C) that was directly driven with sine signals. The motion of the skull was measured using a Laser Doppler vibrometer (A, C). A Hydrophone was placed lateral (B, E). (D) Example of a motion pattern of a skull (superior view) at 2 kHz (left) and 8 kHz (right).

I.IV Development of the ear in humans

The ear is a complex sensory organ of multiple embryonic origin; different structures derive from different germ layers (see Figure I.96). Structures of the developing ear are visible for the first time around day 22 as a swelling of the ectoderm surface (otic placode); at this stage the embryo has implanted itself into the uterine wall and starts the process of gastrulation (see Figure I.96). Six distinct hillocks arise from the branchial arches; three hillocks arise from the first (mandibular) arch and three from the second branchial (hyoid) arch. These six hillocks will form the external ear (pinna) (see Figure I.96). The external ear canal is derived from the first branchial arch (Sadler 2008) (see Figure I.96). Two layers adjoin each other at the tympanic membrane; the ectoderm of the first branchial arch and the endoderm of the first branchial arch. The tympanic cavity develops from the first branchial arch (endoderm). The connection between the tympanic cavity and epipharynx persists as the auditory tube. The middle ear ossicles malleus and incus derive from the first branchial arch, unlike the stapes, which derives from the second arch (Sadler 2008). In the early stages, the auditory ossicles development all occurs within the solid mesenchyme of the branchial arches. This mesenchyme dissolves around the eighth month of development, change to a fluid-filled space for the final month, and finally to the air-filled tympanic cavity in neonates (Hill 2014). Therefore, prenatal conduction to the cochlea must be mediated through bone conduction; the prenatal middle ear does not function correctly. Additionally, there are two muscles (tensor tympani and stapedius) formed from mesenchyme (Hill 2014). The membranous labyrinth of the inner ear derives from the ectodermal otic placodes (see Figure I.96), which soon invaginate into the mesenchymal tissue to form the otic pit. The invaginated portion then enlarges, fuse and convert into a closed sac in the fourth week; the otic vesicle (otocyst). Subsequently, the otic vesicle undergoes a complex morphogenesis; subdivided into a dorsal part (resulting in utricle, semicircular canals and endolymphatic duct) and a ventral part (resulting in saccule, and organ of Corti ‘snail’) (Sadler 2008).

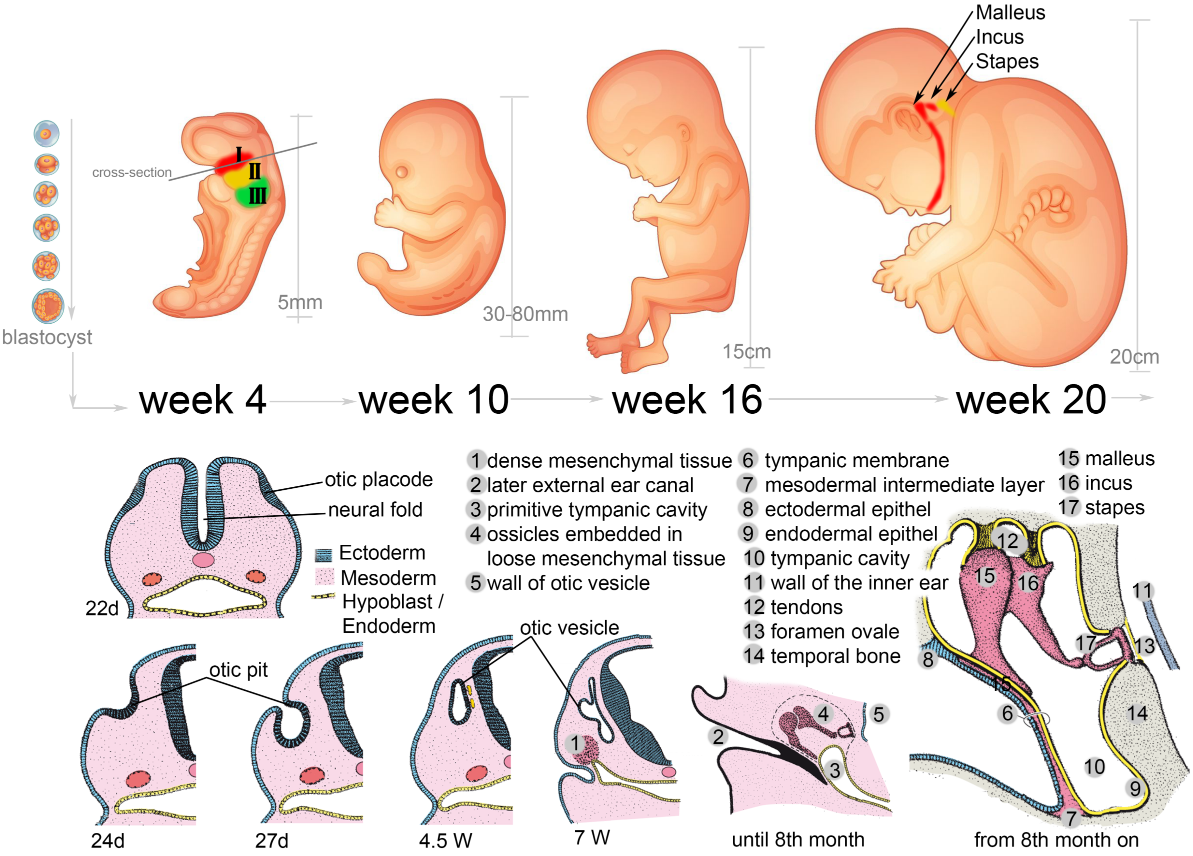

Figure I.96 (upper part) Development of the ear: Fetus 4, 10, 16 and 20 weeks old. Branchial arches I (I), II (II), III (III). (lower part) Development of the otic placode: day 22 to 8th month in comparison to fully developed middle ear (right). Lower part is modified after (Sadler 2008) with kind permission of Wolters Kluwer Health.

I.IV.1 Development of the joints in the ossicular chain

This chapter mainly focuses on the development of the IMJ (see chapter I.IV.1.1). In the interests of completeness a short description of the development of the ISJ and stapediovestibular joint is presented as well.

The Whyte et al. studied described the development of all three joints (IMJ see chapter I.IV.1.1, ISJ, and stapediovestibular joint) of human fetuses (n=25, between 7th and 29th week). (Whyte et al. 2002). The ISJ showed “typical characteristics of a diarthrosis and spheroidal joint with a homogenous interzone at the 7th week, showing similar characteristics for 12 weeks, and completed its cavitation at the 16th week (Whyte et al. 2002).” They observed hyaline cartilage on articular surfaces of the ISJ from 29 weeks on. The stapediovestibular joint showed typical characteristics of a syndesmosis (Whyte et al. 2002) (=fibrous joint in which two adjacent bones are linked by a strong membrane or ligaments (Hermans et al. 2010)). “The annular ligament primordium derived from cartilage differentiation, both from stapedial footplate and from the surrounding otic capsule, into mesenchyme and its subsequent transformation into fibrous tissue, reaching definitive characteristics from the 12th week (Whyte et al. 2002)”.

I.IV.1.1 Development of the IMJ

The development of the IMJ has been studies in detail by Whyte et al. (Whyte et al. 2002) and Cisneros Gimeno et al. (Cisneros Gimeno et al. 2009). Both explored the development of the IMJ in histological cuts: Whyte et al. from cuts of 25 temporal bones between 7th (21 mm) and 29th week (270 mm) (fixed in 10% formol, decalcified with 2% nitric acid, embedded in Paraplast, sectioned in a sequence of 7 µm, and then stained with Martin’s trichrome), Cisneros Gimeno et al. from cuts of 46 temporal bones between 9 mm and newborns (Martins' trichrome technique as well).

The IMJ showed diarthrosis and saddle joint characteristics. During the development of the IMJ several steps can be distinguished:

- **7th week (21 mm)** Figure 1.97 A**:** homogenous interzone: blastemas of malleus and incus were separated by means of a very homogenous condensated mesenchyme interzone (Whyte et al. 2002)
- **8th week (36 mm)** Figure 1.97 B: a three-layered interzone: the IMJ primordium showed its classical morphology of saddle joint, characterized by the presence of articular surfaces, concave in one sense and convex in the other; the interzone at this moment of development was in a three-layered phase formed by two chondrogenic sheets, separated by an intermediate looser sheet (Whyte et al. 2002)
- **9th week (42 mm)** Figure 1.97 C: first cavitation signs in the joint: the IMJ showed a cavitation phenomenon in the interzone that was more pronounced in the peripheral than in the central zones (Whyte et al. 2002)
- **10th week (50 mm)** Figure 1.97 D: characteristics of a saddle joint (Cisneros Gimeno et al. 2009), presence of an articular cavity, development of the diarthrosis characteristics, cartilaginous structure of the ossicles and of the articular surfaces, condensation of the synovial mesenchyme in the outer layer, and loose in the inner layer, observation of the joint capsule ligament and the synovial tissue (Whyte et al. 2002)
- **11th to 13th week** Figure 1.97 E**:** endochondral ossification of the ossicles from one unique center situated in the head of the malleus and the long limb of incus (Whyte et al. 2002)
- **14th week:** the articular surfaces organized in one stratum (layer) (Cisneros Gimeno et al. 2009, Whyte et al. 2002), where small size cells were restricted to collagen fibers and disposed horizontally with the surface (Whyte et al. 2002)
- **15th-18th week** Figure 1.97 F**:** cartilage increased in thickness and showed two well-defined stages (1st stage: cells arranged in horizontal layers, 2nd stage: oval or round cells with a random disposition), reinforcement of the joint capsule with collagen fibers inserted into the cartilaginous matrix (Whyte et al. 2002)

- **18th week:** internal surface developed the synovial membrane, primordium (=tissue in its earliest recognizable stage of development) of meniscus (Cisneros Gimeno et al. 2009)
- **19th week** Figure 1.97 G: endochondral bone appeared in incus and malleus, three stages of cartilage that covered the articular (1^{st} stage: superficial stage with cells arranged horizontally, 2^{nd} stage: cells arranged at random, 3^{rd} stage: deepest, cells arranged in perpendicular columns and continued with bone (Whyte et al. 2002)
- **20th week** Figure 1.97 H: presence of a hyaline cartilage covering joint surfaces (Whyte et al. 2002)
- **25th-28th week** Figure 1.97 H & I: ossification of ossicles completed, hyaline cartilage completely covered the articular surface, visible capsular ligament and synovial membrane

Schmidt (Schmidt 1903) found the cartilaginous disk between the malleal and incudal cartilage to be present already in a 1.6 cm long fetus, but neither at this stage of development nor in the adult stage was this meniscus totally detached from the cartilaginous surfaces of both ossicles.

The ossicles show a very early ossification (Cisneros Gimeno et al. 2009). The adult size of the ossicles is already reached in the fetus (Cisneros Gimeno et al. 2009). The growth of the ossicles ends at the 4th year, changing from cavity structure to a compact structure (Cisneros Gimeno et al. 2009). They lack of a epiphysis (filled with red bone marrow, which produces erythrocytes) and a metaphysis (zone of growth between during development of a bone) as the only large bones in the human body (Cisneros Gimeno et al. 2009). Their growth remains constant with minimum remodeling (Cisneros Gimeno et al. 2009).

The morphological changes of the IMJ with age are described in chapter I.III.2.4.4.1.4.

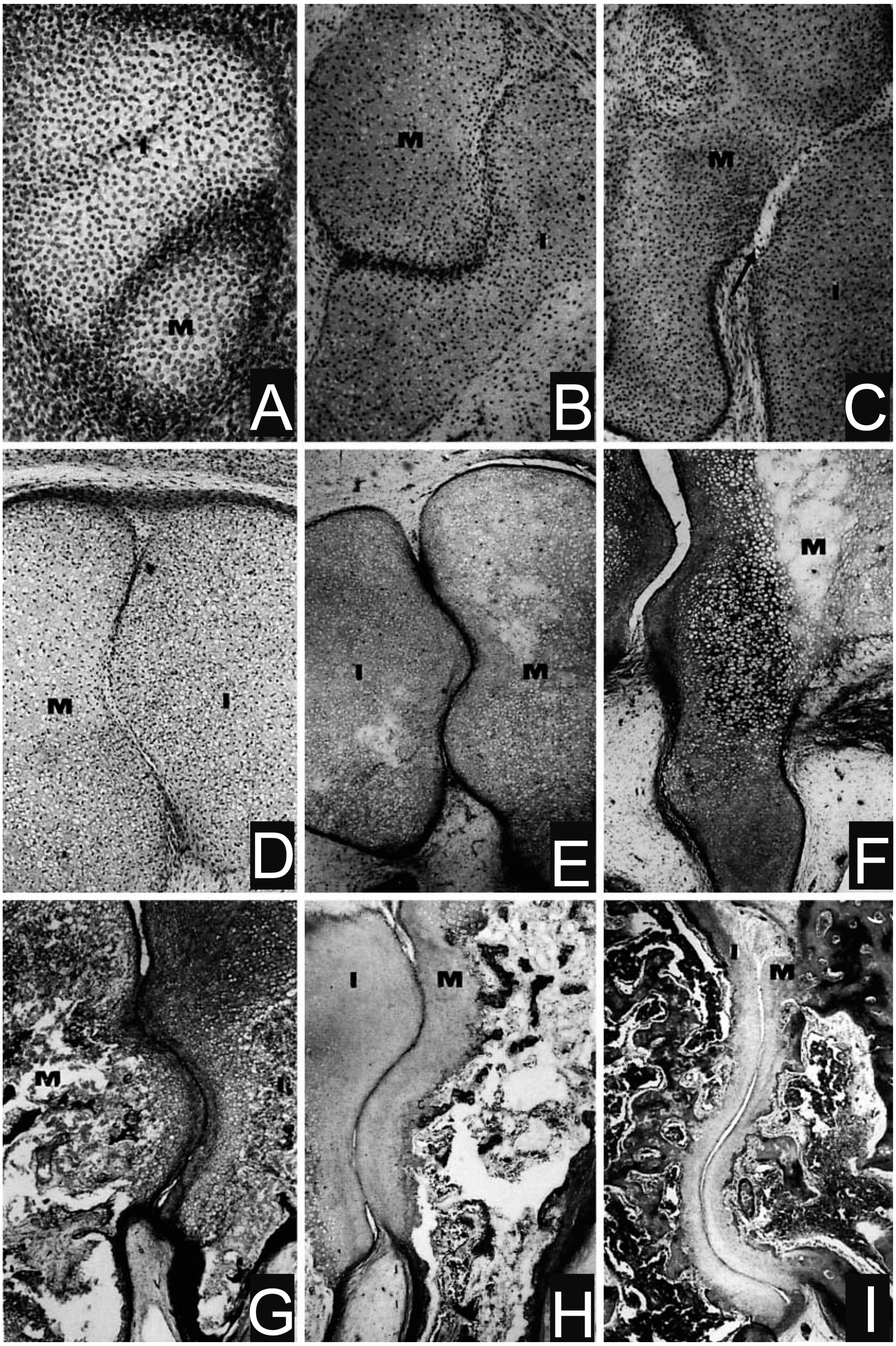

Figure I.97 Development of the IMJ: (A) week 7, (B) week 8, (C) week 9, (D) week 10, (E) week 12, (F) week 16, (G) week 19, (H) week 21, (I) week 26. Reprinted from (Whyte et al. 2002) and permission achieved from Copyright © 2002 Karger Publishers, Basel, Switzerland. "Fetal Development of the Human Tympanic Ossicular Chain Articulations", J.R. Whyte L. Gonzàlez A.I. Cisneros C. Yus A. Torres R. Sarrat, Cells Tissues Organs 2002;171:241–249, figure 1.

II Methodological approach

The projects of this dissertation include the construction of the 3-D motion of the ossicles. The construction is based on the assumption that the human middle-ear ossicles behave as rigid bodies. This chapter includes the description of rigid body motion in general (see chapter II.II.1), as well as the behavior of the ossicles as rigid bodies up to a certain frequency (see chapter II.II.1.2). It also focuses on the excitation signals used for the stimulation of the ossicular motion (see chapter II.III), the velocity measurements of the ossicles using Laser Doppler Vibrometry (see chapter II.IV), and on necessary procedures for the 3-D motion construction e.g. frame registration with micro-CT data (see chapter II.V).

II.I Temporal bone preparation and measurement

The middle ear is not accessible without any preparation; the ossicular chain is embedded in the middle-ear cavity surrounded by bone and the tympanic membrane (see chapter I.III.2). Therefore, two different temporal bone preparations were realized for the different projects of this work. For the measurements described in chapters III.I and III.III, a posterior tympanotomy was performed (see chapter II.I.1). The malleus-incus complex (MIC) was removed from fresh human temporal bones for the project described in chapter III.II (see Figure 2.5).

II.I.1. Posterior tympanotomy

The temporal bones used for the measurement of the stapes motion for the projects of chapters III.I and III.III were prepared such that the view on the malleus head, incus body, and stapes footplate was unobstructed. The preparation was as follows: First, all connective tissues and muscles were removed from the temporal bone. Then, the external ear canal was drilled down to 2 mm from the tympanic annulus. A simple mastoidectomy with posterior tympanotomy was performed in order to obtain a clear and near-perpendicular view of the stapes footplate. The posterior tympanotomy included the removal of the mastoid (see Figure 1.94 Nr. 4) and a part of the tympanic segment of the facial nerve (see Figure 1.18 B Nr. 6) and surrounding bone. The tympanic membrane, ossicles, stapedius muscle, and tendons were left intact. An example of a prepared temporal bone is shown in Figure 2.2.

An artificial ear canal (AEC, see Figure 2.2, AEC) was mounted on the tympanic annulus: a syringe was mounted with a small amount of plasticine on the tympanic annulus to avoid any leakage of air through the attachment surfaces. Plaster was applied on the inferior side of the ear canal to stabilize the AEC (see Figure 2.1 and Figure 2.2). The loudspeaker and the reference microphone were mounted with foam in the AEC (see Figure 2.1 and Figure 2.2). Then, the velocity of the stapes footplate was measured with the scanning LDV system at different frequencies. The same measurement was repeated after the IMJ was immobilized by opening of the joint capsule and replacing the synovial fluid with glue (see Figure 2.3). The immobilization was checked by measuring the area around the IMJ of the malleus head and incus body before and after immobilization of the joint. For the measurement of the stapes velocity, the laser beam of the LDV came from posterolateral (see Figure 2.1, Figure 2.4, and Figure 3.5). The areas on malleus and incus around the IMJ were measured from superior (see Figure 2.1 and Figure 2.4).

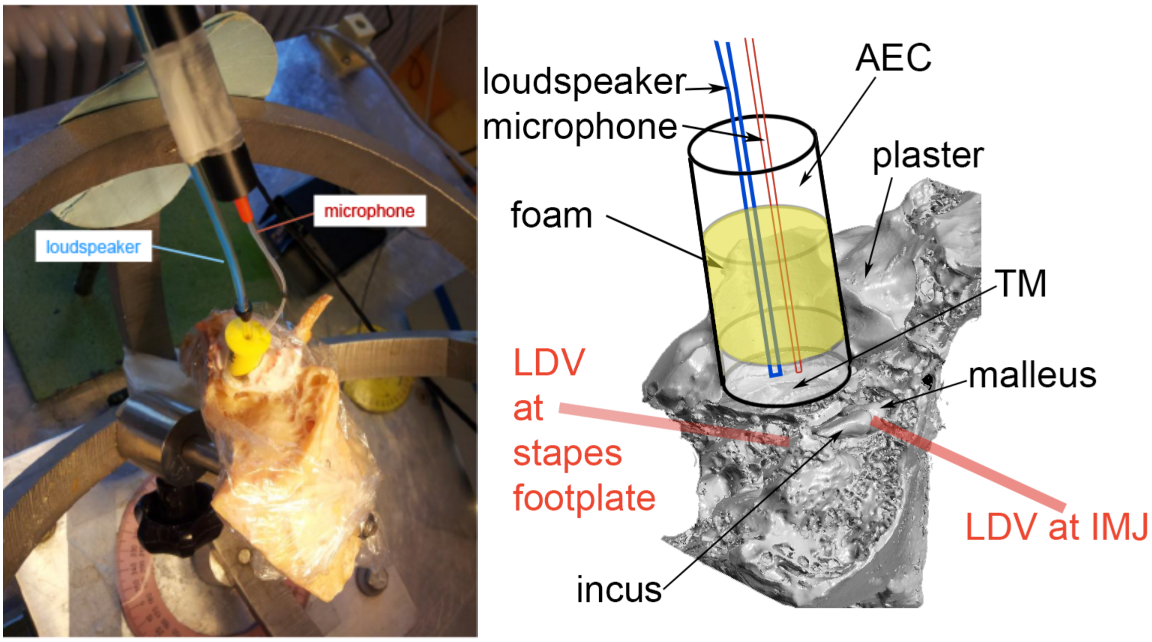

Figure 2.1 Measurement setup for the measurements of the contribution of the IMJ to middle-ear sound transmission: (left) Measurement setup for the LDV measurements on the stapes footplate and IMJ (malleus head and incus body). (right) Illustration of the temporal bone after preparation: the tympanic membrane (TM) is still intact (not visible in this 3-D reconstruction of the micro-CT scan), the microphone (ER-7) and loudspeaker (ER) are placed close to the TM in the foam placed in the artificial ear canal (AEC). LDV measurements were possible from the posterior side on the stapes footplate and from the superior side to the IMJ (malleus head and incus body).

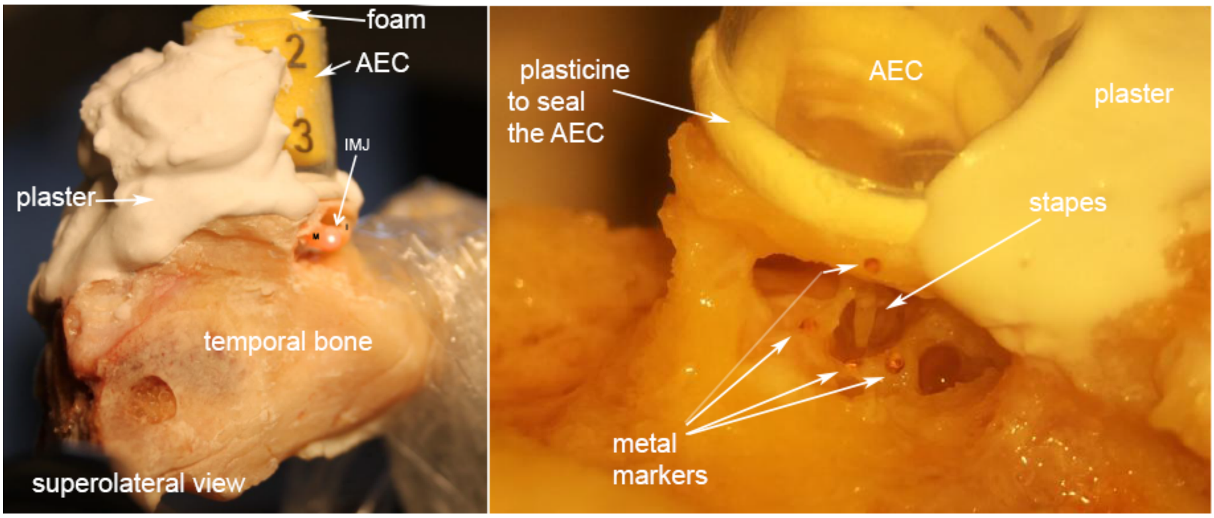

Figure 2.2 Prepared temporal bone: (left) superolateral view of the human temporal bone. The artificial ear canal (AEC) is mounted with plaster and plasticine to seal it. The malleus (M), incus (I) and the IMJ between the two ossicles are visible.

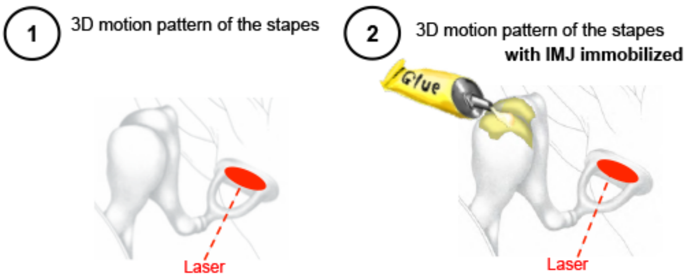

Figure 2.3 The stapes motion was measured before and after the immobilization of the IMJ. By comparing the two measurements, the influence of the IMJ on the sound transmission in the middle ear was described (see chapter III.I).

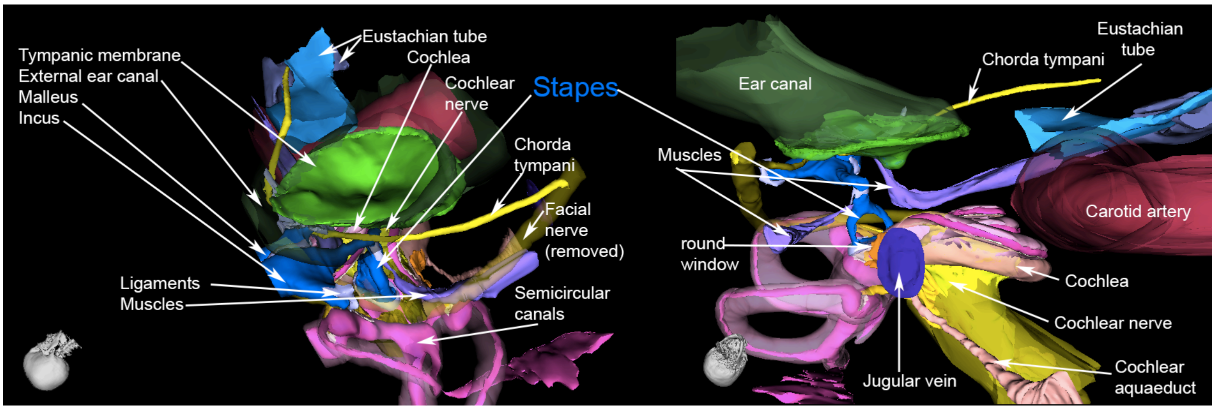

Figure 2.4 Two different views on the structures of the ear. These illustrations were modified after the model of the Massachusetts Eye and Ear (MIT, Boston, USA). "The model was made under the supervision of Drs. M. Charles Liberman and Saumil Merchant by Haobing Wang and Clarinda Northrop. Model development was supported by a core grant from the NIDCD (P30 DC05209)". http://www.masseyeandear.org/research/otolaryngology/investigators/laboratories/eaton-peabody-laboratories/epl-imaging-resources/3-d-model-of-human-temporal-bone/. With kind permission of Haobing Wang.

II.I.2. Isolated malleus-incus-complex

Isolated malleus-incus complexes (MICs) were used for the project described in chapter II.II. The middle-ear cavity was assessed with a posterior tympanotomy. Additionally, the tendons connecting the MIC to the middle-ear cavity (see chapter I.III.2.4) were cut and the MIC removed. It was taken great care that the IMJ was not injured during the process of the removal (see Figure 2.5).

The isolation of the MIC is important to model the biomechanics of the human middle ear; decoupling the MIC from the surrounding components reveals the individual role of the IMJ. This methodology has previously been used by several authors (Wever & Lawrence 1954, Tonndorf & Pastaci 1986, Puria & Allen 1998). The underlying assumption of this approach is that the biomedical properties in the malleus-incus-complex are not altered from its physiological operation. Sim and Puria (2008) described that, in normal middle ears, "it is assumed that preloads in suspensory structures are present and those preloads are balanced with eardrum and stapes preloads. The pulling forces of the eardrum along the medial-to-lateral direction will cause rotation and translation of the MIC about an axis along the anterior–posterior direction, resulting in pretension in the tensor tympani tendon and twist in the anterior ligament and the incus ligament pp 20 (J.H. Sim & Puria 2008)." These pretensions of the suspensory attachments (tendons/ligaments) will affect the biomechanics of the middle ear and should be taken into account in future models of the healthy middle ear.

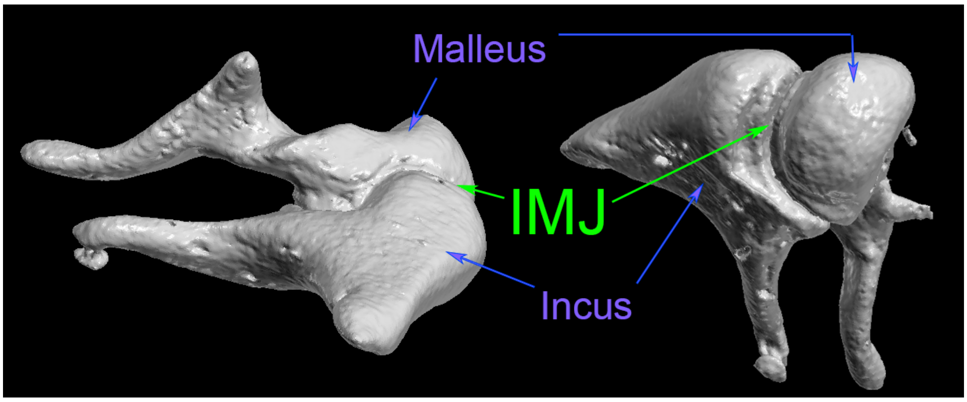

Figure 2.5 3-D reconstruction of the malleus-incus-complex from micro-CT data (see chapter II.V).

II.II Measurement of the three-dimensional ossicular motion

The measurement of the three-dimensional ossicular motion is described in detail in the following subchapters. The general introduction to rigid body motion (II.II.1) is followed by a chapter focusing on the rigid body motion of malleus and incus (II.II.2), and on the rigid body motion of the stapes (II.II.3).

II.II.1. Description of rigid body motion

A rigid body is defined as a particular system of particles, which does not deform. Let A and B be any two of its particles, then, in a rigid body the distance between A and B will remain without change (see Figure 2.6, A). The limits of this assumption are elasticity and break of the rigid body. Forces acting on rigid bodies can be separated in two groups: external and internal forces. External forces can change a motion to the rigid body in form of translation or rotation or both.

II.II.1.1 General plane motion

Any general plane motion of a rigid body can be considered as a translation plus a rotation. In the three-dimensional space, the rigid body motion (of a free body) consists of three translational motions and three rotational motions (see Figure 2.6, B1 and B2).

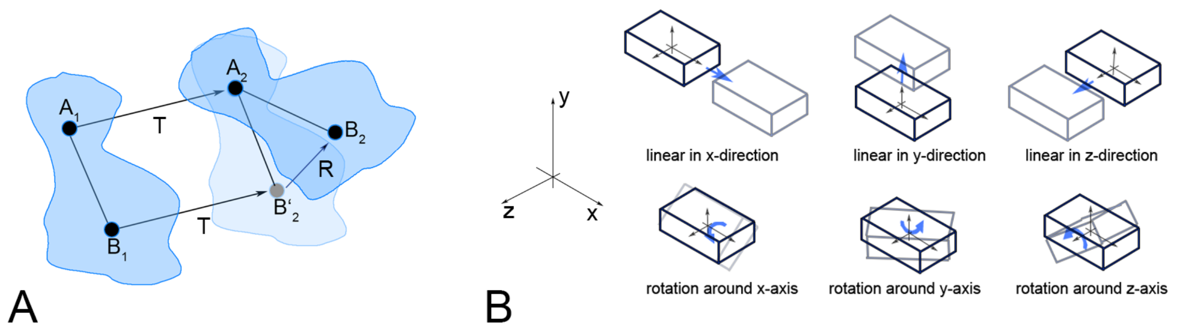

Figure 2.6 Illustrations of rigid body motion: (A) Illustration showing a plane motion A_1 to A_2 and B_1 to B_2 with translation (T) and rotation (R) in the two-dimensional space. (B) The six motion components in the three-dimensional space are: 3 translational (in x-, y-, and z-direction) and 3 rotational (rotation around x-, y-, and z-axis) components.

II.II.1.2 Are the middle-ear ossicles rigid bodies?

Some authors doubt that the ossicles behave as rigid bodies for all frequencies. Beer et al. (Beer et al. 1999) found with natural mode shape calculations that the ossicles can be treated as rigid bodies only for frequencies below about 3.5 kHz. Consequently, the ossicles have been modeled as elastic bodies in their finite element model, which requires much more computation time. An alternative approach is to model the ossicles as elastic bodies incorporating just the first two or three modes in each body (J. H. Sim et al. 2004). Funnell (Funnell et al. 1992) found bending at higher frequencies in cat ossicles in a finite-element model.

However, the middle-ear ossicles are assumed to behave as rigid bodies under acoustic stimulation in the physiological range (Willi 2003, Willi et al. 2002, J.H Sim 2007, J. H. Sim et al. 2010a, J. H. Sim et al. 2012, Huber et al. 1997). In a recent publication, Decraemer et al. (W.F. Decraemer et al. 2014) reported that the ossicles of living gerbils are rigid bodies and only show "a minor bending at the neck of the malleus" at the highest frequencies (>30 kHz) (see Figure 2.7).

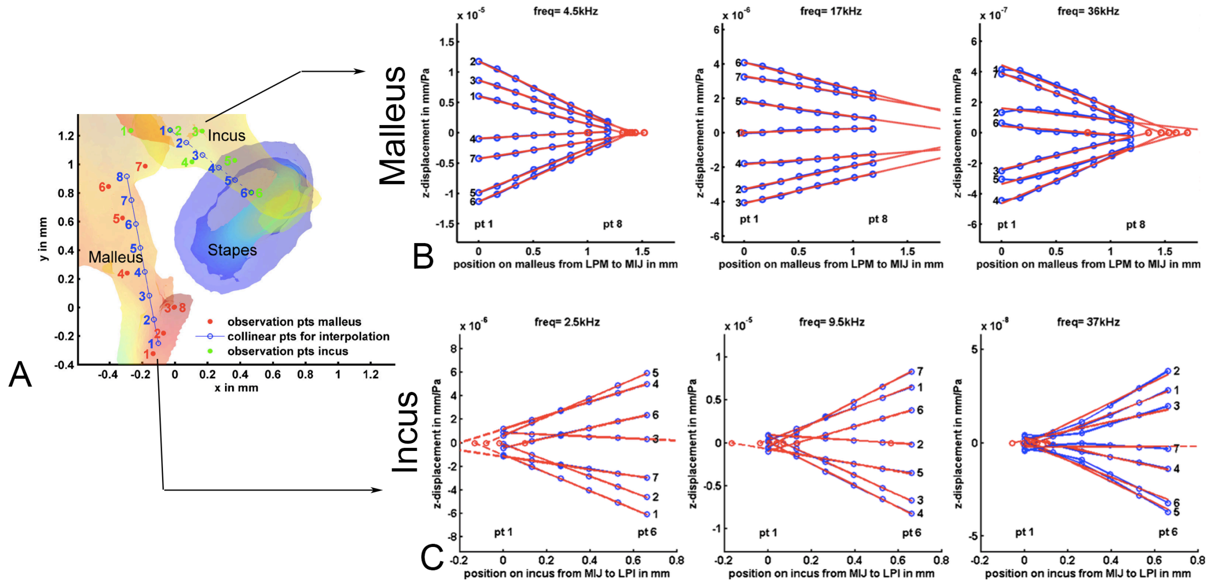

Figure 2.7 Rigid-body fit of malleus and incus for one gerbil: (A) Observation points on the malleus and on the incus, and collinear points for interpolation. (B and C) The solid straight line in red

shows the rigid-body fit to the blue experimental data points (phases plotted as a function of position) for the malleus (B) and the incus (C). For the malleus (B), the displacements at the "experimental points" (blue) align nearly perfectly with the straight line segments of the rigid-body fit (red), except for the highest frequency (36 kHz, right panel) where a small deviation from linearity in the region of the malleus neck (C, collinear points 1-3) suggests some bending. Illustrations are combined and reprinted after Springer and JARO - Journal of the Association for Research in Otolaryngology, 15, 2014, 483–510, "Three-Dimensional Vibration of the Malleus and Incus in the Living Gerbil", Decraemer W.F., de La Rochefoucauld O., Funnell W. R., Olson E. S., figure 3, figure 4, figure 5 © Springer Science and Business Media, with kind permission from Springer Science and Business Media (W.F. Decraemer et al. 2014).

II.II.2. Measurement of the malleus and incus motion

Spatial motions of the malleus-incus complex in mammals have been described by the classical ''hinging" motion i.e., rotation about the anterior–posterior axis (see Figure 2.8). However, during last two decades, it has appeared that spatial motion of the malleus and the incus has more complex patterns, especially at high frequencies. It has been revealed that the rotational axis of the "hinging" motion changes with frequency, and the rotational axis does not remain fixed even during the cycle at high frequencies (W. Decraemer & Khanna 1995, W.F. Decraemer et al. 2014). Moreover, it is presumed that spatial motion of the malleus-incus complex in human ears is more complex because the mobile IMJ allows relative motions between the malleus and the incus. Sim et al. (2004) showed that spatial motion of the isolated malleus-incus complex of human ears has complicated mode patterns with relative motion between the malleus and incus at high frequencies. Puria and Steele (2010a) proposed that in larger mammals (e.g. human and cat), the malleus performs ''twisting" motion along the inferior–superior axis of the malleus at higher frequencies to transmit sound effectively. Their proposition was based on the non-symmetric shape of the eardrum in humans and cats, which can produce excitation for the "twisting" motion, and the mobile IMJ, which can transfer the "twisting" motion of the malleus to the incus. Willi et al. (2002) also observed large relative motion between the malleus and incus with complicated motion patterns of the two bones at high frequencies. Considering complex spatial motion of the malleus and the incus, it is generally accepted nowadays that full six degrees of freedom (DOF) are required to describe spatial motion of the malleus and the incus.

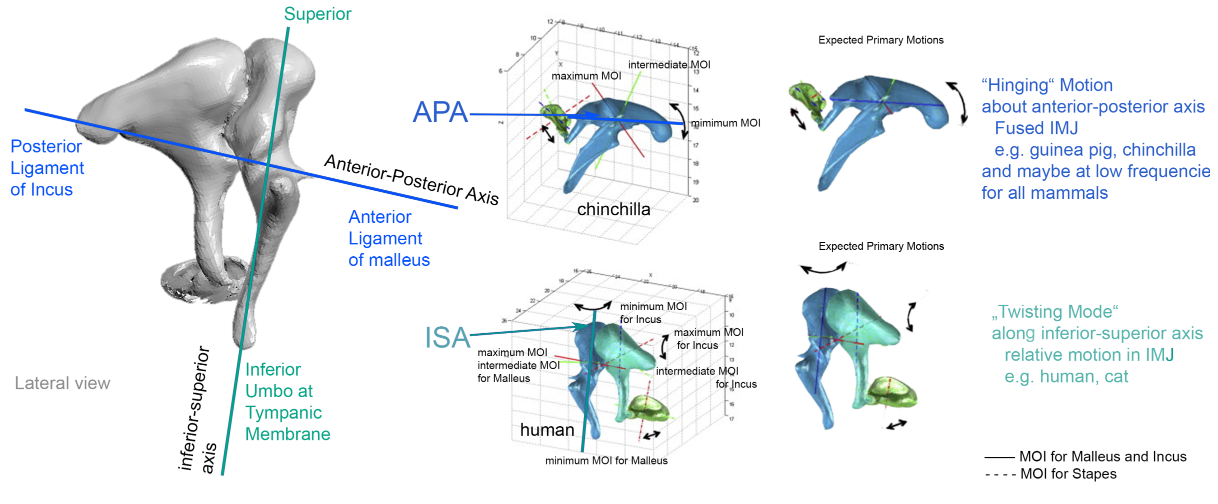

Figure 2.8 "Hinging" motions around the anterior-posterior axis (APA) and "twisting mode" along the inferior-superior axis (ISA) of the malleus-incus complex. The illustrations on the right side are modified after Hearing research, Vol. 263, S. Puria and C. Steele, "Tympanic-membrane and malleus-

incus-complex co-adaptations for high-frequency hearing in mammals", figure 6, pp. 183-90. Copyright 2009, with permission from Elsevier. (Puria & Steele 2010a).

II.II.2.1 Construction of the three-dimensional motion of the malleus-incus-complex

Considering rigid-body motion of each of the malleus and the incus with six degrees of freedom (DOF) of three translations and three rotations in a reference frame, the six rigid-body motion components in a reference frame can be determined with the 3-D motion components if the motion of three or more non-co-linear points on the rigid body is known.

To obtain the 3-D motion components at a point, the motion of that point must be measured from at least three different angles. In a work by Decraemer et al. (2004), they mounted temporal bones on two stacked goniometers which provide rotations about horizontal and vertical axes, and measured velocities using a 1-D LDV from several different angles. The 3-D LDV systems with recent technology already have built-in three laser beams with three different measurement angles, and provide real-time measurements of the 3-D motion components at a measurement point.

Once the 3-D motion components are measured at several points on an ossicle, assuming small magnitudes of motions, the velocity vector $\mathbf{v}_m$ of the 3-D motion components at a point m is related to the rigid-body motion components by

$$\mathbf{v}_m = \mathbf{v}_o + \boldsymbol{\omega} \times \mathbf{x}_m,$$

where $\mathbf{v}_o$ and $\boldsymbol{\omega}$ indicate translational and rotational velocity vectors of rigid-body motion components, and $\mathbf{x}_m$ indicates the position vector of the point m with respect to the reference point o. The equation can be rewritten as

$$\mathbf{v}_m = \mathbf{A}_m \mathbf{v}_r,$$

with $\mathbf{A}_m = \begin{bmatrix} 1 & 0 & 0 & 0 & z_m & -y_m \\ 0 & 1 & 0 & -z_m & 0 & x_m \\ 0 & 0 & 1 & y_m & -x_m & 0 \end{bmatrix}$ and $\mathbf{v}_r = \begin{Bmatrix} \mathbf{v}_o \\ \boldsymbol{\omega} \end{Bmatrix} = \begin{Bmatrix} v_{ox} \\ v_{oy} \\ v_{oz} \\ \omega_x \\ \omega_y \\ \omega_z \end{Bmatrix}.$

Combining all n measurement points ($n \geq 3$), the equation above leads to

$$\mathbf{v} = \mathbf{B}\mathbf{v}_r,$$

with $\mathbf{v} = \begin{Bmatrix} \mathbf{v}_1 \\ \mathbf{v}_2 \\ \vdots \\ \mathbf{v}_n \end{Bmatrix}$ and $\mathbf{B} = \begin{Bmatrix} \mathbf{A}_1 \\ \mathbf{A}_2 \\ \vdots \\ \mathbf{A}_n \end{Bmatrix}.$

Then, the vector $\mathbf{v}_o$ of the rigid-body motion components can be determined by the method of least square errors by

$$\mathbf{v}_r = \left(\mathbf{B}^T\mathbf{B}\right)^{-1}\left(\mathbf{B}^T\mathbf{v}\right).$$

II.II.3. Measurement of the stapes motion

II.II.3.1 Piston-like and rocking-like motion of the stapes

In several previous works (Hato et al. 2003, J. H. Sim et al. 2010a, J. H. Sim et al. 2010b, Eiber et al. 2012), spatial motion of the stapes was described only by three elementary motion components; a translation along the longitudinal axis of the stapes (i.e., axis perpendicular to the footplate plane through the center of the footplate) and two rotations about the short and long axes of the footplate. The translational motion is called piston-like motion and the two rotational motions rocking-like motions. The baseline for such simplification is that the annular ligament of the stapes restricts in-plane motions of the stapes along the footplate plane. Lauxmann et al. (Lauxmann et al. 2012b) found the in-plane motion to be only 4.2 ± 1.4 % of the piston-like motion of the stapes when the footplate plane is precisely determined within the footplate. The comparison of the literature and our results of the different motion components is discussed in chapter IV.III.3.

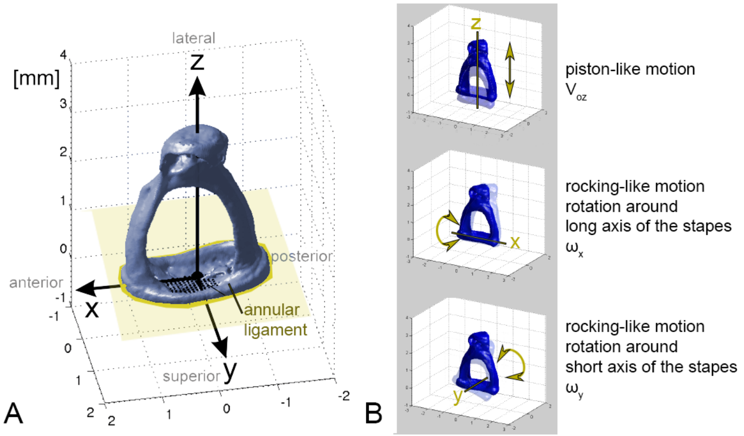

Figure 2.9 Stapes motion. The stapes motion can be described with three motion components: a piston-like motion and two rotational motions rocking-like motions.

II.II.3.2 Construction of the three-dimensional motion of the stapes

Assuming the three elementary components (i.e., piston-like motion and two rocking-like motions) are dominant components of the spatial stapes motion, measurements of the spatial stapes motion can be simplified. A method using a scanning laser Doppler vibrometry (SLDV) system has been developed and has been used in a project of this dissertation (see chapter III.I).

The *xyz* coordinate system is set up such that the *x* axis is along the long length of the footplate, the *y* axis is along the short axis of the footplate, and the *z* axis is along the longitudinal direction of the stapes. With such a coordinate system, the origin *o* is located at the center of the footplate. Then, the rigid body motion components v_{oz} (translational velocity of the footplate center), ω_x (rotational velocity along the long axis of the footplate), and ω_y, (rotational velocity along the long axis of the footplate) are related to the velocity component $\boldsymbol{v_{mz}}$ in *z* direction at a point *m* on the footplate plane as

$$v_{mz} = v_{oz} + \omega_x y_m - \omega_y x_m$$

Since it was assumed that in-plane motions along the footplate plane are negligible, the motion of the point *m* has only a *z*-component ($v_{mx} = v_{my} = 0$). Therefore, the measured motion v_m of the point *m* with an angle θ_L between the laser beam direction and the *z* axis is related to the velocity component $\boldsymbol{v_{mz}}$ in *z* direction as

$$v_m = v_{mz} \cos\theta_L$$

Combining the two equations,

$$v_m = \cos\theta_L \left(v_{oz} + \omega_x y_m - \omega_y x_m \right).$$

For *n* measurement points on the footplate,

$$\mathbf{v_m} = \cos\theta_L \cdot \mathbf{A} \cdot \mathbf{v_r},$$

with
$$\mathbf{v_m} = \begin{bmatrix} v_1 \\ v_2 \\ \vdots \\ v_n \end{bmatrix}, \quad \mathbf{A} = \begin{bmatrix} 1 & y_1 & -x_1 \\ 1 & y_2 & -x_2 \\ \vdots & \vdots & \vdots \\ 1 & y_n & -x_n \end{bmatrix}, \quad \mathbf{v_r} = \begin{bmatrix} v_{oz} \\ \omega_x \\ \omega_y \end{bmatrix}.$$

Finally, the vector of the rigid-body motion components can be obtained by the method of least squares error as

$$\mathbf{v_r} = \frac{1}{\cos\theta_L} \left(\mathbf{A}^{\mathrm{T}} \mathbf{A} \right)^{-1} \left(\mathbf{A}^{\mathrm{T}} \mathbf{v_m} \right).$$

II.III Excitation

In a healthy ear, the ossicles are excited by acoustic energy during hearing of sounds. To simulate the behavior of the ossicles during this process of hearing, several excitation forms were applied for the several projects in the context of this work. The different excitation forms are described in the following subchapters.

II.III.1. Quasi-static excitation

A quasi-static load is time dependent (contrary to a time-independent static load), but the excitation frequencies are much smaller compared to the natural frequency (Younis 2011).

Thus, the effect of damping or inertia is negligibly small. This quasi-static excitation allows to measure the stiffness coefficient of the system, if the amplitude of vibration is measured (Younis 2011).

For the project described in chapter III.II, quasi-static forces were applied on the malleus (of an isolated malleus-incus-complex) with a needle mounted on a force meter. Simultaneously, the spatial motion of the malleus was measured with a 3-D LDV system. The measurement setup is described in detail in chapter III.II.2.2.

II.III.2. Dynamic excitation

The dynamic excitation is time- and frequency dependent. For the project described in chapter III.I the ossicles were dynamically excited by acoustic simulation with a loudspeaker (see chapter II.III.2.1), and in the project described in chapter III.II.2.1 with a shaker (see chapter II.III.2.2).

II.III.2.1 Acoustic excitation

The contribution of the IMJ on middle-ear sound transmission was measured for project III.I. The ossicular chain was excited by acoustic stimulation with a loudspeaker in the artificially mounted ear canal (see Figure 2.1). The applied sound pressure was monitored with a reference microphone in the artificial ear canal. More details about the measurement setup are described in chapter III.I.4. The sound pressure level of the acoustic excitation was in the physiological range (90 – 110 dB SPL).

II.III.2.2 Excitation with a shaker

The isolated malleus-incus-complex was excited with a shaker from different excitation directions for the project described in chapter III.II. Simultaneously, the spatial motion of the malleus was measured with a 3-D LDV system. The details of the measurement setup are described in chapter III.II.2.1.

II.IV Velocity measurement using Laser Doppler Vibrometry

Vibrations of middle-ear ossicles were measured for the projects presented in this work. If the human middle ear is stimulated at threshold sound pressure level, the in and out movement of the umbo is about 0.1 nm peak-to-peak (which is less than a diameter of an atom) (Huber et al. 1997). Thus, a special measurement system is necessary to assess these very small vibrations: a Laser Doppler vibrometry system (see chapter II.IV.1). Furthermore, the middle ear is not direct visually accessible. The temporal bones need to be prepared (see chapter II.V.1) such that the laser beam of the laser Doppler vibrometer has access to the middle-ear structures. Every change may influence the acoustic properties and the middle-ear function (see chapter IV.II.3). For these reasons, an advanced measurement setup and a validated preparation of the samples are needed for informative measurements.

II.IV.1. Laser Doppler Vibrometry

A laser Doppler vibrometer (LDV) is an optical system that is used to perform non-contact vibration measurements of a surface. Several other optical techniques were used to measure displacements of ossicular vibrations. Contrary to previous methods, the LDV system allows measurements without adding load to the ossicles. Additionally, no direct contact to the vibrating surface is needed, as it would be the case by attached transducers. Any kind of load on the ossicles was an influence on their dynamic behavior and, thus biases the obtained results.

Since the output of the LDV is directly proportional to the instantaneous surface velocity, the technique is used for any kind of mobility measurements like in research, R&D in industry and for daily use (see Table 2.1). The LDV allows measuring a wide dynamic range of vibration amplitude and frequency.

Field	Examples
Hearing Research	Motion of the tympanic membrane, ossicular motion, motion of the skull, promontory
Acoustic	speaker design, performance of musical instruments (Bissinger & Oliver 2007)
Aerospace	non-destructive inspection of aircraft components (Kilpatrick & Markov 2008)
Architectural	bridge and structure vibration tests (Polytec_GmbH 2015a)
Automotive & Transportation	structural dynamics measurements (R&D), quality control in production processes; structural dynamics, brake diagnostics, and quantification of Noise, vibration, and harshness (NVH), measurement of accurate speed
Biological	insect communication (Fonseca & Popov 1994)
Calibration	Calibration of all types of transducers (since LDV measure motion that can be directly calibrated to the wavelength of light) (Sutton 1990)
Hard Disk Drive Diagnostics	analysis of hard disk drives, specifically in the area of head positioning (Mamun et al. 2006)
Landmine detection	detection of buried landmines; an audio source (loudspeaker) is used to excite the ground (causing the ground to vibrate), resulting in a enhanced ground velocity at the resonance frequency of the areas above a buried mine (Xiang & Sabatier 2000, Burgett et al. 2003, Lal et al. 2006)
Security	remote voice acquisition; with assistance of a visual sensor (camera) audio events can be detected by an LDV (Mamun et al. 2006)

Table 2.1 Adapted from Wikipedia (Wikipedia 2015c).

Vibrations of structures can be measured relatively quickly and with only little or no surface manipulations. Another advantage of LDV systems is that the power of the laser is on a low level (~1 mW), nevertheless, direct eye exposure should be avoided. The performance of the LDV greatly depends on the vibration characteristics of the selected target surfaces (Rui et al. 2011), which is discussed later in this work.

II.IV.1.1 The basic principle of lasers

Laser is an acronym for **L**ight **A**mplification by **S**timulated **E**mission of **R**adiation (Halliday et al. 2003)). The basic principle behind lasers is the “stimulated emission of a photon of electromagnetic radiation” (Yanoff et al. 2009). Thus, laser light has can be derivated from the nature of light. Light shows both, characteristics of waves and particles (wave-particle dualism) (Zahnert 2003). The ‘wave theory of light’ describes all characteristics of light, that describe the propagation of light, while the ‘quantum theory’ describes the conversion of energy at formation and annihilation of light on the atomic scale (Westphal 1947). Atoms can gain, store and lose again a defined amount of energy. For the gain of energy, an electron (that revolves around the atom-nucleus) leaves its orbit to an orbit further away of the atom-nucleus (see Figure 2.10) (quantum leap). If the energy is lost, the electron jumps back to the lower level orbit, and a defined amount of energy is released. The gain or loss of energy happens in form of energy quanta (photons) (see Figure 2.10). The loss of energy is controllable from extern (stimulated emission), and this effect can then be used to produce laser light (Zahnert 2003). Spontaneous emission leads to a photon that is directed to another atom, which leads to emission of further photons in this atom (see Figure 2.10). Electromagnetic radiation is produced in this process (Zahnert 2003). A resonator affects this radiation in a way that it is directed in only one direction, contrary to the scattered visible light of a light bulb. "Each photon has a characteristic frequency, and it's energy is proportional to its frequency" (Reed 1990).

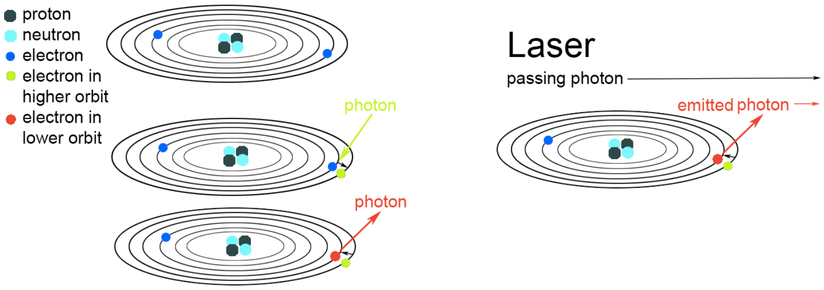

Figure 2.10 Illustration of a simple model of a helium atom at a single point in time: two electrons orbit around the atom-nucleus of protons and neurons. Each orbit has unique energy levels. In the example shown in this illustration, the electrons occupy two different orbits. The electron moves to a higher orbit if the atom absorbs a photon (green photon). Contrary, during spontaneous emission of a photon (red photon) the electron 'falls' to a lower orbit. In the case of a laser, "stimulated emission is not a random process. The electron drops at the moment a passing photon stimulates the electron to drop and emit a photon. Importantly, the stimulating photon and the emitted photon will be identical in frequency and phase. In other words, the two photons are coherent (Lipson et al. 1995)" pp. 41 (Yanoff et al. 2009).

The stimulating photon and the emitted photon will be identical in frequency and phase (see Figure 2.10). Thus, all emitted laser beams have the same frequency and wavelength (monochromasia), the beams are almost parallel (collimation), and the waves have a fixed phase and space relationship (coherence) (Zahnert 2003).

The basic principle of helium-neon lasers

A helium–neon laser is a type of gas laser that mostly operates wavelength of 632.8 nm in the red part of the visible spectrum up to 1152 nm. The gain medium consists of a mixture of helium and neon (approximately 10:1 for 1152 nm, and 5:1 for 633 nm) inside of a small bore capillary tube, usually excited by a direct current electrical discharge (discharging voltage ~ 1–2 kV, current ~ 1–30 mA) (Wikipedia 2015a). The gas inside the capillary is under a pressure of about 100 Pa (Wikipedia 2015b). The gas discharge brings the helium atoms in a state of 'higher energy' (see Figure 2.10, and Figure 2.11), the helium atoms transfer this impact to the neon atoms, and cause a 'population inversion' between the higher and lower energy states (see Figure 2.11). The laser light is generated because of the different energy states of the neon atoms (see Figure 2.11).

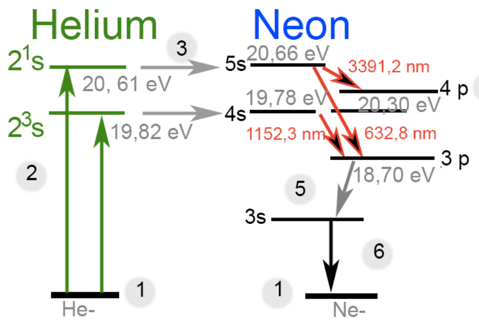

Figure 2.11 Illustration of the energy diagram of ha helium-neon laser: (1) initial state, (2) impulse due to electron impact, (3) electron bombardment, (4) stimulated emission, (5) spontaneous emission, (6) recombination at the wall of the capillary tube. Modified after (Wikipedia 2015b).

II.IV.1.2 The principle of Laser Doppler Vibrometry (LDV)

The basic principle of the LDV measurement technique is the Doppler effect. The laser beam is directed at the surface of interest of a moving sample, and the vibration amplitude and frequency (or phase) are extracted from the Doppler shift of the reflected laser beam. Based on the interferometer technique used in this system, the laser beam is first divided into a reference and a measurement beam. Thus, the frequency (or phase) is extracted from the difference between these two beams (see Figure 2.12). The LDV beams are mixed electronically with a carrier frequency resulting in a single frequency shifted Doppler signal, which is then converted to an analog voltage directly proportional to the instantaneous velocity of the moving sample. Therefore, the LDV can only provide information of the relative position and no absolute values. The relative position like change of the position or displacement can be calculated from the changes in velocity.

For the measurements presented in this dissertation, the amplitude and phase of the ossicular velocity were measured under dynamic (acoustic) stimulation at different frequencies (see chapter II.II).

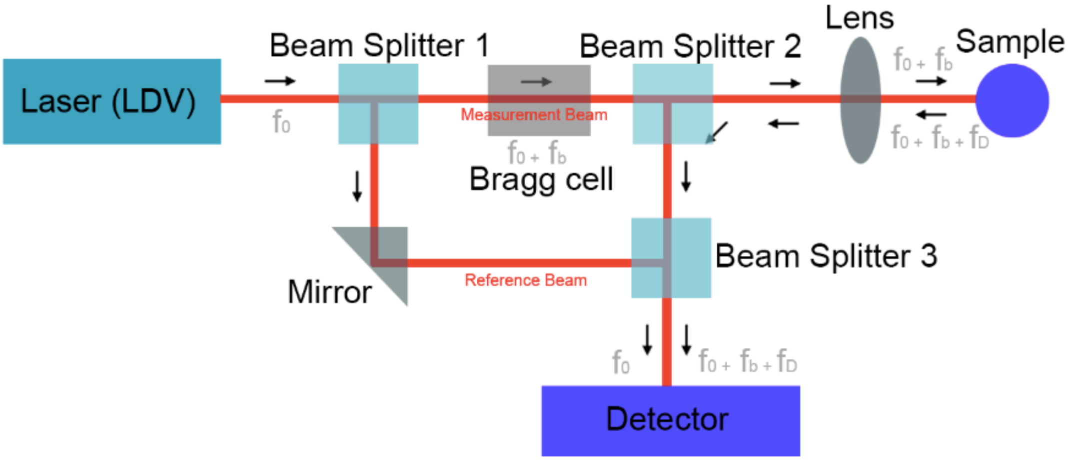

Figure 2.12 Schematic of a laser Doppler vibrometer: the beam from the helium neon laser (with corresponding frequency f_0), is divided into a reference beam and a measurement beam with a beam splitter (beam splitter 1). The measurement beam then passes through the Bragg cell (which adds a frequency shift f_b). This frequency shifted beam then is directed to the sample. The motion of the sample ads a Doppler shift to the beam ($f_D=2*v(t)*\cos(\alpha)/\lambda$, where $v(t)$ is the velocity of the

sample as a function of time, α is the angle between the laser beam and the velocity vector, and λ is the wavelength of the light). The wavelength λ is shortened when the sample moves towards the laser head and elongated when it moves away from the laser head (see Figure 2.13). To be able to determine the velocity of an object, the Doppler-frequency shift (f_D*) has to be measured at a known wavelength. This is done in the LDV by using a laser interferometer. The beam reflected from the sample scatters in all directions, but some portion is collected by the LDV and reflected by the beam splitter (beam splitter 2 and 3) to the photodetector (detector) (frequency = *$f_0 + f_b + f_D$*). In the photodetector, this measurement beam (frequency = *$f_0 + f_b + f_D$*) is compared to the reference beam (frequency = *f_0*). The resulting respond of the detector (frequency = *$f_b + f_D$*) is lower than the initial frequency of the laser (> *10^{14}* Hz). The Bragg cell necessary for the system, because the movement away from the LDV generates the same interference pattern like the movement toward the LDV. Thus, the acousto-optic modulator (Bragg cell) shifts the beam frequency by 40 MHz (by comparison, the frequency of the laser light is 4.74 to *10^{14}* Hz). If the sample moves now towards the LDV, this frequency is reduced and if it moves away from the LDV it is higher than 40 MHz. Consequently, it is possible to detect not only the amplitude but also the direction of the movement. Adapted from (Wikipedia 2015c, Polytec_GmbH 2015b).*

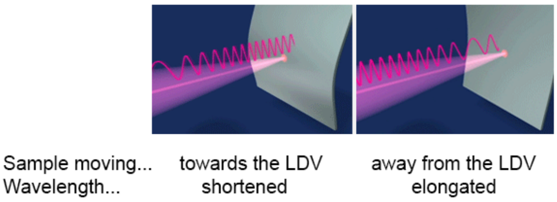

Figure 2.13 The motion of the sample adds a Doppler shift to the beam. The wavelength λ is shortened when the sample moves towards the laser head and elongated when it moves away from the laser head. Adapted from (Polytec_GmbH 2015b).

The vibrometers of Polytec GmbH attain a resolution of 2 nm, and with digital demodulation techniques even down to the picometer range (Polytec_GmbH 2015b).

Different LDV systems are nowadays on the market (Polytec_GmbH 2015d, Polytec_GmbH 2015c, Wikipedia 2015c):

1. Single-point vibrometers
   measurements only in one direction out of plane possible
2. **Scanning vibrometers** (see chapter II.IV.1.3 scanning laser Doppler vibrometer SLDV)
   a single laser beam can be moved across the surface of interest due to a set of X-Y scanning mirrors implemented in the system
3. Continuous Scan Laser Doppler Vibrometry (CSLDV)
   sweeps the laser continuously across the surface of the target to capture the motion of a surface at many points simultaneously
4. **3-D vibrometers** (see chapter III.II and III.III)
   allows to measure all three components of the target's velocity (contrary to single-point LDV and SLDV) with three independent beams, which strike the target from three different directions
5. Rotational vibrometers
   to measure rotational or angular velocity
6. Differential vibrometers
   to measure the out-of-plane velocity difference between two locations on the target
7. Multi-beam vibrometers
   to measures the target velocity at several locations simultaneously
8. Self-mixing vibrometers
   including a ultra-compact optical head that are generally based on a laser diode with a built-in photodetector

II.IV.1.3 Scanning Laser Doppler Vibrometry (SLDV)

A scanning laser Doppler vibrometer (SLDV) PSV-200-1 (Polytec GmbH, Waldbronn, Germany) was used to investigate the dynamic behavior of the middle-ear ossicles presented in this work.

The advantage of this system is the possibility of a rapid non-contact measurement of any vibration. A SLDV integrates computer-controlled X,Y scanning mirrors and a video camera inside an optical head. The laser beam scans point-by-point over samples surface to provide a large number of very high spatial resolution measurements. This data can then be used to visualize deflection shapes in the relevant frequency bands from *frequency domain* analysis – or it can be acquired in the *time domain* to show, for example, animations of wave propagation across the sample.

The system used for this work (see Figure 2.14) is composed of a laser head (OFV 303, Polytec GmbH, Waldbronn, Germany), a vibrometer controller (OFV 3001-S, Polytec GmbH, Waldbronn, Germany), a scanning unit (OFV 040, Polytec GmbH, Waldbronn, Germany), a scanning controller (OFV 042, Polytec GmbH, Waldbronn, Germany) and a computer (Windows XP). A video camera (VCT 24, Polytec GmbH, Waldbronn, Germany) coaxial to the laser beam constantly streamed an image of the scanning area.

The laser head (OFV 303) contains the helium neon laser (wavelength 622 nm, cavity length 203 mm, laser safety class 2, laser output power < 1mW, power consumption ca. 15 W, output center frequency 40 MHz). If two laser beams reach the surface of a sample, they can theoretically be discriminated down to 10 microns center-to-center distance. Thus, for the present work this high performance spatial resolution is abundant.

The vibrometer controller (OFV 3001-S) allows the computer to control the laser head. The processing of the signal coming from the laser head leads to a delay. Therefore, the vibrometer controller synchronizes the velocity signal from an external device e.g. a microphone.

The scanning unit (OFV 040) is mounted in front of the senor head. It contains fast scan mirrors to move the laser beam within an angular range of ±15° in the x and y directions. The delay between two measurement points is reduced to 10 ms by dampening the drivers of the mirrors to prevent vibrations in the mirror during a measurement. The scanning controller (OFV-042) controls voltage and power of the mirrors.

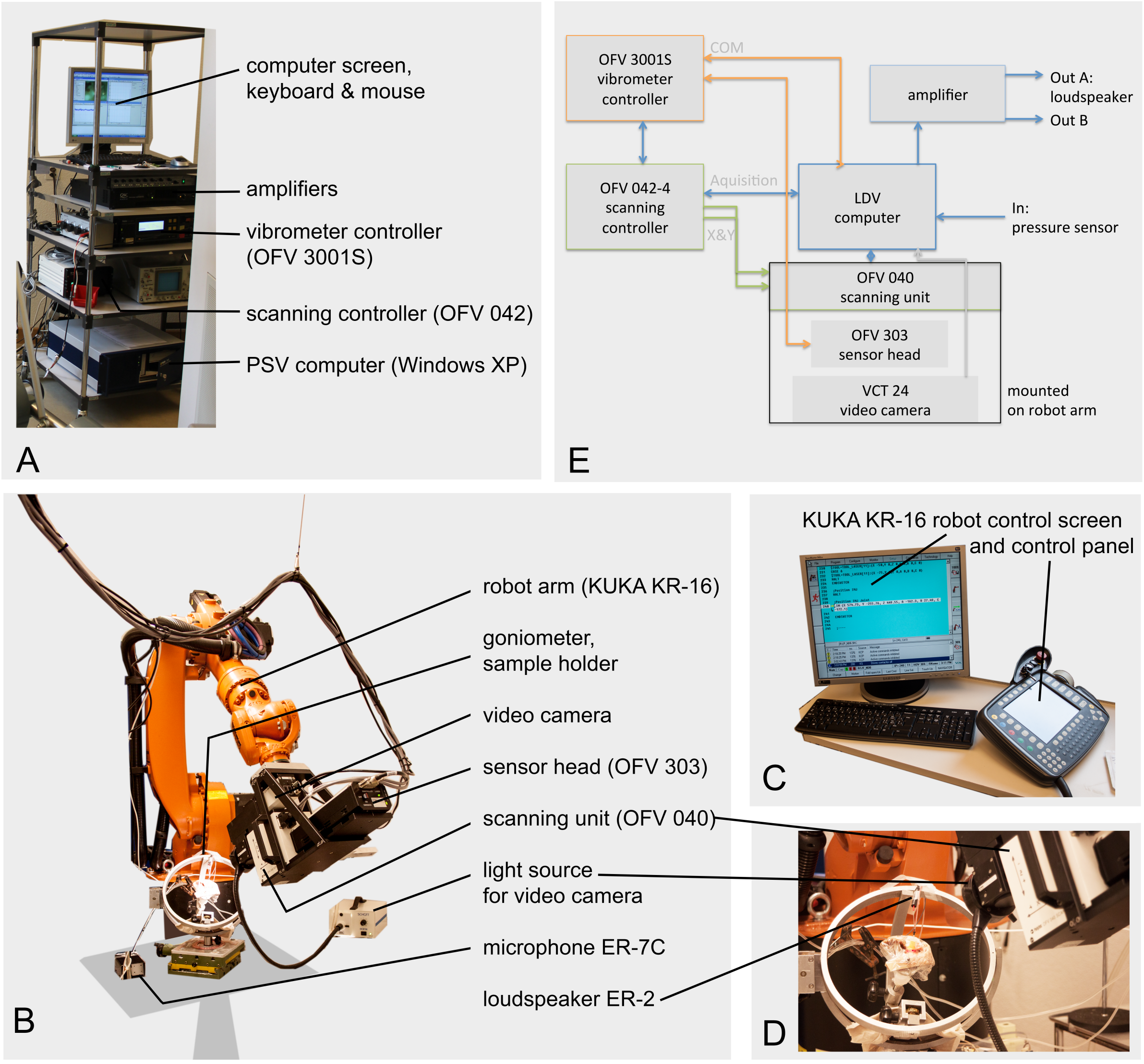

Figure 2.14 Setup of the scanning laser Doppler vibrometer (SLDV) system PSV-200-1 from Polytec GmbH (Waldbronn, Germany).

The video camera (VCT 24) includes a half-silvered mirror, inserted at a 45° angle to the laser beam. It is primarily diaphanous for the wavelength of the emitted laser beam (λ = 622 nm). The scanning area is then finally visible for the user in a video image on the computer screen. A small portion of the reflected laser beam is deflected by the mirror and, therefore, also visible on the video image. The video camera allows zooming and focusing the video image. This facilitates the adjustment of the area of interest on the sample and the laser beam. If the area of interest is visible in the video image and the laser beam is not, a re-positioning of the LDV has to be considered, because a lug could block the laser beam.

II.IV.1.4 Software of the LDV system

The software package (PSV 9.0, Polytec) controls the measurement system (PSV-200-1). It can operate in two modes; an acquisition and a presentation mode. The software allows to control the hardware, defining the scan points, setting the parameters for data acquisition, generating an excitation signal (as an option), acquiring digital data, saving data and displaying data and evaluating it (Polytec_GmbH 2014).

Acquisition mode of the PSV Software

In the acquisition mode the software controls the signal generator and two input channels during the measurement.

II.IV.1.4.1.1 Calibration

First, the surface of the area of interest has to be zoomed in and focused with the laser control tool of the acquisition mode of the PSV software in order to calibrate the system (see Figure 2.15). First, the laser beam needs to be arbitrarily positioned on the area of interest on the sample surface. Then, the cursor is placed in the center of the laser beam visible in the video image, and with a mouse click this position is marked (see Figure 2.15, Nr. 1). Therewith, x-, y-coordinates are assigned to this position. This procedure is repeated three times in minimum to successfully accomplish the calibration.

II.IV.1.4.1.2 Measurement grid

Single point measurements can be performed in real time at a single 'manually' selected point. This helps to check the quality of the laser signal at a certain point of interest. A grid with several points of interest has to be defined for a measurement. The system then automatically scans along the defined grid, and saves the data automatically to a file. If the video image is zoomed in or out, or the focus is changed, the system needs to be re-calibrated before the next measurement. Both angular deflection of the beam and the x-,y-position change. This is due to the changes in the distance between the sample surface and the laser head since the mirrors of the scanning unit automatically position the laser beam by angular deflection. The application window in the acquisition mode and video mode is shown in Figure 2.16.

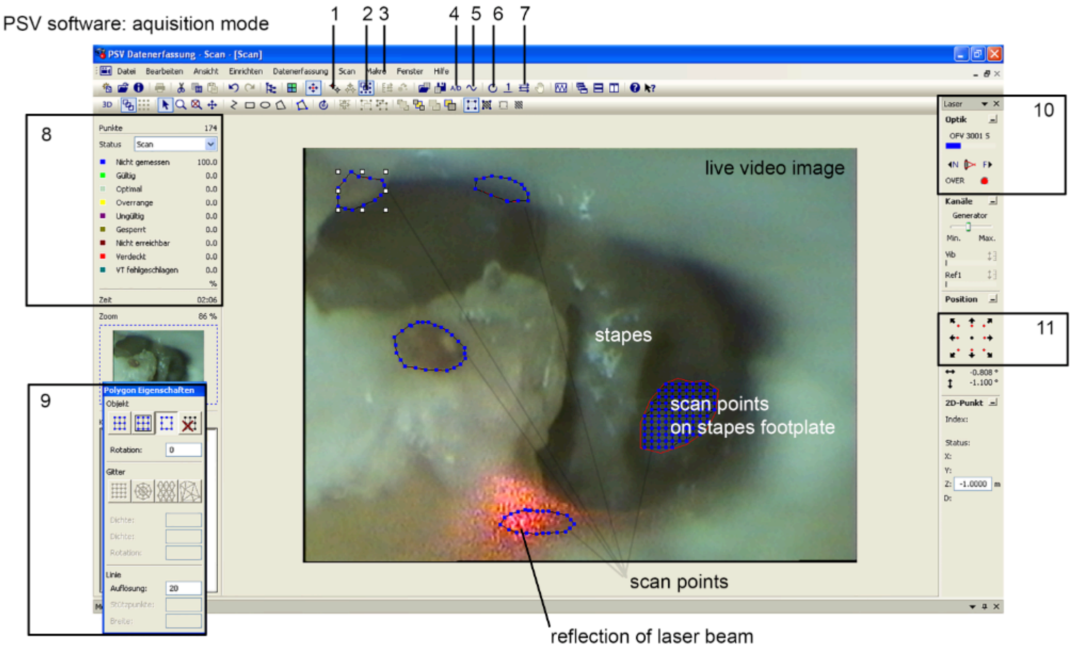

Punkte	174
Status	Scan
Nicht gemessen	100.0
Gültig	0.0
Optimal	0.0
Overrange	0.0
Ungültig	0.0
Gesperrt	0.0
Nicht erreichbar	0.0
Verdeckt	0.0
VT fehlgeschlagen	0.0
	%
Zeit	02:06
Zoom	86 %

Rotation: 0
Dichte:
Dichte:
Rotation:
Auflösung: 20
Stützpunkte:
Breite:

OFV 3001 S
N F
OVER
-0.808 °
-1.100 °
Index:
Status:
X:
Y:
Z: -1.0000 m
D:

Figure 2.15 Example of the application window in acquisition mode with live video image during a scan: (1) laser focus setting, (2) scan points scatter, (3) macro tool, (4) scan properties (preferences), (5) stimulus on/off, (6) acquisition, (7) scan storage properties, (8) scan points and scan information (valid scan point, not valid scan point, etc.), (9) scatter properties, (10) quality of laser signal information, (11) control field for laser direction manipulation.

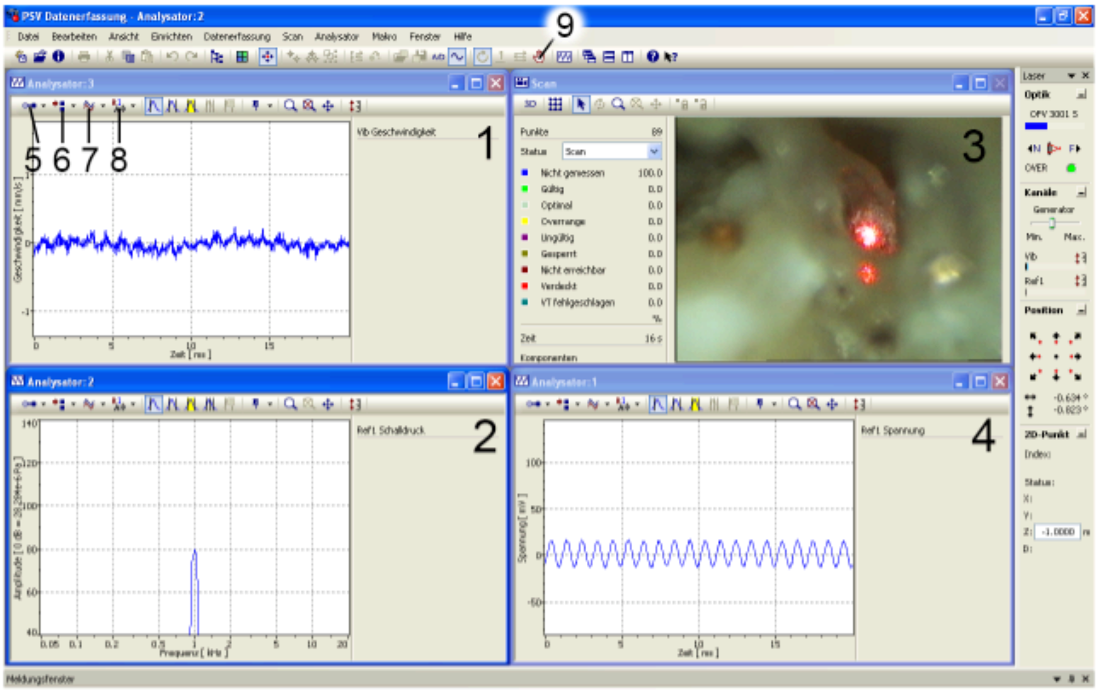

Figure 2.16 Example of the application window in acquisition mode with live video image during a scan: (1) signal from LDV (velocity of vibration), (2) reference pressure, (3) live video image of measurement of stapes footplate vibration, (4) reference voltage, (5) select domain (6) select channel (A or B), (7) select signal, (8) select display mode, (9) stop acquisition.

An example for a stapes footplate motion measurement is shown in Figure 2.17 and for a IMJ motion measurement in Figure 2.18.

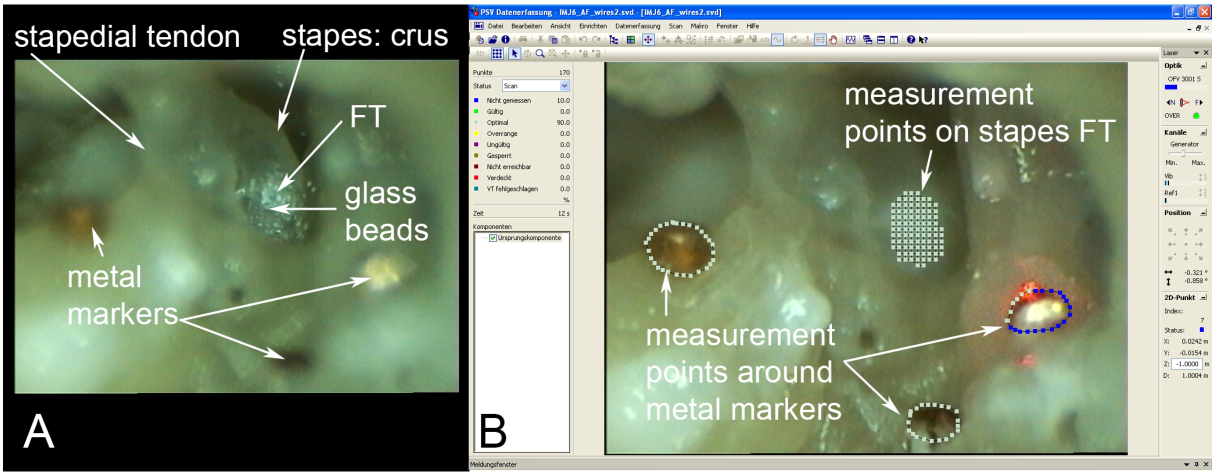

Figure 2.17 Example of a measurement of the stapes footplate motion with the LDV. (A) Microscope image shows the footplate (FT) of the stapes with glass beads, the stapedial tendon, and the metal markers. (B) Acquisition mode of the PSV software for a measurement of the stapes footplate vibration. The grid of the measurement points is shown for the footplate and around the metal markers. The laser beam is visible on the right side on the metal marker.

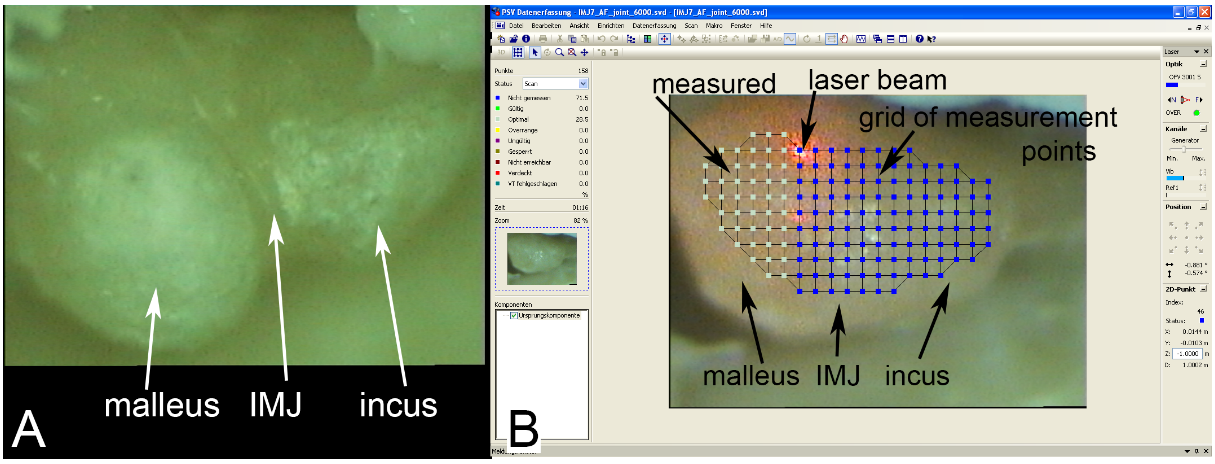

Figure 2.18 Example of a measurement of the IMJ motion with the LDV. (A) Microscope image of the mobile IMJ. (B) Acquisition mode of the PSV software for a measurement of the immobilized IMJ.

II.IV.1.4.1.3 Scan properties

The scan properties (preferences) need to be defined prior to a measurement for an optimal outcome. It includes (see Figure 2.19):

1. General properties
2. Canals
3. Filters
4. Frequencies
5. windows
6. Trigger
7. SE
8. Generator

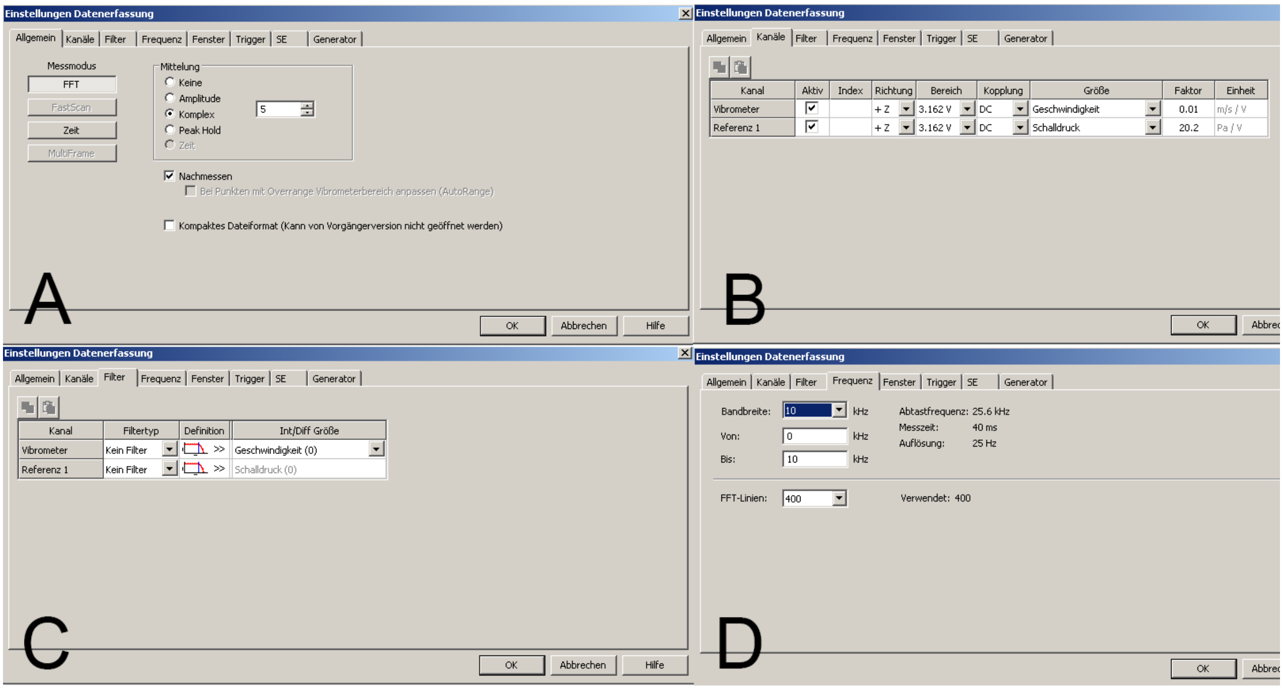

Messmodus: FFT

FastScan

Zeit

MultiFrame

Mittelung

○ Keine

○ Amplitude

● Komplex 5

○ Peak Hold

○ Zeit

☑ Nachmessen

☐ Bei Punkten mit Overrange Vibrometerbereich anpassen (AutoRange)

☐ Kompaktes Dateiformat (Kann von Vorgängerversion nicht geöffnet werden)

Kanal	Aktiv	Index	Richtung	Bereich	Kopplung	Größe	Faktor	Einheit
Vibrometer	☑		+ Z	3.162 V	DC	Geschwindigkeit	0.01	m/s / V
Referenz 1	☑		+ Z	3.162 V	DC	Schalldruck	20.2	Pa / V

Kanal	Filtertyp	Definition	Int/Diff Größe
Vibrometer	Kein Filter	>>	Geschwindigkeit (0)
Referenz 1	Kein Filter	>>	Schalldruck (0)

Bandbreite: 10 kHz

Von: 0 kHz

Bis: 10 kHz

Abtastfrequenz: 25.6 kHz

Messzeit: 40 ms

Auflösung: 25 Hz

FFT-Linien: 400

Verwendet: 400

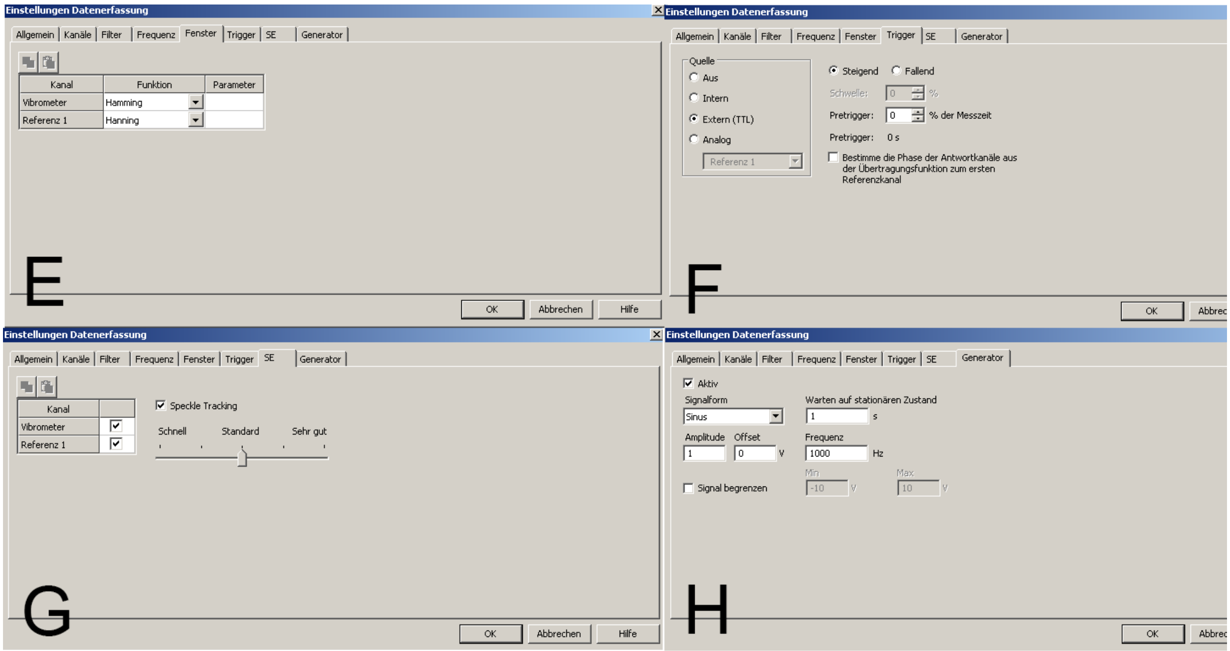

Kanal	Funktion	Parameter
Vibrometer	Hamming	
Referenz 1	Hanning	

Quelle
○ Aus
○ Intern
● Extern (TTL)
○ Analog
Referenz 1

● Steigend ○ Fallend
Schwelle: 0 %
Pretrigger: 0 % der Messzeit
Pretrigger: 0 s
☐ Bestimme die Phase der Antwortkanäle aus der Übertragungsfunktion zum ersten Referenzkanal

Kanal	
Vibrometer	☑
Referenz 1	☑

☑ Speckle Tracking
Schnell Standard Sehr gut

☑ Aktiv
Signalform: Sinus
Warten auf stationären Zustand: 1 s
Amplitude: 1 Offset: 0 V
Frequenz: 1000 Hz
☐ Signal begrenzen Min: -10 V Max: 10 V

Figure 2.19 Properties of the PSV Software: (A) general properties, (B) canals, (C) filters, (D) frequencies, (E) windows, (F) trigger, (G) SE, (H) generator.

II.IV.1.4.1.4 Control of signal generation

The signal control is included in the first category 'devices'. This property of the PSV software allows controlling the acoustic signal, which is produced by the signal generator. The signal type (sinus, periodic chirp, sweep, noise, user defined etc.), the frequency resolution (number of FFT-lines) and the frequency range is defined here as well (see Figure 2.19). For this work, a custom-made macro was programmed that allowed to measure the ossicular motion under a stepped-sine stimulation. The macro automatically changed the stimulation frequency and saved the data. It reduced the measurement time essentially, since it replaced the manual naming and storage of every single frequency.

II.IV.1.4.1.5 Measurement and data storage

The measurement of a single point can be followed in real time in the time or frequency domain. The measured data is processed using Fast Fourier Transform (FFT). Afterwards the data including coordinates, amplitude and phase information is stored as complex numbers at each point and frequency (see Figure 2.20). The z-coordinate has always the same value since the SLDV only measures the x and y component that is measurable with one laser beam. To measure all three motion components a 3-D LDV would be needed. Additionally, the file name, sound pressure, band number, measured frequency and information about interpolation and filter are stored in the header of every output data file (see Figure 2.20).

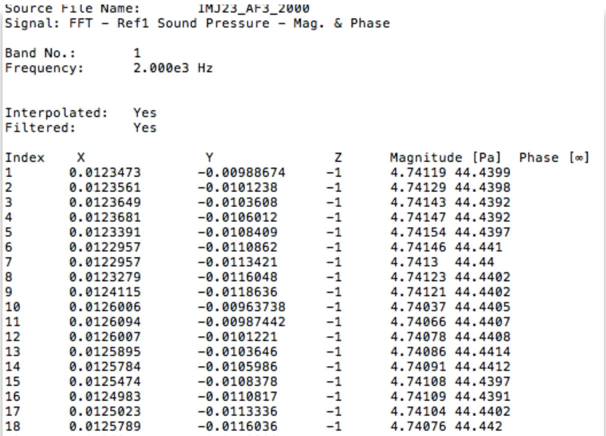

```
Source File Name:       IMJ23_AF3_2000
Signal: FFT - Ref1 Sound Pressure - Mag. & Phase

Band No.:       1
Frequency:      2.000e3 Hz


Interpolated:   Yes
Filtered:       Yes

Index    X               Y               Z       Magnitude [Pa]  Phase [∞]
1        0.0123473       -0.00988674     -1      4.74119 44.4399
2        0.0123561       -0.0101238      -1      4.74129 44.4398
3        0.0123649       -0.0103608      -1      4.74143 44.4392
4        0.0123681       -0.0106012      -1      4.74147 44.4392
5        0.0123391       -0.0108409      -1      4.74154 44.4397
6        0.0122957       -0.0110862      -1      4.74146 44.441
7        0.0122957       -0.0113421      -1      4.7413  44.44
8        0.0123279       -0.0116048      -1      4.74123 44.4402
9        0.0124115       -0.0118636      -1      4.74121 44.4402
10       0.0126006       -0.00963738     -1      4.74037 44.4405
11       0.0126094       -0.00987442     -1      4.74066 44.4407
12       0.0126007       -0.0101221      -1      4.74078 44.4408
13       0.0125895       -0.0103646      -1      4.74086 44.4414
14       0.0125784       -0.0105986      -1      4.74091 44.4412
15       0.0125474       -0.0108378      -1      4.74108 44.4397
16       0.0124983       -0.0110817      -1      4.74109 44.4391
17       0.0125023       -0.0113336      -1      4.74104 44.4402
18       0.0125789       -0.0116036      -1      4.74076 44.442
```

Figure 2.20 Output data from the PSV software for a measurement at 2 kHz. The data includes coordinates, magnitude and phase of each LDV measurement point.

Presentation mode of the PSV Software

In the presentation mode, the velocity data of one measurement (all points of the measurement grid) can be visualized (see Figure 2.21). The displacement mode can be changed: 'topographic map' or as an iso-displacement map to show the given velocity, displacement or acceleration on a linear or logarithmic (dB) scale. The quality of each point on the measurement point grid can be assessed by displaying the intensity of the reflected signal and the coherence between the excitation signal and the measured signal. The coherence was judged as 'sufficient' if it was larger than 80 %. The PSV software allows animating the vibrations of the measured points (see Figure 2.21). The dynamic motions of the ossicles were visualized directly after the measurements to have a first impression of the motion patterns.

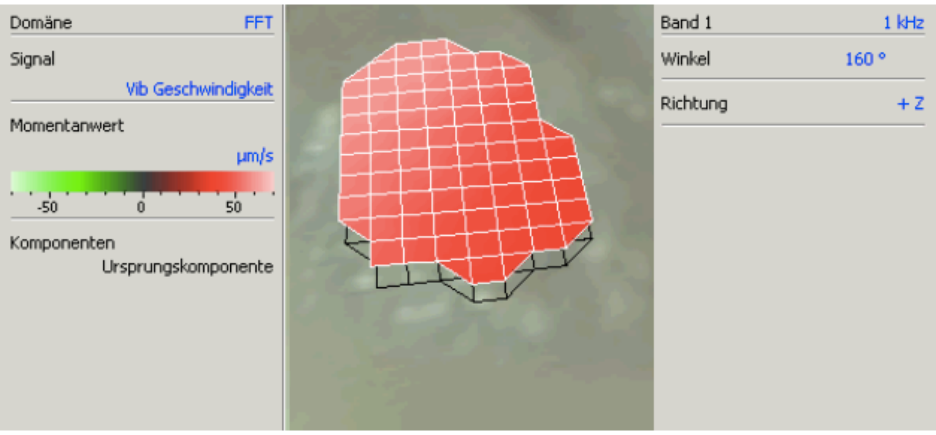

Domäne FFT
Signal Vib Geschwindigkeit
Momentanwert µm/s
Komponenten Ursprungskomponente
Band 1 1 kHz
Winkel 160 °
Richtung + Z

Figure 2.21 Animation of the motion of the stapes footplate by the PSV software in the presentation mode.

II.IV.2. Robot arm

For the first preliminary measurements, the LDV has been manually controlled on a stand of a microscope. Changing the position of the LDV was difficult, due to the required precision in the millimeter range (long length of stapes footplate 2.81 ± 0.158 mm) and the weight of the LDV system (12 kg, 58 cm x 29 cm x 24 cm). A robot arm KUKA KR 16 (KUKA Roboter Schweiz AG, Neuenhof, Switzerland) and the corresponding controller KR C4 are now installed since July 2013 in the laboratories of our 'biomechanics of hearing' group to control the position of the LDV system (see Figure 2.14). The advantages of the robot arm are: easier and more precise positioning of the LDV, the possibility for a partly automatized change of the LDV position (known position of spatial coordinates), a time saving aspect, and the possibility to change the angle of the laser beam and, therefore, the possibility to calculate the 3-D motion of the 2-D LDV and angle information. The KUKA KR 16 has six axes, and the repeatability is <±0,05 mm. A function was programmed together with INSYS Industriesysteme AG (Münsingen, Switzerland) to move the robot arm to a previously saved position. This function allowed measuring the motion of the stapes footplate, move to the IMJ, and then back to the first position to measure again the stapes footplate motion (see chapter III.I).

II.V Micro-CT imaging and frame registration

II.V.1. Preparation of the sample for the micro-CT scan

If retro-reflective glass beads of a micron size were used to enhance the LDV signals, they were removed prior the micro-CT scans to avoid artifacts later on in the micro-CT images by carefully flushing the beads out with water by a syringe. Additionally, the water was sucked out of the middle ear cavity with a vacuum pump. Then, the middle ear cavity was filled with glue to be sure that mainly the metal markers are well fixed. This is important for a frame registration, which is needed to reconstruct the 3-D components of ossicular motion later on (see chapter II.V.4.1). The sample was further prepared; bony tissue was removed such that it fitted into the sample holder (holder size: 36 mm) of the micro-CT with an inner diameter of 33 mm (see Figure 3.1). Great cares were taken to not to drill close to the middle-ear structures and the metal markers.

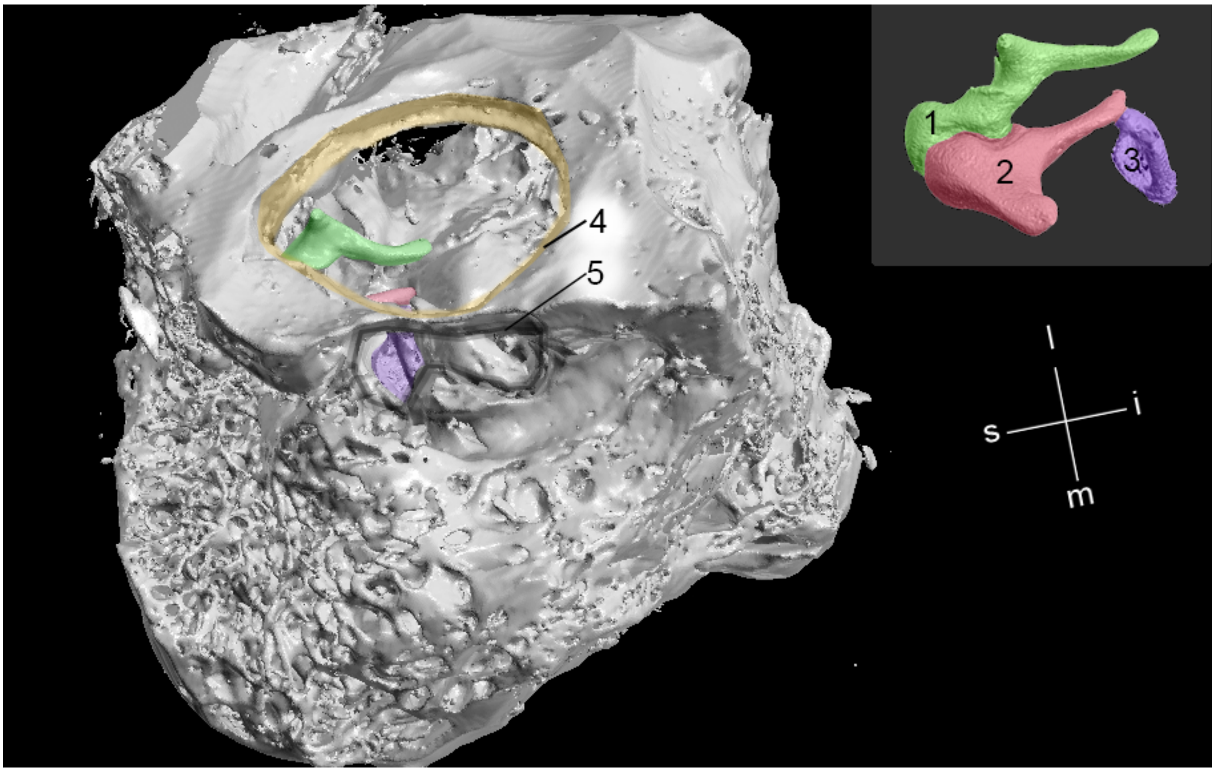

Figure 3.1 Prepared temporal bone sample for the holder of the micro-CT machine shown by a micro-CT 3-D reconstruction of the middle-ear and surrounding structures: (1) malleus, (2) incus, (3) stapes, (4) tympanic annulus (tympanic membrane is not visible in the micro-CT reconstruction), (5) access to the stapes footplate after the posterior tympanotomy. On the upper right side the ossicular chain is shown with same size and angle as in the temporal bone sample on the left side. (m) medial, (l) lateral, (s) superior, (i) inferior.

II.V.2. Micro-CT scan (micro-scale x-ray computed tomography)

The micro-scale x-ray computed tomography (micro-CT) is a non-destructive imaging method with a high resolution (10 µm). Therefore, it has been used to measure the geometry of the ossicular chain by several authors (Lane et al. 2004, Lane et al. 2005, J.H Sim et al. 2013, J.H Sim et al. 2007, J.H. Sim & Puria 2008, J.H Sim 2007).

II.V.2.1 Basics of micro-CT processes

The x-ray absorption is dependent on the material, resulting in different gray-scale values for different tissues e.g., bone absorbs more x-ray than soft tissue and, therefore, bone appears brighter in the 2-D slice images. Consequently, “the 3-D internal structure can be inferred from the images, and internal features can be uniquely positioned. The resulting 3-D images are typically displayed as a series of 2D slices” (Landis & Keane 2010). The process is schematically illustrated in Figure 3.2.

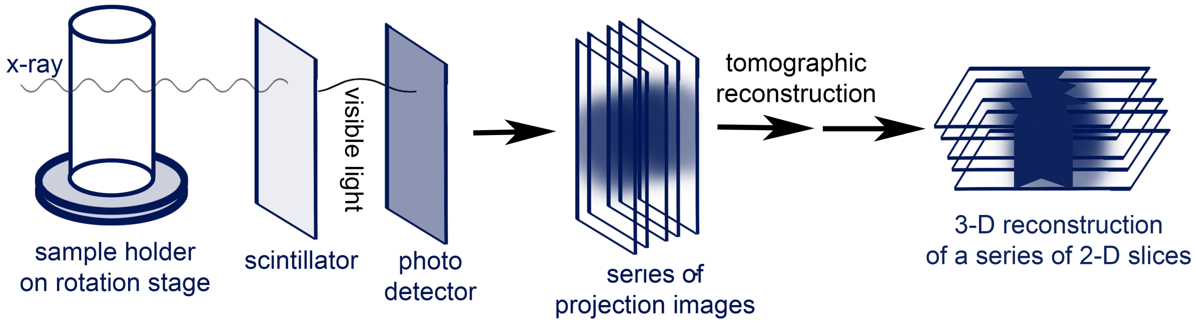

Figure 3.2 Illustration of the micro-CT processes (acquisition and reconstruction). The sample is placed in a sample holder, which is then placed on a rotation stage. The rotation stage constantly rotates during the scan. A mathematical reconstruction produces a 3-D map of the X-ray absorption in the volume out of the series of the X-ray projection images. The software of the micro-CT machine displays the 3-D map a series of 2-D slices, where the user (with or without additional software) can reconstruct the 3-D image of the region of interest e.g, middle ear ossicles. Modified after (Landis & Keane 2010).

II.V.3. Micro-CT scan properties

The SCANCO µCT40 micro-CT scanner of the company SCANCO Medical AG (Dietikon, Zurich, Switzerland, www.scanco.ch) and the ‘SCANCO vivaCT 40’ micro-CT scanner of the Division of Surgical Research (University Hospital & University of Zurich, Switzerland) developed by SCANCO Medical AG (Dietikon, Zurich, Switzerland, www.scanco.ch) were used in this work. The main window of the micro-CT computer is shown in Figure 3.3. This CT-machine permits to control the resolution, the photon energy level, the current intensity of the x-ray beam, and the integration time as conditions for CT scanning (see Figure 3.3, Nr. 2). By changing these factors, the quality of the resulting micro-CT images can be optimized. The achievement of the optimal image quality of middle-ear structures was discussed in the doctoral thesis and in a publication of Dr. Jae Hoon Sim (J.H Sim 2007, J.H Sim et al. 2007). Sim (J.H Sim 2007) obtained the maximal resolution of the middle ear structures using a 21.5 mm diameter sample holder and the highest possible resolution of the vivaCT 40 (2048 x 2048 pixels per image slice), which was in this case 10.5 µm. For the samples in this study a maximal possible resolution of 17 µm (diameter of sample holder divided by 2048 x 2048 pixels per image slice) was obtained. This lower resolution, compared to Sim 2007, was obtained due to the larger size of the sample holder (36 mm). The photon energy level was 70 kVp, the current intensity was 114 µA, the voxel size was 11.4 X 11.4 X 11.4 µm, and the integration time (number of average) was 300 µs. The time for each scan was approximately 4-6 hours, followed by several hours of reconstruction calculation of the CT-computer.

The quality of the micro-CT image depends on the signal-to-noise ratio, which is directly affected by the x-ray intensity. The disadvantage of the increase of this x-ray intensity is the often require larger focal spot, which results in degrading image sharpness (Ketcham & Carlson 2001). For our scans a photon energy level of 70 kVp with a current intensity of 114 µA showed the best possible image quality for our samples including the reference markers.

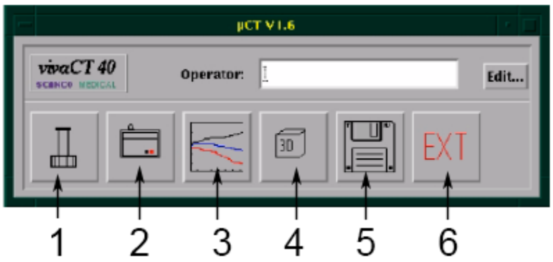

Figure 3.3 Main window of micro-CT software. Before scan: (1) define sample name, (2) choose properties for scan and start scan. After scan: (3) evaluate measurements, (4) show 3-D reconstruction of in (3) reconstructed 3-D shape of region of interest, (5) save scan data externally e.g., magnet band, server, external disk, (6) exit the software.

II.V.4. Segmentation of the micro-CT images and construction of 3-D surface model (STL file)

Once the scan is done, the micro-CT machine generates an 'ISQ file'; a file type that is primarily associated with micro-CT scans by SCANCO Medical AG. These files contain layers representing CT 2-D image slices (see chapter II.V.2.1). Because the sample is not scanned slice by slice (see Figure 3.2) but rather in series of projection images, the full tomographic reconstruction (see Figure 3.2) has to be completed before the 2-D slices (ISG file) are available for further analysis. For the segmentation, the contour of the stapes in each slide has to be determined (see Figure 3.4). The 3-D reconstruction can be obtained by the micro-CT software using the information of the contours of the structure that was manually defined before (see Figure 3.5 B). It also exists a semi-automatic command in the software that follows the defined contours from slice to slice. However, this command can only be used if the gray-scale value of the structure of interest is different from the surrounding structures – which is sometimes difficult in case of the stapes, because of the tendons, ligaments and the bony tissue close to it with similar gray-scale values (see Figure 3.4).

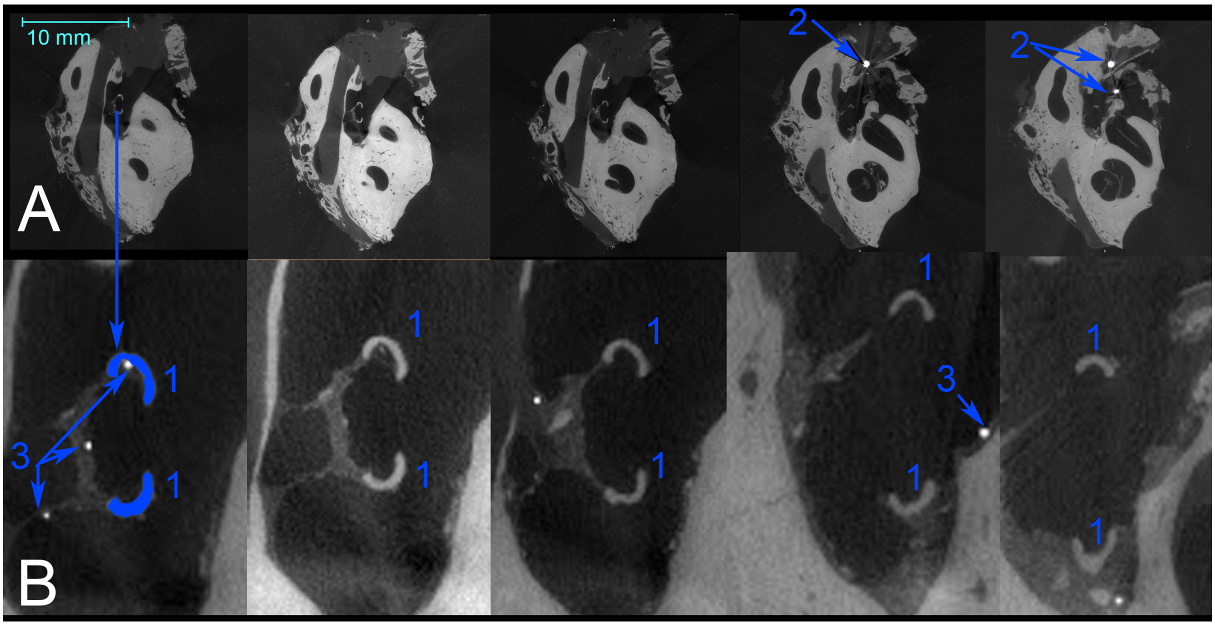

Figure 3.4 Output data of the micro-CT machine: 2-D slices. (A) 2-D slices showing a cross-section trough the whole sample. (B) Zoomed-in view of (A) showing the area with the stapes. (1) Contours of the stapes structure, (2) metal markers, (3) glass beads (remaining after washing out the most glass beads, see II.V.1).

Once the 3-D file is generated, the 3-D surface model can be generated and saved as a STL-file (STereoLithography, format for CAD/ Computer-aided design software). For further calculations in Matlab, the dimensions and position of the generated 3-D model of e.g. the stapes and the metal markers (see Figure 3.5 B) has to be read from the STL format using the 'examine geo' function in the micro-CT software. This then shows the face (F), vertex (V) and color (C) values (see Figure 3.5 A).

A

```
ipl > examine in geo
/examine
        -input  in
        -item   geo
!> dim                      56            80            37
!> off                      0             0             0
!> pos                      514           1360          2249
!> element size in mm       0.0150 0.0150 0.0150
!> phys dim in mm           0.8400 1.2000 0.5550
```

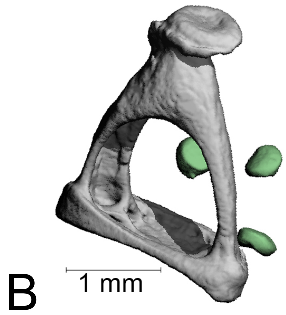

Figure 3.5 (A) Output of the 'examine geo' command showing the dimension, the offset, the position and the element size of the sample. This info is needed for later calculations of the footplate frame registration (see chapter III.V.5.1). (B) Result of the 3-D reconstruction of the stapes (grey) and three metal markers (green). This information is needed for the later frame registration (see chapter III.V.4.1).

II.V.4.1 Frame registration

Reference markers (pieces of copper wire) were mounted on the sample during the preparation (see Figure 3.5 B). Once the 3-D volumes of the stapes and reference markers were constructed, the anatomically-fixed intrinsic frame was obtained, and relation between the anatomical intrinsic frame and the LDV measurement frame was calculated, based on coordinates of the reference markers in both frames.

Anatomical intrinsic frame

Two anatomical frames were defined and were used as the intrinsic frame in this dissertation.

The first anatomical frame was defined based on the median surface of the stapes footplate and was used to describe spatial motion of the stapes. The anatomical frame was defined such that the xy-plane was fit to the median surface of the stapes footplate with the centroid of the median surface set as the origin. Such procedures were performed using a commercial software RapidForm (3-D Systems Inc.). The *x*-axis was aligned along the long length, the *y*-axis was aligned along the short length of the footplate, and consequently the *z*-axis was aligned along the longitudinal direction of the stapes (i.e., direction of the piston-like motion of the stapes) as shown in Figure 2.22 A. The superior direction was set as the positive y direction, and the anterior direction was set as the positive *x* direction. The right panel of Figure 2.23 shows the stapes and the reference markers in the anatomical intrinsic frame.

The second anatomical frame was defined to describe spatial motions of the malleus and the incus. The *x, y,* and *z* directions in the first anatomical frame was maintained in the second anatomical frame, but the origin of the second frame was located the center of mass of the malleus-incus complex (see Figure 2.22 B).

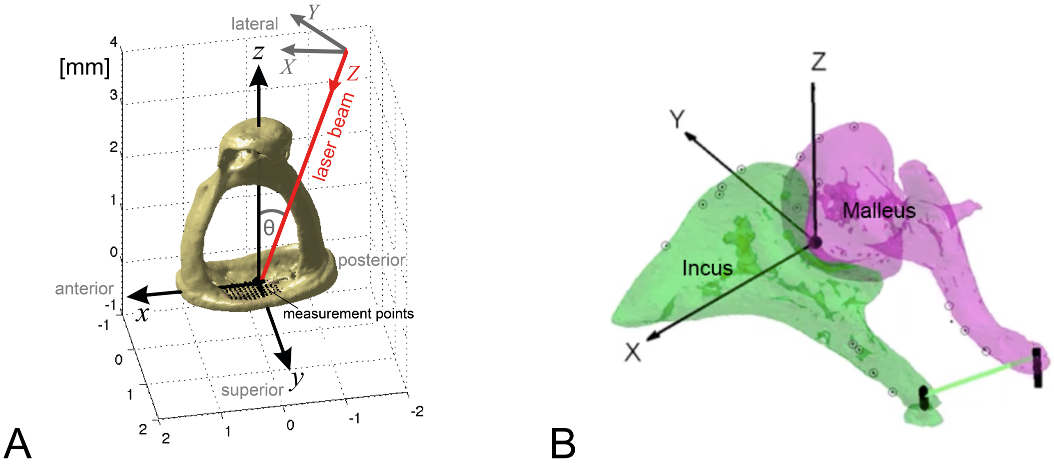

Figure 2.22 (A) Orientation of the stapes in the anatomically fixed frame (see III.I). (B) Orientation of the malleus-incus complex (MIC) in the anatomically fixed frame.

Registration to the anatomical intrinsic frame

Correlation between the anatomical intrinsic frame and LDV measurement frame was obtained by two-dimensional matching of the reference markers between both frames. Denoting the *XYZ* coordinate system as the LDV measurement frame (see left panel in Figure 2.23) and *xyz* coordinate system as the anatomical intrinsic frame (see right panel in Figure 2.23), the *XY* coordinates of the outlines of the reference markers in the LDV measurement frame were recorded during the measurement of vibrational motion of the ossicles, and the *xyz* coordinates of the reference markers were obtained from the 3-D features of the reference markers, which were reconstructed from the micro-CT images and were registered into the intrinsic frame. To obtain the relation between the two frames, the 3-D features of the ossicles and the markers in the intrinsic frame were transformed by means of rotations and translations such the XY coordinates of the outlines of the reference markers in the LDV measurement frame fitted to the actual shapes of the reference markers obtained from micro-CT imaging (see middle panel in Figure 2.23). The rotations and translation for the transformation were calculated as

$$\begin{Bmatrix} X \\ Y \end{Bmatrix} = \begin{bmatrix} \cos\varphi\cos\theta & \sin\varphi\cos\theta & -\sin\theta \\ \cos\varphi\sin\theta\sin\phi - \sin\varphi\cos\phi & \sin\varphi\sin\theta\sin\phi + \cos\varphi\cos\phi & \cos\theta\sin\phi \end{bmatrix} \begin{Bmatrix} x - x_{shift} \\ y - y_{shift} \\ z - z_{shift} \end{Bmatrix},$$

Base lines for these techniques have been developed in our group (Sim et al. 2010, Sim et sl. 2012). The middle panel of Figure 2.23 shows the 3-D features of the ossicles and the markers finally aligned to the LDV measurement frame by the procedures described above.

After the transformation from the anatomical intrinsic frame to the LDV measurement frame was defined by rotational angles and translations in the equations above, by reversing the transformation, the transformation from the LDV measurement frame to the anatomical intrinsic frame is obtained, and all measurement points and measured velocities were registered to the intrinsic frame for further processing and analysis.

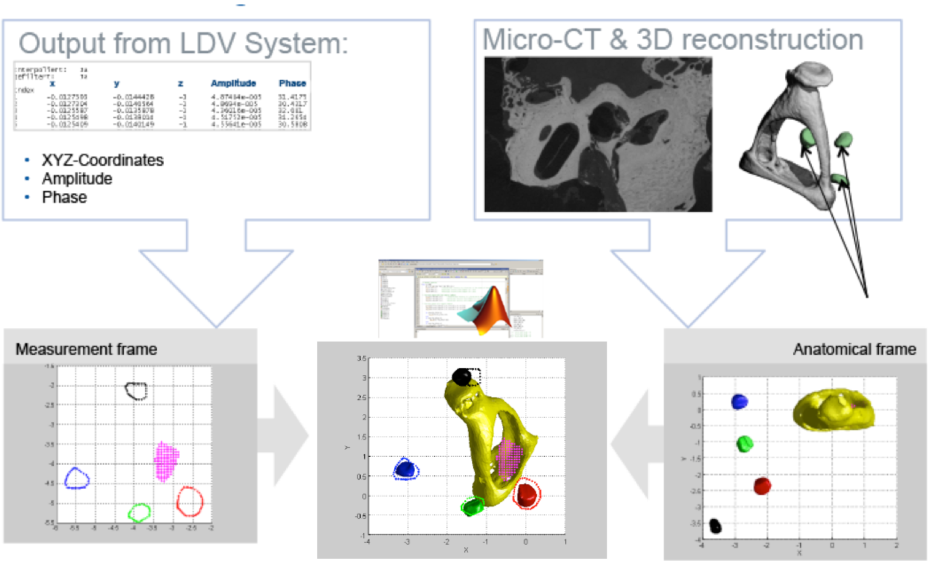

Figure 2.23 Process of frame registration: the measurement frame is obtained from the LDV-data, and the anatomically fixed frame is obtained from the micro-CT-data. The two frames are then overlapped during the process of frame registration with Matlab; Alignment of the measurement frame (dots) and the anatomical intrinsic frame (markers and stapes) is shown in the middle panel.

II.VI Audiometric measurements and assessment of distorted sound perception for reconstructed ears

The quality of the perceived hearing after stapedotomy surgery is in focus for the project described in chapter III.IV. One factor that can influence the patient's satisfaction of the hearing quality after surgery is the perception of distorted sounds. This factor cannot be assessed with the standard pure tone audiometry. Pure tone audiometry serves as a diagnosis tool before surgery and is also standardly performed after ear surgery for the qualitative and quantitative analysis of the patients hearing (see chapter II.VI.1). To assess the perception of distorted sound after stapedotomy, a new test was performed additionally to the standard pure tone audiometry (see II.VI.1). To evaluate the perception of distorted sounds in the daily live, a questionnaire (Amsterdam Post Operative Sound Evaluation: APOSE) (see chapter II.VI.2).

II.VI.1. Pure tone audiometry (PTA)

Pure tone audiometry (PTA) aims an analysis of the patient's hearing (conductive hearing loss, sensorineural hearing loss or mixed loss) for pre-operative and post-operative evaluations or the fit of hearing aids. It is carried out in a sound proof room of the University Hospital Zurich for our studies. The frequency range tested is 125 Hz to 8000 Hz for air conduction, and 250 Hz to 4000 Hz for bone conduction. Depending on the audiometer (measurement apparatus for pure tone audiometry), the patient is told to raise her/his finger or press the signal-button when she/he appreciates the slightest sound. The bone conduction hearing is indicative for the cochlear function, showing the sensorineural component of the hearing loss. The difference between the thresholds of air and bone conduction (Air-Bone-Gap (ABG)= air conduction threshold – bone conduction threshold) represents the conductive hearing loss. This conductive hearing loss can appear due to pathologies of the external ear (see chapter I.III.1) or the middle ear (including the tympanic membrane) (see chapter I.III.2). The audiometers are calibrated regularly. The audiometry of the University Hospital Zurich is certificated according to the DIN EN ISO 8253 norm.

To assess the perception of distorted sound after stapedotomy, a new test was performed additionally to the standard pure tone audiometry. This additional test is described in detail in chapter III.IV.3.1.5; the subjects were told to raise her/his finger if the sound was perceived distorted at different sound levels and frequencies.

II.VI.2. Questionnaire: Amsterdam Post Operative Sound Evaluation (APOSE)

The patient's quality of hearing during the everyday life is assessed with a questionnaire: Amsterdam Post Operative Sound Evaluation (APOSE). This questionnaire asks about the quality of hearing for different sounds e.g., music, own voice, and about hearing after surgery in general (better, worse, unchanged). The questionnaire is described and reprinted in chapter III.IV.3.3.

III. Projects

The following subchapters show the achieved results of the different projects:

III.I	Contribution of the incudo-malleolar joint to middle-ear sound transmission
III.II	Quasi-static and dynamic behavior
III.III	Characterization of spatial incudo-malleolar-joint motions under acoustic stimulation
III.IV	Middle-ear sound transmission in reconstructed ears: Distortion product after stapedotomy surgery

Chapter III.I was the main project of this dissertation. The corresponding manuscript was submitted to the journal 'Hearing Research' and is presented in chapter III.I.

Chapters III.I, III.II, and III.III focus on the behavior and functionality of the IMJ. The morphology (see chapter I.III.2.4.4.1), and the mobility and functionality (see chapter I.III.2.5.3) of the IMJ were broadly described previously in the background chapter of this dissertation. The data analysis of the projects in chapter III.II and chapter III.III is still in progress. The patient recruitment and data analysis of the project in chapter III.IV are still in progress as well.

III.I Contribution of the incudo-malleolar joint to middle-ear sound transmission

The study about the 'contribution of the incudo-malleolar joint to middle-ear sound transmission' is the main project of this work. The detailed morphology of the IMJ is described in chapter (see chapter I.III.2.4.4.1). The pervious works about the physiology and function of the joint are chronologically listed in chapter I.III.2.5.3 and summarized in Table 1.7.

Non-peer reviewed articles about this study in the main were published in the InFocus Magazines of Polytec GmbH (Waldbronn, Germany) (Gerig 2014b, Gerig 2014a).

The following manuscript (chapters III.I.2 to III.I.12) was submitted as – [1]Rahel Gerig, [2]Sebastian Ihrle, [1]Christof Röösli, [1]Adrian Dalbert, [1]Ivo Dobrev, [1]Flurin Pfiffner, [2]Albrecht Eiber, [1]Alexander M. Huber, [1]Jae Hoon Sim (2015). ([1]University Hospital Zurich, University of Zurich, [2]University of Stuttgart), Contribution of the incudo-malleolar joint to middle-ear sound transmission, Hearing Research (Hear Res. 2015 Sep;327:218-26. doi: 10.1016/j.heares.2015.07.011. Epub 2015 Jul 21). The graphical abstract in Figure 3.1 serves as an overview of this project.

Additionally to the published data, the data of the trial measurements (see chapter III.I.1) and linearity data (see chapter III.I.13) are presented.

The contributions of the author of this dissertation to this project were:

Preparation of the samples:

- Preparation of the fresh human temporal bones from the pathology department of the University Hospital Zurich, except the posterior tympanotomy that was performed by Dr. Röösli and Dr. Dalbert.
- Mounting metal markers and artificial ear canal on the samples.
- Adding retroreflective beads to the stapes footplate for improvement of the LDV signal.

Measurements:

- Setup installation (based on experience of Dr. Eiber, MSc. Ihrle and Prof. Huber).

- LDV measurements of stapes motion.
- LDV measurement of motion of malleus head and incus body.
- Artificial immobilization of the IMJ.

Micro-CT:
  - Preparation of the samples for the holder of the micro-CT machine.
  - Micro-CT scans of each sample.
  - 3D-Reconstruction of micro-CT images for each sample.

Data analysis:
  - Adaption of Matlab code programmed by Dr. Sim and Dr. Dobrev for the corresponding measurements.
  - Data analysis for each measurement.
  - Statistical analysis of the data supported by Prof. Seifert and Dr. Pfiffner.
  - Presentation of the data in the weekly group meetings of Prof. Huber.
  - Presentation of data at different conferences.

Manuscript:
  - Manuscript writing in collaboration with Dr. Sim.
  - Correction of the manuscript based on proofreading and comments of the other authors.

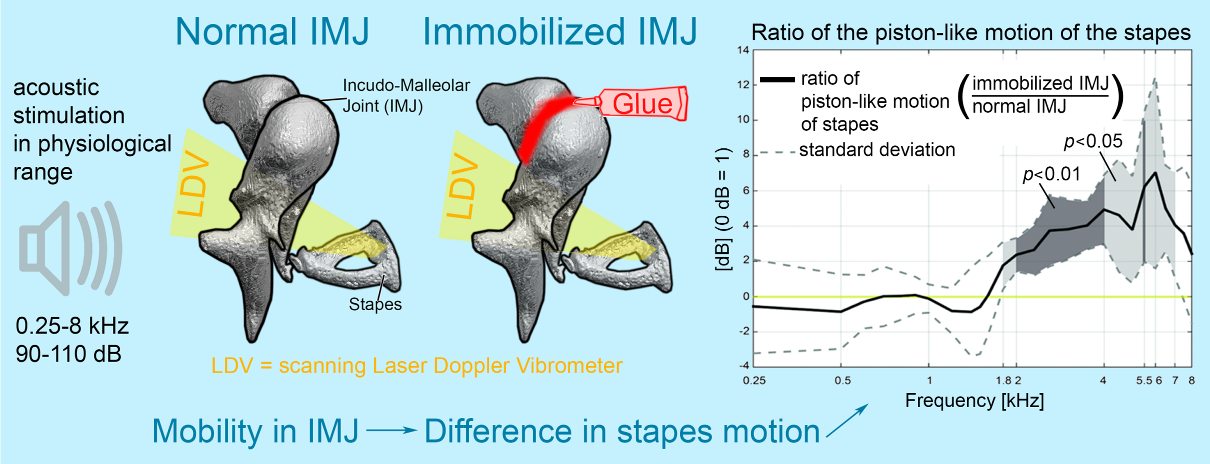

Figure 3.1 Graphical abstract: the goal of this study was to describe the influence of the IMJ on the sound transmission in the middle ear. The piston-like motion of the stapes changes after immobilization of the IMJ at higher frequencies.

III.I.1 Trial measurements

Trial measurements were performed without rehydration of the samples by immersion into saline solution prior to the stapes-motion measurements with immobilized IMJ. The ratio of the rocking-motion with immobilized IMJ to the rocking-motion with mobile IMJ showed a difference due to the immobilization of the joint, but the inter-individual difference was large and showed no trend (see Figure 3.3). The ratio of the translational motions with immobilized IMJ to the translational motions with the mobile IMJ showed a trend to decrease at low frequencies and increase at high frequencies after immobilization of the joint (see Figure 3.4). This trend was similarly described for the drying effect of the middle-ear structures. Thus, the resonant frequency of the middle-ear ossicular chain increased, similarly like reported physiological changes of the middle-ear tissues due to drying that was reported by previous studies (Rosowski et al. 1990, Voss et al. 2000, Willi et al. 2002, J. H. Sim et al. 2004). Two samples were re-measured for several hours to monitor the changes in the piston-like motion of the stapes due to effect of drying of the middle-ear structures; TBT 13 (temporal bone; trial measurements) is shown in Figure 3.2, and TBT 15 in Figure 3.3. The effect of drying is described in chapter III.I.9.1. Therefore, the samples were carefully rehydrated (at least after 30 min) to be sure that the effect of drying was reduced to a minimum.

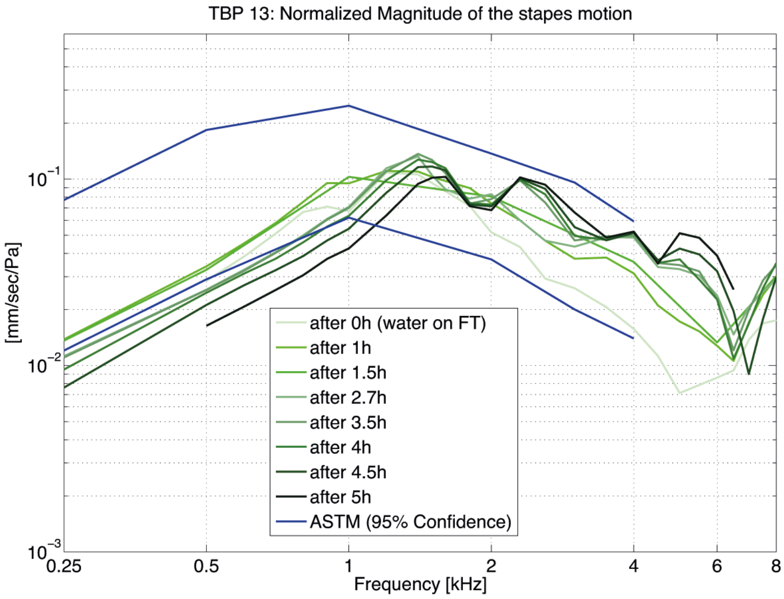

Figure 3.2 Effect of drying of the middle-ear structures on the normalized magnitude of the stapes motion. After 0 hours (0 h) corresponds to approximately 10 min after removal from the saline solution; therefore, water was still on the stapes footplate and the first measurement appeared noisy. Despite the first measurement at high frequencies, the measurements seem to be stable up to 1.5 hours after the removal of the saline solution. The resonant frequency of the middle-ear ossicular chain was shifted to higher frequencies with increasing drying effect.

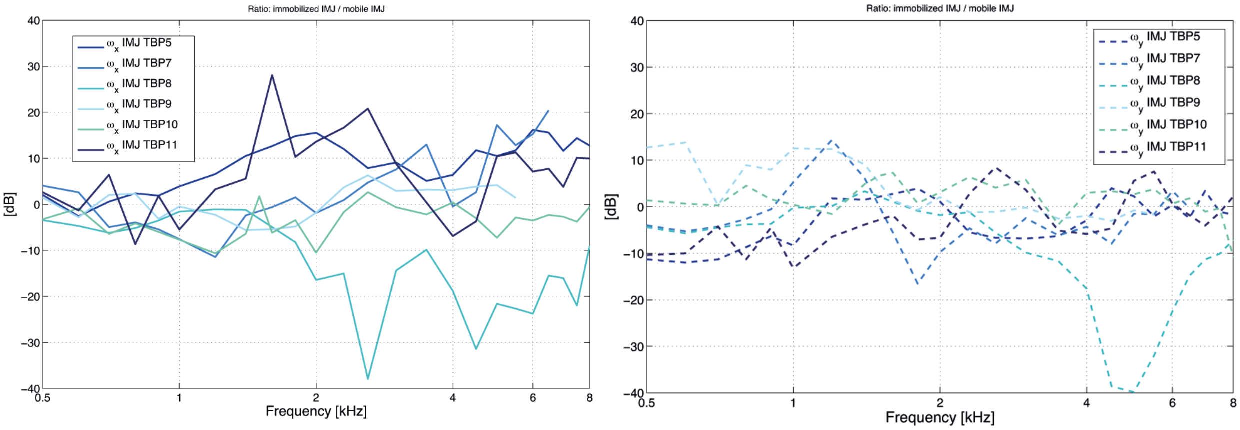

Figure 3.3 Ratio of the rocking motions with immobilized IMJ to the rocking motions with the mobile IMJ of six TBs (trial measurements).

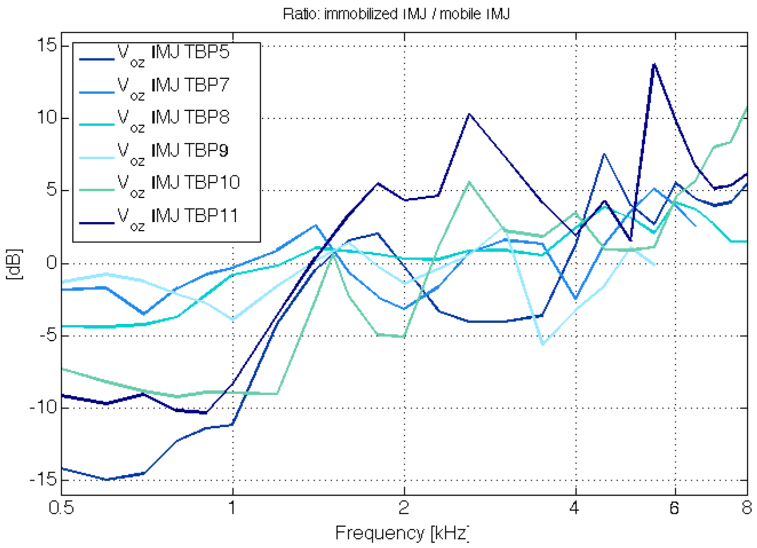

Figure 3.4 Ratio of the translational motions with immobilized IMJ to the translational motions with the mobile IMJ of 6 TBs (trial measurements).

III.I.2 Abstract

The malleus and incus in the human middle ear are linked with the incudo-malleolar joint (IMJ). The mobility of the human IMJ under physiologically relevant acoustic stimulation and its functional role in middle-ear sound transmission are still debated. In this study, spatial stapes motions were measured during acoustic stimulation (0.25-8 kHz) in six fresh human temporal bones for two conditions of the IMJ: (1) normal IMJ and (2) IMJ with experimentally-reduced mobility. Stapes velocity was measured at multiple points on the footplate using a scanning laser Doppler vibrometry (SLDV) system, and the 3-D motion components were calculated under both conditions of the IMJ. The artificial reduction of the IMJ mobility was confirmed by measuring the relative motion between the malleus and the incus. The magnitudes of the piston-like motion of the stapes increased with the reduced IMJ mobility above 2 kHz. The increase was frequency dependent and was prominent from 2-4 kHz and at 5.5 kHz. The magnitude ratios of the rocking-like motions to the piston-like motion were similar for both IMJ conditions. The frequency-dependent change of the piston-like motion after the reduction of the IMJ mobility suggests that the IMJ is mobile under physiologically relevant levels of acoustic stimulation, especially at frequencies above 2 kHz.

Keywords: Incudo-malleolar joint (IMJ); incudo-malleal joint (IMJ); malleo-incudal joint; incudo-mallear joint; articulatio incudomallearis; middle ear; malleus; incus; stapes; piston-like motion; rocking-like motion; Laser Doppler Vibrometer (LDV); micro-CT

Abbreviations: 3-D: three dimensional; AEC: artificial ear canal; IMJ: incudo-malleolar joint; ISJ: incudo-stapedial joint; LDV: laser Doppler vibrometry; Micro-CT: micro–computed tomography; SLDV: scanning laser Doppler vibrometry; TB: temporal bone; TM: tympanic membrane

III.I.3 Introduction

The ossicular chain in the human middle ear transmits sound-induced mechanical vibrations of the tympanic membrane (TM) to the inner ear. The middle-ear ossicular chain comprises three bones -- the malleus, incus, and stapes, which are connected via the incudo-malleolar joint (IMJ) and incudo-stapedial joint (ISJ).

The IMJ connects the articular surfaces of the malleus and incus and has a twisted saddle shape (Helmholtz 1863; Etholm and Belal, 1974; Sim and Puria, 2008). It has previously been described in the literature as a synovial joint (diarthrodial joint/diarthrosis) (Politzer, 1884; Harty, 1953, 1964; Etholm and Belal, 1974; Schuknecht, 1974; Marquet, 1981; Hüttenbrink and Pfautsch, 1987; FICAT, 1998; Sim and Puria, 2008). According to the literature, the IMJ is encapsulated by fibrous structures along its borders and contains synovial fluid inside the capsule, without the muscular components that are present in skeletal joints. The thickness of the IMJ tissue structures between the articular surfaces of the malleus and the incus varies from 0.04 mm to 0.32 mm along the intra-articular space, with maximal thickness on the medial and lateral aspects (Sim and Puria, 2008). The anatomical features of the IMJ may allow it to be deformed, resulting in relative motions between the malleus and incus.

The role of the IMJ as a protection mechanism against large static pressure changes has been proposed. For example, Kirikae (1960) argued that the IMJ is immobile up to 140 dB SPL, after which relative motion between the malleus and the incus could occur. Hüttenbrink (1988a) found that the IMJ is mobile under static pressure change. Such relative shear motions between the malleus and incus in human temporal bones (TBs) has been found in other studies as well (Kobrak, 1959; Cancura, 1980; Hüttenbrink, 1988b; Dahmann, 1929; Politzer, 1873; Mach and Kessel, 1874).

While relative displacement between the malleus and the incus under static pressure change of large magnitudes is generally accepted, flexibility of the human IMJ under acoustic stimulation at physiologically-relevant levels and its functional role in middle-ear sound transmission are still under debate.

Several previous works have proposed frequency-dependent behavior of the IMJ, which allows considerable relative motion between the malleus and incus only for the high frequencies. Elpern et al. (1965) observed relative motion above 4 kHz in human TBs, Guinan and Peake (1967) more relative motions at "higher frequencies" in cats and Willi et al. (2002) above 2 kHz in human TBs. Such high-frequency dominant slippage was also observed in three-dimensional measurements of ossicular motion in one human TB (Decraemer and Khanna, 2004). "Slippage" of the IMJ was observed in a study with two human TBs even for the low frequencies (Decraemer and Khanna, 2001), but in their study, the slippage was dominant at the high frequencies.

While some previous studies have argued that the IMJ is functionally immobilized during middle-ear sound transmission under physiological acoustic stimulation, the methods used in these studies did not account for factors that we realize today can influence the results resulting in potential inaccuracies. Harty (1964) made predictions based solely on morphological examination. Békésy (1960) used TBs with a drained cochlea in his measurements. It is known that absence of impedance of the cochlear fluid with a drained cochlea results in an increase of the middle-ear transfer function, especially above 0.5 kHz (Gyo et al. 1987). Some measurement systems were in contact with the middle-ear ossicles, which may change the natural motions of the ossicles. One example is a capacitive probe (Békésy, 1941), where a piece of metal foil is attached to measure the vibration of the surface of interest. Gundersen and Hogmoen, (1976) performed their measurements only at frequencies below 2 kHz with time-averaged holographic methods. The measurement with an electromagnetic probe in a study reported by Cancura (1980) was only static and not dynamic. In Elpern et al. (1965), the immobilization of the IMJ was not verified; thus the information of the degree of immobilization was missing.

Willi (2003) and Offergeld et al. (2007) have reported that relative motion between the malleus and the incus caused by the mobility of the IMJ resulted in frequency-dependent transmission loss in the middle-ear transfer function. Willi (2003) observed that the transmission loss between the malleus and incus decreased by immobilizing the IMJ with glue. In this study, almost no reduction of the transmission loss was observed below 1.5 kHz, and the reduction increased with frequency above 3 kHz, reaching a 10-dB reduction at 10 kHz. Similarly, an increase (less than 10 dB) of stapes motion amplitude occurred in the high frequencies (from 1.2 kHz to 5 kHz) after immobilization of the IMJ, as reported by Offergeld et al. (2007). However, the work by Willi explored transmission loss between the malleus and incus rather than transmission loss through the entire middle ear, which is defined as motion of the stapes with respect to ear-canal pressure. Further, the measurements and analysis were two-dimensional. In the work by Offergeld et al., motions of the stapes were measured one-dimensionally, and immobilization of the IMJ was not quantitatively examined.

In our study, it is hypothesized based on previous studies that the IMJ is mobile under physiological relevant acoustic stimulation, and the mobility of the IMJ results in transmission loss in the middle-ear transfer function, especially at higher frequencies. Our aim is to assess the contribution of the IMJ to middle-ear sound transmission accurately by using current methodologies that include quantification of artificial immobilization of the IMJ and three-dimensional measurement of stapes motion.

III.I.4 Material and Methods

Fresh TBs from human cadavers were used in this study, and approval was obtained by the Ethical Committee of Zurich (KEK-ZH-Nr. 2012-0007).

To assess the contribution of the IMJ to middle-ear sound transmission in human ears, spatial motions of the stapes, which were measured using a laser Doppler vibrometry (LDV) system, were compared under two different conditions of the IMJ: (1) normal IMJ and (2) IMJ with experimentally reduced mobility. To reduce the mobility of the IMJ, the articular capsule of the IMJ was opened with a surgical hook on the superior side, and the synovial liquid was facilitated by capillary flow to an absorbent tissue. Then, the cavity was filled with glue (Denseal Superior, Prevest Denpro GmbH, Germany) such that the glue replaced the synovial fluid and connected the articular surfaces of the malleus and the incus. For purposes of the study, we refer to the unmodified IMJ as “mobile IMJ,” and the IMJ with reduced mobility following insertion of the glue (reduced by 15-18 dB, see Figure 3.7) as “immobilized IMJ."

The effectiveness of the immobilization of the IMJ was quantified based on the relative motions between the malleus and incus, measured on an area covering the superior parts of the malleus head and the incus body around the IMJ using the LDV system. Once the immobilization was confirmed, spatial motions of the stapes were re-measured and compared to corresponding data with the mobile IMJ. To avoid bias due to physiological changes of middle-ear tissues caused by drying (Rosowski et al., 1990; Voss et al., 2000; Sim et al., 2004), the samples were placed in saline solution for 30 minutes prior to the second stage of the measurement, which was with the immobilized IMJ. The time interval between removing the TBs from the saline solution and the measurements was kept constant at approximately 20 minutes for both stages of the measurement.

III.I.4.1 Temporal Bone Preparation

The fresh TBs were harvested within 24 hours after death and were preserved in thiomersal 0.1 % (thimerosal, $C_9H_9HgNaO_2S$) solution at 4° C. Subsequent measurements were done within 7 days after the TBs were harvested (except for TB 2, which was done at 13 days). One TB, which did not conform with the American Society for Testing and Materials (ASTM) standard (F2504-05, Philadelphia, 2005), was excluded during the first stage of the measurements, resulting in a total of six TBs. The six fresh TBs were from four males and two females, with an average age of 68.2 years (ranging from 48 to 83 years).

Exposure of the middle-ear ossicular chain, which included a near-perpendicular view of the stapes footplate and a superior-medial view of the malleus-incus complex, was made by a mastoidectomy with posterior tympanotomy. The TM, middle-ear ossicles, ligaments, and tendon were left intact. The external ear canal was removed and was replaced by an artificial ear canal (AEC) of about 0.5-ml volume (diameter of 9.65 mm and length of 6-8 mm) (Sim et al., 2010, 2012; Lauxmann et al., 2012).

III.I.4.2 Acoustical stimulation and measurements of ossicular motion

The stapes motions were measured with harmonic excitations at 26 different frequencies in the range of 0.25 to 8 kHz. The excitation signals were provided by a signal generator incorporated within the PSV data acquisition system (Polytec GmbH, Germany). The stimulation, amplified by an amplifier (RMX 850, QSC Audio Products, USA), was delivered by a loudspeaker (ER-2, Etymotic Research, USA) embedded in the AEC. The sound pressure level (SPL) in the AEC was in the range of 90 – 110 dB SPL, measured by a microphone probe (ER-7C, Etymotic Research, USA).

To obtain the spatial components of the stapes motion, velocities at multiple points (approximately 100 points) on the stapes footplate were measured by a scanning laser Doppler vibrometry (SLDV) system (OFV-3001 SLDV system, Polytec GmbH, Germany). To improve the signal-to-noise ratio of the SLDV, retro-reflective glass beads (50 microns) were attached to the stapes footplate. A video camera (VCT 24), oriented coaxially with the laser beam, was used to determine the measurement area on the footplate as well as the 2D coordinates (i.e., X and Y coordinates) of the measurement points in the SLDV measurement frame (corresponds to XYZ coordinate system in Figure 3.5). In the SLDV measurment frame, the XYZ coordinate system was set such that the laser beam was along the Z direction and the XY plane was normal to the laser beam. The angle θ between the laser beam direction (i.e., Z axis of SLDV frame) and the z axis of the anatomical frame (see Figure 3.5) was 34.17 ± 10.99 °.

The mobility of the IMJ was monitored before and after immobilization. Motions of the malleus and incus were measured from a superior-medial view at about 150 points, covering areas on the malleus head and incus body adjacent to the IMJ. The number of measurement points for the malleus and the incus were approximately equal. The acoustic stimulation was by harmonic signals at 0.5, 1, 2, 4, and 6 kHz, in the range of 90 – 110 dB SPL where motions of the human middle-ear ossicular chain as a function of stimulation level are presumed to be linear (Schön and Müller, 1999).

All measurement procedures were controlled by PSV V9.0 software (Polytec GmbH, Germany), and were automated by a custom-made macro within the PSV V9.0 software.

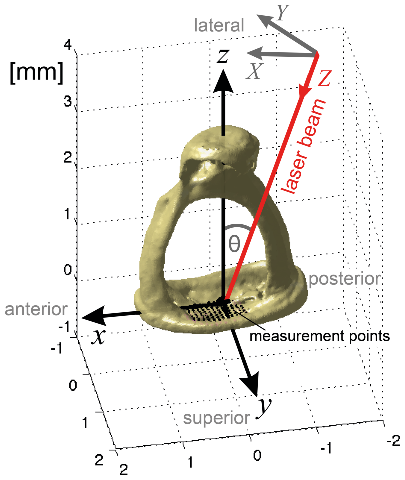

Figure 3.5 SLDV measurement frame (XYZ coordinate system) and footplate-fixed anatomical frame (xyz coordinate system) for the right ear (right-handed frame system). In the SLDV measurment frame, the XYZ coordinate system was set such that the laser beam was along the Z direction and the XY plane was normal to the laser beam. In the footplate-fixed anatomical frame, the xy-plane was fitted to the median surface of the stapes footplate, and the origin at the centroid of the median surface. The anterior direction was set as the positive x-direction, the superior direction as the positive y-direction, and lateral direction as the positive z-direction. The angle θ between the laser beam direction (i.e., Z axis of SLDV frame) and the z axis of the anatomical frame was 34.17 ± 10.99 °.

III.I.5 Registration into anatomical frame (footplate-fixed frame)

After the two stages of the motion measurements of the stapes, all the temporal bones were imaged using the micro-CT 40 (SCANCO Medical AG, Switzerland), with resolutions of 15-18 μm. The 3-D features of the stapes were reconstructed from the micro-CT images, and the footplate-fixed anatomical frame (corresponds to *xyz* coordinate system in Figure 3.5) of each temporal bone was obtained, such that the *xy*-plane was fitted to the median surface of the corresponding stapes footplate, and the origin was located at the centroid of the median surface. The anterior direction was set as the positive *x*-direction, the superior direction as the positive *y*-direction, and lateral direction as the positive *z*-direction. Thereby, a right-handed frame system was made for the right ear (Figure 3.5) and a left-handed frame system for the left ear.

To correlate *XYZ* coordinates in the SLDV measurement frame with *xyz* coordinates in the footplate-fixed frame, four or five reference markers (copper wires of a 0.75-mm diameter) were glued to the peripheral bones, and the *XY* coordinates of their outlines in the SLDV measurement frame were recorded. The 3-D features of the reference markers were also obtained from micro-CT images, and the correlation between the two frames was calculated such that the outline of the reference markers recorded in the SLDV measurement frame was fitted to the outline of the 3-D features from the micro-CT images. Once the correlation between the two frames was obtained, the measurement points and measured velocities at those points in the SLDV measurement frame were registered into the footplate-fixed frame, in order to calculate the 3-D motion components of the stapes in the footplate-fixed frame. Details of the frame registration procedures have been described previously (Sim et al., 2010, 2012).

III.I.6 Transfer function of the middle ear

Spatial motion components of the stapes were calculated by a method that we have used previously (Sim et al., 2010), in which the translation of the footplate's center along the medial-lateral direction (*z*-direction; piston-like motion, V_{oz}) and two rotations about the long (*x*-direction) and short (*y*-direction) axes of the footplate (rocking-like motions) were considered as the dominant rigid-body motion components of the stapes (Lauxmann et al., 2012). Consequently, the velocities of the three rigid-body motion components were normalized by the measured ear-canal pressure to obtain the corresponding transfer-function components.

III.I.7 Quantification of the IMJ mobility

To quantify the relative motion between the malleus and the incus before and after the IMJ immobilization, the relative motion around the IMJ was measured from a superior view, and the magnitude ratios of the relative motion components to the corresponding motion components of the malleus and incus (R_{vO}, $R_{\omega X}$, $R_{\omega Y}$, and R_{TOTAL}) were obtained.

The SLDV system was positioned for the right ear such that the approximate alignments of the direction of each axis were: the *X*-axis, posterior-to-anterior; the *Y*-axis, lateral-to-median; the *Z*-axis, the inferior-to-superior. Since the motions of the malleus and the incus were measured with only one laser beam direction, only three rigid-body motion components for each of the malleus and incus could be obtained in the SLDV measurement frame: translation along the laser beam direction (Z-direction) and two rotations about the *X*- and *Y*-axes of the SLDV measurement frame (Note that the *XYZ* directions of the SLDV measurement frame here are different from the *XYZ* directions of the SLDV measurement frame in stapes motion). The translational motion along the laser beam direction was calculated with respect to the center of the measurement area (denoted as *O*), which was located on the IMJ, for both the malleus and the incus. Next, the relative motions in the three rigid body motion components were calculated by

$$\begin{aligned} |V_{OR}| &= |V_{OM} - V_{OI}|, \\ |\omega_{XR}| &= |\omega_{XM} - \omega_{XI}|, \\ |\omega_{YR}| &= |\omega_{YM} - \omega_{YI}|, \end{aligned} \tag{1}$$

where V_{OM}, ω_{XM}, and ω_{YM} are the translational velocity of the point *O* along the laser beam direction and two rotational velocities for the malleus, V_{OI}, ω_{XI}, and ω_{YI} are the translational velocity of the point *O* along the laser beam direction and two rotational velocities for the incus, and V_{OR}, ω_{XR}, and ω_{YR} are the corresponding relative velocities. In calculation of Eq. (1), all the velocity components were treated as complex numbers to consider the phases. Then, each relative motion component was normalized by the magnitude of the corresponding motion component of the malleus and incus, as an index representing the ratio of the relative motion to motion of the malleus and incus (R_{vO}, $R_{\omega X}$, and $R_{\omega Y}$).

$$R_{vO} = \frac{|V_{OR}|}{(|V_{OM}| + |V_{OI}|)/2},$$

$$R_{\omega X} = \frac{|\omega_{XR}|}{(|\omega_{XM}| + |\omega_{XI}|)/2},$$

$$R_{\omega Y} = \frac{|\omega_{YR}|}{(|\omega_{YM}| + |\omega_{YI}|)/2}. \quad (2)$$

In Eq. (2), the magnitudes of the corresponding motion components of the malleus and incus were obtained as the average of magnitudes of the malleus motion components and the incus motion components. To represent the ratio of the total relative motion to the incus and malleus motion, the ratios of the relative motion components were averaged with the ratio components weighted by portions of the corresponding motion components.

$$R_{TOTAL} = W_{vO}R_{vO} + W_{\omega X}R_{\omega X} + W_{\omega Y}R_{\omega Y}, \quad (3)$$

In Eq. (3), W_{vO}, $W_{\omega X}$, and $W_{\omega Y}$ indicate weighting coefficients of $|V_{OR}|$, $|\omega_{XR}|$, and $|\omega_{YR}|$, which are calculated by portions of the corresponding motion components.

$$W_{vO} = \frac{|V_{OM}| + |V_{OI}|}{D},$$

$$W_{\omega X} = \frac{|\omega_{XM}| \cdot |\overline{Y}_M| + |\omega_{XI}| \cdot |\overline{Y}_I|}{D},$$

$$W_{\omega Y} = \frac{|\omega_{YM}| \cdot |\overline{X}_M| + |\omega_{YI}| \cdot |\overline{X}_I|}{D},$$

with $D = (|V_{OM}| + |V_{OI}|) + (|\omega_{XM}| \cdot |\overline{Y}_M| + |\omega_{XI}| \cdot |\overline{Y}_I|) + (|\omega_{YM}| \cdot |\overline{X}_M| + |\omega_{YI}| \cdot |\overline{X}_I|)$,

where $|\overline{Y}_M|$ and $|\overline{Y}_I|$ are average distances of measurement points from the center point *O* in the *Y* direction, and $|\overline{X}_M|$ and $|\overline{X}_I|$ are average distances of measurement points from the center point *O* in the *X* direction, for the malleus and the incus. The multiplication of the average distances to the magnitudes of the corresponding rotational velocity components was done in order to make the magnitudes of the rotational velocity components equivalent to the magnitudes of the translational velocity components.

III.I.8 Statistical analysis

Frequency-dependence and age-dependence of the normal IMJ mobility were analyzed using an ANOVA for repeated measures (with age as covariate for examination of age dependence). Frequency-dependence and age-dependence of the relative change of the piston-like motion between the mobile and immobilized conditions of the IMJ were also analyzed using an ANOVA for repeated measures (with age as covariate for examination of age dependence), with the two variables as the IMJ condition (i.e., mobile and immobilized) and frequency. Data were logarithmically transformed for this analysis. Deviations from sphericity were addressed using the Greenhouse-Geisser correction. Post-hoc comparison with paired *t*-tests was performed for comparison between the mobile and immobilized conditions of the IMJ at each frequency. The statistical calculations were done with SPSS 20 software (IBM, USA).

III.I.9 Results

III.I.9.1 Drying Effect

Figure 3.6 depicts changes of the motion of the stapes (footplate center) due to drying of the TB tissues. The sample was immersed for 30 minutes in saline solution, and the first measurement (0 min in the figure) took place within 5 minutes after removal from the saline solution. There is a trend for the first natural frequency to increase with time, indicating a stiffening of the suspensory structures due to the drying. The clear phase shift with drying was observed as well. Consequently, over time, there is a reduction in the magnitudes of motions at frequencies below the resonance and an increase of motions above the resonance. The change in the lower frequencies between 90 – 150 minutes of drying was larger than the change during other time intervals. The changes for the higher frequencies were also minimized after 150 minutes. Then, the sample was re-hydrated by immersion in the saline solution for 30 minutes, and the measurement was repeated within 5 minutes after removal from the saline solution ('Rehydration' in the figure). The magnitude of the motion of the stapes with rehydration recovered to approximately the same levels as before drying.

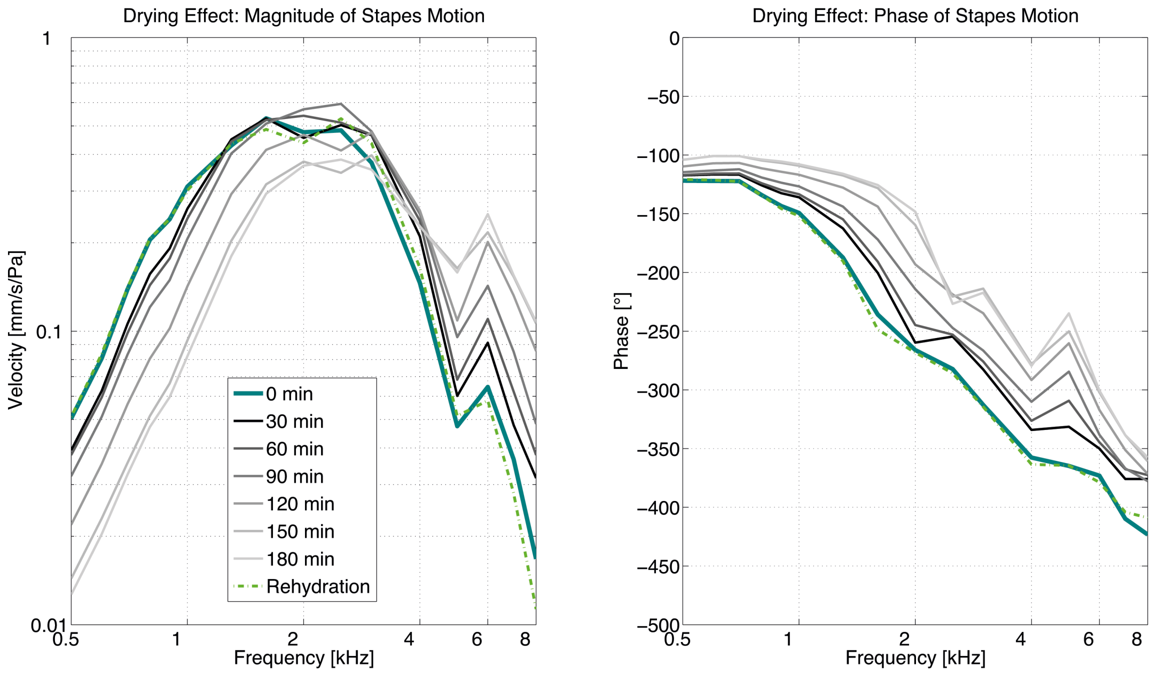

Figure 3.6 Changes in the magnitudes (left) and phases (right) of motions of the stapes footplate (center) with drying. After the sample was dried for 180 minutes, it was rehydrated by immersion in saline solution.

III.I.9.2 Immobilization of the IMJ

Figure 3.7 displays the index for the ratios of the relative motion components between the malleus and the incus to the corresponding motion components of the malleus and incus, calculated using Eqs. (1) - (3), before (solid) and after (dashed) the IMJ was immobilized. Before the IMJ was immobilized, the averaged relative motion ratios (R_{TOTAL}) were small in the low frequency range (-17.5±2.9 dB at 0.5 kHz), and increased with frequency, reaching 0.1±1.9 dB at 6 kHz. The relative motion ratio of ω_Y ($R_{\omega Y}$) was larger than the relative motion ratios of the other components, but its contribution to the weighted average ratio (R_{TOTAL}) was smaller than the contribution of the relative motion ratios of the other components because the motion components ω_{YM} and ω_{YI} of the malleus and incus had smaller magnitudes than other motion components (i.e., $W_{\omega Y}$ was smaller than W_{vO} and $W_{\omega X}$). No dependence of the relative motion on age was observed with the six temporal bones used in this study (ANOVA with age as covariate). After the IMJ was immobilized, the averaged relative motion ratios were reduced by 10 to 15 dB (i.e., R_{TOTAL} was reduced to 18 – 30 % of the values before immobilization of the IMJ), along the frequency range of 0.5 – 6 kHz ($p < 0.05$ at 1 kHz and $p < 0.01$ at all other frequencies with paired t-test). The immobilization of the IMJ was more effective for higher frequencies, where the IMJ had more relative motion before the immobilization (R_{TOTAL} was reduced by 10 dB at 0.5 kHz and by 15 dB at 6 kHz).

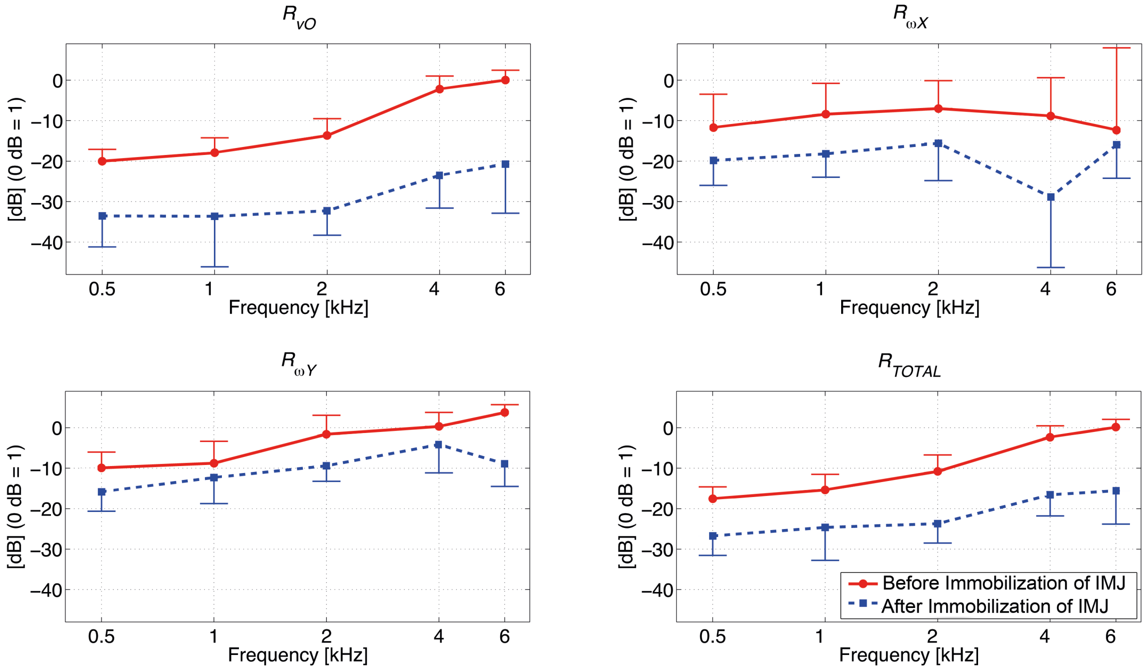

Figure 3.7 Relative motion between the malleus and incus represented by the ratios of the relative motion components to the corresponding motion components of the malleus and incus, before IMJ was immobilized (solid) and after the IMJ was immobilized (dashed). The relative motion ratios for V_O *(*R_{vO}*, left upper),* ω_X *(*$R_{\omega X}$*, right upper),,* ω_Y *(*$R_{\omega Y}$*, left below), and average with the ratio components weighted by portions of the corresponding motion components (*R_{TOTAL}*, right below).*

III.I.9.3 Stapes Motion Before/After the IMJ Immobilization

Figure 3.8 illustrates the magnitude of the translational motions of the footplate's center along the z-axis (i.e., piston-like motions, V_{oz}) normalized by the ear canal pressure, before (solid) and after (dashed) the IMJ was immobilized, for all six temporal bones used in this study (TB1-TB6).

To determine the effect of the IMJ immobilization on the translational motions, changes of the translational motion with immobilized IMJ relative to the translational motion with mobile IMJ were calculated, and the results are shown in Figure 3.9. In the figure, the relative change was calculated for each temporal bone, then the relative changes were averaged over all the temporal bones (n = 6). An ANOVA for repeated measures on the magnitude change revealed that the difference of the magnitude between the two IMJ conditions was frequency-dependent ($p = 0.004$). While the magnitudes were similar for both IMJ conditions at frequencies below 1.8

kHz, the magnitudes were generally higher for the immobilized IMJ for the higher frequencies. The paired *t*-test resulted in *p*-values less than 0.05 for frequencies in the 1.8 to 7 kHz range and *p*-values less than 0.01 for frequencies from 2 to 4 kHz and at 5.5 kHz (shaded with dark gray in Figure 3.9). The immobilization of the IMJ also tended to cause an increase in phase between 1.5 and 4 kHz. Because of the age range of the TBs and the proposition that mobility could change as a function of age, we examined dependence of the results on age, and no dependence of age on the relative change was observed (ANOVA with age as covariate).

To observe the changes in magnitude ratios of the two rotational velocities (i.e., rocking-like motions) relative to the translational velocities of the footplate-center (i.e., piston-like motion) following immobilization of the IMJ, the linear velocities at the inferior and posterior edges of the footplate generated by the two rotational velocities were calculated, and were normalized by the footplate-center velocity in the *z*-direction (Heiland et al. 1999; Hato et al. 2003; Sim et al. 2010), for mobile and immobilized IMJ conditions (Figure 3.10). The mean values and corresponding standard deviations for each of the mobile and immobilized IMJ conditions were calculated after the relative ratios were obtained for each of the temporal bones (n = 6). The inferior-edge velocities were calculated by multiplication of half of the footplate's short length to the rotational velocity components along the long axis of the footplate, and the posterior-edge velocities by multiplication of half of the footplate's long length to the rotational velocity components along the short axis of the footplate (Sim et al., 2010). The short and long lengths of the footplate were measured from the reconstructed shapes of the stapes, which were obtained from micro-CT imaging for each of the temporal bones. The lengths were 2.86 ± 0.250 mm along the long axis and 1.40 ± 0.101 mm along the short axis, and were slightly longer than the lengths of specimens used in Sim et al. 2013 (2.81 ± 0.158 mm along the long axis and 1.27 ± 0.109 mm along the short axis).

The mean ratio of the inferior-edge velocity to the footplate-center velocity was approximately -18 dB at 0.25 kHz and increased with frequency, for the both mobile (solid) and immobilized IMJ (dashed) conditions. The trends were similar for the ratio of the superior-edge velocity to the footplate-center velocity. While Figure 3.10 shows the ratios of the edge velocities to the footplate-center velocity separately for each of the mobile and immobilized IMJ conditions, post-hoc comparison with paired *t*-tests was performed for comparison of the ratios between the mobile and immobilized IMJ conditions. No significant difference between the mobile and immobilized IMJ conditions was observed for both the ratio the inferior-edge velocity to the footplate-center and the ratio of the superior-edge velocity to the footplate-center velocity.

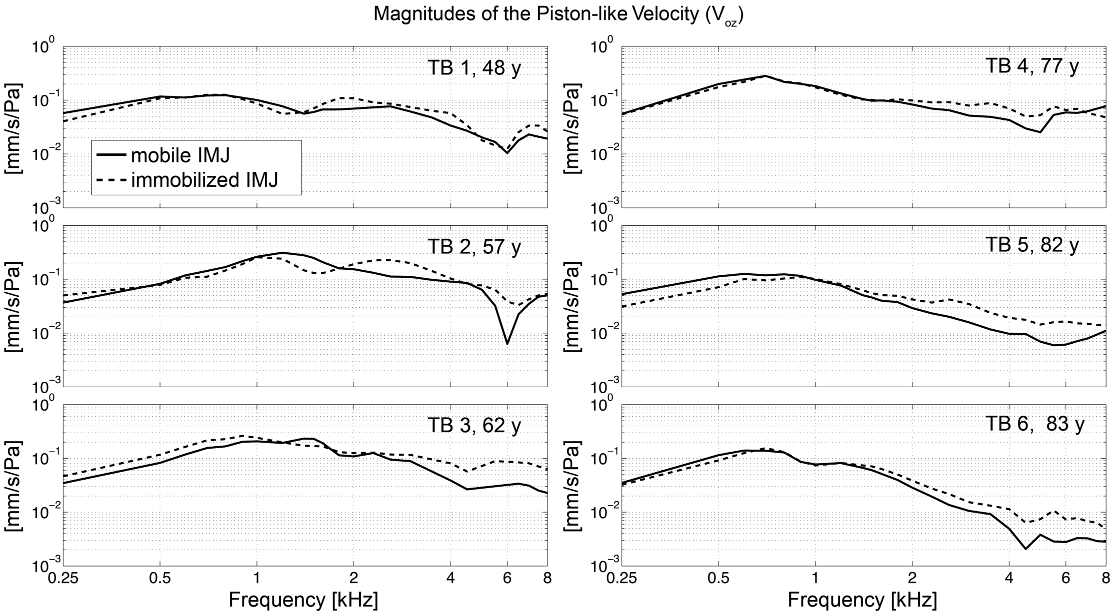

Figure 3.8 Magnitudes of the translational motions of the footplate center along the z-axis (i.e., piston-like motions, V_{oz}) normalized by the ear canal pressure, before (solid) and after (dashed) the IMJ is immobilized.

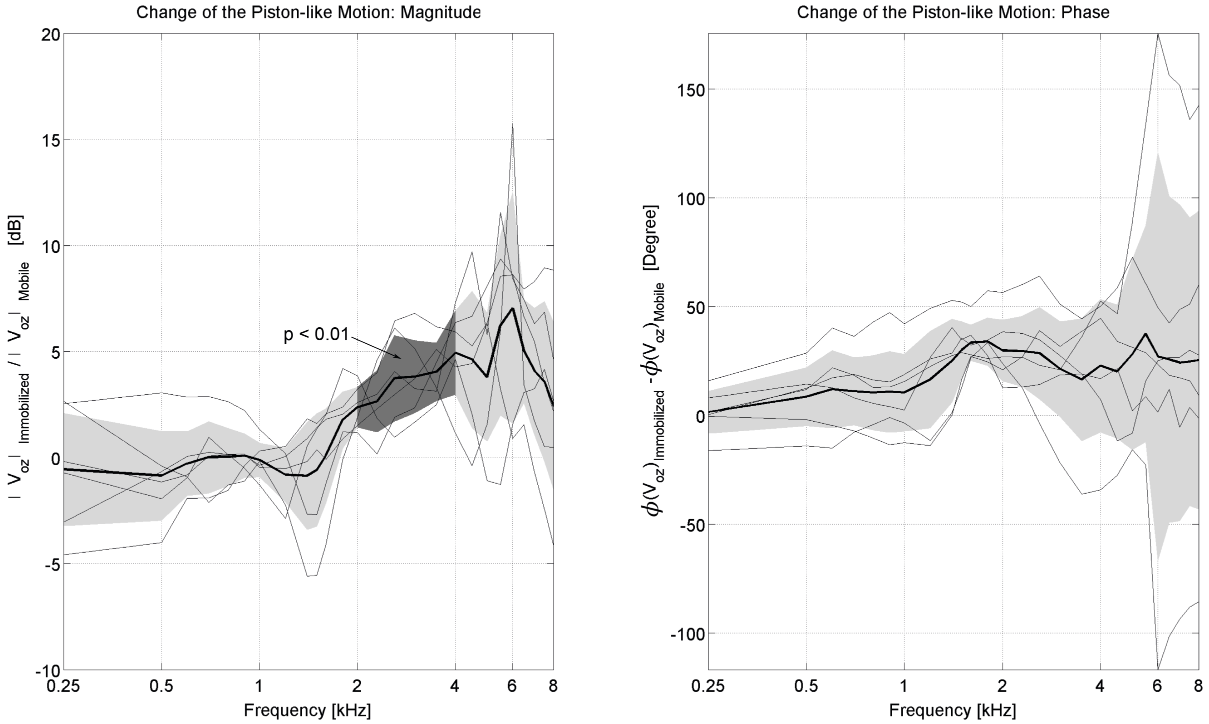

Figure 3.9 Change of the translational motion with immobilized IMJ relative to the translational motion with mobile IMJ. Relative magnitude ratios (left) and relative phase difference (right) with the mean values (thick lines) and standard deviations (shaded). Prominent differences in magnitude between the mobile and immobilized conditions of the IMJ are shown as shaded with dark gray (2- 4 kHz and 5.5 kHz, $p < 0.01$ with paired t-test).

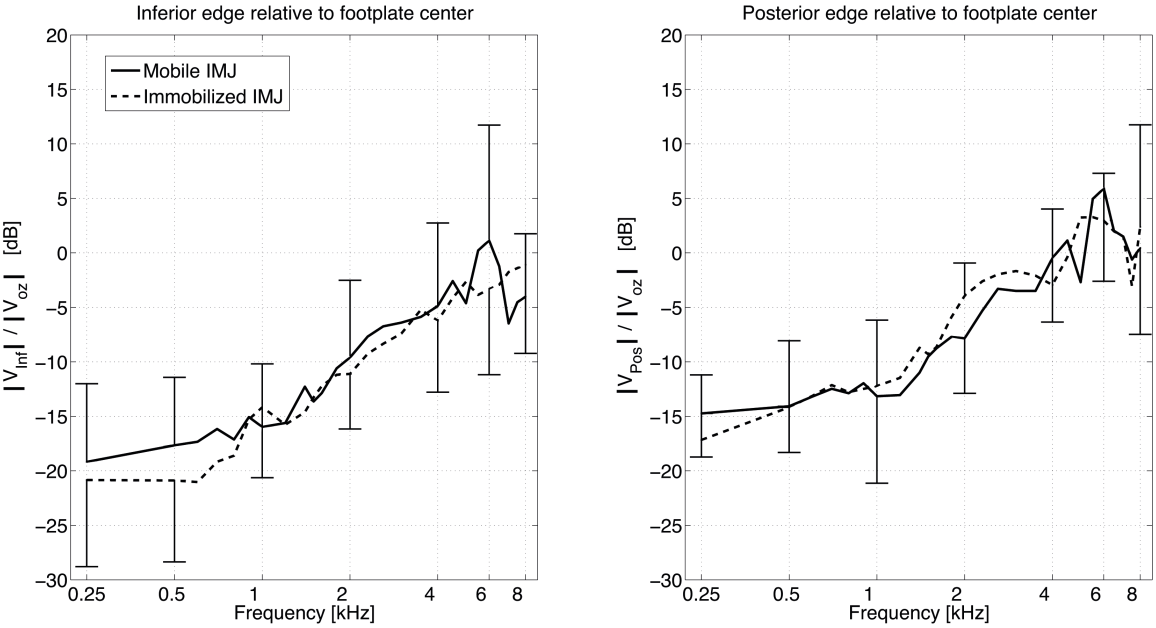

Figure 3.10 Relative magnitudes of the edge velocities generated by the rocking-like motions (i.e, two rotational motions along the long and short axes of the footplate) with respect to the piston-like motion (i.e., the footplate-center velocity in the z-direction), before (solid) and after (dashed) the IMJ immobilization. The inferior-edge velocity due to the rocking-like motion of the footplate along the long axis (left), and the posterior-edge velocity due to the rocking-like motion of the footplate along the short axis (right).

III.I.10 Discussion

The goal of this study was to investigate the role of the IMJ in middle-ear sound transmission under physiologically-relevant acoustic stimulation. We controlled for bias due to a drying effect of the TBs in two ways. Each specimen was periodically moisturized during the measurements, and they were placed in a saline solution for 30 minutes prior to the measurement with the immobilized IMJ. Previous studies (Rosowski et al. 1990; Voss et al., 2000; Willi et al., 2002; Sim et al., 2004) have reported that physiological changes of the middle-ear tissues due to drying result in significant increase of the resonant frequency of the middle-ear ossicular chain. These studies have also found that the shift of the resonant frequency is accelerated with time. Voss et al. (2000) have argued that measurements with TBs are typically presumed to be stable for a "couple of hours," but there is large variability across TBs in the rate of acceleration of the physiological changes of the middle-ear tissues. Our examination of the drying effect (Figure 3.6) shows similar trends. We also found that the effect can be reversed by immersing the TBs in saline solution, thus the motion of the stapes recovers to approximately the same levels as before being dried. Such restoration of the mechanical properties of the middle-ear tissues by immersing the TBs in saline solution has been observed in other studies (Voss et al., 2000; Willi et al., 2002; Nakajima et al., 2005).

Artificial immobilization of the IMJ in this study was performed under the microscope by applying glue to the inner space of the IMJ capsule after removal of the synovial fluid. The effectiveness of the artificial immobilization procedures was confirmed by measurements of the relative motion between the malleus and incus before and after the artificial immobilization (Figure 3.7). The relative motion was reduced by 10 to 15 dB after the artificial immobilization.

Our results indicate that a mobile IMJ attenuates the magnitude of middle-ear sound transmission, especially for frequencies above 2 kHz. The mean piston-like motion (Voz) increases after immobilization by less than 7 dB for the frequencies from 1.8 to 8 kHz. Specifically, the prominent difference occurs from 2 to 4 kHz, and at 5.5 kHz ($p < 0.01$ with paired t-test). With the mobile IMJ, the ratios of the two rocking-like motions to the piston-like motion were frequency-dependent ($p < 0.001$ with ANOVA test), that is to say, there were relatively large rocking-like motions at higher frequencies. This is in agreement with results from previous studies (Heiland et al., 1999; Hato et al., 2003; Sim et al., 2010). The two ratios showed no significant difference between the mobile and immobilized IMJ conditions, suggesting that there are no important changes in relative magnitude ratios of the rocking-like motions to the piston-like motion caused by immobilization of the IMJ.

The larger difference of the piston-like stapes motion between the mobile and immobilized IMJ conditions at higher frequencies is presumed to be due to relatively large loss of motion from malleus to incus at higher frequencies for the normal IMJ as compared to the immobilized IMJ. With the normal condition of the IMJ (i.e., before the IMJ immobilization), the index for the ratio of the relative motion (R_{TOTAL}) increased with frequency (Figure 3.7), indicating more relative motion at higher frequencies. Therefore, the mobility of the IMJ will not affect the middle-ear sound transmission at low frequencies considerably. At frequencies above 4 kHz, the R_{TOTAL} reaches almost 0 dB, indicating that the magnitude of the relative motion is almost the same as the motion of the malleus and the incus. Therefore, in this frequency range, the immobilization of the IMJ is expected to affect the middle-ear transmission significantly.

The high-frequency dominant change in middle-ear sound transmission due to mobility of the IMJ in human TBs has been described previously. Huber et al. (1997) reported a transmission loss from the malleus to the incus of about 6 dB at frequencies above 2 kHz under acoustic stimulation at moderate SPLs. Offergeld et al. (2007) observed an increase of less than 10 dB in the amplitude of the stapes motion after immobilization of the IMJ for frequencies from 1.2 - 5 kHz. Willi et al. (2003) described that a decrease of 5.5 dB per octave above 1 kHz may be caused by the mobility of the IMJ, based on the transmission loss observed in his two-dimensional measurements of motions of the malleus and the incus.

Mobility of the human IMJ has been found in many previous studies (Helmholtz, 1868; Mach and Kessel, 1874; Frank, 1923; Dahmann, 1930; Stuhlman, 1937; Kobrak, 1959; Marquet, 1981; Schön and Müller, 1999; Huber et al., 1997; Decraemer and Khanna, 1999, 2001; Willi et al., 2002, 2003; Sim et al, 2004; Nakajima et al., 2005; Offergeld et al., 2007). Decraemer et al. (2014) also observed large slippage in the IMJ in TBs, and addressed two possible reasons for the slippage: 1) there are post-mortem changes in the cadaveric TBs that were used to examine the mobility of the IMJ in most studies; 2) the cadaveric TBs are from elderly people. They doubted that large slippage in the IMJ "really happens in the healthy living ear (pp. 508)".

It is known that cadaveric TBs have fast and slow post-mortem changes. The *fast* post-mortem changes, which are presumed to be caused mainly by a stoppage of blood flow and changes of the inner ear pressure in cadaveric ears, occur immediately after death (Brenkman and Grote, 1987). Békésy (1960), from his anatomical studies for human TBs, described that no considerable change of the elasticity of the ligaments, the joint capsule or the tympanic membrane occurs within several hours after death, indicating that the fast post-mortem changes probably do not affect middle-ear mechanics significantly. Several other studies have reported the fast post-mortem changes in animals as well, and found no considerable difference from living animals up to 1h in guinea pigs (Gilad et al. 1967), 1-2 hours in cats (Tonndorf and Khanna

1967, 1968), 17 hours in rabbits (Gill 1951), and 48 hours in rabbits (Onchi 1961).

The *slow* post-mortem changes, which may be caused by dehydration and autolysis, are important for the repeatability and stability of the measurements. According to previous studies, the slow post-mortem changes do not necessarily occur in all human TBs, and the effects are not accentuated for a specific frequency range. Goode et al. (1993) measured umbo displacement 2 weeks and 4 weeks after death, and obtained almost the same frequency responses. Rosowski et al. (1990) observed considerable post-mortem changes before 100 days only in two out of nine TBs investigated. Brenkman and Grote (1987) observed from their measurement with two TBs that the umbo velocity was stable up to 45 hours after death and then decreased with post-mortem time for the investigated frequencies of 0.6, 2 and 5 kHz. Zwislocki and Feldman (1963) observed that the changes start in the low-frequency range. Effects of the slow post-mortem changes on the measurements in this study were unavoidable. However, they were minimized by preserving the fresh TBs in thiomersal 0.1 % solution at 4° C within 24 hours after death and by performing most measurements within a week after death (with the exception of TB2, which was measured 13 days after the death). No major differences in terms of stapes motion between live human subjects and fresh human TBs were obtained in intraoperative measurements (Huber et al. 2001, Chien et al. 2009), which strongly argues against large post-mortem effects. Therefore, our observation that the immobilized IMJ generates larger piston-like motions than the mobile IMJ only at frequencies above 2 kHz is not likely to be from the post-mortem changes of the TBs.

The fact that the temporal bones in this study are mostly from elderly subjects (average of 68 years) could have influenced the results. Although we did not observe an age dependency in our results, the number of samples is too small to draw a definitive conclusion. Decraemer and Khanna (2004) noted that their experiments also may have been biased due to use of temporal bones from elderly subjects. Willi (2003) describes a trend of a decrease of sound transmission at higher frequencies (> 3 kHz) with age in fresh human temporal bones, which would have to be confirmed in further measurements. Several morphological parameters of the IMJ may change with age including hyalinization or calcification of the joint capsule, thinning and calcification of the articular cartilage, thinning and calcification of the disc, and arthritis resulting in narrowing or obliteration of the joint space (Gussen, 1971; Etholm and Belal, 1974). In addition, the amount of elastic fibers in the joint capsule tends to decrease with age (Harty, 1953), which may result in a reduction of the joint tension. Savić and Djerić (1988) describe degenerative changes in 40 % of their samples from persons between 40 and 60 years. While the reduction of the joint tension is expected to increase the mobility of the IMJ, effects of other morphological changes such as calcification and obliteration on the mobility of the IMJ have not been investigated, to our knowledge. With a possibility that the age-related morphological changes of the IMJ increase its mobility, we cannot rule out that the large mobility of the IMJ that we observed may have been due to the TBs from elderly people used in this study.

Another possibility is that the mobility of the IMJ exists as part of a protection mechanism, and the transmission loss at the high frequencies under moderate sound pressures is an unavoidable side effect of this mechanism. That is, the mobility of the IMJ that exists to protect the sensitive structures of the inner ear against high static pressure change also affects normal sound transmission with acoustic sound simulation of moderate levels. The protection mechanism has been proposed previously by several investigators (Dahmann, 1929, 1930; Békésy, 1936; Stuhlman 1937; Kobrak, 1959; Hüttenbrink, 1988a, 1988b, 1997; Cancura, 1980; Offergeld et al., 2000).

Puria and Steele (2010) predicted that the mobility of the IMJ could provide flexible adaptation to the complex motion of the malleus such as a twisting motion at high frequencies. However, our results that artificial immobilization of the IMJ increased the middle-ear transfer function of the piston-like motion without change in the pattern of the stapes motion do not provide evidence for such a role of adaptation of the IMJ, at least up to 8 kHz, which is the frequency range considered in this study.

III.I.11 Conclusion

The IMJ was shown to be mobile at frequencies above 2 kHz under physiologically relevant acoustic stimulation of 90-110 dB SPL. A prominent frequency-dependent difference of the piston-like motion of the stapes between the mobile and immobilized IMJ conditions was observed; whereas, the ratio of the rocking-like motions relative to the piston-like motion of the stapes showed no significant difference. The prominent frequency-dependent change of the piston-like motion above 2 kHz is presumed to be due to large mobility of the IMJ at high frequencies. It is still questionable whether the mobility of the IMJ exists as part of a protection mechanism, regardless of age, or occurs only in elderly people due to aging effects. Since the sample size of six in this study is not sufficient to reveal the effects of age on middle-ear sound transmission, further measurements are required to clarify these open questions.

III.I.12 Acknowledgement

This study was funded by SNF (Swiss National Foundation) Project No. 138726, and has been supported by the German Research Foundation (DFG) within the Ei 231/6-1 Grant. The authors thank Prof. B. Seifert, Division of Biostatistics, Institute of Social- and Preventive Medicine, University of Zurich for the statistical consulting.

III.I.13 Linearity measurements of the stapes motion (not included in the manuscript)

Figure 3.11 shows two types of linearity; (1) linearity of the ear canal pressure versus the input voltage of the loudspeaker (left) and (2) linearity of the stapes motion versus the ear canal pressure (right). In the right figure, the ear canal pressure has a slight deviation from linear relation with the input voltage to the loudspeaker for 4-kHz simulation, but the graphs generally show good linear relation between the input to the loud speaker and the ear canal pressure. In relation between the stapes motion and the ear canal pressure, linear relations were broken for stimulation of high frequencies at 6 and 8 kHz. However, the deviation was not large.

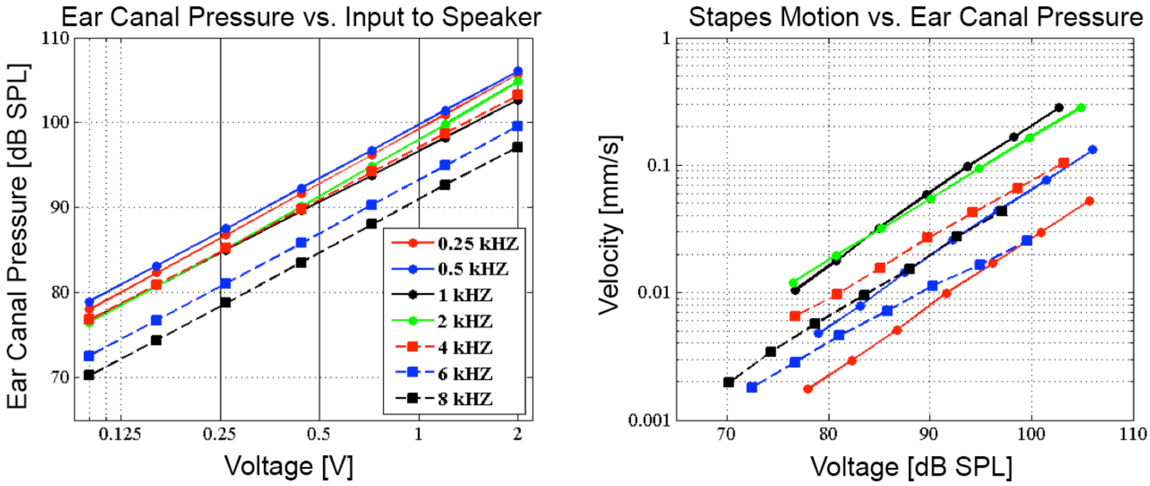

Figure 3.11 Linearity of the ear canal pressure versus the input voltage of the loud speaker (left) and stapes motion versus the ear canal pressure (right). Note that horizontal and vertical axes are in log scale because dB SPL (sound pressure level) already represents pressures in log scale.

III.II Quasi-static and dynamic behavior of the incudo-malleolar joint

The work of this section has been performed as a cross-border co-operation project with Institute of Engineering and Computational Mechanics, University of Stuttgart (Dr. Albrecht Eiber and MSc. Sebastian Ihrle). Preliminary results are presented in this chapter. Dipl.-Ing. Sebastian Ihrle will present the final results in his dissertation.

The contributions of the author of this dissertation to this project were:
Sample preparation:

- Fresh human temporal bone preparation, except posterior tympanotomy performed by Dr. Röösli.
- Mounting the malleus of the malleus-incus-complex on a crystal block.

Measurements:

- Measurements of the quasi-static and dynamic behavior of the incudo-malleolar joint together with MSc. Ihrle at the University of Stuttgart for each sample.

Micro-CT:

- Sample preparation for the micro-CT.
- Micro-CT scans of each sample.
- 3-D reconstruction of the micro-CT data.

Data analysis:

- Discussion of the analyzed data with Dr. Eiber, Dr. Sim, MSc. Ihrle and Prof. Huber.
- Presentation of the data at different conferences.

Manuscript:

- Co-authorship and proofreading of the manuscript.

III.II.1 Background and aim of the study

The malleus and incus are held together by a joint capsule called the incudo-malleolar joint (IMJ) (see chapter I.III.2.4.4.1.2.2). The IMJ is encapsulated by fibrous tissue along its boundaries, and contains synovial fluid inside the capsule (see chapter I.III.2.4.4.1.2.1). With such compositions, the IMJ presumably causes a viscoelastic behavior. Under static loads, occurring for example with change of static air pressure in the ear canal, the IMJ is expected to show a mainly elastic compliance due to the fibrous structures. Under dynamic excitation, additionally the influence of the viscosity of the synovial fluid is supposed to increase as the frequency increases. This viscoelastic characteristic of the IMJ can be integrated into a comprehensive mechanical model to answer questions about functional roles of the IMJ in middle-ear sound transmission.

The aim of this study is to identify the mechanical properties of the IMJ under quasi-static and dynamic excitation. A measurement setup was established to characterize the three-dimensional (3-D) behavior of the IMJ motions by measuring the spatial displacement and velocity at different points on the malleus and incus, (Ihrle et al. 2015). While static and dynamic excitation patterns were applied, the 3-D motions of the ossicles were recorded. Then, the mechanical properties of the IMJ are derived from the measurements to build up a mathematical model of the IMJ. The experimentally determined IMJ model will also be integrated into a comprehensive middle-ear model with multi-bodies (Ihrle et al. 2013). The simulation of the comprehensive middle-ear model can be a base for the improvement and development of hearing aids (e.g., middle-ear prostheses), a better interpretation in medical diagnostics, and progress of diagnostics procedures.

III.II.2 Experimental approach

In total, five fresh human temporal bones were used for this study. To reduce complexity of mechanism by other middle-ear structures, the malleus-incus complex was surgically isolated (see Figure 3.12). For measurements of the *static behavior* of the IMJ, the malleus was fixed to a custom-made frame (crystal block, sample holder, 15x15x18 mm^3, 5.8 g), and the incus was excited by applying a quasi-static force while measuring the resulting spatial displacement subsequently at several points on the incus. For measurement of the *dynamic* behavior, the isolated malleus-incus complex was excited by an electrodynamic shaker using different test signals (e.g. sweep of harmonic tones and band-limited white noise) and 3-D velocity components were measured at several points on the malleus-incus complex. The measurements of 3-D behavior of the ossicles were performed using a 3-D Laser Doppler Vibrometry (LDV) system with three independent LDVs (OFV-5000/OFV-534, Polytec, Waldbronn) as described by Ihrle et al. (Ihrle et al. 2015). The three LDVs were mounted in linearly-independent directions to obtain the spatial motion information. The combination of velocity and displacement decoders allows recording static and dynamic measurements. The LDVs have an integrated camera coupled with the laser beams and are fitted with microscope optics (see Figure 3.13 A). This setup allows positioning the LDV measurement points precisely on the ossicles. Furthermore, the LDV system was coupled with electric micro-positioning stage (PI Physik Instrumente M-126.CG1, Karlsruhe, Germany) to allow a precise positioning of the laser measurement points on the ossicles (see Figure 3.13 A).

The three single LDV beams were orientated angularly; thus, the intensity of the reflected signal is clearly smaller than a 1-D LDV with a mainly orthogonal laser beam (see Figure 3.13 A, B). This leads to different incremental raw signals (different heights) of the LDV during displacement measurements. These differences were identified with the ‘Wavelet analysis’ and gradient-based methods, and then the signal was corrected. The performance of this correction was verified on the technical substitute model. Because the displacements under static loads were large, the rotation could not be described with a linear rotation matrix. Therefore, the reconstruction of the 3-D motion of the incus was calculated based on incremental methods (for more information see (Ihrle et al. 2015)).

The function of this measurement system was confirmed on a mechanical substitute model, see (Ihrle et al. 2015). This substitute model consists of artificial ossicles obtained from micro-CT data of real ossicles and produced with a rapid-prototyping process with a selective laser-sinter. The artificial ossicles were joined with a viscoelastic material ('rubber-cement'). This viscoelastic material should substitute the tissue of the IMJ with presumed viscoelastic properties such as ligaments, fibrous tissues on the joint surface and synovial fluid.

The ossicles are assumed to be rigid bodies in these measurements (see chapter II.II) based on the assumption that elastic deformations of the ossicles can be neglected when compared to the rigid body motions. Thus, the motion of the points on the surface of the ossicles can be calculated by three coordinates, and the ossicular motion by six coordinates (three rotation and three translation). Therefore, a minimum of three non-collinear measurement points per ossicle are needed for the reconstruction of these coordinates.

The measurement procedure for all measurements was as follows:

1. A measurement-point grid (non-collinear points) is defined.
2. The laser is moved to each of the measurement points.
3. A defined force is applied with the load cell to define the start-load '0' (for the quasi-static measurements later on).

These preparations allow an automatized and faster measurement procedure later on and, thus, diminish the drying effects of the MIC (biological material). Manual interventions of the user are then only necessary for the definition of the measurement points.

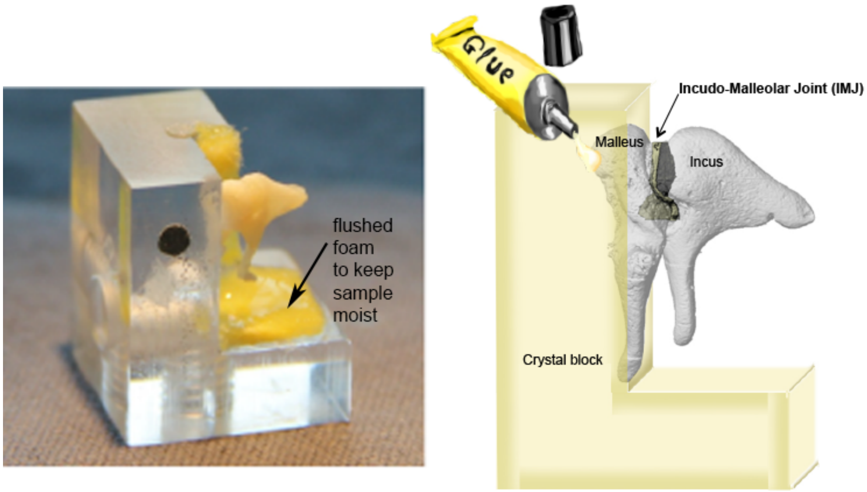

Figure 3.12 The malleus-incus complex was isolated from human temporal bone, and then the malleus was glued to a crystal block. Foam material was placed on the crystal block and flushed with water to keep the sample moist during the measurements. Additionally, drops of saline solution were applied with a syringe to the IMJ in-between the different measurements steps. The 3-D reconstruction of the MIC in the illustration on the right side is reprinted with kind permission of Jae Hoon Sim and was created within the context of his dissertation (J.H Sim 2007).

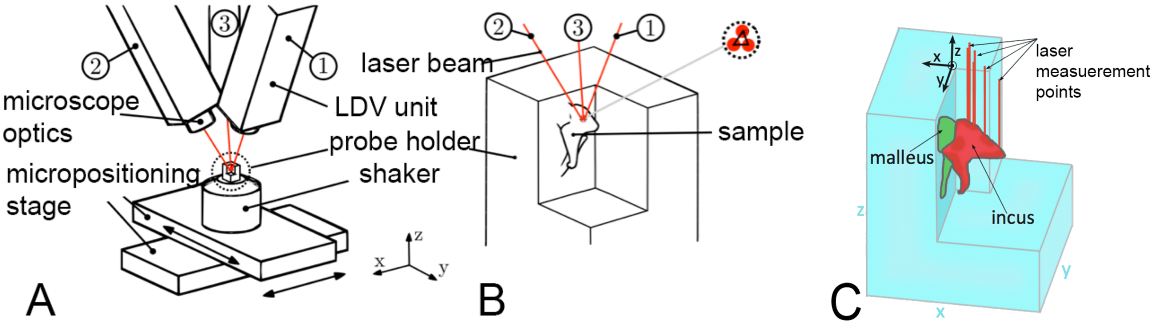

Figure 3.13 Schematic illustration of the measurement setup: (A) Setup of the 3-D laser consisting of three single lasers (1D-LDV): 1, 2 and 3. (B) The position of the three measurement points (1, 2, 3) in the measurement frame is adapted by the micropositioning stage. This illustration is modified after (Ihrle et al. 2015) with kind permission of Sebastian Ihrle and 'Journal of Sound and Vibration'. (C) Spatial velocity is measured at different measurement points to calculate the 3-D rigid body motion of the incus.

Finally, the relative motion between the malleus and incus of the isolated malleus-incus complex is calculated, and spatial behavior of the IMJ is characterized. Different intensities and directions of excitation are used, and their influence on the IMJ motion is analyzed as well.

III.II.2.1 Dynamic excitation

Five isolated malleus-incus complexes (MICs) from fresh human temporal bones were used. As described above, the malleus was fixed on the sample holder (crystal block, acrylic glass), such that the incus and the IMJ were still free to move (see Figure 3.12, Figure 3.14). This sample holder was mounted on an electro-dynamic mini-shaker (Brüel&Kjær 4810, Nærum, Denmark) by a screw, and stimulated with different patterns of excitation (sweep, multisinus, single sine) in three different excitation directions (see Figure 3.15). The shaker was driven by the signal generated by the real-time computer and amplified by a Brüel&Kjær type 2718 amplifier. Then, spatial velocity of malleus and incus was measured with the three single LDVs at several different measurement points (see Figure 3.13 C). The rigid body motion of the ossicles is obtained from measurements of the spatial velocity at several non-collinear points on the ossicles for a given excitation.

The measurement procedure was as follows:

1. The sample holder is mounted on the shaker for one excitation direction (see Figure 3.15): inferior-superior, anterior-posterior, or lateral-medial excitation direction.
2. A measurement-point grid (non-collinear points) is defined on the ossicles (see Figure 3.17).
3. The measurement is repeated for each measurement point on the grid.
4. All points of the measurement-point grid are as well measured for the other excitation directions.

As described in chapter III.I.10, the IMJ is nowadays assumed to allow relative motion between malleus and incus in the frequency region of human hearing. The spatial rigid body motion is calculated from subsequent velocity measurements at different points on the malleus and incus to clarify the still open question how the relative motion looks like and how the spatial vibration pattern of the ossicles changes as the excitation frequency varies. The ossicles are excited in three linearly-independent directions (see Figure 3.15) with the shaker, since the excitation direction may influence this vibration pattern. Parameters for a simulation model of the IMJ can be derived with the set of spatial transfer functions.

The malleus performs a uniaxial vibration during excitation induced by the shaker, because it is rigidly connected to the sample holder, which is fixed on the shaker by a screw. The transfer function between the malleus and the incus is calculated between the uniaxial vibration of the malleus (input) and the spatial vibration of the incus (output). This information is given for all three different excitation directions. Thus, at this point three reference signals of the transfer function, namely the uniaxial vibration of the malleus for each of the three excitation directions are known. The spatial vibration of the incus can now be determined for each excitation direction from subsequent measurements on the incus surface of the predefined measurement grid. The coordinate system of these measurements is shown in Figure 3.16. The coordinate system of the sample is shown in Figure 3.16 A, and the generalized coordinates in Figure 3.16 B. The generalized coordinates are calculated from the exact positions of the measurement point on the incus surface, which are reconstructed from the data of the incremental encoders. An example of the LDV measurement points on the incus is illustrated in Figure 3.17 A: the LDV beams are projected on the surface of the incus Figure 3.17 B.

At this time, the spatial motion of the incus for three excitation directions of the malleus is known and the spatial transfer functions can be calculated. The transfer functions are calculated between the uniaxial vibration of the malleus and the spatial vibration of the incus described by its generalized coordinates (Ihrle et al. 2015).

Further information of the measurement setup for dynamic excitations can be found in Ihrle et al. (Ihrle et al. 2015).

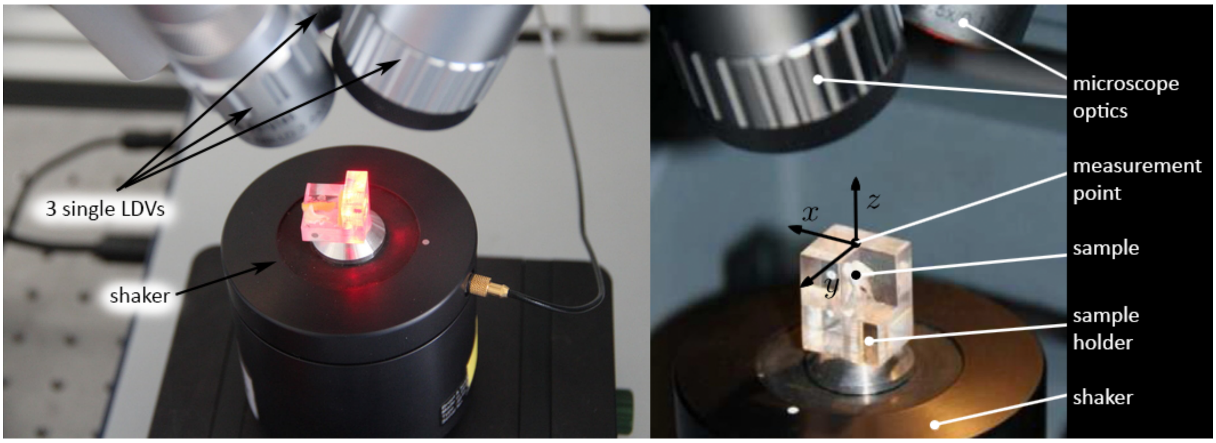

Figure 3.14 Dynamic excitation: measurement setup. This illustration (right side) is modified after (Ihrle et al. 2015) with kind permission of Sebastian Ihrle and 'Journal of Sound and Vibration'.

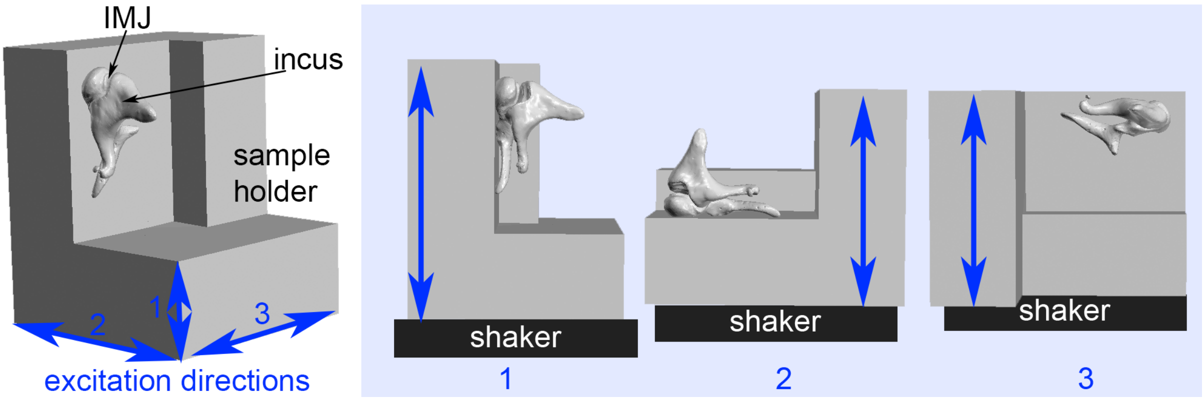

Figure 3.15 Excitation directions of the dynamic excitation with a shaker: (1) inferior-superior excitation direction (z-direction), (2) anterior-posterior excitation direction (x-direction), and (3) from lateral-medial (y-direction) excitation direction. Combination of the 3-D reconstruction of the MIC (micro-CT data) and the sample holder (CAD construction).

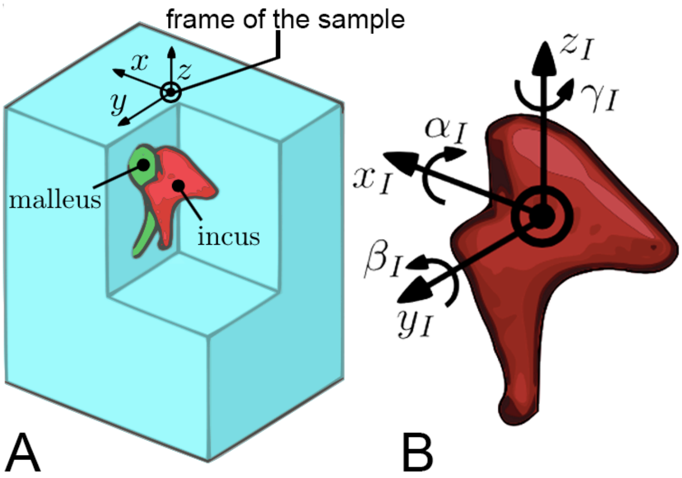

Figure 3.16 Dynamic excitation measurements: Coordinate system. (A) Sample holder an frame of the sample (= sample frame). (B) Generalized coordinate system; the coordinate system describing the motion of the incus has a that is located at the center of gravity of the incus (B) and orientated like the sample frame (A). This illustration is modified after (Ihrle et al. 2015) with kind permission of Sebastian Ihrle and 'Journal of Sound and Vibration'.

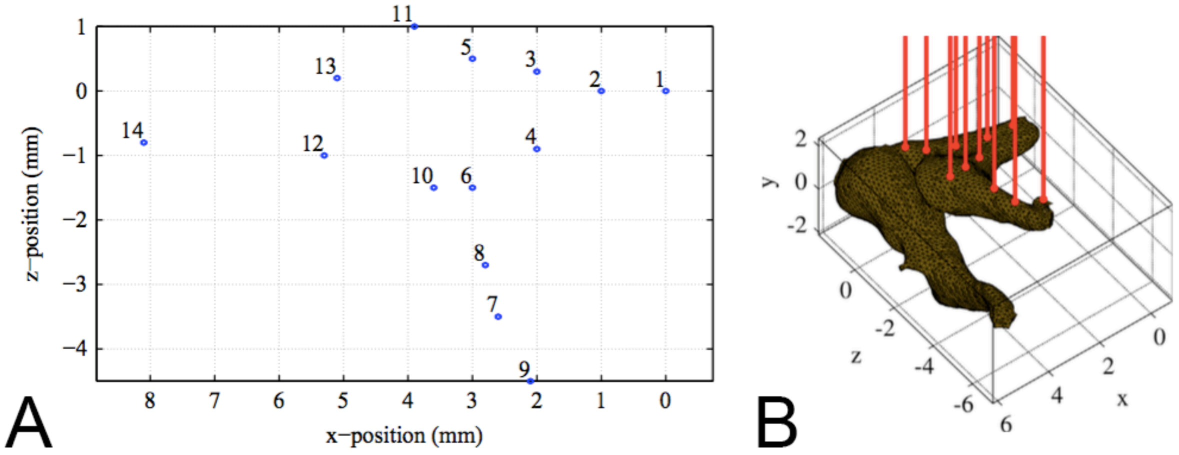

Figure 3.17 Measurement points on the specimen surface in the case of an excitation in the y-direction (lateral-medial excitation direction). The measurement points 1–11 are positioned on the surface of the incus. (A) Position of the measurement points in the x–z reference plane. (B) Reconstruction of the spatial coordinates of the measurement points. The red lines show the LDV laser beams and measurement point on the incus. This illustration is modified after (Ihrle et al. 2015) with kind permission of Sebastian Ihrle and 'Journal of Sound and Vibration'.

III.II.2.2 Quasi-static excitation

Following the dynamic measurements, the quasi-static measurements were performed in the five samples. A sinusoidal force was applied at different points on the incus. Thus, the incus was excited by applying a quasi-static force (see Figure 3.18 and Figure 3.19) while measuring the resulting spatial displacement subsequently at several points on the incus (see Figure 3.13 C). The quasi-static force was applied with a stylus that was connected to a load cell and driven by a micropositioning stage. Two different excitation patterns were applied: the low-frequency sine excitation (Figure 3.19, C1) and the stepped excitation (Figure 3.19, C2). The low-frequency sine excitation allows calculating several parameters as for example: the damping capacity, and the loss factor and loss of each cycle. Thus, the velocity-proportional properties of the joint capsule of the IMJ can be characterized. The stepped excitation allows analyzing the viscoelastic relaxation and creep phenomena.

The measurement procedure was as follows:

5. A measurement-point grid (non-collinear points) is defined on the ossicles.
6. The force application points (FAPs) are defined on the incus.
7. For each FAP (after one another): excitation of the incus with the identical excitation pattern and different LDV measurement points.

The measurement is completed, if for each force application point (FAP) all LDV measurement points were measured.

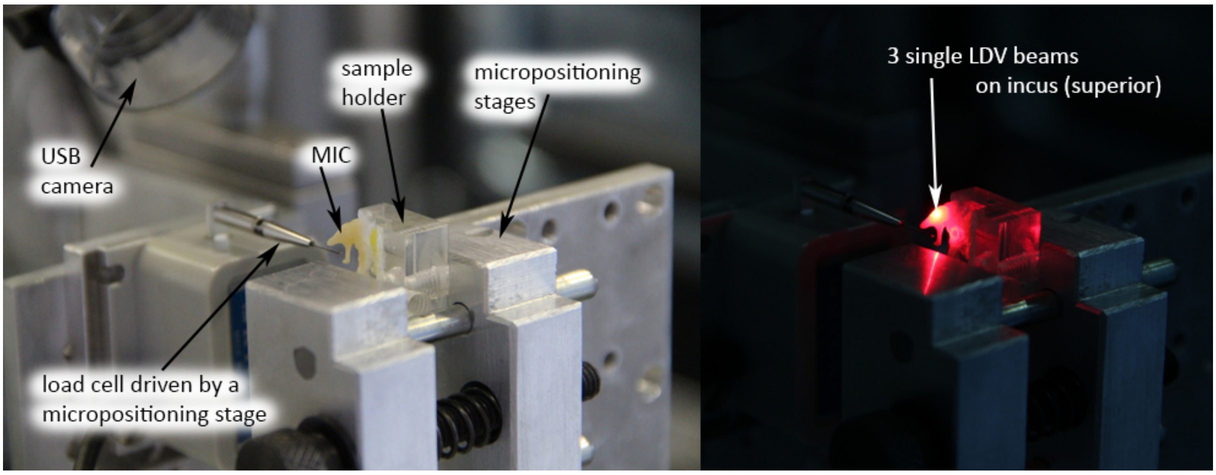

Figure 3.18 Quasi-static excitation: measurement setup (left) and photo during measurement with LDV lasers on (right). MIC = malleus-incus complex.

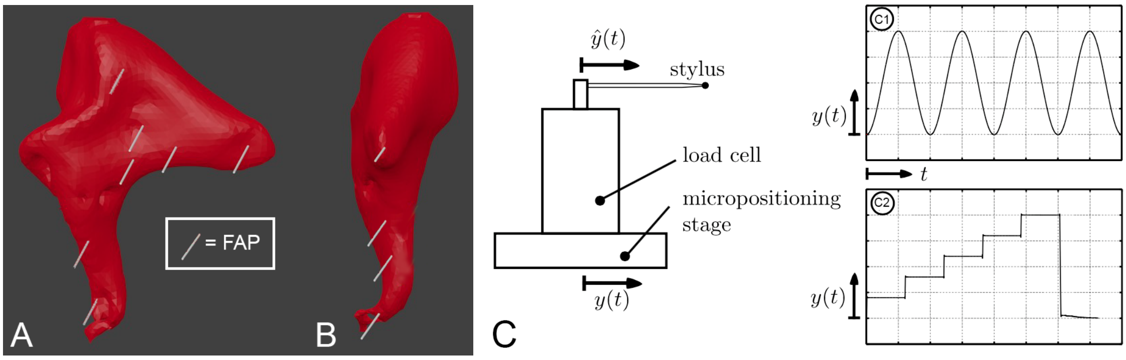

Figure 3.19 Quasi-static excitation: Force application points (FAPs) (for the load cell driven by a micropositioning stage) on the incus. (A) Incus form medial view with FAPs marked in grey. (B) Incus from posterior view with FAPs marked in grey. (C) The stylus connected to the load cell is driven by a micropositioning stage: the displacement of the micropositioning stage is in the direction of the long axis of the stylus. C1 and C2 show the displacement of the micropositioning stage for the low-frequency sine excitation (C1) and the stepped excitation (C2). The illustration (C) is modified after (Ihrle et al. 2015) with kind permission of Sebastian Ihrle and 'Journal of Sound and Vibration'.

III.II.2.3 Micro-CT scans of the malleus-incus-complexes

After the dynamic and the quasi-static measurements, the MIC and the sample holder were prepared with a metallic marker (edding 780 Glanzlack-Marker, edding Vertrieb GmbH, Wunstorf, Germany) for the micro-CT scans (for details about the micro-CT scans see chapter II.V.3). Due to the metallic marker, the sample holder was visible in the micro-CT scans later on. The ossicles were visible as well. Additionally, metal markers (pieces of copper wire) were glued on the sample holder for orientation, which were then visible in the micro-CT scans as well.

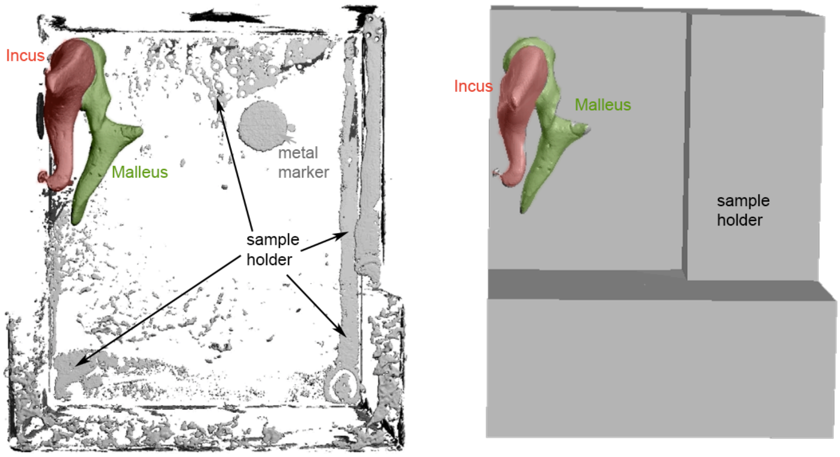

Figure 3.20 The MIC fixed to the sample holder (painted with a metal marker) is imaged in a micro-CT machine and then reconstructed, such that all structures are visible in the 3-D reconstruction: ossicles, sample holder (metallic paint on it), metal markers on the sample holder.

The method of the combination of a spatial 'LDV measurement point frame' and 'anatomical frame' reconstructed from the micro-CT allows calculating the rigid body motion of the ossicles at a single point of for the whole ossicle (see Ihrle et al. 2015 for further information about the calculation of the frame registration).

III.II.3 Preliminary Results of the malleus-incus complex (MIC) measurements

The exact positions of the FAPs were reconstructed based on the 3-D reconstruction of the micro-CT data (see chapter III.II.2.3) and the laser measurement points (see Figure 3.17 B). The dynamic as well as the quasi-static excitation resulted in a relative motion between the malleus and incus. The preliminary results are presented in chapter III.II.3.1 for the dynamic measurements and in chapter III.II.3.2 for the quasi-static measurements.

III.II.3.1 Results of the dynamic measurements

The goal of the dynamic measurements is to investigate the spatial transfer behavior between the malleus and the incus of the specimen for three independent directions of excitation. Thus, the frequency dependent transfer behavior of the IMJ was investigated. By combining the data, the response of the specimen for any excitation direction can be calculated. Finally, the data set of spatial transfer functions will be used for the parameter estimation of a model of the joint connecting the malleus and the incus (Ihrle et al. 2015).

Only incomplete preliminary results are presented in this work. The main analysis of these measurements is performed by Dipl.-Ing. Sebastian Ihrle (Institute of Engineering and Computational Mechanics, Stuttgart, Germany) and will be finally presented in his dissertation.

In the focus of the analysis are:

- The relative motion not orientated in the excitation direction.
- The rotational components of the incus.
- The changes of the motion pattern depending on the frequency.

Figure 3.21 shows the magnitude of the transfer function between the piston motion of the sample holder (malleus rigidly fixed to the sample holder) and the generalized coordinates of the incus for two different excitation directions.

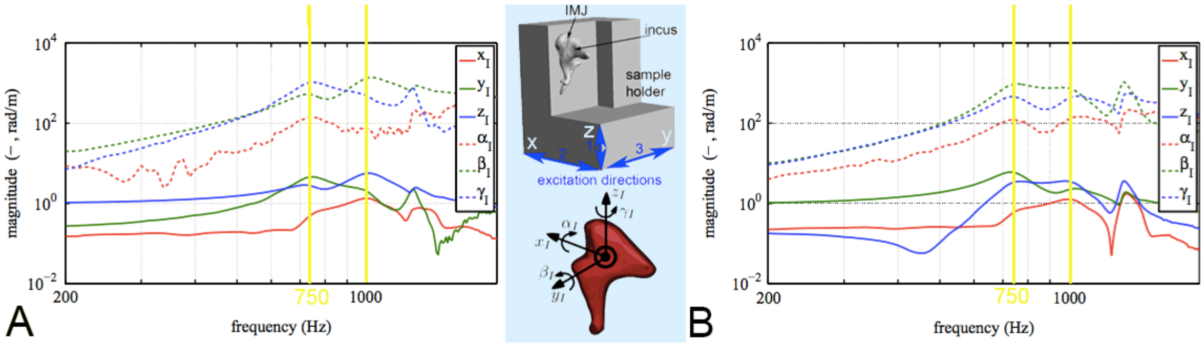

Figure 3.21 Magnitude of the transfer function between the piston movement of the probe holder (malleus rigidly connected to the sample holder) and the generalized coordinates of the incus. The incus exhibits a spatial movement with two prominent resonance peaks near 750 Hz, 1000 Hz. The peaks at 1.3 kHz are caused by a bending mode of the shaker. (a) Excitation in the z-direction (inferior-superior excitation direction). (b) Excitation in the y-direction (lateral-medial excitation direction). This illustrations (A & B) are modified after (Ihrle et al. 2015) with kind permission of Sebastian Ihrle and 'Journal of Sound and Vibration'.

No significant relative motion between malleus and incus is visible below 300 Hz. The relative motion increases with increasing frequency. The motion of the malleus is as assumed only translational because it is rigidly fixed to the sample holder.

The preliminary results show a frequency dependent spatial relative motion of the ossicles. An example of a reconstruction of the motion trajectories for one sample at two different frequencies is shown in Figure 3.21. There is a significant amount of rotational motion of the incus for frequencies above 600 Hz, which are the relevant frequencies for hearing (Ihrle et al. 2015). If the excitation patterns changes, the motion pattern changes as well – the motion is strongly influenced by the malleus head. The motion depends on the excitation frequency, and is composed as follows (Ihrle et al. 2015):

- translational motion
    - along the malleus head
- rotational components
    - around the long axis of the malleus head
    - or the short axis of the malleus head

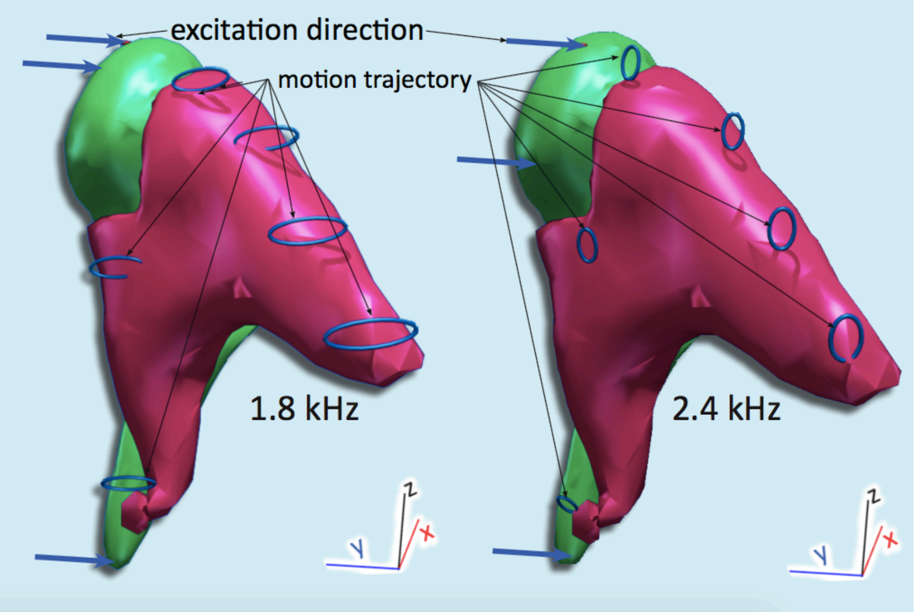

Figure 3.22 Example of a dynamic excitation measurement for 1.8 kHz and 2.4 kHz. The motion trajectories are illustrated in blue circles. The excitation direction (y-direction, lateral-medial excitation direction) is marked in blue arrows. The rotational motion causes the elliptic form of the trajectories.

III.II.3.2 Results of the quasi-static measurements

The quasi-static measurements aim to show the flexibility of the IMJ under large quasi-static excitation. The analysis including the setup of a stiffness matrix and the analysis of effects of the IMJ on middle-ear sound transmission is in progress. Like for the dynamic measurements, only incomplete preliminary results of quasi-static measurements are presented here. The analysis of these measurements is performed mainly by Dipl.-Ing. Sebastian Ihrle (Institute of Engineering and Computational Mechanics, Stuttgart, Germany) and will be finally presented in his dissertation.

It was not possible to describe the obtained preliminary results with a mechanical spare model. The simplified spare model with (non-linear) spring-damper elements vertical to the surface was not able to reproduce the quasi-static measurement results and thus, parameter fitting was not possible for several measurement points. Motion in the joint was observed; the analysis of the reconstructed spatial motion showed that saddle-shaped spatial curved surfaces induce a change of the widths of the joint clefts as well as the tangential position during excitation. Thus, an exact simulation model furthermore takes into account the spatial shape of the joint. Therefore, the 3-D reconstruction model of the micro-CT data was used to obtain the geometry of the joint, and implemented into a multi-body model of the IMJ (see chapter III.II.4). This integration of the contact force on the joint surfaces into the multi body model allows recreating the actual motion of the IMJ. Hence, it is important to include the geometry of the joint into the mathematical model to characterize large quasi-static motions.

Figure 3.23 shows an example of all relevant components for one measurement point. The displacement of the stylus (and the load cell) is sinusoidal with amplitude of 380 µm and a frequency of 0.05 Hz (Figure 3.23 A). The force signal shows a non-symmetric force for the inward and outward displacement of the load cell (Figure 3.23 B). The displacement signal of the measurement point measured by the LDVs (Figure 3.23 C) show significant changes in all three spatial directions (x,y,z). Comparing the displacement and the force changes shows a decrease of the force to zero until the half of the outward motion. Contrary, the measurement point moves slowly back to the origin position (outward motion). Thus, the IMJ moves the incus slowly back to its (non-preloaded) origin position. An example of two different FAPs is shown in Figure 3.24 for FAP 1 (Figure 3.24 A, B, C, D) and FAP 2 (Figure 3.24 E, F, G, H).

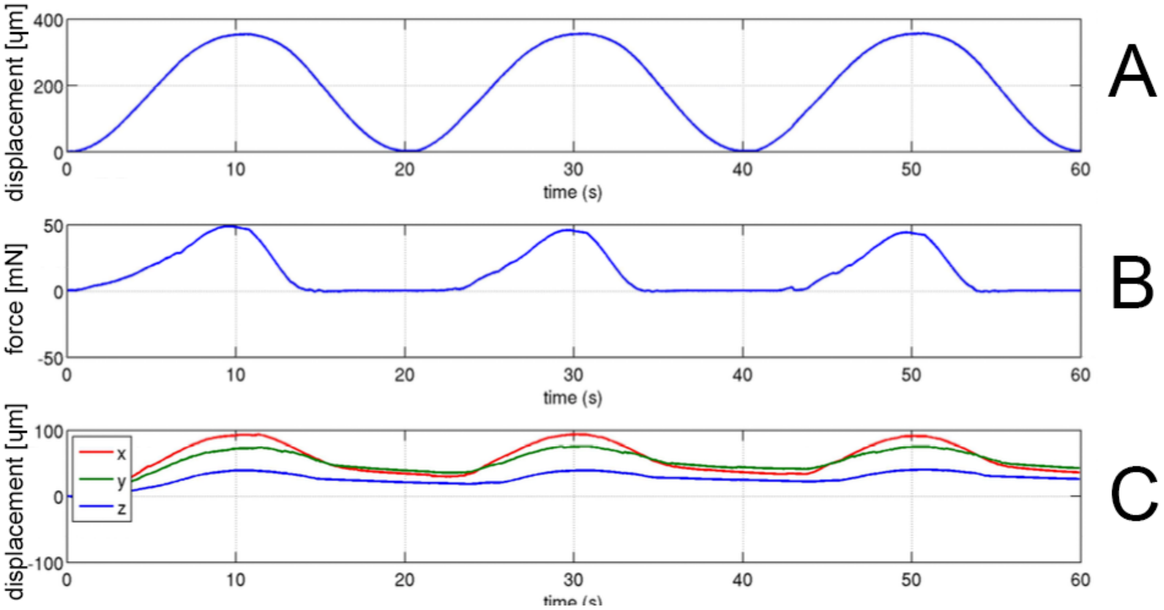

Figure 3.23 Example for signals of the quasi-static measurements of one measurement point with a low-frequency sinusoidal excitation: the force increases non-linear. The measurement point shows displacement components in all three spatial directions. (A) Displacement of the stylus by the micropositioning stage. (B) Force measured by the load cell. (C) Displacement of a point on the ossicles measured by the three single LDVs. This graph is printed with kind permission of Sebastian Ihrle.

The motion of the incus can be reconstructed by the displacement measured for all the measurement points on the incus, together with the coordinates of the measurement points. The spatial coordinates of the measurement points were reconstructed by the position of the micropositioning tables and the micro-CT scan data (see chapter II.V) for details about micro-CT scans). Details about this procedure are explained for example by Ihrle et al. 2015 (Ihrle et al. 2015). The results of two different FAPs are shown in Figure 3.23.

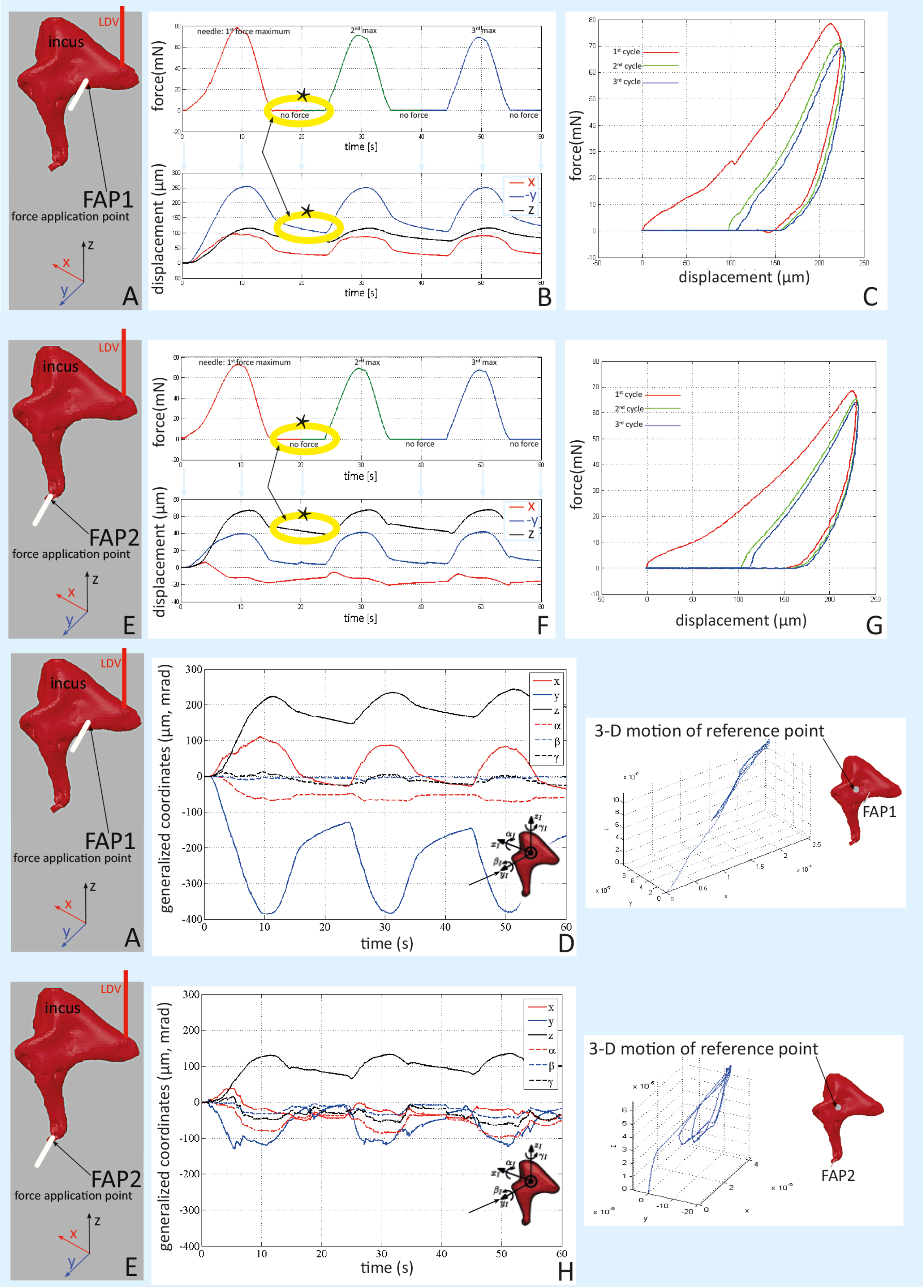

Figure 3.24 Example of the results of two different FAPs: FAP 1 (A, B, C, D) and FAP 2 (E, F, G, H). The force was applied in y-direction. As the viscous part is prominent, the relaxation is not fully completed in one cycle and the needle touches the incus before it reaches the initial position. This is

*indicated by the change of the slope of the spatial displacement (yellow slope, *) in B for FAP 1 and F for FAP 2. Spatial motion components calculated for FAP 1 (D) and FAP 2 (H). FAP 1 (D) moves mainly in positive x-direction, contrary, FAP 2 (H) moves mainly in negative x-direction and shows lover motion amplitudes. The force displacement curves for the two FAPs (C, G) shows an elastic hysteresis and a nonlinear behavior of the IMJ under quasi-static excitation. This large hysteresis shows the typical behavior of soft tissues (Fung 1993) with a large hysteresis showing the large damping of the tendons in the IMJ.*

An example of the reconstructed spatial displacement is shown in Figure 3.25. The trajectory shows a complex spatial motion of the incus (Figure 3.25 B). The direction of the displacement changed due to the complex geometry of the joint surfaces of the IMJ (see chapter I.III.2.4.4.1) during the load curve. The motion direction changes with increasing excursion. This is mainly visible at 180 µm in x-direction in Figure 3.25 B.

In conclusion, the preliminary results indicate that the isolated MICs show a complex spatial motion pattern under large quasi-static excitation. The spatial motions show different displacement patterns during one cycle with different dominant motion directions. This difference in the dominant motion direction may derive directly from the complex geometry of the articular surfaces of the IMJ.

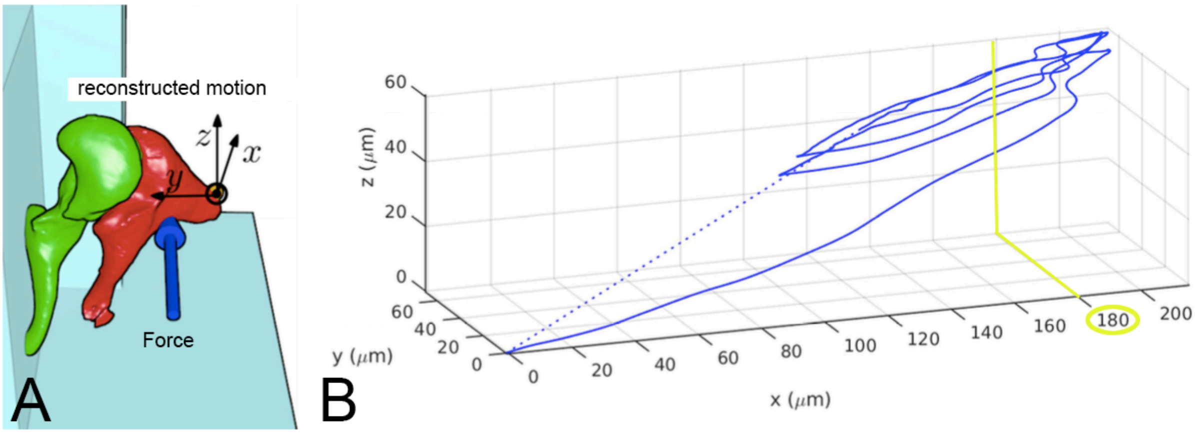

Figure 3.25 Example of a reconstruction of the spatial displacement at one FAP. (A) Illustration of the measurement setup with the MIC; malleus in green and incus in red, the FAP in blue, and the LDV measurement point (reconstructed motion). (B) The trajectory shows a complex spatial motion of the incus. This graph is modified and printed with kind permission of Sebastian Ihrle.

The preliminary data of the MIC measurements shows that the spatial motion of the ossicles has to be considered to obtain the properties and function of the IMJ, and that the measurement setup used for our measurements is capable to do so.

III.II.4 Modelling of the IMJ

The already existing elastic multi-body model was expanded by our co-group from Stuttgart with a detailed model of the IMJ. More details can be found in Ihrle et al. 2013 (Ihrle et al. 2013). The knowledge gained from these quasi-static excitation and dynamic excitation measurements will be integrated in this model.

For the dynamic measurements with small movements, the characterization of the ligaments by a spring-damper-element is adequate, as for example in the model of the IMJ of the dissertation of Dr. Jae Hoon Sim (J.H Sim 2007). For large quasi-static motions, the geometry of the joint has to be considered in the simulation model (contact formulations) to characterize the physical behavior of the joint (see chapter III.II.2.2).

III.III Characterization of spatial incudo-malleolar-joint motions under acoustic stimulation

This work has been performed as a cross-border co-operation project of Dr.-Ing. Albrecht Eiber and Dipl.-Ing. Sebastian Ihrle (Institute of Engineering and Computational Mechanics, University of Stuttgart, Germany) and our group 'Biomechanics of Hearing' (Division of Otorhinolaryngology, Head and Neck Surgery University Hospital Zurich, University of Zurich). Preliminary data is presented in this work. The manuscript 'Sound transmission via the malleus-incus complex' will be submitted to Hearing Research in August 2015 including the following authors: Ivo Dobrev, Sebastian Ihrle, Rahel Gerig, Christof Röösli, Albrecht Eiber, Alexander M Huber, and Jae Hoon Sim.

The contributions of the author of this dissertation to this project were:
Sample preparation:

- Fresh temporal bone preparation, except posterior tympanotomy performed by Dr. Röösli and Prof. Huber.
- Mounting of the metal markers and the artificial ear canal.

Measurements:

- Measurements of the 3-D motion of malleus and incus together with the other authors for each sample.
- Placement of retro-reflective glass beads to enhance LDV signal.

Micro-CT:

- Sample preparation for the micro-CT.
- Micro-CT scans of each sample.
- 3-D reconstruction of the micro-CT data.

Data analysis:

- Discussion of the analyzed data with the other authors.

Manuscript:

- Co-authorship and proofreading of the manuscript.

III.III.1 Background and aim

The malleus-incus complex (MIC) plays a crucial role in the hearing process as it transforms and transmits acoustically-induced motion of the tympanic membrane, through the stapes, into the inner-ear. However, the transfer function of the MIC under physiologically-relevant acoustic stimulation is still under debate, especially due to insufficient quantitative data of vibrational behavior of the MIC. This study focuses on the investigation of the sound transformation through the MIC, based on measurements of three-dimensional motions of the malleus and incus with full six degrees of freedom (6 DOF).

Acoustically-induced motions of the tympanic membrane cause three-dimensional vibrations of the middle-ear ossicles. Sophisticated techniques are needed to measure the vibrational motions of the middle-ear ossicles because the amplitude of the ossicular vibration is of nanometer scale. Previous investigations (Puria 2003, W. Decraemer et al. 1999c) have revealed that the Laser Doppler Vibrometer (LDV) provides a sufficiently sensitive, reliable and accurate measurements for determining vibration modes of the middle-ear bones.

Considering motion of each of the middle-ear ossicles (i.e., the malleus, inucs, and stapes) as a rigid body motion under physiologically-relevant acoustical stimulation, three-dimensional (3-D) motions of each ossicle has six degrees of freedom (DOF) of three translations and three being rotations, and thereby the ossicular motion of the middle-ear bones can be described in a common reference frame. From a theory of classical dynamics, the six rigid-body motion (RBM) components can be determined when spatial motion components and coordinates of at least three non-co-linear points on the rigid body are known. Decraemer (W.F. Decraemer et al. 1994) presented a method for determining three translational components at a specific point on the middle-ear bone from measurements using an one-dimensional (1D) LDV. They mounted temporal bones on two stacked goniometers, and measured velocities using a laser Doppler vibrometer from several different angles, which were provided by rotations of the two goniometers. Recent developments and commercialization of 3-D LDV systems with three built-in laser beams, oriented at three independent measurement angles, allow for convenient and simultaneous measurements of all three translational components at a measurement point.

In previous studies, spatial motion of the stapes was measured for humans (Hato et al. 2003, J. H. Sim et al. 2010a) and for guinea pigs (J. H. Sim et al. 2010b) with an assumption that in-plane motion of the stapes along the footplate plane is restricted due to anatomy of the annular ligaments, and thus motion of the stapes has only three dominant spatial motion components. Lauxmann et al. (2012) measured motion of the human stapes with the full six DOF, but in their measurements, the cochlea was drained. They measured 3-D motion components at nine points on the medial side of the footplate using a 3-D LDV system, and constructed the six rigid-body motion components from the measurement. Decraemer et al. (2007) also measured motion of the gerbil stapes with the full six degrees of freedom. In the study, the measurement points were aligned at the center of the rotations of the goniometers, and thus the location of the measured points could be maintained during the rotations by the goniometers.

While spatial motion of the stapes was measured in several previous works, measurements of spatial motion of the malleus or the incus include technical difficulties. First, the spatial motions malleus and incus are expected to have full six degrees of freedom, and thus simplification of the spatial motion is not possible. Second, surgical opening for access to malleus and incus is limited because the malleus-incus complex is suspended by several ligaments and tendons and those must not be damaged to measure physiological motion of the malleus-incus complex. Sim et al. (2004) measured spatial motion of the malleus-incus complex with full six degrees of freedom, but in their measurements, the malleus-incus complex was isolated with the stapes and extraneous bones were removed to obtain sufficient access of the LDV beam to the malleus and the incus.

In this study, a method to measure and determine spatial motion of middle-ear ossicles with the full six DOF using a three-dimensional (3-D) LDV system is introduced, and the method is applied to three cadaveric temporal bones. The 3-D LDV system is positioned by several different angles with respect to the specimen due to limited access of the laser beam to the malleus and the incus. To identify spatial coordinates of the measurement points on the ossicles with different orientations of the 3-D LDV system, techniques using micro-CT imaging are used.

III.III.2 Experimental approach

The motion of the MIC was measured in three cadaveric human temporal bones with intact middle-ear structures excited via a loud speaker embedded in an artificial ear canal, in the frequency range of 0.5-5 kHz. Three-dimensional (3-D) shapes of the middle-ear ossicles were obtained by sequent micro-CT imaging, and an intrinsic frame based on the middle-ear anatomy was defined. All data were registered into the intrinsic frame, and rigid body motions of the malleus and incus were calculated with full six degrees of freedom. Then, the 3-D transfer function of the MIC, defined as velocity of the incus lenticular process relative to velocity of the malleus umbo, was obtained and analyzed.

III.III.2.1 Temporal bone preparation

Two fresh cadaveric temporal bones (TBs) within 7 days after death (TB1 and TB2) and a frozen TB (TB3) were used for this study. The fresh TBs were harvested within 24 hours after death and were preserved in thiomersal 0.1 % ($C_9H_9HgNaO_2S$) solution at 4° C. The frozen TB was also harvested within 24 hours after death and was frozen immediately.

The temporal bone preparation was similar as described for the first project (see III.I.4.1): A canal-wall-up mastoidectomy including posterior tympanotomy and a wide epitympanectomy were performed subsequently to expose the malleus-incus complex. After the surgical opening, the superior part of the malleus head and incus body, the manubrium of the malleus, and the long process of the incus were exposed (see Figure 3.28 B). The intact tympanic membrane (TM) was confirmed by microscopic view, and all suspensory attachments to the middle-ear ossicles, which include ligaments and tendons, were left intact, during the preparation. The external ear canal was removed and was replaced by an artificial ear canal (AEC) of about 0.5-ml volume (see Figure 3.27) (J. H. Sim et al. 2010a, J. H. Sim et al. 2012, Lauxmann et al. 2012b).

Several custom-made markers were glued on the peripheral bones (see Figure 3.28 C) as references for identification of the LDV measurement frame, and were held in position during the measurements. The marker consists of a silica glass tube (diameter of 0.3 mm and length of 1-3mm) and a copper wire (diameter of 0.05 mm) embedded in the silica glass tube.

III.III.2.2 Measurement of vibration of the malleus and incus

Figure 3.26 illustrates the measurement setup of this study schematically. The TBs were mounted on a custom-made test rig, and a 3-D LDV system (CLV-3000, CLV-3-D, Polytec, Germany) with electrically-driven micro-positioning translation stages (PI Physik Instrumente M-126.CG1/DG1, Karlsruhe, Germany) was mounted on the test rig as well. The position of the 3-D LDV laser spot was controlled by the translational stages and was identified by displacement encoders integrated into the translational stages, with a bidirectional repeatability of 2.5 µm. The control of the translational stages and recording of the position of the 3-D LDV system from the displacement encoders were done in a real-time environment with dSPACE (Paderborn, Germany). A USB microscopic camera (Digimicro 1.3, DNT, Germany) was coupled into the head of the 3-D LDV system by means of a reflective prism for visual observation of the laser spot on the surface of the malleus and the incus (Lauxmann et al. 2012).

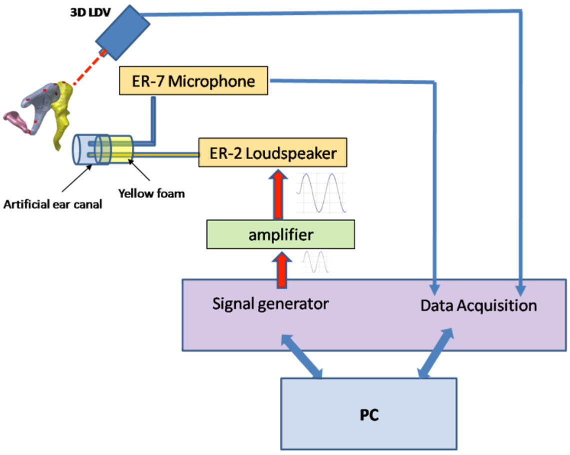

Figure 3.26 Schematic illustration of the measurement setup for the spatial motion measurements of the malleus and incus with a 3-D LDV.

A loud speaker (ER-2, Etymotic Research, USA) and a microphone (ER-14C, Etymotic Research, USA) were placed in the AEC (see Figure 3.27), in order to generate the sound stimuli and monitor the sound pressure levels inside the AEC. Two sets of multi-frequency harmonic signals (0.5- 2 kHz and 2-5 kHz) were generated by a function generator embedded in the dSPACE data acquisition system, and were delivered to the loud speaker via an amplifier. To reduce the crest factor of the resulting signal, the phases of the sinusoidal components were optimized using a Schroeder multisine (Gatto et al. 2010). The frequency steps were 12.5 Hz through the stimulation frequency range. With the multi-frequency harmonic signals, AEC pressure levels of 80-95 dB SPL were obtained.

With the acoustic stimulation, spatial motion components (i.e., XYZ components) of each measurement point were measured by the 3-D LDV system. The measurements at each point were repeated 20 times (20 measurement blocks), and were averaged. All the measurement procedures were controlled by an external computer with a custom-made algorithm.

The measurements of the vibrational motion were performed at 6-8 points on the malleus, and 8-9 points on the incus (see Figure 3.28 A). The measurement points were located on the superior part of the malleus head and incus body, the manubrium of the malleus, and on the long process of the incus. Access of the laser beams from the 3-D LDV system could be obtained with several different orientations of the TBs: three orientations for TB1 and TB2 (see Figure 3.29) and two orientations for TB3.

During the velocity measurement, *XY* coordinates of the measurement points in the 3-D LDV measurement frame (*XYZ* coordinate system), in which the Z-axis along the laser beam and the *XY* plane is perpendicular to the laser beam, were recorded by the displacement encoders of the translational stages. *XY* coordinates of one end of the markers in the 3-D LDV measurement frame were also recorded. The recorded *XY* coordinates of the measurement points and markers were used for identification of the 3-D LDV measurement frame and measurement frame.

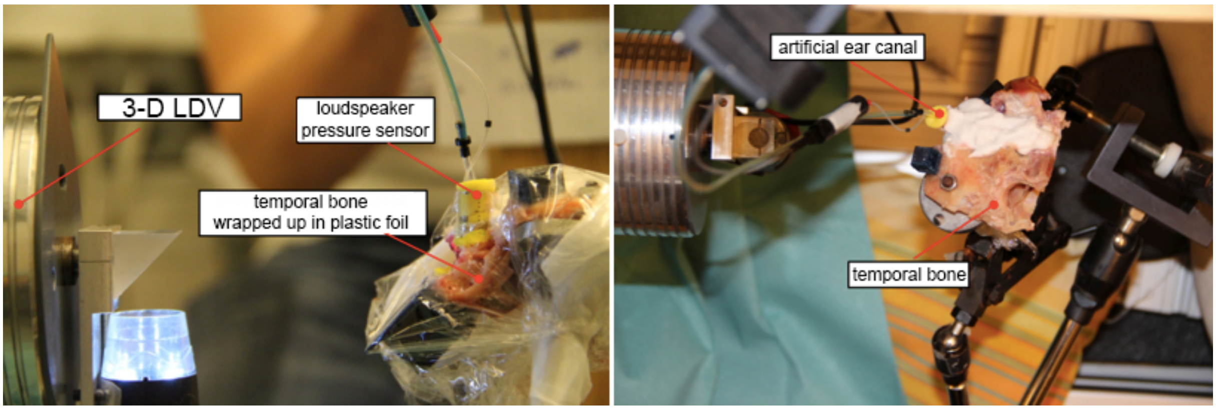

Figure 3.27 Measurement setup of the 3-D LDV spatial motion measurements of malleus and incus.

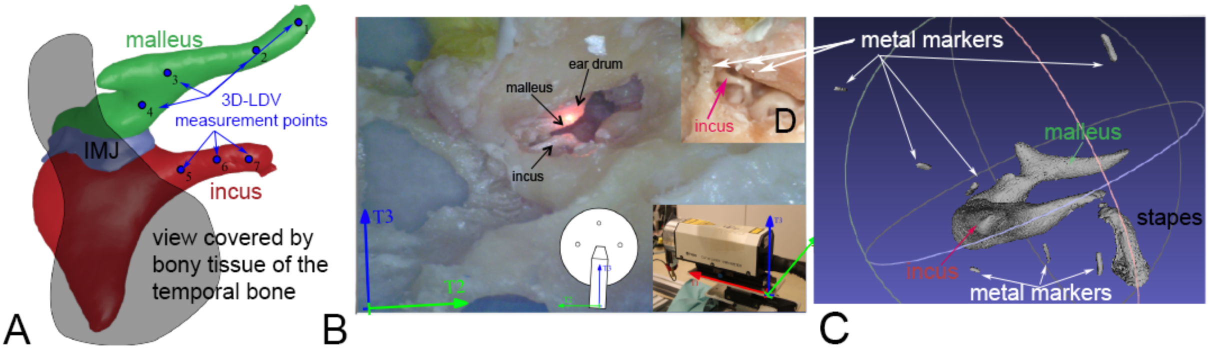

Figure 3.28 Measurement of the spatial motion of malleus and incus in a prepared temporal bone: (A) 3-D reconstruction from micro-CT data: the 3-D LDV measurement points are marked in blue on the incus and the malleus. IMJ = incudo-malleolar-joint. (B) View via the USB-camera on the measurement field showing the malleus, incus and tympanic membrane (eardrum). The laser is reflected and visible on the umbo in this picture. The 3-D LDV with the corresponding measurement axis is shown on the lower right corner. (C) 3-D reconstruction of the middle-ear ossicular chain and the metal markers.

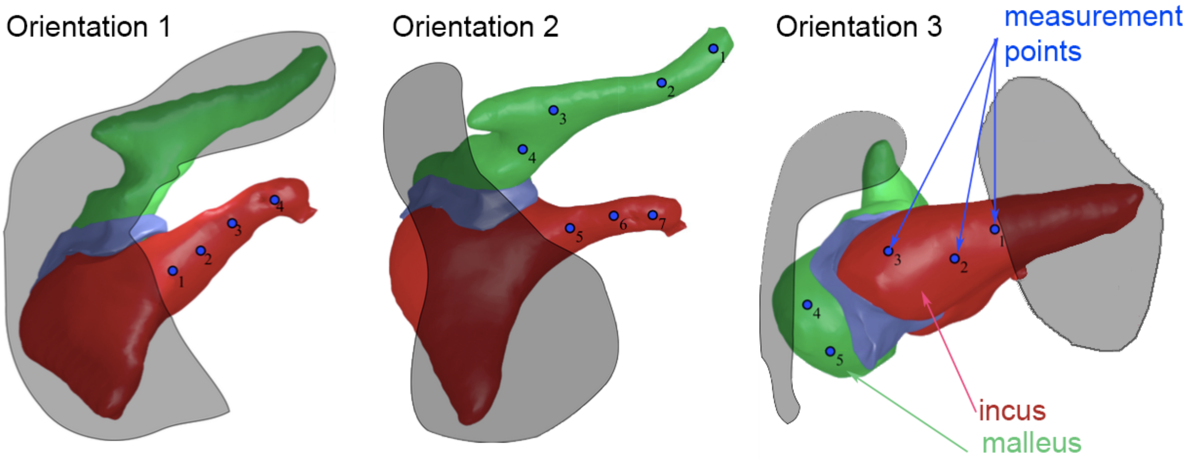

Figure 3.29 The motion of malleus and incus was measured with three different orientations of the 3-D LDV to have all information to calculate the six rigid body motion components (6 DOF) in the three dimensional space.

III.III.2.3 Frame registration

III.III.2.3.1 Micro-CT imaging

After the velocity measurement, the TBs with the markers were scanned by a high-resolution micro-CT scanner (vivaCT 40, SCANCO Medial AG). The resolution was set to 15 µm, and the photon energy level was set to 55 keV (J.H. Sim & Puria 2008). The 3-D volumes of the malleus, the incus, and the markers were reconstructed from the micro-CT slice images (see Figure 3.28 C). The copper wires in the markers were clearly visible and distinguishable from bones in the micro-CT images (see Figure 3.28 C) because the copper had much larger x-ray attenuation than the bones and soft tissues (Sim et al. 2010a).

III.III.2.3.2 Intrinsic Frame (anatomical frame)

The *xyz* coordinate system of the intrinsic frame (i.e. anatomical frame) was defined based on the geometry of the medial surface of the stapes footplate (J.H Sim et al. 2013) and the center of mass of the malleus-incus complex. First, in order to determine the directions of the intrinsic frame axes, surface models of the stapes in STL format were obtained from micro-CT images. The surface models were imported to a commercial software (RapidForm XOS2) and a plane which best fits to the medial surface of the footplate was obtained. On the plane, the posterior-anterior direction along the long axis of the footplate was set as the x-direction, the inferior-superior direction along the short axis of the footplate as the y-direction, and the medial-lateral direction (i.e., the direction normal to the plane) as the z-direction. To follow up the right-hand rule, the anterior, superior, and lateral directions for the right ears and the posterior, superior, and lateral directions for the right ears were set as the positive *x, y*, and *z* directions. The directions of the long and short axes of the footplate were determined such that the ratio of the length along the short axis to the length along the long axis was the minimum.

While the *xyz* directions of the intrinsic frame were determined with surface models of the stapes, the center of mass of the malleus-incus complex, which was calculated from 3-D volume data of the malleus-incus complex, was set as the origin of the intrinsic frame. In the calculation, only the high-density bony parts were considered with a uniform density (Sim et al. 2013).

III.III.2.3.3 Registration into intrinsic frame

Once the 3-D features of the middle-ear ossicles and the markers reconstructed from micro-CT frame is registered into the intrinsic frame, correlation between the LDV measurement frame and the intrinsic frame (anatomical frame) was obtained from coordinates of the markers in both frames. The 3-D features of the middle-ear ossicles and the markers in the intrinsic frame were transformed to the LDV measurement frame by rotations and translations, such that the *XY* coordinates of the markers recorded in the LDV measurement frame are fitted the 3-D features of the markers. Thereby, transformation from the intrinsic frame to the LDV measurement frame was defined by the rotations and translations preformed during the transformation.

Then, since only the *XY* coordinates of the measurement points were recorded in the LDV measurement frame, the *Z* coordinates of the measurement points need to be identified. The *Z* coordinates of the measurement points were determined such that the measurement points are located on the surface of the ossicles. That is, each measurement point was moved along the *Z* direction to find the point which contacts the surface of the ossicle.

After the transformation from the intrinsic frame to the LDV measurement frame was identified including the *Z* coordinates of the measurement points in the LDV measurement frame, transformation of the measurement points from the LDV measurement to the intrinsic frame was performed by reversing the transformation from the intrinsic frame to the LDV measurement frame.

III.III.2.4 Construction of rigid body motion (RBM) components

Once all the measurement points on the malleus and the incus are registered to the intrinsic frame, the vector v_r of the six rigid-body motion components of each of the malleus and the incus is related to the velocity vector v_m at the point m on the bone in the intrinsic frame (see chapter II.II.1).

To determine the six rigid-body motion components, at least three non-collinear points are needed for each of the malleus and the incus (i.e., $n \geq 3$).

In calculation of the rigid-body motion components (see chapter II.II.1), the measured velocity components which have the average signal-to-noise ratio (SNR) of less than 20 dB were excluded. Once the vector v_r of the six rigid-body motion components was calculated, the velocity vector of each measurement point was reversely calculated from the obtained rigid body motion components, and the reversely-calculated velocity components was compared with the originally measured velocity components. In the case that any reversely-calculated velocity component showed a large difference from the corresponding measured velocity component, the velocity component was removed and the rigid-body motion components were recalculated.

III.III.3 Preliminary results

The data processing of these measurements is still in progress. Preliminary results are presented in this chapter.

Based on the transfer function of the MIC, the motion of the lenticular process of the incus relative to the umbo of the malleus reduces with frequency, particularly in the 2-5 kHz range. Analysis of the individual motion components of the transfer function indicates a predominant medial-lateral component at frequencies below 1 kHz, with low but considerable anterior-posterior and superior-inferior components that become prominent in the 2-5 kHz range (see Figure 3.31). While the magnitude of the transfer function decreases with frequency, its spatio-temporal complexity increases significantly (see Figure 3.30).

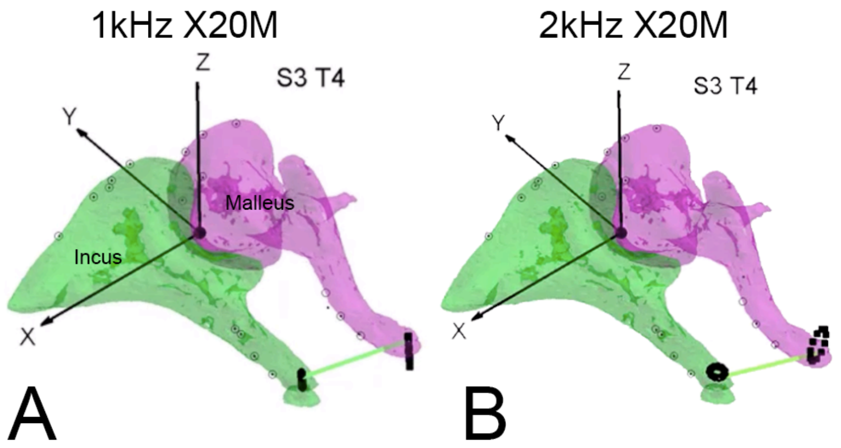

Figure 3.30 Example of the MIC motion at one particular orientation: (A) At 1 kHz, mainly piston-like motion of the lenticular process of the incus is observed. The motion patters of the malleus and

incus are similar. (B) At 2 kHz, the motion is more complex. The motion pattern of the malleus and incus clearly differ. Thus, motion in the joint is expected.

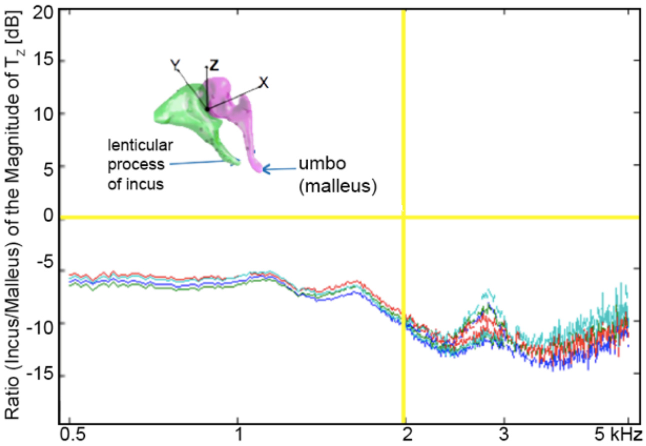

Figure 3.31 Ratio of the piston-like component (T_z direction; Z-coordinate in the Figure) at on orientation: a transmission loss from malleus to incus is shown, especially above 2 kHz.

III.IV Middle-ear sound transmission in reconstructed ears: Distortion product after stapedotomy surgery

III.IV.1 Background

Conductive hearing loss occurs if the stapes footplate is fixed in position, e.g. caused by otosclerosis, rather than being normally mobile. This conductive hearing loss is usually corrected with hearing aids or by stapes surgeries such as stapedotomy surgery. During stapedotomy surgery, the pathologically immobile stapes bone is removed and replaced with a piston prosthesis that conveys the sound stimulus from the incus to the cochlear fluid.

The procedure of a stapedotomy surgery is as follows: first, an incision in ear canal is made and the tympanic membrane is reflected (Figure 3.32 Nr. 2.2) to enter the middle ear. Then, the superstructures (head and crurae) of the stapes are mechanically separated (Figure 3.32 Nr. 3) and removed (Figure 3.32 Nr. 4). The remaining sessile stapes footplate on the oval window of the cochlea is then perforated with a diode-pumped solid-state laser (Figure 3.32 Nr. 6). The stapes prosthesis is placed on the long process of the incus (Figure 3.32 Nr. 7).

Several different types of stapes prostheses are commercially available. Our group was involved in the development of the stapes piston prosthesis NiTiBOND® (see Figure 3.32, Nr. 7) in collaboration with KURZ® (Heinz Kurz GmbH Medizintechnik, Dusslingen, Germany) and the Institute of Engineering and Computational Mechanics of the University of Stuttgart. NiTiBOND® consists of 2 different materials: a pure titanium piston and a nitinol part. Nitinol is a shape-memory alloy (SMA) material, which allows a heat-activated fixation on the incus. Thus, the common 'manual crimping' at the time was replaced by a laser and thereby facilitated and standardized the surgical procedure.

Mainly NiTiBOND® stapes prosthesis are implanted in the University Hospital Zurich. A clinical evaluation of the NiTiBOND® stapes prosthesis was published in 2012 (Huber et al. 2012) suggesting safety and reliability for the new NiTiBOND® stapes prosthesis in short-term results. An air-bone gap (ABG, see chapter III.IV.3.1.3) closure within 10 dB was achieved in 71% and within 20 dB in 93% of the subjects (n=38, 3 months after surgery). In the year 2012, approximately 50 NiTiBOND® stapes prostheses were implanted at the University Hospital Zurich.

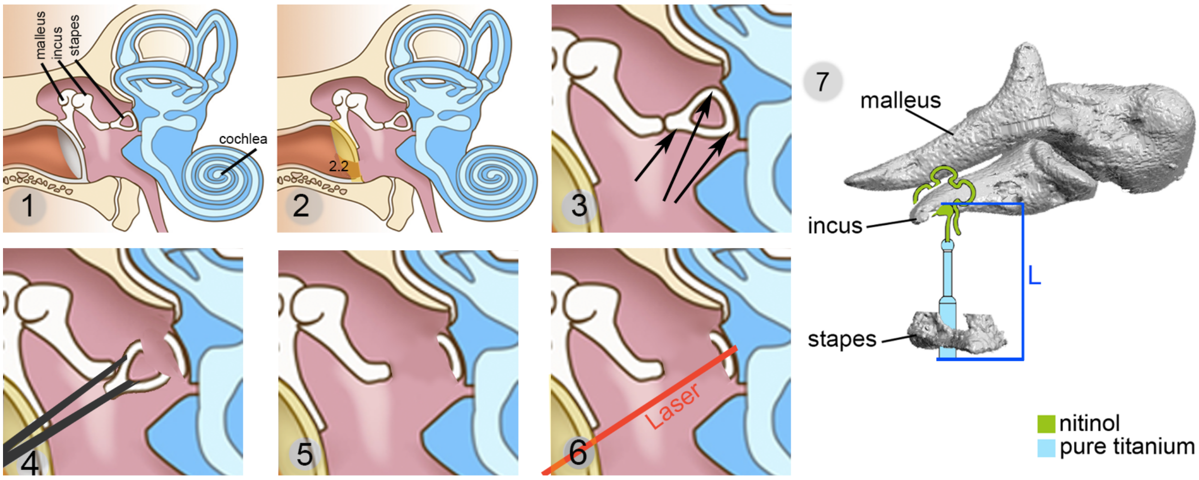

Figure 3.32 Schematic illustration of a stapedotomy surgery: (1) the stapes is fixed due to otosclerosis, (2) Incision in ear canal, and reflection of tympanic membrane (2.2) to enter the middle ear, (3) separation of superstructure, (4) removal of superstructure; head and crurae of the stapes, (5) the stapes footplate is still fixed on the oval window of the cochlea, (6) A perforation into the stapes footplate is made with a laser, and the stapes prosthesis is placed on the long process of the incus (7). The length (L) of the NiTiBOND® stapes prosthesis can be modified by the surgeon for each patient individually. The shape of the NiTiBOND® stapes (7) is modified after (Huber et al. 2012).

A stapedotomy surgery is defined as 'successful' if the air-bone gap (ABG, see chapter III.IV.3.1.3) diminishes by improving the air conduction, or if the speech understanding score improves compared to the preoperative score. Several studies reported a success rate of 78 % to 80 % for the postoperative ABG of < 10 dB and 94 to 97 % for ABG < 20 dB (Somers et al. 1994, de Bruijn et al. 1999, Raske et al. 2001, Zuur et al. 2003).

Most of the subjects profit from stapedotomy surgery in daily life e.g., the 'Operation Benefit Profile Questionnaire' showed an overall subjective median satisfaction score of 75 (scala 0-100), which may be interpreted as patients were "very satisfied" (Tan et al. 2007). In a recent prospective multicenter study, 70 % of 54 subjects had a postoperative air-bone gap less than 10 dB – with an average air conduction hearing thresholds (AC) less than 30 dB in 49% of the subjects (Hazenberg et al. 2013). Reports of subjective quality of life questionnaire after surgery shown to be excellent (pre- and 6 month postoperatively, score ≥9 in 45 % from a scala of 0–10) (Hazenberg et al. 2013). This postoperative questionnaire showed a correlation between postoperative audiometric parameters and subjective quality of life after surgery (Operation Benefit Profile questionnaire).

It is important to focus also on the postoperative quality of sound as well, because subjects sometimes state that the quality of hearing is suboptimal although their hearing ability has been improved significantly. Thus, an improvement in the audiometric test does not necessarily mean an improvement in perceived sound and vice versa (e.g, Hearing Disability and Handicap Score (HDHS) assessed by Meyer & Megerian (2000)). The quality of sound is not assessed routinely in the clinics after stapedotomy surgery nowadays. However, only a few studies focused on the actual quality of perceived sound after stapedotomy surgery (Ramsay et al. 1997, Lundman et al. 1999, Arnold et al. 2000, Meyer & Megerian 2000, Tan et al. 2007, Hazenberg et al. 2013).

The primary aim of this study is to assess the quality of perceived sound after stapedotomy with the focus on distorted sound perception (DSP). For the first time, we collect data of subjective perception of distortion at different frequencies and loudness levels at different time points up to a 1-year follow-up. The secondary aim is to assess the quality of hearing after stapedotomy surgery with a questionnaire (Amsterdam Post Operative Sound Evaluation: APOSE).

III.IV.2 Subject assessment and methods

This ongoing prospective case control study is targeted to include 50-60 subjects. The study was approved by the Ethical Committee of Zurich (KEK-ZH-Nr. 2014-0012). All subjects underwent stapedotomy surgery after clinical evidence of otosclerosis. Twenty-two subjects were included between October 2014 and May 2015. The preliminary subject demographics are summarized in table (see Table 3.1). None of the included subjects had revision stapes surgery. All but one implanted stapes prostheses are NiTiBOND® prostheses (Heinz Kurz GmbH Medizintechnik, Dusslingen, Germany). One titanium-prosthesis was implanted in a subject suffering from a nickel allergy which is contained in the NiTiBOND® prosthesis (Nitinol = Nickel Titanium Naval Ordnance Laboratory) (see Figure 3.32 Nr 7).

Subject characteristics	**First measurement session: Total number of subjects = 22 N (N %)**
Gender	
Male	8 (26 %)
Female	14 (64 %)
Age (mean)	45 years range, 25 to 69 years
Operated otosclerosis	
Unilateral	14 (64 %)
Bilateral	8 (36 %)
Prostheses	
NitiBond®	21 (95 %)
Other	1 Titan (5 %)

Table 3.1 Table of subject characteristics.

Audiometric data is obtained at six different time points as a follow-up after stapedotomy surgery (see Table 3.2). Additionally to the pure tone audiogram including air conduction hearing thresholds (AC) and bone conduction hearing thresholds (BC), the uncomfortable level (UCL) and subjective changes of distorted sound perception (DSP) were assessed. The distortions were assessed up to the thresholds of the uncomfortable level (UCL). The audiometric data is expressed in decibel hearing level (dB HL). The assessment of audiometric data is certificated according to the DIN EN ISO 8253.

A standard 'measure' to assess DSP does not exist. Therefore, a custom measurement method was used: subjects were asked at the different frequencies and loudness levels whether the sound was ‘clear/normal’ or ’distorted/noisy/clanking’ to assess the perceived distorted sound. The stimulus was a pulsed pure tone. The frequencies included to the assessment of AC, BC, UCL and DSP were: 125 Hz, 250 Hz, 500 Hz, 1 kHz, 2kHz, 3 kHz, 4 kHz, 6 kHz, and 8 kHz.

Additionally, a questionnaire on quality of hearing after stapedotomy (Amsterdam Post Operative Sound Evaluation, APOSE) was evaluated at each of the five postoperative measurement sessions (see Table 3.2). The APOSE questionnaire is reprinted in Figure 3.33 in the original English (A) version of Tan et al. (2007) and in the customized translated German version (B). It covers the overall postoperative hearing and the quality of perceived sound that are to be judged in terms of “good,” “too loud,” “too soft,” “distorted,” or “other.” (“high pitched sound,” “low pitched sound,” “loud sound,” “male voice,” “female voice,” “one’s own voice,” “radio,” “television,” “phone conversations” and “music”).

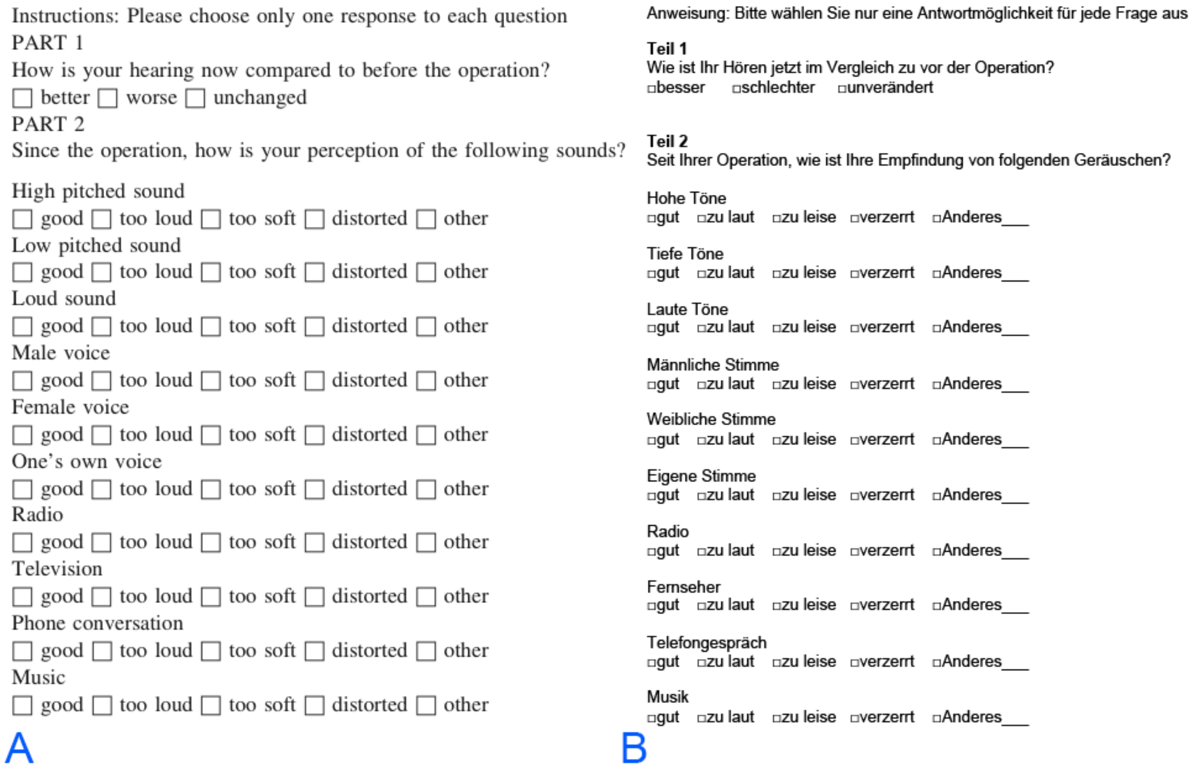
Instructions: Please choose only one response to each question
PART 1
How is your hearing now compared to before the operation?
☐ better ☐ worse ☐ unchanged
PART 2
Since the operation, how is your perception of the following sounds?

High pitched sound
☐ good ☐ too loud ☐ too soft ☐ distorted ☐ other
Low pitched sound
☐ good ☐ too loud ☐ too soft ☐ distorted ☐ other
Loud sound
☐ good ☐ too loud ☐ too soft ☐ distorted ☐ other
Male voice
☐ good ☐ too loud ☐ too soft ☐ distorted ☐ other
Female voice
☐ good ☐ too loud ☐ too soft ☐ distorted ☐ other
One’s own voice
☐ good ☐ too loud ☐ too soft ☐ distorted ☐ other
Radio
☐ good ☐ too loud ☐ too soft ☐ distorted ☐ other
Television
☐ good ☐ too loud ☐ too soft ☐ distorted ☐ other
Phone conversation
☐ good ☐ too loud ☐ too soft ☐ distorted ☐ other
Music
☐ good ☐ too loud ☐ too soft ☐ distorted ☐ other

Anweisung: Bitte wählen Sie nur eine Antwortmöglichkeit für jede Frage aus

Teil 1
Wie ist Ihr Hören jetzt im Vergleich zu vor der Operation?
☐besser ☐schlechter ☐unverändert

Teil 2
Seit Ihrer Operation, wie ist Ihre Empfindung von folgenden Geräuschen?

Hohe Töne
☐gut ☐zu laut ☐zu leise ☐verzerrt ☐Anderes___

Tiefe Töne
☐gut ☐zu laut ☐zu leise ☐verzerrt ☐Anderes___

Laute Töne
☐gut ☐zu laut ☐zu leise ☐verzerrt ☐Anderes___

Männliche Stimme
☐gut ☐zu laut ☐zu leise ☐verzerrt ☐Anderes___

Weibliche Stimme
☐gut ☐zu laut ☐zu leise ☐verzerrt ☐Anderes___

Eigene Stimme
☐gut ☐zu laut ☐zu leise ☐verzerrt ☐Anderes___

Radio
☐gut ☐zu laut ☐zu leise ☐verzerrt ☐Anderes___

Fernseher
☐gut ☐zu laut ☐zu leise ☐verzerrt ☐Anderes___

Telefongespräch
☐gut ☐zu laut ☐zu leise ☐verzerrt ☐Anderes___

Musik
☐gut ☐zu laut ☐zu leise ☐verzerrt ☐Anderes___

Figure 3.33 APOSE questionnaire in (A) English from (Tan et al. 2007) and (B) German. This questionnaire (see also http://journal.entnet.org) was developed by the Amsterdam ear department (Tan et al. 2007).

Measurement session	Time point of measurement session	Assessments	Included subject until May 2015
Before surgery	Within one month before surgery	Pure tone audiogram	22
1	7 to 14 days post surgery	Pure tone audiogram Distorted sound perception (DSP) APOSE questionnaire	22
2	21 to 25 days post surgery	Pure tone audiogram	21

		Distorted sound perception (DSP) APOSE questionnaire	
3	3 months after surgery	Pure tone audiogram Distorted sound perception (DSP) APOSE questionnaire	15
4	6 months after surgery	Pure tone audiogram Distorted sound perception (DSP) APOSE questionnaire	5
5	12 months after surgery	Pure tone audiogram Distorted sound perception (DSP) APOSE questionnaire	0

Table 3.2 Table of subject characteristics.

III.IV.3 Results

The presented results of the ongoing study include the first, second and third post-operative measurement sessions. No results are presented in this chapter for the fourth and fifth measurement sessions, because only 5 and no subjects, respectively, were included in the study until May 2015 (see Table 3.2). All subjects had surgery only at one ear during the study period, but 36% of the subjects had also stapedotomy surgery at the contra-lateral ear before the study started. The pre-operative data was available for all subjects included. For two out of 22 subjects, the first measurement session could not be realized. For the second session 3 out of 21 subjects were not assessed. Missing data occurred due to pain while wearing the headphones for the audiometric measurements or remaining material such as e.g. absorbent cotton in the external ear canal due to clinical treatment. For the third session all 15 included subjects were assessed.

III.IV.3.1 Audiometric outcomes

III.IV.3.1.1 Air conduction (AC)

The comparison of the preoperative air-conduction (AC) to the postoperative AC threshold is illustrated in Figure 3.34 for the third measurement session. All pure tone averages (PTA) improved after surgery (see Table 3.3). To allow comparisons with other studies (e.g. to Tan et al. 2007) several PTAs were calculated:

PTA 0.5, 1, 2 = $(AC_{05kHz} + AC_{1kHz} + AC_{2kHz})/3$

PTA 0.5, 1, 2, 3= $(AC_{05kHz} + AC_{1kHz} + AC_{2kHz} + AC_{3kHz})/4$

PTA 0.5, 1, 2, 3, 4= $(AC_{05kHz} + AC_{1kHz} + AC_{2kHz} + AC_{3kHz} + AC_{4kHz})/5$

PTA 1, 2, 4= $(AC_{1kHz} + AC_{2kHz} + AC_{4kHz})/3$

III.IV.3.1.2 Bone conduction (BC)

The pre-and postoperative BC thresholds and the mean gain for each frequency are illustrated in Figure 3.34 for the third measurement session. The PTAs are listed in Table 3.3.

	Frequency kHz	**Pre-surgery** [dB HL] ± SD	**Post-surgery 3rd session** [dB HL] ± SD	**Mean gain [dB]**
Air conduction (AC)	**PTA 0.5, 1, 2**	56±20	34±16	22±12
	PTA 0.5, 1, 2, 3	55±20	34±16	21±12
	PTA 0.5, 1, 2, 3, 4	55±20	36±17	19±13
	PTA 1, 2, 4	55±21	38±19	17±13
Bone conduction (BC)	**PTA 0.5, 1, 2**	28±19	23±18	5±10
	PTA 1, 2, 4	28±20	21±19	4±11
Air-Bone-Gap (ABG)	**ABG 0.5-1-2-4 kHz**			
	0-10 dB	0	4	
	10-20 dB	3	6	
	20-30 dB	3	1	
	> 30 dB	5	0	

Table 3.3 Audiometric result pure tone averages for air conduction, bone conduction and air-bone gap before surgery compared to three months after surgery (third measurement session) (n= 11).

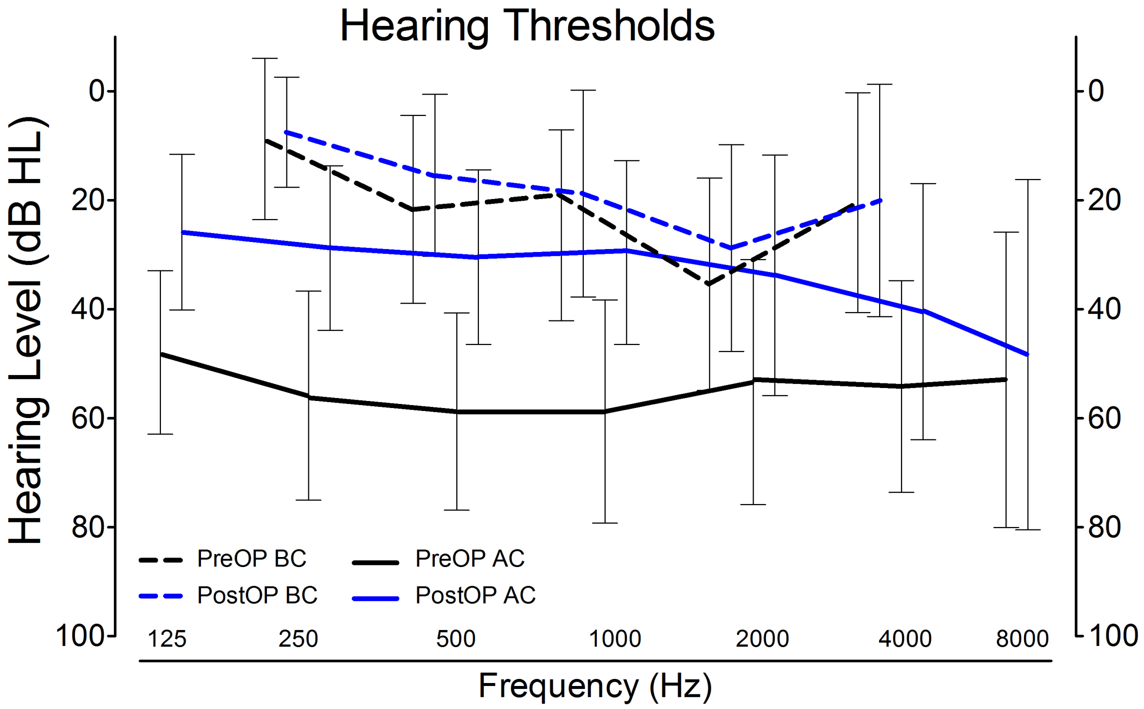

Figure 3.34 Audiometric results (AC, BC): Comparison of the pre-surgery data and third post-operative measurement session data (n=15).

III.IV.3.1.3 Air-bone GAP (ABG)

The results for the air-bone GAP (ABG) are listed in Table 3.3. The ABG was calculated as follows:

ABG (0.5-1-2-4 kHz) = ((AC 0.5 kHz – BC 0.5 kHz) + (AC 1 kHz – BC 1 kHz) + (AC 2 kHz – BC 2 kHz) + (AC 4 kHz – BC 4 kHz))) / 4.

III.IV.3.1.4 Distorted sound perception (DSP)

59% (13/22) of the subjects had distorted sounds perception (DSP) in the operated ear in at least one of the five post-operative measurement sessions performed until May 2015. The percentage of DSP differed from 5 % in the second measurement session at 3-6 kHz to 36% in the first measurement session at 125 Hz (see Figure 3.35). In the third measurement session, the maximum of subjects that had DSP was 22 % (4/15) for 125 Hz and 250 Hz. In the fourth measurement session (n=5), one subject still perceived distorted sound at several frequencies, and two subjects only at 1 kHz (see Table 3.4). The subjects perceived distorted sounds mainly at low frequencies (e.g., 36 % at 125 Hz), compared to higher frequencies (e.g., 9 % at 8 kHz).

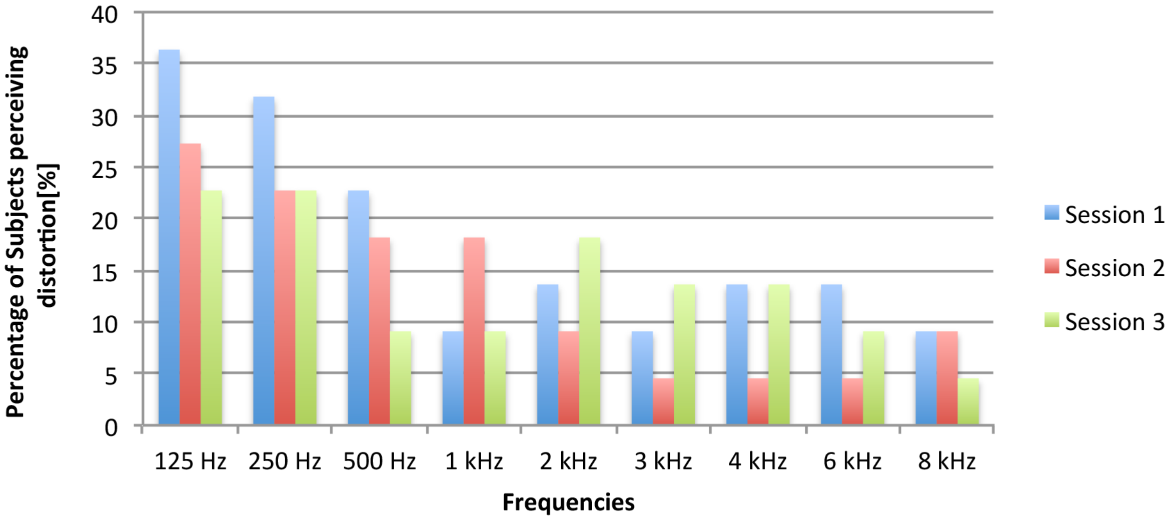

Figure 3.35 Perceived distorted sounds (DSP) at each frequency in percentage of the total study subjects (n=22) for the 1st measurement session (7-14 days after surgery, n=22), 2nd measurement session (21-25 days after surgery, n=21) and 3rd measurement session (3 months after surgery, n=15).

III.IV.3.2 APOSE questionnaire

The subjects received the APOSE questionnaires after each of the five post-operative audiometric-test sessions. The questionnaire was filled in before the audiometric test, or between the audiometric tests and before the UCL and DSP measurement. The first measurement (7-14 days postoperative) was directly performed after the removal of the tamponade after surgery. Therefore, the subjects were often uncertain in choosing the best answer, because the perception of the operated ear is new and unfamiliar for them. Additionally, the questions about perception of music, phone, and television was mainly answered with ‘other’ due to the missing experience of these sounds in the short time between removal of the tamponade and the survey.

In general, most of the subjects (76-80%) stated to hear 'better' then before the surgery (see Figure 3.36). None of the subjects heard 'worse', and 9-13.3% heard 'unchanged' since after the surgery.

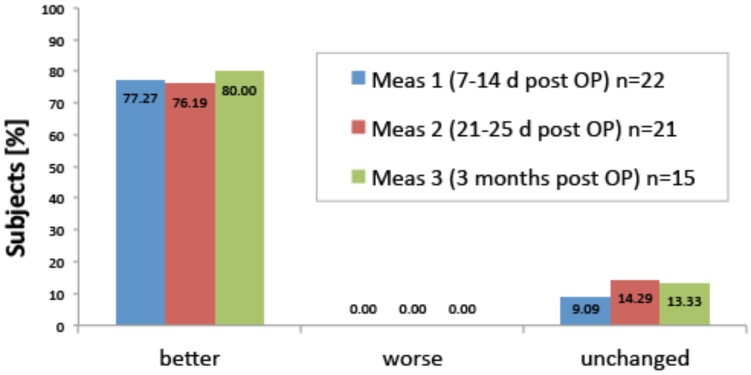

Figure 3.36 Results of the APOSE questionnaire about the hearing quality after stapedotomy surgery in general. Most of the subjects (>76%) stated to hear better then before the surgery for all three assessments after surgery. The recruitment of subjects and the measurements are still in progress. Therefore, the results of the 4th and the 5th measurement are not shown in this graph, and for the 3rd measurement only data of 15 subjects is available until today.

The results of the APOSE questionnaire showing all assessed categories of perceived sounds are illustrated in Figure 3.37. Except for 'loud sounds', the answers were mainly 'good' for all categories (see Figure 3.37) – the percentage of 'good' answers for each category in the third session (3 months after surgery) were: high pitched sound 60%, low pitched sound 87%, loud sound 20 % (47 % 'too loud', 33% 'distorted'), male voice and female voice 87%, own voice 80%, radio 87%, television 67%, phone 60% and music 73%.

The result for the DSP per category is illustrated in Figure 3.38. The most perceived distorted sound was 'loud sound' (33 %). 'High pitched sound', 'low pitched sound', 'male voice', 'female voice', 'one's own voice' and 'Music' were perceived as distorted for less then 10% of the subjects. No subject perceived radio and television distorted. Phone conversations were perceived distorted for 20% of the subjects three months after surgery.

According to Table 3.4, 69.2% (9/13) of the subjects perceived the distorted sounds from the first measurement session on. Four of these subjects (4/13) still perceived distortions at the third measurement session. The other 23% (3/13) perceived distortions from the second measurement session on; one subject of this group also perceived distortions at the third measurement session, two subjects of the third measurement session are still pending, and one didn't perceive distortions anymore at the third measurement session. Only one of the subjects perceived distorted sounds at the third measurement session for the first time.

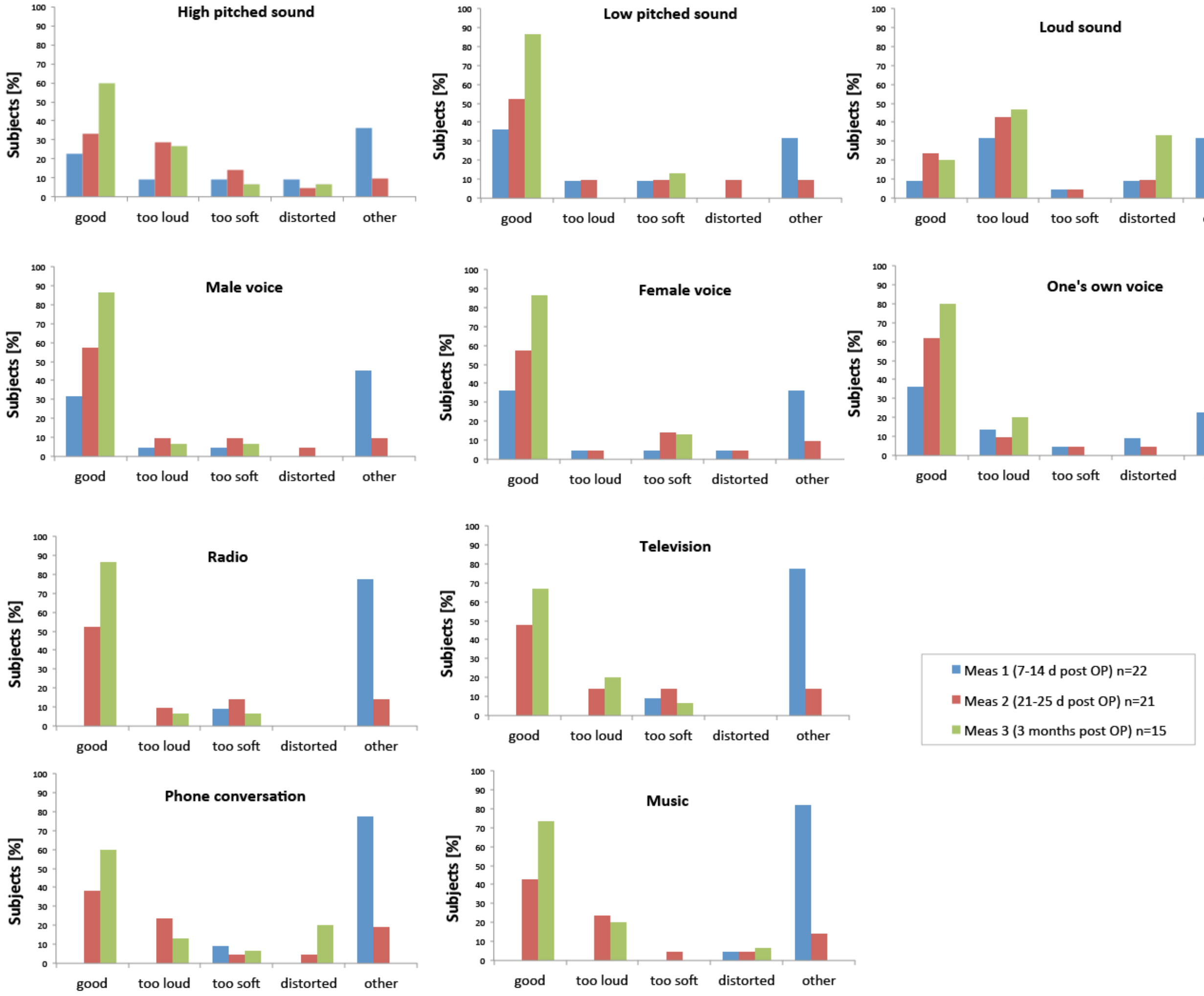

Figure 3.37 Results of the APOSE questionnaire showing all assessed categories of perceived sounds. Except for 'loud sounds', 'good' was the most chosen answer for all categories. The distorted sound category is shown in a separate figure (see Figure 3.38).

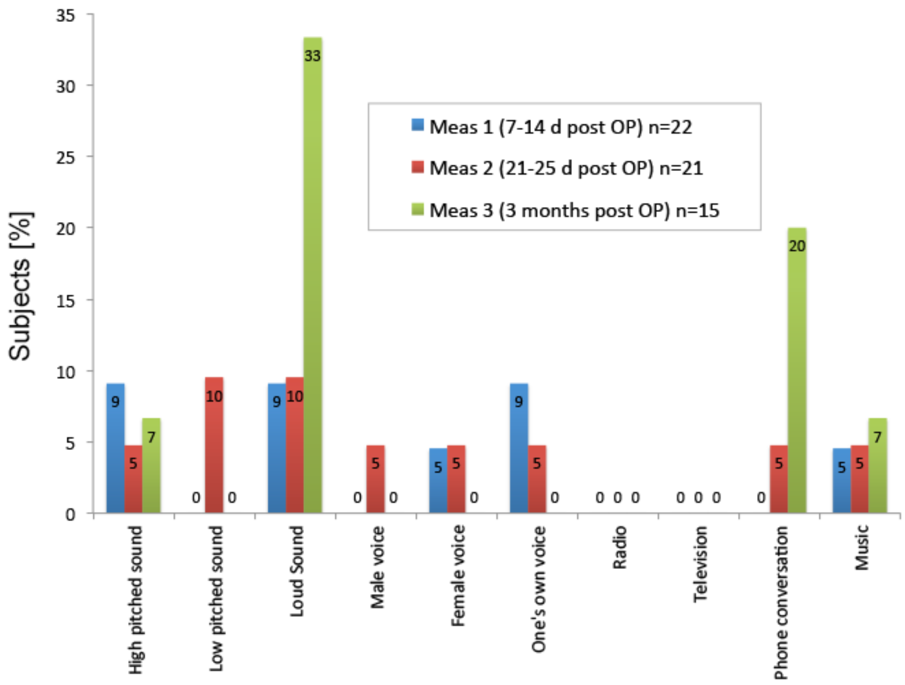

Figure 3.38 Results of the APOSE questionnaire showing the perceived distorted sounds in the different categories.

III.IV.3.3 Audiometric outcome versus APOSE questionnaire

In Table 3.4, the results of the audiometric data and the APOSE questionnaire are compared. 53.3% of the 15 subjects perceived the distorted sound in both, the audiometric test and the APOSE questionnaire. 26.6% of the subjects perceived distorted sound only in the audiometric test, and 20% of the subjects only perceived distorted sound in their daily life (APOSE questionnaire) and not in the audiometric test.

Subject Nr. N=21	Audiometric data: Distortions in at least two sessions	APOSE: Distortions in at least two sessions	Perceived distortions (audiometric) at session #	Perceived distortions (APOSE) at session #
1	no	-	-	3
2	yes	-	2, 3, 4	3
5	yes	-	1, 2 (not assessed), 3	-
6	yes	-	1, 2	3
7	yes	+	1, 2, 3	2,3
	no	+	-	2,3
11	no	-	3	-
13	yes	+	2 (not assessed), 3	1,2
14	yes	-	1,2 (not assessed), 3	1
15	no	-	2	1,3
16	no	-	1	-
17	yes	-	1, 2, 3? (in progress)	-
18	yes	+	1, 2, 3? (in progress)	2,3? (in progress)

19	yes	+	1, 2, 3? (in progress)	2,3? (in progress)
21	yes	+	1, 2, 3? (in progress)	1,2,3? (in progress)

Table 3.4 Overview of patients perceiving distortions for measurement sessions 1, 2 and 3. The subjects who reported distorted sounds in the daily life in the APOSE questionnaire are marked with a '+'. Subjects perceiving distorted sounds in the audiometric measurement and reporting distorted sounds in the APOSE questionnaire (both in at least two measurement sessions) are shaded in green.

Looking at the percentage of subjects that received distorted sounds, maximum 33% of the APOSE responders stated to hear distortions, and similarly maximum 31% of the audiometric tests were positive for distortions (see Table 3.5).

	1st session: **7 to 14 days postoperative** **N=22**	**2nd session:** **21 to 25 days postoperative** **N=21**	**3rd session:** **3 months postoperative** **N=15**	**4th session:** **6 months postoperative**	**5th session:** **12 months postoperative**
Perceived distortions	9-36% of the subjects at the different frequencies	5-29%	6-31%	Measurements in progress	Measurements in progress
APOSE: distortions	0–9 % of subjects at the different categories of distorted sounds	0-10%	0-33%	Measurements in progress	Measurements in progress

Table 3.5 Perceived distorted sounds: comparison of the audiometric data and the data of the APOSE questionnaire.

III.IV.4 Discussion

Preliminary results with varying numbers of subjects at different measurement sessions have been collected. Nevertheless, the reader will be introduced to previous works about quality of hearing after stapes surgery compared with our preliminary results (see chapter III.IV.4.1) and about possible reasons why distortions may occur after stapes surgery (see chapter III.IV.4.2).

Several authors reported DSP in subjects after stapes surgery (Tan et al. 2007, Lundman et al. 1999, Arnold et al. 2000, Ramsay et al. 1997). In our study, subjects mainly perceived distortions at low frequencies in audiometric tests. In contrast, none of the subjects stated to hear 'low pitched sounds' distorted in the APOSE questionnaire. Contrary to Tan et al. (2007), who reported distorted sounds as well at 'low pitched' sound. DSP generally tend to disappear over time (Lundman et al. 1999, Arnold et al. 2000). It will be interesting to compare the long-time follow up results of Lundman et al (1999), Arnold et al. (2000), and Ramsay et al. 1997 with our 1-year follow up data.

Our findings of a subjective hyperacusis after surgery (e.g. 'too loud' for loud sounds in the APOSE questionnaire) do agree with previous works of Tan et al. 2007, Lundman et al. 1999, Arnold et al. 2000, and Ramsay et al. 1997. This phenomenon is assumed to originate from the loss of the stapedius muscle function (Ramsay et al. 1997) or mechanical causes due to the smaller diameter size of the stapes prosthesis with a higher hydraulic lever action, even though the prosthesis is not fixed at the lenticular process of the incus (Raman 1999). The hydraulic lever is presumably 10-28 times larger in the reconstructed ear compared to the normal ear (see III.IV.4.2).

III.IV.4.1 Quality of perceived sound after stapedotomy surgery

Tan et al. (2007) investigated the quality of perceived sound after stapedotomy from retrospective audiometric data and the APOSE questionnaire. Similar to our results, Tan et al. (2007) found in 98 subjects (4-6 months postoperative) the highest percentage of DSP according the APOSE questionnaire were 'high pitched sound' (15% compared to 7% in our study 3 months after surgery), 'loud sound' (13% compared to 33% in our study), and 'music' (10% compared to 7% in our study). Contrary to our results, Tan et al. reported highest percentage of distortion also in 'low pitched sound' (11% compared to 0% in our study).

Lundman et al. (1999) showed in 33% of in total 95 subjects severe hearing disabilities postoperatively including tinnitus, dizziness and sound distortion/hyperacusis. Changes in sound quality occurred in 80% (sound-distortion/hyperacusis) of the operated ears in the early period after surgery, and tended to disappear over time. In our study, 59% of the subject perceived distortions in at least one of the tested frequencies in the DSP test (from 0.15 to 8 kHz), and 52% of the subjects reported at least once DSP in the APOSE questionnaire. In Lundman's study, in 20% of subjects hyperacusis and distortion were still present at follow up (3-8 years) (Lundman et al. 1999). A comparison of our 1-year follow-up data to Lundman's data will be informative. However, Lundman et al. concluded that "sound distortion and hyperacusis are not major problems after otosclerosis surgery, but patients must be informed that it might occur, and that it may even be permanent after surgery." They assumed that normally patients accustomed to the different sound perception after surgery regarding loudness and character of sound in general.

Arnold et al. (2000) found that patients perceiving distortions often had an increased loudness perception. They could determine hyperacusis and distortion of speech by conventional audiometry in 50 % of the cases. The subjectively perceived sound perception by means of hearing level was confirmed with pure tone audiogram and speech audiometry. Contrary, the quality of perceived sound (perceived distortions, loudness sensitivity) did not always match with the audiometric tests. More subjects stated to perceive distorted sounds (18%, n= 11) than assessed with the audiometric tests (10%, n= 6) of in total 61 subjects. Although the percentage of subjects perceiving DSP at least once during the first three months after surgery is similar in both audiometric DSP tests (59%, n=22) and APOSE questionnaires (52%, n=22), the answers in the questionnaire were not consistent with the audiometric DSP for every subject; 19% of the subjects perceived distortions only in the audiometric test, and 10% of the subjects only reported distortions in the APOSE questionnaire. Statistical tests will be performed with the completed data set to evaluate the correlation between DSP in the audiometric tests and the APOSE questionnaires. In 55% of the cases (6/11), the distorted sounds were not perceived any more after 6 months (Arnold et al. 2000). Subjects temporary perceiving distortions showed different loudness levels in the different frequencies; this sensitivity to the loudness was not for all cases visible in the speech audiometry test. Our 6-month follow-up data will be compared with Arnold's results.

More than 5 years after surgery (mean: 55.8 months, n=246), Ramsay et al. (Ramsay et al. 1997) found that, despite of good hearing assessed in the pure tone audiogram, subjects complain about e.g, loud noise intolerance, "caused by the absence of the stapedius reflex", and/or DSP –

which they assumed was caused by 'loose wire syndrome' (see chapter III.IV.4.2). 4.1 % responded to have 'considerable limitation in daily life' and perceived significantly more distorted sounds. Occasional DSP was found in 26.3 % of the subjects; only 1.9 % constantly complained about perceiving distorted sounds. Our one-year follow up data will be compared to these data.

An improvement of the BC thresholds after surgery compared to before surgery may result in studies of stapedotomy patients, because the post-operative BC outcome may be influenced by a phenomenon called "Carhart notch" (Carhart 1950) – a hallmark of otosclerosis. A recent study showed that it is likely "that the morphology of the Carhart notch is variable and is not exclusively at 2 kHz as originally described" (Perez et al. 2009). Thus, the resulting BC threshold is a mechanical artifact and does not necessarily indicate the true cochlear function. In our preliminary results the BC threshold does not change significantly.

III.IV.4.2 Possible reasons for perception of distorted sound after stapedotomy surgery

Why do subjects perceive distorted sound in a 'linear system' of the middle ear (see also Figure 3.39)?

One possible reason may be the signal processing in the brain. Studies have shown, that the time for the adaption of the loudness levels at different frequencies may correlate with the DSP (Arnold et al. 2000). Also Hornig et al. and Kollmeier (Hornig et al. 1996, Kollmeier 1997) found the distorted sounds to correlate with the change in loudness-growth functions and the loss in the speech understanding. In general, subjects may perceive a different sound after surgery and get used to this new kind of sound perception (loudness, new character of sound) already in the early postoperative period (Lundman et al. 1999). Lundman did not go into more detail than reporting changes of perceived sound over time after surgery. However, it is imaginable that this adaption is due to the plasticity of the brain. It was shown that an input from impaired auditory pathways to the brain result in significant changes in the central auditory system (Lee et al. 2003). Several studies obtained additional plasticity of the brain after cochlear implantation induced by reintroducing auditory input to the brain (e.g., Ito et al. 2004, Peterson et al. 2013). A recent study by Firszt et al. (2013) showed in one study subject (female, 40 years old, unilateral, mixed, moderately-severe to profound hearing loss, hearing loss for > 30 years) that the auditory cortex reorganized after stapedotomy surgery. Hearing improved significantly after the surgery; the air-conduction thresholds improved 35–45 dB through the low and mid frequencies (Firszt et al. 2013). Several tests and functional magnetic resonance imaging (fMRI) measurements were performed before surgery, and 3 and 9 months after surgery. The fMRI data, obtained with a monaural stimulation at the normal ear, showed an increase in the operated-ear-auditory-cortex response after hearing recovery. The extent of activated cortex was bilateral and, thus, binaural hearing restored (Firszt et al. 2013). The same subject substantially improved in sound localization and speech recognition in noise (Firszt et al. 2013).

Another possibility of DSP is that otosclerosis still progresses over time and results in an impaired bone conduction and deteriorates the function of the cochlear in both operated and non-operated ears (Pirodda et al. 1995). "This deterioration may explain why after stapes surgery, patients often state that although their hearing ability has improved considerably, the quality of sound is different (Lundman et al. 1999)".

Another possible reason for DSP is that the prosthesis itself causes distorted sound like e.g. by the fixation of the prosthesis on the long process of the incus – in pronounced cases known as the ”loose wire syndrome” described by other authors (McGee 1981, Ramsay et al. 1997). McGee originally described this syndrome in patients “who have had stapedectomy surgery and insertion of a prosthesis which attaches to the long process of the incus by means of a crimped wire (McGee 1981)”. He also stated that the syndrome “consists of a triad of one or more symptoms which improve temporarily with middle ear inflation. These include improvements in auditory acuity, in distortion of sound, and in speech discrimination (McGee 1981)”. In his study, all 43 subjects with this symptom showed a loose wire at its attachment to the incus, and therefore, corrective surgery (tightening of the wire) was performed. All but two patients were relieved of their symptoms (subjectively and objectively). The conclusion of McGee (1981) also fits to our results showing a decrease of perceived distortions at ‘low pitched sounds’ with time. With regards to our results, an effect of the prosthesis fixation (see “loose wire syndrome” above) seems plausible. The relative motion of the prosthesis to the long process of the incus may decrease with time due to tissue growth e.g. mucosa of the incus. This could explain why often distortions disappear with time. However, it is only a hypothesis and needs to be investigated in the future.

A possible reason for DSP can be mechanical causes due to the smaller diameter size of the stapes prosthesis compared to the normal stapes footplate. The diameter of a stapes prosthesis (usually 0.4-0.6 mm^2) results in a functional area of the base of the prosthesis of approximately 0.13 to 0.3 mm^2 functional area. Thus, the functional area is around 10 to 28 times smaller than the diameter of a physiological stapes footplate (around 3-3.2 mm^2 (J.H Sim et al. 2013, Ludman 1988)) and thus, the hydraulic lever action is up to 10-28 times larger in the reconstructed ear than in the normal ear.

An additional reason for DSP can be a suboptimal position of the prosthesis may cause DSP as suggested by Tan et al. 2007. The sound quality may be diminished if the prosthesis does not allow smooth movement in the remnant of the stapes footplate and even result in DSP. This effect may influences the quality of the perceived sound without being visible in the audiometric tests.

III.IV.5 Conclusion and Outlook

The preliminary results show a subjective satisfaction after stapedotomy surgery: 80 % (3 months after surgery, n=12/15) reported better hearing than before surgery. The subjective satisfaction six months after surgery was good for 89% of the 9 subjects assessed until June 29th 2015. The distortions were mainly perceived at low frequencies at high hearing levels, with a maximum of 27 % of the subjects that perceived distortions at 85 dB at 125 Hz. Three months after surgery, the perceived distortions decreased for the low frequencies (125 Hz, 250 Hz, 500 Hz, 1 kHz) compared to the first and second measurements.

However, distortions are reported in the APOSE questionnaire by < 34% for the ‘loud sounds’, and < 10% in all other nine categories three months after surgery (n=15). Subjectively, the distorted sounds in three months after surgery are reported in the categories ‘high pitched sound’ and ‘loud sound’.

Thus, the audiometric results do not directly match with the APOSE questionnaire answers: whereas in the audiometric test mainly the low frequencies are noticeable, ‘low pitched sounds’ were not reported to be subjectively affected by distortions. It is likely that the DSP correlates with the loudness level of sound. In the audiometric test, DSP was mainly observed at high hearing thresholds (close to the uncomfortable level), and the 33% of the subjects reported 'loud sound' to be distorted three months after surgery.

It is not clarified until today why subjects perceive distorted sound (see Figure 3.39) after stapedotomy surgery, which mostly recovers with time.

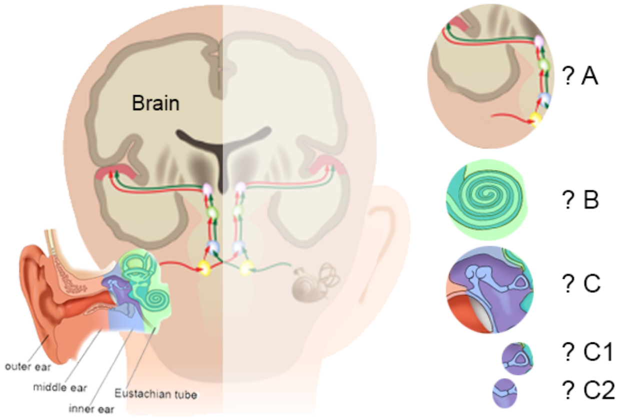

Figure 3.39 It is not clear until today where the perceived distortions after stapedotomy originate. Possible areas are (A) the brain (adaption of the brain to the new character of sound), (B) the cochlea (progressing otosclerosis even after surgery), (C) the middle ear by (C1) placing of the prosthesis such that the prosthesis can not move smoothly in and out the in the remnant of the stapes footplate (e.g. friction of the prosthesis on the footplate due to location or angulation), or (C2) the fixation of the prosthesis on the long process of the incus (relative motion between prosthesis and incus at the beginning – maybe corrected by growth of tissue e.g. mucosa with time).

Our hypothesis is that the perceived distortions often recover over time. After completion of the study (40-50 subjects), the discussed parameters will be carefully analyzed again. The result of the questionnaire is then compared with the results of Tan et al. (2007).

In a second step, objective measurements of distortions could be interesting to measure in the subjects that still perceive distortions after the 1-year follow-up, e.g. by measuring distortions with a microphone in the external ear canal of the subjects. Eldredge (1951) reported that healthy subjects exposed to loud tones perceived subharmonics when the level was ~140 dB SPL, and subharmonics were also detected in the subjects' ear canal pressure. Several authors assumed that these prominent even-order subharmonics (with frequency one half or one quarter of the fundamental) are produced in the middle ear, mainly in the coupling of the tympanic membrane and the malleus (Dallos and Linnell 1966, Huang et al. 2012) and above ~110 dB (Huang et al. 2012). No study is known to the author that focused on distortions in the ear canal of reconstructed ears.

Huber et al. (2008b) measured the motion of the head of the stapes and the area around on the long process of the incus using a laser Doppler vibrometer system. A next step could be to measure the 3-D motion of stapes prostheses close to the contact area with the inner ear in a temporal bone model using 3-D laser Doppler vibrometry. This could give an insight in the motion direction of the functional area of the stapes prosthesis. Additionally, intracochlear pressure measurement with the recently developed pressure sensor by our group (see Figure 1.91 in chapter I.III.3.2.3) in the reconstructed middle ear may follow in the future.

III.V Additional work

The results of the additional studies where the author of this dissertation significantly supported the colleagues of the group 'Biomechanics of hearing' of the University Hospital Zurich are integrated in the introduction part of this work:

- Whole head measurement regarding bone conduction via the skull and soft tissue (see chapter I.III.6).
    - Organization and preparation of cadaver heads.
    - Preparation of measurement setup for cadaver head measurements.
    - Measurements of skull vibration and intracranial pressure.
- Intra-acoustic receiver project (ICAR) for the later development of a fully implantable cochlear implant (see chapter I.III.3.2.3).
    - Support in sheep and human temporal bone organization and preparation.
    - Micro-CT scans and 3-D reconstruction of the temporal bones.
    - Active participation at workshops and meetings including company-internal workshops at Cochlear AG (Basel, Switzerland) and Cochlear Benelux NV (Mechelen, Belgium) related to this project.
- Monitor changes in cochlear function after cochlear implant surgery using electrocochleography (ECoG) (see chapter I.III.3 in subchapter 2.2.1.3.3)
    - Data management (Matlab, Excel), discussion and presentation of achieved results.
    - Support for manuscript preparation and manuscript revision.

IV Discussion and Conclusion

IV.I. Overall findings

The works in this dissertation provide physiological behaviors and functional roles of the incudo-malleolar joint (IMJ) in human ears. The investigations were made with a series of four measurements, which include 1) middle-ear sound transfer function, 2) behavior of the IMJ under directional dynamic forces, 3) behavior of the IMJ under quasi-static loads, and 4) relative motion between the malleus and incus under sound-induced acoustic stimulation. While it appeared that the IMJ is mobile under all the different types of stimulation in the investigations, the four different approaches provide different aspects of the functional roles of the IMJ.

In the *first measurement* (see chapter III.I), six fresh human temporal bones were acoustically stimulated via an artificial external ear canal with physiologically relevant levels (90-110 dB, 0.25-8 kHz). The 3-D motion of the stapes was constructed from motions of about 100 measurement points on the stapes footplate, measured using a scanning LDV (SLDV) system. The measurements were made for two different conditions of the IMJ: (1) normal IMJ and (2) artificially immobilized IMJ. The artificial immobilization of the IMJ was confirmed by measuring the relative motion between the malleus and the incus before and after the immobilization. Comparison between the measurements under two different IMJ conditions revealed that the immobilization of the IMJ causes increase in the magnitudes of the piston-like motion of the stapes, and the increase is frequency-dependent. The increase was prominent at high frequencies above 2 kHz. The magnitude ratios of the rocking-like motions to the piston-like motion were similar for both IMJ conditions. Such results suggest that the mobility of the IMJ in normal ears causes middle-ear transmission loss under physiologically relevant levels of acoustic stimulation without change of stapes motion pattern, especially at frequencies above 2 kHz.

In the *second measurement* (see chapter III.II), five isolated malleus-incus-complexes (MICs) from fresh human temporal bones were used. The isolated malleus-incus complex (MIC) was glued to a custom-made holder in a way that the malleus is fixed but the incus is still mobile, and thus relative motion between the two bones is possible. The excitation was dynamic using an electro-dynamic shaker (0.01–10 kHz, sweep, multi-sine, single sine) with three different excitation directions: inferior-superior, anterior-posterior, and lateral-medial. Simultaneously, the 3-D motion of the MIC was measured using a 3-D LDV system. No relative motion between malleus and incus below 3 kHz was observed in the preliminary data analysis. However, above 3 kHz, relative motion through the IMJ was observed, which increased with increasing frequency. The pattern of the relative motion was dependent on the excitation direction, suggesting that the mobility of the IMJ is directional allowing larger relative motion for specific directions (see chapter III.II.3.1).

In the *third measurement* (see chapter III.II) five isolated MICs were used. The MIC was glued to the custom-made holder by the same way used in the second measurement, but the incus was excited with quasi-static forces. The quasi-static forces were applied to multiple points on the incus with the magnitude of the force increasing gradually. The amplitudes of the quasi-static forces were controlled and measured by a load cell. Simultaneously, the 3-D motion of the incus was measured using a 3-D LDV system. The preliminary results show spatial motion patterns different from the corresponding patterns under dynamic excitation. Viscous behavior of the IMJ was also observed, indicating energy dissipation at the IMJ. When the large magnitude of the quasi-static force was applied, the surfaces of the two ossicles contacted and slid against each other. Patterns of the sliding motion followed the surface profiles of the two ossicles at the IMJ. The observations in this measurement are considered behavior of the IMJ as a role of protective mechanism under large static pressure change.

In the *fourth measurement* (see chapter III. III), there-dimensional (3D) spatial motions of the malleus and incus were constructed by measuring the 3D motion components of several points on each of the two ossicles using a 3-D LDV system, in one frozen and two fresh human temporal bones. The stimulation was delivered via a loudspeaker to an artificial ear canal (90-110 dB, 0.5-5 kHz). Relative motion between malleus and incus was observed. This relative motion increased with increasing frequency. The incus motion at the lenticular process was smaller than the malleus motion at the umbo at high frequencies.

Overall, these findings suggest a frequency-dependent mobility of the human IMJ under acoustic stimulation in the physiological range, especially above 2-3 kHz. Thus, the IMJ induces a loss in middle-ear sound transmission at higher frequencies.

The middle-ear sound transmission in reconstructed ears may differ from the physiological situation. For example during stapes surgery as a treatment for otosclerosis, the fixed stapes structure is removed and replaced with a stapes prosthesis. In our ongoing study about the quality of hearing after stapedotomy surgery (n=21), audiometric tests (pure tone audiogram, test for distortions at different frequencies and loudness levels) and a questionnaire (APOSE) are assessed. The subjective satisfaction of the subjects is positive three months after surgery: 80 % of the 15 subjects state to hear better and none of the subjects hear worse compared to before surgery. This finding is confirmed with the audiometric results: the pure tone average (for 0.5, 1, 2, and 3 kHz) gain is 21 ±12 dB three months after surgery compared to before surgery. However, 52 % subjects report distortions in the questionnaire and 59% in the audiometric tests at least once during the three months follow up. Most distortions are subjectively reported at 'loud sounds', which is consistent with the audiometric observations.

IV.II. Validity of the applied techniques

IV.II.1. Validity of the temporal bone model

Temporal bones (TBs) extracted from human cadavers (within 24 hours after death) were confirmed to be useful models of the human middle ear function. The middle-ear input impedances (defined by the ratio of the pressure and the acoustic volume velocity at the tympanic membrane) were shown to be indistinguishable from those of live subjects (Rosowski et al. 1990). This result is also supported by the studies of Goode et al. (1993), who reported similar umbo velocity in live subjects and in the temporal bone model. Several other authors previously used the temporal bone model to investigate the ossicular motion (Gyo et al. 1987, Vlaming & Feenstra 1986, Gundersen & Høgmoen 1976, Sim et al. 2010a, Willi et al. 2002, Nakajima et al. 2005, Zahnert 2003, C. Offergeld et al. 2007, C.F.E. Offergeld 2000, Decraemer & Khanna 2001, Decraemer & Khanna 1997, Decraemer & Khanna 2000, Goode et al. 1993, Tay & Mills 1996, Schön & Müller 1999). A standard for acceptance as mechanically normal human TBs is defined for the stapes motion: ASTM standard (F2504-05, Philadelphia, 2005) (displacement limits 5%/95% percentile interval) (see Figure 4.1). The stapes motions measured in our studies were in the ASTM range (see chapter III.I.4.1). For the measurements presented in chapter III.II, the MICs were isolated from fresh human temporal bones. Nevertheless, factors such as the drying effect of the middle-ear structures (see chapter IV.II.3.1), the post-mortem effect (see chapter IV.II.3.2), the *ex vivo* temperature (see chapter IV.II.3.3) and the age or gender of the donor (see chapter IV.II.3.4) could bias the mechanical properties of the middle ear.

IV.II.2. Validity of the measurement system

Laser Doppler Vibrometry (LDV, see II.IV) is a powerful measurement system to measure the ossicular motion due to its high measurement resolution (0.3 µm/s). This means for example that the LDV system is able to measure a displacement of ≈ 0.008 nm at 6000 Hz and of ≈ 0.1 nm at 500 Hz ($d = \frac{0.3\ \mu\mathrm{m/s}}{2*\pi*f}$). An advantage of the LDV system is that the sensor does not need to be in contact with the sample. Any contact of the measurement system with the sample may affect the mechanical properties of the ossicles due to e.g. additional load. The LDV system is the most adequate system available at the moment to measure ossicular motions, although access of the laser beam to the ossicles is required and, therefore, surgical preparation for exposure of the ossicles is needed (e.g. posterior tympanotomy or isolated MICs (see II.I)).

The scanning feature of the Scanning Laser Doppler Vibrometer (SLDV, see chapter II.IV.1.3) allows to measure motions of multiple points in a short period of time (around 100 points in 2 minutes), with coordinates of the multiple points recorded. The SLDV system was used for automated measurements of motions at multiple points on the stapes footplate, and spatial motion components of the stapes were constructed from the measured motions of the multiple points (see III.I.5). The 3-D LDV system, with three built-in laser beams, allows measurement of the 3D motion components at the measurement point. The 3D motion components were measured at several points on the malleus and the incus, and the full 3-D rigid-body motion components of the ossicles were reconstructed (see projects in chapters III.II and IIII.III). The rigid body motion of an ossicle can be constructed with full six degrees of freedom from minimum three non-collinear measurement points.

IV.II.3. Possible biases and challenges

IV.II.3.1. Drying out of the samples

Drying of the middle-ear structures effects the mechanical properties of the middle ear. This effect is described in chapter III.I.9.1 in detail. The rehydration of the sample in saline solution (30 min) was shown to be an adequate method to recover the magnitude of the motion of the stapes to approximately the same levels as before drying (see chapter III.I.9.1). The isolated MICs were rehydrated after each measurement step (approximately every 4 minutes) with water during the measurements. The drying effect is though minimized in the presented studies and not assumed to have significant effects on the presented results.

IV.II.3.2. Post-mortem effect

Post-mortem effects occur directly after death. Thus, these effects may influence the mechanical properties of the middle ears from fresh human temporal bones. This topic is extensively discussed in the discussion part of the submitted work about the contribution of the IMJ to middle-ear sound transmission in chapter III.I.10. Most notably, our observations are not likely to be from the post-mortem changes of the TBs, because no major differences in terms of stapes motion between live human subjects and fresh human TBs were obtained in intraoperative measurements (Huber et al. 2001, Chien et al. 2009). The dash-dotted line (▪ ▪) in Figure 4.1 represents the results of Chien et al. (2009) controlled for measurement angle and location, which fit to our stapes motion measurements in temporal bones and the ASTM norm. Goode et al. (Goode et al. 1993) compared the umbo motion in temporal bones and live subjects and did not find remarkable changes.

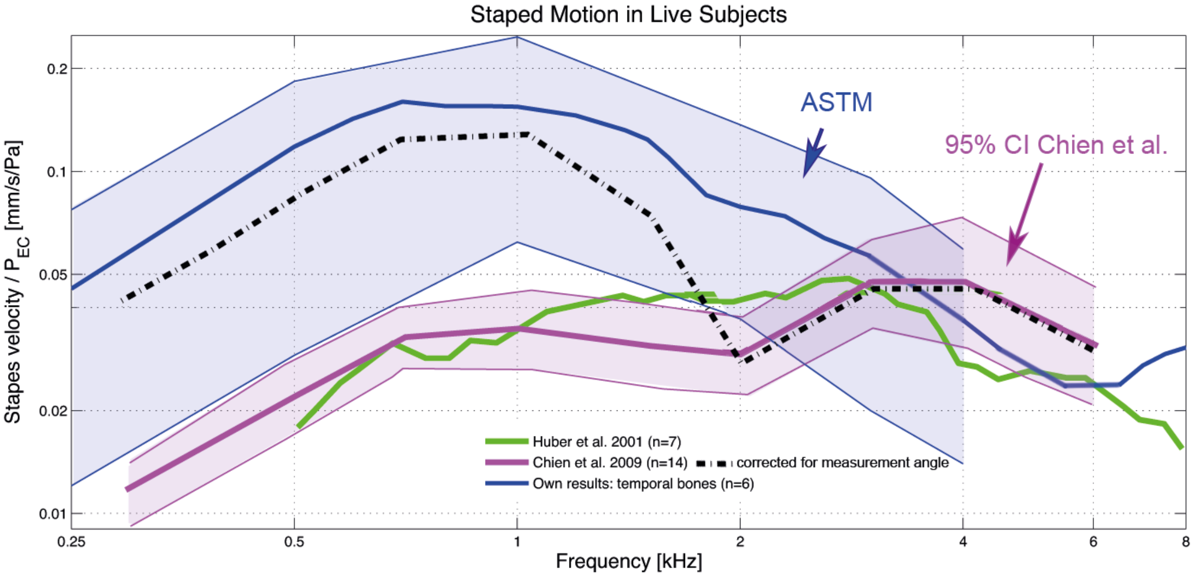

Figure 4.1 Stapes motion in live subjects (Huber et al. 2001, Chien et al. 2009) compared to own results in temporal bones. The stapes velocity was normalized by the ear canal pressure. The ASTM is marked in shaded blue and the 95 % CI of Chien et al. (2009) is shaded in purple. The dotted line represents the stapes velocity measured by Chien et al. after correction for the measurement angle and location.

IV.II.3.3. Ex vivo temperature

The body temperature of a living human is about 37°C. Thus, the temperature differs from the room temperature (20-22°C) where the measurements are performed for the presented studies. The question arises whether this temperature-difference affects the mechanical properties of the middle ear, especially the ligaments, tendons and muscles. No study investigated this effect in the middle ear until today. Some studies focused on the effect of temperature changes on the mechanical properties of ligaments or elastin: no temperature-changes are reported in bovine elastin (Gosline & French 1979), and an inverse relationship between stiffness and temperature are reported in ligaments of the knee (Woo & Young 1991, Akeson et al. 1984). Contrary, measurements *in vivo* show similar stapes motion (Huber et al. 2001, Chien et al. 2009) (see Figure 4.1) and umbo displacement as (Goode et al. 1993, Nishihara & Goode 1997) in the temporal bone model, which clearly contradicts to the effect of the temperature on the ossicular motion.

IV.II.3.4. Age and gender of the donor

The sample size of our measurements is to small to find a correlation of the stapes motion with age or gender.

The results presented by Willi (2003) suggested that middle-ear transmission decreases (from malleus to incus) with age with more pronounced effects at higher frequencies, but he was also convinced that the large inter-individual differences and the large scattering with advanced age would have required a much larger sample size to answer that question in his study.

However, changes in the morphology of the IMJ were described by several authors (Glorig & Davis 1961, Harty 1953, Etholm & Belal 1974, Gussen 1971, Savić & Djerić 1988) (see chapter I.III.2.4.4.1.4). Harty (1953) found that the capsule of the IMJ and ISJ were composed entirely of elastic tissue which showed a tendency to fragment and split with advancing age. Etholm and Belal (1974) classified the changes (including hyalinization and calcification of the joint capsule, fraying, vacuolation, fibrillation, thinning and calcification of the articular cartilage, hyaline and calcium deposits in the articular disc, and narrowing and obliteration of the joint space) of the middle-ear joints (IMJ and ISJ) into three grades: I mild, II moderate and III severe (see Table I.3). The gradual changes increased with advancing age; none of the individuals under one year of age showed arthritic changes, while all individuals over 70 years showed grade II to III in the joints. Etholm and Belal (1974) did not believe in a relation between the arthritic changes in the joints and the age-related hearing loss. They only found one case (out of 26 over the age of 70) of arthritic changes that correlated with conductive hearing loss. Contrary, Glorig and Davis (1961) found in their audiometric study (164 men, 25-80 y) a consistent air bone gap (ABG) for high frequencies and attributed this finding to an age-related conductive hearing loss in the middle ear (see Figure I.40). Similarly, Gussen (1971) described a progressing degenerative arthritis of the IMJ with advancing age; including the loss of surface demarcation, focal surface defects, and foci of thinning and absence of the intra-articular disc with approximation of uneven, calcified joint surfaces. Savić & Djerić (1988) studied the histopathologic features of degenerative changes in the IMJ in adults. They found degenerative changes in 40% of the cases; including atrophy, fibrosis, hyalinization and calcification. In agreement with Harty, they only noted obliteration of the articular space in few cases.

It remains unclear until today whether the effects of age and gender of the donor influence the middle-ear sound transmission.

IV.III. Related literature

An overview of previous works with focus on the mobility of the human IMJ back to the year 1851 is presented in chapter I.III (see chapter I.III.2.5.3.4). Since then, the measurement methods improved drastically. Nowadays, the LDV systems enable to measure the ossicular motion in the nanometer range without any contact to the samples, and thus, without changing the middle-ear properties with additional load or the like.

IV.III.1. Disagreements with previous works

Earlier studies assumed the IMJ to be generally immobilized based on morphology, macroscopical findings or rough mechanical testing (Weber 1851, von Helmholtz 1869, Marquet 1981), measurements with optical systems at lower frequencies (Buck 1869, Gill

1951, Gundersen 1971, Gundersen & Høgmoen 1976, Gyo et al. 1987), the assumption of a fixed rotational axis although relative motion in the joint was observed in the same studies (Dahmann 1930, Dahmann 1929), measurements with a capacitive probe (Bárány 1938, Bárány 1910, G Békésy 1936b, G. Békésy 1939, G. Békésy 1960, Fischler et al. 1967), measurements with a condenser microphone at the round window (Elpern et al. 1965), or measurements with a SQUID system – a contact sensor that measures displacements (see chapter I.III.2.5.3.2.20) (Brenkman et al. 1987). Other authors reported that the IMJ is mobile at high sound pressure levels and immobile under stimulation in the physiological range (Kirikae 1960, Harty 1964, Cancura 1980, Hüttenbrink & Pfautsch 1987, Hüttenbrink 1988c, Hüttenbrink 1988d, Goode et al. 1994, Goode et al. 1993, Tay & Mills 1996). Hudde and Engel (Hudde & Engel 1998) measured the changes of the middle-ear impedance between the mobile and immobilized IMJ and concluded that the differences (5 dB between 0.3 and 2 kHz) were negligible small.

IV.III.2. Agreements with previous works

The very early publications showing a mobile IMJ were based on macroscopic morphology studies or rough mechanical testing (von Helmholtz 1869, Harty 1964), optical methods that only allowed low-frequency conclusions (Politzer 1873, Politzer 1864, Buck 1869, Mach & Kessel 1874, Dahmann 1930, Dahmann 1929, Kobrak 1959), an oversized model (20x) of the middle-ear (Stuhlman 1937), early mathematical models (Frank 1923), mechanical models (Marquet et al. 1973), excitation tests at very high sound pressure levels (Kirikae 1960, Kobrak 1959, Cancura 1980, Gyo et al. 1987, Hüttenbrink 1988d, Hüttenbrink 1988c, Hüttenbrink & Pfautsch 1987), or on optical findings at extremely high sound pressure levels (Tay & Mills 1996).

The measurement of ossicular motions comparable to our results using dynamic excitation and a LDV system were first reported in the nineties. Goode et al. (1993, 1994) stated that the IMJ is immobile under physiological excitation, although they found a difference in malleus and incus motion. They assumed that this relative motion was caused by ‘translational displacement of the rotational axis’. Later, the IMJ was described as ‘mobile’ under dynamic excitation by several authors using a LDV system (Schön & Müller 1999, Decraemer & Khanna 1999b, Decraemer & Khanna 2001, Decraemer et al. 2014, Willi 2003, Willi et al. 2002, Zahnert 2003, Sim et al. 2004, Nakajima et al. 2005). Some authors stated that this mobility is unlikely to happens in the living human, although they found relative motion in the joint (Schön & Müller 1999, Decraemer et al. 2014), and that the mobility of the IMJ only originates from post-mortem effects (see IV.II.3.2) (Decraemer et al. 2014), or is clinically irrelevant (C.F.E. Offergeld 2000, C. Offergeld et al. 2007).

Our main finding is that the IMJ is mobile under physiological stimulation, especially at high frequencies (>2-3 kHz). The high-frequency dominant change in middle-ear sound transmission due to mobility of the IMJ in human TBs has been described previously by Huber et al. (1997), Offergeld (2007) and Willi et al. (2003) (see III.I.10). Only a few previous works compared the stapes motion with a mobile versus immobilized IMJ excited in the physiological range (see Figure 4.2). The increase of the stapes motion after fixation was in the range of 6 dB (above 2 kHz, Huber et al. 1997) to 10 dB (1.2-5 kHz, Offergeld 2007), compared to our result of < 7 dB from 1.8 to 8 kHz. Willi et al. (2003) described that a decrease of 5.5 dB per octave above 1 kHz may be caused by the mobility of the IMJ, based on the transmission loss observed in his two-dimensional measurements of motions of the malleus and the incus. Willi (2003) also supports our finding of an increased relative motion with increasing frequency (see chapters III.II and III.III). Zahnert (2003) (see chapter I.III.2.5.3.3.8) measured the stapes motion assumable only in one TB under both conditions (mobile IMJ versus immobilized IMJ). The method how the IMJ was artificially immobilized is not described – acrylic adhesive was used for the immobilization of the reported ISJ immobilization in the same publication. After the IMJ immobilization, the motion magnitude of the stapes shows an increase in sound transmission at around 1 kHz of approximately 5 dB, and a decrease in sound transmission (< 5 dB) at around 2-5 kHz (see Figure 4.2). Offergeld (2000) found a decrease of the stapes motion at low frequencies, and a small increase at high frequencies with an artificially immobilized IMJ (n=10). Thus, Offergeld (2000) stated due to this resonance shift that the ossicular chain may not be 'absolutely stiff for acoustic sound transfer'. Although he assumed that "in general the ossicular joints have a negligible effect on the acoustic transfer function of the middle ear during physiological pressure conditions (Offergeld 2000)". The method of the joint immobilization is described in detail in chapter I.III.2.5.3.3.8: Similar to our immobilization, the IMJ joint capsule was opened from superior and the synovial fluid was removed, and replaced with glue. Although they reported that the 'specimens were kept moist' throughout the experimental investigations, the results are comparable at lower frequencies to our measurements showing the drying effect (see chapter III.I.9.1). Seven years later, Offergeld et al. (2007) presented similar measurements (n=6) of the stapes motion with the IMJ mobile versus immobilized IMJ. The same artificial immobilization was used as in 2000. In contrast to the previous measurements, the stapes motion increased at higher frequencies up to approximately 10 dB above 1.2 kHz. This results fit to our findings of an increase of the stapes motion (< 7 dB) at higher frequencies (>2-3 kHz) with the immobilized IMJ (see chapters III.I, III.II, and III.III).

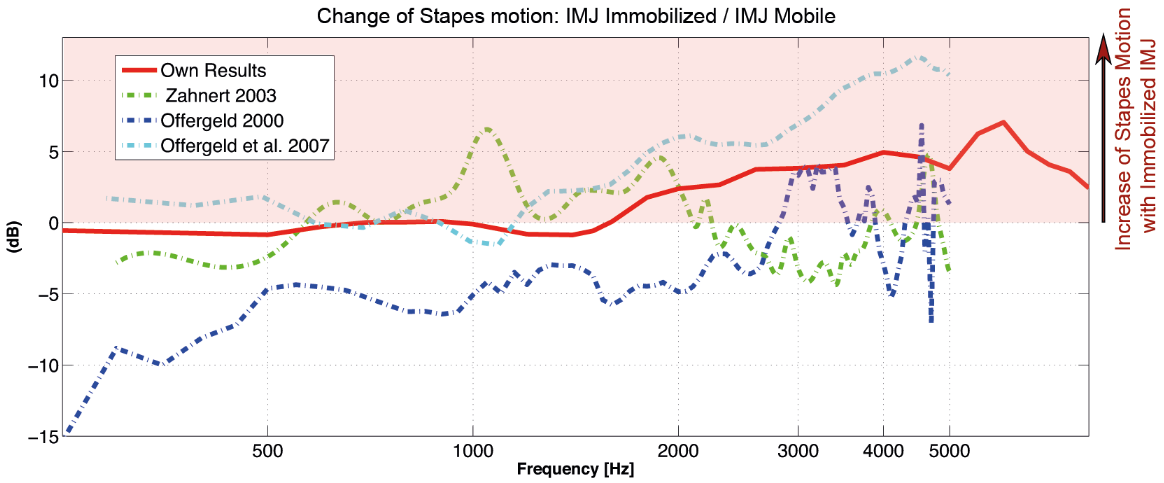

Figure 4.2 Change in stapes motion with a mobile IMJ versus immobilized IMJ. Own results (red) compared to previous measurements by Zahnert 2003 n=1 at 94 dB, Offergeld 2000 n=10, and Offergeld et al. 2007 n=6.

IV.III.3. Piston-like and rocking-like motion of the stapes

At the beginning of the 20th century, Bárány (Bárány 1938) and Békésy (G. Békésy 1939) described the motion of the stapes as a piston-like motion perpendicular to the oval window.

Békésy (1960) found the stapes to rotate about the vertical axis (e.g., in the superior-inferior direction); he described this axis to run through a point close to the posterior edge of the footplate, where the anatomy of the annular ligament show its thicker portion (see chapter I.III.2.4.3.1). Kirikae (1960) described the stapes motion to consist of three motion components (piston-like motion, hinged motion around a posterior axis, rotation around the long axis). Several years later, Gundersen (1972) showed that the piston-like motion is preserved up to 2 kHz, but at higher frequencies also rocking-like motions appear (see chapter I.III.2.5.3.2.17). The electromagnetic-measurement method of Gundersen my have influenced the results due to the contact of the measurement device to the stapes (added load to pick-up needle). Also Gyo et al. (1987) (see chapter I.III.2.5.3.2.18) found mainly piston-like motion in the lower frequencies and complex motions at high frequencies.

More recent studies performed with LDV agree with this finding of spatial modes of the stapes, especially at high frequencies in human (A Huber et al. 2001, Hato et al. 2003, Heiland et al. 1999, Voss et al. 2000, Sim et al. 2010a), cat (Decraemer et al. 2000, Decraemer & Khanna 1999b), and gerbil (Decraemer et al. 2007, Ravicz et al. 2008). The results of the rocking-like motion as a ratio to the piston-like motion are compared with the own results of the project described in chapter III.I in Figure 4.3.

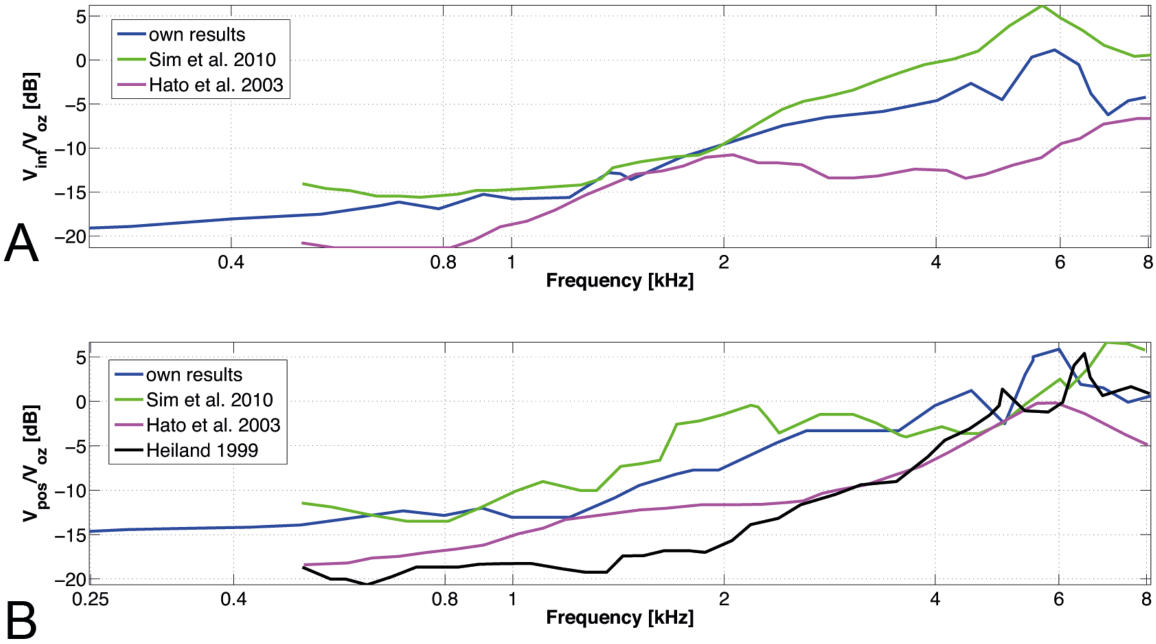

Figure 4.3 Relative magnitudes of the edge velocities due to the rocking of the footplate with respect to the footplate-center velocity (piston-like motion). (A) Relative magnitude of the inferior-edge velocity v_{inf} due to the rocking of the footplate along the long axis (ω_x). (B) Relative magnitude of the posterior-edge velocity v_{pos} due to the rocking of the footplate along the short axis (ω_y).

However, most of the current middle-ear models do not represent these rocking-like motions and assume that that they are negligible (Kolston & Ashmore 1996, Lim & Steele 2002), which needs to be adapted in future works.

A study reported that non-piston-like motions did not change the scala-vestibuli pressure in gerbil ears (de la Rochefoucauld et al. 2008). Contrary in guinea pigs, Huber et al. (A. Huber et al. 2008) found an influence of the rocking-like motions on the response of the cochlea (compound action potentials (CAP)). Edom et al. (Edom et al. 2013) recently showed in a numerical model the effect of the rocking-like stapes motion on the fluid flow in the cochlea (see Introduction chapter I.III.3.1.2.2.1). They concluded that the basilar motion was dominated by the piston-like motion under normal conditions (when the cochlea was activated by both stapes movements at the same time), and however, that the rocking-like motion may lead to hearing if no piston-like motion is present or possible (see Figure 1.89).

Most of the previous measurements did not reconstruct the 3-D motion of the stapes taking into account the anatomy of the stapes by reconstruction with micro-CT data. Thus, the described stapes motion of these works corresponds mainly to the piston-like motion of the stapes. An overview of the stapes motion measurements reviewed by Rosowski et al. (Rosowski et al. 2007) is shown in Figure 4.4 B, and recent publications are compared to the results of our stapes motion measurements (chapter III.I) in Figure 4.4 A. In the literature, the vibration amplitude of the stapes showed a similar first resonance of the middle-ear motion in different studies; 0.8 – 1.2 kHz (Silman & Silverman 1991) and 1.17 ± 0.27 kHz (n = 275 live human subjects, air conduction) (Wada et al. 1998).

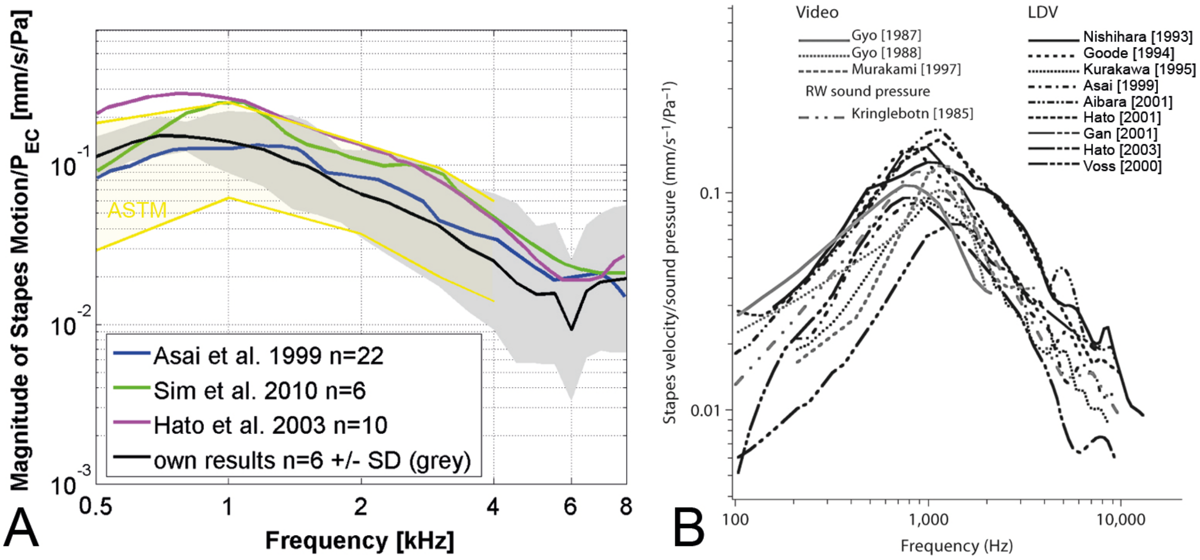

Figure 4.4 Stapes velocity normalized with the sound pressure level in the ear canal (P_{EC}): (A) own results compared to the ASTM standard F2505.24930 (displacement limits 5%/95% percentile interval) for acceptance as mechanically normal human TBs. (B) Stapes velocity in cadaver ears measured with laser-Doppler measurements (Nishihara et al. 1993, Goode et al. 1994, Kurokawa & Goode 1995, Asai et al. 1999, Voss et al. 2000, Aibara et al. 2001, Hato et al. 2003, Hato et al. 2001, Gan et al. 2001), 3 videostroboscopic measurements (Gyo et al. 1987, Gyo & Goode 1988, Murakami et al. 1997), and 1 round window sound pressure estimate (Kringlebotn & Gundersen 1985). Illustration (B) is reprinted from Rosowski et al (Rosowski et al. 2007). Permission for reprint of (B) achieved from Karger Publishers. Copyright © 2007 Karger Publishers, Basel, Switzerland.

IV.III.4. Advantage of our measurement method

In the author’s opinion, the advantages of the presented studies compared to previous works are as follows:

- Fresh human temporal bones were used as a model for the human middle-ear sound transmission (see chapter IV.II.1). This model is widely accepted as a good model for middle-ear sound transmission measurements in human.
- For the temporal bone preparation, a posterior tympanotomy was performed with an intact cochlea, and all middle-ear structures were preserved.
- The acoustic excitation was in the physiological range (90-110 dB) and, therefore, reflects the sound transmission of normal hearing.
- The used measurement method (LDV) is a non-contact system that does not influence the sound transmission in the middle ear (see chapter IV.II.2).
- The samples were controlled for the drying effect (see chapter IV.II.3.1) and it was avoided by consequent rehydration of the samples.
- The drying affect was also avoided for the isolated MICs by frequent rehydration.
- The MIC is a good model to test the material properties and the behavior of the IMJ.
- Modeling of the malleus and incus motion in the 3-D space is an important step to improve the existing models of the middle-ear sound transmission.
- The assessment of perceived distortions after stapedotomy surgery gives an interesting insight in the quality of hearing of the tested subjects. It never been assessed before at which frequencies and which sound pressure levels the distortions are perceived

IV.IV. Function of the IMJ

What could be the function of such an IMJ-induced transmission loss in the living human at higher frequencies? The mobility of the IMJ in human seems to be a disadvantage for the high frequency hearing. Thus, do mammals with an immobilized IMJ have better high frequency hearing? In animals, e.g. the guinea pig and chinchilla, the IMJ is immobilized by bony fusion of the malleus head and incus body (Puria & Steele 2010a, Puria et al. 2007, Kobayashi 1955, Dallos 1973). Indeed, the high frequency hearing is much more pronounced in many small mammals (e.g. guinea pigs) than in humans. There also exists a theory that the IMJ is immobilized in animals that depend on high frequency hearing (Henson 1974). The fact that the mobile IMJ causes high-frequency sound transmission loss, which is a disadvantage in hearing, suggests that it developed for other purposes.

A reasonable function is a protection mechanism (see chapter I.III.2.5.3.6) of the IMJ that prevents the inner ear and the middle ear from high static pressure changes (e.g. blow one's nose, sneezing, explosions, in a air plane) and at very high sound pressure levels (e.g. loud music, noise). It may be that this protection mechanism cannot be fulfilled without transmission losses at higher frequencies. Several other others suggested a protection mechanism as the function of the IMJ (Dahmann 1930, Dahmann 1929, G Békésy 1936b, Stuhlman 1937, Kobrak 1959, Kirikae 1960, Gundersen & Høgmoen 1976, Hüttenbrink & Pfautsch 1987, Hüttenbrink 1988a, Hüttenbrink 1988b, Hüttenbrink 1997, Cancura 1980, C.F.E. Offergeld 2000).

At low frequencies (< 1.8 dB), the immobilization of the IMJ showed no effect on the middle-ear sound transmission. The capsule of the IMJ mainly consists of elastic tissue (Davies 1948, Harty 1953, Harty 1964). It may be that the joint capsules store and release energy very efficient at low frequencies (< 1kHz) based on the viscoelastic properties of elastic biological tissue described by Fung (Fung 1993). This is in agreement with our finding of a high viscoelastic damping of the joint capsule in the isolated malleus-incus complex (MIC) during quasi-static excitation (see chapter III.II.3.2); the low frequencies (or quasi-static pressure changes) are not immediately transmitted from malleus to incus due to the viscoelastic properties of the joint capsule of the IMJ. Willi (2003) found transmission losses (<3 dB) also at the low frequencies in the normal IMJ by measuring the 2-D motion of the malleus an incus that were not affected by the immobilization of the joint. The IMJ seems to protect the ear-structures with a minimal sound transmission loss.

The protective role of the IMJ may be related to the suspensory attachments of the ossicles (see chapters I.III.2.4.1.1, I.III.2.4.2.1, and I.III.2.4.3.1), which are assumed to affect the middle-ear sound transmission. The middle-ear muscles enable independent muscular control of the position of the tympanic membrane related to the malleus, and the stapes. Kobrak (1959) found a correlation between the tone intensity and the strength of muscle contraction: “the stronger the tone, the greater the contraction”. Several authors support the idea that the middle-ear muscles prevent excessive displacement of the ossicles (von Helmholtz 1869, Wever & Lawrence 1954). Two muscles are present in the middle ear. The contracting *tensor tympani muscle* (see chapter I.III.2.4.1.1) pulls the manubrium of the malleus inward, displacing the tympanic membrane inwards by stretching it (Møller 2000). It is also assumed to dampen sounds conducted through bone, such as those produced from chewing or even speech (Peggy Mason 2011). The inward motion of the malleus compresses the IMJ. Because of the presence of the ossicular joints, the tensor tympani can produce changes in the static position of the tympanic membrane without excessively affecting the stapes displacement (Marquet 1981, Hüttenbrink 1988d). The contracted *stapedius muscle* (see chapter I.III.2.4.3.1.2) pulls the stapes in a direction that is perpendicular to its piston-like motion (Møller 2000), and thus dislocate the incudo-stapedial joint. This reflexive contraction of the stapedius muscle is also assumed to protect the cochlea against acoustic trauma evoked by loud sounds (Hilding & Fletcher 1960, Zakrisson & Borg 1974, Zakrisson et al. 1975). Thus, the stapedius muscle can significantly stiffen the connection between the stapes footplate and the oval window of the cochlea without producing large changes in the position of the malleus and tympanic membrane (Pang & Guinan 1997). It is possible for both muscles that they increase the stiffness of the middle ear and, thus, increase the impedance and reduce the sound transmission. Therefore, mobile middle-ear joints (IMJ, ISJ) seem to play an important role for the function of the muscles in human.

IV.V. Advantages of a mobile IMJ

Are though three ossicles (human) better than one (columella in birds, reptiles) or two (guinea pigs, chinchilla) ossicles? It is generally thought that the middle ear of mammals developed independently of the columellar ears of birds and reptiles, thus, one might argue that both columellar and three-ossicle middle ears allow the animals to function in the environmental niche to which they have adapted (Puria et al. 2013). Puria et al. (2013) summarized the advantage and disadvantage of three middle-ear ossicles compared to one ossicle, according the presence of a moment of inertia about the rotational axis of the ossicular chain, (e.g. (Puria & Steele 2010a, Lavender et al. 2011)) as follows: the advantage of the three ossicles is the reduction of the contribution of ossicular mass to the middle ear function in case of a coincidence of the rotational axis and the center of gravity of the ossicle. The disadvantage of the three ossicles is that the ossicular specializations (that lead to significant differences between the location of the ossicular center of gravity and the rotational axes) could enhance the middle ear's response to sounds conducted through the bone by substrate and other vibrations (Bárány 1938, M.J. Mason 2003, Puria & Rosowski 2012).

But why did three ossicles develop during evolution? It is nowadays generally assumed that the malleus and incus developed from the bones of the jaw of early reptiles in a manner that was independent of the development of the reptilian and avian ossicular system (see, Chapter 2 'The Evolution and Development of Middle Ears in Land Vertebrates' by Manley and Sienknecht in (Puria et al. 2013)). One hypothesis is that the multiple degrees of freedom, allowed by the coupling of separate ossicles due to the mobility of the joints, allow adaptions in the mode of ossicular motions to favor sound transmission in different frequency ranges (Fleischer 1978, Puria & Steele 2010a, Lavender et al. 2011, Puria et al. 2013).

IV.VI. Clinical cases of immobilized IMJs

The clinical role of the mobility of the IMJ is still under debate. Would it be beneficial to include a joint mechanism to middle ear prostheses (that replace the whole middle-ear chain) to mimic the assumed protection function of the IMJ and avoid hyperacusis (= loudness intolerance of patients)? It is doubtful that the perceived hyperacusis could be avoided. Subjects after stapes surgery sometimes suffer from hyperacusis (see chapter III.IV.4). This phenomenon is assumed to originate from the loss of the stapedius muscle function (Ramsay et al. 1997) or mechanical due to the smaller diameter of the stapes (10-28x higher hydraulic lever action), even though the prosthesis is not fixed at the lenticular process of the incus (and therefore, the ossicular lever action is reduced) (Raman 1999).

Ankylosis of the IMJ, a pathological immobility of the joint e.g. due to arthritis, was described for several cases in the literature (Belal & Stewart 1974, Etholm & Belal 1974, Hüttenbrink & Pfautsch 1987). A case report recently showed an immobilized IMJ due to a rare case of a symptomatic malleo-incudal osteoma (= benign bone forming tumor) (Ramdoo et al. 2011). The osteoma arose from the incus and attached to the malleus head. The symptoms mimicked those of other otological causes of conductive hearing loss, such as otosclerosis. The pure tone audiometry showed a 70 dB mixed hearing loss, with a large conductive component, and a 10 dB reduction in the bone conduction thresholds at 2 kHz ('Carhart's notch'). Due to the clinical findings, a stapedectomy was planned, where the surgeons found the intact but immobile ossicular chain. Only four cases of symptomatic osteomas of the incus have been described in the English-language literature (Ramdoo et al. 2011, Jang & Cho 2009). Thus it is assumed that incudal osteomas very rarely become symptomatic. For human speech, the range of frequency spans over 0.3 and 3 kHz. This may explain why patients with an immobilized IMJ rarely complain about symptoms.

However, this case is not similar to our situation with an isolated IMJ-immobilization. According to our findings an immobilized IMJ would even improve hearing above 2 kHz of about 7 dB.

The physiological function of the IMJ is still not fully understood. Thus, until today, an artificial immobilization of the IMJ in patients that suffer from high-frequency hearing loss is not considered at this point. Nevertheless, the understanding of the physiological role and function of the IMJ may be of great importance for hearing improvement in the future.

IV.VII. Conclusion

The findings of each project are listed in chapter IV.I.

The conclusion from several approaches is that the human IMJ is mobile under physiologically relevant acoustic stimulation, especially above 2-3 kHz. The mobility of the IMJ measured by the spatial relative motion between the malleus and incus is frequency dependent and increases with increasing frequencies. A frequency-dependent difference of the piston-like motion of the stapes between the mobile and immobilized IMJ conditions is observed from 1.8 kHz to 8 kHz. This difference is prominent between 2-4 kHz and at 5.5 kHz; whereas, the ratio of the rocking-like motions relative to the piston-like motion of the stapes shows no significant difference. The prominent frequency-dependent change of the piston-like motion above 2 kHz is presumed to be due to the mobility of the IMJ at high frequencies.

The stapes motion is linear under physiologically relevant acoustic stimulation (see chapter III.I.13). If this system is altered for example by stapes surgery, the middle-ear properties may change.

Subjects with implanted stapes prostheses sometimes perceive distorted sounds, mainly at high sound pressure levels, which tend to disappear over time. Several subject subjectively report the perception of distorted sound for ‘loud sound’. The origin of these distortions remains unclear from the presented preliminary results.

IV.VIII. Outlook

It is still questionable whether the mobility of the IMJ exists as part of a protection mechanism, regardless of age, or occurs only in elderly people due to aging effects. Since the sample size of six in this study is not sufficient to reveal the effects of age on middle-ear sound transmission, further measurements are required to clarify these open questions. In the future, it will be noteworthy to investigate the effect of age on the IMJ to clarify the function of the IMJ.

The data analysis of several projects is still ongoing (see chapter III.II and III.III) – as well as the subject recruiting for the project described in chapter I.IV. It will be interesting to integrate the new findings into the presented results of this thesis.

Abbreviations

AEC	artificial external ear canal
AC	air conduction, air conduction thresholds in the pure tone audiogram
BC	bone conduction, bone conduction thresholds in the pure tone audiogram
DSP	distorted sound perception
DOF	degrees of freedom
IMJ	incudo-malleolar joint
ISJ	incudo-stapedial joint
LDV	Laser Doppler Vibrometry
LPI	lenticular process of incus
MIC	Malleus-Incus-Complex
Micro-CT	micro–computed tomography
SLDV	scanning Laser Doppler vibrometry
SPL	sound pressure level
TB	temporal bone
TM	tympanic membrane

References

AERNOUTS, J., AERTS, J. R. and DIRCKX, J. J. 2012. Mechanical properties of human tympanic membrane in the quasi-static regime from in situ point indentation measurements. Hear Res, 290, 45-54.

AHN, T. S., BAEK, M. J. and LEE, D. 2013. Experimental measurement of tympanic membrane response for finite element model validation of a human middle ear. Springerplus, 2, 527.

AIBARA, R., WELSH, J. T., PURIA, S. and GOODE, R. L. 2001. Human middle-ear sound transfer function and cochlear input impedance. Hear Res, 152, 100-9.

AIKEN, S. J., ANDRUS, J. N., BANCE, M. and PHILLIPS, D. P. 2013. Acoustic stapedius reflex function in man revisited. Ear Hear, 34, e38-51.

AKESON, W. H., WOO, S. L., AMIEL, D. and FRANK, C. B. 1984. The chemical basis of tissue repair. , In: Hunter LY, Funk FJ (eds.). Rehabilitation of the injured knee. St. Louis: Mosby.

ALIAN, W., MAJDALAWIEH, O., KIEFTE, M., EJNELL, H. and BANCE, M. 2013. The effect of increased stiffness of the incudostapedial joint on the transmission of air-conducted sound by the human middle ear. Otol Neurotol, 34, 1503-9.

ALTMANN, F. 1965. The finer structure of the auditory ossicles in otosclerosis. Arch. Otolaryng., 82, 569-574.

AMERICAN SOCIETY FOR TESTING AND MATERIALS (ASTM) F2504-05 (2005). Standard practice for describing system output of implantable middle ear hearing devices. Philadelphia.

ANSON, B. J. and DONALDSON, J. A. 1967. Surgical anatomy of the temporal bone W.B. Saunders & Co, Philadelphia.

ARITOMO, H. 1989. [Ossicular vibration in human temporal bones]. Nihon Jibiinkoka Gakkai Kaiho, 92, 1359-70.

ARNOLD, B., BAUMANN, U., PFANNENSTIEL, S. and SCHORN, K. 2000. Einsatz der Hörfeldmessung bei Patienten mit Otosklerose [Use of auditory field measurement in patients with otosclerosis]. Laryngo-Rhino-Otol., 79, 14-20.

ARS, B. 1989. Organogenesis of the middle ear structures. J Laryngol Otol, 103, 16-21.

ASAI, M., HUBER, A. M. and GOODE, R. L. 1999. Analysis of the best site on the stapes footplate for ossicular chain reconstruction. Acta Otolaryngol, 119, 356-61.

BÁRÁNY, E. 1910. Versuche über die Wirkung des künstlichen Trommelfells. Verhandl. d. dtsch. Otol.-Ges. , 81.

BÁRÁNY, E. 1938. A Contribution to the Physiology of Bone Conduction. Supplementum 26, 96–111.

BARKOW 1841. Syndesmologie. Breslau, 29.

BECK, C. 1978. Anatomie und Histologie des Ohres. In: Hals-Nasen- und Ohrenheilkunde in Praxis und Klinik. Berendes, J., Link R., Zöllner F., Thieme Stuttgart, 2. Auflage.

BEER, H. J., BORNITZ, M., DRESCHER, J., SCHMIDT, R., HARDTKE, H. J., HOFMANN, G., VOGEL, U., ZAHNERT, T. and HÜTTENBRINK, K. B. 1996. Finit element modelling of the human eardrum and application. Proceeding of the International Workshop on MEMRO. 40-47.

BEER, H. J., BORNITZ, M., DRESCHER, J., SCHMIDT, R., HARDTKE, H. J., HOFMANN, G., VOGEL, U., ZAHNERT, T. and HUTTENBRINK, K. B. 1997. Finite element modeling of the human eardrum and applications. . In: Hüttenbrink KB, ed. Middle Mechanics in Research and Otosurgery: Proceedings of the International Workshop on Middle Ear Mechanics. Dresden, Germany. Dresden University of Technology, 40-7.

BEER, H. J., BORNITZ, M., HARDTKE, H. J., SCHMIDT, R., HOFMANN, G., VOGEL, U., ZAHNERT, T. and HUTTENBRINK, K. B. 1999. Modelling of components of the human middle ear and simulation of their dynamic behaviour. Audiol Neurootol, 4, 156-62.

BÉKÉSY, G. 1936. Über die Hörschwelle und Fühlgrenze langsamer sinusförmiger Luftdruckschwankungen. Ann. Physik, 26, 554-566 [257-267].

BÉKÉSY, G. 1936b. Zur Physik des Mittelohres und über das Hören bei fehlerhaftem Trommelfell. Akust. Zeits., 1, 13–23.

BÉKÉSY, G. 1939. Über die mechanisch-akustischen Vorgänge beim Hören. Acta Oto-Laryngologica, 27, 281-296.

BÉKÉSY, VON G., 1941. Über die Messung Schwingungsamplitude der Gehörknöchelchen mittels einer kapazitiven Sonde [About the vibration amplitude of the ossicles measured by means of a capacitive probe] Akust Zeits. 6, 1–16.

BÉKÉSY, G. 1960. Experiments in hearing, New York, McGraw-Hill.

BÉKÉSY, G. V. 1942. Über die Schwingungen der Schneckentrennwand beim Präparat und Ohrenmodell. Akust. Zeits., 7.

BÉKÉSY, G. V. 1949. J. Acoustical Soc. of America, 13, 217-231.

BÉKÉSY, G. V. and WEVER, E. G. 1960. Experiments in hearing, New York, McGraw-Hill.

BÉKÉSY, VON G., 1936. Zur Physik des Mittelohres und über das Hören bei fehlerhaftem Trommelfell. Akust. Zeits. 1, 13–23.

BÉKÉSY, VON G., 1960. Experiments in hearing. McGraw-Hill, New York.

BELAL, A. and STEWART, T. J. 1974. Pathologocal changes in the middle ear joints. Ann Otol Rhinol Laryngol, 83, 159-67.

BENNEMANN, J., FREIGANG, C., SCHROGER, E., RUBSAMEN, R. and RICHTER, N. 2013. Resolution of lateral acoustic space assessed by electroencephalography and psychoacoustics. Front Psychol, 4, 338.

BEZOLD, F. 1880. Experimentelle Untersuchungen über den Schalleitungsapparat des menschlichen Ohres. Arch Ohrenheilkd., 16, 1-50.

BISSINGER, G. and OLIVER, D. 2007. 3-D Laser Vibrometry on Legendary Old Italian Violins [Online]. SOUND AND VIBRATION. Available: http://www.sandv.com/downloads/0707biss.pdf JULY 2007].

BLAUERT, J. 1997. Spatial hearing : the psychophysics of human sound localization, Cambridge, Mass., MIT Press.

BOCKERS, A. 2013. [Anatomy of the eustachian tube]. Hno, 61, 462-6.

BOLZ, E. A. and LIM, D. J. 1972. Morphology of the stapediovestibular joint. Acta Otolaryngol, 73, 10-7.

BORG, E. 1968. A Quantitative Study of the Effect of the Acoustic Stapedius Reflex on Sound transmission Through the Middle Ear of Man. Acta Oto-laryngologica, 66, 461-472.

BRÉMOND, G. and COQUIN, A. 1972. Ultrastructure of normal and pathological middle ear mucosa. J Laryngol Otol, 86, 457-72.

BRENKMAN, C. J., GROTE, J. J. and RUTTEN, W. L. 1987. Acoustic transfer characteristics in human middle ears studied by a SQUID magnetometer method. J Acoust Soc Am, 82, 1646-54.

BRENKMAN, C.J., Grote, J.J., 1987. Acoustic transfer characteristics in human middle ears studied by a SQUID magnetometer method. J. Acoust. Soc. Am. 82, 1646-1654.

BROMAN, I. 1899. Die Entwickelungsgeschichte der Gehörknöchelchen beim Menschen. Anatomy and embryology, 11, 507-670.

BRONZINO, J. D. and PETERSON, D. R. 2006. Biomedical Engineering Fundamentals, Taylor & Francis.

BROWNSON, R. J. and MAROVITZ, W. F. 1972a. Comparative scanning electron microscopy of rodent and human ossicles. Laryngoscope, 82, 598-606.

BROWNSON, R. J. and MAROVITZ, W. F. 1972b. Scanning electron microscopy of normal human ossicles. Laryngoscope, 82, 355-62.

BRUNNER, G. 1870. Beiträge zur Anatomie und Histologie des mittleren Ohres: Diss. Inaug, Habilitationsschrift Zürich, Engelman.

BUCK, A. 1869. Untersuchungen über den Mechanismus der Gehörknöchelchen. Arch Augen Ohrenheilkd., 1, 121-136.

BURGETT, R. D., BRADLEY, M. R., DUNCAN, M., MELTON, J., LAL, A. K., ARANCHUK, V., HESS, C. F., SABATIER, J. M. and XIANG, N. 2003. Mobile mounted laser Doppler vibrometer array for acoustic landmine detection.

BUUNEN, T. J. and VLAMING, M. S. 1981. Laser--Doppler velocity meter applied to tympanic membrane vibrations in cat. J Acoust Soc Am, 69, 744-50.

BUYTAERT, J. A., SALIH, W. H., DIERICK, M., JACOBS, P. and DIRCKX, J. J. 2011. Realistic 3D computer model of the gerbil middle ear, featuring accurate morphology of bone and soft tissue structures. J Assoc Res Otolaryngol, 12, 681-96.

CABLE, H. R. and TADROS, S. 1982. Tympanic membrane retraction and middle-ear pressure. J Laryngol Otol, 96, 113-7.

CANCURA, W. 1980. On the statics of malleus and incus and on the function of the malleus-incus joint. Acta Otolaryngol, 89, 342-4.

CANCURA, W., 1980. On the statics of malleus and incus and on the function of the malleus-incus joint. Acta Otolaryngol. 89 (3-4), 342-344.

CARHART, R. 1950. Clinical application of bone conduction audiometry. Archives of Otolaryngology, 51, 798-808.

CASSELBRANT, M. 1979. Indirect Determination of variations in the inner ear pressure in man. An experimental study. Acta Otolaryngol, Suppl. 362.

CHEN, H., OKUMURA, T., EMURA, S. and SHOUMURA, S. 2008. Scanning electron microscopic study of the human auditory ossicles. Ann Anat, 190, 53-8.

CHENG, J. T., AARNISALO, A. A., HARRINGTON, E., HERNANDEZ-MONTES MDEL, S., FURLONG, C., MERCHANT, S. N. and ROSOWSKI, J. J. 2010. Motion of the surface of the human tympanic membrane measured with stroboscopic holography. Hear Res, 263, 66-77.

CHENG, J. T., HAMADE, M., MERCHANT, S. N., ROSOWSKI, J. J., HARRINGTON, E. and FURLONG, C. 2013. Wave motion on the surface of the human tympanic membrane: holographic measurement and modeling analysis. J Acoust Soc Am, 133, 918-37.

CHENG, J. T., RAVICZ, M., GUIGNARD, J., FURLONG, C. and ROSOWSKI, J. J. 2015. The Effect of Ear Canal Orientation on Tympanic Membrane Motion and the Sound Field Near the Tympanic Membrane. J Assoc Res Otolaryngol.

CHERUKUPALLY, S. R., MERCHANT, S. N. and ROSOWSKI, J. J. 1998. Correlations between pathologic changes in the stapes and conductive hearing loss in otosclerosis. Ann Otol Rhinol Laryngol, 107, 319-26.

CHIEN, W., NORTHROP, C., LEVINE, S., PILCH, B. Z., PEAKE, W. T., ROSOWSKI, J. J. and MERCHANT, S. N. 2009a. Anatomy of the distal incus in humans. J Assoc Res Otolaryngol, 10, 485-96.

CHIEN, W., ROSOWSKI, J. J., RAVICZ, M. E., RAUCH, S. D., SMULLEN, J. and MERCHANT, S. N. 2009b. Measurements of stapes velocity in live human ears. Hear Res, 249, 54-61.

CHIEN, W., Rosowski, J., J., Ravicz, M., E., Rauch, S., D., Smullen, J., Merchant, S., N., 2009. Measurements of stapes velocity in live human ears. Hear. Res. 249, 54-61.

CHOU, C. F., YU, J. F. and CHEN, C. K. 2011. The natural vibration characteristics of human ossicles. Chang Gung Med J, 34, 160-5.

CISNEROS GIMENO, A. I., WHYTE OROZCO, J. R., OBON NOGUES, J. A., YUS GOTOR, C., CROVETTO DE LA TORRE, M. A. and WHYTE OROZCO, A. 2009. Contribution to morphological knowledge of the development of the human incudo-mallear joint. Acta Otolaryngol, 129, 1380-7.

COVELL, W. P. and FEINMESSER, M. 1959. Further studies on the pathology of ossicles in otosclerosis. Laryngoscope, 69, 164-173.

DAHMANN, D. 1929. Zur Physiologie des Hörens; experimentelle Untersuchungen über die Mechanik der Gehörknöchelchenkette, sowie über deren Verhalten auf Ton und Luftdruck. . Kongressbericht "zur Physiologie des Hörens" (S ds Z), 24, 462-497.

DAHMANN, D. 1930. Zur Physiologie des Hörens; experimentelle Untersuchungen über die Mechanik der Gehörknöchelchenkette sowie über deren Verhalten auf Ton und Luftdruck. Z f Hals-Nasen-Ohrenheilk, 27, 329-368, 462 - 488.

DALBERT, A., SIM, J. H., GERIG, R., PFIFFNER, F., ROOSLI, C. and HUBER, A. 2015a. Correlation of Electrophysiological Properties and Hearing Preservation in Cochlear Implant Patients. Otol Neurotol.

DALBERT, A., SIM, J. H., PFIFFNER, F., GERIG, R., RÖÖSLI, C. and HUBER, A. 2015b. Abstract: Electrocochleography During and After Cochlear Implantation. Association for

Research in Otolaryngology, 38th Annual MidWinter Meeting. Saturday, February 21 - Wednesday, February 25. Baltimore.

DALLOS, P. J.and LINNELL, C. O. 1966. Even-order subharmonics in the peripheral auditory system. J Acoust Soc Am, 40, 561-4.

DALLOS, P. 1973. The auditory periphery, biophysics and physiology. Academic Press.

DALLOS, P., BILLONE, M. C., DURRANT, J. D., WANG, C. and RAYNOR, S. 1972. Cochlear inner and outer hair cells: functional differences. Science, 177, 356-8.

DANCER, A. and FRANKE, R. 1980. Intracochlear sound pressure measurements in guinea pigs. Hear Res, 2, 191-205.

DAPHALAPURKAR, N. P., DAI, C., GAN, R. Z. and LU, H. 2009. Characterization of the linearly viscoelastic behavior of human tympanic membrane by nanoindentation. J Mech Behav Biomed Mater, 2, 82-92.

DAVIES, D. V. 1948. A note on the articulations of the auditory ossicles and related structures. J Laryngol Otol, 62, 533-6.

DAVIS, H. 1983. An active process in cochlear mechanics. Hear Res., Jan;9(1):79-90.

DE BRUIJN, A. J., TANGE, R. A. and DRESCHLER, W. A. 1999. Comparison of stapes prostheses: a retrospective analysis of individual audiometric results obtained after stapedotomy by implantation of a gold and a teflon piston. Am J Otol, 20, 573-80.

DE LA ROCHEFOUCAULD, O., DECRAEMER, W. F., KHANNA, S. M. and OLSON, E. S. 2008. Simultaneous measurements of ossicular velocity and intracochlear pressure leading to the cochlear input impedance in gerbil. J Assoc Res Otolaryngol, 9, 161-77.

DE LA ROCHEFOUCAULD, O., KACHROO, P. and OLSON, E. S. 2010. Ossicular motion related to middle ear transmission delay in gerbil. Hear Res, 270, 158-72.

DE LA ROCHEFOUCAULD, O. and OLSON, E. S. 2010. A sum of simple and complex motions on the eardrum and manubrium in gerbil. Hear Res, 263, 9-15.

DECRAEMER W.F., ROCHEFOUCAULD O., FUNNELL W.R.J., OLSON E.S., 2014. Three-dimensional vibration of the malleus and incus in the living gerbil. Journal of the Association for Research in Otolaryngology 15, 483-510.

DECRAEMER, W. F., DE LA ROCHEFOUCAULD, O., DONG, W., KHANNA, S. M., DIRCKX, J. J. and OLSON, E. S. 2007. Scala vestibuli pressure and three-dimensional stapes velocity measured in direct succession in gerbil. J Acoust Soc Am, 121, 2774-91.

DECRAEMER, W. F., DE LA ROCHEFOUCAULD, O., FUNNELL, W. R. and OLSON, E. S. 2014. Three-dimensional vibration of the malleus and incus in the living gerbil. J Assoc Res Otolaryngol, 15, 483-510.

DECRAEMER, W. F., DIRCKX, J. J. and FUNNELL, W. R. 2003. Three-dimensional modelling of the middle-ear ossicular chain using a commercial high-resolution X-ray CT scanner. J Assoc Res Otolaryngol, 4, 250-63.

DECRAEMER, W. F., KHANNA, S. M. and DIRCKX, J. J. 2002. The integration of detailed 3-dimensional anatomical data for the quantitative description of 3-dimensional vibration of a biological structure. An illustration from the middle-ear. In: Tomasini EP (ed) Vibra- tion Measurements by Laser Techniques: Advances and Applications. SPIE, Bellingham, WA, 4872, 148-158.

DECRAEMER, W. F., KHANNA, S. M. and FUNNELL, W. R. 1989. Interferometric measurement of the amplitude and phase of tympanic membrane vibrations in cat. Hear Res, 38, 1-17.

DECRAEMER, W. F., KHANNA, S. M. and FUNNELL, W. R. 1991. Malleus vibration mode changes with frequency. Hear Res, 54, 305-18.

DECRAEMER, W. F., KHANNA, S. M. and FUNNELL, W. R. 1994. A method for determining three-dimensional vibration in the ear. Hear Res, 77, 19-37.

DECRAEMER, W. F., KHANNA, S. M. and FUNNELL, W. R. 2000. Measurement and modeling of the three-dimensional vibration of the stapes in cat. Proceeding of the Symposium on Recent Developments in Auditory Mechanics. In: Wada H, Takasaka K, Ikeda K, Phyama K, Koike T (eds). World Scientific. , 36–43.

DECRAEMER, W. F. and KHANNA, S. M. 1997. Vibrations on the Malleus measured trough the ear canal, Dresden, Middle ear mechanics in research and otosurgery. In: Hüttenbrink, K-B (ed) Proc. Internat. Workshop, Dresden, 1996 Sep 19–22. Dept. Oto-rhinolaryngol., Univ. Hosp. Carl Gustav Carus, Dresden Univ. Technology,.

DECRAEMER, W. F. and KHANNA, S. M. 1999. New insights in the functioning of the middle-ear. In: Rosowski JJ, Merchant S, editors. The function and mechanics of normal, diseased and reconstructed middle-ears. . The Hague, The Netherlands: Kugler Publications, 23–38.

DECRAEMER, W. F. and KHANNA, S. M. 1999b. Measurement and modelling of the three-dimensional vibrations of the stapes in cat. Abstract of the Symposium on Recent Developments in Auditory mechanics, Sendai, Japan, 20-21.

DECRAEMER, W. F. and KHANNA, S. M. 2000. New insights into vibration of the middle ear. In: JJ Rosowski, SN Merchant, eds. The Function and Mechanics of Normal, Diseased and Reconstructed Middle Ears. , Boston, MA.

DECRAEMER, W. F. and KHANNA, S. M. 2001. Measurement and animation of the 3-dimensional motion of the ossicular chain in a human temporal bone. Abstract. . In: PROCEEDINGS OF THE TWENTY-FOURTH ANNUAL MIDWINTER RESEARCH MEETING OF THE ASSOCIATION FOR RESEARCH IN OTOLARYNGOLOGY 24 (ed.). St. Petersburg, FL, USA.

DECRAEMER, W. F. and KHANNA, S. M. 2004. Measurement, visualization and quantitative analysis of complete three-dimensional kinematical data sets of human and cat middle ear. In: Gyo, K., Wada, H., Hato, N., Koike, T. (Eds.), Middle Ear Mechanics in Research and Otology. World Scientific, Singapore. Proceedings of the 3rd Symposium on Middle Ear Mechanics in Research and Otology, Gyo et al (eds) World Scientific, 3–10 July 2003, Matsuyama, Ehime, Japan, 9–12 3-10.

DECRAEMER, W., M., K. S. and FUNNELL, W. R. J. Vibrations at a fine grid of points on the cat tympanic membrane measured with a heterodyne interferometer. 1999c. In EOS/SPIE International Symposia on Industrial Lasers and Inspection, Conference on Biomedical Laser and Metrology and Applications.

DECRAEMER, W. and KHANNA, S. 1995. Malleus vibration modelled as rigid body motion. Acta Otorhinolaryngol Belg, 49, 139-45.

DECRAEMER, W.F., KHANNA, S.M., 1999. New insights in the functioning of the middle ear. In: Rosowski, J.J., Merchant, S.N. (Eds.), The Function and Mechanics of Normal, Diseased and Recon- structed Middle Ears. Kugler Publications, The Hague, 23-38.

DECRAEMER, W.F., KHANNA, S.M., 2001. Complete 3-dimensional motion of the ossicular chain in a human temporal bone. Abstract. Proceedings of the twenty-fourth Annual Midwinter Research Meeting of the Association for Research in Otolaryngology 24, 221.

DECRAEMER, W.F., KHANNA, S.M., 2004. Measurement, visualization and quantitative analysis of complete three-dimensional kinematical data sets of human and cat middle ear. In: Gyo, K., Wada, H., Hato, N., Koike, T. (Eds.), Middle Ear Mechanics in Research and Otology. World Scientific, Singapore. 3–10.

DJERIC, D., SAVIC, D. and POLIC, D. 1987. A scanning electron microscopic study of the incudostapedial joint. Rev Laryngol Otol Rhinol (Bord), 108, 463-6.

DJUPESLAND, G. and ZWISLOCKI, J. J. 1973. Sound pressure distribution in the outer ear. Acta Otolaryngol, 75, 350-2.

DORAN, A. H. G. 1876. Morphology of the Mammalian Ossicula Auditus: Extracted from the "Transactions of the Linnean Society of London.", Linnean Society of London.

DORAN, A. H. G. 1878. XVIII. Morphology of the Mammalian Ossicula auditûs. Transactions of the Linnean Society of London. 2nd Series: Zoology, 1, 371-497.

DRUSS, J. G. 1928. Zur Histologie und Pathologie der Verbindungen der Gehörknöchelchen. Monatsschrift f. Ohrenheilk u Lar Rhin 62, 257-267.

EALY, M. L., SMITH, R. J. H. and UNIVERSITY OF IOWA. INTERDISCIPLINARY GRADUATE PROGRAM IN GENETICS. 2011. Otosclerosis - identifying genetic contributions to a complex hearing disorder. Iowa City, Iowa: University of Iowa.

ECKERDAL, O. 1991. The petrotympanic fissure: a link connecting the tympanic cavity and the temporomandibular joint. Cranio, 9, 15-22.

EDOM, E., OBRIST, D., HENNIGER, R., KLEISER, L., SIM, J. H. and HUBER, A. M. 2013. The effect of rocking stapes motions on the cochlear fluid flow and on the basilar membrane motion. J Acoust Soc Am, 134, 3749-58.

EIBER, A., HUBER, A. M., LAUXMANN, M., CHATZIMICHALIS, M., SEQUEIRA, D. and SIM, J. H. 2012. Contribution of complex stapes motion to cochlea activation. Hear Res, 284, 82-92.

ELDREDGE, D.H. (1951) Some responses of the ear to high frequency sound. Am Soc Exp Biol Fed Proc A 9:37

ELPERN, B. S., GREISEN, O. and ANDERSEN, H. C. 1965. Experimental Studies on Sound Transmission in the Human Ear: VI. Clinical and Experimental Observations on Non-Otosclerotic Ossicle Fixation. Acta Oto-Laryngologica, 60, 223-230.

ELPERN, B.S., GREISEN, O., ANDERSEN, H.C., 1965. Experimental studies on sound transmission in the human ear. VI. Clinical and Experimental Observations on Non-Otosclerotic Ossicle Fixation. Acta Otolaryngol. 60 (1-6), 223-230.

ERIXON, E., HOGSTORP, H., WADIN, K. and RASK-ANDERSEN, H. 2009. Variational anatomy of the human cochlea: implications for cochlear implantation. Otol Neurotol, 30, 14-22.

ETHOLM, B., BELAL, A., 1974. Senile changes in the middle ear joints. Ann. Otol. 83 (1), 49-54.

ETHOLM, B. and BELAL, A., JR. 1974. Senile changes in the middle ear joints. Ann Otol Rhinol Laryngol, 83, 49-54.

EVEREST, F. A. and POHLMANN, K. C. 2009. Master handbook of acoustics, New York, McGraw-Hill.

EYSELL, A. 1870. Beiträge zur Anatomie des Steigbügels und seiner Verbindungen. Arch. Ohrenheilk., 5, 237-249.

FARAHANI, R. M. and NOORANIPOUR, M. 2008. Anatomy and anthropometry of human stapes. Am J Otolaryngol, 29, 42-7.

FASTL, H. and ZWICKER, E. 2007. Psychoacoustics. Facts and models. , Berlin, Springer

FAUSCH, C. and RÖÖSLI, C. 2015. The incudomalleolar articulation in Down syndrome (trisomy 21): a temporal bone study. Otol Neurotol, 36, 348-53.

FAY, J., PURIA, S., DECRAEMER, W. F. and STEELE, C. 2005. Three approaches for estimating the elastic modulus of the tympanic membrane. J Biomech, 38, 1807-15.

FEDERATIVE COMMITTEE ON ANATOMICAL TERMINOLOGY (FICAT)and INTERNATIONAL FEDERATION OF ASSOCIATIONS OF ANATOMISTS 1998. Terminologia anatomica, Stuttgart, G. Thieme.

FERRAZZINI, M. 2003. Virtual middle ear: a dynamic mathematical model based on [the] finite element method. Diss , Technische Wissenschaften ETH Zürich, Nr 15294, 2003.

FETTIPLACE, R. and HACKNEY, C. M. 2006. The sensory and motor roles of auditory hair cells. Nat Rev Neurosci, 7, 19-29.

FICAT, 1998, Federative Committee on Anatomical Terminology (FICAT), International Federation of Associations of Anatomists. Terminologia anatomica. Stuttgart: G. Thieme.

FIRSZT, J. B., REEDER, R. M., HOLDEN, T. A., BURTON, H.and CHOLE, R. A. 2013. Changes in auditory perceptions and cortex resulting from hearing recovery after extended congenital unilateral hearing loss. Front Syst Neurosci, 7, 108.

FISCHLER, H., FREI, E. H., SPIRA, D. and RUBINSTEIN, M. 1967. Dynamic response of middle-ear structures. J Acoust Soc Am, 41, 1220-31.

FLEISCHER, G. 1978. Evolutionary principles of the mammalian middle ear. Adv Anat Embryol Cell Biol, 55, 3-70.

FLINT, P. W. and CUMMINGS, C. W. 2010. Cummings Otolaryngology - Head and Neck Surgery, Mosby/Elsevier.

FONSECA, P. J. and POPOV, A. V. 1994. Sound radiation in a cicada: the role of different structures. Journal of Comparative Physiology A, 175, 349-361.

FRANK, O. 1923. Die Leitung des Schalles im Ohr, Bayerische Akademie der Wissenschaften.

Frank, O., 1923. Die Leitung des Schalles im Ohr. Bayerische Akademie der Wissenschaften. 1923.

FREY, H. 1911. Vergleichend-anatomische Studien ueber die Hammer-Amboss-Verbindung der Saeuger, J.F. Bergmann.

FUNG, Y. C. 1993. Biomechanics mechanical properties of living tissues, New York etc., Springer.

FUNNELL, W. R., DECRAEMER, W. F. and KHANNA, S. M. 1987. On the damped frequency response of a finite-element model of the cat eardrum. J Acoust Soc Am, 81, 1851-9.

FUNNELL, W. R., HENG SIAH, T., MCKEE, M. D., DANIEL, S. J. and DECRAEMER, W. F. 2005. On the coupling between the incus and the stapes in the cat. J Assoc Res Otolaryngol, 6, 9-18.

FUNNELL, W. R., KHANNA, S. M. and DECRAEMER, W. F. 1992. On the degree of rigidity of the manubrium in a finite-element model of the cat eardrum. J Acoust Soc Am, 91, 2082-90.

GAN, R. Z., DYER, R. K., WOOD, M. W. and DORMER, K. J. 2001. Mass loading on the ossicles and middle ear function. Ann Otol Rhinol Laryngol, 110, 478-85.

GAN, R. Z., SUN, Q., DYER, R. K., JR., CHANG, K. H. and DORMER, K. J. 2002. Three-dimensional modeling of middle ear biomechanics and its applications. Otol Neurotol, 23, 271-80.

GAN, R. Z., SUN, Q., FENG, B. and WOOD, M. W. 2006. Acoustic-structural coupled finite element analysis for sound transmission in human ear--pressure distributions. Med Eng Phys, 28, 395-404.

GAN, R. Z., YANG, F., ZHANG, X. and NAKMALI, D. 2011. Mechanical properties of stapedial annular ligament. Med Eng Phys, 33, 330-9.

GELFAND, S. A. 2009. Essentials of audiology, New York, Thieme.

GERHARDT, K. J., RODRIGUEZ, G. P., HEPLER, E. L. and MOUL, M. L. 1987. Ear canal volume and variability in the patterns of temporary threshold shifts. Ear Hear, 8, 316-21.

GERIG, R. 2014a. Dem Hören auf der Spur - Schwingungsmuster vom kleinsten Knochen des Menschen. Polytec InFocus, Magazin für Optische Messsysteme, Ausgabe 2014, ISSN 1864-9181, Polytec GmbH, 40-42.

GERIG, R. 2014b. Fascination of Hearing - Vibration patterns of the smallest bone in the human body. Polytec InFocus, Optical measurement Solutions, Issue 2014, ISSN 1864-9203, Polytec GmbH, 40-42.

Gilad, P., Shtrikman, S., Hillmann, P., 1967. Application of the Mössbauer method to ear vibrations. J. Acoust. Soc. Am. 41, 1232-1236.

GILL, N. W. 1951. Some observations on the conduction mechanism of the ear. J Laryngol Otol, 65, 404-13.

GLORIG, A. and DAVIS, H. 1961. Age, noise and hearing loss. Ann Otol Rhinol Laryngol, 70, 556-71.

GOODE, R. L., BALL, G. and NISHIHARA, S. 1993. Measurement of umbo vibration in human subjects--method and possible clinical applications. Am J Otol, 14, 247-51.

GOODE, R. L., KILLION, M., NAKAMURA, K. and NISHIHARA, S. 1994. New knowledge about the function of the human middle ear: development of an improved analog model. Am J Otol, 15, 145-54.

GOODE, R.L., BALL, G., NISHIHARA, S., 1993. Measurement of umbo vibration in human subjects - method and possible clinical applications. Am J Otol. 103 (5), 565-569.

GOSLINE, J. M. and FRENCH, C. J. 1979. Dynamic mechanical properties of Elastin. Biopolymers. , 18, 2091-2103.

GOYCOOLEA, M. V. and DE SOUZA, C. 2012. Atlas of Otologic Surgery and Magic Otology: The International Team Approach Based on Pathogenesis, Jaypee Brothers Medical Publishers.

GRABOYES, E. M., HULLAR, T. E. and CHOLE, R. A. 2011. The lenticular process of the incus. Otol Neurotol, 32, 1600-4.

GRAHAM, J. M. 2009. Ballantyne's deafness, Chichester, Wiley.

GRAHAM, M. D. 1985. The annular ligament attachment to the normal human stapes footplate. A scanning electron microscopic study. Ann Otol Rhinol Laryngol, 94, 171-5.

GRAHAM, M. D., REAMS, C. and PERKINS, R. 1978. Human tympanic membrane--malleus attachment. Preliminary study. Ann Otol Rhinol Laryngol, 87, 426-31.

GRAY, H. and LEWIS, W. H. 1918. Anatomy of the human body, Philadelphia, Lea & Febiger.

GUINAN, J. J., JR. and PEAKE, W. T. 1967. Middle-ear characteristics of anesthetized cats. J Acoust Soc Am, 41, 1237-61.

GUINAN, J.J., PEAKE, W.T., 1967. Middle-ear characteristics of anesthetized cats. J. Acoust. Soc. Am. 41, 1237-1261.

GULYA, A. J. and SCHUKNECHT, H. F. 1995. Anatomy of the temporal bone with surgical implications, New York, NY <etc.>, Parthenon.

GUNDERSEN, T. 1971. Prostheses in the Ossicular Chain: Experimental and Clinical Studies, Universitetsforlaget.

GUNDERSEN, T., HOGMOEN, K., 1976. Holographic vibration analysis of the ossicular chain. Acta Otolaryngol. 82, 16-25.

GUNDERSEN, T. and HØGMOEN, K. 1976. Holographic vibration analysis of the ossicular chain. Acta Otolaryngol, 82, 16-25.

GUSSEN, R. 1971. The human incudomalleal joint. Chondroid articular cartilage and degenerative arthritis. Arthritis Rheum, 14, 465-74.

GYO, K., ARITOMO, H. and GOODE, R. L. 1987. Measurement of the ossicular vibration ratio in human temporal bones by use of a video measuring system. Acta Otolaryngol, 103, 87-95.

GYO, K., GOODE, R. L. and MILLER, C. 1986. Effect of middle ear modification on umbo vibration. Human temporal bone experiments with a new vibration measuring system. Arch Otolaryngol Head Neck Surg, 112, 1262-8.

GYO, K. and GOODE, R. L. 1988. Measurement of stapes vibration driven by the ceramic vibrator of a middle ear implant – human temporal bone experiments. Middle ear implant: implantable hearing aids. Adv Audiol, 4, 107–116.

HAAS, J. 2003. An Acoustics Primer, Chapter 8

HALLIDAY, D., RESNICK, R., WALKER, J. and KOCH, S. W. 2003. Physik, Wiley.

HARTY, M. 1953. Elastic tissue in the middle-ear cavity. J Laryngol Otol, 67, 723-9.

HARTY, M. 1964. The joints of the middle ear. Z Mikrosk Anat Forsch, 71, 24-31.

HASS, J. 2003. An Acoustics Primer [Online]. http://www.indiana.edu/. Available: http://www.indiana.edu/~emusic/acoustics/amplitude.htm [Accessed 12.04.2014 2014]. [Online]. Center for Electronic and Computer Music, School of Music, Indiana University, Bloomington, Indiana. . Available: http://www.indiana.edu/~emusic/acoustics/phase.htm [Accessed 28. March 2015].

HASSMANN, E. and CHODYNICKI, S. 1978. Scanning electron microscopy of human ossicles. Arch Otorhinolaryngol, 220, 175-85.

HATO, N., STENFELT, S. and GOODE, R. L. 2003. Three-dimensional stapes footplate motion in human temporal bones. Audiol Neurootol, 8, 140-52.

HATO, N., WELSH, J. T., GOODE, R. L. and STENFELT, S. 2001. Acoustic role of the buttress and posterior incudal ligament in human temporal bones. Otolaryngol Head Neck Surg, 124, 274-8.

HAWKELIBRARY. 2014. http://otoscopy.hawkelibrary.com. Available: http://otoscopy.hawkelibrary.com/album06/Anat_14_001 [Accessed June 10th 2014].

HAZENBERG, A. J. C., MINOVI, A., DAZERT, S. and HOPPE, F. F. 2013. Predictors of Listening Capabilities and Patient Satisfaction After Stapes Surgery in Otosclerosis. Otology & Neurotology, 34.

HEILAND, K. E., GOODE, R. L., ASAI, M. and HUBER, A. M. 1999. A human temporal bone study of stapes footplate movement. Am J Otol, 20, 81-6.

HELLSTRÖM, P. A. 1995. The relationship between sound transfer functions and hearing levels. Hear Res, 88, 54-60.

HELMHOLTZ, H. 1863. Die Lehre von den Tonempfindungen als physiologische Grundlage für die Theorie der Musik,[On the Sensations of Tone as a Physiological Basis for the Theory of Music], Sensations of Tone. J. Vieweg, Bayerische Staatsbibliothek.

HELMHOLTZ, H. 1868. Die Mechanik der Gehörknöchelchen und des Trommelfells. Archiv für die gesamte Physiologie des Menschen und der Tiere, 1, 1-60.

HELMHOLTZ, H. V. 1896. Die Lehre von den Tonempfindungen als physiologische Grundlage für die Theorie der Musik, Braunschweig, Friedrich Vieweg.

HELMHOLTZ, H., BUCK, A. H. and SMITH, N. 1873. The mechanism of the ossicles of the ear and membrana tympani, New York, W. Wood & Co.

HENSON, O. W. 1974. Comparative anatomy of the middle ear. In: Kiedel, W.D., Neff, W.D. (Eds.), Handbook of Sensory Physiol- ogy: Vol. V: The Auditory System., Springer Verlag, New York.

HERMANS, J. J., BEUMER, A., DE JONG, T. A. and KLEINRENSINK, G. J. 2010. Anatomy of the distal tibiofibular syndesmosis in adults: a pictorial essay with a multimodality approach. J Anat, 217, 633-45.

HILDING, D. A. and FLETCHER, J. L. 1960. The protective value of the middle ear reflex. Int Rec Med, 173, 369-74.

HILL, M. A. 2014. Embryology, http://php.med.unsw.edu.au/embryology/index.php?title=Hearing_-_Middle_Ear_Development [Online]. Retrieved May 19, 2014].

HOFMAN, P. M., VAN RISWICK, J. G. and VAN OPSTAL, A. J. 1998. Relearning sound localization with new ears. Nat Neurosci, 1, 417-21.

HOLLER, F. C. and GREENBERG, L. M. 1972. Incudostapedial joint disarticulation. Arch Otolaryngol, 95, 182-4.

HORNIG, S., SCHÖNFELD, R. and KOLLMEIER, B. 1996. Sprachaudiometrische Befunde bei Patienten mit positivem Recruitmentnachweis in der Hörfeldskalierung. . In: Gross, M (Hrsg). Aktuelle phoniatrisch-pädau- diologische Aspekte. R Gross Verlag.

HUBER, A. M., SCHREPFER, T. and EIBER, A. 2012. Clinical evaluation of the NiTiBOND stapes prosthesis, an optimized shape memory alloy design. Otol Neurotol, 33, 132-6.

HUBER, A., ASSAI, M., BALL, G. and GOODE, R. L. 1997. Analysis of ossicular vibration in three dimensions. In: Middle ear mechanics in research and otosurgery. Dresden. 82-87.

HUBER, A., LINDER, T., FERRAZZINI, M., SCHMID, S., DILLIER, N., STOECKLI, S. and FISCH, U. 2001. Intraoperative assessment of stapes movement. Ann Otol Rhinol Laryngol, 110, 31-35.

HUBER, A., SEQUEIRA, D., BREUNINGER, C. and EIBER, A. 2008. The Effects of Complex Stapes Motion on the Response of the Cochlea. Otology & Neurotology, 29, 1187-1192.

HUBER, A. M., VERAGUTH, D., SCHMID, S., ROTH, T.and EIBER, A. 2008b. Tight stapes prosthesis fixation leads to better functional results in otosclerosis surgery. Otol Neurotol, 29, 893-9.

HUDDE, H. and ENGEL, A. 1998. Measuring and Modeling Basic Properties of the Human Middle Ear and Ear Canal. Part III: Eardrum Impedances, Transfer Functions and Model Calculations. Acta Acustica united with Acustica, 84, 1091-1108.

HUDDE, H. and ENGEL, A. 1998a. Measuring and Modeling Basic Properties of the Human Middle Ear and Ear Canal. Part I: Model Structure and Measuring Techniques. Acta Acustica united with Acustica, 84, 720-738.

HUDDE, H. and ENGEL, A. 1998b. Measuring and Modeling Basic Properties of the Human Middle Ear and Ear Canal. Part II: Ear Canal, Middle Ear Cavities, Eardrum, and Ossicles. Acta Acustica united with Acustica, 84, 894-913.

HUDDE, H. and ENGEL, A. 1998c. Measuring and Modeling Basic Properties of the Human Middle Ear and Ear Canal. Part III: Eardrum Impedances, Transfer Functions and Model Calculations. Acta Acustica united with Acustica, 84, 1091-1108.

HUANG, S., DONG, W.and OLSON, E. S. 2012. Subharmonic distortion in ear canal pressure and intracochlear pressure and motion. J Assoc Res Otolaryngol, 13, 461-71.

HÜTTENBRINK, K. B. 1988a. Die Mechanik der Gehörknöchelchen bei statischen Drucken. I Normales Mittelohr. . Laryngol. Rhinol. Otol. , 67, 45-52.

HÜTTENBRINK, K. B. 1988b. Die Mechanik der Gehörknöchelchenkette bei statischen. Drucken II. Behinderte Gelenkfunktion und operative Kettenkonstruktion. Laryngol Rhinol Otol, 67, 100-105.

HÜTTENBRINK, K. B. 1988c. [Mechanics of the ear ossicles in static pressures. II. Impaired joint function and surgical reconstruction of the ossicle chain]. Laryngol Rhinol Otol (Stuttg), 67, 100-5.

HÜTTENBRINK, K. B. 1988d. The mechanics of the middle-ear at static air pressures: the role of the ossicular joints, the function of the middle-ear muscles and the behaviour of stapedial prostheses. Acta Otolaryngol Suppl, 451, 1-35.

HÜTTENBRINK, K. B. 1992. [The mechanics and function of the middle ear. Part 1: The ossicular chain and middle ear muscles]. Laryngorhinootologie, 71, 545-51.

HÜTTENBRINK, K. B. 1997. The middle ear as a pressure receptor. Middle ear mechanics in research and otosurgery. In: Hüttenbrink, K-B (ed) Proc. Internat. Workshop, Dresden, 1996 Sep 19–22. Dept. Oto-rhinolaryngol., Univ. Hosp. Carl Gustav Carus, Dresden Univ. Technology, pp 15–20, p 259, 1997.

HÜTTENBRINK, K. B. and PFAUTSCH, M. 1987. [The ear ossicle joints in the scanning electron microscopy image]. Laryngol Rhinol Otol (Stuttg), 66, 176-9.

IHRLE, S., EIBER, A. and EBERHARD, P. 2015. Experimental investigation of the three dimensional vibration of a small lightweight object. Journal of Sound and Vibration, 334.

IHRLE, S., LAUXMANN, M., EIBER, A. and EBERHARD, P. 2013. Nonlinear modelling of the middle ear as an elastic multibody system — Applying model order reduction to acousto-structural coupled systems. Journal of Computational and Applied Mathematics, 246, 18-26.

ITO, K., MOMOSE, T., OKU, S., ISHIMOTO, S., YAMASOBA, T., SUGASAWA, M.and KAGA, K. 2004. Cortical activation shortly after cochlear implantation. Audiol Neurootol, 9, 282-93.

JAHN, G. 1960. Über den Unterschied zwischen den Kurven gleicher Lautstärke in den ebenen Welle und im diffusen Schallfeld, Akademische verlagsgesellschaft Becker & Erler kom.-ges.

JANG, C. H. and CHO, Y. B. 2009. Osteoma of the incus with congenital cholesteatoma: a case report. Auris Nasus Larynx, 36, 349-52.

JENSEN, J. H. and BONDING, P. 1993. Experimental pressure induced rupture of the tympanic membrane in man. Acta Otolaryngol, 113, 62-7.

JONAS, J. B., SCHNEIDER, U. and NAUMANN, G. O. 1992. Count and density of human retinal photoreceptors. Graefes Arch Clin Exp Ophthalmol, 230, 505-10.

KARMODY, C. S., NORTHROP, C. C. and LEVINE, S. R. 2009. The incudostapedial articulation: new concepts. Otol Neurotol, 30, 990-7.

KETCHAM, R. A. and CARLSON, W. D. 2001. Acquisition, optimization and interpretation of x-ray computed tomographic imagery: Applications to the geosciences, . Computers and Geosciences, 27, 381-400.

KEY, J. A. 1932. The synovial membmns of joints and bursae. Cowdny's special Cybology, 2nd Ed., Hoeber, New York.

KHANNA, S. M., KOESTER, C. J., WILLEMIN, J. F., DÄNDLIKER, R. and ROSSKOTHEN, H. 1996. A noninvasive optical system for the study of the function of inner ear in living animals. SPIE 2732, 64–81.

KHANNA, S. M. and TONNDORF, J. 1972b. Tympanic membrane vibrations in cats studied by time-averaged holography. J Acoust Soc Am, 51, 1904-20.

KIANG, N. Y.-S. 1965. Discharge patterns of single fibers in the cat's auditory nerve, Cambridge, MIT Press.

KILLION, M. C. and CLEMIS, J. D. 1981. An engineering view of middle ear surgery. J Acoust Soc Am, 1.

KILPATRICK, J. M. and MARKOV, V. Matrix laser vibrometer for transient modal imaging and rapid nondestructive testing. 2008. 709809-709809-12.

KIRIKAE, I. 1960. The Structure and Function of the Middle Ear, University of Tokyo Press.

KOBAYASHI, M. 1955. The articulation of the auditory ossicles and their ligaments of various species of mammalian animals. Hiroschima J Med Sci, 4, 319-349.

KOBRAK, H. G., 1941. J. Acoustical Soc. of America 13, 179-181.

KOBRAK, H. G., 1959. The Middle Ear. University of Chicago Press.

KOIKE, T., WADA, H. and KOBAYASHI, T. 2002. Modeling of the human middle ear using the finite-element method. J Acoust Soc Am, 111, 1306-17.

KOLLMEIER, B. 1997. Grundlagen der Lautheitsskalierung. In: Kollmeier, B (Hrsg). Hörflächenskalierung. Grundlagen und Anwendungen der kategorialen Lautheitsskalierung für Hördiagnostik und Hörgeräteversorgung. Buchreihe Audiologische Akustik. Median- Verlag von Killisch-Horn GmbH.

KOLSTON, P. J. and ASHMORE, J. F. 1996. Finite element micromechanical modeling of the cochlea in three dimensions. J Acoust Soc Am, 99, 455-67.

KÖRNER, E. 1878. Die Gelenke der Gehörknöchelchen und die Knorpel des Ohres: Inaug. Diss. der Univ. München. (Separat-Abd. aus der "Monatsschrift für Ohrenheilkunde" No 10, 1878).

KRINGLEBOTN, M. 1988. Network model for the human middle ear. Scand Audiol, 17, 75-85.

KRINGLEBOTN, M. and GUNDERSEN, T. 1985. Frequency characteristics of the middle ear. J Acoust Soc Am. , 77, 159-164.

KUROKAWA, H. and GOODE, R. L. 1995. Sound pressure gain produced by the human middle ear. Otolaryngol Head Neck Surg, 113, 349-55.

LADAK, H. M. and FUNNELL, W. R. 1996. Finite-element modeling of the normal and surgically repaired cat middle ear. J Acoust Soc Am, 100, 933-44.

LAL, A., ARANCHUK, S., DOUSHKINA, V., HURTADO, E., HESS, C., KILPATRICK, J., L'ESPERANCE, D., LUO, N., MARKOV, V., SABATIER, J. and SCOTT, E. 2006. Advanced LDV instruments for buried landmine detection. Proc. SPIE 6217, Detection and Remediation Technologies for Mines and Minelike Targets XI, 621715.

LANDIS, E. N. and KEANE, D. T. 2010. X-ray microtomography. Materials Characterization, 61, 1305-1316.

LANE, J. I., WITTE, R. J., DRISCOLL, C. L. W., CAMP, J. J. and ROBB, R. A. 2004. Imaging microscopy of the middle and inner ear, Part I: CT microscopy. Clinical Anatomy, 17, 607–612.

LANE, J. I., WITTE, R. J., HENSON, O. W., DRISCOLL, C. L. W., CAMP, J. and ROBB, R. A. 2005. Imaging microscopy of the middle and inner ear - Part II: MR microscopy. Clinical Anatomy, 18 (6), 409-415.es.

LANG, F., VALLON, V., KNIPPER, M. and WANGEMANN, P. 2007. Functional significance of channels and transporters expressed in the inner ear and kidney. Am J Physiol Cell Physiol, 293, C1187-208.

LAUXMANN, M., EIBER, A., HECKELER, C., IHRLE, S., CHATZIMICHALIS, M., HUBER, A. and SIM, J. H. 2012b. In-plane motions of the stapes in human ears. J Acoust Soc Am, 132, 3280-91.

LAUXMANN, M., HECKELER, C., BEUTNER, D., LUERS, J. C., HUTTENBRINK, K. B., CHATZIMICHALIS, M., HUBER, A. and EIBER, A. 2012a. Experimental study on admissible forces at the incudomalleolar joint. Otol Neurotol, 33, 1077-84.

LAVENDER, D., TARASKIN, S. N. and MASON, M. J. 2011. Mass distribution and rotational inertia of "microtype" and "freely mobile" middle ear ossicles in rodents. Hear Res, 282, 97-107.

LEE, C. F., CHEN, P. R., LEE, W. J., CHEN, J. H. and LIU, T. C. 2006. Three-dimensional reconstruction and modeling of middle ear biomechanics by high-resolution computed tomography and finite element analysis. Laryngoscope, 116, 711-6.

LEE, J. S., LEE, D. S., OH, S. H., KIM, C. S., KIM, J. W., HWANG, C. H., KOO, J., KANG, E., CHUNG, J. K.and LEE, M. C. 2003. PET evidence of neuroplasticity in adult auditory cortex of postlingual deafness. J Nucl Med, 44, 1435-9.

LEMPERT, I. 1945. Histopathology of the incus and the head of the malleus in cases of stapedial ankylosis. Arch. Otolaryng., 79, 780-799.

LESSER, T. H., WILLIAMS, K. R. and BLAYNEY, A. W. 1991. Mechanics and materials in middle ear reconstruction. Clin Otolaryngol Allied Sci, 16, 29-32.

LESSER, T. H. and WILLIAMS, K. R. 1988. The tympanic membrane in cross section: a finite element analysis. J Laryngol Otol, 102, 209-14.

LEUWER, R. and KOCH, U. 1999. [Anatomy and physiology of the auditory tube. Therapeutic possibilities in chronic disorders of tubal function]. Hno, 47, 514-23.

LIM, D. J. 1970. A scanning electron microscopic investigation on otosclerotic stapes. Ann Otol Rhinol Laryngol, 79, 780-99.

LIM, K. M. and STEELE, C. R. 2002. A three-dimensional nonlinear active cochlear model analyzed by the WKB-numeric method. Hear Res, 170, 190-205.

LIPSON, S. G., LIPSON, H. and TANNHAUSER, D. S. 1995. Optical physics Cambridge University Press.

LOCKHART, R. D. 1965. Anatomy of the Human Body, Faber & Faber.

LORD, R. M., ABEL, E. W., WANG, Z. and MILLS, R. P. 2001. Effects of draining cochlear fluids on stapes displacement in human middle-ear models. J Acoust Soc Am, 110, 3132-9.

LUCAE, A. 1901. Arch. Ohrenheilk, 53, 39-51.

LUDMAN, H. 1988. Physiology of hearing and balance, Mawson's Diseases of the Ear, 5th edition, Edward Arnold- Hodder, Sroughton, London, Baltimore, Melbourne, Aukland.

LUDWIG, C. 1852. Lehrbuch der Physiologie des Menschen, C. F. Winter.

LUNDMAN, L., MENDEL, L., BAGGER-SJOBACK, D. and ROSENHALL, U. 1999. Hearing in patients operated unilaterally for otosclerosis. Self-assessment of hearing and audiometric results. Acta Otolaryngol, 119, 453-8.

LUSCHKA, H. 1858. Die Gelenke und Halbgelenke des menschlichen Körpers. Z Ohrenheilkd. 153.

LYNCH, T. J. 1981. Signal Processing by the Cat Middle Ear: Admittance, and Transmission, Measurements and Models Doctoral thesis. . Massachusetts Institute of Technology.

MACH, E. and KESSEL, J. 1874. Beiträge zur Topographie und Mechanik des Mittelohres. Sitz. ber. Kais. Akad. Wiss. Math. Nat. wiss. Kl. 3, 221-245.

MACPHERSON, E. A. and MIDDLEBROOKS, J. C. 2002. Listener weighting of cues for lateral angle: the duplex theory of sound localization revisited. J Acoust Soc Am, 111, 2219-36.

MAFTOON, N., FUNNELL, W. R., DANIEL, S. J. and DECRAEMER, W. F. 2014. Effect of opening middle-ear cavity on vibrations of gerbil tympanic membrane. J Assoc Res Otolaryngol, 15, 319-34.

MAGNUS, A. 1861. Beiträge zur Anatomie des mittleren Ohres. Archiv für pathologische Anatomie und Physiologie und für klinische Medicin, 20, 79-132.

MAMUN, A. A., GUO, G. X. and BI, C. 2006. Hard Disk Drive: Mechatronics and Control, CRC Press.

MANOUSSAKI, D., DIMITRIADIS, E. K. and CHADWICK, R. S. 2006. Cochlea's graded curvature effect on low frequency waves. Phys Rev Lett, 96, 088701.

MAROTTI, G., BALLI, R., REMAGGI, F. and FARNETI, D. 1987. [Morphofunctional study of the osteocytes in the tympanic ossicles under normal conditions]. Acta Otorhinolaryngol Ital, 7, 347-63.

MAROTTI, G., FARNETI, D., REMAGGI, F. and TARTARI, F. 1998. Morphometric investigation on osteocytes in human auditory ossicles. Ann Anat, 180, 449-53.

MARQUET, J. 1981. The incudo-malleal joint. J Laryngol Otol, 95, 543-65.

MARQUET, J. 1985. "Stapedotomy" technique and results. Am J Otol, 6, 63-7.

MARQUET, J., VAN CAMP, K. J., CRETEN, W. L., DECRAEMER, W. F., WOLFF, H. B. and SCHEPENS, P. 1973. Topics in physics and middle ear surgery. Acta Otorhinolaryngol Belg, 27, 139-319.

MASON, M. J. 2003. Bone conduction and seismic sensitivity in golden moles (Chrysochloridae). Journal of Zoology, 260, 405-413.

MASON, P. 2011. Medical neurobiology, New York, Oxford University Press.

MCELVEEN, J. T., GOODE, R. L., MILLER, C. and FALK, S. A. 1982. Effect of mastoid cavity modification on middle ear sound transmission. Ann Otol Rhinol Laryngol, 91, 526-32.

MCGEE, T. M. 1981. The loose wire syndrome. Laryngoscope, 101, 810-814.

MCKNIGHT, C. L., DOMAN, D. A., BROWN, J. A., BANCE, M. and ADAMSON, R. B. 2013. Direct measurement of the wavelength of sound waves in the human skull. J Acoust Soc Am, 133, 136-45.

MCMANUS, L. J., DAWES, P. J. and STRINGER, M. D. 2012. The orientation of the tympanic membrane. Clin Anat, 25, 260-2.

MEHRGARDT, S. and MELLERT, V. 1977. Transformation characteristics of the external human ear. J Acoust Soc Am, 61, 1567-76.

MERCHANT, S. N., INCESULU, A., GLYNN, R. J. and NADOL, J. B., JR. 2001. Histologic studies of the posterior stapediovestibular joint in otosclerosis. Otol Neurotol, 22, 305-10.

MERCHANT, S. N. and NADOL, J. B. 2010. Schuknecht's Pathology of the Ear, People's Medical Publishing House-USA.

MERCHANT, S. N. and ROSOWSKI, J. J. 2003. Auditory physiology (middle-ear mechanics). . In: Gulya, A.J., Glasscock, M.E. IIIIII (Eds.), Surgery of the Ear, fifth ed. BC Decker, Hamilton, Ont.,, 59-82.

MEYER, S. E. and MEGERIAN, C. A. 2000. Patients' perceived outcomes after stapedectomy for otosclerosis. Ear Nose Throat J, 79, 846-8, 851-2, 854 passim.

MICHAELS, L. and HELLQUIST, H. B. 2001. Ear, Nose and Throat Histopathology, Springer.

MIDDLEBROOKS, J. C. 1992. Narrow-band sound localization related to external ear acoustics. J Acoust Soc Am, 92, 2607-24.

MIDDLEBROOKS, J. C. and GREEN, D. M. 1991. Sound localization by human listeners. Annu Rev Psychol, 42, 135-59.

MILLS, A. W. 1958. On the Minimum Audible Angle. Journal of the Acoustical Society of America, 30, 237-246.

MØLLER, A. R. 1961. Network model of the middle ear. J Acoust Soc Am, 33, 168-176.

MØLLER, A. R. 1963. Transfer function of the middle ear. J Acoust Soc Am, 35, 1526-1534.

MØLLER, A. R. 2000. Hearing : its physiology and pathophysiology, San Diego, Calif., Academic Press.

MÖLLER, P. 1982. Incus in normal ears and in chronic otitis media. Acta Otolaryngol, Suppl. 386, 64-67.

MURAKAMI, S., GYO, K. and GOODE, R. L. 1997. Effect of middle ear pressure change on middle ear mechanics. Acta Otolaryngol, 117, 390-5.

MUSIEK, F. E. and BARAN, J. A. 2007. The auditory system : anatomy, physiology and clinical correlates, Boston, Pearson.

NAKAJIMA, H. H., DONG, W., OLSON, E. S., MERCHANT, S. N., RAVICZ, M. E. and ROSOWSKI, J. J. 2009. Differential intracochlear sound pressure measurements in normal human temporal bones. J Assoc Res Otolaryngol, 10, 23-36.

NAKAJIMA, H. H., RAVICZ, M. E., MERCHANT, S. N., PEAKE, W. T. and ROSOWSKI, J. J. 2005. Experimental ossicular fixations and the middle ear's response to sound: evidence for a flexible ossicular chain. Hear Res, 204, 60-77.

NATIONAL PARK SERVICE. 2010. Gateway Arch [Online]. U.S. Department of the Interior, 1849 C Street NW, Washington, DC 20240: National Historic Landmarks Program. Available: http://www.webcitation.org/5uynJZKkF [Accessed September 2014].

NEDZELNITSKY, V. 1980. Sound pressures in the basal turn of the cat cochlea. J Acoust Soc Am, 68, 1676-89.

NIH PUBLICATION NO. 11-4798. 2013. NIH Publication No. 11-4798 (2013-11-01). "Cochlear Implants". National Institute on Deafness and Other Communication Disorders. [Online]. Available: https://http://www.nidcd.nih.gov/health/hearing/pages/coch.aspx [Accessed 25. April 2015].

NISHIHARA, S., ARITOMO, H. and GOODE, R. L. 1993. Effect of changes in mass on middle ear function. Otolaryngol Head Neck Surg, 109, 899-910.

NISHIHARA, S. and GOODE, R. 1997. Measurement of tympanic membrane vibration in 99 human ears, In: Hüttenbrink KB. Proceedings of the international workshop on middle ear mechanics in research and otosurgery.

NOBEL MEDIA AB. 2014. Web. 3 Jan 2015. . "The Nobel Prize in Physiology or Medicine 1961" [Online]. Available: http://www.nobelprize.org/nobel_prizes/medicine/laureates/1961/.

O'CONNOR, K. N. and PURIA, S. 2006. Middle ear cavity and ear canal pressure-driven stapes velocity responses in human cadaveric temporal bones. J Acoust Soc Am, 120, 1517-28.

OFFERGELD, C. F. E. 2000. Experimental investigations of ossicular joint ankylosis In: Rosowski, J.J. and Merchant, S.N. (eds.), The function and mechanics of normal, diseased and reconstructed middle ears. Kurger Publication, The Hague, The Netherlands, 177-186.

OFFERGELD, C., LASURASHVILI, N., BORNITZ, M., BELEITES, T. and ZAHNERT, T. 2007. Experimental investigations on the functional effect of ossicular joint fixation. In: Huber, A. and Eiber, A. (eds.), The 4th Symposium on Middle Ear Mechanics in Research and Ootology. World Scientific Publishing, Singapore. 102-108.

OGANDO, P. B., ROOSLI, C., KARMODY, C. S. and NORTHROP, C. C. 2013. The incudostapedial articulation in Down's syndrome (trisomy 21): a temporal bone study. Otol Neurotol, 34, 1489-95.

OLDFIELD, S. R. and PARKER, S. P. 1984. Acuity of sound localisation: a topography of auditory space. II. Pinna cues absent. Perception, 13, 601-17.

OLSON, E. S. 1998. Observing middle and inner ear mechanics with novel intracochlear pressure sensors. J Acoust Soc Am, 103, 3445-63.

OLSZEWSKI, J. 1990. [The morphometry of the ear ossicles in humans during development]. Anat Anz, 171, 187-91.

ONCHI, Y., 1961. Mechanism of the middle ear. J. Acoust. Soc. Am. 33, 794-805.

PANG, X. D. and GUINAN, J. J., JR. 1997. Effects of stapedius-muscle contractions on the masking of auditory-nerve responses. J Acoust Soc Am, 102, 3576-86.

PAPARELLA, M. M. 2009. Location of the ventilation tube. Ear Nose Throat J, 88, 963.

PAPPENHEIM 1840. Die spezielle Gewebelehre des Gehörorgans nach Sruktur, Entwicklung, Krankheit, Breslau 1840.

PEAKE, W. T., ROSOWSKI, J. J. and LYNCH, T. J., 3RD 1992. Middle-ear transmission: acoustic versus ossicular coupling in cat and human. Hear Res, 57, 245-68.

PEREZ, R., DE ALMEIDA, J., NEDZELSKI, J. M. and CHEN, J. M. 2009. Variations in the "Carhart notch" and overclosure after laser-assisted stapedotomy in otosclerosis. Otol Neurotol, 30, 1033-6.

PERLMAN, H. B. 1945. Ann. Otol. etc., St. Loius, 54, 483 ‐ 494.

PETERSEN, B., GJEDDE, A., WALLENTIN, M.and VUUST, P. 2013. Cortical plasticity after cochlear implantation. Neural Plast, 2013, 318521.

PFIFFNER, F., PROCHAZKA, L., THOELE, K., PARIS, F., WALRAEVENS, J., SIM, J. H., GERIG, R., DOBREV, I., OBRIST, D., RÖÖSLI, C. and HUBER, A. 2015. Abstract: Intracochlear Acoustic Receiver for Totally Implantable Cochlear Implants: Concept and Preliminary Temporal Bone Results. Association for Research in Otolaryngology, 38th Annual MidWinter Meeting

PIRODDA, E., MODUGNO, G. C. and BUCCOLIERI, M. 1995. The problem of the sensorineural component in otosclerotic hearing loss: a comparison between operated and non-operated ears. Acta Otolaryngol, 115, 427-32.

POLITZER A, 1873. Zur physiologischen Akustik und deren Anwendung auf die Pathologie des Gehörorgans. Arch Ohrenheilkd. 6, 35-44.

POLITZER, A. 1862. Wiener med. Wochenschrift, No. 13 and 14.

POLITZER, A. 1864. Untersuchungen über Schallfortpflanzung und Schallleitung im Gehörorgane im gesunden und kranken Zustande. Arch Ohrenheilkd.

POLITZER, A. 1884. Traite des Maladies de l'Oreille. Paris, ed. Octave Doin.

POLYTEC_GMBH 2014. Software Manual, Polytec Scanning Vibrometer, Software 8.4. In: POLYTEC GMBH, H. P.-P.-D.-W. (ed.) 41031-Man-Vib-PSV-Soft8.4-0706-01e.

POLYTEC_GMBH. 2015a. Applications & Markets [Online]. Available: http://www.polytec.com/us/applications/ [Accessed 3. March 2015].

POLYTEC_GMBH. 2015b. Basic Principles of Vibrometry [Online]. Available: http://www.polytec.com/se/solutions/vibration-measurement/basic-principles-of-vibrometry/ [Accessed 23. March 2015].

POLYTEC_GMBH. 2015c. Scanning Vibrometers [Online]. Available: http://www.polytec.com/us/products/vibration-sensors/scanning-vibrometers/ [Accessed 23. March 2015].

POLYTEC_GMBH. 2015d. Single-Point Vibrometers [Online]. Available: http://www.polytec.com/us/products/vibration-sensors/single-point-vibrometers/ [Accessed 23. March 2015].

PRENDERGAST, P. J., FERRIS, P., RICE, H. J. and BLAYNEY, A. W. 1999. Vibro-acoustic modelling of the outer and middle ear using the finite-element method. Audiol Neurootol, 4, 185-91.

PROCTOR, B. 1989. Surgical Anatomy of the Ear and Temporal Bone, Thieme Medical Publisher.

PUJOL RÉMY, N. R. L. M. 2013. Hair cells: overview [Online]. NeurOreille. Available: http://www.cochlea.eu/en/hair-cells [Accessed 21.05 2014].

PURIA, S. 2003. Measurements of human middle ear forward and reverse acoustics: implications for otoacoustic emissions. J Acoust Soc Am, 113, 2773-89.

PURIA, S., FAY, R. R. and POPPER, A. 2013. The Middle Ear: Science, Otosurgery, and Technology, Springer.

PURIA, S., PEAKE, W. T. and ROSOWSKI, J. J. 1997. Sound-pressure measurements in the cochlear vestibule of human-cadaver ears. J Acoust Soc Am, 101, 2754-70.

PURIA, S., SIM, J. H., SHIN, M., TUCK-LEE, J. and STEELE, C. R. 2007. Middle ear morphometry from cadaveric temporal bone micro-CT imaging. Middle Ear Mechanics in Research and Otology Eds. A. Eiber and A. Huber. Zurich, SW, World Scientific.

PURIA, S. and ALLEN, J. B. 1998. Measurements and model of the cat middle ear: evidence of tympanic membrane acoustic delay. J Acoust Soc Am, 104, 3463-81.

PURIA, S. and ROSOWSKI, J. J. 2012. Bekesy's contributions to our present understanding of sound conduction to the inner ear. Hear Res, 293, 21-30.

PURIA, S. and STEELE, C. 2010a. Tympanic-membrane and malleus-incus-complex co-adaptations for high-frequency hearing in mammals. Hear Res, 263, 183-90.

PURIA, S. and STEELE, C. R. 2010b. Mechano-acoustical transformations. Handbook of the Senses.

PURVES, D. and WILLIAMS, S. M. 2001. Neuroscience, Sunderland, Mass., Sinauer Associates.

PUTZ, R. and PABST, R. 2005. Sobotta, Atlas der Anatomie des Menschen Band 1, Urban & Fischer in Elsevier

RAMAN, R. 1999. Post stapedotomy hyperacousis — a mechanical explanation. Indian J Otolaryngol Head Neck Surg., 51, 64-65.

RAMDOO, K., DALE, O. T. and HERDMAN, R. C. 2011. Malleo-incudal osteoma: an unexpected finding during surgery for presumed otosclerosis. J Laryngol Otol, 125, 968-9.

RAMIREZ-GARCIA, E. 1980. In Vitro investigations of the mechanics of the middle ear and implications in ossicular chain reconstruction surgery. .

RAMSAY, H., KARKKAINEN, J. and PALVA, T. 1997. Success in surgery for otosclerosis: hearing improvement and other indicators. Am J Otolaryngol, 18, 23-8.

RAPHAEL, Y. and ALTSCHULER, R. A. 2003. Structure and innervation of the cochlea. Brain Res Bull, 60, 397-422.

RASK-ANDERSEN, H., LIU, W., ERIXON, E., KINNEFORS, A., PFALLER, K., SCHROTT-FISCHER, A. and GLUECKERT, R. 2012. Human cochlea: anatomical characteristics and their relevance for cochlear implantation. Anat Rec (Hoboken), 295, 1791-811.

RASKE, M., WELLING, J. D., GILLUM, T. and WELLING, D. B. 2001. Long-term stapedectomy results with the McGee stapes prosthesis. Laryngoscope, 111, 2060-3.

RAUBER, A. and KOPSCH, F. 1987. Anatomie des Menschen Lehrbuch und Atlas, and Leonhardt, Helmut Töndury, Gian Zilles, Karl, Stuttgart, Thieme.

RAVICZ, M. E., COOPER, N. P. and ROSOWSKI, J. J. 2008. Gerbil middle-ear sound transmission from 100 Hz to 60 kHz. J Acoust Soc Am, 124, 363-80.

REED, B. C. 1990. Quantum mechanics: a first courdes. Winnipeg: Wuerz, 1-35.

ROADS, C. 1994. The computer music tutorial, Cambridge, Mass., MIT Press.

RÖÖSLI, C., J.H., S., XIE, Y. and HUBER, A. Abstract: Correlation between intracranial pressure and skull vibration in bone conduction of cadaveric human whole heads. Association for Research in Otolaryngology, 36th Annual MidWinter Meeting, February 16-20, 2013 Baltimore.

RÖÖSLI, C., SIM, J. H., GERIG, R., DALBERT, A., FAUSCH, C., STENFELT, S. and HUBER, A. 2014a. Abstract: Wave propagation in the skull bone during bone conduction stimulation 8th International Symposium on Objective Measures in Auditory Implants, October 15-18. Toronto, Ontario, Canada.

RÖÖSLI, C., SIM, J. H., GERIG, R., DALBERT, A., FAUSCH, C., STENFELT, S. and HUBER, A. 2014b. Abstract: Wave propagation in the Skull Bone During Bone Conduction Stimulation. Association for Research in Otolaryngology, 37th Annual MidWinter Meeting, Feburary 22-26. San Diego.

RÖÖSLI, C., SIM, J. H., GERIG, R., STENFELT, S. and HUBER, A. 2015. Abstract: Bone conduction pathway through non-osseous contents. Association for Research in Otolaryngology, 38th Annual MidWinter Meeting, Saturday, February 21 - Wednesday, February 25. Baltimore.

ROSOWSKI, J. J., CHENG, J. T., MERCHANT, S. N., HARRINGTON, E. and FURLONG, C. 2011. New data on the motion of the normal and reconstructed tympanic membrane. Otol Neurotol, 32, 1559-67.

ROSOWSKI, J. J., CHENG, J. T., RAVICZ, M. E., HULLI, N., HERNANDEZ-MONTES, M., HARRINGTON, E. and FURLONG, C. 2009. Computer-assisted time-averaged holograms of the motion of the surface of the mammalian tympanic membrane with sound stimuli of 0.4-25 kHz. Hear Res, 253, 83-96.

ROSOWSKI, J. J., CHIEN, W., RAVICZ, M. E. and MERCHANT, S. N. 2007. Testing a method for quantifying the output of implantable middle ear hearing devices. Audiol Neurootol, 12, 265-76.

ROSOWSKI, J. J., DAVIS, P. J., MERCHANT, S. N., DONAHUE, K. M. and COLTRERA, M. D. 1990. Cadaver middle ears as models for living ears: comparisons of middle ear input immittance. Ann Otol Rhinol Laryngol, 99, 403-12.

RUAH, C. B., SCHACHERN, P. A., ZELTERMAN, D., PAPARELLA, M. M. and YOON, T. H. 1991. Age-related morphologic changes in the human tympanic membrane. A light and electron microscopic study. Arch Otolaryngol Head Neck Surg, 117, 627-34.

RÜDINGER, N. 1870. Beiträge zur Histologie des Gehörorganes: Mit 5 Tafeln, Lentner.

RUI, L., TAO, W., ZHIGANG, Z. and WEN, X. 2011. Vibration Characteristics of Various Surfaces Using an LDV for Long-Range Voice Acquisition. Sensors Journal, IEEE, 11, 1415-1422.

RUTHERFORD, W. 1886. A New Theory of Hearing. J Anat Physiol, 21, 166-8.

RUTTEN, W. L. C., PETERS, M. J., BRENKMAN, C. J., MOL, H., GROTE, J. J. and MAREL, L. C. V. D. 1982. The use of a SQUID magnetometer for middle ear research. Cryogenics, 22, 457-460.

RUTTEN, W. L., BAKKER, D., KUIT, J. H., MAES, M. A. and GROTE, J. J. 1986. The use of a SQUID magnetometer in the study and development of normal and artificial middle ear. Acta Otolaryngol Suppl, 432, 11-4.

SADE, J. 1992. The correlation of middle ear aeration with mastoid pneumatization. The mastoid as a pressure buffer. Eur Arch Otorhinolaryngol, 249, 301-4.

SADLER, T. W. 2008. Medizinische Embryologie: die normale menschliche Entwicklung und ihre Fehlbildungen, Thieme.

SALADIN, K. S. 2012. Anatomy & Physiology: The Unity of Form and Function, McGraw-Hill.

SALIH, W. H., BUYTAERT, J. A., AERTS, J. R., VANDERNIEPEN, P., DIERICK, M. and DIRCKX, J. J. 2012. Open access high-resolution 3D morphology models of cat, gerbil, rabbit, rat and human ossicular chains. Hear Res, 284, 1-5.

SALVINELLI, F., MAURIZI, M., CALAMITA, S., D'ALATRI, L., CAPELLI, A. and CARBONE, A. 1991. The external ear and the tympanic membrane. A three-dimensional study. Scand Audiol, 20, 253-6.

SAVIĆ, D. and DJERIĆ, D. 1988. [Histopathological characteristics of degenerative modifications of the incudomalleolar joint]. Ann Otolaryngol Chir Cervicofac, 105, 203-6.

SCHMIDT, C. 1903. Zur Anatomie und Entwicklungsgeschichte der Gelenks- verbindung der Gehörknöchelchen beim Menschen. , Zeitschrift für Öhrenheilkunde, Bergmann.

SCHMIEDEKAM, D. 1868. Experimentelle Studien zur Physiologie des Gehörorgans. Arbeiten aus dem Kieler physiologischen Institut 1868. Herausgegeben von Dr. V. Hensen. .

SCHÖN, F. and MÜLLER, J. 1999. Measurements of ossicular vibrations in the middle ear. Audiol. Neurootol. 4 (3-4), 142-149.

SCHUKNECHT, H. F. 1974. Pathology of the ear, Cambridge, Mass., Harvard University Press.

SCHUKNECHT, H. F. and BARBER, W. 1985. Histologic variants in otosclerosis. Laryngoscope, 95, 1307-17.

SCHUKNECHT, H.F., 1974. Pathology of the ear. Cambridge, Mass.: Harvard University Press.

SEIKEL, J. A., KING, D. W. and DRUMRIGHT, D. G. 2005. Anatomy & physiology for speech, language and hearing, Clifton Park, NY, Thomson Delmar Learning.

SEIKEL, J., DRUMRIGHT, D. and SEIKEL, P. 2013. Essentials of Anatomy and Physiology for Communication Disorders, Cengage Learning.

SHAHNAZ, N. and BORK, K. 2006. Wideband reflectance norms for Caucasian and Chinese young adults. Ear Hear, 27, 774-88.

SHAW, E. A. 1974. Transformation of sound pressure level from the free field to the eardrum in the horizontal plane. J Acoust Soc Am, 56, 1848-61.

SHAW, E. A. G. and STINSON, M. R. 1981. Network concepts and energy flow in the human middle-ear. J Acoust Soc Am, 69, 69:S43.

SHERA, C. A. and ZWEIG, G. 1992. Middle-ear phenomenology: the view from the three windows. J Acoust Soc Am, 92, 1356-70.

SIEBENMANN, F. 1898. Anatomie des Mittelohres. . Handbuch der Anatomie des Menschen, 5, 284.

SILMAN, S. and SILVERMAN, C. A. 1991. Auditory Diagnosis: Principles and Applications Academic, San Diego, Chap. 3, 79.

SIM, J. H. 2007. Imaging, physiology, and biomechanics of the malleus- incus complex.

SIM, J. H., CHATZIMICHALIS, M., LAUXMANN, M., ROOSLI, C., EIBER, A. and HUBER, A. M. 2010a. Complex stapes motions in human ears. J Assoc Res Otolaryngol, 11, 329-41.

SIM, J. H., CHATZIMICHALIS, M., ROOSLI, C., LASKE, R. D. and HUBER, A. M. 2012. Objective assessment of stapedotomy surgery from round window motion measurement. Ear Hear, 33, e24-31.

SIM, J. H., LAUXMANN, M., CHATZIMICHALIS, M., ROOSLI, C., EIBER, A. and HUBER, A. M. 2010b. Errors in measurement of three-dimensional motions of the stapes using a laser Doppler vibrometer system. Hear Res, 270, 4-14.

SIM, J. H., PURIA, S. and STEELE, C. 2007. Calculation of the inertial properties of the malleus–incus complex from micro-CT imaging. J Mech Mater Struct., 2, 1515–1524.

SIM, J. H., PURIA, S. and STEELE, C. R. 2004. Three-dimensional measurement and analysis of the isolated malleus-incus complex. In K. Gyo & H. Wada (Eds.),. In: OTOLOGY, T. R. I. S. O. M. E. M. I. R. A. (ed.) World Scientific. Singapore.

SIM, J. H., RÖÖSLI, C., CHATZIMICHALIS, M., EIBER, A. and HUBER, A. M. 2013. Characterization of stapes anatomy: investigation of human and guinea pig. J Assoc Res Otolaryngol, 14, 159-73.

SIM, J. H. and PURIA, S. 2008. Soft tissue morphometry of the malleus-incus complex from micro-CT imaging. J Assoc Res Otolaryngol, 9, 5-21.

SIM, J., RÖÖSLI, C., GERIG, R., DALBERT, A., FAUSCH, C., STENFELT, S. and HUBER, A. 2014. Abstract: Distribution of Intra-Cranial Sound Pressure During Bone Conduction Stimulation. Association for Research in Otolaryngology, 37th Annual MidWinter Meeting, Feburary 22-26. San Diego.

SIM, J.H., PURIA, S., 2008. Soft tissue morphometry of the malleus-incus complex from micro-CT imaging. J Assoc Res Otolaryngol. 9, 5-21.

SIM, J.H., PURIA, S., STEELE, C.R., 2004. Three-dimensional measurement and analysis of the isolated malleus-incus complex. In: Gyo K and Wada H (eds.), The 3rd International Symposium on Middle Ear Mechanics in Research and Otology. World Scientific Publishing, Singapore. 61-67.

SIM, R. J. and CHANG, P. 2008. Incudostapedial ankylosis from temporomandibular joint disruption. Otolaryngol Head Neck Surg, 139, 166-7.

SMELT, G., HAWKE, M. and PROOPS, D. 1988. Anatomy of the external ear canal: a new technique for making impressions. J Otolaryngol, 17, 249-53.

SOHMER, H. 2012. Two types of cochlear hair cells with two different modes of activation are better than one. J Basic Clin Physiol Pharmacol, 23, 1-3.

SOMERS, T., GOVAERTS, P., MARQUET, T. and OFFECIERS, E. 1994. Statistical analysis of otosclerosis surgery performed by Jean Marquet. Ann Otol Rhinol Laryngol, 103, 945-51.

SPROAT, R., BURGESS, C., LANCASTER, T. and MARTINEZ-DEVESA, P. 2014. Eustachian tube dysfunction in adults. Bmj, 348, g1647.

STENFELT, S. 2014. Inner ear contribution to bone conduction hearing in the human. Hear Res.

STENFELT, S. and GOODE, R. L. 2005. Bone-conducted sound: physiological and clinical aspects. Otol Neurotol, 26, 1245-61.

STUHLMAN, O. 1937. The nonlinear transmission characteristics of the auditory ossicles. J Acoust Soc Am., 9, 119–128.

SUN, Q., GAN, R. Z., CHANG, K. H. and DORMER, K. J. 2002. Computer-integrated finite element modeling of human middle ear. Biomech Model Mechanobiol, 1, 109-22.

SUTTON, C. M. 1990. Accelerometer Calibration by Dynamic Position Measurement Using Heterodyne Laser Interferometry. Metrologia, 27.

SUZUKI, M., KANEBAYASHI, H., KAWANO, A., HAGIWARA, A., FURUSE, H., YAMAGUCHI, T. and SHIMIZU, M. 2008. Involvement of the incudostapedial joint anomaly in conductive deafness. Acta Otolaryngol, 128, 515-9.

SWARTZ, J. D. and LOEVNER, L. A. 2011. Imaging of the Temporal Bone, Thieme.

SZPUNAR, J. and MISZKE, A. 1970. Fibrous ankylosis of the incudostapedial joint. Arch Otolaryngol, 92, 138-40.

SZYMANSKI, M., RUSINEK, R., ZADROZNIAK, M., MORSHED, K. and WARMINSKI, J. 2014. The influence of incudostapedial joint separation on the middle ear transfer function. Clin Exp Otorhinolaryngol, 7, 250-3.

TAN, F. M., GROLMAN, W., TANGE, R. A. and FOKKENS, W. J. 2007. Quality of perceived sound after stapedotomy. Otolaryngol Head Neck Surg, 137, 443-9.

TANNER-THIES, R. 2011. Physiology - An Illustrated Review, Thieme.

TAY, H. L. and MILLS, R. P. 1996. The mobility of the malleus and incus with varying middle ear pressures. Clin Otolaryngol Allied Sci, 21, 256-8.

TERRAHE, K., FROMME, H. G. and SCHULZ, J. 1970. [Electron microscopy scanning examinations of the histology of the ear ossicles]. Z Laryngol Rhinol Otol, 49, 733-42.

TERRAHE, K., FROMME, H. G. and SCHULZ, J. 1971a. [Sound conduction chain of the middle ear in chronic epitympanal otitis. A scanning electron microscopy study]. Z Laryngol Rhinol Otol, 50, 548-56.

TERRAHE, K., FROMME, H. G. and SCHULZ, J. 1971b. [Sound conduction chain of the middle ear in chronic epitympanal otitis. Scanning electronic microscope studies]. Z Laryngol Rhinol Otol, 50, 548-56.

TILLAUX, A. 1980. The external ear canal. Wiliams PL, Wawrick R, eds. Gray's Anatomy, 36th edn. London: Churchill & Livingstone, 1194.

TODD, N. W. 2009. Tympanum-canal angles anteriorly, anteroinferiorly, and inferiorly: a postmortem study of 41 adult crania. Ear Nose Throat J, 88, E22-7.

TODD, N. W. and CREIGHTON, F. X., JR. 2013. Malleus and incus: correlates of size. Ann Otol Rhinol Laryngol, 122, 60-5.

TONNDORF, J. 1960. Shearing motion in scala media of cochlear models. Proj Rep USAF Sch Aviat Med, 60, 1-10.

TONNDORF, J. and KHANNA, S. M. 1966. Ein Beitrag zur Funktion des Mittelohres. Archiv für klinische und experimentelle Ohren-, Nasen- und Kehlkopfheilkunde, 187, 431-438.

TONNDORF, J., KHANNA, S.M., 1967. Some properties of sound transmission in the middle and outer ears of cats. J. Acoust. Soc. Am. 41, 513–521.

TONNDORF, J., KHANNA, S.M., 1968. Submicroscopic displacement amplitudes of the tympanic membrane (cat) measured by a Laser interferometer. J. Acoust. Soc. Amer. 44, 1546-1554.

TONNDORF, J. and KHANNA, S. M. 1970. The role of the tympanic membrane in middle ear transmission. Ann Otol Rhinol Laryngol, 79, 743-53.

TONNDORF, J. and KHANNA, S. M. 1972a. Tympanic-membrane vibrations in human cadaver ears studied by time-averaged holography. J Acoust Soc Am, 52, 1221-33.

TONNDORF, J. and PASTACI, H. 1986. Middle ear sound transmission: a field of early interest to Merle Lawrence. Am J Otolaryngol, 7, 120-9.

TOTH, M., MOSER, G., ROSCH, S., GRABMAIR, G. and RASP, G. 2013. Anatomic parameters of the long process of incus for stapes surgery. Otol Neurotol, 34, 1564-70.

TOYNBEE, J. 1865. The diseases of the ear: their nature, diagnosis, and treatment. Philadelphia : Blanchard & Lea.

TRUAX, B. 1999. Phon, Second Edition 1999, Originally published by the World Soundscape Project, Simon Fraser University, and ARC Publications, 1978 [Online]. © Cambridge Street Publishing, 1999. Available: http://www.sfu.ca/sonic-studio/handbook/Phon.html [Accessed 31. March 2015].

V. BÉKÉSY, G. 1953. Description of Some Mechanical Properties of the Organ of Corti. The Journal of the Acoustical Society of America, 25, 770-785.

VALSALVA 1707. De aure humana tractatus. Trajecti ad Rhenum, 32.

VAN DER JEUGHT, S., DIRCKX, J. J., AERTS, J. R., BRADU, A., PODOLEANU, A. G. and BUYTAERT, J. A. 2013. Full-field thickness distribution of human tympanic membrane obtained with optical coherence tomography. J Assoc Res Otolaryngol, 14, 483-94.

VLAMING, M. S. and FEENSTRA, L. 1986. Studies on the mechanics of the normal human middle ear. Clin Otolaryngol Allied Sci, 11, 353-63.

VOLANDRI, G., DI PUCCIO, F., FORTE, P. and CARMIGNANI, C. 2011. Biomechanics of the tympanic membrane. J Biomech, 44, 1219-36.

VOLANDRI, G., DI PUCCIO, F., FORTE, P. and MANETTI, S. 2012. Model-oriented review and multi-body simulation of the ossicular chain of the human middle ear. Med Eng Phys, 34, 1339-55.

VON BÉKÉSY, G. 1960. Experiments in Hearing, McGraw.

VON BÉKÉSY, G. 1980. Experiments in hearing, R. E. Krieger Pub. Co.

VON HELMHOLTZ, H. 1869. Die Mechanik der Gehörknöchelchen und des Trommelfells, M. Cohen & Sohn.

VON SÖMMERRING, S. T. 1791. Vom Baue des menschlichen Körpers, Bd1 Knochenlehre & Bd2 Bänderlehre, Varrentrapp und Wenner.

VOSS, S. E., HORTON, N. J., WOODBURY, R. R. and SHEFFIELD, K. N. 2008. Sources of variability in reflectance measurements on normal cadaver ears. Ear Hear, 29, 651-65.

VOSS, S. E., ROSOWSKI, J. J., MERCHANT, S. N. and PEAKE, W. T. 2000. Acoustic responses of the human middle ear. Hear Res, 150, 43-69.

WADA, H., KOIKE, T. and KOBAYASHI, T. 1998. Clinical applicability of the sweep frequency measuring apparatus for diagnosis of middle ear diseases. Ear Hear, 19, 240-9.

WADA, H., METOKI, T. and KOBAYASHI, T. 1992. Analysis of dynamic behavior of human middle ear using a finite-element method. J Acoust Soc Am, 92, 3157-68.

WAJNBERG, J. 1987. The true shape of the tympanic membrane. J Laryngol Otol, 101, 538-41.

WANG, D. and BROWN, G. J. 2006. Computational auditory scene analysis : principles, algorithms and applications, Hoboken, N.J. John Wiley distributor. Chichester, Wiley interscience

WANG, H., NORTHROP, C., BURGESS, B., LIBERMAN, M. C. and MERCHANT, S. N. 2006. Three-dimensional virtual model of the human temporal bone: a stand-alone, downloadable teaching tool. Otol Neurotol, 27, 452-7.

WEBER, E. 1851. Über den Mechanismus des Gehörorgans. Verhandl. d. Kgl. Sächs. Gesellsch. d. Wissenschaften (Leipzig), 29-31.

WEISTENHÖFER, C. and HUDDE, H. 2000. Schwingungsformen der menschlichen Ossikelkette bei Luftschallanregung. Fortschritte der Akustik - DGA'2000.

WESTPHAL, W. H. 1947. Physik, Berlin, Heidelberg, Springer-Verlag.

WEVER, E. G., LAWRENCE, M. and SMITH, K. R. 1948. The middle ear in sound conduction. Arch. Otolaryngol., 48, 19-25.

WEVER, E. G. and LAWRENCE, M. 1954. Physiological acoustics, Princeton,, Princeton University Press.

WHITTEMORE, K. R., JR., MERCHANT, S. N. and ROSOWSKI, J. J. 1998. Acoustic mechanisms: canal wall-up versus canal wall-down mastoidectomy. Otolaryngol Head Neck Surg, 118, 751-61.

WHYTE, J. R., GONZALEZ, L., CISNEROS, A. I., YUS, C., TORRES, A. and SARRAT, R. 2002. Fetal development of the human tympanic ossicular chain articulations. Cells Tissues Organs, 171, 241-9.

WIENER, F. M. and ROSS, D. A. 1946. The Pressure Distribution in the Auditory Canal in a Progressive Sound Field. The Journal of the Acoustical Society of America, 18, 401-408.

WIGHTMAN, F. L. and KISTLER, D. J. 1989. Headphone simulation of free-field listening. I: Stimulus synthesis. J Acoust Soc Am, 85, 858-67.

WIGHTMAN, F. L. and KISTLER, D. J. 1992. The dominant role of low-frequency interaural time differences in sound localization. J Acoust Soc Am, 91, 1648-61.

WIKIPEDIA. 2015a. Helium-neon laser [Online]. Available: http://de.wikipedia.org/wiki/Helium-Neon-Laser [Accessed 3. May 2015].

WIKIPEDIA. 2015b. Helium-Neon-Laser [Online]. Available: http://de.wikipedia.org/wiki/Helium-Neon-Laser [Accessed 4. May 2015].

WIKIPEDIA. 2015c. Laser Doppler vibrometer [Online]. Wikipedia Foundation, Inc. Available: http://en.wikipedia.org/wiki/Laser_Doppler_vibrometer.

WILLI, U. 2003. Middle-ear Mechanics: The Dynamic Behavior of the Incudo-Malleolar Joint and its Role During the Transmission of Sound. Zurich.

WILLI, U. B., FERAZZINI, M. A. and HUBER, A. M. 2004. The mobility of the incudo-malleolar joint and associated middle-ear transmission losses. In: Gyo, K., Wada, H., Hato, N., Koike, T. (Eds.), Middle Ear Mechanics in Research and Otology. World Scientific, Singapore.

WILLI, U., FERRAZZINI, M. A. and HUBER, A. M. 2002. The incudo-malleolar joint and sound transmission losses. Hear Res, 174, 32-44.

WILLI, U., 2003. Middle-ear mechanics: the dynamic behavior of the incudo-malleolar joint and its role during the transmission of sound. Dissertation in Mathematics and Natural Science. University of Zurich, Zurich.

WILLIAMS, K. R., BLAYNEY, A. W. and LESSER, T. H. 1995. A 3-D finite element analysis of the natural frequencies of vibration of a stapes prosthesis replacement reconstruction of the middle ear. Clin Otolaryngol Allied Sci, 20, 36-44.

WILLIAMS, K. R. and LESSER, T. H. 1990. A finite element analysis of the natural frequencies of vibration of the human tympanic membrane. Part I. Br J Audiol, 24, 319-27.

WILSON, J. P. and JOHNSTONE, J. R. 1975. Basilar membrane and middle-ear vibration in guinea pig measured by capacitive probe. J Acoust Soc Am, 57, 705-23.

WOLFF, D., BELLUCCI, R. J. and EGGSTON, A. A. 1957. Surgical and microscopic anatomy of the temporal bone, Hafner Pub. Co.

WOLFF, D. and BELLUCCI, R. J. 1956. The human ossicular ligaments. Ann Otol Rhinol Laryngol, 65, 895-910.

WOO, S. L. and YOUNG, E. P. 1991. Structures and function of tendons and ligaments, In: Mow VC and Hynes WC (eds,). Basic orthopaetic biomechanics. New York: Raven Press. .

XIANG, N. and SABATIER, J. M. 2000. Land mine detection measurements using acoustic-to-seismic coupling. Proc. SPIE 4038, Detection and Remediation Technologies for Mines and Minelike Targets V, 645.

YAMADA, M., TSUNODA, A., MURAOKA, H. and KOMATSUZAKI, A. 1999. Three-dimensional reconstruction of the incudostapedial joint with helical computed tomography. J Laryngol Otol, 113, 707-9.

YANOFF, M., DUKER, J. S. and AUGSBURGER, J. J. 2009. Ophthalmology, Mosby Elsevier.

YOUNIS, M. I. 2011. MEMS Linear and Nonlinear Statics ans Dynamics, Springer US, Springer Science+Business Media, LLC.

ZAHNERT, T. 2003. [Lasers in ear research]. Laryngorhinootologie, 82 Suppl 1, S157-80.

ZAHNERT, T. 2007. Die Nanowelt des Hörens, The nanoworld of hearing. Wissenschaftliche Zeitschrift der Technischen Universität Dresden, 56, 147 - 151.

ZAKRISSON, J. E., BORG, E., DIAMANT, H. and MLLLER, A. R. 1975. Auditory fatigue in patients with stapedius muscle paralysis. Acta Otolaryngol, 79, 228-32.

ZAKRISSON, J. E. and BORG, E. 1974. Stapedius reflex and auditory fatigue. Audiology, 13, 231-5.

ZHANG, X. and GAN, R. Z. 2011. Experimental measurement and modeling analysis on mechanical properties of incudostapedial joint. Biomech Model Mechanobiol, 10, 713-26.

ZHAO, F., KOIKE, T., WANG, J., SIENZ, H. and MEREDITH, R. 2009. Finite element analysis of the middle ear transfer functions and related pathologies. Med Eng Phys, 31, 907-16.

ZUUR, C. L., DE BRUIJN, A. J., LINDEBOOM, R. and TANGE, R. A. 2003. Retrospective analysis of early postoperative hearing results obtained after stapedotomy with implantation of a new titanium stapes prosthesis. Otol Neurotol, 24, 863-7.

ZWISLOCKI, J. J. 1962. Analysis of the middle ear function. Part I. Input im- pedance. J Acoust Soc Am, 34, 1514-23.

ZWISLOCKI, J. J. 1963. Analysis of the middle ear function. Part II. Guinea-pig ear. . J. Acoust. Soc. Am. , 35, 1034–1040.

ZWISLOCKI, J., FELDMAN. A.S., 1963. Post-mortem acoustic impedance of human ears. J. Acoust. Soc. Am. 35, 104 ‐ 107.